Doctoral Dissertation
Doctoral Program in Energy Engineering (29th Cycle)

Modeling, design, testing and analysis of biogas-fed SOFC power plants

Marta Gandiglio

******

Supervisor(s):
Prof. Massimo Santarelli ,Supervisor
Dr. Andrea Lanzini , Co-Supervisor

Doctoral Examination Committee:
Prof. Blengini Giovanni Andrea, Politecnico di Torino (IT)
Prof. Kivihao Yari, *Referee*, VTT Technical Research Centre of Finland (FI)
Prof. Massardo Aristide, Università degli Studi di Genova (IT)
Prof. Russo Nunzio, Politecnico di Torino (IT)
Prof. Van Herle Jan, *Referee*, École polytechnique fédérale de Lausanne (CH)

Politecnico di Torino
2017

Declaration

I hereby declare that the contents and organization of this dissertation constitute my own original work and does not compromise in any way the rights of third parties, including those relating to the security of personal data.

Marta Gandiglio

2017

Alla mia famiglia.

Abstract

The present work is related to the complete analysis of biogas-fed SOFC system.

The first part of the work has been related to a review on the concept of polygeneration system and on the analysis of the current status of SOFC installations, especially when fed with biogas.

The use of a renewable fuel, coupled with carbon capture, can lead to negative emissions plants, defined as key technologies for reaching the goals set in the Paris Agreement. Furthermore, biogas and SOFC show many affinities which have been discussed in the works: from the high efficiency at low sizes to the availability of already existing subsidy schemes for electricity production. An analysis of the potential biogas production in EU is proposed, with focus on wastewater treatment plants. In this particular area, the work tries to point out the numbers of potential installed power by using SOFCs.

The experimental and modeling activities are then proposed. The PhD activity is linked to two European projects, SOFCOM and DEMOSOFC.

The first project is related to the analysis of biogas fed SOFC system with carbon capture and re-use. In this context, a demonstration plant has been developed and tested in the SMAT Castiglione wastewater treatment plant. Results show an easy process for the CO_2 capture from the SOFC exhaust, thus pointing SOFC as a key technology in the framework of negative carbon emissions plants. More

criticalities have been found in the choice of CO_2 utilization for production of algae in a photobioreactor: the unstable quality of the inlet wastewater coming from the plant, the fluctuating algae productivity as function of the weather conditions, and the algae attachment to the pipe, pointed out a need for improvements and research on this technology.

The experimental activity has been coupled with a modeling activity on the same concept of biogas fed SOFC, with the possibility of a downstream carbon capture and use/ sequestration. Different plant layout and different system sizes have been analyzed from a technical and economical point of view.

Finally, the analysis of a real industrial size SOFC system is proposed. This activity has been developed in the framework of the DEMOSOFC EU project, where the first industrial size biogas fed SOFC system will be installed. Being the first installation of its kind, many issued and improvements have been detected. The analysis is related to the system design and description, for what concerning plant integration (electrical and thermal), system operation, and biogas processing. Biogas processing has been especially pointed out as a key component in a biogas-fed SOFC system. Because of the low admissible contaminants levels for fuel cell, a new and dedicated cleaning unit is required, which is not currently available on the market. The processing unit design is proposed and ongoing experimental activity on the adsorption with activated carbons are proposed. The main harmful contaminants found in wastewater biogas are sulphur (in the form of H_2S) and siloxanes (mainly D4 and D5).

Contents

List of Figures

List of Tables

Nomenclature

AC	Alternate Current (if electrical)	ICE	Internal Combustion Engine
	Annual Costs (if economical)	IIR	Indirect Internal Reforming
	Activated Carbons (in Chapter 5)	LMTD	Log Mean Temperature
AD	Anaerobic Digestion		Difference
AP	Annual Production	MCFC	Molten Carbonate Fuel Cell
ASR	Area Specific Resistance	MOO	Multi-Objective Optimization
ASU	Air Separation Unit	MSC	Multi-Stage Compressor
ATR	Auto-Thermal Reforming	NETL	National Energy Technology
BEC	Bare Erected Cost		Laboratory
CCS	Carbon Capture and	NLPM	Normal Litres Per Minute
	Sequestration	NPV	Net Present Value
CCU	Carbon Capture and Use	OCV	Open Circuit Voltage
CF	Capacity Factor	OSR	Oxy-steam Reforming
CHP	Combined Heat and Power	OFMSW	Organic Fraction of
CMP	Compressor	Municipal Solid Waste	
CRR	Carbon Recovery and Re-	POx	Partial Oxidation
	utilization	PSA	Pressure Swing Adsorption
DC	Direct Current	SLPM	Standard Litres Per Minute
DIR	Direct Internal Reforming	SOFC	Solid Oxide Fuel Cell
DOE	Department Of Energy	SC	Steam to Carbon
EPCC	Engineering, Procurement and	SR	Steam Reformer/Reforming
	Construction Cost	TASC	Total As-Spent Capital
EPCM	Engineering, Procurement and	TOC	Total Overnight Capital
	Construction Management	TPC	Total Plant Cost
EU	European Union	VOC	Volatile Organic Compound
FC	Fuel Cell	WACC	Weighted Average Cost of
GHSV	Gas Hourly Space Velocity		Capital
HX	Heat Exchanger	WWTP	Waste Water Treatment Plant

Chapter 1

Introduction

The International Energy Agency (IEA), in the 2016 World Energy Outlook on Energy Climate and Change, stated that '*The mainstreaming of renewable energies has happened in recent years, with historically low costs of renewables contributing to the confidence that enabled agreement in Paris: costs for utility-scale solar photovoltaic (PV) are down by two-thirds, and for onshore wind by 30% compared with five years ago. However, serious challenges have also presented themselves. First off, countries will need to implement what they have pledged under the Agreement – their Nationally Determined Contributions (NDCs) – ensuring that their paper commitments are translated into real-world policies and actions. The ultimate success of the Paris Agreement will depend on the underlying ambition of the individual country contributions and the actions taken to realize them*'. (International Energy Agency (IEA) 2016)

A common and challenging goal is the results of the ongoing climate change international events, but national and international actions are required if we want to reach the final goal (see Figure 1, where ESCII past and 'theoretical' future trend are shown). At mid-2016, 163 NDCs have been officially submitted to the UNFCCC, representing 190 countries and corresponding to almost 99% of global GHG emissions. In the World Energy Outlook Special Briefing for COP21, the IEA estimated that if NDCs are implemented fully (the INDC Scenario, Figure 2), annual growth in energy sector GHG emissions slows dramatically by 2030 to around 0.5%, but does not yet come to a halt, which is a prerequisite for limiting temperature rise to 2°C or less. (International Energy Agency (IEA) 2016)

IEA analysis has pointed out that limiting temperature rise to 2°C will require a peaking of near-term global emissions and a marked decline after that (e.g. the 450 Scenario through 2030, Figure 2).

The IEA has also proposed a <u>Bridge Scenario</u> (Figure 2) using existing technologies that could deliver a peak in global energy-related emissions by 2020 at no cost to global economic activity compared with the INDC Scenario.
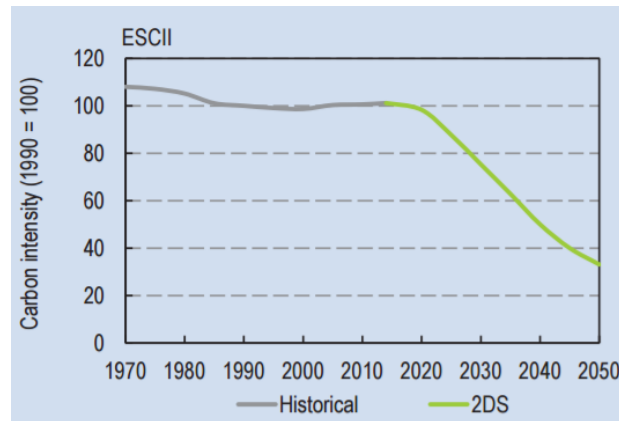
Figure 1. The Energy Sector Carbon Intensity Index (ESCII) since 1970, compared to 2DS targets. (European Commission 2016)
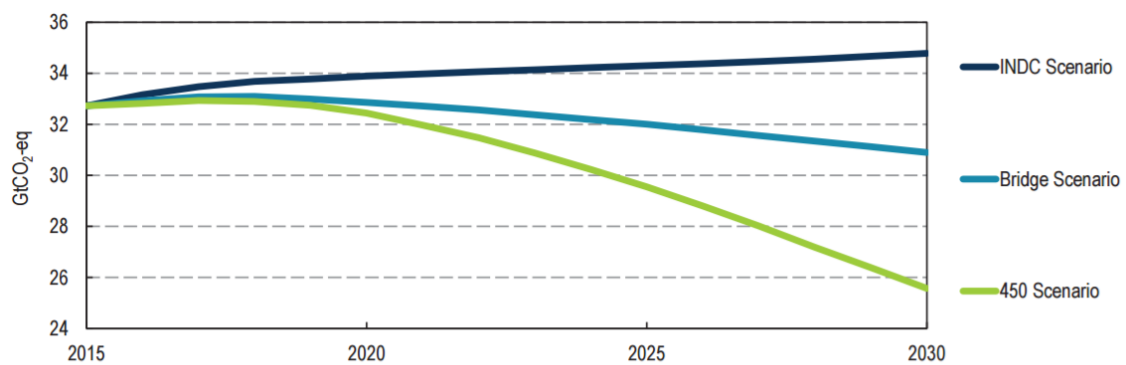
Note: The INDC Scenario depicted in this graph covers NDCs submitted up to 14 May 2015.

Figure 2. Global energy-related CO2 emissions under the INDC, Bridge, and 450 Scenarios through 2030. (International Energy Agency (IEA) 2016)
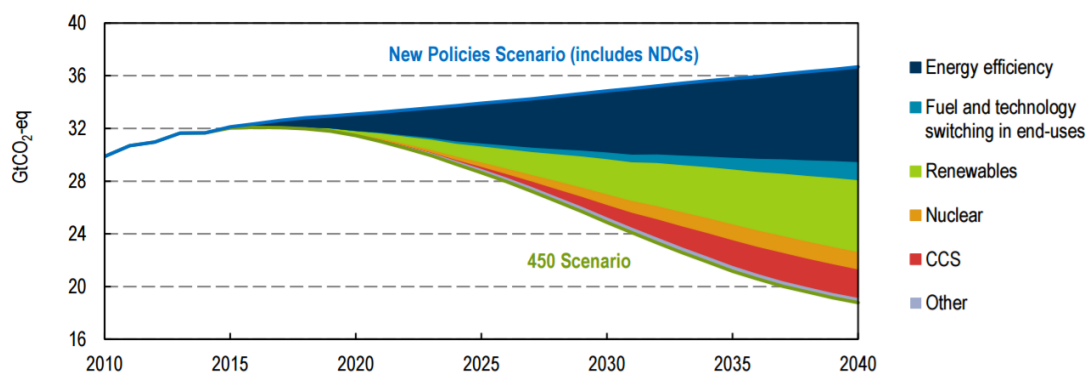
Note: The New Policies Scenario (NPS) is the central scenario of the World Energy Outlook and includes the energy-related components of NDCs submitted by 1 October 2015.

Figure 3. Measures needed to surpass current NDCs to reach 2°C trajectory (<u>450 Scenario</u>), through 2040. (International Energy Agency (IEA) 2016)

In Figure 3, measures required to move from the current NDCs to the 2°C trajectory are shown. Main efforts should be devoted to increasing energy efficiency, renewable, carbon capture and nuclear.

From the COP21 guidelines and agreements, domestic EU (2020 and 2030 Climate and Energy) plans have been defined, as shown in Figure 4. The Paris Agreement set an emission reduction target of -40% in 2030 respect to 1990, while 2030 EU target is more challenging for ETS (Emissions Trading System, -43% compared to 2005), and similar for non-ETS systems (-30% compared to 2005).

	International commitments		EU domestic legislation			
	Kyoto Protocol	Paris Agreement	2020 Climate and Energy Package		2030 Climate and Energy Framework	
			EU ETS	ESD	EU ETS (as proposal COM(2015) 337 final)	ESR (as proposal COM(2016) 482)
Target year of period	Second commitment period (2013-2020) (target for EU-28)	Already in force – covers the period post 2020	2013-2020	2013-2020	2021-2030	2021-2030
Emission reduction target	-20%	at least -40% in 2030	-21% compared to 2005 for ETS emissions	Annual targets by MS. In 2020 -10% compared to 2005 for non-ETS emissions	-43% compared to 2005 for ETS emissions	Annual targets by MS. In 2030 -30% compared to 2005 for non-ETS emissions
			Overall target: -20% GHG emissions reduction vs 1990"		Overall target: "at least -40% domestic GHG emissions reduction vs 1990"	
Further targets	-	• limiting global warming to well below 2°C.; • every 5 years to set more ambitious targets as required by science; • report on implementation/ track progress towards the long-term goal through a robust transparency and accountability system. • balance between anthropogenic emissions by sources and removals by sinks of greenhouse gases in the second half of this century	✓Renewable Energy Directive: 20% share of renewable energy of gross final energy consumption; ✓Energy Efficiency Directive : Increase energy efficiency by 20 %		✓At least 27% share of renewable energy in EU energy consumption; ✓At least 27% improvement in energy efficiency (to be reviewed by 2020, having in mind an EU level of 30%)	

Figure 4. Overview of Climate targets (European Commission 2016).

It is in this context that the author has developed the thesis work. With a worldwide goal of reducing emissions, biogas-fed SOFC systems are a potential key technology for

1) increase in energy efficiency (because of the high-efficiency electrochemical conversion within the fuel cells)

2) larger use of renewable sources (since biogas is produced from wastes)

3) and potentiality for an 'easy' CO_2 capture towards negative CO_2 emissions.

This study is linked with the concept of bio-energy with carbon capture and storage (BECCS), discussed by the International Energy Agency as a carbon reduction technology offering permanent net removal of carbon dioxide (CO_2) from the atmosphere (International Energy Agency 2011; Rhodes & Keith 2008). The advantages of the system are clearly show in Figure 5. The European Biofuels Technology Platform also confirm that there is an urgent need for carbon-negative solutions such as Bio-CCS – the only largescale technology that can efficiently remove CO_2 from the atmosphere (European Technology Platform for Zero Emission Fossil Fuel Power Plants 2012).

The concept of BECCS is drawn from the integration of trees and crops, which extract carbon dioxide (CO_2) from the atmosphere as they grow, the use of this biomass in processing industries or power plants, and the application of carbon capture and storage via CO_2 injection into geological formations. In the IPCC Fourth Assessment Report by the Intergovernmental Panel on Climate Change (IPCC). BECCS was indicated as a key technology for reaching low carbon dioxide atmospheric concentration targets (Fisher, B.S., N. Nakicenovic, K. Alfsen, J. Corfee Morlot, F. de la Chesnaye, J.-Ch. Hourcade, K. Jiang, M. Kainuma & A. Matysek, A. Rana, K. Riahi, R. Richels, S. Rose, D. van Vuuren 2007). The negative emissions that can be produced by BECCS has been estimated by the Royal Society to be equivalent to a 50 to 150 ppm decrease in global atmospheric carbon dioxide concentrations (The Royal Society 2009).
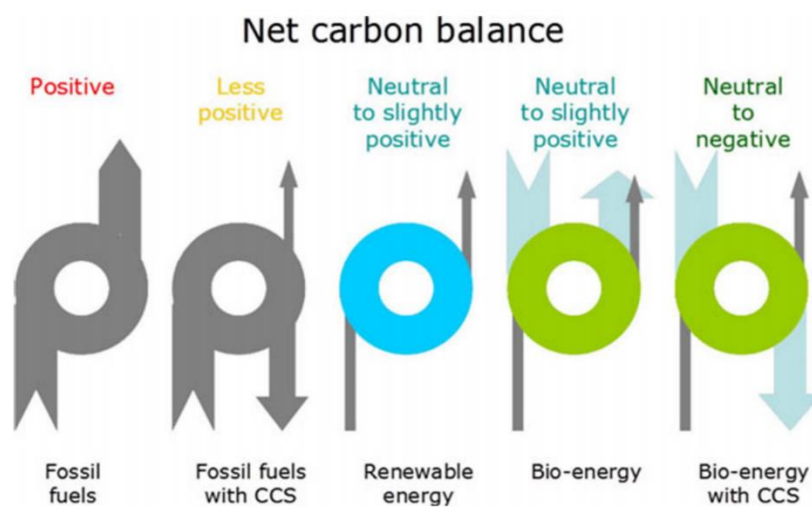
Figure 5. Net carbon balance for different plant concepts. (Jasmin Kemper 2016; European Technology Platform for Zero Emission Fossil Fuel Power Plants 2012)

The three-year studies have focused on the analysis of specific SOFC installations in biogas production sites (Waste Water Treatment Plants, WWTP), modeling and techno-economic analysis of biogas-fed SOFC systems and analysis of the potential for SOFC systems in the biogas market. Furthermore, the possible use of SOFC for polygeneration has also been analyzed, by studying a specific installation where carbon capture and re-use was performed, achieving a final tetra-generation plant.

The introduction section will discuss the novelty around the concept of polygeneration and the start-of-the-art of polygeneration systems based on fuel cells. The current scenario for biogas-fed fuel cell systems, from a scientific and industrial point of view, is then reviewed.

1.1 The polygeneration concept

'*One major drawback of single products processes is their low adaptability to the fluctuations of market prices, especially the crude oil price. With polygeneration, economic risks can be reduced by diversification of product portfolios, and potentially higher profits can be achieved compared to the single-product plants by optimization of portfolios*' (Y. Chen, Adams II & Arton 2011).

Thomas A. Adams II has widely analyzed Polygeneration concept in his works. In hise first two works, both published in 2011 (Y. Chen, Adams II & Barton 2011; Y. Chen, Adams II & Arton 2011), the author analyzed in detail a coal/biomass-based polygeneration system. He demonstrated that this process exhibits better economic performance and lower CO_2 emissions than conventional energy production processes. The analyzed system includes a gasifier, a cleaning unit, and upgrading unit and an air separation unit. It can be fed by two streams (Illinois coal and straw); the systems is then able to produce power (from a gas turbine a steam turbine), liquid fuels (naphtha and diesel from Fischer-Tropsch (FT)) and chemicals (methanol from a synthesis process). Key decision variables for the plant operation are inlet stream flow rates, split fractions among the different units and conversion rates in the reactors. Economic variables are indeed prices for input and output streams, the cost of carbon capture and storage and the carbon tax. Two case studies are presented here: (1) for the power production (higher power price) and (2) for the liquid fuel production (higher liquid fuels price). Results for case (1) show that the optimal configuration leads to a 100% power production, while for case (2) a different share is pointed out: 85% methanol, 13% liquid fuels and 2% power. The preference of power and liquid fuels generation are strongly based on the ratio of naphtha price to power price. Biomass use is depending both on feedstock price and carbon tax, while carbon tax policy is also influencing the products distribution. Finally, the system (both with and without CCS) is compared to single-product plants showing a higher NPV compared to traditional plants for different liquid fuel prices.

Previous scientific works on polygeneration have also been developed: (Meerman et al. 2009) analyzes and integrated gasification cogeneration system able to produce multiple products (chemical) from multiple fuels. (Mantripragada & Rubina 2009) and (Hamelinck et al. 2004) present the analysis of a polygeneration plant (liquid fuels and power) with the option of carbon capture. A combination of Gas Turbine (GT) and FT is indeed available in (Wang et al. 2008).

Furthermore, a large number of literature works is related to the optimal operation of polygeneration systems: as stated again by Thomas A. Adams II in (Y. Chen, Adams II & Barton 2011), in flexible systems, the various product rates change throughout the lifetime of the plant in response to market conditions in different scenarios. These flexible polygeneration systems can achieve higher net present values than static ones for the same oil price and the carbon tax. From this work, it is clear that one of the advantages of

polygeneration systems is related to the definition of the optimal operating strategy. Different Mixed-Integer Linear Programming (MILP) and Mixed-Integer NonLinear Programming (MINLP) methods have been analyzed for the optimal operation of multi-products systems, such as (Liu et al. 2007; Liu et al. 2010b; Liu et al. 2010a; Liu et al. 2009).

(Rong & Lahdelma 2016) also presented another recent and interesting discussion on polygeneration systems. The work from the authors in mainly devoted to the analysis of CHP and CCHP plants able to produce power, heat, and cold. Chicco et al. have deeply analyzed similar poly-generation systems for what concerning the operation and the control (Chicco & Mancarella 2007; Chicco & Mancarella 2009; Chicco & Mancarella 2008). A typical feasible operating region for a simple CHP system, defined by power production, heat production, and costs, is shown in Figure 6.
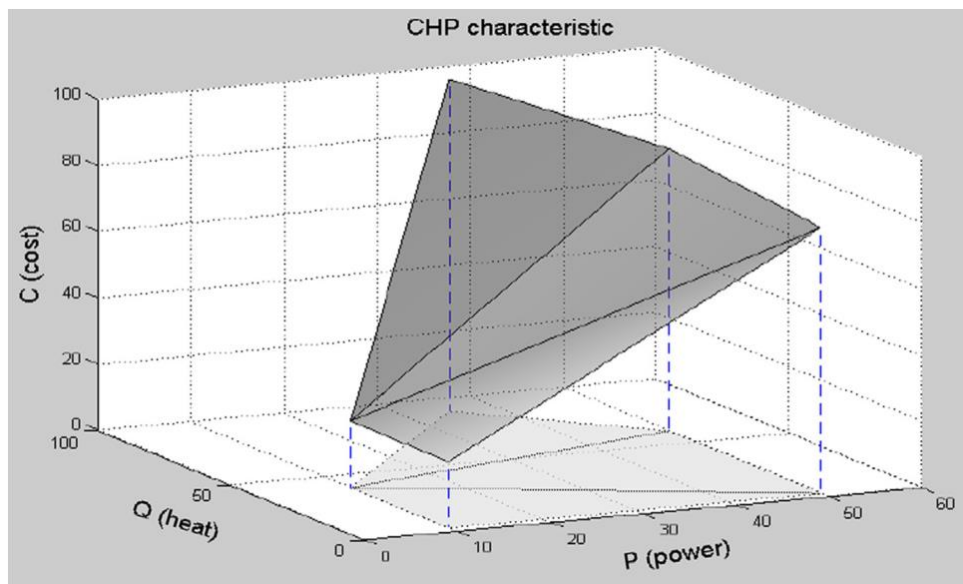
Figure 6. The feasible operating region of a convex CHP plant (Rong & Lahdelma 2007).

The coupling of a renewable feed and cogeneration systems has also been studied and reviewed by (Raj et al. 2011) and (Dong et al. 2009), where heat&power only was analyzed. In fact, even if we analyze a cogeneration system (the simplest form of polygeneration) it is pointed out that plants do not always include CHP, even if it is an 'easy' way to increase an overall system efficiency by heat recovery from exhaust. (Rong & Lahdelma 2016) shows the distribution of CHP share for national power production in Europe (taken from (International Energy Agency (IEA) 2011)). Northern countries, such as Denmark, Finland, and Netherlands has achieved a share among 30 and 50%, while the average EU value is around 10%. In the US, polygeneration in power production sites accounts for only 9% (Jradi & Riffat 2014).

As already discussed, one of the main criticalities in the adoption of polygeneration systems is the requirement of an optimization of products generation, because of the strong interdependence among them (Bazmi & Zahedi 2011). Production strategies should include long-term planning (to determine capacity investments and types of production technologies), medium-term planning (to find the allocation of fuel, emissions, and maintenance) and short-term planning (for the unit commitment and economic dispatch) (Rong & Lahdelma 2016). Other interesting considerations of the presented review paper are related to the refinery concept: refineries are poly-generation plants producing various fuels and chemicals from crude oil.

1.1.1 CO$_2$ capture and re-use

The presented SOFCOM tetra-generation plant was combining the advantages of a poly-generation system with the concept of carbon capture. Carbon capture is one of the key efforts for the achievement of the COP21, as discussed in the first paragraph and shown in Figure 3. The SOFCOM prototype plant, as will be discussed in Subchapter 3.5, was designed to produce pipeline quality CO$_2$, suitable for sequestration. Carbon sequestration seems, in fact, the first option to deal with the separated carbon dioxide at large scale and in large quantities. Furthermore, a tubular photobioreactor was installed to demonstrate, at least at a technical level, the carbon re-use and re-fixation in the form of fuel is an achievable target. In this way, inside the SOFCOM plant, the carbon cycle was closed, and no carbon was emitted to the atmosphere or send to the underground (Figure 7).

A similar concept, without the biogas feeding and algae production, and especially without experimental activities, can be found in (Kuramochi et al. 2011), where the authors proposed an SOFC based system with carbon capture.
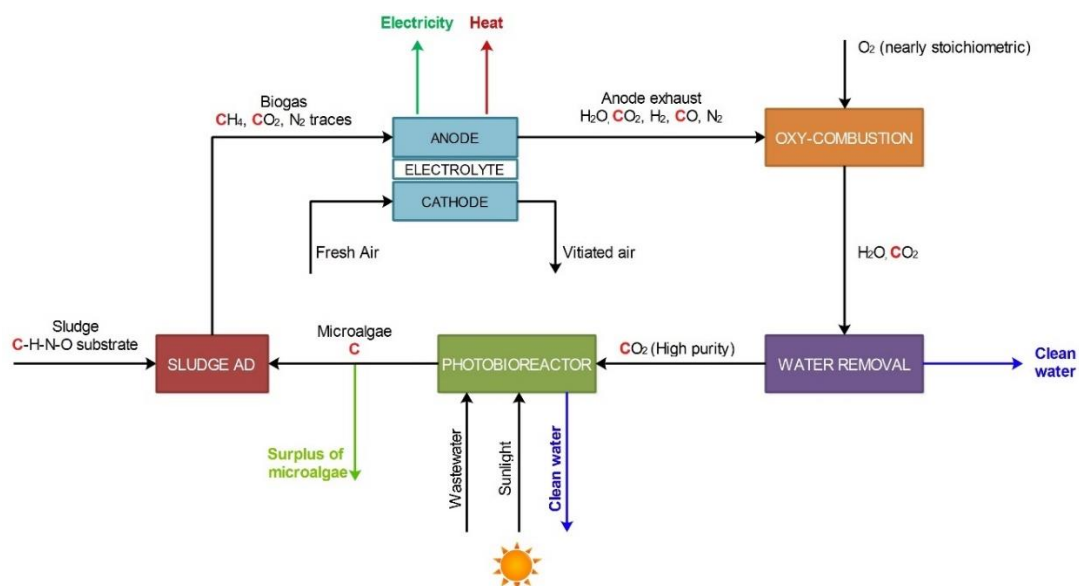
Figure 7. Carbon cycle (red C in the figure) in the SOFCOM proof-of-concept.

Carbon dioxide capture and storage (CCS) is considered a crucial strategy for meeting CO_2 emission reduction targets. (Leung et al. 2014) analysed the different technologies for CCS. Over the past century, the atmospheric CO_2 level has increased more than 39%, from 280 ppm during the pre-industrial time to the record high level of 400 ppm in May 2013 with a corresponding increase in global surface temperature of about 0.8 °C. CO_2 capture technologies are available in the market but are costly in general, and contribute to around 70–80% of the total cost of a full CCS system including capture, transport, and storage (Leung et al. 2014).

Figure 8 resumes the available technologies for carbon capture:

- Post-combustion of CO_2. It is the most mature and tested technology, even in large scale plants. The typical area of application is coal-fired and gas-fired plants. One of the main disadvantages is related to the low efficiency at low CO_2 concentrations in the exhaust gas.
- Pre-combustion of CO_2: this is also a commercially viable technology, usually devoted to coal-gasification plants. Criticalities are related to efficiency reduction at low CO_2 concentrations and temperature associated heat transfer problems since the process is performed before the combustion.
- Oxy-fuel carbon capture: this process is again applicable to coal-fired and gas-fired plants. The use of pure oxygen reduces the total flow sent to the CO_2 separation process with consequent lower component size. On the contrary, the production of pure oxygen, even if commercially available, can reduce the total process efficiency.
- Chemical looping carbon capture: this process has a potential higher efficiency than commercial carbon capture technologies because of the non-direct mix between air and fuel, thus avoiding the nitrogen. However, demonstrations at large scale are required to prove the potential advantages.

In any of the chosen cases, there are then the different technological option for the carbon dioxide separation: absorption, adsorption, chemical looping combustion, membrane separation and cryogenic distillation.
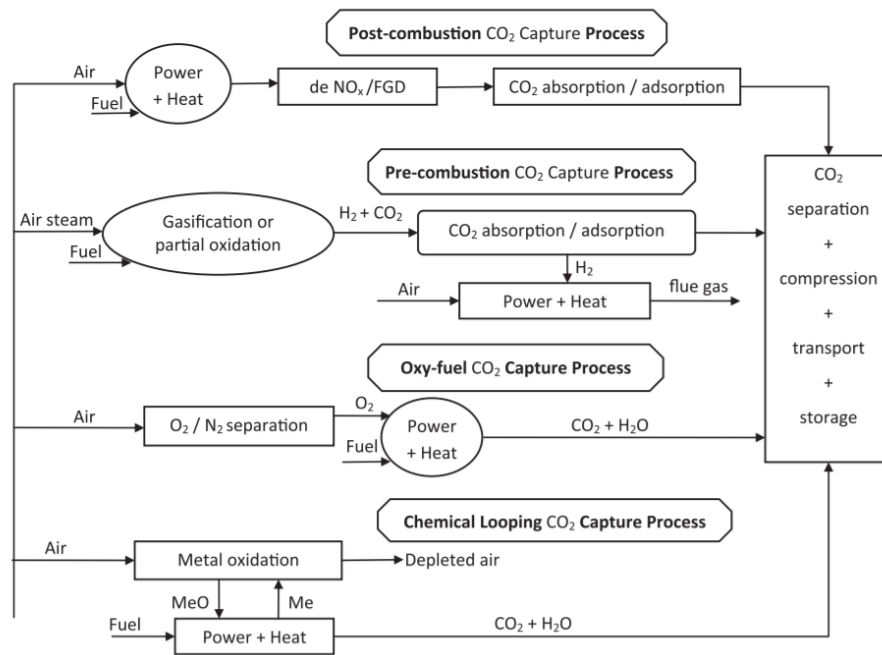
Figure 8. CO_2 capture technologies. (Leung et al. 2014)

The SOFCOM plant was performing an oxy-fuel carbon capture with CO_2 separation through a pressurized membrane. Use of membranes could lead to high efficiency and avoid high costs (economic and environmental) for sorbents replacement and regeneration. On the contrary, fouling and operational problems could occur.

After the first separation step, whatever the chosen final fate of CO_2, a reliable, safe and economically feasible system of transport is a key feature of any CCS project. Depending on the volumes involved a variety of means of transport may be utilized, ranging from road tankers to ships and pipelines (Leung et al. 2014). In the same review paper, the authors stated that the best option for CO_2 transport would depend on a variety of parameters including:

- volumes of CO_2 to be transported
- planned lifetime of the CO_2 source (e.g. power plants, steel and cement factories)
- the distance between CO_2 source and storage area
- onshore vs. offshore transport and storage
- typology of transporting infrastructure available (i.e. road and rail networks, pipelines trunks, shipping docks facilities)

By now, the pipeline is considered to be the most viable solution if large volumes of CO_2 are available for a long time.

The third step for CO_2 capture is related to the utilization or sequestration. Concerning the use of carbon dioxide, the review proposed different options:

- Production of ammonia and urea
- Enhanced oil recovery (EOR)
- CO_2 as a cushion gas for energy storage
- Use through mineralization, a process based on the accelerated reaction of CO_2 with Mg/Ca-rich silicate rocks or inorganic wastes to form stable carbonates
- MCFC for CO_2 capture. Molten Carbonate Fuel Cells requires a high concentrated stream at the cathode side. If located close to a carbon capture site, this combination could partially (because of the limited carbon utilization at the cathode) capture the CO_2. (Hill et al. 2015)
- Large scale, economic photocatalytic conversion of CO_2 into methane (CH_4) and methanol (CH_3OH) represents a formidable scientific and technical challenge.
- In a more general view, the use of CO_2 for the production of new fuel (re-fixation of the carbon atom) could be a powerful way to enhance the carbon capture process. (Aresta et al. 2013). In (Styring et al. 2011) the authors discussed the use of CO_2 for the chemical industry, for mineral carbonation and to grow microalgae (Chiu et al. 2008). Although these options are for the most part in the R&D phase, they offer the potential for value-added applications of carbon dioxide captured from an industrial installation or power plant.

Currently, CO_2 utilization accounts for only 2% of emissions. The second option for carbon dioxide is the sequestration: CO_2 can be stored in geological formations such as deep saline aquifers which have no other practical use, and oil or gas reservoirs. From the Life Cycle Assessment (LCA) of CCS and CCU performed in (Cuéllar-Franca & Azapagic 2015), it is clear that, depending on the analysed scenario, environmental impacts related to the CCU are not always lower than the ones related to CCS, because of the low efficiency and high costs for carbon utilization.

(Leung et al. 2014) conclude their review by declaring that, although technologies regarding the capture and storage of CO_2 exist, we should reduce the overall cost of using current CCS procedures, which is still high, before we can widely deploy similar systems. There are multiple hurdles to CCS deployment that need to be addressed in the coming years, including the absence of a clear business case for investment in CCS, and the absence of robust economic incentives to support the additional high capital and operating costs associated with CCS (Rubin et al. 2013).

1.2 Commercial fuel cell systems for stationary use

The Fuel Cell & Hydrogen Annual Review (4th Energy Wave 2016) and the Fuel Cell Industry Review (E4Tech 2015) recently analyzed the commercial status of stationary fuel cell system.

The main area of interest for the fuel cell market are Asia, North America, and Europe. The rest of the world is always presented but negligible regarding production and installations. In all the three mentioned regions, there are around 100 fuel cell companies (Figure 9), but only 50-60% has a commercial product available on the market. Half of them are probably still working on R&D to develop a commercial product in the next years.

The share of shipments by region (Figure 10) is dominated by Asia, with nearly 54'000 units shipped over around 65'000, and 246 MW over 479 MW globally shipped. Japan is producing and installing stationary fuel cell systems and FCEV, together with Korea and China, which is rapidly accelerating the development of FCEV. This trend is mainly due to the high Government investment in fuel cells, as is happening in Japan for the Ene.farm project. An increasing trend, regarding MW (but not units), is also seen in North America, thanks to the Toyota Mirai FCE, the success of lift trucks and the ongoing installation of stationary systems (especially in countries where dedicated incentives are available).

Figure 9. Global fuel cell system and stack company, by region, 2015. (4th Energy Wave 2016)

The stationary area dominates the share between the different fuel cell applications (portable, stationary and transport) regarding units shipped (Figure 11): data show an increase in 2016 (around 65'000 units) after a sensible decrease in 2015. The same trend is also confirmed by the transport sector. Regarding power shipped (MWs), the transport sector has surpassed the stationary one during 2016.

Among different fuel cell types, PEMFC is dominating the shipments because of the residential micro-CHP systems and FCEV, followed by SOFC (Figure 12). Regarding

MWs shipped, PEMFC show again the major share, while SOFC, MCFC, and PAFC all show similar values.
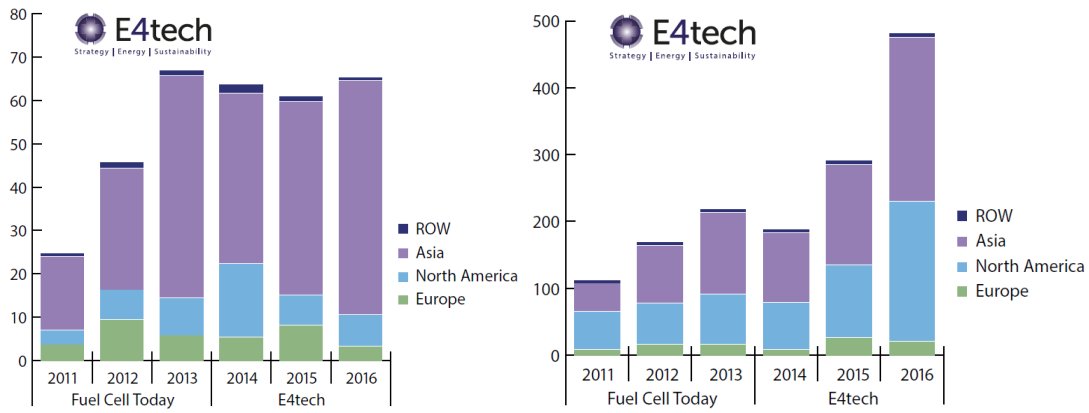
Figure 10. Units (1'000 units, on the left) / Megawatts (on the right) shipped by region 2011 - 2016 (1,000 units). (E4Tech 2015)
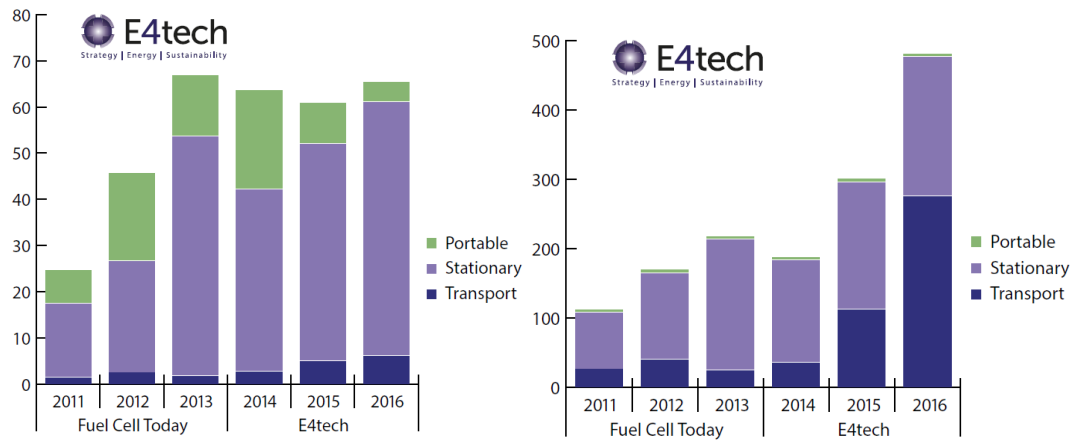
Figure 11. Units (1'000 units, on the left) / Megawatts (on the right) shipped by application 2011 – 2016. (E4Tech 2015)
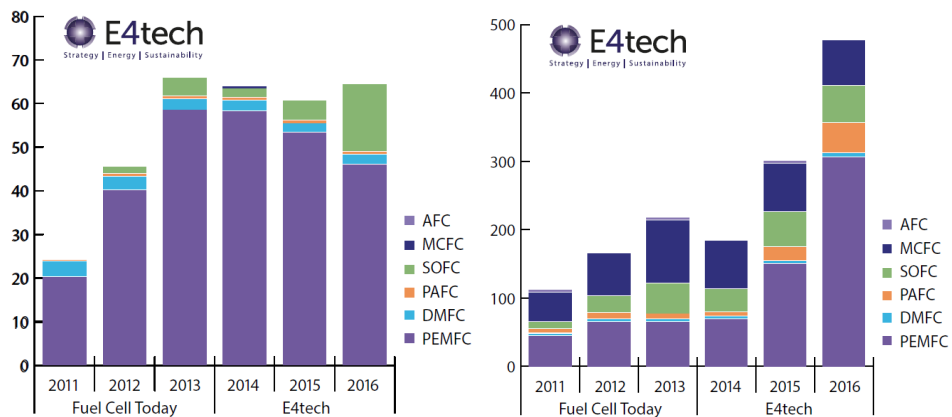
Figure 12. Units (1'000 units, on the left) / Megawatts (on the right) shipped by fuel cell type 2011 – 2016. (E4Tech 2015)

The 4th Energy Wave report describe the fuel cell industry as a pyramid where at the top, with commercial products and the current focus on costs, only few industry are located (FuelCellEnergy, Hydrogenics, and others for a total number of around 30 companies). In the middle layer, companies close to a commercial product and cost aware can be found (such as Powercell and Sunfire. All the rest of the industry is located at the bottom of the pyramid, with no commercial product and no incomes from the fuel cell selling.

From a business point of view (Figure 13), the fuel cell market is, as happens for new technologies, blocked between the adoption and the production. Because of the low production volumes, fuel cell costs are still high, and so the adoption is not increasing; on the contrary, because of the low adoption (installations), the production volumes are reduced and so costs are high. A dedicated subsidy system is the only answer to start a growing trend of installations and production volumes.
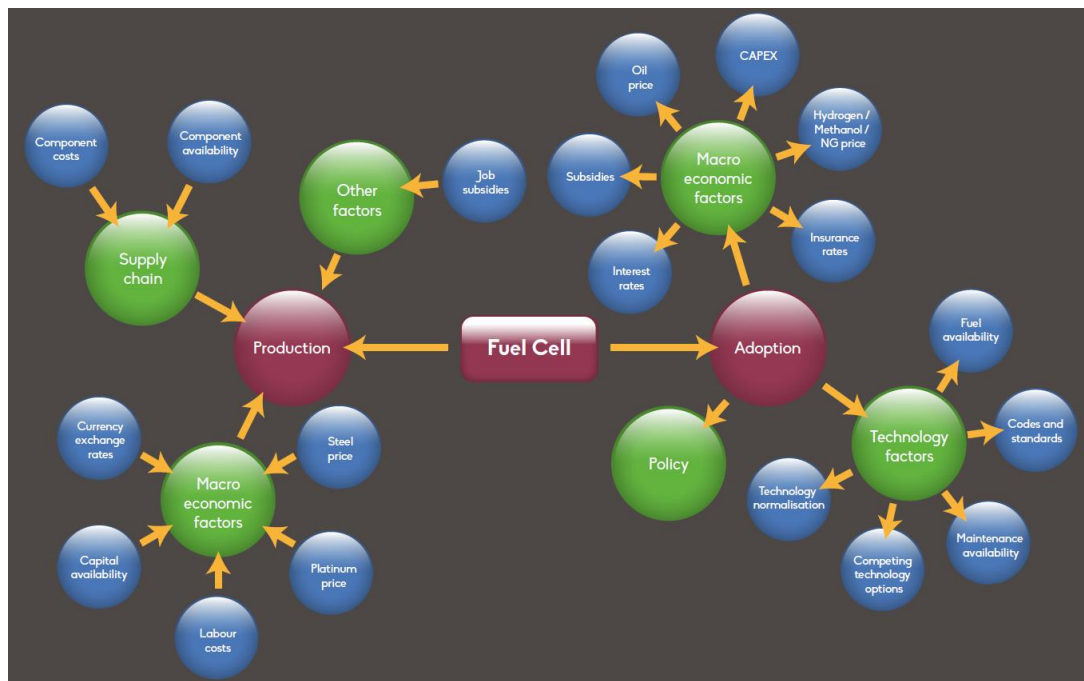
Figure 13. Influencing Factors and Pain Points. (4th Energy Wave 2016)

(4th Energy Wave 2016) also presents the attractiveness indexes for the four analyzed geographical areas: higher values are related to the focus on energy pollution and decarbonisation, growing market demand for fuel cells and removal of barriers to the adoption of the systems. Currently, low indexes refer to dedicated policies and subsidies, which are not present in most of the area analyzed.

As will be discussed later, currently, the most growing area for fuel cells, with investments and installations under development, is Asia. Here, thanks to the Ene.Farm project (Figure 14), a high number of installations has been performed (50'000 only in 2016, for a cumulative number of installations equal to 180'000 during September 2016)

and fuel cells (PEM and SOFC) costs have been more than halved in the last decades. The cost for the residential FC-based micro-CHP system is now around 15'000 $ of CAPEX (for SOFC), while in 2009 the value was higher than 25'000 $ (the units are 0.7-1 kW each). The payback period for the investment is around 18 years at full price, and this is the reason why incentives are still ongoing to further reduce costs. The target for 2010 is a CAPEX around 9'250 $ with a payback time of 7/8 years.

For larger systems, such as the ones analyzed in this work, we expect the same trend. The Roland Berger Consultancy has developed the analysis of the current and future stationary SOFC costs (for industrial application) for the European Union (Roland Berger Strategy Consultants 2015). Here, the author shows cost trends for the 1 kW, 50 kW, and multi-MW SOFC. Figure 15 shows the SOFC cost trajectories: the 'as is' case study refers to an early commercial product in the EU market. Production volumes, even if reduced, could strongly help companies in reducing (more than 50%) that cost. Currently, stack purchasing or assembling is, in fact, dominating the cost.
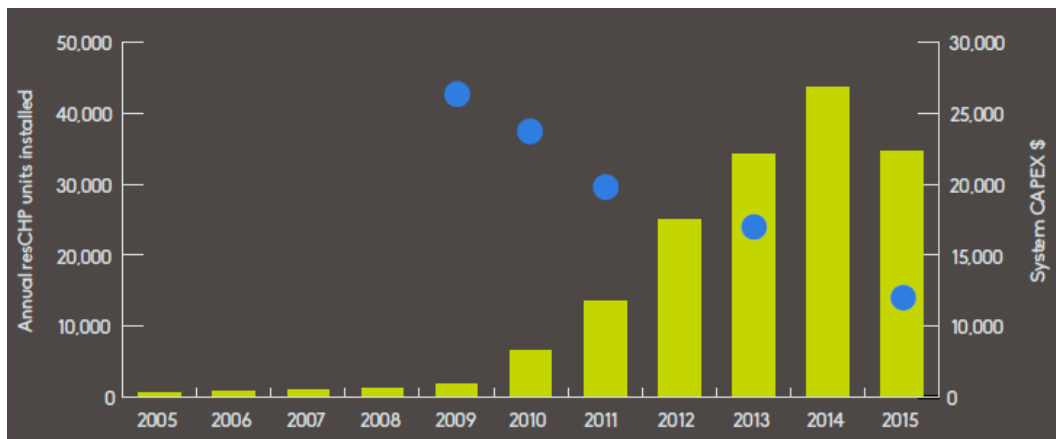
Figure 14. Japanese ENE-FARM Deployments and System Cost: 2005 – 2015. (4th Energy Wave 2016)

Some specific countries have seen a strong increase in industrial fuel cell installations because of specific and dedicated incentives (for medium-large size stationary applications, in the US):

- Beginning in 2017, the State of California Self-Generation Incentive Program (SGIP) will provide partial reimbursement of the capital costs for FC power plants. The reimbursement is 50 percent up-front, and 50 percent over time-based on $0.60/watt ($600/kW) for CHP configured plants operating on natural gas and up to $1.20/watt ($1,200/kW) for CHP configured plants operating on renewable biogas (Figure 16).
- The State of Connecticut has a performance-based renewable energy program divided into two categories including low emission renewable energy credits (LREC's) that FC plants are eligible for and zero emission renewable energy

credits (ZREC's) for solar and wind. Under the program, the two major electric utilities in the State enter into 15-year contracts to purchase renewable energy certificates from renewable power generation installations.

- New York's Clean Energy Standard is structured to fight climate change, reduce air pollution, and ensure a diverse and reliable energy supply. Fuel cells operating on natural gas or renewable biogas are eligible. The Renewable Portfolio Standard Program Purchase of Renewable Energy Attributes utilizes renewable energy credits (REC's) under a structure where the State purchases the environmental attributes of a power generation project at a fixed price over a 15-year term. (FuelCellEnergy 2017)
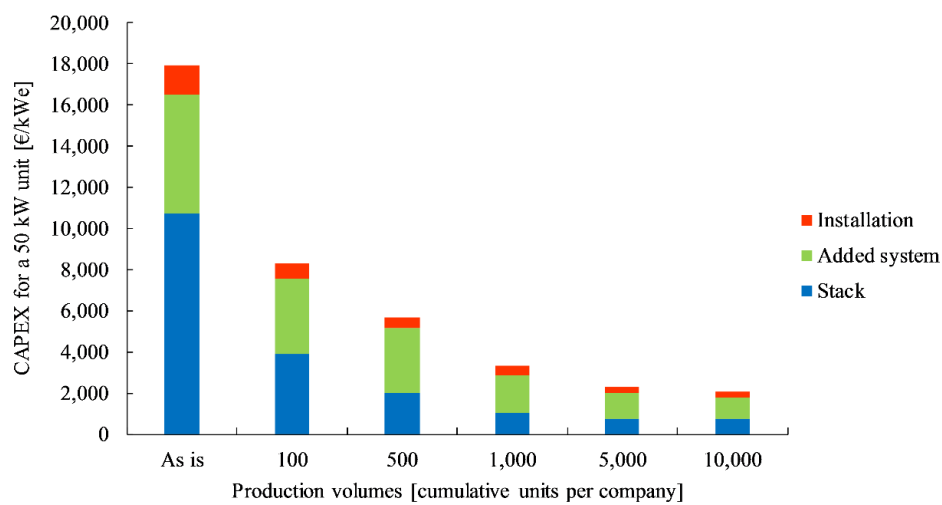
Figure 15. Investment costs trajectories for a 50 kW SOFC module. Author's elaboration of (Roland Berger Strategy Consultants 2015)
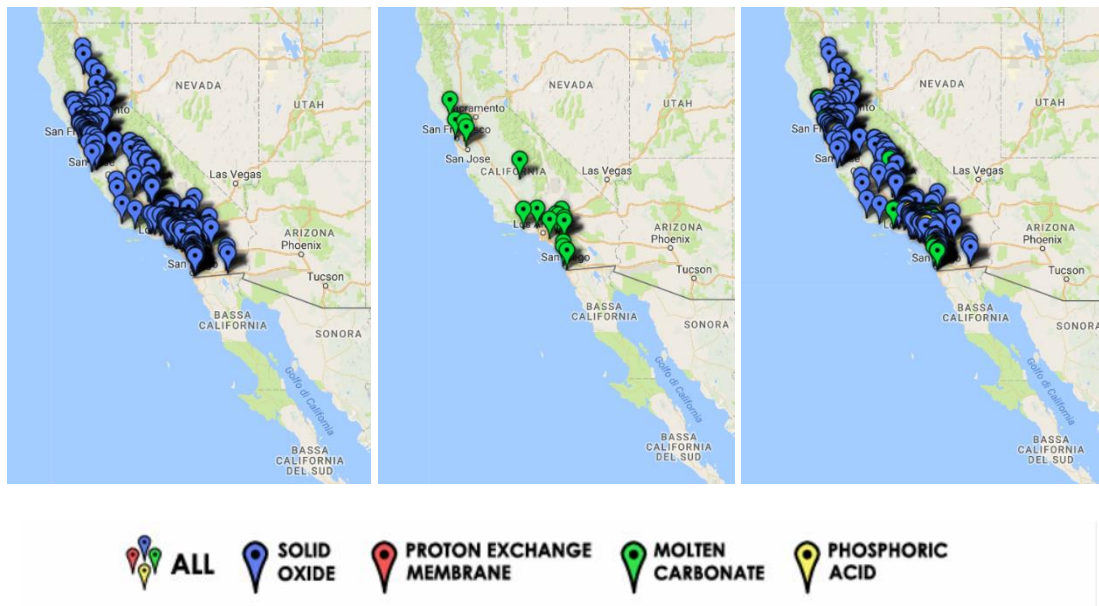
Figure 16. Fuel cell installations in California. (California Stationary Fuel Cell Collaborative (CaSFCC) 2016)

Analyzing only SOFCs, an analysis of the potential market in EU has been developed by (Roland Berger Strategy Consultants 2015). The authors define three application groups for stationary SOFC:

1) Power security (data centers, base stations)
2) Power and heat intensity (pharmaceuticals, chemicals, pulp industry)
3) Availability of fuel (WWTP biogas, breweries biogas)

The defined potential for distributed generation applications is defined around 1'500 MWel, calculated starting from the current installed capacity and accounting for the exchange time of current systems and the non-gas fired technology. Among the wide possible applications for SOFCs, biogas is a near-term approachable market. The Roland Berger study focuses on WWTP and breweries.

Bloomenergy, the only large size SOFC producer is US (California), declared an installed power around 200 MW installed, with 150 MW only in the US. Bloom Energy Servers produce power for companies including Apple, Wal-Mart, AT&T, eBay and FedEx, as well as notable non-profit organizations such as Caltech and Kaiser Permanente. Also, with its Mission Critical Systems practice, Bloom Energy provides grid-independent power for critical loads in data centers and manufacturing. (Anon n.d.)

Chapter 1.3 will present the potential use of fuel cells for polygeneration production, while Chapter1.4 will analyze the specific case study of biogas-fed fuel cells, providing a state of the art of the proposed concept and by introducing the potential of this market, which will be then deeply analyzed in Chapter 2.

1.3 Polygeneration with fuel cell systems

Among the different technologies available for polygeneration, fuel cells are one of the most promising choices for an emission-free generation of electricity, heat, and chemicals.

The key advantage of fuel cells is the electrochemical power production, which leads to an ion transfer without having any combustion, and consequently any direct contact between the anode (fuel) and the cathode (usually air) stream. For this reason, the production of chemicals from the anode exhaust is easier, since the anode outlet present a high concentrated and non-diluted exhaust gas.

At the Orange County Sanitation District, a trigeneration system based on Molten Carbonate Fuel Cells (MCFC) has been installed in the last years (from September 2010). The system, fed by biogas from the local WWTP, was able to produce electricity, heat, and hydrogen simultaneously. Hydrogen was feeding a hydrogen vehicle fueling station, located on the premises. The project was funded by the Department Of Energy (DOE) and developed with the cooperation of the National Fuel Cell Research Center (NFCRC) at the University of California Irvine. Main industrial partners were Air Products and FuelCell Energy.

Key to the system was a 300 kW MCFC that performed the direct fuel-to-energy conversion. The project was the first in the world to use digester gas for a fuel cell, which generates the hydrogen for automotive fuel, electricity for the clean-water plant, and heat for different possible purposes such as heating the anaerobic digesters that produce the biogas. The wastewater plant's hydrogen fuelling station is one of four in Orange County and the only one that makes hydrogen for dispensing - the others receive hydrogen produced from natural gas (Day 2014). The system layout and performance are discussed in detail in (Margalef et al. 2011b; Margalef et al. 2011a), where the FC-base polygeneration for the production of electricity, heat, and hydrogen is completely analyzed. Results pointed out that the efficiency of the products generation in the innovative polygeneration plant is always higher than the single product production only.
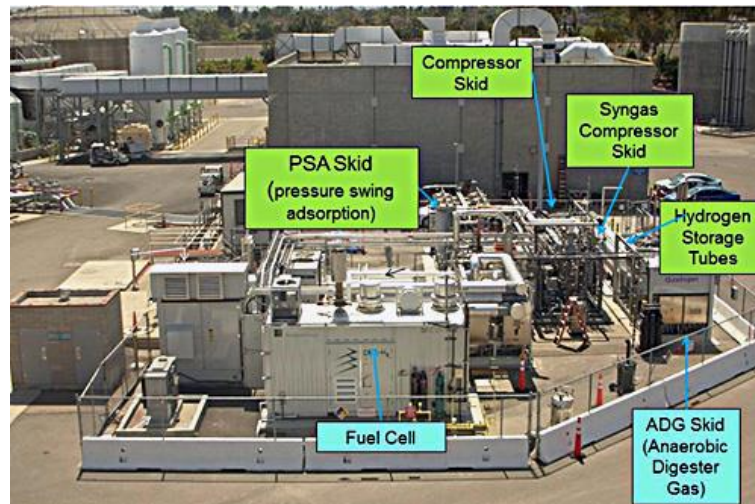
Figure 17. Layout of the trigeneration plant. (Advanced Power and Energy Program 2012; Brouwer et al. 2012)

Figure 18. Hydrogen Fuelling station. (Advanced Power and Energy Program 2012; Brouwer et al. 2012)

1.4 Biogas fed fuel cell systems

The present work deals with the analysis of biogas-fed Solid Oxide Fuel Cell (SOFC) systems.

Biogas is an interesting potential market for fuel cells, since the average biogas plant size, according to the waste distribution, is made of a large number of small-medium size plants in the range of hundreds of kW. The current CHP system usually installed for the exploitation of biogas is the Internal Combustion Engine (ICE). ICEs show interesting efficiencies (up to 42-43%) at MW scale (Jenbacher 1.4 MWe) under biogas feeding and can work in continuous operation with reduced maintenance in the first years of lifetime. When going from MW to kW scale, ICE efficiency is reduced up to 30-35% (MAN 60-100 kWe) and both CAPEX and OPEX specific costs, which are usually lower than 1'000 €/kW (CAPEX), start increasing. This reduction is the reason why in Europe, in the last years, many centralized 1 MW plants have been constructed and installed to benefit from the high subsidies for the electrical production from biogas. However, a problem arises related to these installations. During the 2010-2012 period, at least in Italy, a fixed subsidy of 28 c€/kWh was available despite the substrate used (wastes or energy crops), which led to a high number of biogas installations around 1 MW. This high incentive creates the centralization of wastes, by the collection and transport of different substrates in a unique site with a consequent increase in costs. With the reduction of the biogas incomes (Ministero dello Sviluppo Economico 2012; Ministero dello Sviluppo Economico 2016) in the following years, the economic sustainability of this type of plants starts decreasing. Currently, biogas installations in Italy have slow down their growing rate.

Furthermore, ICEs start showing problems with current emission limits to the atmosphere (for what concerning NOx, SOx, and organic compounds). Table 1 shows the measurements for the SMAT Castiglione WWTP ICE emissions. Results (1 to 4) refer to the 4 ICEs installed in the plant, fed by biogas locally produced. As can be seen, results are close or above the limits for what concerning the above-mentioned species.

Table 1. SMAT Emission measurements from ICE, November 2014.

	Test 1	Test 2	Test 3	Test 4	Average	Limit	
Total Powders	3.67	1.25	5.01	5.31	**3.81**	**10**	mg/m^3
Total NOx	437.67	427	307.67	469	**410.34**	**450**	mg/m^3
Total SOx	50.4	47.3	47.33	50.33	**48.84**	**50**	mg/m^3
Sulfuric acid	< 0.2	< 0.2	< 0.2	< 0.2	**< 0.2**	**2**	mg/m^3
Carbon Monoxide	274.67	143	257.67	201	**219.09**	**500**	mg/m^3
TOC	786	695	1229.33	825	**883.83**	**150**	mg/m^3
TOC (not methane)	232.67	165	341.67	212.67	**238.00**	**150**	mg/m^3
Hydrochloric acid	< 0.2	< 0.2	< 0.2	< 0.2	**< 0.2**	**10**	mg/m^3

On the contrary, SOFCs show no direct emissions to the atmosphere as can be seen from the Convion product datasheet shown in Table 2.

Table 2. Convion SOFC module datasheet. (Convion Fuel Cell Systems 2016)

Performance	Targets
Net power output	58kW (3x400-440V AC 50/60Hz)
Energy efficiency (LHV)	
Electrical (net , AC)	> 53 %
Total (exhaust 40°C)	> 80 %
Heat recover	
Exhaust gas flow	650 kg/h
Exhaust gas temperature	222 °C
Emissions	
NOx	< 2 ppm
Particulates(PM10)	< 0.09 mg/kWh
CO_2 (NG, nominal load)	354 kg/MWh
CO_2 (with heat recovery)	234 kg/MWh
Fuels	Natural gas, City gas, Biogas
Dimensions (L x W x H)	
power unit	3,5 x 1,9 x 2,3 m
aux. equipment	2,4 x 0,6 x 2,2 m
Noise level	< 70 dB(A) at 1 m
Installation	Indoor / outdoor
Temperature	-20 – +40°C

Roland Berger, in his report on SOFC potential markets, stated that *"Once a new technology exceeds the economic attractiveness (in terms of financial, operational and environmental criteria) of the currently used technology, switching to the new technology becomes high probable."* (Roland Berger Strategy Consultants 2015)

The advantages given by this technology in comparison with traditional ICEs, especially at small-medium sizes, motivate the analysis of biogas-fed SOFC systems. Chapter 2 will try to analyze the potential market for SOFCs in the biogas sector, with a special focus to WWTPs in Europe.

Many scientific works recently analyzed SOFC systems fed by biogas for what concerning:

- The biogas purification system, which needs to be beyond traditional levels of purifications because of the high risk of catalyst poisoning. Even parts per billion of sulphurs and siloxanes could damage the fuel cell irreversibly; for this reason researchers are looking for high removal efficiency and high duration

material able to guarantee near zero outlet contaminants (Sigot et al. 2016; Papurello et al. 2014; Shiratori & Sakamoto 2016).

Biogas cleaning, usually performed with adsorption on activated carbon, is a wide field of research and Chapter 5 will provide a brief discussion on the topic.

- Laboratory tests on simulated biogas and SOFCs in CHP configuration have been analyzed in (Kupecki et al. 2016; De Lorenzo et al. 2016; Wu et al. 2016).

- From lab tests, Valderrama et al. also analyzed an interesting 2.8 kWe pilot scale SOFC fed by sewage biogas, operated for more than 700 hours. (De Arespacochaga, Valderrama, Peregrina, Mesa, et al. 2015; De Arespacochaga, Valderrama, Peregrina, Hornero, et al. 2015)

- Biogas from WWTP is, among different biogases, a relatively 'clean' gas regarding sulfur and siloxanes, since water purification is usually a controlled and stable process during the time. For this reason, the coupling of WWTP and SOFC has been proposed by (Lackey et al. 2016): here, a specific stack testing is performed with varying biogas compositions and SOFC performance are presented. (Hauptmeier et al. 2016) also, present an economic analysis on WWTP biogas and. Braun et al. also proposed complete techno-economic modeling for the analysis of biogas-fed SOFC systems. (Trendewicz & Braun 2013; Becker et al. 2011)

State of the art on biogas-fed SOFC systems has deeply analyzed the modeling of the SOFC, the performance of the cells under biogas conditions, the methane reforming process, and the cleaning section.

Few works have proposed the coupling of a biogas-fed SOFC and the carbon capture process, which is the main focus of the thesis. Furthermore, the concept, presented in Chapter 3 and 4, has been analyzed not only through a detailed techno-economic modeling but also with the development of the first proof-of-concept with a biogas-fed SOFC and a carbon capture and re-use system. The thesis is thus proposing a novel concept, discussed with both experimental and modeling approaches. Furthermore, the last part of the thesis (Chapter 5) will be devoted to the analysis of real large industrial size biogas-fed SOFC installations, thanks to the involvement in the DEMOSOFC European project, where we will install the first European biogas-fed SOFC system (at industrial level). This analysis, still under development, pointed out that research efforts are still required to reach a real commercial level biogas-fed SOFC system, which should not be limited to the stack itself, but should include all the BoP and auxiliaries system required to guarantee a continuous and stable operation of the system.

1.4.1 Polygeneration with biogas fed SOFC systems

The presented thesis is focused on a polygeneration proof-of-concept, developed in the framework of the SOFCOM European project (Http://www.sofcom.eu. n.d.) where a

biogas-fed SOFC was installed. The system was fed with biogas and was able to produce electricity, heat and to separate CO_2. The core component was a 2 kWe SOFC system. The pure carbon dioxide was only an intermediate product since the carbon was fixed again in the form of a fuel (microalgae) in a tubular photobioreactor. Algae were growing by use of carbon, sunlight, and nutrients (nitrates and phosphates) contained in the waste water. Clean water (with reduced/zero nitrogen and phosphorus content) was also another output of the system. As an overall system, the plant was a tetra-generation system able to produce electricity, heat, micro-algae and clean water. Chapter 3 will fully describe the plant layout.

Chapter 2

Potential for SOFC in biogas applications

The chapter focuses on the analysis of the potential biogas market in Europe. The analysis starts with a literature review on the available scientific works related to the calculation of the biogas potential and continues with a simple but general potential calculation to understand the order of magnitude of the biogas sector in Europe. Finally, the work provides a specific focus on the WWTP sector.

2.1 Biogas potential calculation

Different works are available related to the analysis of the biogas potential in different EU countries. If it is relatively "easy" to estimate the biogas production from agriculture crops, municipal wastes, and sewage sludges, the calculation is more difficult in the case of residual for agriculture (corn straw for example), from food and alcoholic beverage industries and landfill. For the first two substrates, the struggle is related to the availability of collecting the wastes (maybe with modification to the current production/cropping procedure) and in the knowledge of a mean yield to be used for calculations. Furthermore, the possible suitable processes in which biogas substrates are collected is wide and full of small differentiations. For the landfill gas, the struggle is different since it is related to the non-constant gas production of a landfill site, which presents a real life trend for what concerning the gas and leachate production. For the reasons mentioned above, literature works often limit the calculation of the biogas potential to a small number of substrates. Among the available literature works, the most interesting are listed below.

- (Murphy & McKeogh 2004): the paper discusses the different available pathways for the MSW exploitations, from gasification to anaerobic digestion + CHP or biofuel for vehicles production.
- (Appels et al. 2011): the paper investigates the biogas potential related to different sources. The analysis shows biogas yields for energy crops, livestock effluents, MSW and food waste, but without including the methodology for the energy potential calculation.
- (Aebiom 2009): this is one of the most cited reports when working on biogas potential. The European Biomass Association shows in the report the current scenario for the biogas production in 2009 and the 2020 potential.

Origin (according to template for National Renewable Energy Action Plans)	Potential Billion m³ Biomethane	2020		
		Assumed percentage of use until 2020	Primary energy Billion m³ Biomethane	Primary energy Mtoe
Agriculture	58,9	62%	36,4	31,3
Agricultural crops directly provided for energy generation (5% of arable land; calculation in annex)	27,2	100%	27,2	23,4
Agricultural by-products / processed residues	31,7	28%	9,2	7,9
• straw	10,0	5%	0,5	0,4
• manure	20,5	35%	7,2	6,0
• rest (landscape management)	1,2	40%	0,5	0,4
Waste	19,0	50%	9,5	8,2
Biodegradable fraction of municipal solid waste including biowaste (biodegradable garden and park waste, food and kitchen waste from households, restaurants, caterers and retail premises, and comparable waste from food processing plants) and landfill gas	10,0	40%	4,0	3,4
Biodegradable fraction of industrial waste (including paper, cardboard, pallets)	3,0	50%	1,5	1,3
Sewage sludge	6,0	66%	4,0	3,4
Total	77,9	59%	45,9	39,5

Figure 19. Biogas potential for 2020 according to AEBIOM. (Aebiom 2009)

As can be seen, the considered substrates are:

- Energy crops (5% of arable land)
- Agricultural by-products (straw, livestock effluents, and others)
- Waste (OFMSW, grass waste, kitchen/food waste, LBG, WTTP)

The report gives little detail on the methodology and hypothesis used. AEBIOM assumes that 25 million ha agricultural land (arable land plus green land) can be used for energy in 2020 without harming the food production and the national environment. This land will be needed to produce raw materials for the first generation fuels, for heat, power and second generation fuels and biogas crops. In the AEBIOM scenario:

- o 15 million ha land is used for first generation biofuels (wheat, rape, sugar beet)
- o 5 million ha for short rotation forests, miscanthus, and other solid biomass production
- o 5 million ha for biogas crops.
- (Foreest 2012): the report shows a detailed analysis of the potential use of biogas in EU, with data on the economic feasibility and the current production
- (Berhad 2009): the report is done by IEA Bioenergy, an international collaborative agreement set up in 1978 by the International Energy Agency (IEA) and is full of information on the bioenergy market. The report gives no detail on the potential.
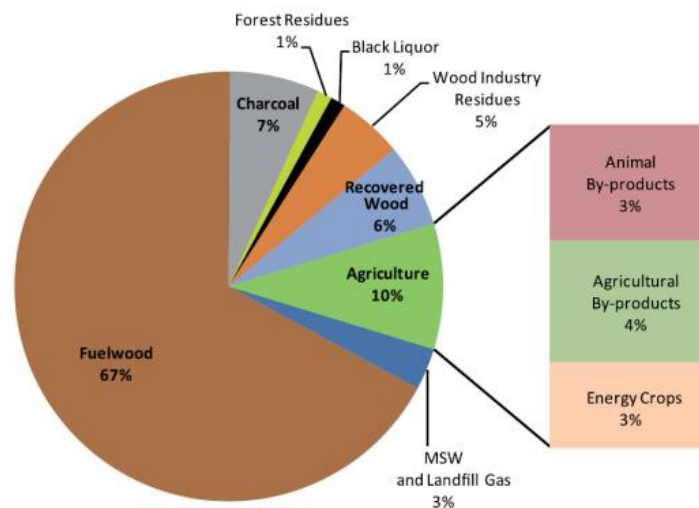
Figure 20. The share of the biomass sources in the primary bioenergy mix (Berhad 2009).

- (Pöschl et al. 2010): the paper is dedicated to the calculation and discussion of biogas yields from different substrates. The work also presents the influence of the different stages of the substrates production and collection line.

  Figure 21 shows how, in the case of crops as corn silage, the crop cultivation is highly influencing the energy input to the system. The feedstock preparation is also a fundamental step in the MSW and food residues, while cattle manure and pomace, for example, are more dominated by collection and transport and plant operation. The digested biomass processing can also be a high percentage of the energy input. On the other side, looking at the output/input ratio (Figure 22), crops show a higher production and thus a lower ratio, while manure and wastes have a higher energy consumption.

- (NREL 2013): also for the US, a biogas potential has been evaluated by the National Renewable Energy Laboratory and results are shown as Mtoe/yr for WWTP, LBG, and wastes.
- (Bilek 2011): for single countries, for example for Germany, reports can also be found. This document is related to the analysis of the biogas exploitation in Germany, which is one of the countries which has exploited more the potential during last years.
- (Rechberger & Lötjönen 2009), (European Environmental Agency (EEA) 2007), (Witzke et al. 2009): most of the reports in the last years focused on the discussion of biogas from energy crops. As will be discussed later, a proper balance between the use of land for food production and land for bioenergy should be defined and respected.

  The presented analysis is developed in different stages:

  1) Definition of the possible **biogas substrates**, with details on production yields.
  2) Calculation of the **biogas theoretical potential** from different substrates, trying to consider all the possible source for biogas production.
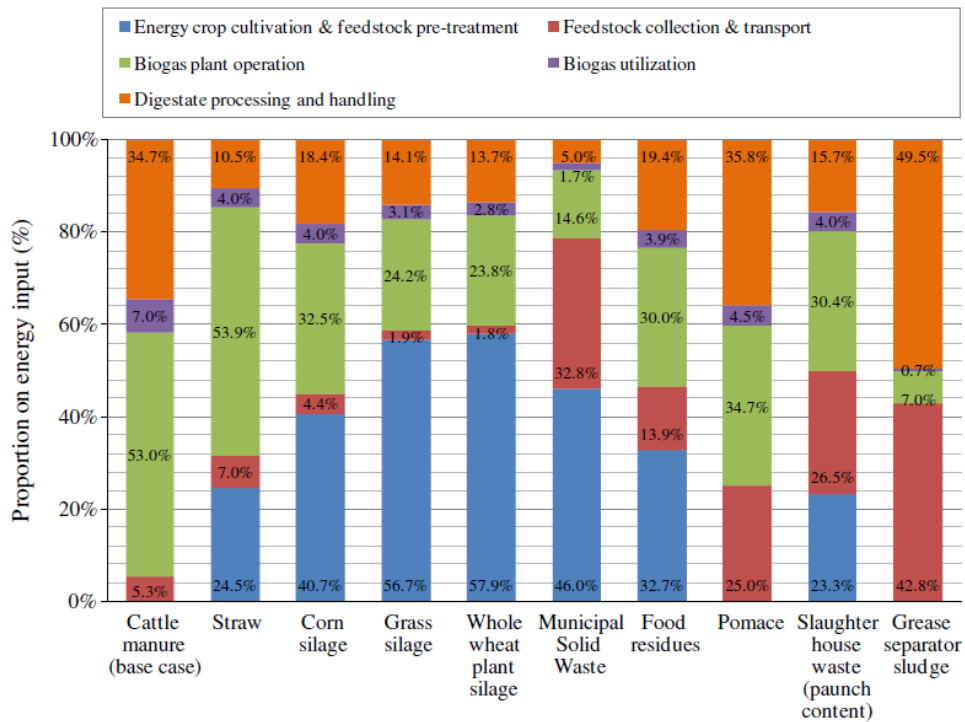
Figure 21. The proportion of the energy input to each process step for the digestion of different organic substrates.
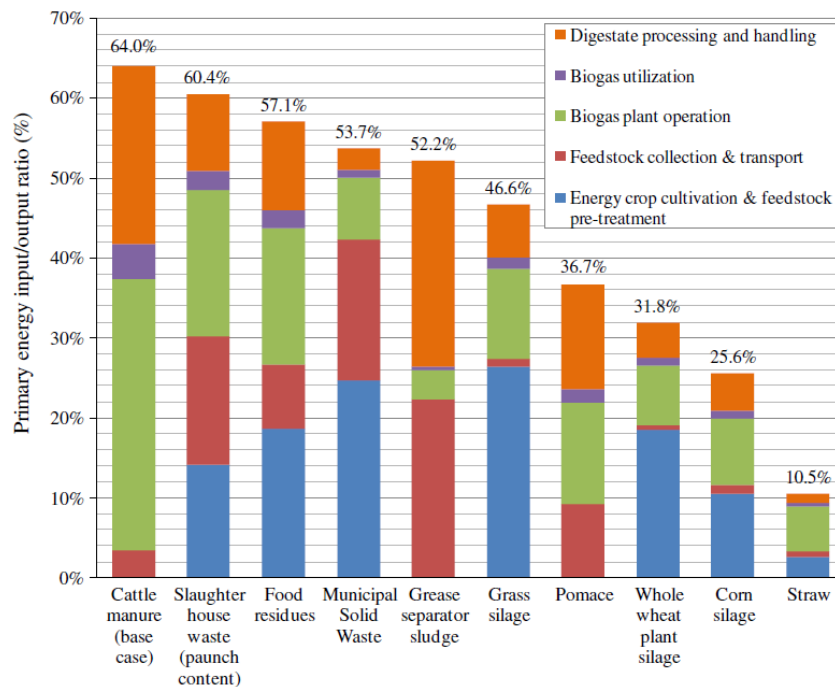
Figure 22. Primary Energy Input/Output ratio in single feedstock digestion scenario
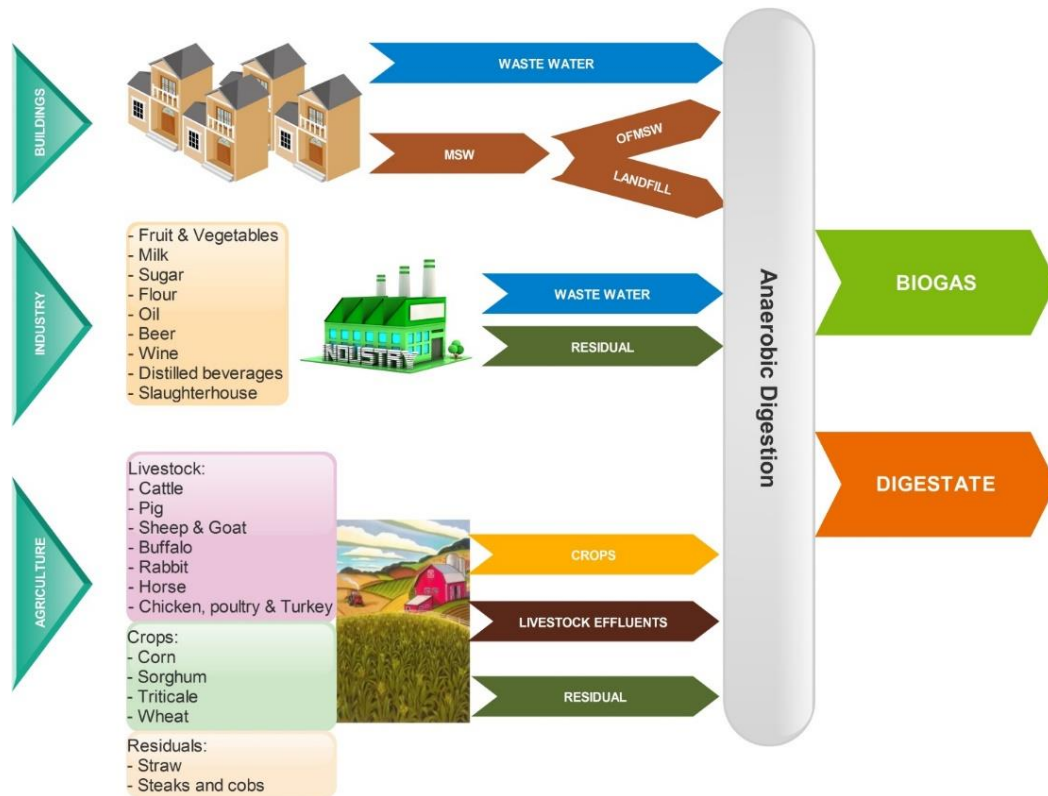
Figure 23. Biomass available for biogas production in different sectors.

The analysis of the possible biogas substrates and the general AD plant layout is presented in "Appendix 1 – Biogas potential calculation method", section "A1.1 Biogas substrates". The work is developed to analyze biogas production from a high number of available substrates (Figure 23). The second section of the appendix is devoted to the methodology presentation (A1.2 Methodology for biogas potential evaluation)

Results of the overall biogas potential per country are shown in the figures below. Energy crops are the largest share of the biogas potential, for all the analyzed countries (Figure 24). This is due, as expected, to the unexploited organic matter contained in the crops. On the contrary, 'waste-related' substrates always show reduced biogas yields. The largest crops contributions are related to Central and Southern Europe, where the largest part of the arable land and agricultural activities are located. Contributions related to Northern Countries are the lowest one. This trend is also confirmed by the total potential by country (Figure 25): the highest contribution is related to France, followed by Germany, Spain, and Poland. Eastern Europe, represented by Poland, is usually pointed out as a potentially large source for biogas, currently almost fully unexploited.
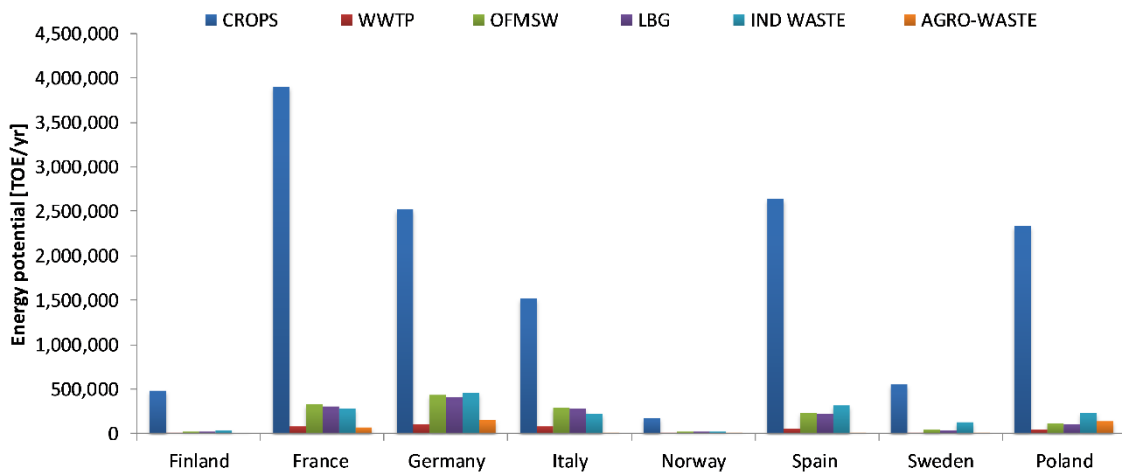
Figure 24. Total biogas potential by substrate in selected EU countries.

Figure 26 shows the share among all the waste-related substrates for biogas production. Food industry waste is, as already shown in the previous section, a large potential source, together with the residential sector waste (LBG and OFMSW). Agro-waste has the same behavior of energy crops: the contribution is relevant only in countries where a relevant portion of arable land is detected (Central and Southern EU). WWTP show a reduced potential in biogas mainly because of the low biogas yield of the substrate: improvements are possible in terms of efficiency of the anaerobic digester and sludge pre-treatments to enhance the biogas production rate.
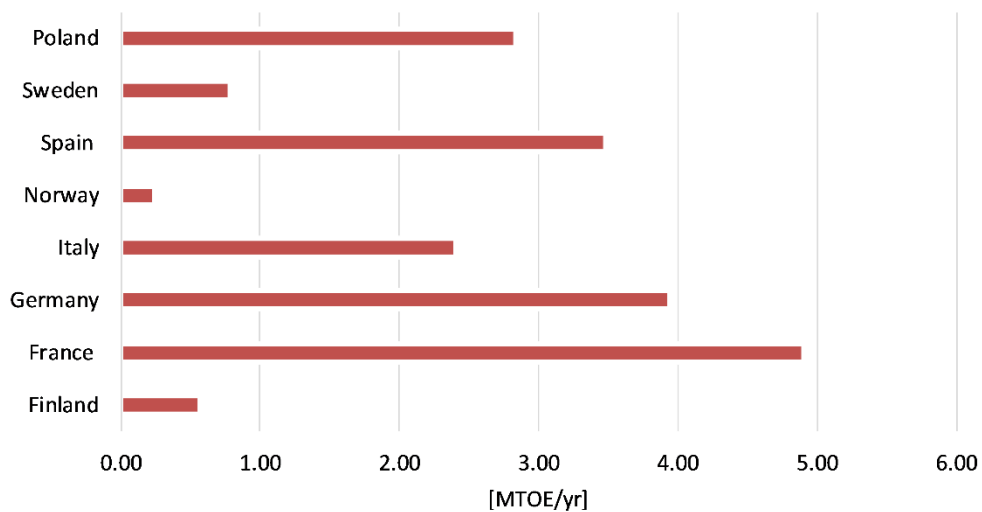
Figure 25. Total biogas potential in selected EU countries
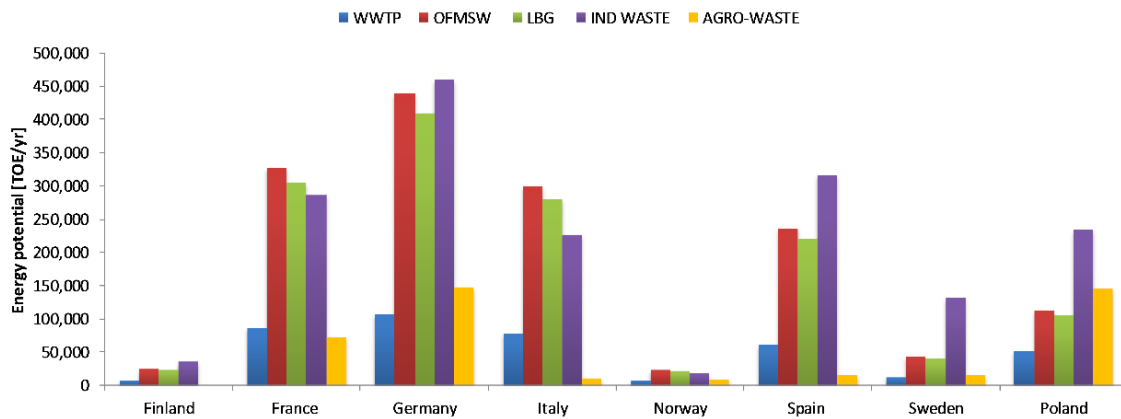
Figure 26. Total biogas potential by substrate (excluding crops) in selected EU countries.

Figure 27 is representing the biogas potential result for all the EU area. Results confirm the largest share related to energy crops (around 25%), followed by landfill and organic municipal solid wastes. The overall theoretical potential in EU has been estimated around 36 Mtoe/yr. It is fundamental to underline that this is a theoretical potential, which is not accounting for the economic feasibility of the biogas plants: this could be related to geographical limitations (rural and remote areas), micro-plants (too small size) and other limiting factors.

When comparing these results with the ones available from the Aebiom report some comments can be developed:

-   The value rated to the agricultural crops is in line with the presented value. This work has been based on FaoSTAT databased and has obtained a final result of 24.6 Mtoe/yr. Aebiom data is 27.2 Mtoe/yr.
-   The main difference in the 'agricultural' section, looking at the proposed share seems to be related to the manure, which accounts for 20 Mtoe/yr in the Aebiom report, and only for 1.35 Mtoe/yr in the present work. The difference is probably located in the yield used for the biogas production. The presented work has developed the analysis on the total number of animals from FAOstat, but assumptions have been made on the % of available manure for biogas production (fixed at 50%) and the biogas specific yield. The specific biogas production from livestock effluents is strongly varying according to the process and is especially subjected to the influence of co-digestion. If livestock effluents are treated together with other substrates (crops, industrial wastes), their specific production yield can be increased. This has been found as the main motivation for the strong discrepancy. For further comments, a better detail on the Aebiom calculation methodology should be available.
-   Concerning the biogas from OFMSW potential production, a value of 10 Mtoe/yr is proposed by Aebiom, while this work generate a potential of 2.40 Mtoe/yr.

- Concerning WWTP biogas, results from this work are again lower if compared to the Aebiom report, with a potential of 0.67 against 6 Mtoe/yr. This difference could be derived, as described above, from the assumptions on the biogas specific production, which can strongly change according to the process analyzed, and the percentage of 'eligible' plants considered for biogas production.
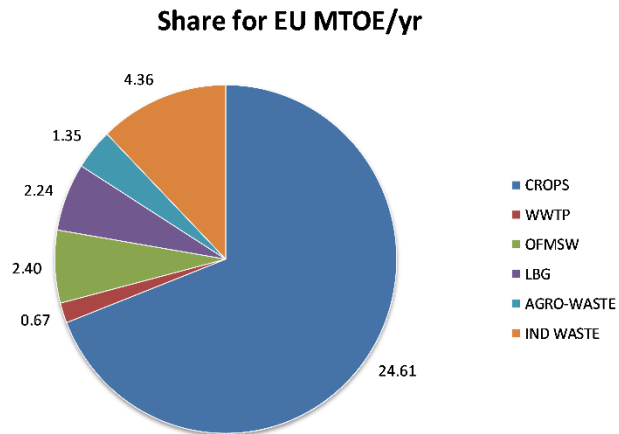
Share for EU MTOE/yr

Figure 27. Share for EU (total EU potential: 35.63 Mtoe/yr).

2.2 Biogas potential in WWTP

A more detailed biogas potential analysis has been performed for the WWTP sector.

2.2.1 WWTP – Waste Water Treatment Plants

Biogas is currently produced in medium and large size WWTPs in order to reduce the organic load of sludge. Sludges are produced for the treatment (gravitational, chemical and biological) of the waste water entering the plant. The main goal of a WWTP is the cleaning of waste water (reduction in terms of bacteria, nitrates, phosphates, etc.). Sludge are usually considered a by-product which cannot be dismissed in its current composition because of the high organic load. Anaerobic digestion is thus seen as a solution to this problem, since the organic fraction is strongly reduced while biogas is produced. Biogas is usually exploited in boiler or internal combustion engines, with the aim of providing heat for the digester and producing electricity for the plant itself.

Because of the reduced solid content, sludges are usually approximated, inside the models, with pure water, from a thermodynamic point of view. For the same reason, the specific heat requirement inside the digester (kW/kg biomass) is higher compared to a similar plant where a more dense substrate is used. This criticality has been detected in all the SMAT plants analyzed during the thesis. Specific analysis on the WWTP can be found in one of the author scientific publication (Marta Gandiglio et al. 2016). The author also studies the integration of the DEMOSOFC concept (Chapter 5) with a solar system to have a full coverage of the digester thermal load in (Mehr et al. 2017)

The SMAT Castiglione plant (Figure 28) is the fifth largest WWTP in Europe by entering load, with a capacity of 3'800'000 Person Equivalent (P.E.) and a entering water flow of 600'000 m³/day. The plant has six anaerobic digesters (shown in Figure 28), where biogas is produced (usually only four digester are operative and two under maintenance to avoid discontinuities in the production). Biogas is then fed to four Jenbacher Internal Combustion Engines (ICEs), able to provide 1.4 MWe each, for a total installed power of 5.6 MWe. All the electricity produced is self-consumed by the plant itself, together with the renewable electricity produced by a group of PV panels. In this plant, the SOFCOM demonstration plant (Chapter 3) was installed, in a dedicated area close to the water final filtration. The SOFCOM plant was fed by a tiny portion of the biogas produced within the plant. In the framework of the project, an analysis on biogas composition was performed (as shown in Chapter 3.1 and published in (Gandiglio et al. 2013).

The SMAT Collegno WWTP (Figure 29) is a medium size plant, and it located at number 50 in the EU WWTP classification by entering load.

Figure 28. SMAT Castiglione WWTP.

Figure 29. SMAT Collegno WWTP.

All the experimental activities performed during the thesis has been on WWTP biogas fed SOFC systems. In both the EU funded project involved (SOFCOM and DEMOSOFC), the largest Italian WWTP owner and manager, SMAT s.p.a., was involved. Thanks to the collaboration with SMAT, a more detailed knowledge has been developed on WWTP biogas respect to other sources. Furthermore, a detailed database on all the European waste water treatments plants is available from the European Environment Agency (European Environment Agency 2015). The main reasons for the development of a more specific biogas potential calculation for WWTP (respect to the previous section) are:

- The theoretical biogas potential calculation for WWTP was based on the population of each country. This method includes all the population across EU, without taking into account presence of rural or remote areas where waste water is treated in a different way respect to urban area. Furthermore, from literature, a minimum entering load for the economic sustainability of biogas production is usually found. In very small WWTPs there is no economic convenience in the installation of an anaerobic digester, and this should be considered in the analysis. For this reason, the biogas potential calculated could be overestimated by using the total country population.
- On the contrary, a risk of underestimation could also occur because WWTPs are usually treating also industrial waste waters, which have not been considered in the previous calculation.

By knowing the exact distribution of WWTPs around Europe and, for each of them, the entering load (in terms of Person Equivalent, PE), and the treatments involves, a more detailed biogas potential calculation can be performed.

Figure 30 and Figure 31 show how the EEA database is provided on the website. All the data for Europe have been downloaded in an excel form and have been elaborated to obtain the biogas potential.
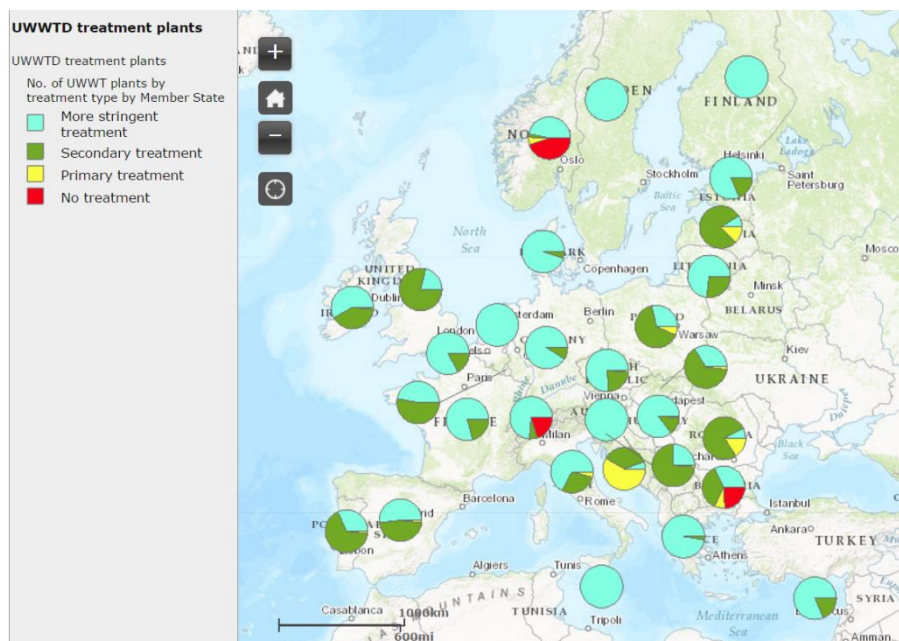
Figure 30. WWTPs distribution by treatment in EU countries. (European Environment Agency 2015)
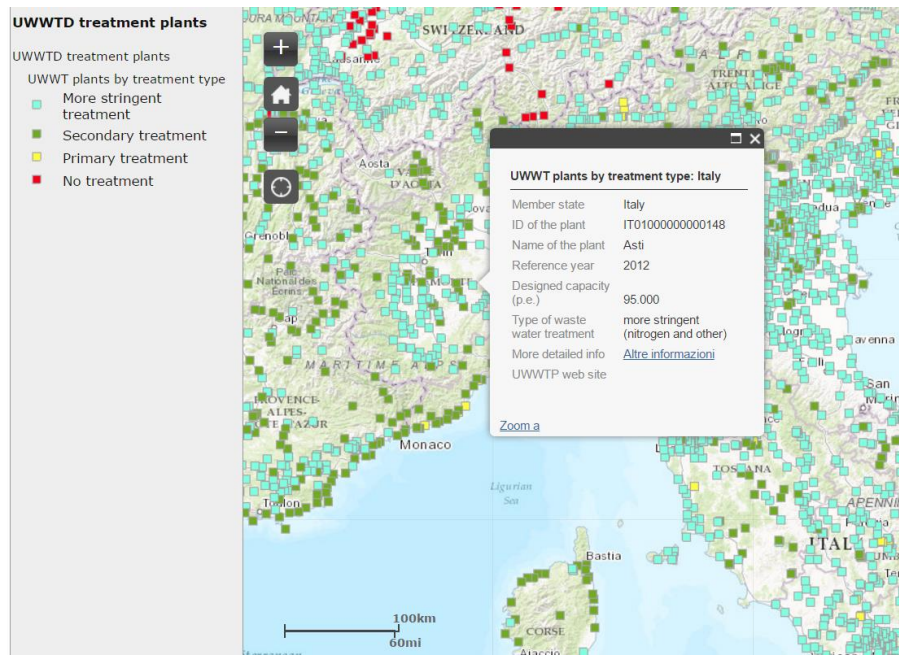
Figure 31. Focus on WWTPs location and specifications (European Environment Agency 2015).

2.2.2 Methodology

The above-mentioned database is able to provide, for all the WWTPs in Europe, values of the location (country), entering load (P.E.), plant capacity (P.E.) and information on the treatments performed (primary, secondary, tertiary, others..). For the biogas potential calculation, the entering load has been used as a starting point for the evaluation. For the plants for which the entering load was not available, the capacity has been used (even if these plants account only for 11% of the total number of plants). The plants for which both entering load and capacity were not available, have been excluded from the analysis.

The biogas potential from WWTP has been calculated according to a simple method, based on available data from the literature (Table 3):

- Biogas yield: this is the most influencing data, as will be seen later. Ongoing work with Imperial College (in the framework of the DEMOSOFC project, see Chapter 5), has detected a feasible range of 10-30 l biogas/ PE/ day. In the SMAT Collegno WWTP, the biogas yield can be determined from the knowledge of the average biogas production (70 m^3/h), and the P.E. served (around 170'000): the resulting value is 9.88 l biogas/ PE/ day. In this context, it is well known, from the operators and from the dedicated analysis (Marta Gandiglio et al. 2016), that the biogas yield could be increased by means of a better digester thermal management and sludge pre-treatments. For this reason, a 'safety' value of 15 l biogas/ PE/ day has been used for the analysis. This value can be considered realistic or slightly overestimated in existing plants,

where anaerobic digester is already installed, while higher values could be obtained in the case of new constructions with particular attention to the biogas production yield. A sensitivity analysis will be performed at the end to see the influence of the biogas yield on the EU potential.

- Methane content in biogas: from SMAT measurement during 2014, 2015 and 2016 in both Collegno and Castiglione WWTPs, methane content was always between 60 and 65%. A 'safety' and the standard value of 60% has been assumed for this analysis.

- Biogas LHV: the Lower Heating Value is calculated based on the methane content discussed above.

- SOFC electrical efficiency: the SOFC efficiency has been assumed according to the current Convion module datasheet (Convion Fuel Cell Systems 2016). Future short-term developments in the stacks and BoP integration could lead to an even higher efficiency, up to 60%.

- Minimum plant size for biogas production: this is also a fundamental value for the analysis. With the chosen biogas yield, 20'000 P.E. corresponds to a 40 kWe CHP system. This number, always defined during the ongoing analysis with Imperial College, can vary between 10'000 and 30'000 P.E., depending on the country, the WWTP layout and the biogas production efficiency. The chosen value has also been confirmed by a member of the IEA Task 37 on biogas. By considering all the WWTPs in Europe with an entering load equal or higher than 20'000 P.E., the analysis is including both plants where anaerobic digestion is performed and plants where is not.

Table 3. Input parameters for the potential calculation.

Parameter	Value	Unit
Biogas yield, $BioY$	15	l biogas/ P.E./ day
Methane content in biogas	60	%
Biogas LHV, LHV_{biogas}	481'404	kJ/mol
SOFC electrical efficiency, $\eta_{el,SOFC}$	53	%
Minimum size for biogas production in WWTP	20'000	P.E.

Starting from the entering load (EL, in PE), the biogas production (BP, flow rate of biogas, in l/day) can be calculated as:

$$BP = EL \cdot BioY \qquad \text{Eq. 1}$$

From the knowledge of the biogas production, the SOFC size can be estimated. This equation includes the hypothesis of having the biogas flow stable during all the year, with the SOFC, sized directly on the potential biogas flow produced.

$$W_{el,SOFC} = \eta_{el,SOFC} \cdot W_{biogas} = \eta_{el,SOFC} \cdot BP \cdot LHV_{biogas} \qquad \text{Eq. 2}$$

The method has been applied to the overall Europe and to some specific countries:

- Italy, France and Germany and the United Kingdom, representative of the largest EU countries. Except the UK; these countries are also representative of central EU.
- Spain, representative of Southern EU.
- Finland, representative of Northern EU (Scandinavian peninsula)
- Poland, representative of Eastern EU.

2.2.3 Results

In Europe, a total number of 26'900 WWTPs has been found. The number includes only plants where information on entering load and/or capacity were available. The EU average entering load per plants is 22'500 P.E.

Figure 32 shows the top 10 largest WWTPs in Europe: the SMAT Castiglione WWTP, where the SOFCOM project was installed (see Chapter 3) is #5 in Europe, while the DEMOSOFC site (SMAT Collegno, see Chapter 5) is # 50. The largest WWTP in Europe is the Paris Seine Aval WWTP, with an entering load of around 6'500'000 P.E. The top 10 largest plants treat about 5.4% of the overall demand in Europe. Plants ranking from 11 to 1000 (3% of the overall WWTPs) treat 46% of the overall entering load. The geographical distribution of WWTPs is made of a small number of larger plants, which are treating the largest part of waste waters, and a high number of small-medium size plants, with a reduced entering load. This is confirmed by the average value of entering load in EU, 22'500 P.E.

In EU, 5'141 plants with an entering load > 20'000 P.E. have been found. They are 19 % of total WWTPs in Europe. This value is confirmed by the specific country percentage, which is ranging from 11.62% (Italy) to 31.58% (Finland). This value is strongly related to the average entering load per WWTPs, as will be shown later. The largest number of plants involved is related to Germany, followed by Italy, France, and the UK with similar values. Slightly lower results are shown in Spain and Poland, while the potential in Finland, in terms of plants, is only 54. This is due to the overall small number of plants in the country. Of course part of the potential plants already has anaerobic digestion installed, while part of them have not. Unfortunately, no data on the anaerobic digestion was available on the database to compare the results. An interesting analysis on the current status of biogas production from sewage sludges has been presented in 2016 by F. Malpei at a biogas

congress in Como (IT) (Malpei 2016). The author shows the current biogas production per country in terms of liters of biogas per inhabitants per day.
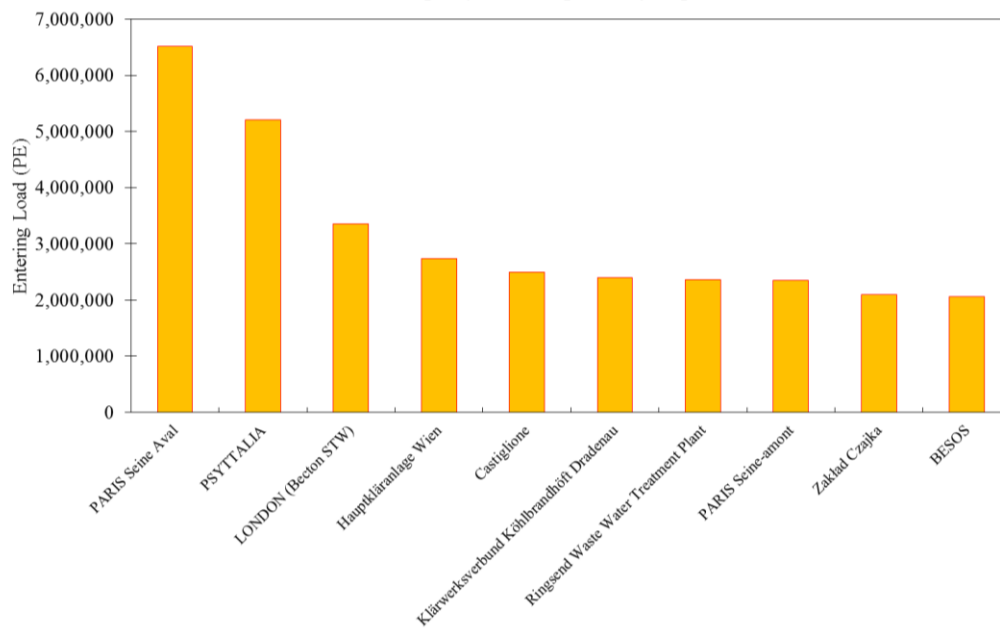
Figure 32. WWTP in Europe by size – Top 10 largest plants.

Country	EU	IT	DE	FR	UK	ES	FI	PL
% of eligible WWPTs	19.12%	11.62%	25.91%	16.83%	28.10%	21.92%	31.58%	24.11%
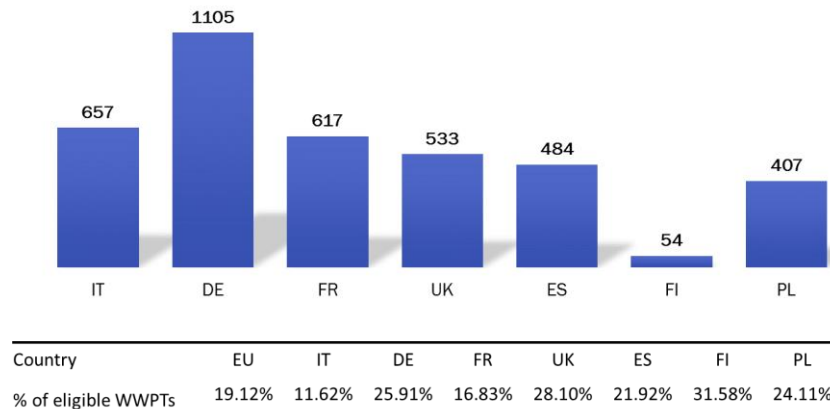
Figure 33. Eligible WWTPs for biogas production.

The ratio between P.E. per country and number of inhabitants, calculated on the database, has an average value for EU of 1.15. Consequently, the potential in liters per P.E. or liters per inhabitants should not show a high discrepancy. If the potential is exploited entirely, this number should be equal to the theoretical biogas yield (10-15 l biogas/ P.E./ day), at least if considering only plants larger than 20'000 P.E. On the contrary, the author shows an average value for EU of 3 Nm^3 CH_4/capita/yr. If converted, this number is equal to 13 l biogas/capita/day, which is lower than the 10-30 potential range found in our analysis. As a consequence, the exploitation of biogas production in WWTPs seems to be

already developed but not fully exploited, especially in specific countries. In fact, 3 Nm^3 CH_4/capita/yr is an average value with peaks of 10 in Sweden and 2.5 in Spain.

The potential for SOFC in EU is shown in Figure 34. The total number of eligible plants is again around 5'200, with a total installed number of MWs of 983. This value corresponds to a number of 50kW units of 19'665.
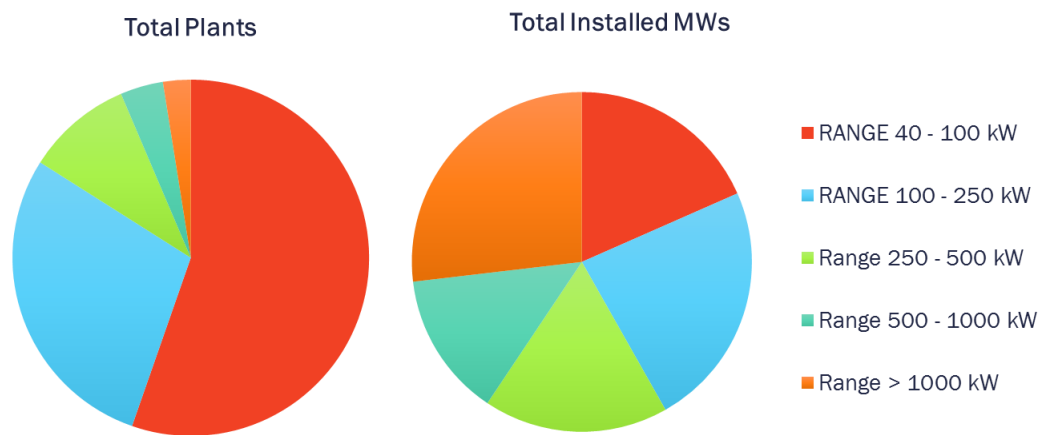
Figure 34. EU potential for SOFC in WWTPs. Results for different ranges in terms of plants and MWs.

The selected countries are covering 72-73% of the EU potential in terms of plants and MWs installed, as cab be seen in Figure 35 and Figure 36. The largest share in terms of a number of installations is related to the small size systems (40 – 100 kW and 100 – 250 kW). From the analysis of the MWs installed, large size systems are giving a high contribution: this is due to the presence of very large WWTPs (mainly in the main cities of each country) which show an entering load higher compared to the average value and could lead to MW-size system installation.

The final map is a view of the specific EU countries: results pointed out that eligible plants % is directly linked to the average entering load (in P.E.) per WWTP. Furthermore, larger potential is related to central Europe, in particular, Germany, France UK, Spain, and Italy, where a large population is found. These countries would be able to cover more than 70% of the total EU biogas potential.
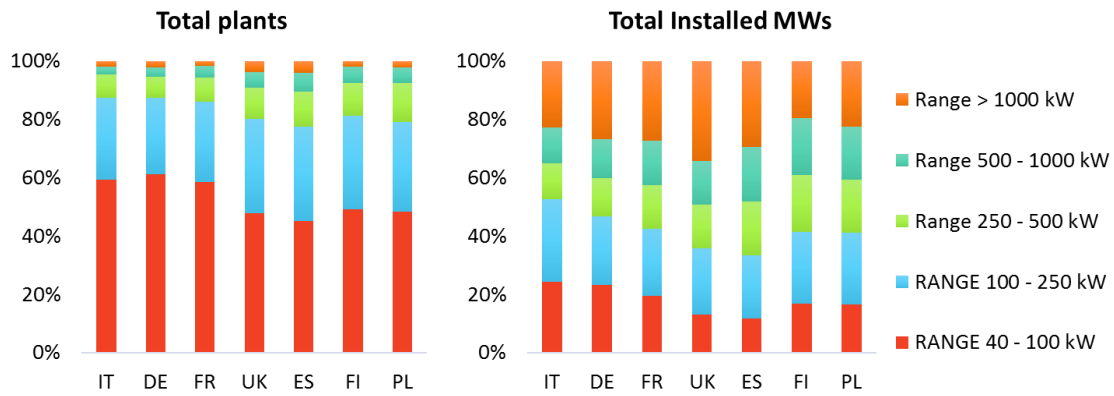
Figure 35. Potential for SOFC in WWTPs for specific countries. Results for different ranges in terms of plants and MWs.

Country	FI
Average WWTP entering load	35'045 PE
% of plants larger than 20'000 PE	31.58%
Total number of plants	53
Total MWs	10

Country	UK
Average WWTP entering load	36'944 PE
% of plants larger than 20'000 PE	28.10%
Total number of plants	530
Total MWs	119

Country	PL
Average WWTP entering load	28'813 PE
% of plants larger than 20'000 PE	24.11%
Total number of plants	402
Total MWs	77

Country	FR
Average WWTP entering load	19'968 PE
% of plants larger than 20'000 PE	16.83%
Total number of plants	610
Total MWs	112

Country	DE
Average WWTP entering load	26'727 PE
% of plants larger than 20'000 PE	25.91%
Total number of plants	1'081
Total MWs	179

Country	ES
Average WWTP entering load	29'727 PE
% of plants larger than 20'000 PE	21.92%
Total number of plants	474
Total MWs	110

Country	IT
Average WWTP entering load	12'395 PE
% of plants larger than 20'000 PE	11.62%
Total number of plants	653
Total MWs	100

Figure 36. Potential for SOFC in WWTPs for specific countries. Final map.

Chapter 3

The   SOFCOM   proof-of-concept: Experimental activities

One of the important targets of climate mitigation is the control and management of CO_2 in the Earth's biosphere. In fact, the Conference of the Parties Twenty-first session (COP21), held in Paris from November 30 to December 11 of 2015, declared in the Adoption of the Paris Agreement under the United Nations Framework Convention on Climate Change document (FCCC United Nations 2015):

"Recognizing that climate change represents an urgent and potentially irreversible threat to human societies and the planet and thus requires the widest possible cooperation by all countries, and their participation in an effective and appropriate international response, with a view to accelerating the reduction of global greenhouse gas emissions."

"Also recognizing that deep reductions in global emissions will be required in order to achieve the ultimate objective of the Convention and emphasizing the need for urgency in addressing climate change."

"Emphasizing with serious concern the urgent need to address the significant gap between the aggregate effect of Parties' mitigation pledges in terms of global annual emissions of greenhouse gases by 2020 and aggregate emission pathways consistent with holding the increase in the global average temperature to well below 2 °C above pre-industrial levels and pursuing efforts to limit the temperature increase to 1.5°C above pre-industrial levels"

The world is already at 1°C above pre-industrial levels, and the carbon budget (the amount of atmospheric carbon we can emit before reaching 1.5°C) is half what is allowable under a limit of 2°C. In a very short time, we will be out of carbon budget to stay below 1.5°C, so regardless of how fast we limit fossil fuels, we will need to invest in third-way

technologies to capture CO_2 from the atmosphere, which is difficult due to the low concentration in absolute values. Carbon sequestration in forests, crops, rangelands, biochar and wood industry products can play a role.

However, another paradigm based on the sequestration of CO_2 before its emission into the atmosphere, and especially on the re-fixation of the Carbon content of the CO_2 molecule, can be of high interest and effectivity. This is the paradigm of Carbon Recovery and Re-utilization (or CRR).

In fact, the carbon atom can be of higher interest in the case of recovery than in the case of sequestration, for the energy sector but also for other market applications such as the green chemicals. The carbon atom contained in the CO_2 can be used to produce synthetic fuels, green chemicals, materials and also new biomass. In this way, the carbon, not oxidized in CO_2 but embedded in a synthetic or natural product, can be re-used in the technological sector and play a useful role in the society. This recovery is not free in terms of energy, of course: to recover carbon from the CO_2 molecule, chemical, biological, or electrochemical processes have to be driven, with an expenditure of energy, as the Gibbs free energy has to increase again. Nonetheless, this expenditure can be linked to the increase of the role of renewables in the energy arena, and these procedures can be considered at the same time: (1) a way to remove CO_2 from the biosphere; (2) a way to embed Carbon in synthetic chemicals or in new biomass; (3) to store the renewables in form of stock products; (4) finally, a way to use renewables not only to produce energy, but also synthetic products in other markets, thus increasing even more their role in the human society (Santarelli et al. 2017).

Carbon recovery from CO_2 is certainly not an easy task to accomplish. The typical CO_2 concentration in the exhaust gas of an NG-fired combined cycle power plant and a pulverized coal power plant are about 4% and 15% vol., respectively; these values are high compared to the atmospheric concentration (around 400 ppm at the beginning of the XXI century). Still, the concentration is quite low to allow an easy and economic recovery of CO_2. Other routes are available, such as the combustion in oxygen (oxy-combustion). However, this requires the preliminary separation of O_2 from N_2 from an air stream, which also entails a considerable amount of energy.

Nevertheless, it is possible to perform some type of oxy-combustion even without a preliminary $O_2 - N_2$ separation. This is allowed by structures that use membranes with a selective conductivity of ions, such as the case of solid oxide fuel cells (SOFC). In SOFC systems – electrochemical generators operating at high electrical efficiency – oxygen ions are selectively extracted from cathode air because the electrolyte layer allows only the conduction of O^{2-} ions toward the anode (fuel) electrode. In the anode electrode, the primary fuel undergoes "electrochemical oxidation" in the absence of N_2. The main constituents of a standard anodic fuel (with the generic formula $C_xH_yO_z$) are thus oxidized into H_2O and CO_2, which constitute the main part of the SOFC anode exhaust stream. Some

residual H_2 and CO is still available in the anode exhaust, as the fuel cell cannot reach 100% reactants' utilization due to concentration losses. However, the fuel utilization can reach values up to 85-90%. Hence, the residual fuel can be oxy-combusted in a subsequent burner to achieve an $H_2O - O_2$ stream only. The exhaust CO_2 is eventually cooled, and water is separated by condensation. CO_2 recovery from the SOFC anode exhaust is thus relatively straightforward. Once a stream of very concentrated CO_2 is available, it is ready to be used again (Santarelli et al. 2017).

The conclusion is that CRR is an easier and cheaper task from SOFC anode exhausts. This opportunity is not common to other technologies generating power, such as the thermal cycles (ICE, GT, etc.).

This generates an interest in the application of fuel cells, far beyond their high efficiency in the conversion of chemical energy (of the primary fuels sent to the anode) into electric power. The interest is now connected to the paradigm of CRR, and so to the paradigm of climate change mitigation. This opportunity is available; however, it needs to be designed and demonstrated at the level of proof-of-concept, to study the feasibility of the process, the potential for improvements, and finally measures to define and reduce problematic steps.

The first demonstration, at international level, of the concept of carbon recovery and re-utilization and has been carried out through a research and demonstration project funded by the European Commission in 2011, named SOFCOM (European Union's Seventh Framework Program (FP7/2007-2013) for the Fuel Cells and Hydrogen Joint Technology Initiative under grant agreement number 278798 'SOFCOM') (Santarelli et al. 2017).

The experimental activities involved in this project have pursued the publication of a first work on the Journal of Fuel Cell Science and Technology (Gandiglio et al. 2013) and a second work, accepted for publication with reviews, on the Journal of CO_2 utilization (Santarelli et al. 2017).

The core component of the SOFCOM proof-of-concept is an SOFC generator fed by biogas. Biogas is converted to electricity through high-efficiency electrochemical reactions (the overall fuel cell electrical efficiency is >50% when running on biogas) and with the characteristic that the only exhausts of the plant are pure CO_2 and water. The as-received biogas is first cleaned to remove harmful contaminants (mostly H_2S and siloxanes), partially steam-reformed in an external fuel processor and then fed to a 2 kW_e SOFC stack. The anode exhaust is oxy-combusted to yield a stream that contains only H_2O and CO_2 (with only traces of H_2 and CO; N_2 is also found depending on the initial concentration of this compound in biogas). A water condensation/drying process is finally carried out to produce pipeline quality CO_2 (Santarelli et al. 2017).

In the SOFCOM plant, CO_2 is thus fully recovered and converted into a "fast growing" biomass as micro-algae. Therefore, the Carbon content of the CO_2 is embedded in a

secondary biomass through a photosynthetic process, which occurs in a closed tubular photobioreactor that fixes CO_2 into algae biomass through solar radiation and nutrients (nitrates and phosphates), found in locally available wastewater. The algae production leads to a high nutrients removal from inlet water generating two products: a potential fuel (biomass from algae) and a purified water stream (Santarelli et al. 2017).

From an energy strategy point of view, the proof-of-concept plant aimed at demonstrating how smart fuel cell based systems are key-enabling technologies that run on renewable fuels with best-in-class electric conversion efficiency and the potential for a closed-loop cycle on C-H-O atoms (carbon, hydrogen, and oxygen). Such paradigm is that of new poly-generating systems for co-production of electricity, heat, fuels and chemicals (Santarelli et al. 2017).

From the perspective of climate change mitigation, the SOFCOM proof-of-concept envisaged the innovative opportunity to completely recover CO_2 from an energy process, in an easy and economical way, and to make the carbon available again for other uses in a paradigm of complete CCR (Santarelli et al. 2017).

The SOFCOM demo unit was located inside the wastewater treatment plant of Castiglione Torinese, Torino (IT), the fifth largest WWTP in Europe, where mixed urban and industrial wastewater is treated. The collected sludge is digested in mesophilic-thermophilic anaerobic digesters. Normally, the as-produced biogas is burnt in internal combustion engines that provide a fraction of the overall electricity consumed on-site by the WWTP. In the framework of the SOFCOM project, a portion of the produced biogas is used to feed the SOFC demonstration plant. A biogas blower is required to feed the fuel mixture (found slightly above the atmospheric pressure in the reservoir tanks) across the various plant sections. The biogas is cleaned in order to remove harmful contaminants for the SOFC: according to historical data, cyclic siloxanes (D4 and D5), and sulfur compounds have to be removed carefully to avoid poisoning of the reformer unit and the SOFC. The clean biogas is converted via an external steam reformer to a bio-syngas rich in H_2 and CO that is fed to the SOFC stack. The anode-off gas is burnt with pure oxygen to yield an almost pure CO_2-H_2O stream. The latter is condensed in a dedicated unit to produce a relatively pure CO_2 stream complying also with purity requirements for sequestration. The pure CO_2 stream is finally used (recycled) for carbon bio-fixation in microalgae reactors with additional waste-water treatment via biological nutrients removal. (Gandiglio et al. 2013)

The demonstration plant layout is shown in Figure 37 and Figure 38. The first one shows the first part of the demo plant, from biogas inlet feed to pure CO_2 exhaust. The main components in this section of the demo plant are:

- Clean-up vessels for biogas contaminants removal.

- The processing unit (reformer) for methane conversion into an H_2-CO mixture using demineralize water.
- SOFC for electricity production.
- Air line for feeding oxygen to the SOFC cathode (blower and air pre-heater).
- Oxy-combustor for oxygen combustion of unreacted fuels from SOFC.
- Two heat recovery sections.
- Condenser for water removal.

Figure 38 shows the photobioreactor unit. Wastewater is filtered and then flowed through the recirculation loop. CO_2 is injected into this loop to promote algae growing. In the degasification tank, suspended microalgae are gradually precipitated and removed from the bottom of the reactor. From the degasification tank, the water purification loop also starts. In fact, the water / micro-algae mixture is fed to an ultra-filtration membrane to extract purified water that is eventually collected in the permeate tank. (Santarelli et al. 2017)

The same concepts represented in the schemes are also shown in Figure 39 and Figure 40, where the real installation setup is shown. The nominal operating conditions are listed in Table 4.
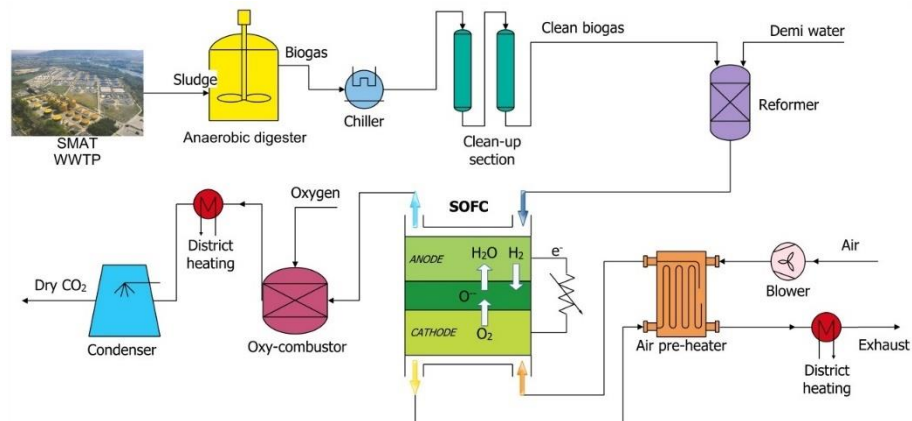
Figure 37. Demonstration plant layout: from biogas to electricity, heat, and CO2.
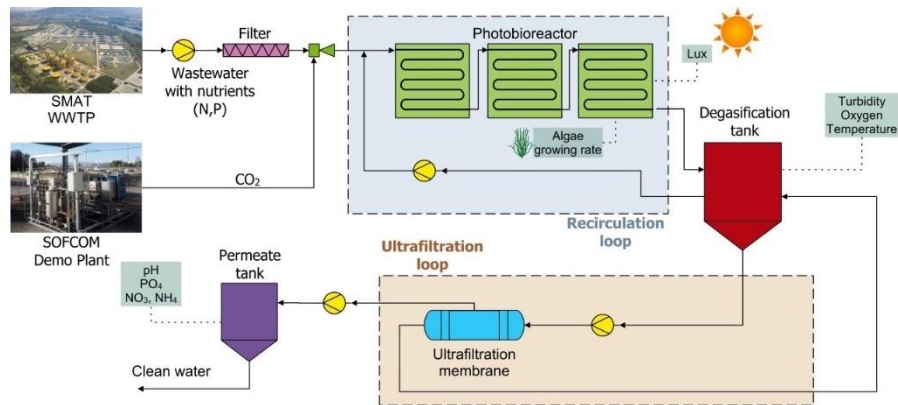
Figure 38. Photobioreactor layout: from CO_2 to algae and clean water.

Table 4. Nominal operating conditions of the SOFCOM proof-of-concept.

Parameter	Value	Unit
Biogas flow rate	8.36	NLPM
Demineralized water flow rate	604	g/h
Air flow rate	150-250	NLPM
Biogas inlet pressure	220	mbar
Evaporator temperature	400-450	°C
Reformer temperature	650-850	°C
S/C (steam-to-carbon)	2.5	-
Anode inlet temperature	750	°C
Cathode inlet temperature	650	°C
SOFC working temperature	820-850	°C
Current	24	A
Oxy-combustor temperature	< 1200	°C
O_2 % in oxy-combustor exhaust	1.1	% vol.
Condenser set point	0	bar
Compressor outlet pressure	8	bar
Compressor outlet temperature	200	°C
Water % at the membrane outlet	< 500	ppm(v)

Figure 39. SOFCOM proof-of-concept at the SMAT Castiglione WWTP – from biogas to CO_2.

Figure 40. SOFCOM proof-of-concept at the SMAT Castiglione WWTP –CO_2 utilization for algae growth.

3.1 Clean-up unit

Biogas is currently produced in the SMAT Castiglione WWTP, the largest one in Italy and the fifth in Europe for equivalent inhabitants served.

In the SOFCOM installation, a tiny portion of the overall biogas produced was sent to the proof-of-concept area, located inside the WWTP, closed to the water final filtration

stage. Biogas was derived after the chillers, in order to avoid water condensation in the pipeline.

As well-known from literature and as discussed in Chapter 3, biogas requires a purification stage prior to feeding the SOFC in order to remove harmful contaminants for both reformer and fuel cell stack. In order to identify the most abundant contaminants found in the SMAT sewage gas, a detailed gas analysis was performed over a period of six months (Anon 2012). According to historical data from biogas samples from two of the SMAT digesters (out of six anaerobic digesters of 12,000 m^3 each, and their composition can be considered representative of the whole plant average biogas production) collected in the period going from Jan. 2012 to Sept. 2012, cyclic siloxanes, the most abundant contaminants found are halogens and sulfur compounds, which have to be removed carefully to avoid poisoning of the reformer and the SOFC units.
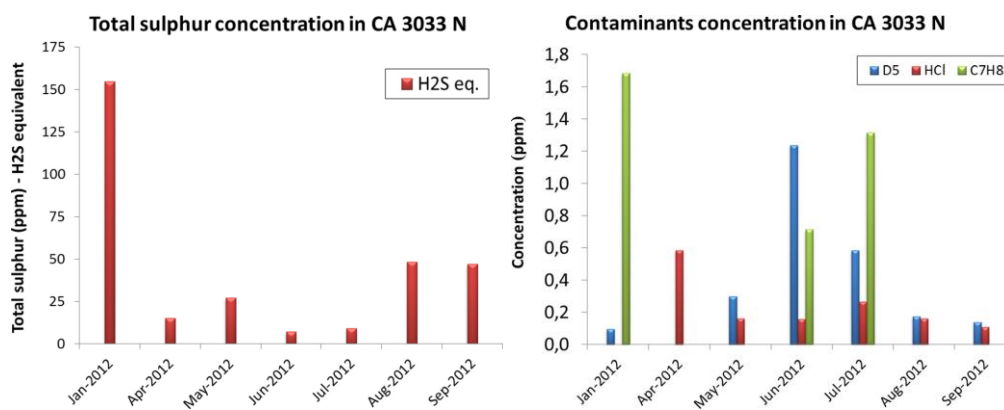
Figure 41. Results from the biogas analysis in SMAT Castiglione, 2012. CA3033 is one of the six anaerobic digesters (Gandiglio et al. 2013).

The clean-up unit was designed and constructed in the Finnish technical research center, VTT, partner of the SOFCOM project.

The cleaning unit was divided into two symmetric cleaning units called "sides" (Figure 42 and Figure 43), A-side and B-side. Both sides have one column filled with Zinc Oxide (ABS-1A and ABS-1B) and one column filled with activated carbons (ABS-2A and ABS-2B). Figure 42 shows the process flow diagram of the cleaning unit.
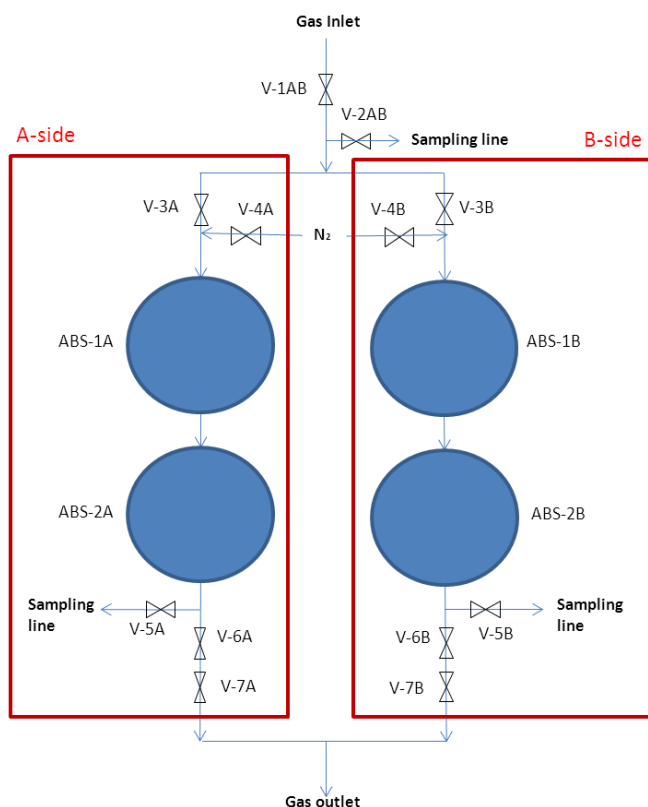
Figure 42. Process flow diagram of the cleaning unit.
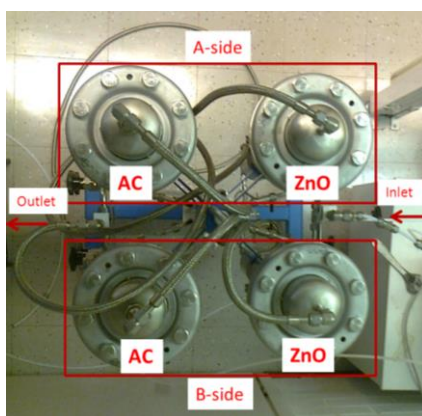
Figure 43. Top view of the cleaning unit.

The cleaning unit had one sample line for the inlet and two sample lines for the outlet (depending on the running side). The cleaning unit also had two lines for flushing with N_2 before and after catalyst replacement.

A biogas pressure sensor (yellow circle in Figure 44) was installed on the inlet line to the system. Biogas reached the plant with a 220/230 mbar overpressure. In order to avoid the use of a blower, which could lead to flows instability, a low delta-P mass flow controller has been installed after the cleaning section to regulate the biogas flow rate. The instrument

position has been defined in order to avoid contaminants or humidity coming to the flow controller. Looking at the bottom part of the system, it also possible to see the nitrogen regulator (red circle in Figure 44). This was a manual system to clean the vessels when adsorption substitution is performed.

Figure 44. Biogas cleaning unit – frontal and lateral view.

The clean-up vessels performance has been measured:

- during the long run operation, with an online portable gas analyzer that was able to detect H_2S in order to check the removal of hydrogen sulfide only;
- With a detailed off-line laboratory analysis of all the micro-contaminants contained in the biogas during the operation period.

Since the H_2S content in the inlet biogas was lower than that one expected and for which the vessels have been designed, the replacement time has been longer than one month.

Experimental tests on the cleaning unit are available in "Appendix 2– SOFCOM units testing", section "A2.1 Clean-up unit test".

3.2 Biogas processing unit

The inlet cleaned and pressurized biogas must be heated before feeding the reformer: electrical heaters are thus provided both for preheating and driving the endothermic

reforming reactions. The fuel processing consisted of mixed dry-steam reforming: this is due to the presence of the carbon dioxide in the inlet biogas. Demineralized water was sourced externally through an auxiliary tank. The reformer worked with a commercial Ni-based catalyst. Its sensitiveness to contaminants is generally very low (e.g.<0.1 ppm for sulfur). The steam to carbon (SC) ratio between CH4 in biogas and external demineralized water has been set to 2 – 2.5 in order to avoid carbon deposition (Gandiglio et al. 2013).

The Steam Reforming (SR) process gives more hydrogen yields compared with dry reforming (DR) reaction (Benito et al. 2007), but, as DR process, it requires an external heat source to supply the endothermic reactions and to preheat the reforming agent (steam), this, reduces the overall efficiency of the fuel processor and of the global system (Processor-SOFC), however, the combustion of the anode off-gas to provide heat for a steam reformer reactor can improve the process efficiency. Another option can be represented by the so-called "CH_4 Tri-Reforming" or Oxy-Steam Reforming (OSR), the process, originally, have been designed for the generation of syngas with a required H_2/CO ratio employing carbon dioxide in the flue gas, from hydrocarbon fuel-based electric power plants (Song & Pan 2004; Lackner 2003; Pino et al. 2014; Vita et al. 2014; Pino et al. 2011).

The biogas reformer reactor was designed and constructed by CNR of Messina, partner of the SOFCOM project. Even if initially designed to work in dry-steam reforming conditions, the reformer was then equipped with an oxygen inlet to drive OSR and reduce the requirement of external heat to be supplied by the electrical heaters.

The reforming unit was developed to reach a nominal hydrogen production of about 2.5 Nm^3/h of syngas (H_2 + CO) from SR or OSR of biogas produced in an industrial wastewater treatment plant. The net size (mm) of the biogas processor was 800 (width), 700 (length), 800 (height). The P&ID of the system is reported in Figure 48. As mentioned above, the oxygen inlet is not drawn in the original system P&ID since was added by the Polito team during the system operation. The main reason for adding oxygen was the insufficient heaters power respect to what required for the endothermic steam reforming reaction. In order to avoid the replacement of the entire reactor, use of oxy-reforming was preferred, because of its exothermic nature which could balance the overall system thermal balance by reducing the external heat requirement.

The reformer was designed to operate, in nominal condition, with a biogas flow of about 10 Nl/min and an H_2O flow of about 725 g/h in SR condition with H_2O/CH_4 ratio between 2-3. The unit can also work under OSR process being equipped with a separate line of oxygen, which is fed in small quantities (O_2/CH_4 molar ratio= 0.05-0.25) to the reactor inlet.

As can be seen from Figure 45, the internal reformer layout is given by:

- Evaporator: horizontal reactor, with water and biogas inlet pipes. The reactor is made of AISI316L and is designed to work at lower temperatures respect to the

reformer, around 400/500 °C. The outlet pipe going to the reformer is placed on the right side of the evaporator. The reactor is heated up by a 4 kW electrical heater.

- Reformer: vertical reactor, the inlet gas from the evaporator enters from the top and the outlet pipe going to the SOFC can be seen on the bottom. The flow is thus moving from top to bottom, in a vertical direction. The reformer, working around 700/800 °C is also heated up by a 4 kW electrical heater.

- Inlet streams flow regulation: the inlet streams going to the reformer (and thus to plant) are measured in flow through Liquid or Gas mass flow controllers. In the bottom part of Figure 45, in the rectangular box on the bottom, the instruments for the flow regulation can be seen: Biogas MFC, Nitrogen MFC, Hydrogen MFC and Demi water MFC. Compressed air (CMP air) is required for the pneumatic valves of the reformer.

The demineralized water required for the reformer is produced directly within the plant. A RioS 5 demineralizer is placed in the demo plant control room (Figure 46). The system is able to produce 5 L/h and feeds the obtained demi water to a 30 L tank where special filters are placed in order to keep the water demineralized during the time. From the indoor tank, an outdoor atmospheric tank (300 L, blue tank in Figure 47) is filled. The filling procedure can be done manually through 25 L small tanks or automatically with a direct connect between the tanks. The first choice has been adopted because of the freezing risk during the winter season.

The demi water is then sent to a pressurized tank (200 L, black tank in Figure 46) through a water pump. The pump is automatically activated when the pressurized tank level goes down the lower level sensors (three level sensors are placed in the tank). The installation of the intermediate atmospheric tank has been requested by the high pump nominal flow, which was not compatible with the demineralizer tank outlet pipe. The pressurized tank is pressurized with nitrogen: pressure around 3-4 bar is required to feed water to the liquid MFC. Higher pressure levels should be avoided since the feeding pump will not be able to fill the tank. The pressurized tank is a steel tank covered with two insulation layers and a heating resistance (working at 65 °C) to prevent freezing accidents during the winter season.
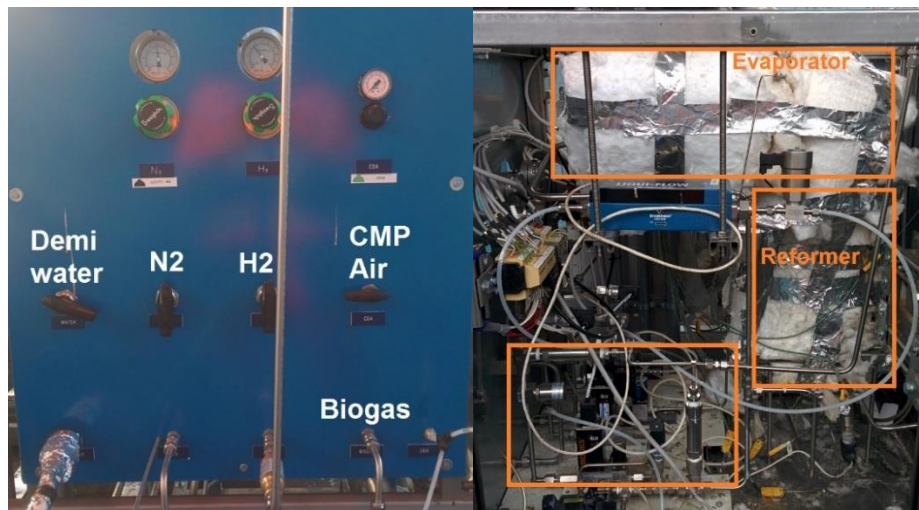
Figure 45. Reformer layout in the SOFCOM demo plant, external and internal view.

All the water pipes where the fluid is not continuously moving have also been heated with the electrical resistance and covered with the insulation layer to prevent freezing episodes.

Figure 46. Tap water demineralizer RioS 5 + 30 L tank

Figure 47. Atmospheric and Pressurized demi water tanks. Demi water pump to feed pressurized tank.

The pipe connecting the reformer outlet and the SOFC stack anode inlet flange is relatively long (around 80 cm) and thus a heating pipe (1 kW) has been installed in order to keep the temperature constant. The reformer nominal outlet temperature is 800 °C while the SOFC anode inlet required temperature is 750 °C. A temperature loss of 50 °C is thus the admissible value in the pipe connection, and the heating pipe works to keep the anode inlet temperature constant through a PID regulator.
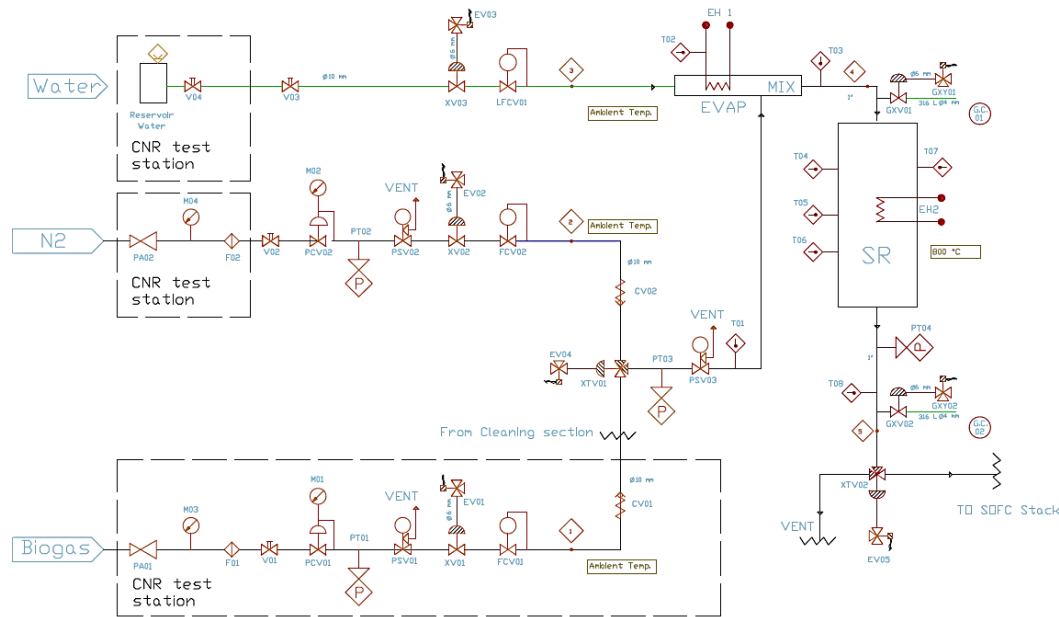
Figure 48. P&ID of the biogas reformer.

Experimental tests of the reformer unit are available in "Appendix 2– SOFCOM units testing" and are presented into two sections: "A2.2 Reformer test session #1" and "A2.3 Reformer test session #2".

3.3 SOFC stack unit

The stack considered for the demo plant is a Sunfire® 2 kW SOFC unit. At the nominal operating point, it will be fed by reformate at 750 °C and cooled by air entering at 650 _C. On the cathode side, the inlet air is flowed by a blower and passes through a gas/gas heat exchanger (air preheater) which recovers heat from the cathode exhaust: the fresh air temperature is increased to 550 °C. The recuperator is followed by an electrical heater which increases the temperature until 650 °C. The air nominal flow rate (390 NLPM) will be varied by the control system in order to keep the temperature inside the stack constant. The SOFC nominal operating temperature is 800°C with a fuel utilization (FU) of 80%, and a cell current of 29 A. The inlet nominal biogas flow is 10.4 SLPM (14 SLPM in the worst operating condition: lower FU and lower CH_4 fraction in the biogas) and the total DC power output is 2 kW.
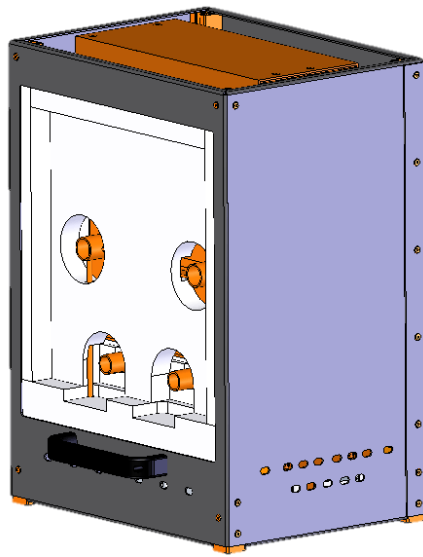
Figure 49. Integrated Stack Module.
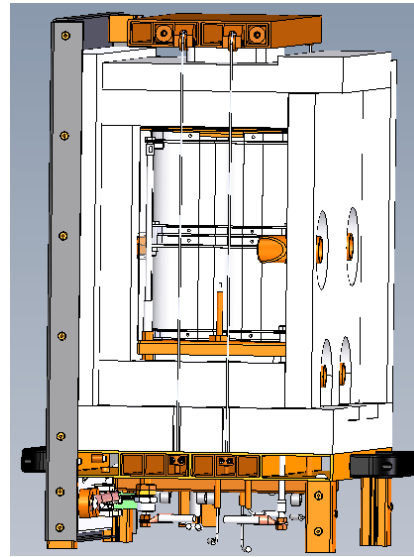
Figure 50. Cut-away view showing stacks.

Table 5. SOFC Module dimensions.

Item	Specification	Comment
N°cell	90	
Height	709 mm	-
Width	436 mm	-
Depth	330.5 mm	Excluding carrying handles and gas connecting tubes/flanges
Volume	102.5 liters	
Mass	≤ 80 kg	-

The cathode exhaust exiting the SOFC found at 800°C is first used to preheat fresh cathode air as explained above and finally sent to a cogeneration system. In the demonstration plant, the hot stream will be used for heating an auxiliary water stream. On nominal conditions, the gas inlet temperature to the CHP heat exchanger is 340 °C, and the water which can be heated is 2.5 l/min (from 65 to 75°C, temperatures suitable for heating digesters) (Gandiglio et al. 2013). The Staxera integrated stack module (ISM) is a solid oxide fuel cell (SOFC) module according to DIN IEC 62282-2. The ISM consists of an SOFC stack within an insulated enclosure. It is intended for integration within an SOFC system or test station. The ISM converts chemical energy to electrical and thermal energy

via an electrochemical process operating at a nominal temperature of between 700°C to 850°C.

Figure 51. SOFC stack, with the four manifold (anode in/out, cathode in/out). Electrical connections where places at the other side of the box.

Table 6. Stack design.

Item	Specification	Comment
Stack	Mk200	60 or 90 layer
Cells	Electrolyte supported	1.3 kW and 1.9 kW: 3YSZ
Seals	Glass / ceramic	-
Interconnectors	Stamped sheet metal	Crofer 22 APU

Table 7. Performance (defined operating point with 75% fuel utilization).

Item	Specification	Comment
Electrical power	≥ 1.9 kW (90 cell option)	At current interface;
Electrical voltage	≥ 38 V/58 V (60/90 cell)	At current interface
Anode gas composition	40% H2 in N2	Without humidification

Anode gas inlet temperature	750°C ± 20 K	T1001 anode inlet
Cathode composition	Atmospheric (ambient air)	Alternative: dry compressor air
Cathode flow rate during full load	≈ 370 Nl/min (1.9 kW)	The flow rate is adjusted to realize stack operating temperature.
Cathode inlet temperature	650°C ± 20 K	T2001 cathode inlet
Operating pressure	5 - 10 mbar gauge	Gauge pressure inside ISM related to ambient pressure
Operating temperature	850 - 860°C	Whichever stack core temperature is the highest.

Table 8. Performance guarantee.

Item	Specification	Comment
Electrical power	1.9 kW (90 cell option)	At defined operating point
Pressure drop anode	≤ 15 hPa	At defined operating point
Pressure drop cathode	≤ 15 hPa	At defined operating point
External temperature	≤ 70°C	At any point of metal housing

Anode gas may be composed of any mixture of fuels (H_2, CO, CH_4) and diluters (N_2, H_2O, CO_2). Other fuels (such as pipeline natural gas, biogas, landfill gas, ethanol, petrol, diesel, etc.) should first be reformed to a gas containing the components listed above.

Fuel composition will influence the power output of the ISM. The rated power output of staxera ISM is achieved with dry fuel gas with the composition 40% H_2 in N_2. Table 9 shows feasible values for power output for typical CPOx- and steam reformate fuel gas compositions (at 75% fuel utilization and 860°C maximum core temperature).

Table 9. Performance changes by different used fuels.

Fuel gas composition	90 cell version
40% H_2 / 60% N_2 staxera reference	1.9 kW
CPOx reformate (typical)	1.6 kW
Steam reformate (typical)	1.5 kW

The ISM is heated up by the anode and cathode process gases, which can be supplied at up to 850°C. Above 700°C, fuel can be supplied, and current can be drawn. Above

820°C, the cathode air temperature is reduced to 650°C. The ISM temperature is controlled by adjusting the cathode air flow rate. To shut down, reduce the current to zero, reduce the air and fuel flow rates to a low value, introduce purge gas (reducing atmosphere recommended, e.g. 5% H_2 in N_2), and then turn off the pre-heaters.

The Staxera ISM generates both thermal and electrical energy during operation. The stack must be cooled to maintain stable operating temperatures. This thermal sink should be dynamically matched to the thermal source, which is proportional to the electrical stack power.

Two methods of cooling are available: convective cooling using cathode air, or partially reactive cooling using internal reforming of methane on the surface of the cell.

Anode line

The inlet gases provided to the SOFCOM plant are nitrogen and hydrogen for the start-up phase and biogas for the stationary operation. There is also an emergency line for nitrogen and a secondary supply oxygen line, used to heat up and sustain the reformer during its operational phase. Demineralized water is the last inlet flow, necessary for the SMR reaction. During stationary conditions, biogas and water are sent together in the evaporator section in order to reach the nominal entering conditions required by the reformer. (see Figure 52)
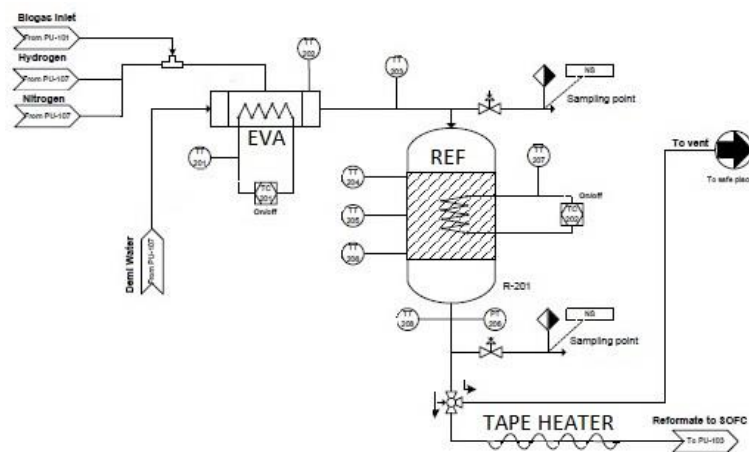
Figure 52. Anode line.

Then, the vaporized water mixed with biogas reach the catalytic bed where the SMR and WGS take place, releasing the hydrogen and carbon monoxide necessary for the subsequent electrochemical reaction. In Figure 53 is shown the electrical tape required to reach the 750 °C requested for the anode inlet temperature. PID block controller unit is used to partially the external thermal power. The power of electrical tape is about 1 kW.
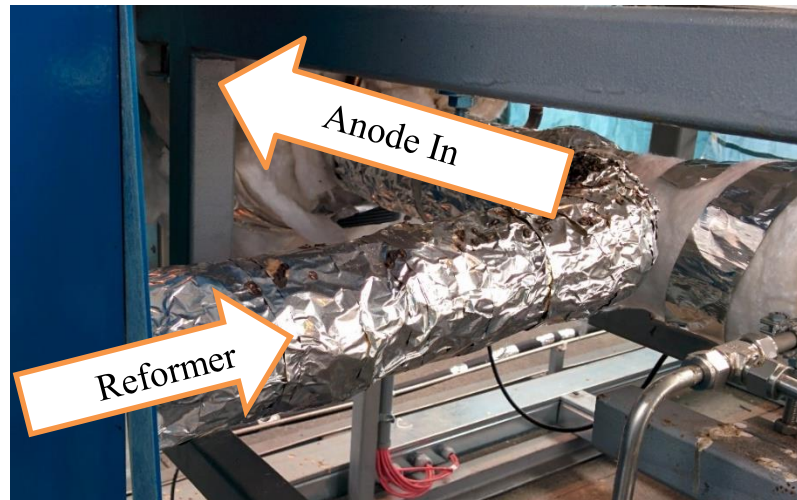
Figure 53. Electrical strip - located under the insulation coating.

Cathode line

The required air for the electrochemical reaction and the thermal control of SOFC stack is pumping in using a motorized air blower equipped with an inverter. The airflow rate is imposed from a PID controller, which must prevent that the temperature of the stack exceeds the maximum allowed. The flow rate is measured with an analogic rotameter (circular shape in Figure 54). The air preheater consists of two sequential sections – a *Heat Exchanger* and an *Electric Heater*. The heat exchanger allows recovering heat from the cathode exhaust, reaching an outlet temperature above 550-600 °C. By manufacturer datasheet, air must be sent at a temperature above 650 °C. Thus a secondary preheater (electric) is installed to reach the final goal. In Table 10 the main parameters of this section are shown.

Table 10. Main parameters of air Pre-heater.

	Parameter	Value	Unit
Heat exchanger Air Pre-Heater	MAX flow rate	300	Nl/min
	MIN flow rate	130	Nl/min
	Exchange heat flow	4,4	kW
	Max_inlet_Temp	830	°C
	Max_out_Temp	650	°C

Figure 54. Air blower and its Rotameter
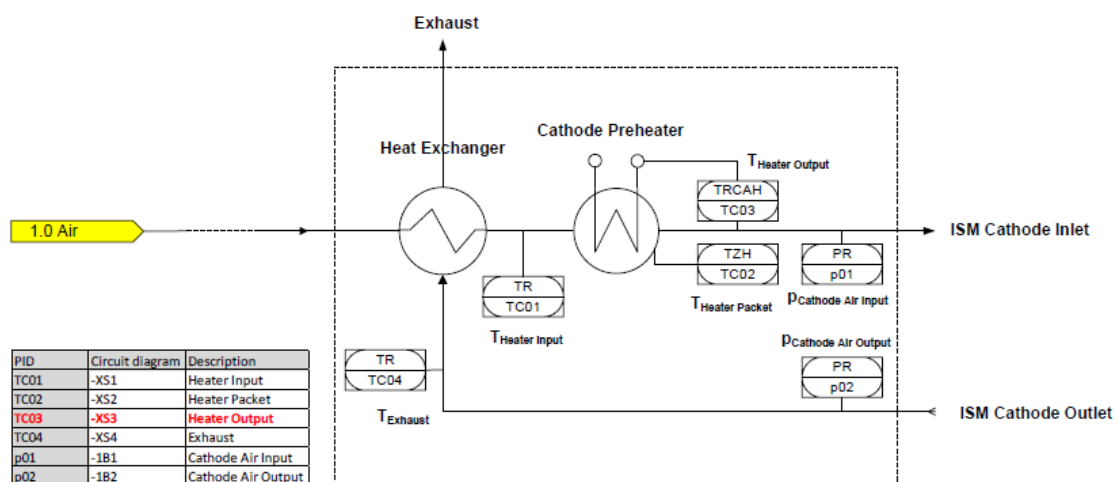
Figure 55. Air Pre-Heater block.

CHP – heat recovery

The exhausted cathode output from the air pre-heater releases the residual heat to the CHP heat exchanger, shown in Figure 56.

Figure 56. CHP water heat exchanger.

An electrical load with variable resistors is used to test the stack module. Thanks to a serial communication port, is possible to change the electric current from its remote control tool.

Figure 57 Electric load.

Experimental tests on the SOFC unit are available in "Appendix 2– SOFCOM units testing", section "A2.4 SOFC unit test results".

3.4 Oxy-combustion unit

The oxy-combustion unit is placed downstream the SOFC stack: the choice of combustion with pure oxygen is in order to have a complete combustion of the excess fuel (H_2 and CO) present in the anode exhaust without adding inert off-gas (i.e., nitrogen in air), to yield an higher CO_2 concentration in the exhaust and, thus, an easier CO_2 separation from water. This is exactly the advantage of the SOFC anode exhaust (no N_2 content) which will be preserved by the oxy-combustion process.

The oxygen is provided in cylinders, because of the low volume flow needed that does not suggest the adoption of an O_2 separator in the demonstrator. After the oxy-combustor the stream temperature has to be decreased until 300–400 °C (condenser maximum inlet temperature) and this is carried out through a water heat exchanger for high temperatures.

The oxy-combustor is designed to regain the chemical energy present in the off-anode gas leaving SOFC stack in the form of not combusted carbohydrates, CO, H_2 and to avoid emissions of those substances to the atmosphere. Moreover, it can be used to produce pure CO_2 for the use of food industry or other purposes.

The current subsection deals with the detailed design of the oxy-combustor. The numbers are summarized in Table 11.

Table 11. Off-anode gas leaving SOFC stack composition range.

Number	Description
1	Inlet of off-anode gases
2	Primary oxygen inlet
3	Primary oxygen pipe
4	Three rows of primary oxygen nozzles
5	Secondary oxygen inlet
6	Five secondary oxygen nozzles
7	Pipe
8	Pipe
9	Pipe
10	SiC porous foam material – mixing zone
11	SiC porous foam material – burnout zone
12	Ignition and outlet zone
13	Cooling air inlet
14	Cooling air outlet
15	Helical baffle enforcing the spiral flow of the cooling air
16	Thermocouple ports
17	Oxygen (lambda) probe ports
18	Igniter port
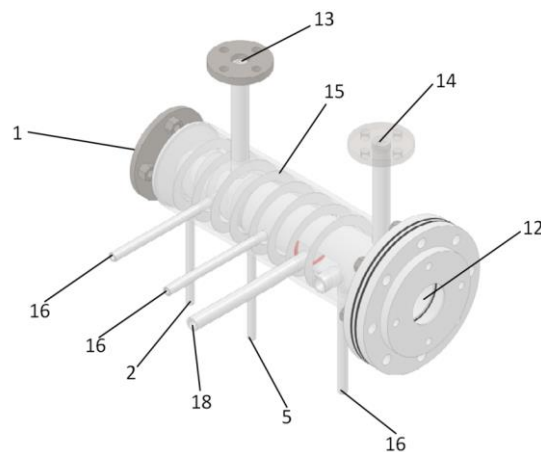
Figure 58. Isometric view of the oxy-combustor. Names corresponding to the numbers are summarized in Table 11.
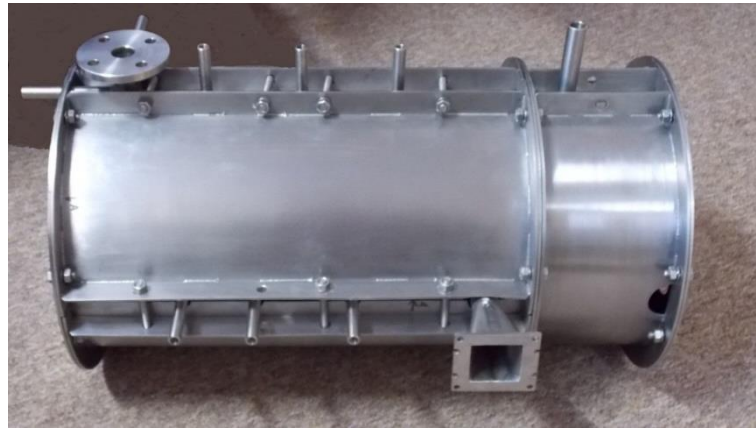
Figure 59. Fully-assembled oxy-combustor.

The oxy-combustor is fed with off-anode gases leaving the SOFC stack. Known solutions are based on initially premixed fuel and oxidizer streams that enter the combustion chamber. However, because of the stack characteristics, the temperature of off-anode gases (that are fuel for oxy-combustor) is > 800 °C. Such high fuel temperature doesn't allow premixing of fuel and oxidizer streams as it may results in uncontrolled self-ignition. In the current oxy-combustor design, the fuel and oxygen streams are initially separated. The oxygen is divided into two streams: primary (2) and secondary (5) and is delivered to the reaction zone by distributors (4)(6). The reaction zone inside the oxy-combustor is divided into two parts: mixing (10) and burnout (11) zones, both filled up with a porous material. The first zone is supplied with primary oxygen, whilst the burnout zone with secondary oxygen. The reason behind the oxygen staging is twofold. Firstly, it allows for the temperature control inside the oxy-combustor. Otherwise, the temperature control would be limited only to the adjustments of the cooling air flow rate. Keeping maximum temperatures of the porous material is important from the view of its thermal strength. SiC porous foams can withstand temperatures as high as 1350 °C. However, in reacting flows, the maximum working temperature should be lowered in order to ensure the required lifetime of the porous material. Therefore in the case of current design, the maximum allowable temperature was set to 1100 °C. The second reason behind the oxygen staging is that it leaves the possibility for making proper adjustments to keep the emissions of H2 and CO low at the outlet. In the mixing zone, only the part of the off-anode gases is burned as only primary oxygen is delivered. The rest of the fuel is combusted in the burnout zone with the use of secondary oxygen.

Another issue that should be emphasized is the flame stabilization. In the known solutions of porous burners, the flame was stabilized by using two porous materials of different porosity and pore size. In the current design, the porous material used in the mixing and burnout zones has the same properties. The flame stabilization is assured by oxygen staging and proper geometrical design of the combustion chamber. The outer diameters of the combustion zones (10)(11) are set in such a way, that inside the mixing zone (10) the flow velocity is higher than the flame propagation speed and in burnout zone

(11) the flow velocity is lower than the flame propagation speed. In this way, the flame is stabilized inside the zone of greater diameter. Moreover, the properties of the porous material and the flow aerodynamics inside it enhance the flame stabilization.

The control application written in NI LabView runs on the main control unit (cRIO-9073). It is responsible for controlling the process, archiving data and visualizing on a panel PC. Its functions are grouped in three tabs, which will now be described.
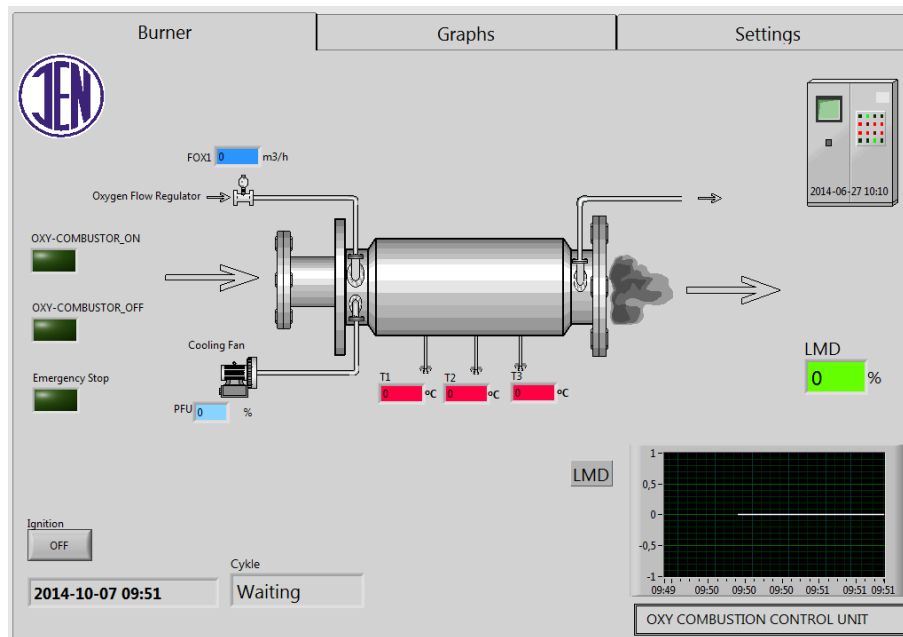
Figure 60. Control application - burner tab.

Overview of the combustor can be seen in this tab, allowing for an easy identification of measurements and control signals. The control system is seen in a "Waiting" mode, as indicated by the box at the bottom.

This tab contains the following elements:

- Numeric indicators of measurements and control signals placed in appropriate locations on the burner schematic (temperatures, oxygen concentration, inlet oxygen flow, cooling fan control),
- Binary indicators for external control signals (parent system ON/OFF signals and emergency stop) on the left side,
- Oxygen concentration graph in the lower right corner,
- Ignition button in the lower left corner,
- Text boxes showing current date, time and operation mode in the lower left corner.

Notice that the flame does not appear on the right side of the burner. This is because the ignition was not detected.
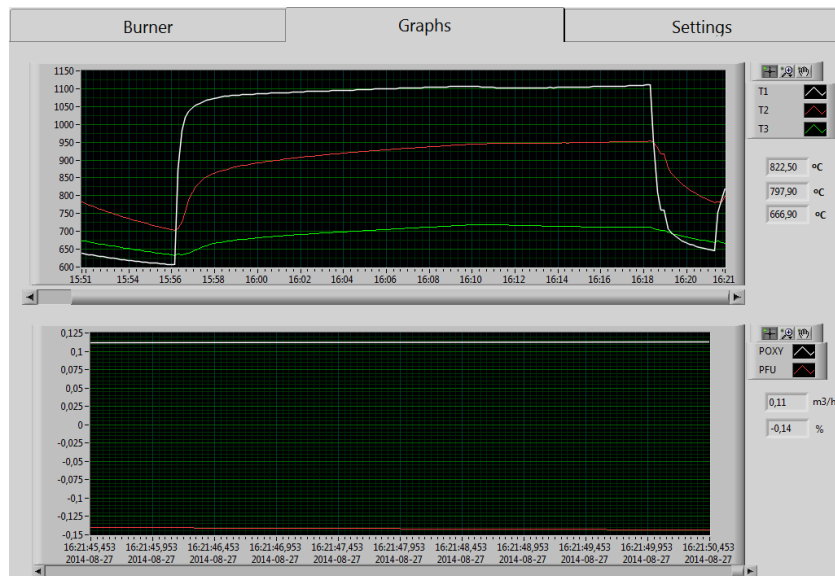
Figure 61. Control application - graphs tab.

This tab is used for plotting of the most important process variables. It contains basic graph tools, allowing for axes zooming, grabbing and scaling . The upper graph contains readings from the thermocouples (T1, T2, and T3); the lower graph contains inlet oxygen flow (POXY) and a cooling fan control signal (PFU).
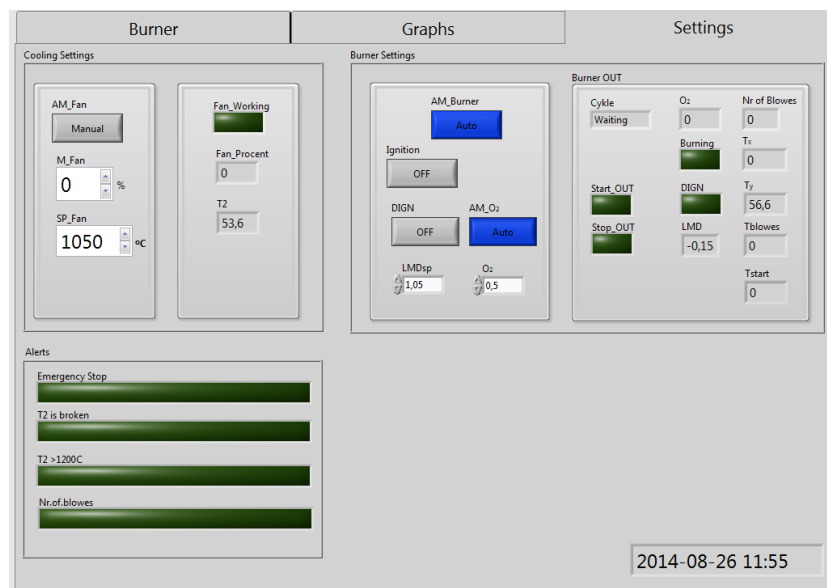
Figure 62. Control application - settings tab.

This tab is used mainly for the configuration of system parameters. It is divided into three main sections:

- Cooling settings – contains controls and indicators for the burner temperature loop (automatic/manual temperature control, temperature set point, fan operation indicators),

- Burner settings – contains controls and indicators for the burner operation (automatic/manual oxygen concentration control, ignition, burner operation indicators, external signals),
- Alert indicators for an emergency stop, T2 fault, the maximum temperature exceeded, the maximum number of ignition attempts exceeded.

Experimental tests on the oxy-combustion unit are available in "Appendix 2– SOFCOM units testing", section "A2.5 Oxy-combustor test results".

3.5 Condenser unit

The water condensation unit is able to remove water from the oxy-combustor outlet stream. The effluent from this unit consists of almost pure CO_2, except traces of inert gas, oxygen, and water. The condensation is first guaranteed by a condenser fed by a demineralized water loop which brings the temperature down until ambient (25–30°C). The condenser is followed by a compressor which increases the stream pressure until 8 bars, required pressure for the downstream stage of membrane separation. The temperature after the compressor is around 150–200°C: the stream is hence re-cooled to ambient temperature (25°C) with a fan driven air cooler. In fact, the membrane cannot stand more than 65°C for a long period of time, and the membrane stage temperature is imposed very close to ambient. The water liquid fraction still present in the stream is taken away by a fog condenser before going into the membrane stage.

Figure 63. Condenser (on the left) and CO2 separation membrane (on the right).

The remaining fraction of water is completely removed by a membrane dryer: the outlet stream will be pure carbon dioxide with some ppm of nitrogen (due to oxygen purity 99.5% in the cylinders), oxygen (due to oxygen excess 1% in the oxy-combustor) and around 500

ppm of water (maximum effectiveness of the membrane). The membrane purge gas is partially recirculated to the condenser inlet. The overpressure valve downstream the membrane guarantees a nominal pressure of 8 bars to the membrane stage and decreases the pressure until 2–3 bar for the photobioreactor module placed downstream. A 2–3 pressure is what required by the mass flow controller feeding CO_2 fed to the photobioreactor.

One major framework condition for the presented work was the gas composition and flow after the oxy-combustion unit. These were derived from the matrix of operation conditions delivered by POLITO in Figure 64.

Case ID:	1	2	3	4	5	6	7	8	9
Variable:									
1 - Stack current, I	140	120	120	160	160	120	120	160	160
2 - Fuel utilization (FU)	80%	75%	85%	75%	85%	75%	85%	75%	85%
3 - Biogas composition (CH_4/CO_2 vol.)	60/40	55/45	55/45	55/45	55/45	65/35	65/35	65/35	65/35
Cell voltage, mV	0,64	0,68	0,66	0,62	0,60	0,68	0,67	0,62	0,60
SOFC DC electrical efficiency	49,4%	48,8%	53,9%	44,4%	48,9%	49,4%	54,5%	44,9%	49,4%
Plant AC electrical efficiency	42,9%	43,3%	46,8%	38,5%	41,3%	43,8%	47,3%	39,0%	41,9%
Biogas inlet flow, SLPM	22,3	22,2	19,6	29,6	26,1	18,8	16,6	25,1	22,1
Anode off-gas composition (% vol.):									
CH_4	0,0%	0,0%	0,0%	0,0%	0,0%	0,0%	0,0%	0,0%	0,0%
CO_2	33,7%	33,1%	38,7%	33,1%	38,7%	29,0%	34,6%	29,0%	34,6%
CO	11,7%	14,5%	8,9%	14,5%	8,9%	14,4%	8,9%	14,4%	8,9%
H_2	10,1%	11,7%	6,8%	11,7%	6,8%	13,8%	8,1%	13,8%	8,1%
H_2O	44,5%	40,7%	45,6%	40,7%	45,6%	42,7%	48,4%	42,7%	48,4%
O_2	0,0%	0,0%	0,0%	0,0%	0,0%	0,0%	0,0%	0,0%	0,0%
N_2	0,0%	0,0%	0,0%	0,0%	0,0%	0,0%	0,0%	0,0%	0,0%
total	100	100	100	100	100	100	100	100	100
Molar flow (kmol/s)	3,66E-05	3,48E-05	3,07E-05	4,64E-05	4,10E-05	3,23E-05	2,85E-05	4,30E-05	3,80E-05
Mass flow (kg/s)	9,63E-04	9,13E-04	8,57E-04	1,22E-03	1,14E-03	8,00E-04	7,58E-04	1,07E-03	1,01E-03
Volumetric flow (SLPM)	49,2	46,8	41,3	62,4	55,1	43,4	38,3	57,9	51,1

Figure 64: Matrix of operation conditions

From this matrix, the average and the most demanding operation points were selected with regards to gas flow and gas composition for designing regular operation and maximum performance. Complete conversion of the leftover fuel in the oxy-combustor was assumed for estimating the overall flow, the maximum amount of trace O2 was assumed to be below 2 vol-%. The gas inlet temperature was assumed to be up to 400°C (673K), which could be easily achieved by air cooling after the oxy-combustor. Approximately atmospheric pressure was assumed. The estimated gas composition for regular operation is shown in Table 12.

The main aim of the unit is purification of CO_2 to transportation and storage limits. These were specified in the EU-funded project DYNAMIS to 4 vol-% trace gases and non-condensable, such as O_2, N_2, and others, and 500ppm of H_2O in order to avoid corrosion of equipment. In the case of biogas conversion in an SOFC system, the non-condensable present in the exhaust under normal conditions without leakage are only leftover H_2, CO, and O_2 from incomplete oxy-combustion. However, these are below the limit of 4 vol-% total.

Table 12. Nominal gas composition after oxy-combustor.

Gas	share in [vol.-%]
CO_2	43,2
CO	1,71
H_2	0,42
H_2O	53,5
O_2	1,2
Molar flow [mol/s]	0,037
Mass flow [kg/s]	1,09E-3
Volume flow [SLPM]	49,8

Thus, in order to reach transport requirements the H_2O content of the exhaust, which is around 50%vol depending on the biogas composition, has to be reduced to 500ppm.

Besides the formal requirements some additional goals were set in order to optimize the system concept:

- Minimizing equipment cost
- Using commercially available equipment only
- Maximizing system robustness and safety by introducing a self-controlled system, thus minimizing the remote control effort.
- Designing the system for a broad range of gas parameters

As can be seen from the paragraph cold drying, most of the water content in the process gas can already be removed by condensing to room temperature. This can be done utilizing fairly inexpensive, robust and well-approved tube bundle heat exchangers. However, achieving 500ppm water content would only be possibly by extensive cooling and thus be technically and economically wise, not favorable. Also, with regards to scale-up of the system, no scale effects can be utilized for producing cold. Excluding the cooling-only option, two major other possibilities are left.

The first is adsorption, which is a commercially available technology. However, after a more detailed investigation of possible system designs, several disadvantages were found. Complex line switching, heating cycles makes system control quite difficult and special expertise would be needed e.g. for material choice and designing the system, which alone was found to cost about 20.000€.

The second option is a pressurized system, which can reduce the effort for cooling. Compressors are reliable state-of-the-art equipment and commercially available at almost any size. However, after a rough estimation, a high energetic effort was still found to be

inevitable. As an alternative to further cooling of the gas membranes were found. These also require compression of the gas stream, but at moderate pressures and no further energy demand. As an additional advantage, there are already commercially available solutions for process gas drying in the market today.

Thus it was decided to design a 2 stage system, consisting of a condenser as the first stage and a rest-dehydrator as the second stage, consisting of a compressor and a membrane. For the membrane purge, gas is necessary in order to transport the separated water. In the case of drying air this is done utilizing air, however, for the selected membrane type it is not known how much CO_2 would be lost over the membrane into the purge gas. As a solution to this problem, a recirculation concept was introduced, utilizing dried CO_2 as a purge gas for the membrane and reintroducing the wet purge gas into the condenser inlet, thus increasing the stream through the condenser but avoiding any loss of CO_2. A schematic drawing of the final system concept can be seen in Figure 65.
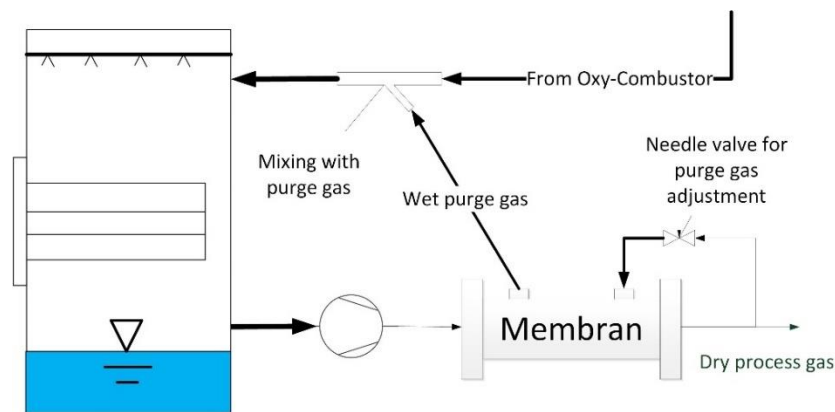
Figure 65: Schematic drawing of the final system configuration

Experimental tests on the condenser unit are available in "Appendix 2– SOFCOM units testing", section "A2.6 Condenser unit test results".

3.6 Photobioreactor unit

The last section of the plant is the treatment of waste water (SMAT secondary treatment water) with algae. Algae have been chosen primarily because they act as a sink to fix (thus recycling) that carbon contained in the CO_2-rich anode exhaust stream. The CO_2 flow, combined with the nutrients of wastewater and sunlight, will grow the algae: output streams are consequently biomass (algae), treated water, O_2 and unfixed CO_2 that is vented with O_2 to the atmosphere, while a continuous mixture of microalgae suspended in water flows from the outlet to the inlet of the system. CO_2 is controlled and pumped with a mass flow controller, then mixed with the waste water which contains nutrients (phosphates and nitrates) and then sent to the photobioreactor. The photobioreactor is a tubular one, made of 3 modules, in which the algae grow thanks to the light, CO_2 and nutrients; the mixture of

algae and water is sent to a tank in which the remaining CO_2 and the O_2 generated are vented. The tank outlet stream is thus sent to a ultrafiltration membrane in which the algae purge is separated from the treated water (outlet streams of the demo plant). The algae purge will be analyzed, and it can close the carbon loop of the plant if it is sent to the digester again. Power is required in the plant for the four water pumps.

At the SMAT facility, the photobioreactor system was installed and connected to the SOFC stack system through the CO_2 exhausted line, to the power supply, the feeding water, and the draining system. The plant was orientated versus the sun cycle, south position and the panels were inclined at 45 °.

Figure 66. Front view of the plant with the 3 modules exposed to the sun.

Figure 67. Back view of the plant with the 3 modules exposed to the sun.

The inlet flow is connected through the 50 μm and washable filter to the system. In Figure 68 is depicted the wastewater inlet and the 50 μm filter to remove the particles in suspension.

Figure 68. Inlet wastewater flow to the system.

Figure 69 shows the water analysis probes included into the degasification tank of the wastewater before the recirculation.
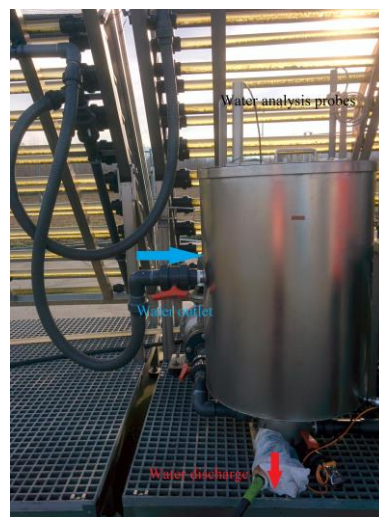
Figure 69. Water analysis probes, degasification tank.

Figure 70 shows the clean water tank that flows from the CO_2 membrane. It was installed a T-tube to allow the water discharge avoiding the water overflow. In Figure 71 is depicted the wastewater analyser: it is possible to monitor the evolution of pH, phosphate, chlorides, nitrates, temperature, turbidity and oxygen dissolved in the water.

Figure 70. Clean water tank.

Figure 71. Wastewater analyzers.

In Figure 72 is depicted the CO_2 injection section: a backup is guaranteed by two CO_2 gas cylinders while the main CO_2 injection is allowed from the SOFC stack.
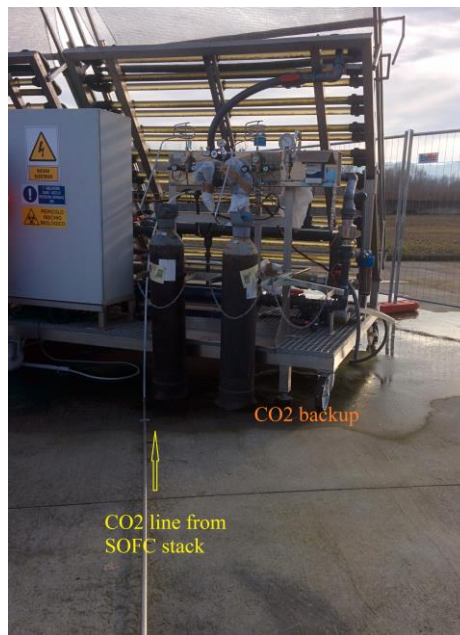
Figure 72. CO2 injection system: from the SOFC stack (main line) and from two CO2 gas cylinders (backup line).

Experimental tests on the PBR unit are available in "Appendix 2– SOFCOM units testing", section "A2.7 Photobioreactor test".

3.7 Overall plant operation

The demonstration plant has been operated continuously for more than 600 operating hours during March and April 2015. Data have been logged through the control system every 2 seconds and analysed in the presented work.

The whole plant set point was always depending on the SOFC operation point, since the value set to the current on the electronic load had an influence on the flow rates and operation of all other equipments. Figure 73 and Figure 74 show the current and voltage profiles for the long run operation. As can be seen, the system operation can be analysed as the sum of different operating intervals:

1. **Hours 0-350 → day/night operation**. Since a problem was detected in the connection between the control system and the electronic load, safety procedures to remove current in case of emergency were not available. For this reason a day/night operation was chosen: the system was working @ 12A (half of the total current) with half of the nominal flow (100% operation) during the day and was moved to 6 A (with the same flow rates, thus 50% operation) during the night and weekends. Three very short blackout also occur during this first period, due to a ruined heating pipe for the reformer outlet, which was then substituted in the second period.

2. **Hours 350-400 → OCV conditions.** Some days before the SOFCOM final meeting, the demo plant was brought to OCV to have a 'safe' operation before the meeting.
3. **Hours 400-520 → Continuous operation**. Since the problem on the electrical load control system was fixed, the system operated for more than 100 hours on continuous operation at 50% with half of the nominal flow (100% operation).
4. **Hours 520-600 → Specific tests**. The last hours were devoted to specific tests on the demo. As can be seen, the current was increased to 27 A first with a N-H mix feeding and then with biogas. The system was then shut-down.
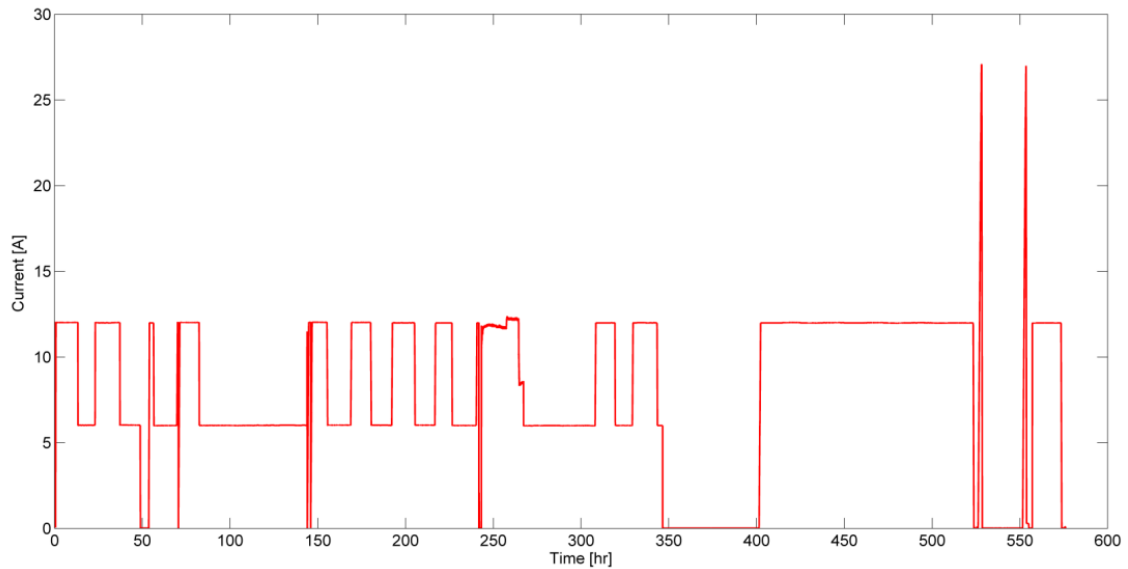
Figure 73. Current profile during long run.
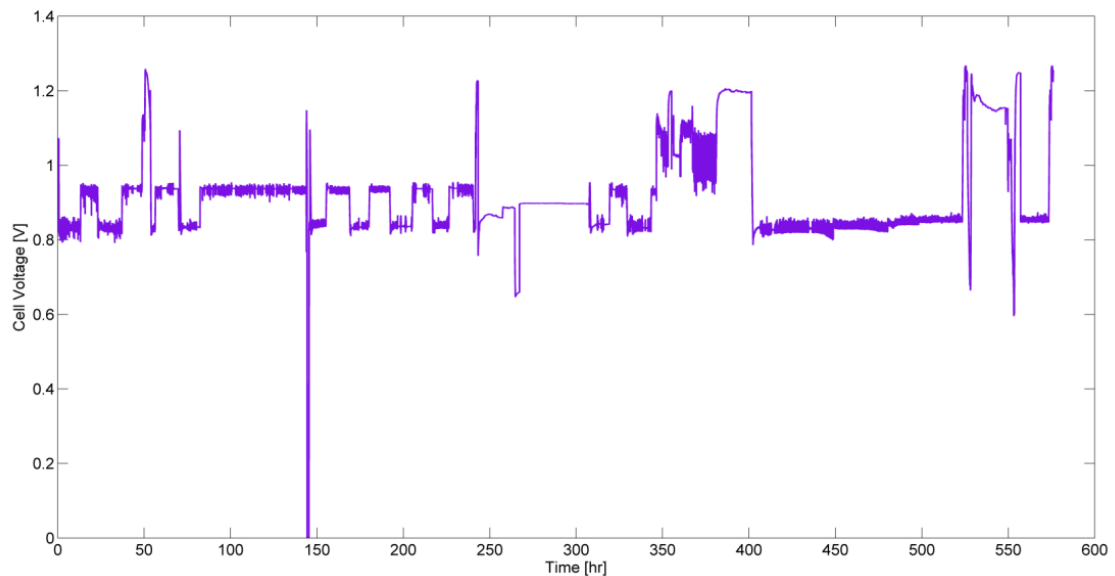
Figure 74. Mean single cell voltage profile during long run.

The choice of keeping the current at 12 A at reduced flow rates was mainly due to maintain a suitable temperature in the reformer reactor. The SOFC performance were tested also in this scenario (because the FU was the nominal one, 80%, even if at half load), but in these conditions the reformer was less stressed and temperatures higher than 700 °C were maintained in the reactor.

The bottom process (oxy-combustor + condenser) was on during most of the long run tests. The first 100 hours were devoted to set the oxy-combustor control system, especially for what concerning the oxygen flow rate through the measurement from sonda lambda, which operation was unstable during transients. The condenser has been operated with a day/night operation since its control system was already supplied from the partner and was not included in the overall demo panel: for this reason, in case of an SOFC failure, the risk of filling the condenser with an explosive mixture was possible. Thus, a day/night operation was preferred.

3.7.1 Algae production and CO_2 fixation

The photobioreactor was operated for many months, with different starts and stops. The first start-up was performed during January 2015, when the cold weather was not optimal both for algae growth and for avoiding freezing problems. Many electro-valves and pipes indeed had problems due to ice formation in the coldest hours of the day. For this reason pumps were switched on 24 hours per day.

PBR control system

The PBR control system is show in Figure 75.
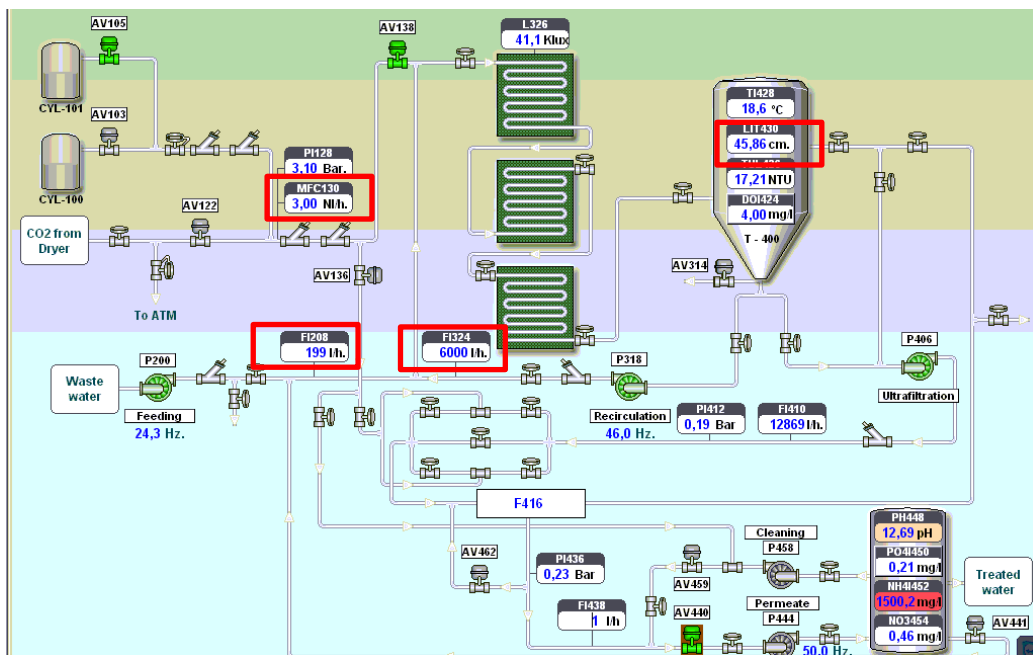
Figure 75. PBR control panel.

The INPUT parameters for the PBR control system are:

- CO_2 flow rate. This is the chosen operating value: the PBR works at a fixed CO_2 flow rate. The control system was able to operate also at constant nitrates/phosphates but, since the analyser were measuring quite unstable values, the operation at constant CO_2 was suggested by the producer. The feeding source for the CO_2, gas cylinders or demo plant, could be directly chosen from the control panel. The value was calculated depending on the inlet CO_2/water ratio chosen: different CO_2% have been tested during the operation.

- **Inlet water flow rate**. The inlet waste water flow was also an input variable. This value was fixed at around 200 l/h even if the system was not always able to maintain a constant flow rate. The unstable flow rate was due to sludge particles inside the water which obstruct the inlet filter. Problems related to filter obstruction have been detected several time during the PBR operation and should be further optimized in future tests.

- **Recirculation flow rate**. The recirculation flow rate is also an input of the control system. A nominal value around 6000 l/h was chosen and maintained during the operation.

- **Degasification tank level.** The nominal level of the tank was also an input. Depending on this value and on the amount of inlet waste water, the ultrafiltration loop was activated/deactivated.

- **Timetables.** Two operating mode were available, day and night, and the system automatically switched from one to the other at certain hours of the day, defined by the user. These values were changed moving from winter to spring weather, increasing the daily operation respect to the night one. The two operating modes are the following:
  - **Day operation.** CO_2 and waste water are sent to the system. Recirculation is ON and clean water is extracted from the system through the ultrafiltration loop. The cleaning procedure of the membrane is also ON at time intervals defined by the user. Thanks to sun irradiation, nutrients from the waste water and CO_2, the algae are able to grow.
  - **Night operation.** The system is OFF except the recirculation pump which is kept always ON to guarantee a continuous mixing effect and avoiding problems of algae attachments to the pipes. Algae are not growing and the system is kept on stable conditions.

The system has always been operated in auto mode with automatic day/night switch, since this regulation was able to guarantee a stable operation to the PBR.

The analyses were conducted both with the PBR instrumentation and with SMAT laboratory testing.

The PBR control system was continuously measuring the nitrates and phosphate outlet content. When algae were growing, the ratio of removal was often so high that the outlet nutrients value was lower than the detection limit. Different samples were collected and analysed in the SMAT laboratories. Every two days inlet and water samples were taken from the PBR to analyse nitrates and phosphates. Furthermore, during the growing period, every 15 days, an algae sampling was performed. This operation was done removing a sampling pipe and collecting attached and suspended algae.

Figure 76. From the left to the right hand. Samplings: 1. PBR inlet water. 2. Water recirculating in the PBR. 3. Algae attached to the pipe. 4. PBR outlet water.

The objective was to measure the bio-fixation and nutrients removal capacity of the demonstration photobioreactor during the demonstration trials in Torino. The following values were calculated.

For the **CO₂ bio-fixation:**

- Microalgae growing rate: Mass of microalgae grow per day

$$R_{algae} = n_{tubs} * \frac{DM_{algae}}{n_{sampling\ tubes} * t_{sampling}}$$ Eq. 3

- Microalgae growing productivity: Mass of microalgae per day and illuminated surface

$$P_{algae} = \frac{R_{algae}}{S_{photobioreactor}} \qquad \text{Eq. 4}$$

- CO_2 capture yield: Percentage of the feed CO_2 which is fixed in the algae and dissolved in the water

$$Y_{CO2\ capture} = \frac{[C]_{algae} * R_{algae} + [CO2]_w * \frac{MW_C}{MW_{CO2}} * F_w}{\frac{MW_C}{MW_{CO2}} * F_{CO2}} \qquad \text{Eq. 5}$$

For the **Nitrogen removal:**

- Residual nitrogen: nitrogen concentration at the outlet of the treatment
- Total nitrogen removal Capacity: Concentration of Nitrogen removed by the treatment, considering same inlet and outlet flow

$$R_N = [NO_3^-]_i + [NH_4^+]_i - [NO_3^-]_o - [NH_4^+]_o \qquad \text{Eq. 6}$$

- Total nitrogen removal yield: Percentage of the inlet total nitrogen which has been removed by the photobioreactor, considering same inlet and outlet flow

$$Y_N = \frac{R_N}{[NO_3^-]_i + [NH_4^+]_i} \qquad \text{Eq. 7}$$

For the **Phosphorous removal:**

- Residual Phosphorous: Phosphorous concentration at the outlet of the treatment
- Total Phosphorous removal Capacity: Concentration of Phosphorous removed by the treatment, considering same inlet and outlet flow

$$R_P = [PO_4^{3-}]_i - [PO_3^{3-}]_o \qquad \text{Eq. 8}$$

- Total Phosphorous removal yield: Percentage of the inlet total phosphorous which has been removed by the photobioreactor, considering same inlet and outlet flow

$$Y_P = \frac{R_P}{[PO_4^{3-}]_i} \qquad \text{Eq. 9}$$

Nomenclature for the above-mentioned equations

P_{algae}: Microalgae productivity or Mass of microalgae growth per day and illuminated surface.

R_{algae}: Growing rate or Mass of microalgae growth per day

n_{tubs}: Total number of tube (2 or 3 modules) running in the photobioreactor

$n_{sampling\ tubes}$: Number of tubes of the photobioreactor used to sample, collect and weight the algae

DM_{algae}: Mass of algae collected during the clean-up of the tube and dried at 105 C for one or two night in an oven

$t_{sampling}$: Number of days since the sampling tubes were cleaned for last time

$S_{photobioreactor}$: Illuminated surface of the photobioreactor

$Y_{CO2\ capture}$: CO_2 capture yield or percentage of the fed CO_2 which is fixed in the algae and dissolved in the water

$[C]_{algae}$: Carbon concentration in the collected algae

$[X]_i$: Concentration of the chemical X in the inlet water

$[X]_o$: Concentration of the chemical X into the outlet water

F_o : Outlet water flowrate

F_{CO2}: Injected CO2 flowrate

R_N: Mass of removed dissolved nitrogen in water

Y_n: Removal yield of nitrogen

R_p: Mass of removed dissolved phosphorous

Y_p: Removal yield of Phosphorous

Analysis of actual CO_2 capture in micro-algae

The main result achieved during the PBR operation, in the long run, is the growing rate of algae. The growing rate was calculated with algae sampling and elementary analysis done by SMAT laboratories.

The growing rate is calculated by dividing the measured dry algae quantity per the time required for the growth and the total PBR surface (area of the system exposed to sun radiation, equal to 9 m^2). (Santarelli et al. 2017)

The working operation of the system can be divided into different operation intervals:

- **Test A (January-February 2015)**: almost no algae growth was observed. This was mainly due to the cold weather with few sunny days and a consequent unstable operation of the system due to maintenance and freezing problems.

- **Test B (March 2015)**: during March 2015 the algae started to grow, and pipes started to become green. A high irradiation was reached in mid-March leading to the maximum growing rate. After the 6 g/m^2/day maximum value, the system had a decrease of the performance. This was due to a high attachment of the algae to the pipes, probably because of a too high irradiation (no protective system for reducing sunlight irradiation was used). The system was completely dark and full of algae, and no sunlight was able to penetrate the surface and reach the inlet water. A degradation was thus observed.

- **Test C (April 2015)**: the system degradation was increasing, and algae changed their color from green to brown, probably because of starvation, as previously observed in the lab experiments. The PBR was thus cleaned and re-started until the end of April. A new but reduced (because of the time length), growth was observed. Sunlight protective systems were also included in this second phase.

Moving from January to April, the average maximum temperature in Turin usually increases from 6 to 17°C. The temperature increase has played a fundamental role in the PBR operation and algae growth.

The cumulative growing rate (Table 13) for the longest performed test (test B, from 25/02/2015 to 15/04/2015) is shown. The first growing period was strongly influenced by the temperature and thus by the sun irradiation. From March on, despite higher temperatures, problems related to the algae attachments were the reason for the decrease in the growing rate. A maximum cumulative growing rate of 6 g/m^2/day was reached on the second sampling point.

Table 13. Cumulative growing rate.

Star time		End time		Growing rate [g/m^2/day]
t_0	25/02/2015	t_1	13/03/2015	1,34
t_0	25/02/2015	t_2	19/03/2015	6,13
t_0	25/02/2015	t_3	02/04/2015	3,14
t_0	25/02/2015	t_4	07/04/2015	1,54
t_0	25/02/2015	t_5	13/04/2015	1,66

When algae sampling was performed by cleaning a pipe of the PBR, not only the growing rate was measured but also the elemental analysis was performed in the WWTP laboratories at SMAT.

As can be seen in Figure 77, the total carbon content was always close to 40%. Other elements were nitrogen, hydrogen, and sulfur.

Furthermore, the quota of carbon related to organic C has been calculated and can be seen in Figure 78. The ration C_{org}/C_{tot} is almost kept constant during the tests and the C_{org} percentage is around 34-35%.

The fact that algae prefer to grow attached to the pipes, confirmed by the PBR producer, the lab experiments explained in the previous section, and by literature, has also been confirmed during two sampling points in which the percentage of algae attached to the pipe and suspended in the contained water were measured separately. Results can be seen in Figure 79 and show that 90% of the algae are found to be attached to the pipe.
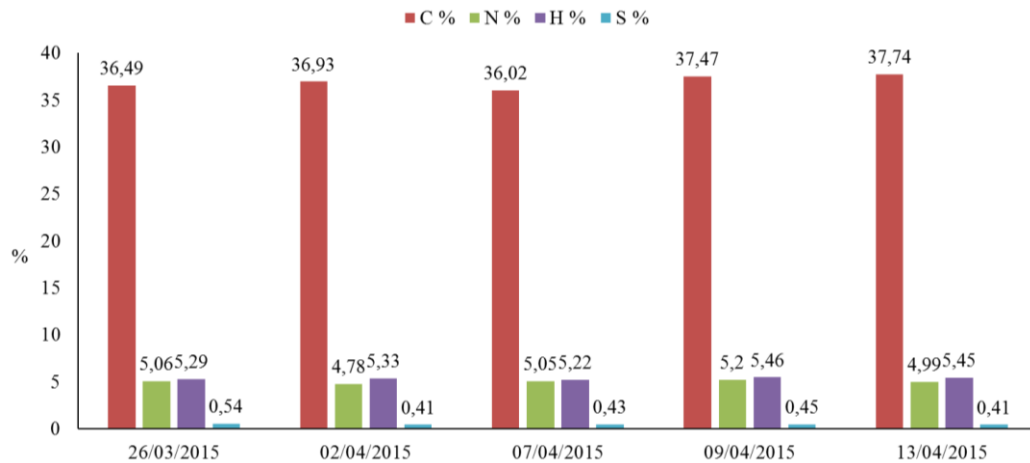
Figure 77. Single element analysis for the algae. (Santarelli et al. 2017)
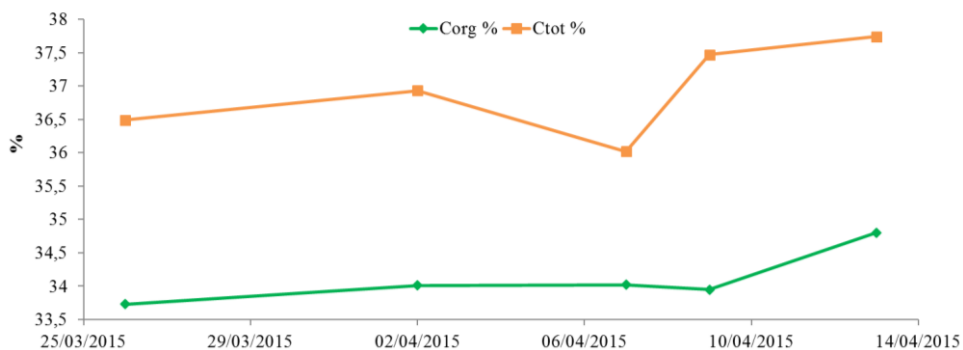
Figure 78. Total and organic carbon ratio. (Santarelli et al. 2017)
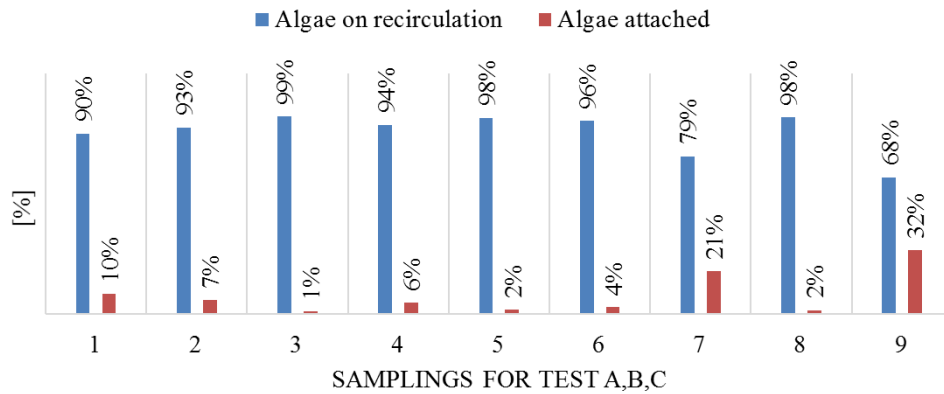
Figure 79. Distribution of detected algae in the PBR. (Santarelli et al. 2017)

Water nutrients removal analysis

An important output of the systems was the removal of nitrated and phosphates contained in the waste water. The PBR control system was continuously measuring the outlet water composition while SMAT laboratories were measuring both inlet and outlet water composition.

During the first month of operation, as discussed before, algae were not growing faster and thus a reduced nutrients removal was observed: the decrease in the N,P content is thus due to the algae production reaction. As can be seen on Figure 80 and Figure 81, the nitrates removal is very limited in this period with outlet contents close to the inlet ones. For the phosphates the reduction is higher but still not constant.
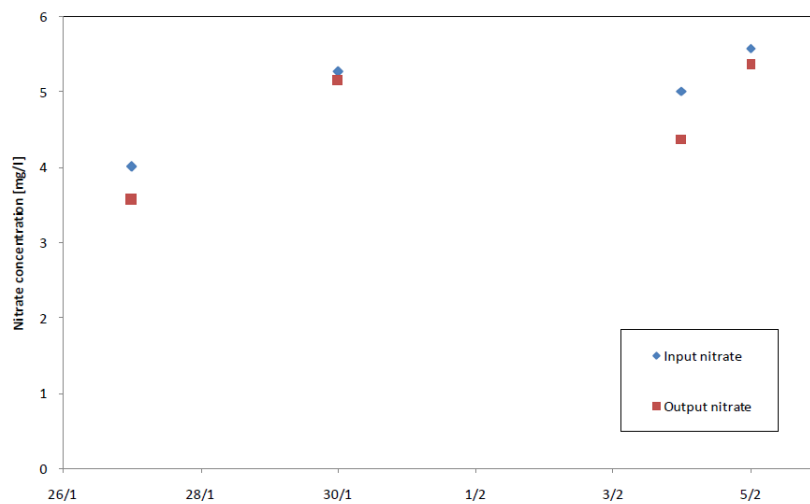
Figure 80. Nitrates analysis for Jan/Feb.

Moving to the central operating period, from end of March to April, the situation is different. Results are shown on Figure 82 and Figure 83. In the first one, the nitrates reduction can be clearly seen with an output trend similar to the input one but with a lower average value. The same can be seen for the phosphates, which are generally already low

in the inlet water. Furthermore, the outlet trend from mid-March on was always below the detection imit.
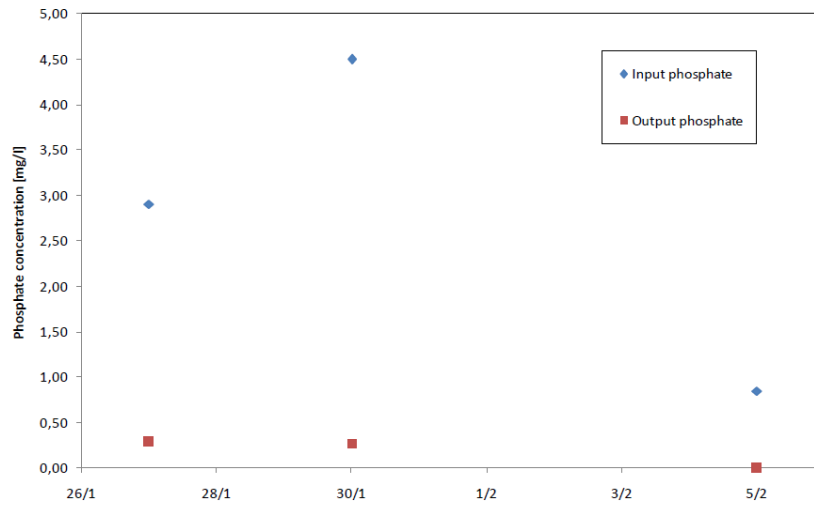
Figure 81. Phosphates analysis for Jan/Feb.
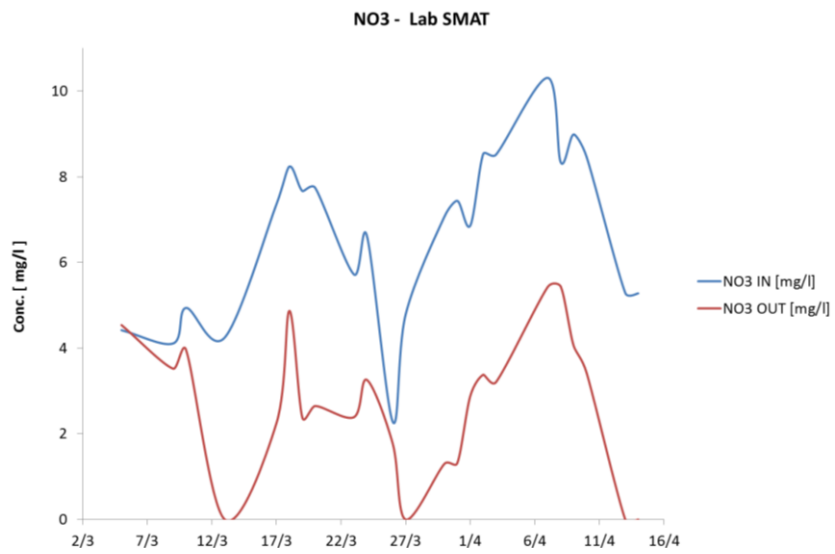
Figure 82. Nitrates analysis for Mar/Apr.
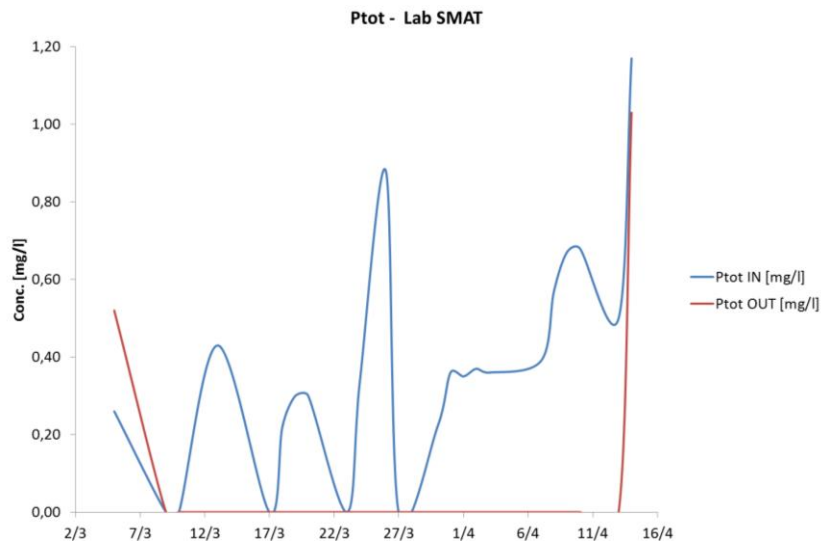
Figure 83. Phosphates analysis for Mar/Apr.

A comparison between the lab values and the online sensors values is shown on Figure 84. The trends are similar even if the lab analyses often go to zero because the instrument detection limit was higher than the one of the analyser installed inside the PBR.
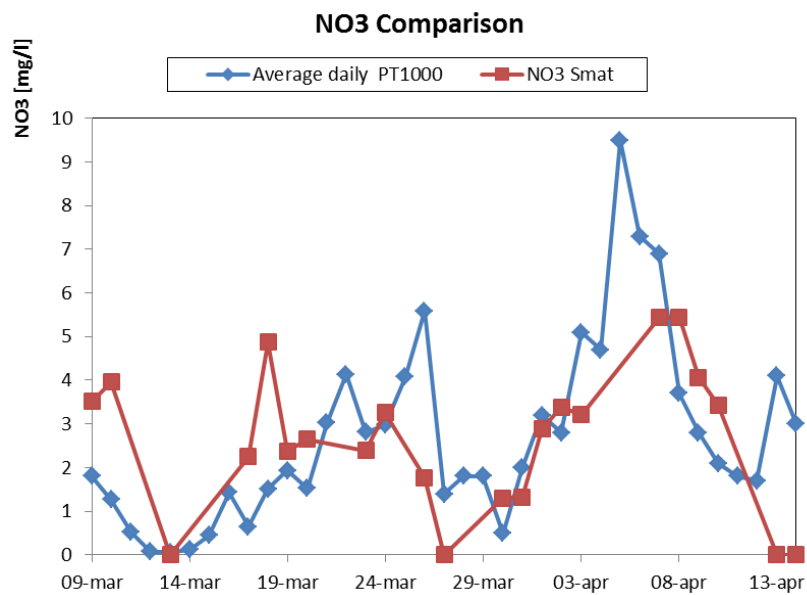
Figure 84. Comparison between SMAT lab data and online sensor data.

Specific test session

Photobioreactor specific tests have been performed related to the direct feeding of biogas and non-combusted exhaust to the system, to check if the feeding with purified CO_2 was indeed a more effective solution.

Results from the biogas feeding test are shown in Figure 85. As can be seen, the injection of biogas in the autochthone algae species Chlorella Vulgaris for Turin cause

growth inhibition. The oxygen curve (oxygen production means that algae are growing), which is normally following the temperature/irradiation trend during the day, presents a decrease when biogas is fed. This standard Chlorella is thus not suitable, in its current operating conditions, for biogas feed.

When biogas feeding was stopped, the PBR was able to recover the inhibition phase, and the trend was again proportional to the irradiation one. When the system growing phase was started again (O_2 proportional to temperature), the non-combusted stream was fed to the PBR.

The choice of analyzing the effect of non-combusted fuel feeding to the PBR was due to the following reasons:

- In different literature works, it is shown how the CO_2 feed to PBR does not need to be 100% pure. A more diluted CO_2 is also suitable for algae growth. The anode exhaust is a diluted CO_2 stream, even if carbon dioxide is diluted with fuels such as hydrogen and carbon monoxide.
- To avoid the oxy-combustion stage would be interesting from and economic point of view, since pure oxygen is required with a consequent energy and economic cost.
- Despite these advantages in feeding the non-combusted stream to the PBR, results in (Figure 85) show again an inhibition of the algae growth. The behavior of the system is the same presented before when biogas was injected.
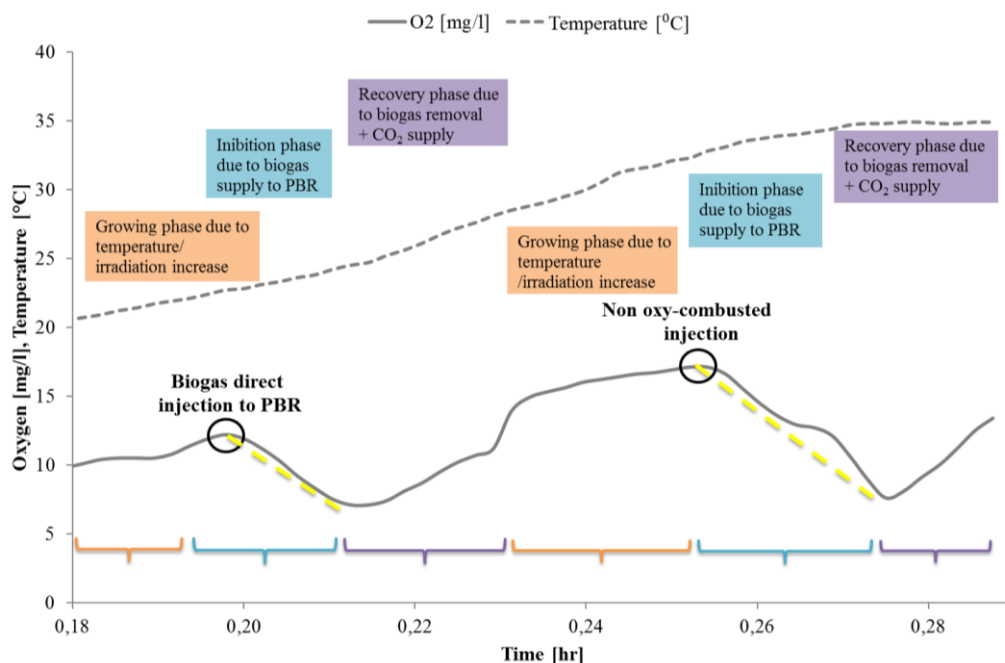
Figure 85. PBR specific tests results.

Furthermore, if the derivative trend is analyzed, the non-combusted stream seems to have a higher slope than the biogas one. The CO_2 content in the anode exhaust, on a dry basis, is 58% on nominal conditions, thus higher than 40% content in pure biogas.

Despite a higher CO_2 stream concentration, the presence of H_2 and CO seems to have a more negative effect on the PBR performance.

3.7.2 Discussion

By considering all the obtained results, it is possible to derive some main conclusions.

The first one is that the oxy-combustion step is not problematic from the technical point of view. The process is very effective in converting the residual H_2, and CO contained in the SOFC anode exhausts into H_2O and CO_2 respectively. Some considerations follow below:

- A way to reduce the amount of residual H_2 and CO in the anode exhaust, could be to operate the SOFC at a higher Fuel Utilization; this can generate a slight reduction of the efficiency of the electrochemical reaction, but this could represent a negligible reduction to accept if the emphasis is given to the effectiveness of carbon recovery from the plant

- the needed reactant is O_2; of course, O_2 would represent a high cost (in terms of energy and economy) if it has to be separated from air (or, even worst, if extracted from cylinder as in our proof-of-concept); a plausible solution could be to use the O_2 recovered from the downstream PBR, coming from the algae photosynthetic reaction; then, the O_2 would be recovered directly from the reduction of the CO_2 into the PBR; in terms of mass balance, the amount of moles of CO_2 inlet into the PBR is by far higher than the amount of moles of H_2 and CO inlet into the oxy-combustor to be oxidized, then the O_2 from PBR is highly in excess compared to the needs of the oxy-combustor; this O_2 would be then available free of charges, and representing another example of strict mass and energy integration inside this poly-generative plant.

The second conclusion, based on the results, is that the H_2O separation step is not problematic from the technical point of view. The process is very effective in separating the H_2O from the CO_2 in the exhaust stream from the oxy-combustion. Some considerations regarding this point are:

- In order to reduce the energy cost related to the compression of the mixture before the membrane separator, a possible solution could be to operate the whole process in pressure; this would generate some higher mechanical requests (and costs) to the structures, but could generate positive effects: (a) the SOFC operating under pressure has a higher conversion efficiency (Singhal & Kendall 2003; Curletti et al. 2015); (b) the oxy-combustion reaction would be more effective; (c) the separation of the H_2O by condensation would be more effective, as a lore amount of H_2O is maintained in equilibrium with the gas when the pressure increases; (d) the separation of the residual H_2O from the CO_2 would not need the necessity of a compressor. Nevertheless, this configuration would have also some drawbacks (due to the more complicated

mechanical behavior): (a) the biogas in origin is usually available at ambient pressure in a gas holder; and so, in absence of a gas already in pressure (standard case), the biogas entering in the plant would have to be compressed (and this would be really a significant energy expenditure); (b) the O_2 sent to the oxy-combustor would have to be compressed as well. Then, as a conclusion, it has to be evaluated if the positive effects (e.g. higher efficiency of the SOFC generator) can compensate the negative effects (e.g. the necessity to compress the biogas).

- The third set of conclusions comes from the PBR, which has revealed as the most problematic component of the chain: the main considerations are:

- the productivity of the PBR in terms of micro-algae is not optimized; the amount of specific productivity is in the order of 6 g/m^2/day in terms of maximum cumulated value and 18.8 g/m^2/day in terms of weekly-average value. From literature, ranges from 20 to 40 g/m^2/day are found for similar PBR (Slade & Bauen 2013), even if peaks up to two orders of magnitude more (more than 3 g/L/day against 0.03 g/L/day in the presented work) have also been reached with PBR in specific operating conditions (C.-Y. Chen et al. 2011). The present test was conducted in an outdoor real environment, with variable nutrients concentrations depending on the inlet waste water, variable irradiation and no initial inoculum for defining a specific algae specie.

- the energy consumptions of the PBR are not negligible: the solutions based on loop recirculation of the water, in order to avoid algae attachment to the pipes and to maximize the effectiveness of the photosynthetic reaction is significant in terms of energy consumption; the amount of energy consumed for gram of micro-algae is around 9 W/m^2, in the current PBR layout, high if compared to the energy contained in the algae. The use of a high flow rate recirculation, operating 24 hours per day, is a key issue to be optimized in future plants (Tredici et al. 2015; Norsker et al. 2012; Sevigné Itoiz et al. 2012; Slade & Bauen 2013), where a less energy intensive way to avoid algae attachments to pipes should be found. Furthermore, an increase in the productivity value (W/m^2) is the second way to reduce the unbalance between energy production and consumption.

- one of the reasons of the low productivity is due to the fact that the micro-algae tend to adhere to the surface of the tubes, forming a screen to the transmission of the solar irradiance and so reducing the specific productivity of the PBR; this adhesion can be reduced in different ways: (a) higher turbulent flow inside the tubes, which means a further increase of the energy consumption for the water recirculation; (b) deposition of coating materials in the inner surface of the tubes to reduce the adhesion; (c) adoption of a screen outside the PBR, but in that way reducing also the specific productivity of the micro-algae. This aspect has to be further analyzed and optimized.

- as it is well know from literature, and from the results obtained in this project, the concentration of CO_2 in the water needs to be controlled in order to avoid a too high reduction of the local pH, because an acidic water is detrimental for the grow up of most of the typologies of algae; in this sense: (a) the research has to be improved in the selection of algae cultures able to grow up fast also in acid water; (b) from the engineering point of view, the solution (also applied in our proof-of-concept) could be to control the mass flow of CO_2 injected inside the water flow, in order to control the pH; so, there is the necessity of accumulating the CO_2 mass flow coming from the upstream SOFC plant in a buffer volume, in order to control its injection in the PBR

- during the dark hours of the day, the micro-algae are not produced; instead they release CO_2; thus, it comes evident the necessity to accumulate the CO_2 coming from the SOFC plant during the dark periods in a storage buffer; this is due to the fact that, of course, the upstream energy plant based on SOFC operates in a continuous way 24/7. This is again related to the need to control the flow of CO_2 before injecting it into the PBR, and so the need to adopt a buffer volume (with related costs of installation and management); also, this depends on the location of these typologies of plant, having on effect on the distribution of light and dark hours during the day and during the year.

Coming to the final target of our discussion, which is related to the evaluation of this innovative opportunity to completely recover CO_2 from an energy process, in a paradigm of complete CCR, the main results and discussions that come from our experience in the SOFCOM proof-of-concept are the following.

Effectiveness of the micro-algae solution

The main results in terms of effectiveness of carbon removal in PBR in our pilot experience is expressed by the quantification of the fact that micro-algae are really a fast growing biomass. In fact, standard biomasses (wood, maize, energy crops, corn) show always growing rates lower than 1 W/m^2; only sugarcanes and tropical plantations are able to reach values close to 2 W/m^2 (MacKay 2009); micro-algae produced during the experimental SOFCOM activities show a cumulative growing rate of 1.36 W/m^2 with a weekly peak of 4.18 W/m^2. These results can be further optimized with the solutions already highlighted here.

Carbon impact of the tested solution

- considering the pathway biogas-SOFC (without CO_2 recovery in PBR), the CO_2 emissions from the SOFC biogas fed system (with optimized sludge pre-thickening) are 0.198 kg$CO_{2,eq}$/kWh$_{el}$ against 0.429 kg$CO_{2,eq}$/kWh$_{el}$ in case of NG feeding;

- taking into account the energy (and environmentally) intensive and not optimized PBR system, the CO_2 emissions from the SOFCOM system are 0

kgCO$_2$/kWh$_{el}$, but only if considering the intermediate buffer able to store the CO$_2$ during the period of null irradiance

- the environmental performance of the PBR has been studied only in reference to the operation mode (the manufacturing and assembly phase has been considered negligible with respect to the operation). At PBR level it is calculated that 60% of the total emissions of CO$_2$ from SOFC are fixed in biomass (because of a limited seasonal buffer). The rest is released into atmosphere.

For the production of 1 kg of biomass this translates in a consumption of 1.84 kg of biogenic CO$_2$ and emissions for 1.23 kg biogenic CO$_2$. To these emissions, using Climate Change impact category for PBR operation, it must be added another 35.9 kg of CO$_2$eq. Overall GHG emissions are thus 20 times higher than the CO$_2$ consumption (presented results have been determined from the Life Cycle Assessment (LCA) analysis of the SOFCOM plant, presented in the related project Deliverable 4.5 (Santarelli et al. 2014)).

Hence, the chosen PBR technology, according to the available information and on the choices made for its operating mode, does not provide neither an energetic nor CO$_2$ sequestration-effective improvement compared to the original energy path (biogas-fed SOFC). However, the conclusions just presented does not imply a negative judgment of the concept of achieving positive effects (energy production, carbon sequestration) in contexts similar to the one presented; more research is required to identify and understand all the parameters involved in the operation of such complex system, and new designs would propose more interesting performances (e.g., hybrid photobioreactors) (Singh & Sharma 2012).

Moreover, in the presented results from SOFCOM plant LCA analysis, the benefit of water purification (nitrates and phosphates removal) is not considered when analyzing the Climate Change impact category. Data on nitrogen and phosphorus balances (available through other LCA impact categories) would underline this positive effect of the PBR system.

Chapter 4

The   SOFCOM   proof-of-concept: Modeling of biogas-fed SOFC systems

The scope of the presented chapter is to "*improve understanding of the energy, environmental, and economic performance of industrial facilities such as sewage treatment plant coupled with an advanced technology producing electricity – the SOFC*", as described in the SOFCOM project proposal. This task was developed in collaboration with the EPFL (École Polytechnique fédérale de Lausanne, Switzerland).

Because of the strong interest of EU countries in biogas plants, not only fed by sewage sludge (as discussed in the biogas potential chapter), the work has been expanded to other biogas substrates such as agricultural waste, energy crops, and landfill gas. A detailed roadmap of possible case studies has been first developed. Several system configurations have been thus designed, simulated and analyzed. Carbon Capture and Sequestration (CCS) or Use (CCU) have been considered as the main innovative process in a carbon constrained future, together with pressurized SOFC for a higher efficiency power generation. The general plant layout is the one represented in Figure 86.

The considered substrate is first converted to biogas in an <u>anaerobic digester</u>: the digestion has not been considered in the models since a biological model of anaerobic digestion was not the main focus of the presented work. Anyway, the heat requirement of the process has been taken into account when analyzing the entire plant.

The biogas, mainly composed of methane and carbon dioxide, is first sent to a <u>cleaning section</u> to remove the contaminants (sulfur, halogens, and siloxanes are highly harmful to

SOFCs) by adsorption material such as activated carbon and Zinc Oxide (ZnO). If a strong cleaning is required, a high temperature polisher could also be included.

The clean biogas in then converted into a hydrogen-rich stream in a <u>processing section</u>, where reforming reactions of methane takes place. The reforming agent can be water, air or a mixture of the two. The reformate is then fed to the <u>SOFC power generator</u>, where electrochemical reactions take place: the stack is fed by the processed fuel and by air, the oxygen carrier for the reactions and the cooling agent of the heat generated within the cells.
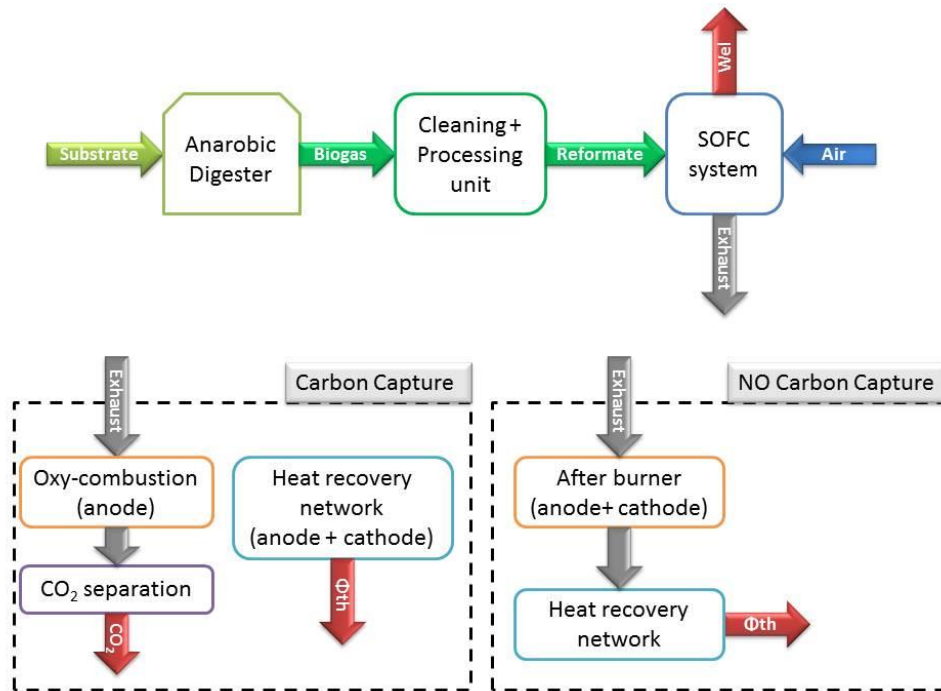
Figure 86. General plant layout.

If carbon capture is avoided, exhaust gases from anode and cathode can be treated together in an <u>afterburner</u> in order to recover the chemical energy still contained in the stream (fuel utilization in the SOFC is always lower than 100%). Chemical energy is thus converted into thermal energy which can be used in the heat-exchanger network to pre-heat the fresh inlet streams and finally for external thermal users.

The choice of carbon capture, on the other side, leads to a more complex system layout: cathode exhaust is used for thermal recovery and the vented while anode exhaust is burned in an <u>oxy-combustor</u> with a pure oxygen stream (usually produced in loco) to yield a CO_2-H_2O stream and avoiding the nitrogen. A condenser is then able to remove a large amount of water, and an adsorption membrane brings the streams to a CO_2 grid quality (water quantity lower than 500 ppm). CO_2 can then be used in loco, shipped to an external user or geologically sequestrated.

A detailed methodology has been developed concerning both the energy and the economical part:

- SOFC electrochemical model
- Energy performance
- Total Plant Cost (TPC)
- Cash flow analysis and Net Present Value (NPV) at the end of life

Figure 87 represents the main steps of the developed methodology.

The work includes a first introduction to the SOFC and biogas world, a presentation of the roadmap and the related case studies, a detailed plant description followed by the methodology which has been applied to all the presented configurations. Finally, results are discussed.
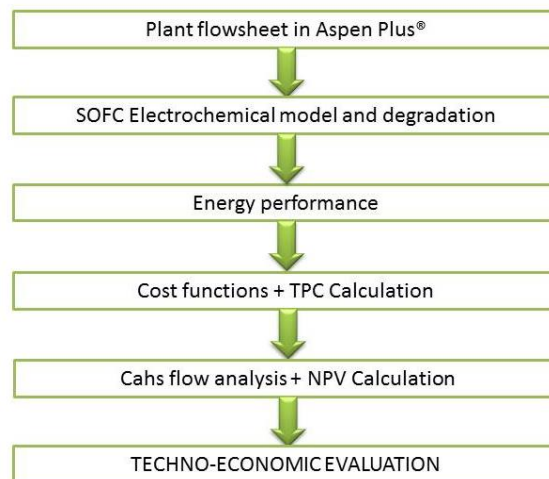
Figure 87. Techno-economic methodology.

The work has been developed for three main case study groups:

- Small size plants: 1-100 kWe. Biogas is produced from agricultural and agroindustrial substrates.
- Medium size plants: 100-1000 kWe. Medium size Waste Water Treatment Plants (WWTP) and anaerobic digestion of Organic Fraction of Municipal Solid Waste (OFMSW).
- Large size plants: > 1 MWe. Large municipal WWTP, landfill gas, and a mixture of different substrates collected in a unique large size power plant.

The analyses brought to interesting results in the coupling between SOFC devices and biogas plants, with a high affinity between the two processes. Carbon capture, despite being

a powerful environmental method for reducing emissions, it is unfortunately not linked with a direct economic convenience since the downstream separation process is expensive and technically not 100% developed.

4.1 Roadmap definition

The first chapter is intended to set the basis of the analysis, with the choice of the case studies, the plant sizes and the motivation for the chosen classification.

SOFC devices lead to a high number of advantages respect to their traditional competitor, Internal Combustion Engines (ICEs), especially when considering biogas plants. Table 14 shows the main advantages/disadvantages of fuel cell systems respect to traditional ICEs. The two most important advantages are:

- SOFC leads to a high reduction in the emissions to the atmosphere, nowadays a very open problem with ICEs. The not-perfect tightness of the cylinder, in fact, has as a consequence a quite high methane compounds emissions, together with NOx and SOx (Table 15).
- The SOFC efficiency is at least 5% points higher that ICEs for large size (1 MWe and above), while is more than 10% points higher when considering lower size (Figure 88).

Looking at the disadvantages, the higher cost of technology, not yet at a commercial level, leads to a non-competitive economic sustainability, especially for large sizes.

Table 14. SOFC vs. ICE.

	SOFC	**ICE**
Reduction in emissions	VVV	V
Efficiency	VVV	VV
High temperature heat recovery	VVV	VV
Flexibility/ Modulation	VV	V
Combined feed biogas + GN	VVV	VVV
Operating cost	V	VV
Investment cost	VVV	V
Tolerance to biogas contaminants	V	VVV

Table 15. Emission levels comparison. Column 1 → Commercial biogas fed ICE, column 2 → Accepted levels from Italian law (Anon 2006), column 3 → Declared emission from an SOFC producer (Bloomenergy n.d.).

Compound	Average emission level from ICE (SMAT Castiglione WWTP site)	Max. acceptable level from D. Lgs. 152/2006	Level from Bloomenegy SOFC stack
Total dusts	5,31 mg/m3	10 mg/Nm3	
Total NOx	469,00 mg/m3	< 450 mg/Nm3	< 1,23 mg/Nm3
Total SOx	50,40 mg/m3	< 50 mg/Nm3	Negligible
Carbon monoxide	201,00 mg/m3	< 500 mg/Nm3	< 12,31 mg/Nm3
Sulfuric acid	< 0,2 mg/m3	< 2 mg/Nm3	-
V.O.C	825,00 mg/m3	< 150 mg/Nm3	< 2,46 mg/Nm3
V.O.C. not methane	212,67 mg/m3	< 150 mg/Nm3	-
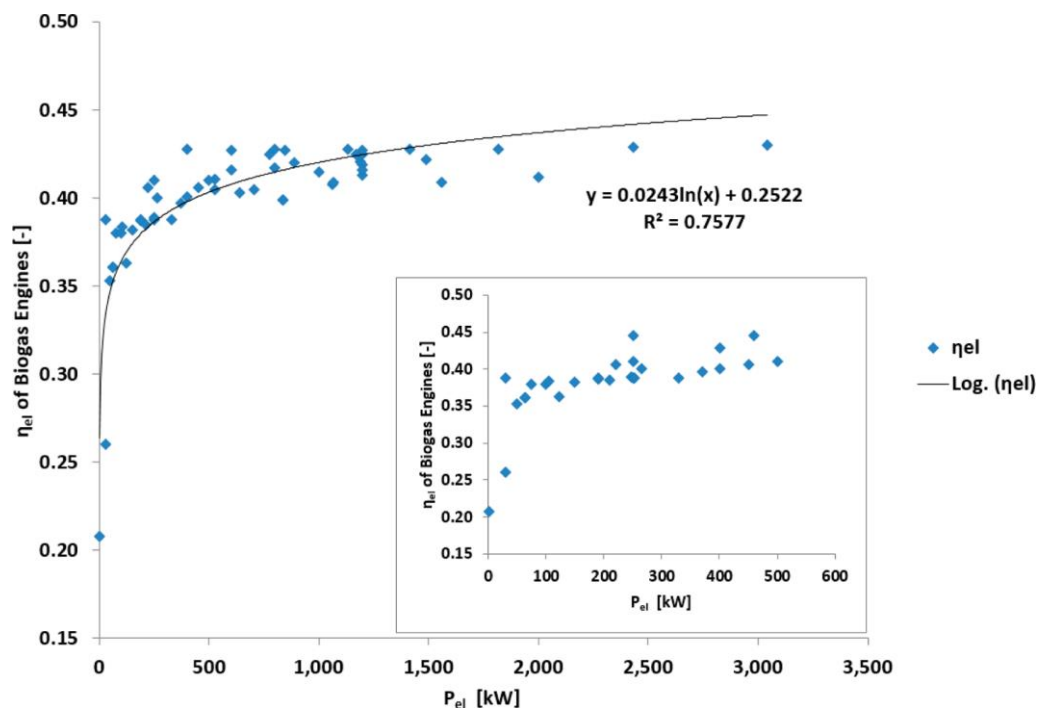
Figure 88. Trend of ICE electrical efficiency depending on the size (author elaboration of reference ICE data from (2G n.d.; General Electric n.d.; SEVA Energy AG n.d.), now available on (Tjaden et al. 2014)).

4.1.1 Biogas substrates

Biogas is a widely available resource which offers a large potential for providing electricity, as shown in Chapter 2.

In the European Union, the biogas production was estimated about 5901 Ktoe (Kiloton of oil equivalent) for 2007, of which 50% coming from urban waste and approximately 8800 Ktoe in 2009 (Eta Florence & Environment Park n.d.). In Italy, 542 biogas plants (61 under construction) and 672 (with 76 under construction) was identified respectively in 2009 and 2010 by CRPA (Piccinini 2010), of which:

- 235 plants in 2009 and 273 in 2010 producing biogas from livestock effluent in co-digestion with energy crops or agro-industrial waste. In Figure 89 the percentage of the number of biogas plants, classified on the basis of different typology of feedstock, has been reported;
- 121 plants producing biogas from anaerobic digestion plant for the stabilization of municipal and industrial sewage sludge;
- 14 plants producing biogas from organic fraction of municipal solid wastes in co-digestion with sewage sludge, partly resulting from the selected collection of urban waste and partly resulting from mechanical sorting;
- 31 plants in 2009 and 32 in 2010 producing biogas from agro-industrial wastewater;
- 141 plants in 2009 and 232 in 2010 from the recovery of biogas from MSW landfills.
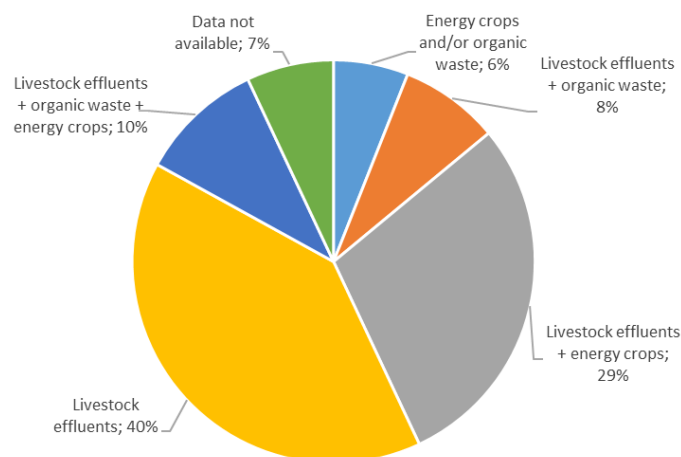
Figure 89. Percentage of number of biogas plants for the different typology of feedstock in 2009.

In 2009, a number of 723 biomass plants was registered for a total of 1491 MWe, including biogas plants, solid biomass plants, and liquid biofuels plants. Figure 90 reports the percentage for each kind of biomass plants according to respectively electrical installed

power and number of specific plants. The gap between the number of plants and the electric power reveals that in Italy a high number of biogas plants is present even if they are mostly small and medium-sized farm-scale. In particular, only the 9% of the total number of the biogas plants from livestock effluents censored in 2007 have installed electrical power of more than 1 MWe.
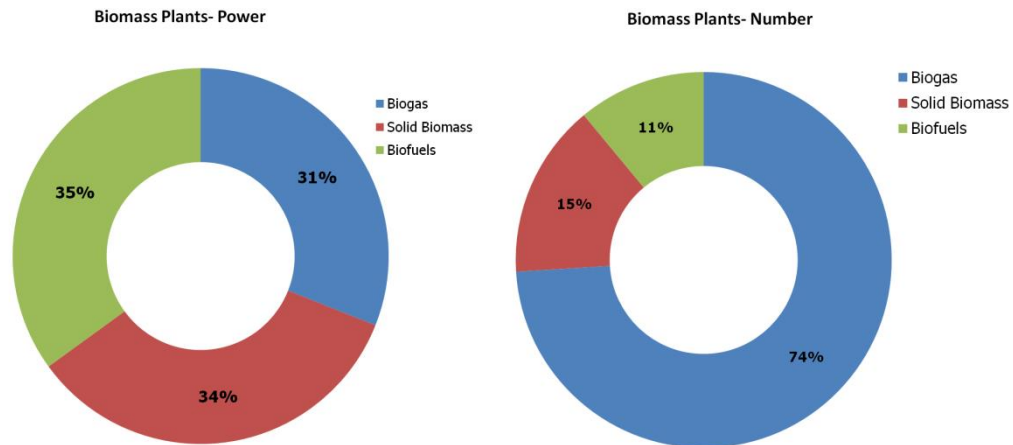
Figure 90.Percentage of number and power of biomass plants in Europe.

The plant size obviously depends on the amount of available biomass (or bio-waste). Biogas can derive from different sources (Seadi et al. 2008): Agricultural biogas plants, Waste Water Treatment plants (WWT), Municipal Solid Waste treatment plants (MSW), Industrial biogas plants, Landfill gas recovery plants.
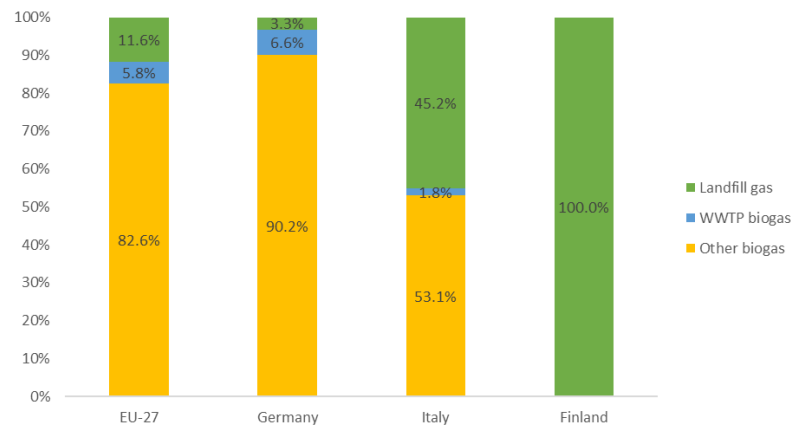
Figure 91. Breakdown of biogas source distribution in electricity mix in 2011.

Biogas data presented by Eurostat gives a distinction of different biogas sources: landfill gas, sewage sludge gas, and other biogas, which presumably refers to biogas produced by anaerobic digestion of biological matter (Eurostat, 2012a). Figure 92 shows that "other biogas" is the main sources of electricity supply stemming from biogas in Germany and Italy. Especially in Germany, the preferred substrates for biogas production

are energy crops and agricultural substances. In Finland, only landfill gas is used to provide electricity which means that either biogas resources produced by other substrates are directly vented to the atmosphere and thus remain untapped or are converted into thermal energy only.

In literature, biogas composition generally constitutes of 60%$_{mol}$ CH_4 and 40 %$_{mol}$ CO_2 (Van Herle et al. 2003). However, such data is not precise enough as different substrates produce biogas with different gas compositions due to their chemical build-up. Such variations are enhanced when different mixtures of substrates are digested in a fermenter simultaneously which in turn makes specific sizing of power plant equipment necessary.

To carry out a first quantitative comparison of CH_4 content in biogas, the "Online European Feedstock Atlas basic version" is used. The atlas lists laboratory-scale experiment results on CH_4 fractions in biogas produced from a wide range of substrates (Jungbluth, T. and De Baey-Ernsten 2012). Figure 92 shows a summarized collection of CH_4 data for the different organic matter. Except for residues of waste water treatment plants (marked as a red bar), all of the plotted substrates fall under the category of the substrate [S]. The graph illustrates that average CH_4 fraction throughout all substrates lies between 0.5 and 0.6 with only a few exceptions surpassing or undercutting this bandwidth. Yet, these CH_4 fractions have been determined in laboratory tests which mean, that they do not reflect real-time data of operating digester plants.
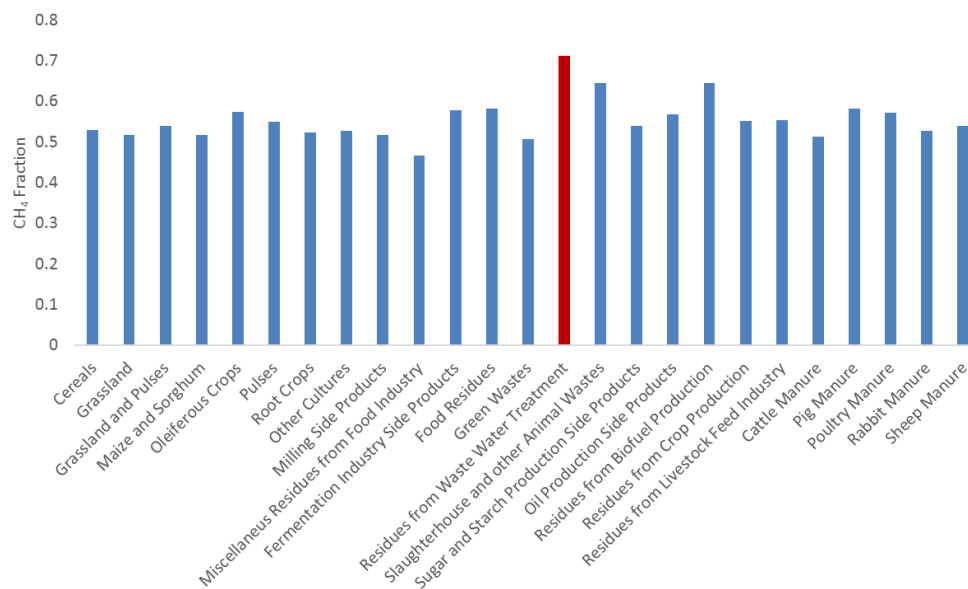
Figure 92. Average CH_4 fraction in biogas of different substrates (Jungbluth, T. and De Baey-Ernsten 2012).

For this reason, different sources of literature are analyzed, and a database of biogas compositions stemming from existing digesters is established in order to carry out a comparative interpretation of biogas data. Figure 92 represents CH_4 contents compiled in

that database for biogas plants with an installed electric power below 200 kW$_{el}$, sorted according to substrate/s.

The data depicted in Figure 93 is comparable with the laboratory-scale test results shown in Figure 92: the average CH$_4$ content lies between 50 %$_{mol}$ and 60 %$_{mol}$ with only a few exceptions and is independent of used substrate. Moreover, Figure 93 clearly shows large variations of methane content even if the biogas is produced from the same biological resources: methane yield of digesting "manure and food waste" ranges from 58.1 %$_{mol}$ to 67.5 %$_{mol}$. It can be concluded, that operating and ambient conditions have a large influence on biogas production and chemical build-up.
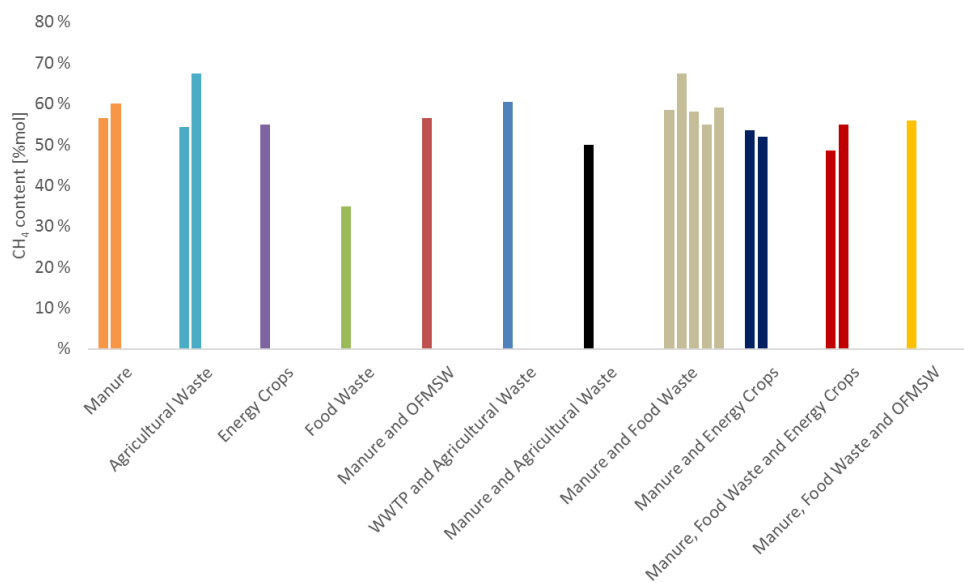
Figure 93. Database on the CH$_4$ content of different biogas plants.

Figure 94 shows such variations of landfill gas composition over an approximately two year period. In this case, CH$_4$ content varied around 10 %$_{mol}$ throughout the measurement period (Jungbluth, T. and De Baey-Ernsten 2012). Such fluctuations are also typical for farm-scale digesters: in an investigation carried out at ten biogas plants in Germany, biogas composition was measured three times over a period of approximately one year, which showed that, measured CH$_4$ content varied in average around 10 %$_{mol}$ (Rasi et al. 2011).

However, not only the composition of biogas is subject to seasonal variations but also the volume flow rate of produced biogas. Figure 95 pictures methane flow rate of two anaerobic digesters located in northern rural India. It can be seen that during cold winter months, the productivity of anaerobic digestion decreases significantly (Bayerisches Institut für Angewandte 2003). This is due to large heat losses during cold seasons where operating temperature of anaerobic digestion cannot be maintained which leads to a decrease and at the worst cease of biogas production.

Distinguishing the challenges going along with varying biogas composition and varying biogas flow rate for SOFC plant operation, it can be concluded, that smaller CH_4 and thus, larger CO_2 content in biogas is a smaller problem compared to biogas flow rate which falls under a certain threshold.

On the other side, when biogas flow rate falls under a certain limit, the amount of reactants in the SOFC decrease and become insufficient to maintain electrochemical reactions and temperature inside the stack.
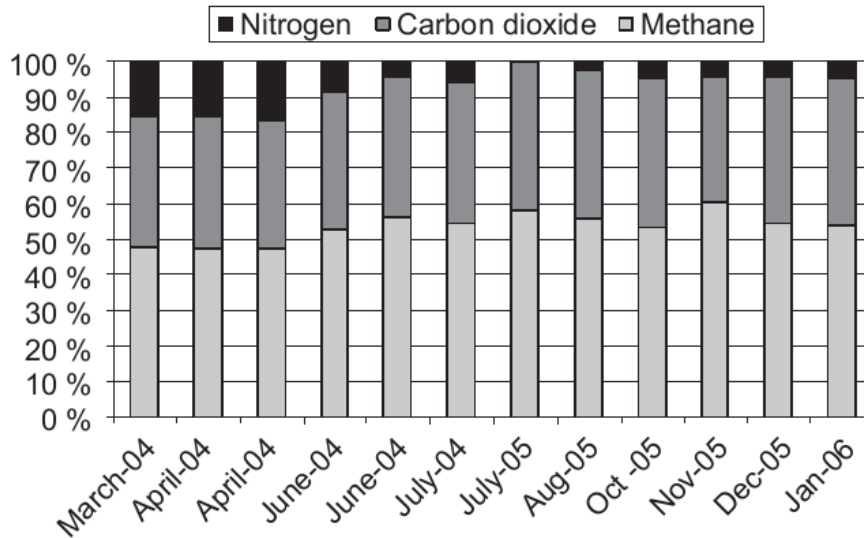
Figure 94. Variation of landfill gas composition throughout different seasons (Rasi et al. 2011).
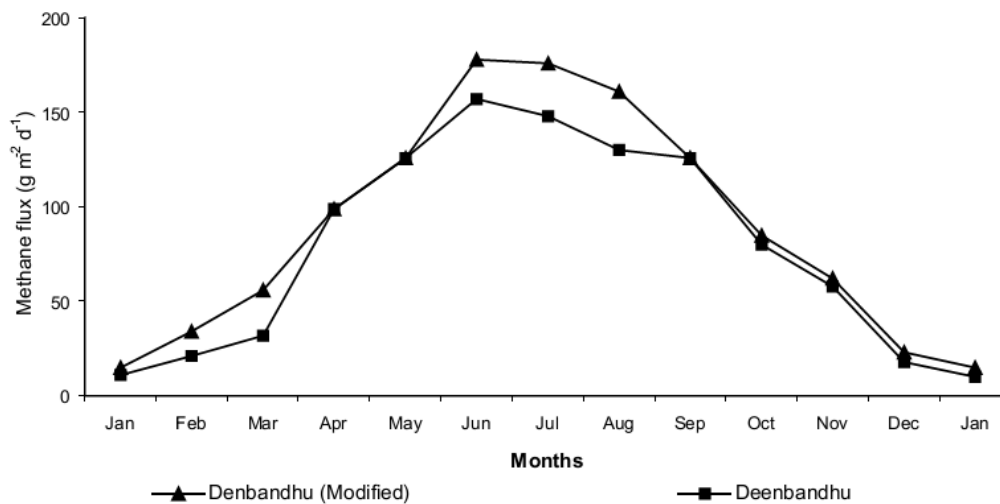
Figure 95. Seasonal variation of CH_4 flow rate of an anaerobic digester (Bayerisches Institut für Angewandte 2003).

Not only seasonal variations in flow rate of produced biogas are observed but also hourly fluctuations occur. Such fluctuations would directly lead to oscillations in power

output of the fuel cell stack. In practice, two strategies are applied to overcome this difficulty (Khoiyangbam et al. 2004):

- Supplement deficit of biogas and methane content by addition of natural gas from gas grid;
- Installation of a short term biogas storage system;

As an intermediate summary, it can be stated, that the chemical build-up of biogas cannot be specified with great accuracy as ambient as well as digester operating conditions has a large influence on anaerobic digestion processes. Looking at the compiled database on CH_4 content, biogas methane content lies between 50 %$_{mol}$ and 60 %$_{mol}$ while large deviations are observed even when using the same substrate.

4.1.2 Plant size

The current status of biogas production in Italy and Europe have been analyzed in order to establish a classification according to the plant size in three main categories. Taking into account all the presented possible choices for the digester feeding and their related electrical power output, the tree sizes which will be analyzed are shown in the table below.

Depending on the availability of substrates for a general plant and on the related size of digester which can be installed, in the framework of the SOFCOM research project, three main groups have been defined related to size and substrate.

Table 16. Plant size groups.

Plant Size		Installed Power	Biogas Substrate
S	Small Size	10 - 100 kWel	Livestock effluents Energy crops Agricultural waste Organic waste
M	Medium Size	< 1 MWel	Livestock effluents + energy crops + agricultural waste Agro-industrial waste Small WWTU
L	Large Size	1 - 10 MWel	Large scale WWTP Landfills

4.1.3 Final Roadmap

By taking into account all the different plant sizes, power generation sources and downstream treatments, the following case studies will be separately modeled on

AspenPlus® , and the results will be finally compared together to identify the more suitable solutions for each plant size.

The roadmap has been developed at the beginning of the project, together with partners of the WP5 (techno-economic analysis of <u>syngas</u> fed SOFC plants).

Furthermore, during the work development, some useful results have been pointed out and used to re-define the roadmap in order to focus the analysis on the most promising solution.
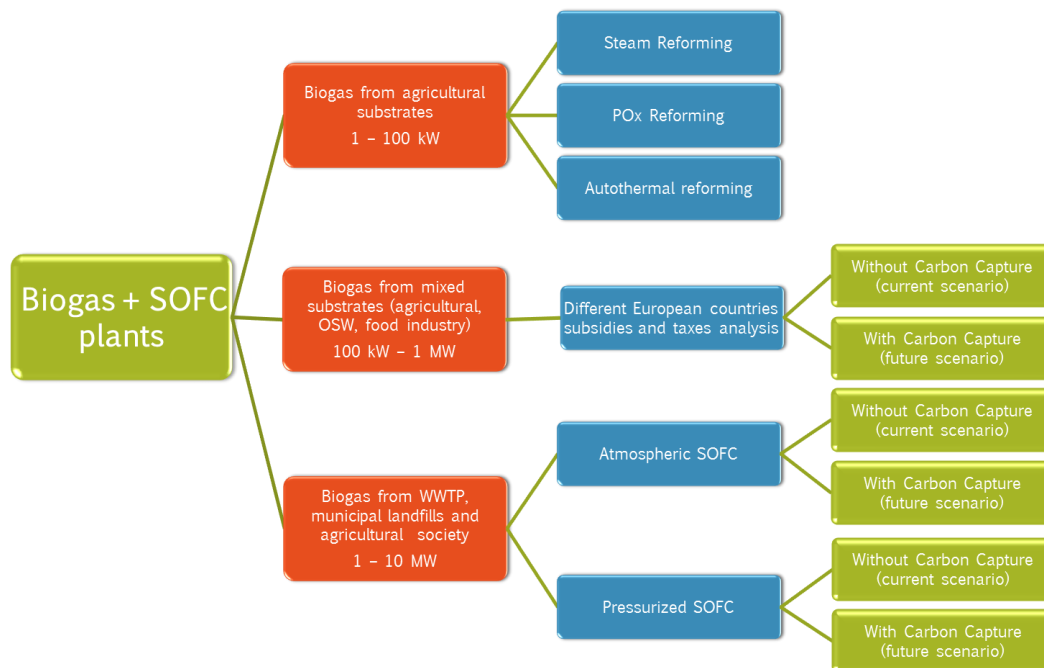
Figure 96. Roadmap for techno-economic analysis.

4.2 Methodology

The second section of the modeling chapter is intended to present the rigorous methodology which has been developed as the first step and followed through all the different analyses.

Concerning the technical part, the main work has been related to the electrochemical model development, starting from literature models and updating the values with more recent experimental results. Furthermore, the processing section has been deeply analyzed taking into account different possible solutions.

After a detailed modeling description, the analysis moves to the economic evaluation of the investment, achieving the most interesting key parameters which can be useful for evaluating the plant.

4.2.1 Scenarios

The general plant layout is changing in relation to the different analyzed layout. Table 17 shows the 7 developed models, on which sub-analysis have been performed:

- For small size plants, the only analyzed configuration is the one without carbon capture and without pressurization, because of the "almost-residential" type of plant. When designing a small plant, a technical complication such as CCS or high-cost new technologies such as pressurized SOFCs should be avoided in order to have a more desirable plant for the private user.
- For the medium size plants, carbon sequestration has been modeled as an alternative to the traditional vented plant. In the case of a future emissions restriction law from the governments, 100 kW – 1 MW plants should be ready for a carbon capture downstream process installation. Pressurization has been not considered since the technological and commercial state of these devices is not at a mature level yet, and thus the price is not sustainable for a medium plant user.
- For the large size plants, considered as a society of users, electricity producers or utilities, all the possible configurations have been analyzed. When installing multi-MW plants, in fact, it is more reasonable to look at the most promising solutions in terms of emissions and efficiency.

Table 17. AspenPlus® developed case studies.

Case ID	Name	Size	Atm./Pres.	CCS	Electrical Generator
1.	S-A-SOFC	Small	Atmospheric	-	SOFC
2.	M-A-SOFC	Medium	Atmospheric	-	SOFC
3.	M-A-SOFC-CCS	Medium	Atmospheric	CCS	SOFC
4.	L-A-SOFC	Large	Atmospheric	-	SOFC
5.	L-A-SOFC-CCS	Large	Atmospheric	CCS	SOFC
6.	L-P-SOFC	Large	Pressurized	-	SOFC-GT
7.	L-P-SOFC-CCS	Large	Pressurized	CCS	SOFC-GT

On Figure 97 and Figure 98 a general plant layout can be found for the vented or CCS solution. The system is composed by the following main macro-units:

→ **Cleaning system**: the scope is the removal of the contaminants contained in the biogas (sulfur compounds, siloxanes, halogens) which can be harmful to the processing and SOFC unit downstream.

→ **Processing unit**: the processing unit is composed by the fuel pre-heater through exhausts and the reforming unit. Here, the conversion of methane into hydrogen and carbon monoxide is performed.

→ **SOFC stack**: the stack is the plant prime electricity generator and is fed by reformate biogas and pre-heated air from external. It is able to generate high-efficiency electrical power and thermal power due to the internal electrochemical reactions.

→ **Downstream process**: the choice of the downstream units depends on the eventual choice of carbon sequestration:

o **No CCS**: the exhaust from the stack are burned in a simple afterburner to recover the chemical energy contained in the anode stream and convert into thermal energy. They are then sent to pre-heat the fresh inlet streams and the to a CHP heat-exchanger.

o **CCS**: to yield a simpler carbon capture anode and cathode exhaust are treated separately in order to avoid the nitrogen contained in the air stream. Cathode exhaust is simply used for preheating the fresh inlet air while anode exhaust is burning with pure oxygen in a special oxy-combustor. The CO2-H2O outlet stream is then sent to a condenser and a membrane stage to remove the water and obtain a pure carbon dioxide stream which can be geologically sequestrated or used.

→ **Pressurization**: in case the system has a pressurized SOFC stack, the inlet blowers are substituted by compressors, and a downstream turbine can be inserted to recover the mechanic power of the exhaust.
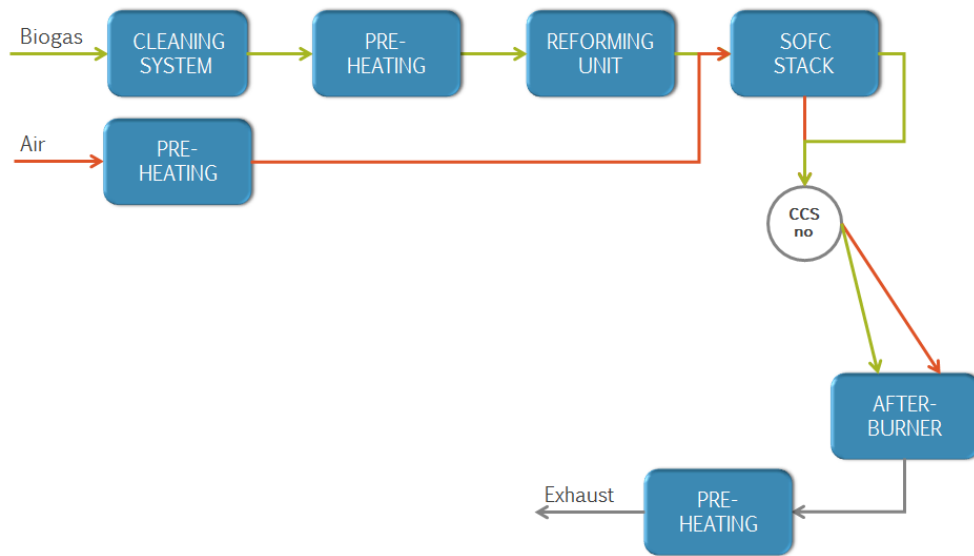
Figure 97. General plant layout without CCS
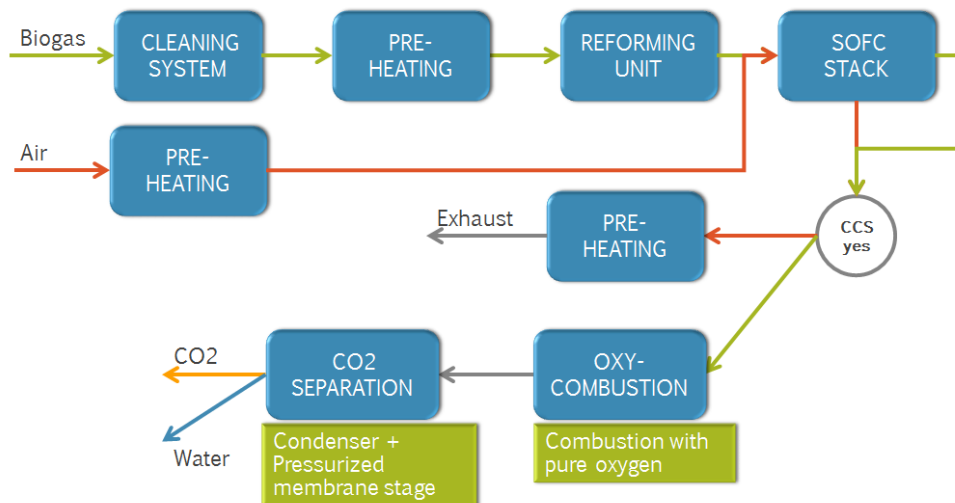
Figure 98. General plant layout with CCS.

The detailed modeling of each plant section is available in "Appendix 3 – Plant modeling", with details on the assumptions and modeling approach for each component of the different analysed layouts.

4.2.2 Plants layout

Figures show the layout of the four analyzed configurations:

ATMOSPHERIC plant WITHOUT carbon capture: this is the simplest possible layout, working at atmospheric pressure and with no recovery of the CO_2. This layout has been analyzed for small, medium and large size plants (Figure 99). Blowers are included at

the beginning of each line just to cover the pressure drops (localized and distributed) until the exhaust reach the chimney. The pressure drops on the components have been taken from real data for commercial components and adjusted to the size of the plant that was under analysis (see Table 18).

Furthermore, the two electrodes of the SOFC should be maintained, as much as possible, at equal pressures because large differences between them may influence the electrochemical activity or even lead to the destruction of electrolyte and of the whole cell. For a correct and an appropriate working, it is thus necessary the presence of a control system which regulates the inlet pressures, so that inside the cell the drop does not exceed the limit value of 500 mbar (Willich et al. n.d.). In this plant the blowers are sized so that:

- The pressure on anode and cathode line never goes below the atmospheric one (the stream will stop flowing)
- The inlet pressure at anode and cathode inlet should be almost the same.

As can be seen from the layout, different reforming agents can be chosen in order to analysis endothermic, and exothermic reforming reactions (air, steam or both) and a by-pass of the reformer can be performed in order to simulate a chosen ratio of internal reforming.

Exhaust are then used for the anode and cathode preheating and then for cogeneration purposes.

ATMOSPHERIC plant WITH carbon capture: this is the second layout analyzed, where carbon sequestration is performed (Figure 100). This layout will be analyzed only for medium and large size plan since a complex system such as the CO_2 removal is not economically feasible for small size plants. The system is the same presented above for what concerning the lines upstream the SOFC, while the treatment of the exhaust downstream is different. The pressure issue is here still more important because the two bottom lines are not burned together (equalization of the upstream pressures) but kept separated; this will require a high precision of the control system device.

PRESSURIZED plant WITHOUT carbon capture: the pressurized layout, even if able to achieve highest efficiencies, is still a non-commercial product (such as the carbon capture system). Furthermore, because of the pressure is very difficult to have the system installed in small and medium size plants. For this reason, the pressurized systems have been analyzed only for the large size plants (1 MW or more). Pressurization is achieved replacing the blowers with a compressor which are able to pressurize the entire plant at a certain value, defined by the SOFC working mode (Figure 101). As explained above, beside compressors, the main difference from the atmospheric plant is the presence of a micro gas turbine, connected in a turbo-compressor group with the air compressor. The turbine is thus

able to recover mechanical power from the exhaust thus increasing the overall electrical efficiency.

PRESSURIZED plant WITH carbon capture (Figure 102): this is the most complex possible layout that will be analyzed, only for large size plants. As already discussed, the pressurization implies two compressors and a turbine, and the carbon capture the downstream CO_2 separation process.

Table 18 summarizes the components pressure drop assumed values.

Table 18. Plant components pressure drops.

Component	Value	Unit
Cleaning Unit	60	mbar
Fuel pre-heater	15	mbar
Reformer	10	mbar
SOFC (anode, cathode)	15	mbar
After-burner	15	mbar
CCS Condenser	15	mbar
CCS Cooler	15	mbar
CHP heat-exchanger	10	mbar
CO_2 pipeline pressure	130 – 150	bar

Figure 99. Atmospheric plant without CCS.
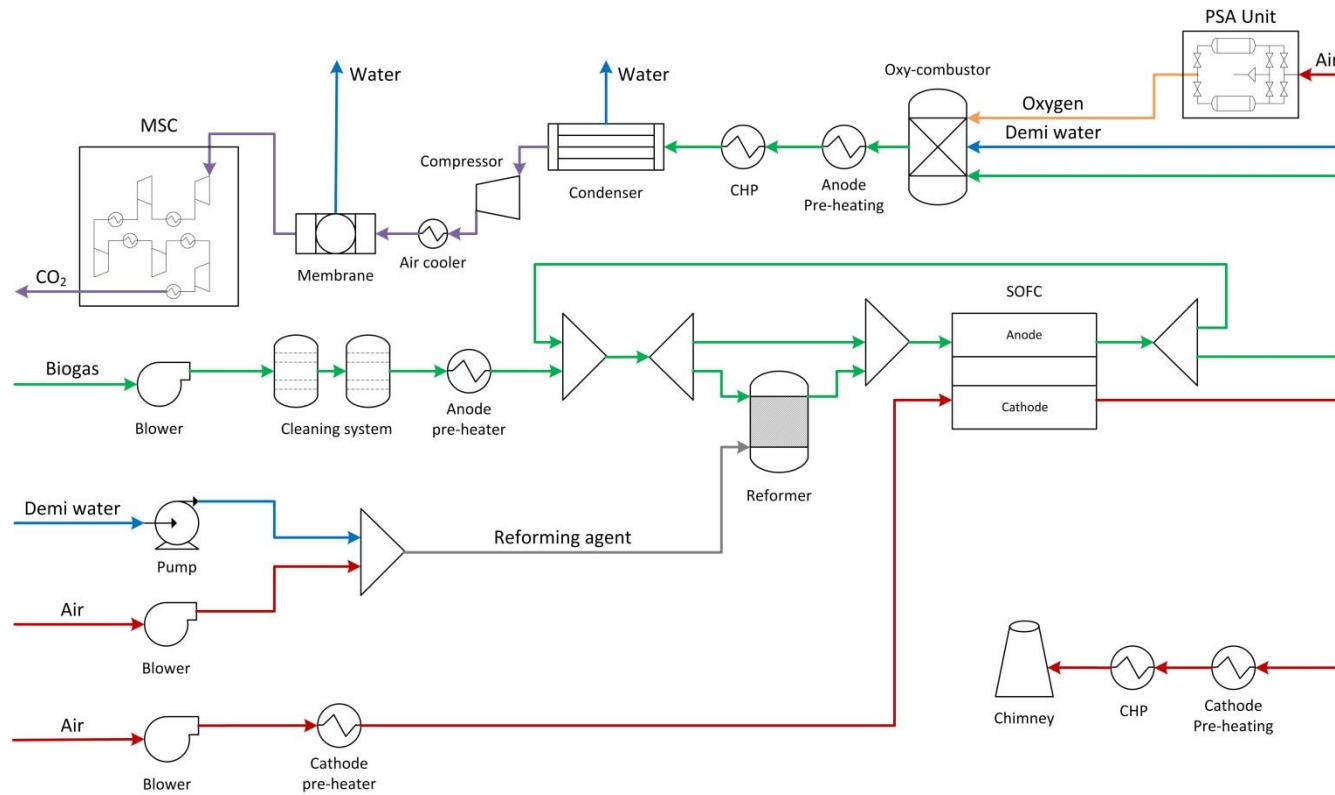
Figure 100. Atmospheric plant with CCS.
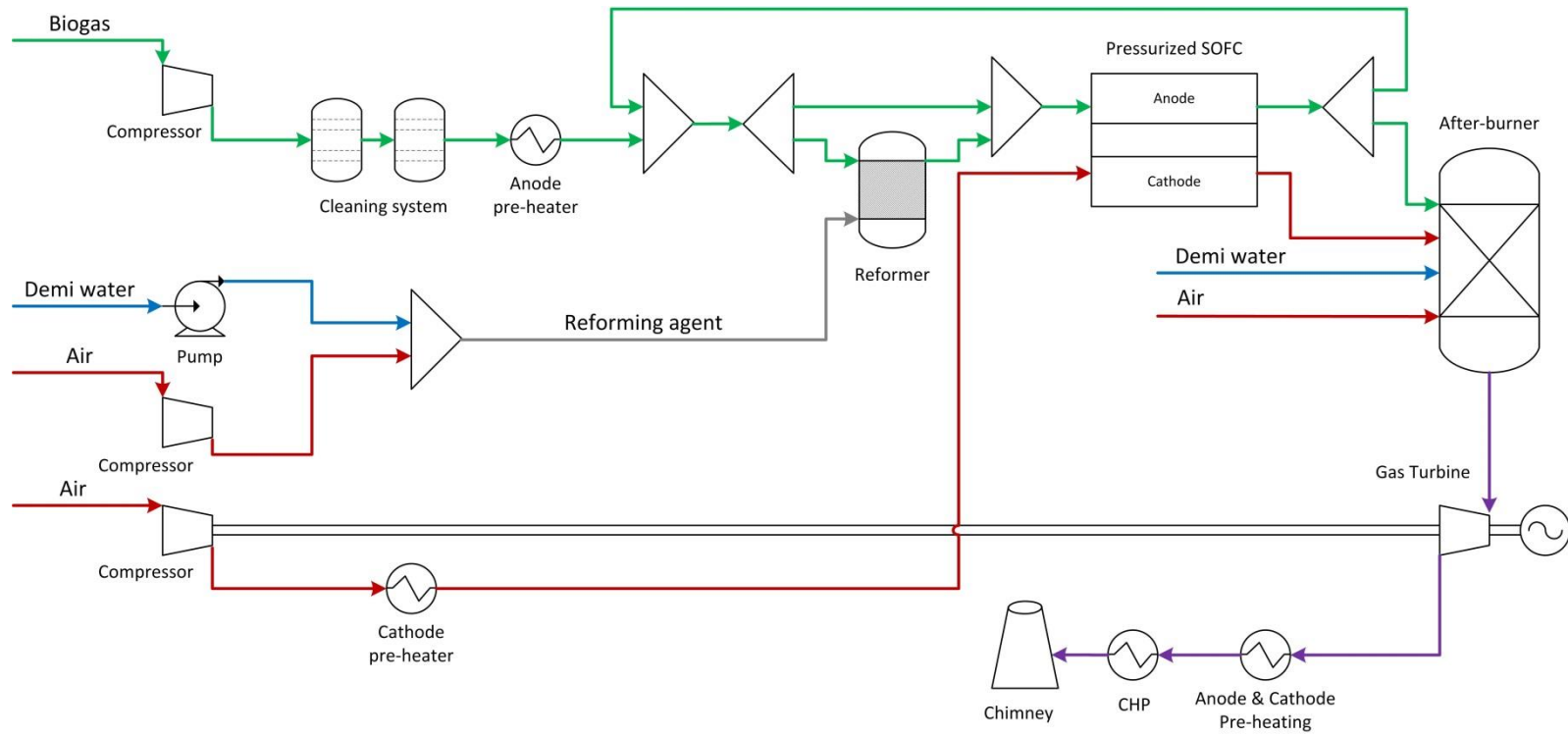
Figure 101. Pressurized plant without CCS.

Figure 102. Pressurised plant with CCS.

4.2.3 Energy analysis

The first analysis made of the modeled plant is the calculation of the energy performance. This includes the mass and energy balance of the plant, performed by the AspenPlus® software, together with the electrical and thermal efficiency.

The electrical efficiency is one of the most important performance parameters that can be used to evaluate the thermodynamic benefits of a fuel cell. As will be seen during the economic evaluations, the efficiency cannot be considered alone during the definition of the most appropriate design of a plant, but certainly is an interesting index of quality, especially from an environmental point of view.

The efficiency can be referred both to the SOFC stack and to the whole plant. In this work, the interest is related to the entire system, and so the useful efficiency is the global one:

$$\eta_{el} = \frac{W_{SOFC,DC} \cdot \eta_{inv} - W_{aux}}{\dot{V}_{biogas} \cdot LHV_{biogas}} \qquad \text{Eq. 10}$$

where:

- $W_{SOFC,DC}$ is the electrical power produced by the SOFC in the form of direct current
- η_{inv} is the efficiency of the inverter (required for the DC/AC conversion), set to 95%
- W_{aux} is the electrical power required by all the auxiliary devices
- $\dot{V}_{biogas}$ is the volume flow of the inlet biogas
- LHV_{biogas} is the lower heating value of the inlet biogas

The auxiliary power consumption is the sum of the requested power from the air blower, the biogas blower, the anode recirculation blower and the water pumps. Because of the high flow rate, the major contribution is related to the air blower. In order to determine the real power consumption from the ideal one, efficiencies have been fixed. General values for efficiencies are:

- Isentropic efficiency: 80% (small/medium size), 86% (large size)
- Mechanical efficiency: 90% (small/medium size), 99.7% (large size)

The total efficiency for auxiliaries is thus 72%; in some models, this values has been reduced for the recirculation blower taking into account the most problematic operation related to the high temperatures. The turbine is not mentioned since the power is subtracted from the air blower consumption (turbo-compressor group), with almost same efficiencies of other auxiliaries.

Furthermore, the auxiliaries have been considered to have AC power supply and thus the inverter efficiency in applied to all the power generated by the SOFC (Figure 103).
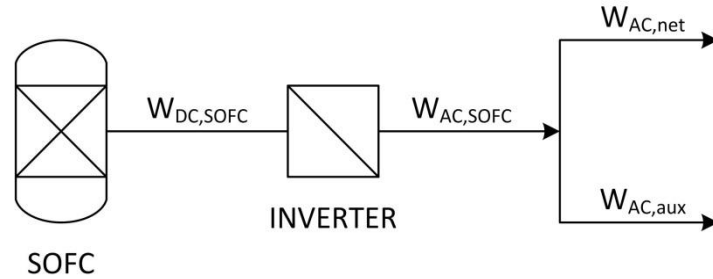
Figure 103. System electrical layout

The thermal efficiency is calculated from the thermal power recovery with CHP heat-exchangers. Depending on the layout (CCS or not) the recovery can be performed using one or two heat exchangers. The thermal efficiency is mainly depending on the chosen water temperatures:

- The water temperatures are always between 60 and 80 °C since these are the current values for heating the digester in the SMAT WWTP plant in Turin (Anon n.d.).
- The exhaust outlet temperature is usually maintained over 100 °C in order to avoid water condensation in the chimney which could lead to steel rusting.

The thermal efficiency can thus be expressed as:

$$\eta_{th} = \frac{\dot{Q}_{CHP}}{\dot{V}_{biogas} \cdot LHV_{biogas}}$$

Eq. 11

The overall plant efficiency will then by the sum of the electrical and thermal efficiencies:

$$\eta_{tot} = \eta_{el} + \eta_{th}$$

Eq. 12

Table 19 shows some of the main input parameters to the model.

Table 19. Main plant input parameters.

Parameter	Value	Unit
Electrical power SOFC, DC	Variable	kW
Operating voltage	0.8	V
Capacity factor	80	%

Annual operating hours	7008	h/y
Plant lifetime	20	y
S/C ratio	2	-
Biogas CH_4 molar frac.	60	%
Biogas CO_2 molar frac.	40	%
Biogas H_2S concentration	100	ppm
Air O_2 molar frac.	21	%
Air N_2 molar frac.	79	%
Internal reforming fraction	50	%
Inverter efficiency	95	%
SOFC heat loss (% power)	1	%
Max. allowable temperature	900	°C
Ambient temperature	25	°C
Ambient pressure	1	bar

4.2.4 Economic analysis

The optimization of the energy performance parameters referred to thermodynamic and electrical features, such as the Areal Specific Resistance (ASR), the electrical efficiency, or the net power sent to the grid, is not sufficient because what really concerns to the investor is the profit that can be achieved from its installation.

The suitability of a plant is usually determined by two economic factors.

The first one is the number of years required to earn back what was initially invested and is defined as **Pay Back Time (PBT)**. From the PBT on, the investor has recovered all the initial investment and started to earn money.

The second one is the total profit achievable at the plant end of life, evaluated with the construction of the annual cash flows actualized to the present year. This procedure that will be described later is called **Net Present Value Analysis (NPV)** and is usually adopted for long-period projects because it allows comparing the analyzed investment with alternative opportunities for the available initial capital.

In this chapter, each component of the power plants has been defined by an appropriate cost function that evaluates its investment costs depending on its main operating conditions. Then each cost is actualized to an appropriate reference year (in this work is 2010 since,

after this year, the actualization indexes were not found) so that the total investment is referred, during the cash-flow analysis, to this year zero. Finally, the annual costs and profits have been calculated so that it as possible to build the monetary cash flows for each year and to define the NPV at the end of life.

Investment costs

The calculation of the capital cost (investment cost) of each component is performed adopting the methodology employed by NETL in its costing models (DOE NETL 2011b). The approach can be adopted for the economic analysis of a generic power generation plant, not depending on the technology to which it is applied.

The total investment cost is defined using five different levels:

(1) **Bare Erected Cost (BEC)**: includes the cost of process equipment, on-site facilities and infrastructure that support the plant, and the direct and indirect labor required for its construction and installation.

(2) **Engineering, Procurement, and Construction Cost (EPCC)**: includes the BEC plus the cost of services provided by the engineering, procurement, and construction (EPC) contractor. The EPC services include detailed design, contractor permitting, and project and construction management costs.

(3) **Total Plant Cost (TPC)**: comprises the EPCC plus project and process contingencies.

(4) **Total Overnight Capital (TOC)**: comprises the TPC plus all other overnight costs, including owner's costs.

(5) **Total As-Spent Capital (TASC)**: is the sum of all capital expenditures as they are incurred during the capital expenditure period including their escalation. It also includes interest during construction.

In Figure 104 a summary of each level of capital cost is reported.
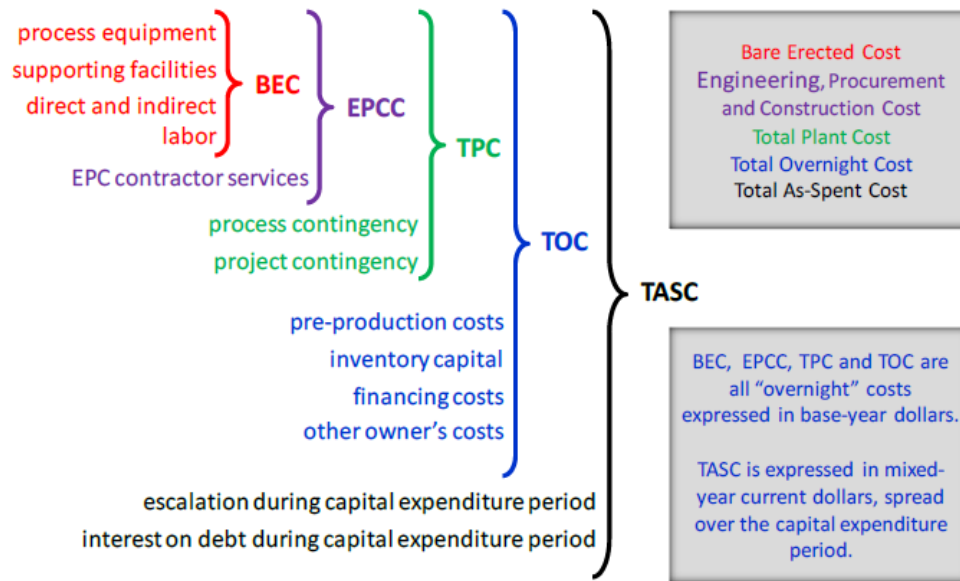
Figure 104. Capital cost levels (DOE NETL 2011b).

The Bare Erected Cost will be determined, for each device, with appropriate cost functions that will consider their most relevant operating conditions, explained below.

For the present analysis, the TPC and the TOC need to be defined, but we are not interested in the calculation of the TASC since the discounting operation is already included in the NPV analysis that will be performed further.

From the value of the BEC, the other cost levels can be found in this way:

$$EPCC = BEC \cdot (1 + f_{EPCC})$$
Eq. 13

$$TPC = EPCC \cdot (1 + f_{TPC})$$
Eq. 14

$$TOC = TPC \cdot (1 + f_{TOC})$$
Eq. 15

where each f represent the increase due to the new cost components included in every cost level. Table 20 shows the fractions suggested by the NETL methodology (DOE NETL 2011b) and, in case are available just ranges, the values actually used in this work.

Table 20. Percentage fractions for the definition of the different cost levels.

Fraction	Components			Result
	Component	Values reported (DOE NETL 2011b)	Values adopted	
f_{EPCC}	EPCM contractor services	8 – 10 %	9 %	9 %
f_{TPC}	Process contingencies (for small pilot plant data)	20 – 35 %	22.5 %	52.5 %
	Project contingencies	15 – 30 %	30 %	
f_{TOC}	Pre-production costs (start-up)	2 %	2 %	20.2 %
	Inventory capital	0.5 %	0.5 %	
	Financing cost	2.7 %	2.7 %	
	Other owner's costs	15 %	15 %	

For the component referred to the EPCM contractor services, the value adopted is simply the average of the range reported. On the other hand, the choice of the two following fractions was taken making some considerations.

The contingencies refer to the uncertainty in the cost definition for a specific technology (process) and for a project. The SOFC technology is quite young, but, at the moment, there are a certain number of applications that uses it. For this reason, we did not want to assume a too high value of the contingencies associated with the technology, so it was chosen 22.5 %, which is not so far from the lower limit.

On the other hand, the knowledge about the cost models, applicable to integrated SOFC power plants of large size, is really limited, so we have assumed to have here the highest project contingencies (30 %).

Cost functions

A <u>cost function</u> is a relationship that estimates the capital cost of a component, using as input one or more reference operating conditions (temperature, pressure, mass flow…):

$$BEC = f(Q_1, Q_2, \dots) \qquad \text{Eq. 16}$$

where Q_i is the *i-th* condition required by the function.

Usually, the cost functions are defined by lower and upper limits of the independent variables: outside these ranges, the resulting investment cost could be completely unrealistic.

When a cost function is not available, it is possible to implement a common procedure based on the use of the costs found for the same device of different size, the <u>scaling method</u>. This approach can be used just if there is one independent variable Q. If, for a device, is known the value of the capital cost BEC_r referred to the operating variable Q_r, the relationship that correlates this information with the operating state (BEC, Q) is:

$$\frac{BEC}{BEC_r} = \left(\frac{Q}{Q_r}\right)^{sc} \qquad\qquad \text{Eq. 17}$$

$$BEC = BEC_r \cdot \left(\frac{Q}{Q_r}\right)^{sc} \qquad\qquad \text{Eq. 18}$$

This simple method is valid just if an appropriate scaling factor is defined. In literature, are available many reference scaling factors, each one for a specific device. In our analysis, if a better scaling factor could not be found, the reference value that will be assumed is 0.7. Furthermore, if more than one reference cost is known, these can be used in equation 67 to determine the scaling factor.

The scaling method can also be used with those cost functions where the independent variable is outside the validity range. Indeed it is sufficient to find the cost referred to one of the two limits (the nearest one to the real condition) and used it for the scaling.

Each cost function defines an accurate capital cost using data available at the moment it was implemented. In the years, this cost tends to change, due to the inflation effect, so the economic analysis requires that every cost component is referred to a specific year. The effect of the inflation can be estimated with the following relationship:

$$BEC(t_r) = BEC(t) \cdot \left(\frac{I(t_r)}{I(t)}\right) \qquad\qquad \text{Eq. 19}$$

where $I(t_r)$ and $I(t)$ are cost indexes defined for the different years.

There are several cost indices used by the chemical industry, for example, the most common are the Chemical Engineering Plant Cost Index (CEPCI) and the Marshall and Swift Equipment Cost Index (MSECI). Table 21 provides the values for both CEPCI and MSECI from 1990 to 2013 and in Figure 105 are shown their trend from 1978 (Anon n.d.).
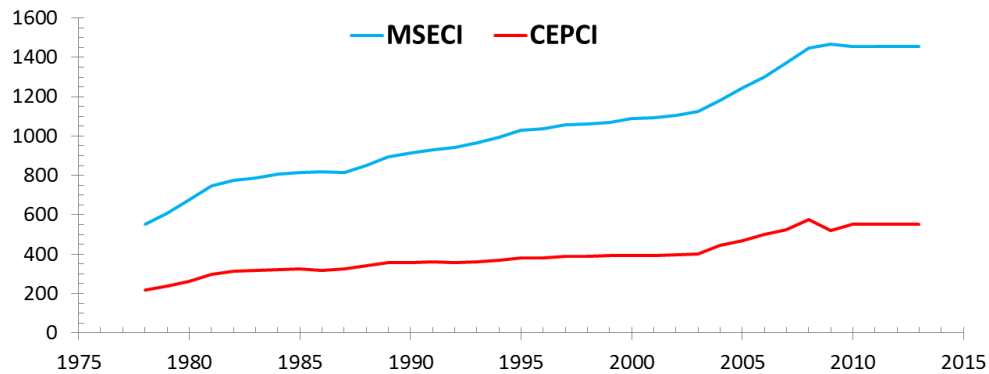
Figure 105. Cost index trend.

It was not possible to find the updated values from 2011 to 2013, so it was hypothesized that they are constant and equal to those referred at 2010. The calculations were made using the indices defined by <u>CEPCI</u> because they can be applied exactly to the power plants, while MSECIs are referred to all industrial plants. Any year can be used as a reference, in this work is adopted 2010.

The cost functions chosen and developed for each plant components are described in "Appendix 4 – Economic analysis: functions, cost of biogas and subsidies", section "A4.1 Cost functions definition".

Table 21. Cost indexes.

Year	MSECI	CEPCI
1990	915	358
1991	931	361
1992	943	358
1993	964	359
1994	993	368
1995	1028	381
1996	1039	382
1997	1057	387
1998	1062	390
1999	1068	391
2000	1089	394
2001	1094	394
2002	1104	396
2003	1124	402

2004	1179	444
2005	1245	468
2006	1302	500
2007	1373	525
2008	1449	575
2009	1469	521
2010	1457	551
2011	1457	551
2012	1457	551
2013	1457	551

Cash flow analysis

The minimization of the total investment cost cannot be used as a target in a well-done economic analysis because it does not let to evaluate the real convenience of the investment through the plant lifetime.

An industrial plant requires periodic costs for its continuous operation but, at the same time, produces profits: thus, an accurate analysis should study the evolution of the cash flows during the time.

In financial analysis, two or more investments are commonly compared using as determining parameter the Net Present Value (NPV) at a defined time. The NPV is defined as the sum of a series of cash flows actualized on the base of the nominal interest rate. The actualization is necessary because, due to the inflation, the monetary values of something estimated in two different years are different. Then, since from the cash flow analysis we obtain the future values of costs and profits, they become present values with the actualization.

For the plants studied in this work, the reference time for the calculation of the NPV is the lifetime (20 years).

The cash flow and NPV analysis are performed with the following steps:

- Calculation of the annual costs
- Calculation of the annual profits
- Construction and actualization of the cash flows
- Definition of the NPV at each year
- Determination of the Pay Back Time (PBT) and of the NPV at end life

Annual cost

The annual costs, required during the life of each SOFC power plant, can be classified in these main components:

- Maintenance costs
- Labor costs
- Annual integration of new spare capacity
- Substitution of the adsorbent materials of the cleaning system
- Substitution of the reformer catalyst
- Fuel costs

The cost methodology implemented by NETL (DOE NETL 2011b) suggests, for the estimation of the maintenance costs of power plants, to consider them as a fraction of the Total Plant Cost (TPC):

$$AC_{O\&M} = f_{O\&M} \cdot TPC$$ Eq. 20

The fraction reported in their work is 3%, but this data was estimated considering both the O&M costs and those associated to the annual consumptions of fuel. In this analysis, was chosen an economic approach that distinguishes these two components, so it was necessary to assume a lower value referred just to the maintenance. The fraction hypothesized is 2%.

The labor costs are really low because these power plants do not require the continuous presence of large groups of workers. If the yearly salary for a person that works for a number of hours around the national average is, more or less, equal to 75000 $ (Rubin et al. 2013), even the hypothesis to have just one worker could overestimate this component. For this reason, it was chosen to use an ideal number of worker lower than 1, and the assumption adopted is 0.3. It is important to understand that this hypothesis is absolutely reasonable because in the power plants based on fuel cells are required employees just for the ordinary maintenance (in this case for the substitution of cleaning adsorbents and catalysts), but no one is necessary during the normal operation.

The annual costs for the integration of spare capacity in the stack of the fuel cell can be easily evaluated from the annual active surface required to cover the degradation effects. The estimation of these costs can be made using the cost function adopted for the initial stack, considering only those components referred to the SOFC integrated block and to the insulation. In fact, the new cells do not require all those accessories that were already

installed during the construction of the power plant (electrical connections, piping, enclosure).

The interesting feature in this last annual cost is that it tends to assume very low constant values for a certain time, then it increases considerably just for a year when the initial stack needs to be replaced and finally returns to low costs.

The NPV and the PBT are strongly influenced by the evolution of the degradation: in fact, as already seen previously, a system that degrades faster could require more than one replacement during its lifetime.

The costs due to the replacement of the adsorbent materials in the cleaning system can be expressed scaling a reference value related to a reference concentration of H_2S in the inlet biogas, just as in the cost function for the BEC of the same device. In Table 22 all the economic data found from the literature are reported (Papadias et al. 2012).

Table 22. Constants for the annual costs of the cleaning system.

Parameter	Value
Reference concentration of H_2S	400 ppm
Annual cost required by the Iron Oxide System	7520 \$/y
Annual cost required by the Low-Temperature Polisher (Active Carbon)	7521 \$/y
Annual cost required by the High Temperature Polisher	150 \$/y

The catalysts of the external reformer have a lifetime around 4 years (DOE NETL et al. 2011), so they do not have to be replaced yearly, even if the annual cost will be spread during every year. The specific cost of the material is expressed as a function of the volume bought, and then the annual cost required is given by the following relationship:

$$ AC_{ref,cat} \left[\frac{\$}{y} \right] = c_{cat} \left[\frac{\$}{4y \cdot m_{cat}^3} \right] \cdot V_{ref} \left[m_{ref}^3 \right] \cdot \frac{1}{1.5} \left[\frac{m_{cat}^3}{m_{ref}^3} \right] \cdot \frac{1}{4y} \qquad \text{Eq. 21} $$

where:

- $c_{cat} = 499 \ \frac{\$}{4y \cdot m_{cat}^3}$ is the specific cost of the catalyst (DOE NETL et al. 2011)
- 1.5 is the ratio between the total volume of the reformer and that of the catalyst, assumed value from experience on real components

The cost of the fuel is an interesting topic in this analysis, even if it is related to some general features of the systems designed. During the definition of the configurations, we

have assumed that the plants studied are all fed by biogas obtained in wastewater treatment systems. In general, in a purification process (such as a wastewater treatment unit) the mixtures of hydrocarbons and carbon dioxide separated do not correspond to the final product but are by-product material of a process that cannot be avoided. The cost of these products is quite difficult to estimate because, first of all, it should be defined their field of application and so the real economic value. However, considering that they should be thrown away if not reused in plants like those proposed in this work, logically their costs should be considered very low or, at the limit, even null.

For this reason, we will assume that this cost component is not included in the analysis: this is not a strong hypothesis, also because, as we have already said, we want to integrate these systems in operating treatment units, so it is absurd to impose a cost for something that has no economic value, and that is sent to the same plant. In any case it is interesting to see how strongly this assumption influences the results and so in Figure 106 and Figure 107 the resulting Cash Flows and NPV for large size plants (1 MW) referred to the same conditions (atmospheric vented plant, FU=80%, T_{SOFC}=800°C) are shown, obtained considering, respectively, a fuel cost null and equal to a value estimated with a simplified approach (described in "Appendix 4 – Economic analysis: functions, cost of biogas and subsidies", section "A4.2 Estimation of the cost of biogas"). The resulting fuel cost estimated is equal to 3.62 c$/kWh.

From these graphs we can see that the cost of fuel has a very strong influence: in fact, considering the fuel cost, the Pay Back Time increases of 6 years, and the NPV at the end life decreases significantly. However, this assumption is absolutely reasonable.

All these cost components found are referred to year 0 of the investment, and, for this reason, they are usually present values. It is necessary to define, with an interest rate i_R, the real monetary values referred at each year (future values):

$$AC(y) = AC_0(y)(1 + i_R)^y \qquad \qquad \text{Eq. 22}$$

where *y* is obviously the generic year.
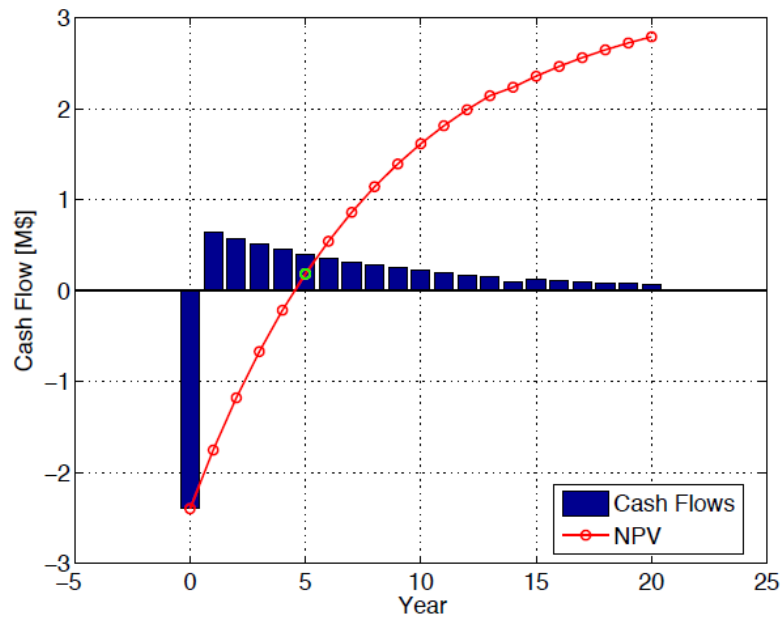
Figure 106. Cash Flows and NPV with a null cost of fuel.
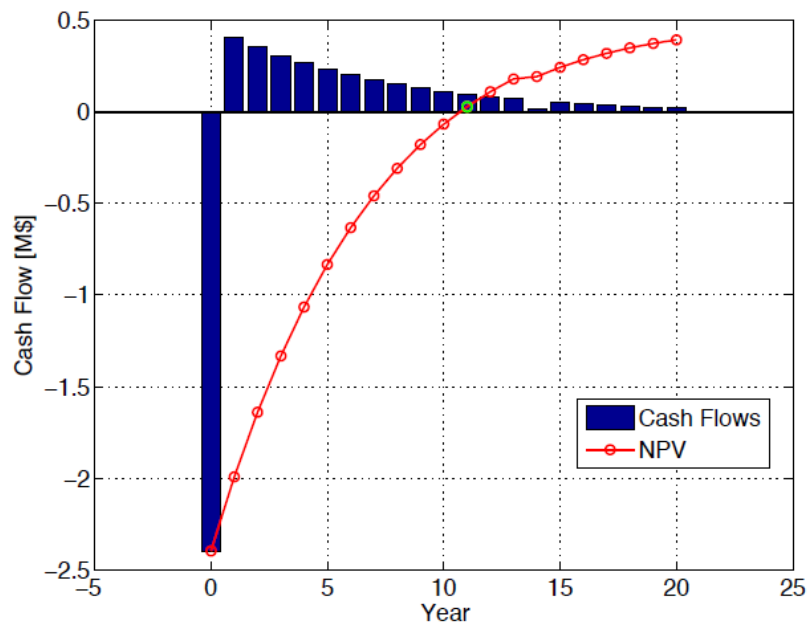
Figure 107. Cash Flows and NPV with an estimated cost of fuel.

Annual incomes

The profits generated during the lifetime of each power plants derive from the sale of electrical power to the grid and to the production of hot water sent to the district heating.

The first component is quite simple to evaluate but requires the definition of the appropriate subsidy that the plant can obtain. A detailed analysis of the subsidies scheme through Europe analyzing some chosen countries can be found in "Appendix 4 – Economic analysis: functions, cost of biogas and subsidies", section "A4.3 Subsidy scheme analysis". The incomes related to subsidies is usually calculated as:

$$AP_{W_{el}} = W_{net} h_y c_{el}$$

<div align="right">Eq. 23</div>

where:

- W_{net} [kW] is the net electrical power produced
- $h_y \left[\frac{h}{y}\right]$ is the number of annual working hours
- $c_{el} \left[\frac{€}{kWh}\right]$ is the subsidies for electricity produces/sold or auto-consumed depending on the subsidy scheme.

The earnings derived from the production of hot water can be evaluated considering the savings of fuel that should be burned, in a traditional thermic plant, for the generation of the same thermal power. For the calculation of these savings has been considered that the hot water is produced in a boiler, fed with methane. Usually, the cost of methane is expressed respect to its internal energy, then the savings of the fuel have to be calculated with the appropriate unit of measure:

$$AP_{CHP} = -c_{CH_4} S_{CH_4}$$

<div align="right">Eq. 24</div>

Where:

- $c_{CH_4} \left[\frac{€}{GJ}\right]$ is the average cost of methane in Italy
- $S_{CH_4} \left[\frac{GJ}{y}\right]$ is the amount of methane (expressed in terms of internal energy) that would be consumed to produce the same thermal energy recovered with a traditional boiler system (95% efficiency).

The cost of methane is the one applied to industrial users operating in Italy (Anon n.d.). The total profits will finally be the sum of the two components. The profits value should then be actualized at each year with an interest rate that depends on the inflation over the incomes, but we have assumed that the inflation on incomes is negligible in those 20 years of life.

Annual cash flows

To calculate the annual cash flows it is necessary to define the taxes that the owner must pay when the power plant produces revenues. First of all, it is important to define the depreciation (*dep*), which expresses the quantity that can be deducted from the taxable income. The depreciation is evaluated during the first years of operation (y_{dep}) when the taxes are lower to allow an easier recovery of the initial investment. In this case, the depreciation is calculated from the Total Overnight Cost (TOC) using:

$$dep = \frac{TOC}{y_{dep}}$$ Eq. 25

When the power plant produces revenues (R), the owner must obviously pay a tax (T) that do not depend on the annual profits but on the revenues themselves.

$$R(y) = AP(y) - AC(y) - dep$$ Eq. 26

$$T(y) = \frac{f_{TAX}}{100} R(y)$$ Eq. 27

where:

- *R(y)* [$] are the annual revenues, which could be either positive or negative
- *T(y)* [$] is the annual tax
- *f_{TAX}* [%] is the fraction of incomes that has to be paid as taxes
- After all these, the cash flows (CF) can be built.

$$CF(0) = -TOC$$ Eq. 28

$$CF(y) = \begin{cases} AP(y) - AC(y) - T(y), & R(y) > 0 \\ AP(y) - AC(y), & R(y) < 0 \end{cases}$$ Eq. 29

As already discussed, the cash flows have to be levelized to the initial year of the investment in order to calculate the *NPV*. The Weighted Average Cost of the Capital is used as a parameter for the actualization and is depending on the initial investment share between equity and debts and on their own value.

$$WACC = \frac{p_e}{100}\frac{c_e}{100} + (1 - f_{TAX})\frac{p_d}{100}\frac{c_d}{100}$$ Eq. 30

$$CF_0(y) = \frac{CF(y)}{(1 + WACC)^y}$$ Eq. 31

Where:

- *WACC* [-] is the Weighted Average Cost of the Capital
- p_e [%] is the percentage of equity
- p_d [% is the percentage of debt
- c_e [%] is the nominal dollar cost of equity
- c_d [%] is the nominal dollar cost of debt

A more detailed description of the meaning of each one of these last economic parameters is available in (DOE NETL 2011b). The percentages of equity and debt can strongly affect the economic models. In this analysis, it was assumed the situation where the initial investment is equally covered by them (50%-50%). Table 23. shows the main economic assumptions adopted in this study.

Table 23. Economic assumptions.

Quantity	Abbreviation	Value	Unit	Reference
Cost of electricity	c_{el}	0.111	€/kWh	(Anon n.d.) for 2013
Cost of methane	c_{CH4}	0.042	€/kWh	(Anon n.d.) for 2013
Conversion Euro/Dollar (March 2014)	$f_{\$€}$	1.3775	\$/€	-
Interest rate	i_R	3	%	-
Percentage of equity	p_e	50	%	-
Percentage of debt	p_d	50	%	-
Nominal dollar cost of equity	c_e	20	%	(DOE NETL 2011b)
Nominal dollar cost of debt	c_d	6.5	%	(DOE NETL 2011b)
Depreciation years	y_{dep}	10	y	-

4.2.5 OSMOSE

Concerning the large size plants analysis, one of the main tool used will be OSMOSE, a Matlab-based package developed by EPFL that allows creating an interface between Matlab® itself and a process modeling software (e.g., Aspen Plus® or Vali®). In this work, OSMOSE is employed to perform thermal integration of hot/cold streams via pinch

analysis methodology, sensitivity analysis and Multi-Object Optimizations (MOO). More details can be found in "Appendix 5 - OSMOSE optimization tool".

4.3 Case studies

4.3.1 Small size plants

Atmospheric plants without CCS/CCU

The analysis of small size plants has been already published in the article from Tjaden, Gandiglio, Lanzini, Santarelli and Jarvinen (Tjaden et al. 2014) and further details on the plant description and analysis can be found directly on the paper. As already shown in the roadmap, small size plants were analyzed only in the atmospheric configuration without CCS since the low size of the system does not justify such higher investment as pressurization or carbon capture.

On the tables below the main system parameters used as model input values and the range of the sensitivity analysis are shown.
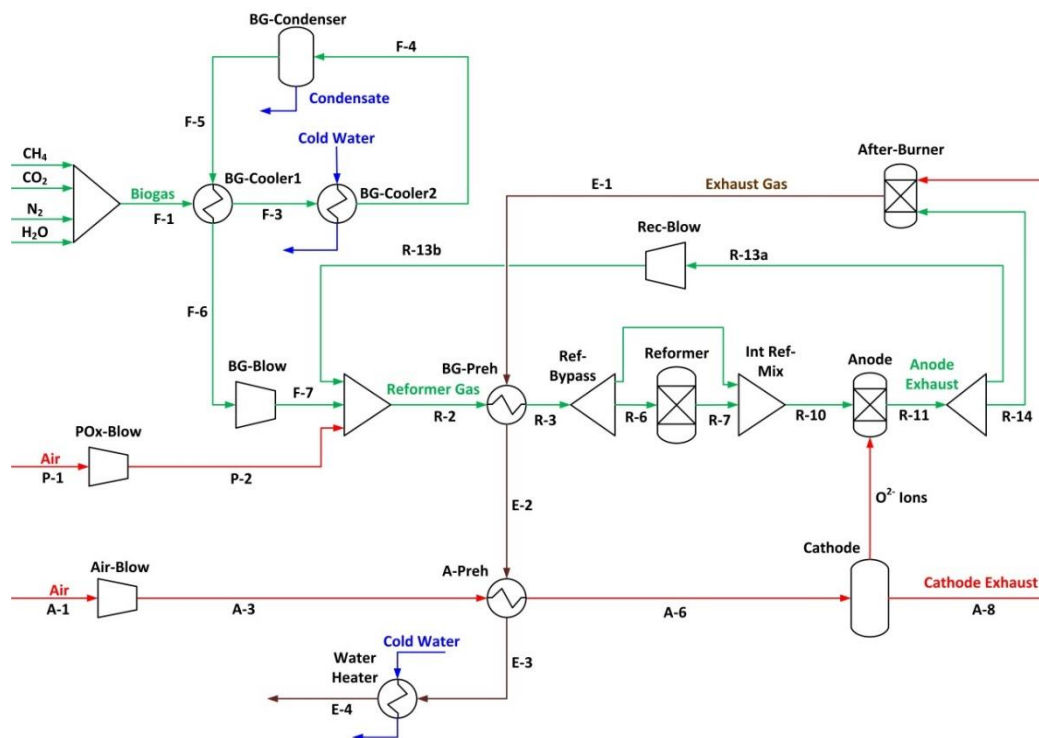
Figure 108. Small size plant layout.

Table 24. Baseline Case Study Main Parameters. (Tjaden et al. 2014)

parameter	value
x_{CH4db}	CH_4 55 mol %
x_{CO2db}	CO_2 45 mol %
x_{N2db}	N_2 0.1 mol %
FU	80%
V_{op}	0.8 V
active area of cell	100 cm^2
S/C ratio	2
λ_{POx}	0.25
reforming temperature	700 °C
SOFC temperature	800 °C
internal reforming ratio (SR)	0%
SOFC DC power output	25 kWe
CHP water inlet temperature	20 °C
CHP water outlet temperature	60 °C
exhaust gas temperature	105 °C

Table 25. Range of Decision Variables for Parametric Study. (Tjaden et al. 2014)

decision variable	baseline value	range
internal reforming with SR (%)	0	0−50
FU (%)	80	70−85
V_{op} (V)	0.8	0.7−0.85
x_{CH4db} (mol %)	55	50−65
x_{N2db} (mol %)	0.1	0.1−25

4.3.2 Medium size plants

Atmospheric plant without CCS/CCU

The work on the medium size plant has been developed analyzing only atmospheric plants but with the study of the carbon capture system. The choice of carbon dioxide sequestration, transportation or on-site use has been analyzed with the different system performance evaluation.
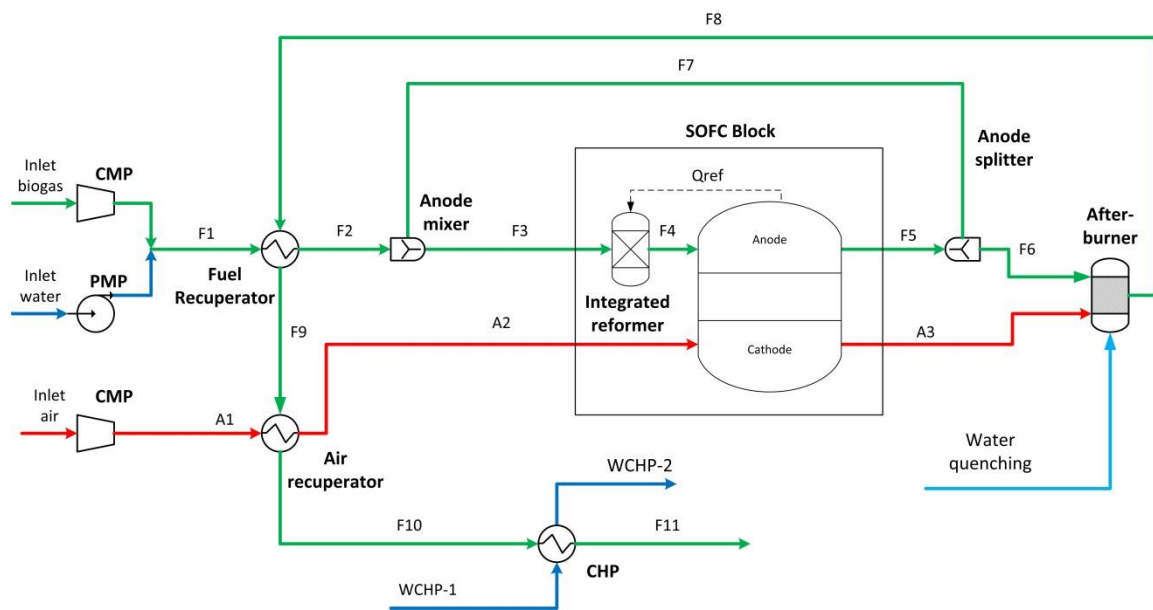
Figure 109. Medium size plant layout without carbon capture.

The three figures above and below show the three analyzed plants with main difference related to the carbon separation unit and the carbon dioxide compression stage.

The table below shows the main input values for the AspenPlus model®.

Table 26. Baseline Case Study Main Parameters.

Nominal conditions				
Vop [V]	WDC [kW]	FU [%]	S/C	$\%CH_4$ - $\%CO_2$
0.8	100	80%	2	60% - 40%

Atmospheric plant with CCS

The AspenPlus® model was defined in order to be able to study in automatic mode without actions on the flowsheet but just working on an input excel file:

- Different biogas composition
- Different reforming agents and related S/C, Pox values
- Different values of internal/external reforming
- Carbon capture or not downstream process
- CCS/CCU pathway
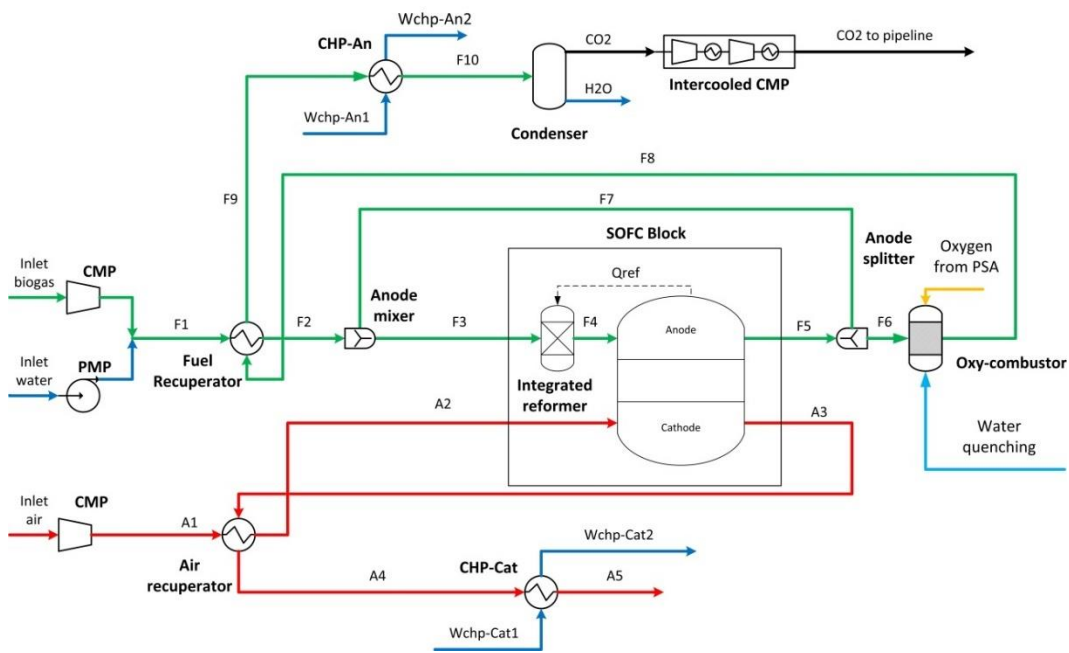
Figure 110. Medium size plant layout with carbon capture and sequestration – CCS

Atmospheric plant with CCU
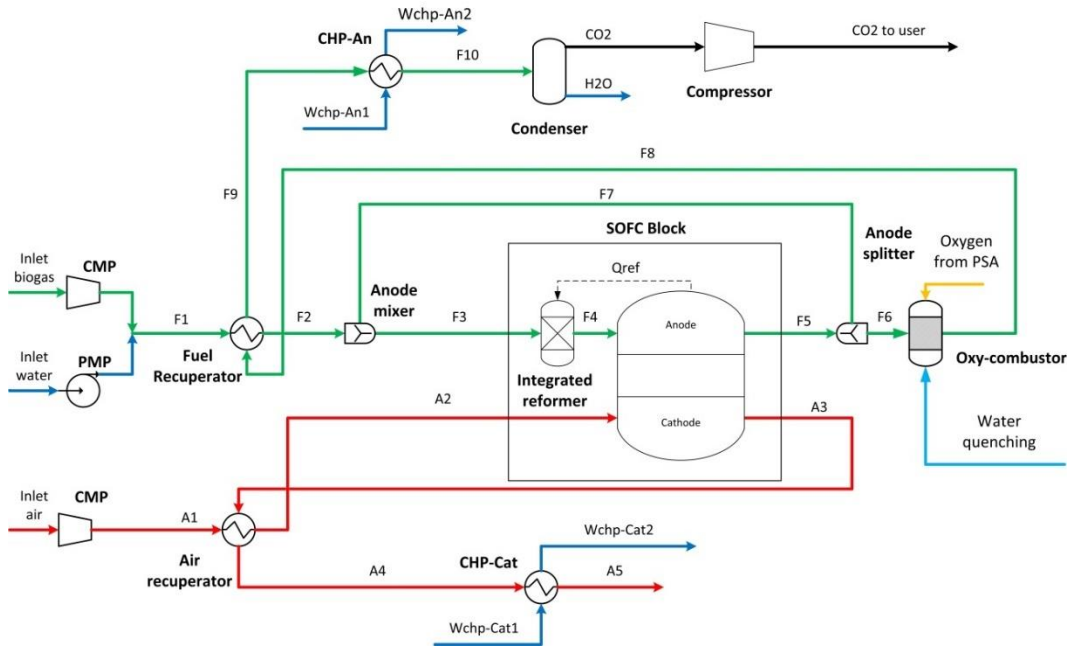
Figure 111. Medium size plant layout with carbon capture and re-use on site.

4.3.3 Large size plants

The works has been published by the author in (Curletti et al. 2015).

Four main different power plants configurations were included in this work, but the last one required two different designs depending on the operating pressure, then five configurations were studied.

In the case of carbon capture just the CCS process has been considered since, even in the case of utilization not on-site as would happen for large power generation plant, the carbon dioxide required pressure is the same as for CCS.

Table 27. Power plants configurations.

Abbreviation	Plant type
A-VENT	Atmospheric SOFC power plant without CCS
A-CCS	Atmospheric SOFC power plant with CCS
P-VENT	Pressurized SOFC power plant without CCS
P-CCS(LP)	Pressurized SOFC power plant with CCS al low pressure
P-CCS(HP)	Pressurized SOFC power plant with CCS al high pressure

AFT-BURN	After Burner	AIR-BLW	Air Blower	AN-CIRC	Anode Circulator
BG-BLW	Biogas Blower	CLEAN	Cleaning system	EXT-REF	External Reformer
FC STACK	Stack of SOFCs				

Figure 112. Large size plant layout, atmospheric without carbon capture.

The atmospheric configurations are supplied with biogas at nearly ambient pressure and ambient air. Blowers are needed cope with the pressure drops due to the streams circulation through the whole plant. On the other hand, the pressurized systems feed reactants to the SOFC stack with a pressure higher than the atmospheric one and compressors replace blowers.

In the power plants without the CCS unit, the post-combustion occurs in an after-burner (AFT-BURN) fed by the anodic (fuel) and cathodic (oxidant) flue gases. The resulting mixture from the burner is richer of water and CO_2, but the concentration of the carbon

dioxide is not sufficient to guarantee an effective and cheap separation of carbon from the exhausts.

Atmospheric plant with CCS

Instead, thanks to the characteristic of the SOFC technology based on an "electrochemical oxy-combustion" at the anode, the anode exhaust results as an almost N_2-free stream (some N_2 can be indeed found in the as received biogas). Therefore, in the case of a CCS system, instead of an after-burner the adopted design foresees the use an oxy-combustor (OXY-COMB) where the anode exhaust is combusted with pure oxygen produced on site through a PSA (Pressure Swing Adsorption) unit. In this configuration, the combustion products consist of mostly water and CO_2, and then the former can be easily separated through condensation. A temperature control system is included in the after-burner and especially in the oxy-combustor so that the inside temperature does not achieve too high values. The limit temperature imposed is 900°C, and the quenching is performed through fresh water injection. The CCS units include two steps of carbon capture: a first condensation (CCS-COND) to remove most of the water from the mixture, and the second separation in a not-porous membrane (CCS-MEMB) that allows a selective diffusion of the CO_2. In fact, the condensation could be sufficient to reach a good separation of the carbon dioxide but, in a CCS unit, also carbon storage is involved, and this requires a high level of purity. The selective diffusion mechanism is effective if driven by an appropriate pressure gradient (here 5 bars is imposed) (Dortmundt & Doshi 1999) and so a compressor (CCS-COMP) is needed.

AIR-BLW	Air Blower	AN-CIRC	Anode Circulator	BG-BLW	Biogas Blower
CLEAN	Cleaning system	CCS	Carbon Capture and Storage	CCS-COND	CCS-Condenser
CCS-COMP	CCS-Compressor	CCS-MEMB	CCS-Selective Membrane	EXT-REF	External Reformer
FC STACK	Stack of SOFCs	MSC	Multi Stage Compressor	OXY-COMB	Oxy-Combustor
PSA	Pressure Swing Adsorption				
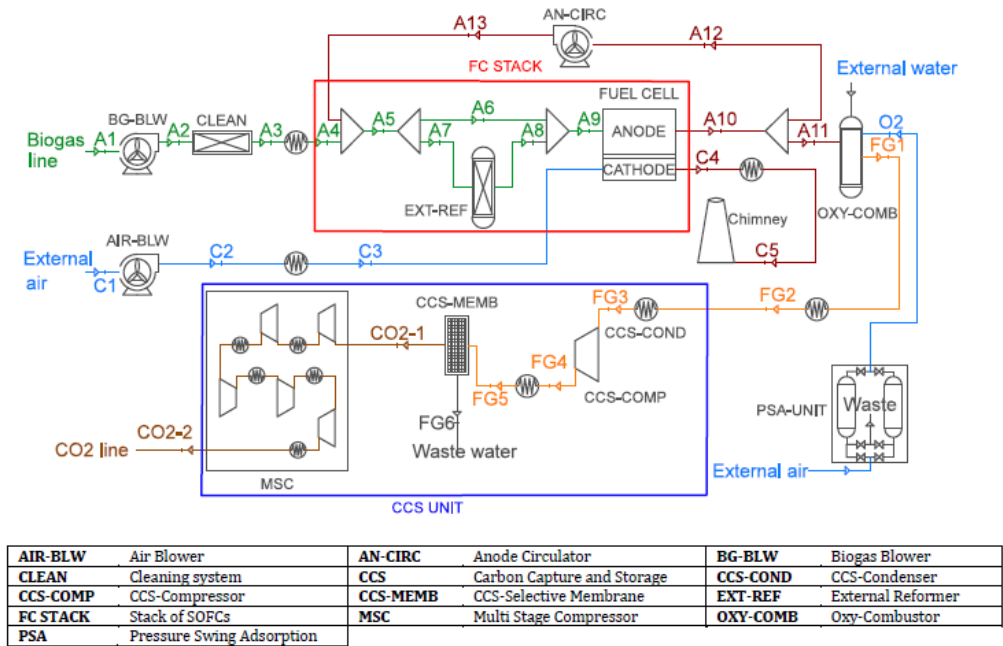
Figure 113. Large size plant layout – atmospheric with CCS.

Pressurized plant without CCS

AFT-BURN	After Burner	AIR-COMP	Air Compressor	AN-CIRC	Anode Circulator
BG-COMP	Biogas Compressor	CLEAN	Cleaning system	EXT-REF	External Reformer
FC STACK	Stack of SOFCs	G-TURB	Gas Turbine		
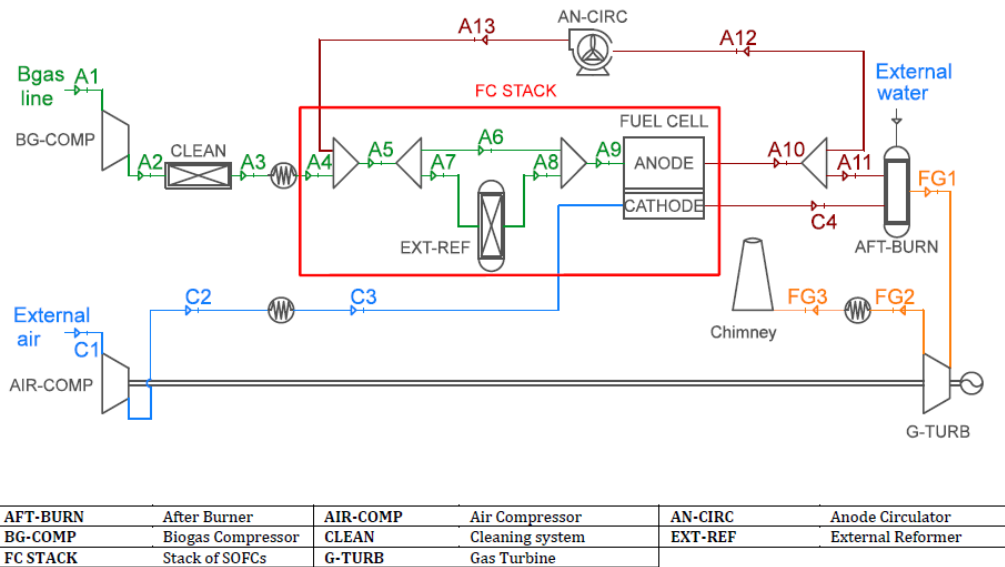
Figure 114. Large size plant layout – pressurized without CCS.

Pressurized plant with CCS – LP ($p_{SOFC} < p_{membrane}$)

In Figure 115, the design is referred to the situation where the pressure of the flue gases is under the value required to the membrane. This plant has the same features already seen before, and then another compressor (CCS-COMP) is required to assure the correct working of the separator. In Figure 116, the pressurization is so intense that the pressure of the flue gases overcomes the value required to the separator. The compressor can be avoided, but the pressure has to be decreased to the one of the membranes, so the gas needs to be expanded.

AIR-COMP	Air Compressor	AN-CIRC	Anode Circulator	BG-COMP	Biogas Compressor
CLEAN	Cleaning system	CCS	Carbon Capture and Storage	CCS-COND	CCS-Condenser
CCS-COMP	CCS-Compressor	CCS-MEMB	CCS-Selective Membrane	EXT-REF	External Reformer
FC STACK	Stack of SOFCs	G-TURB	Gas Turbine	MSC	Multi Stage Compressor
OXY-COMB	Oxy-Combustor	PSA	Pressure Swing Adsorption		
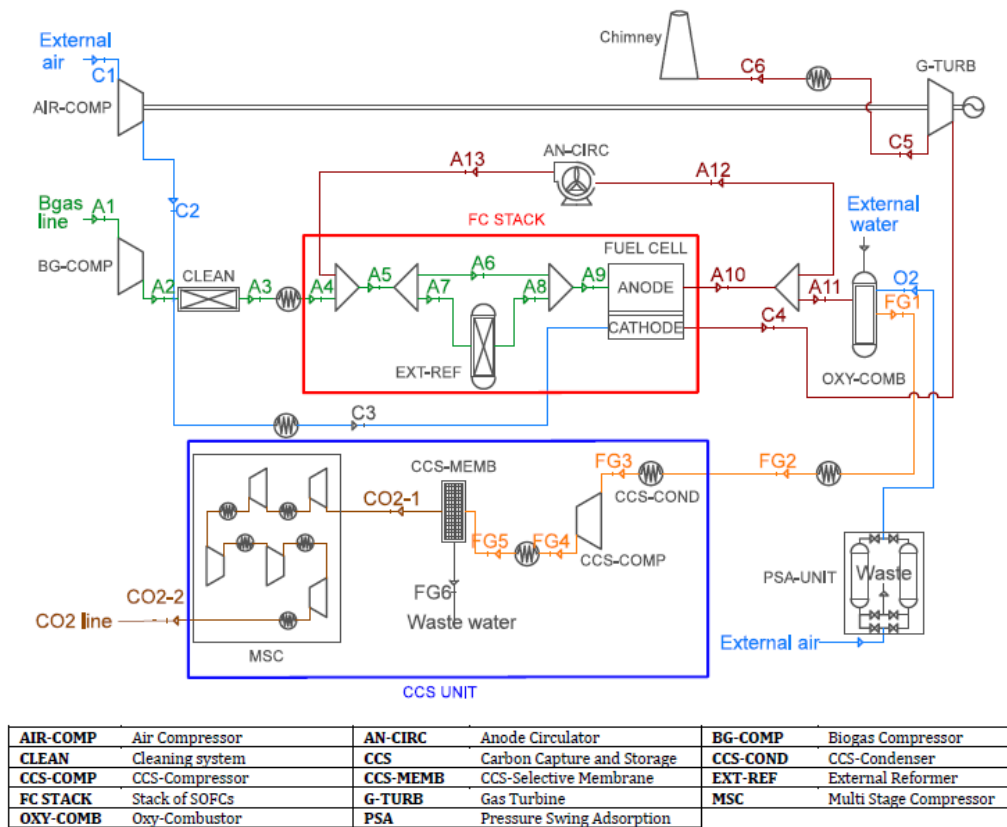
Figure 115. Large size plants layout - Pressurized plant with CCS – LP.

The expansion of the hot flue gases could be done using an expander or another gas turbine. Considering that the membrane works at pressures around 5 bar (this is the value adopted during the simulations), that an SOFC will not be pressurized more than 10 bars (to avoid excessive mechanical stresses) and that the mass flow expanded is much lower than the one sent to the other gas turbine, the energy that can be recovered during the expansion is very low and there isn't a valid motivation to adopt a more complex system. For this reason, an expander (G-EXP) is adopted and, during the simulations, was verified that the mechanical power produced by the expansion is ten times lower than the one produced by the gas turbine.

Pressurized plant with CCS – HP ($p_{SOFC} > p_{membrane}$)
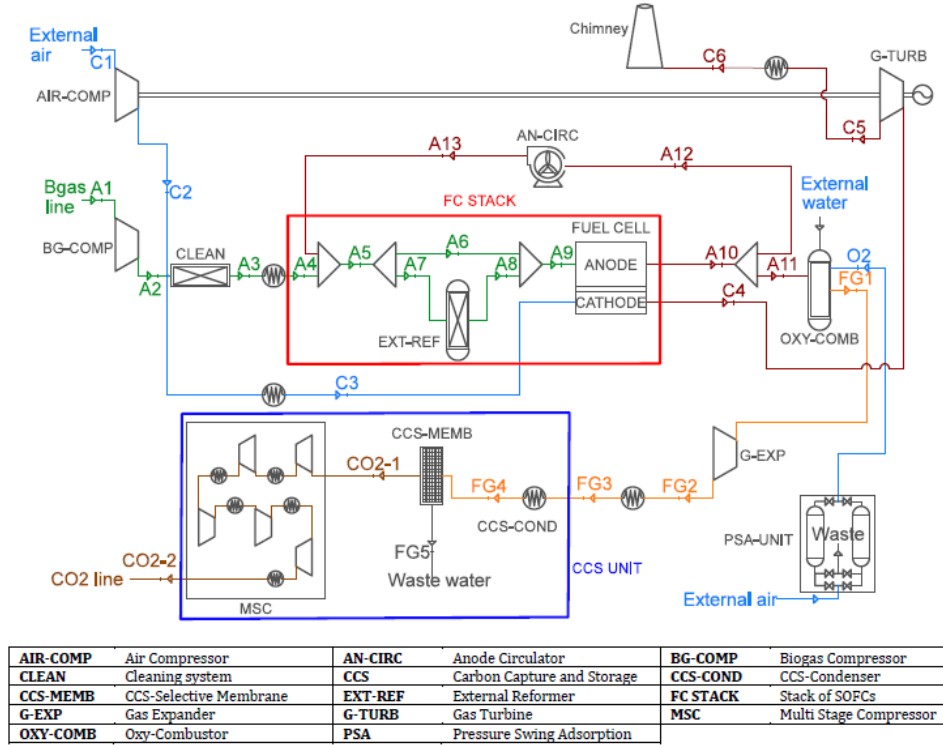
Figure 116. Large size plants layout - Pressurized plant with CCS – HP.

Table 28. Plant specifications.

Parameter	Abbreviation	Value	Unit
Electrical power produced in the stack	W_{el}	1	MW
Operating voltage	V_{op}	0.8	V
Capacity factor	CF	80	%
Life plant	y_L	20	y
Steam-to-Carbon ratio	SC	2	-
Degree of Internal Reforming	IR	50	%
Heat loss ratio from the SOFC	r_{loss}	1	%
Volume fraction of CH$_4$ in the fuel	x_{CH4}	60	%
Volume fraction of CO$_2$ in the fuel	x_{CO2}	40	%
H$_2$S concentration in the fuel	x_{H2S}	100	ppm

Isentropic efficiency of fans and compressors	$\eta_{is,c}$	86	%
Mechanical efficiency for fans and compressors	$\eta_{m,c}$	99.7	%
Electrical generator efficiency	η_{gen}	98.5	%
Inverter efficiency	η_{inv}	95.5	%
PSA efficiency	η_{PSA}	95	%
Oxygen excess (OXY-COMB)	e_{O_2}	1	%
Number of stages in the MSC	n_{MSC}	5	-
Maximum plant acceptable temperature	T_{max}	900	°C
Ambient temperature	T_a	25	°C
Ambient pressure	p_a	1	bar
Exhausts temperature	T_{ex}	60	°C
Operating pressure of the membrane	p_M	5	bar
Pure-CO$_2$ pressure for grid injection	p_{CO2}	110	bar
Pressure drops	Δp	0.01-0.06	bar

Table 29. Design variables - Ranges and reference values.

Plant type		FU (%)	T$_{SOFC}$ (°C)	P$_{SOFC}$ (bar)
A-VENT	*Range*	65-90	750-850	-
	Reference value	75	800	-
A-CCS	*Range*	65-90	750-850	-
	Reference value	75	800	-
P-VENT	*Range*	65-90	750-850	2-10
	Reference value	75	800	6
P-CCS(LP)	*Range*	65-90	750-850	2-5
	Reference value	75	800	2
P-CCS(HP)	*Range*	65-90	750-850	5-10
	Reference value	75	800	6

4.4 Results

4.4.1 Small size plants

The works has been published by the author in (Tjaden et al. 2014).

The performance of the system is evaluated first at baseline and then under varying operating conditions (as described above during the plant layout description), in order to validate and characterize the behavior of the established thermodynamic simulation model.

These values are applied to each reforming option, and the results are then compared. In all cases, the electric power output of the stack, operating temperature, and pressure (i.e., atmospheric) are constant.

Chosen decision variables are characterized below:

(1) **Steam-to-carbon ratio** and **lambda air ratio** are the amounts of reforming agents for POx and SR to be injected into the reformer in order to convert the methane into synthetic gas.

(2) **Internal reforming** determines the amount of gas reformed directly on the anode under steam reforming operation. The higher the amount of internal reformation, the smaller the amount of cooling air needed, which has positive effects on parasitic power demand.

(3) **Operating voltage** is the main parameter for running an SOFC plant under constant voltage operation. Varying V_{op} directly influences the amount of the produced irreversibilities in the SOFC and thus stack efficiency.

(4) **Fuel utilization** affects the productivity of the fuel cell for it indicates how much of the incoming fuel is processed in the fuel cell itself. Thus, FU directly impacts molar flow rate of fuel and the amount heat which is released in the afterburner.

(5) **Molar fraction of CH_4** in biogas underlies significant hourly and seasonal variations for which the flow rate of biogas has to be adapted adequately to supply a constant electric power output.

(6) **Molar fraction of N_2** in biogas depends on the amount of air injected into the digester to reduce H2S. As a consequence, biogas is diluted with a considerable amount of nitrogen, which is compensated by an increase in biogas flow rate. The upper boundary of 25 mol % is chosen in order to account for air leakages in the digester or in the tubing, as well as to account for imprecise air injection for sulfur reduction.

Net electric and total efficiency (electric plus thermal power supply) of the system are the most important thermodynamic parameters when analyzing the performance of an SOFC power plant. Both indicators allow a good interpretation of the performance of the system. Under base conditions, all efficiencies shown in this section are based on the higher heating value of entering biogas. In addition, the total active area of the stack is calculated as well. The reason for this is that overall installed active area of the stack connects thermodynamic parameters with investment costs: the larger the area of the stack, the more expensive the investment costs of the fuel cell.

Reforming options analysis

Table 30 shows the aforementioned performance indicators for each reforming option under baseline simulation conditions. Compared to electric efficiency values from gas engines, it is clear that all reforming options in the fuel cell system surpass the electric efficiency of ICEs by between 5 and 12 percentage points. Steam reforming offers the highest electric efficiency of 50.65% under base-case conditions.

Table 30. Baseline Simulation Results for SR, POx, and ATR. (Tjaden et al. 2014)

reforming option	A_{Act}	η_{el}	η_{tot}
steam reforming	11.35 m^2	50.65%	67.84%
partial oxidation reforming	9.09 m^2	40.62%	74.14%
autothermal reforming	10.62 m^2	38.82%	71.85%

This is around 10 percentage points higher compared to POx and approximately 12 percentage points higher compared to ATR. On the other hand, total plant efficiency for partial oxidation reforming is highest, amounting to 74.14%. High electric efficiency using SR is explained by the fact that in POx as well as ATR, a portion of the biogas is burned prior to feeding it into the SOFC. However, due to endothermic reforming reactions in the steam reformer, heat output is significantly lower compared to the other two reforming options. Under ATR, plant efficiencies are lower compared to POx, which is due to a large amount of CO_2 present in the biogas stream: the large amount of CO_2 present in biogas demands a large amount of heat in order to compensate endothermic dry reforming reactions to reach auto-thermal conditions. For this, a larger quantity of biogas has to be combusted compared to partial oxidation reforming, which reduces electric and total plant efficiency. Hereby, it has to be pointed out that no anode off-gas has to be recirculated as the amount of CO_2 in the biogas is large enough for ATR purposes. Looking at the stack active area, it is visible that under POx the smallest fuel cell area of 9.09 m^2 is needed.
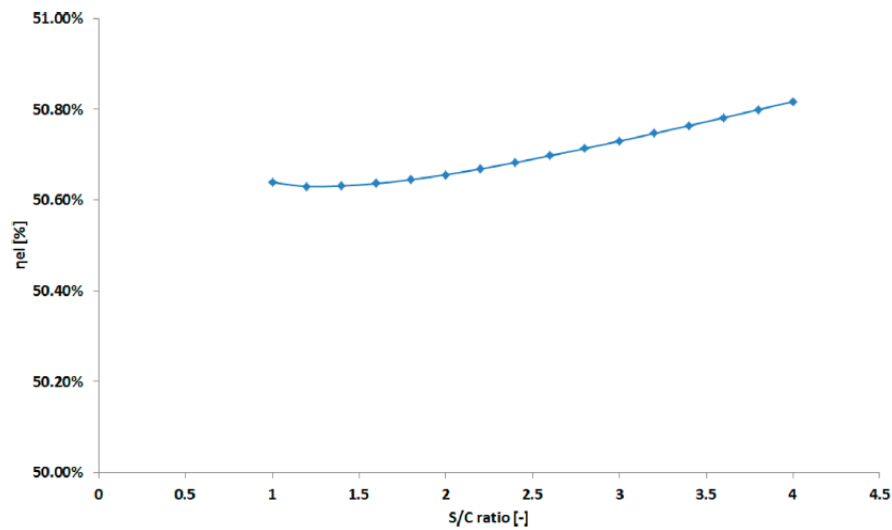
Figure 117. Electrical efficiency trend with S/C variation. (Tjaden et al. 2014)

Under steam reforming and auto-thermal reforming, needed stack area amounts to 11.35 and 10.62m^2, respectively. It can be inferred that the investment cost for a stack with a larger active area is more expensive, resulting in the lowest investment costs under POx.

In order to have a better understanding of the effects of S/C ratio and λ_{POx} on the system performance, a further sensitivity analysis is carried out by varying the ratios for POx and S/C ratio in the ranges of 0.1-0.6 for POx and 1-4 for S/C ratio. Figure 117 shows that by varying the S/C ratio, the electrical efficiency only increases slightly by approximately 0.2%. In relation to analyzing the sensitivity of the system to changes in λ_{POx}, Figure 118 shows that increasing the air flow rate into the reformer results in an increase in thermal power released from the reformer and an increase in hot water production. On the other hand, a drop in electrical efficiency is the direct consequence due to the combustion of biogas in the reformer. A final analysis related to the reforming modeling with the Aspen Plus® software is related to the choice of the reactor model for the partial oxidation simulation: in the analyzed model, the reformer can be modeled either through a stoichiometric reactor in which the POx reaction is predefined or through a Gibbs equilibrium reactor. Figure 119 shows the results of the reformer outlet composition with the two different reactors with a variable air ratio. Under base-case conditions ($\lambda POx = 0.25$), a relatively small difference between the two systems is observed, whereas, at the boundaries of the sensitivity analysis, differences are becoming more significant, which can be explained by different reactions simulated in the Gibbs reactor model.
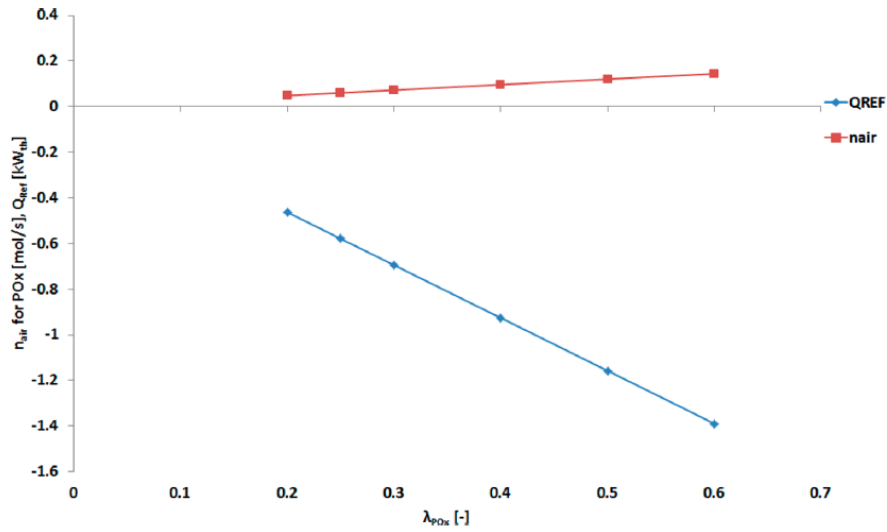
Figure 118. Reformer heat duty Q_{ref} and molar flow rate of air n_{air} for POx for varying λ_{POx}.
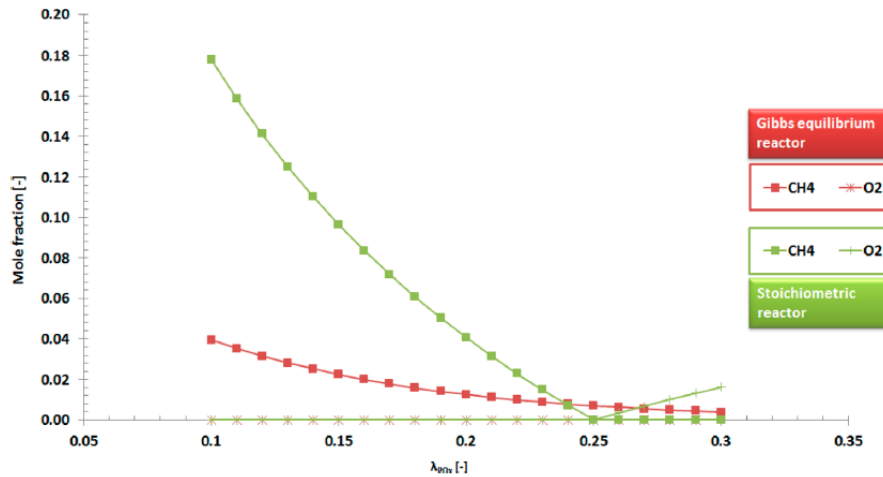
Figure 119. Reformate outlet gas composition for different reactor models.

Operating Voltage Sensitivity Analysis

The behaviour of performance indicators in the parametric study is qualitatively similar throughout each reforming option. Yet, quantitative differences are observed. The decreasing operating voltage from 0.8 to 0.7 V goes along with a decrease in electric efficiency and an increase in thermal efficiency under each reforming option. When operating voltage of the SOFC is increased to 0.85 V, the contrary is the case: lower overpotential generate less waste heat caused by irreversibilities in the stack, which decreases demand for cooling air, thus providing higher electric efficiencies. Consistently, the thermal power output of the plant decreases, leading to lower thermal efficiencies. Yet,

all three reforming options show that total plant efficiency for higher operating voltages increases as the amount of higher electric efficiency compensates decreasing thermal efficiency. Simulation results for varying V_{Op} are presented in Figure 120, which shows the increase and decrease in percentage points compared to results under base-case conditions. It is visible that steam reforming has a higher sensitivity toward varying operating voltage compared to partial oxidation and auto-thermal reforming. It is assumed that due to higher reforming efficiency of SR, response to voltage changes are of higher sensitivity. Development of electric efficiency of POx and ATR as a function of varying V_{Op} is of comparable extent.
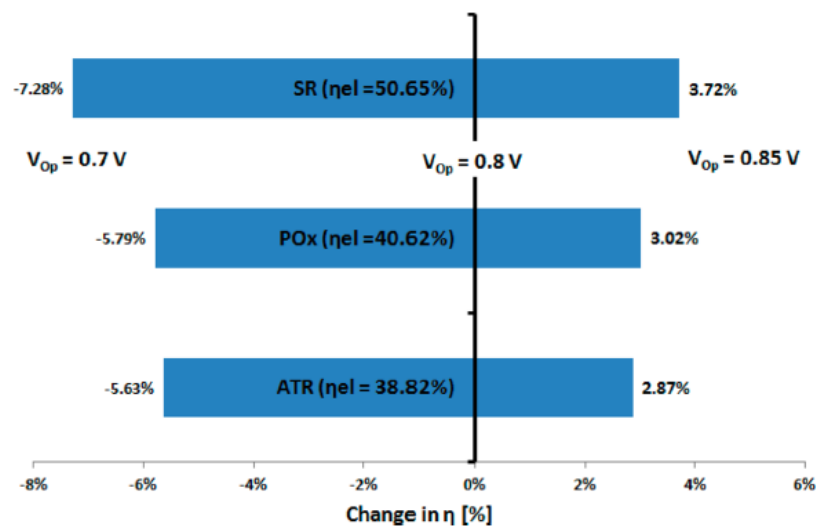
Figure 120. Change in η_{el} as a function of varying V_{Op}. (Tjaden et al. 2014)

Table 31. η_{el} and η_{tot} under Varying V_{Op}. (Tjaden et al. 2014)

| | η_{el} | | | η_{tot} | | |
| | V_{Op} | | | V_{Op} | | |
reforming option	0.7 V	0.8 V	0.85 V	0.7 V	0.8 V	0.85 V
steam reforming	43.36%	50.65%	54.37%	66.10%	67.84%	68.12%
partial oxidation reforming	34.83%	40.62%	43.63%	72.45%	74.14%	74.09%
autothermal reforming	33.18%	38.82%	41.69%	70.61%	71.85%	72.07%

FU Sensitivity Analysis

Manner and extent of variation in performance indicators under changing fuel utilization are comparable with simulation results under varying operating voltage: with higher fuel utilization, less fuel is needed for the same electric power output increasing η_{el}. However, the thermal power output of the plant and thus thermal efficiency decreases. In this case, the slope of decreasing thermal plant efficiency is more negative compared to the slope of increasing electric efficiency. Thus, total plant efficiency decreases. The reason for this is that, with higher FU, less fuel is burned in the afterburner, and therefore, less heat is provided by the system. Results for varying FU are presented in Figure 121 and

Table 32. Furthermore, it is apparent that η_{el} under SR shows the highest sensitivity toward varying fuel utilization. Likewise, POx and ATR show similar results under changing FU as under changing V_{Op}.
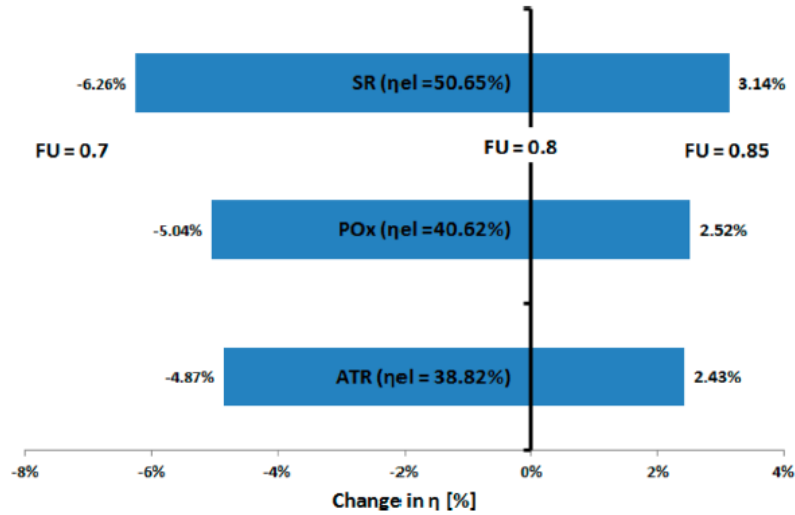
Figure 121. Change in η_{el} as a function of varying FU. (Tjaden et al. 2014)

Table 32. η_{el} and η_{tot} under Varying FU. (Tjaden et al. 2014)

| | η_{el} | | | η_{tot} | | |
| | FU | | | FU | | |
reforming option	0.7	0.8	0.85	0.7	0.8	0.85
steam reforming	44.39%	50.65%	53.78%	71.04%	67.84%	66.28%
partial oxidation reforming	35.58%	40.62%	43.14%	76.41%	74.14%	73.00%
autothermal reforming	33.95%	38.82%	41.25%	74.09%	71.85%	70.73%

Internal reforming ratio Sensitivity Analysis

Internal steam reforming (Int Ref) has positive effects on η_{tot} and, to a lesser extent, positive effects on η_{el}. Endothermic reforming reactions taking place in the anode decrease the amount of cooling air needed in the system. Also, as less heat is needed in the external reformer, a larger amount of thermal power can be provided in the form of hot water. Internal reforming is the only parameter which increases electric as well as thermal efficiency, as depicted in Figure 122.
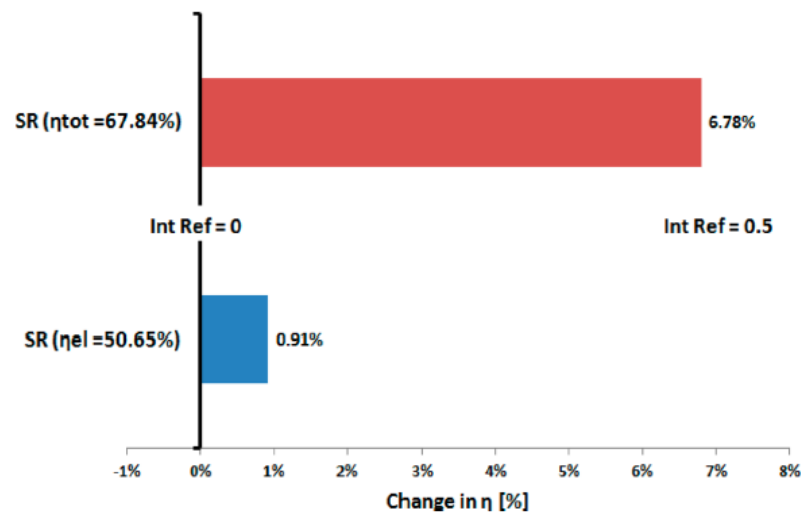
Figure 122. Change in η_{el} (blue) and η_{tot} (red) as a function of a varying degree of direct internal reforming within the SOFC. (Tjaden et al. 2014)

Biogas composition Sensitivity Analysis

Varying biogas composition does not have a large effect on electric as well as total efficiency compared to results in previous sections. Although the amount of overall biogas required must increase when its CH_4 content is lower, the demand for cooling air is reduced. A larger quantity of CO_2 and/or N_2 in the biogas, in fact, has a cooling effect on the stack. Consequently, the higher electric demand for the biogas blower is partly compensated by the smaller demand for cooling air (Figure 123). Connected to this, one peculiarity has to be pointed out: when increasing CH_4 fraction under ATR, the increase of electric and total efficiency is to a larger extent compared to the other two reforming options. The reason for this is that with a lower amount of CO_2 in the biogas stream, less dry reforming reactions are taking place, which in turn means that a smaller amount of biogas has to be combusted to reach auto-thermal conditions. As a result, a smaller amount of air is needed in the reformer. These interrelations have a large effect on the sensitivity of the electric and total efficiency under ATR. In addition, ATR also shows the highest sensitivity toward N2 dilution, as illustrated in Figure 124.
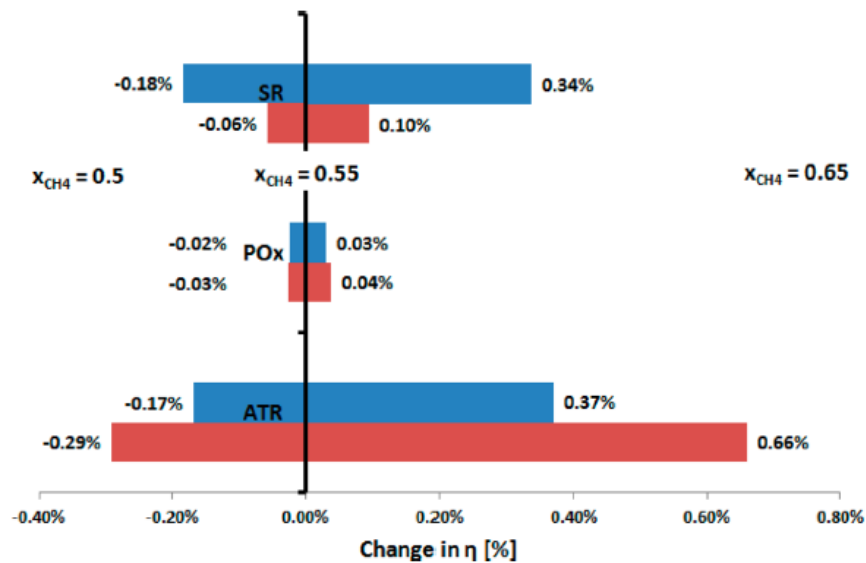
Figure 123. Change in η_{el} (blue) and η_{tot} (red) under varying x_{CH4} (Tjaden et al. 2014)

From a practical point of view, lower sensitivity to varying biogas composition is advantageous as the chemical build-up of biogas underlies significant seasonal as well as hourly variations, as outlined in sections above. As a result, to ensure stable power output and plant efficiency, steam reforming and partial oxidation reforming are more suitable for this area of application.

Coupled with the lowest electric efficiency and larger active area demand for the fuel cell stack compared to POx, auto-thermal reforming seems to be a less effective choice for converting biogas into synthetic gas for small-scale solid oxide fuel cell plants. The presented work contains only sensitivity analyses and not optimizations; even if the AspenPlus® software has the tool for running the optimization, they have not been included in the paper. In fact, looking at all the sensitivity graphs and tables, trends are monotonic increasing/decreasing, and thus, the optimal value is set on one of the sensitivity boundaries. Future work will then be related to multi-objective optimization in order to find the best set of parameters to achieve a maximum efficiency value.
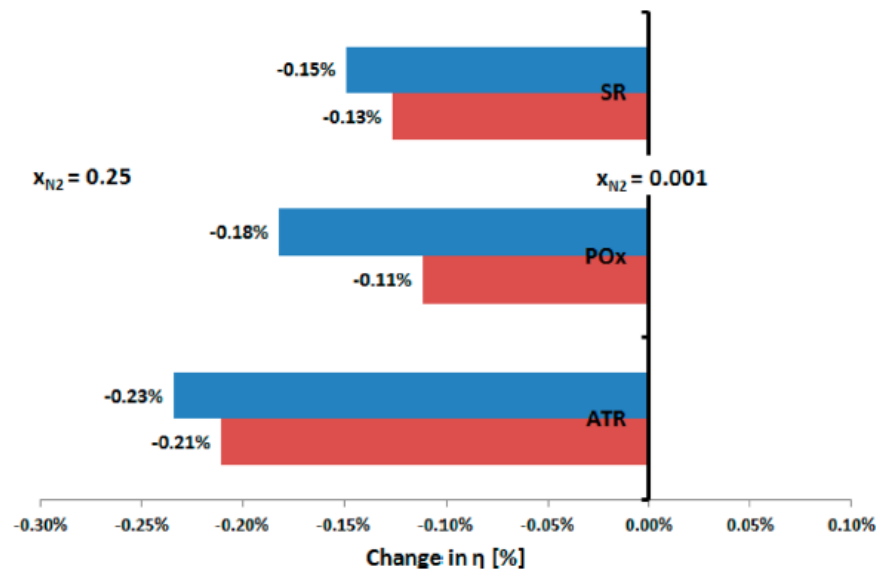
Figure 124. Change in η_{el} (blue) and η_{tot} (red) under varying x_{N2}. (Tjaden et al. 2014)

Economic analysis

Two main performance indicators are analyzed in this chapter: first, the total overnight cost of the system and second, the economic profitability in three European countries. Economic profitability is evaluated by means of net present value and payback period calculation using respective subsidy systems. In order to compare TOC for different plant configurations and operating scenarios, decision variables of the system are changed. The following three graphs show TOC for SR, POx, and ATR for base case conditions as well as for varying decision variables.
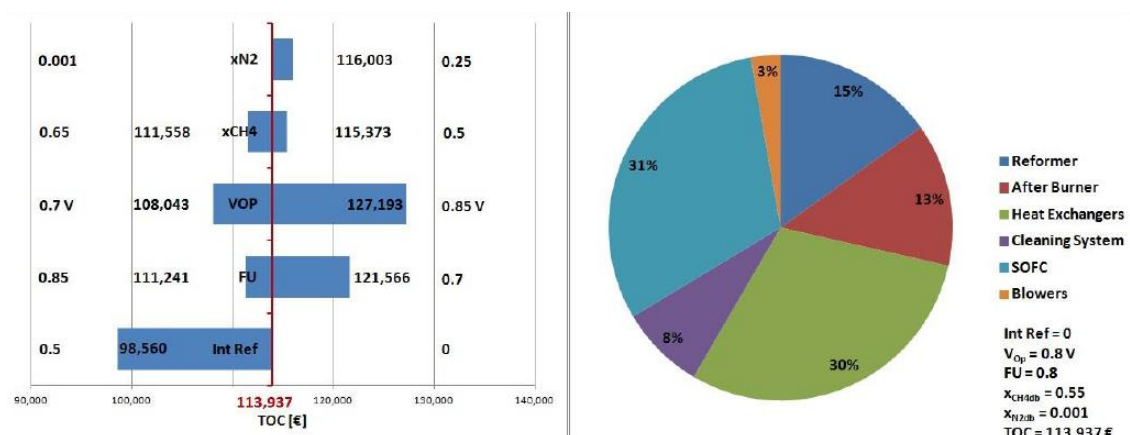
Figure 125. TOC and investment cost distribution for steam reforming.
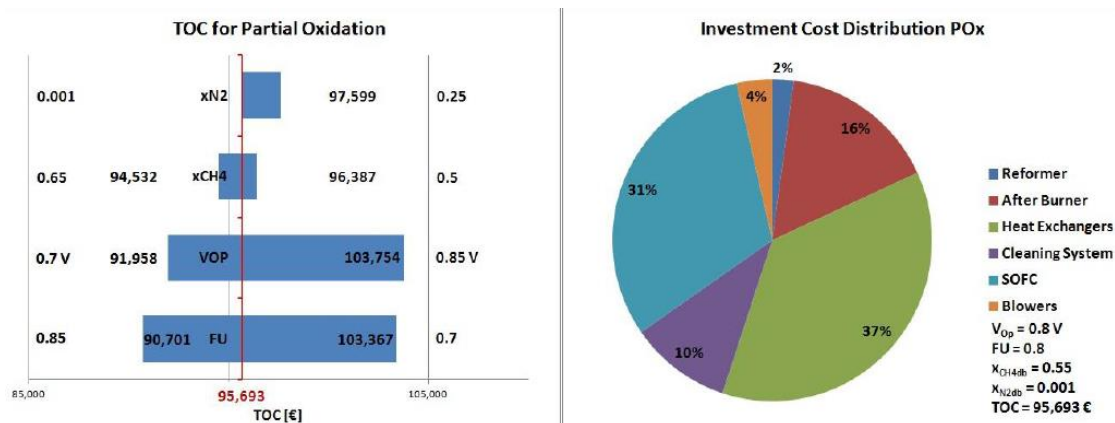
Figure 126. TOC and investment cost distribution for partial oxidation reforming.
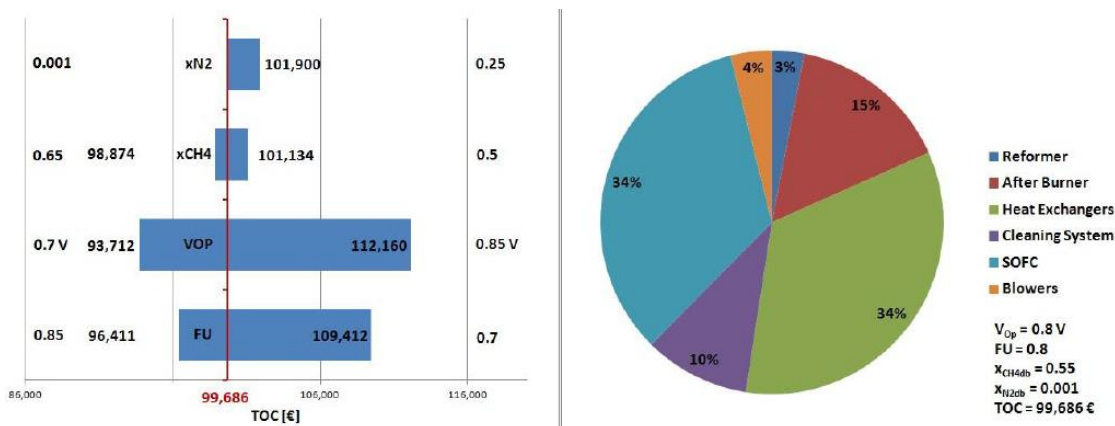
Figure 127. TOC and investment cost distribution for auto-thermal reforming.

It is visible that POx features lowest total overnight cost under base conditions compared to the other two system configurations. Hereby, TOC amounts to 95,693 € and thus, costs of POx lie in the order of 4,000 € and approximately 20,000 € below costs for ATR and SR, respectively. Specific investment costs (TOC divided by Stack price) amounts to 4,557 €/kWel, 3,828 €/kWel and 3,987 €/kWel for SR, POx, and ATR at base case conditions, respectively. It can already be stated, that ATR has lower electric efficiency and higher TOC than POx. Thus, ATR is an unfavorable option when using biogas fuel for SOFC plants from a thermodynamic as well as economic point of view. Again it is visible, that the cost development of all three reforming options under varying operating conditions is of a similar manner.

The figures show that the solid oxide fuel cell and heat exchangers are the most dominant cost items throughout all three reforming options. In addition, reformer cost for steam reforming is significantly higher compared to POx and ATR. This is explained by the sizing parameter used in the reformer cost function: as thermal heat duty is the sizing

parameter for the reformer, the absolute value of endothermic reforming reactions for SR (and parallel DR) are one order of magnitude larger compared to POx.

The three figures indicate that operating voltage and fuel utilization have a large influence on total overnight cost, which coincides with results of thermodynamic sensitivity analysis. A higher fuel utilization goes along with downscaling the afterburner and thus, decreasing component and system cost. On the other hand, an increase in operating voltage has a negative effect on the power density of the SOFC. As a consequence, more cells are needed in the stack to provide the same electric power increasing investment cost. In general, it can be stated, that by decreasing V_{Op} and thus, "sacrificing" electric efficiency, investment costs are reduced.

This makes clear, that the SOFC is the centrepiece of the system, from a thermodynamic as well as economic point of view. Therefore, the area specific resistance is decreased to analyze the effects on investment costs of the system by assuming, that in future development, cell manufacturers are providing an SOFC of lower resistance at the same cost. For this, ASR is reduced by 0.1 Ωcm^2 and 0.2 Ωcm^2. Figure 128 shows TOC and η_{el} for decreasing ASR. When reducing ASR, electric efficiency decreases only slightly. Yet, a decrease in TOC is observed. Both phenomena is explained by an increase in current density in the stack, resulting in a higher biogas flow rate (thus lower η_{el}) and higher power density (thus lower TOC).
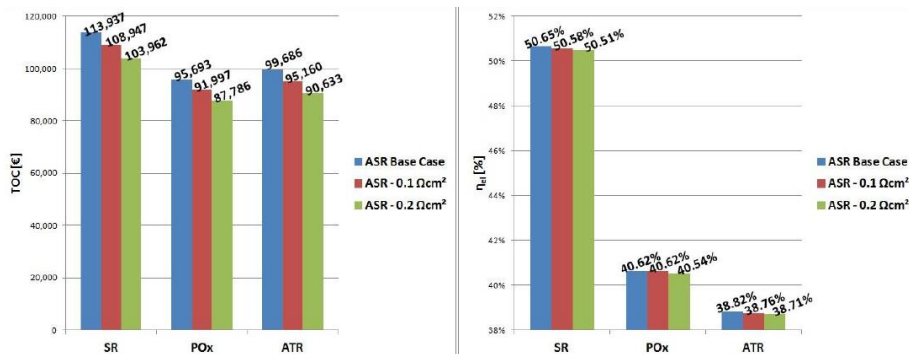
Figure 128. TOC and η_{el} for varying area specific resistance.

Applying the financial assumptions and subsidy schemes for Germany, Italy, and Finland, net present value and payback period for each reforming option under base case conditions is calculated. As in Finland, feed-in tariffs are paid 12 years compared to 20 years in the other two countries; a special finish case is introduced, indicated by Finland*. Hereby, it is assumed, that the feed-in tariff is granted for 20 years and a 40 % investment cost subsidy is paid. Table 33 shows calculation results of NPV and PBT estimation.

Table 33. NPV and PBT for base case scenarios.

Country	SR		POx		ATR	
	NPV [€]	PBP [y]	NPV [€]	PBP [y]	NPV [€]	PBP [y]
Germany	-21,019	-	4,165	17.0	-5,909	-
Italy	32,100	11.1	57,412	7.6	46,868	8.8
Finland	-117,844	-	-91,858	-	-101.839	-
Finland*	-25,922	-	-12,011	-	-19,149	-

It can be stated, that due to highest feed-in tariff provided by Italian subsidy law, all plant configurations are profitable generating positive NPV at the end of project lifetime. In this case, POx features lowest payback period of 7.6 years which is circa 3.5 years shorter compared to SR. Under German subsidy scheme, the project only breaks even after 17 years of operation when applying POx. Due to low subsidies and shorter payment period, a biogas fed SOFC system does seem economically feasible, even if subsidy duration is increased to 20 years and 40 % of investment cost is subsidized.

In addition to NPV and PBT analysis at base case configuration, the following three graphs show discounted cash flow statements for system configurations yielding highest η_{el} (left-hand side) and lowest TOC (right-hand side) for each reforming option. In all analyzed cases, net present values are positive under Italian feed-in tariff. Apart from that, low investment cost cases under SR and POx result in an economically viable project when the German supporting scheme is applied. Finally, Figure 129, Figure 130 and Figure 131 show, that neither Finish nor Finish* subsidies generate enough income to compensate investment and operating costs of the system. Beyond that, as soon as payment period of Finish feed-in tariff ceases, electricity grid prices provide a too little income resulting in a negative cash flow.

Cost functions used to estimate investment costs go along with uncertainties; a final economic sensitivity analysis is carried out at this stage of the report. For this, TOC is varied ± 10 % and NPV as well as PBT under base case conditions are compared with each other. Figure 132 shows NPV for base case conditions as well as varying investment costs. The graph only shows results for German and Italian cases, as within this economic analysis, no positive net present value is generated when using Finish subsidy laws. Values displayed at the bottom of bars with positive NPV indicate PBT in years. It is visible, that even when TOC is increased by 10 %, positive NPV are generated with Italian biogas subsidies. With German subsidies and a reduced TOC, only ATR breaks even compared to base case configuration, rendering SR an uneconomic option.
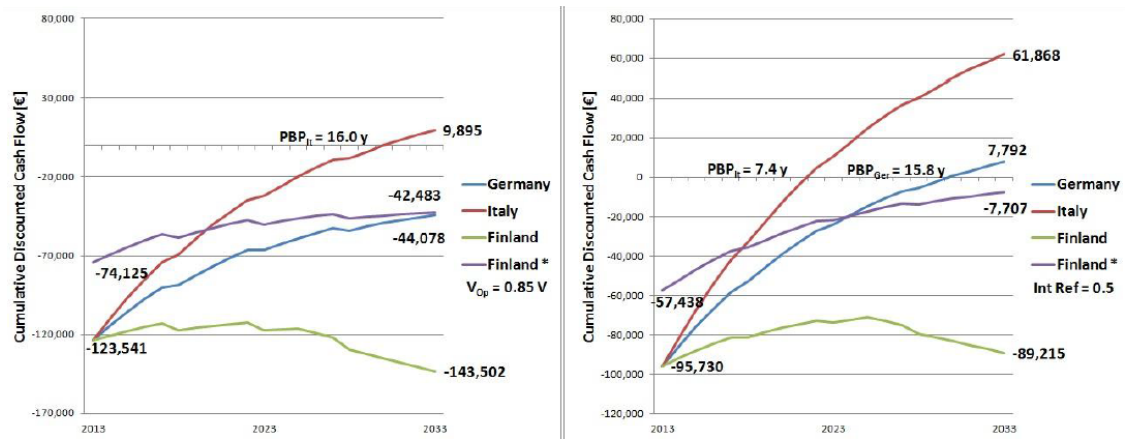
Figure 129. NPV and PBT for $V_{Op} = 0.85$ V and 50 % internal reforming under SR.
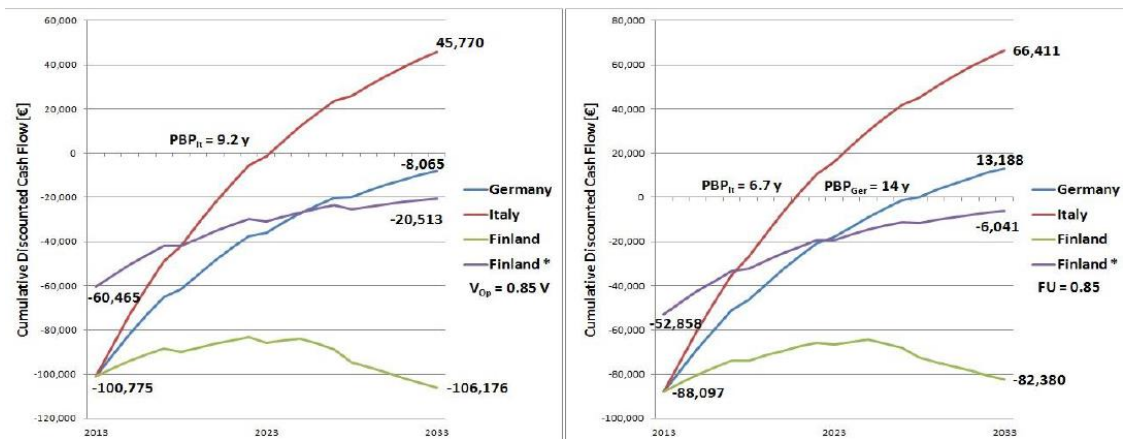
Figure 130. NPV and PBT for $V_{Op} = 0.85$ V and FU = 0.85 under Pox.
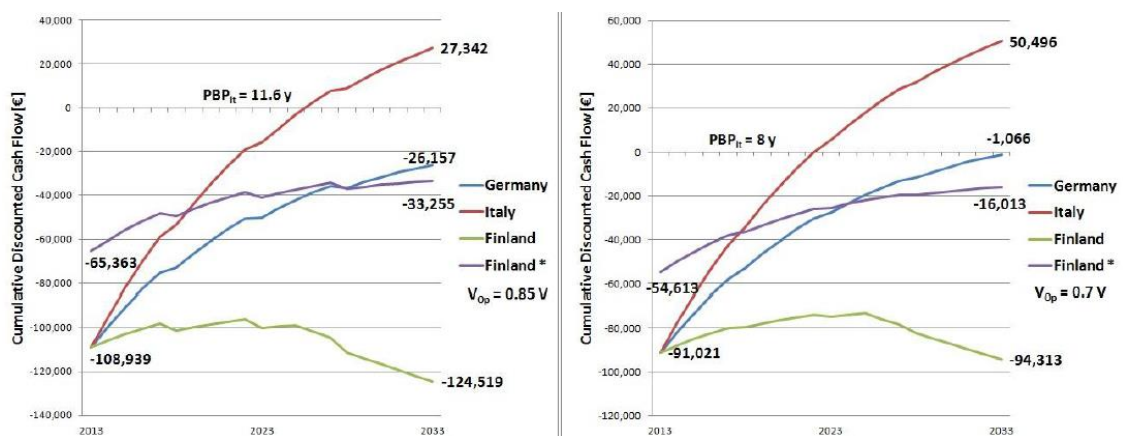
Figure 131. NPV and PBT for $V_{Op} = 0.85$ V and $V_{Op} = 0.7$ under ATR.
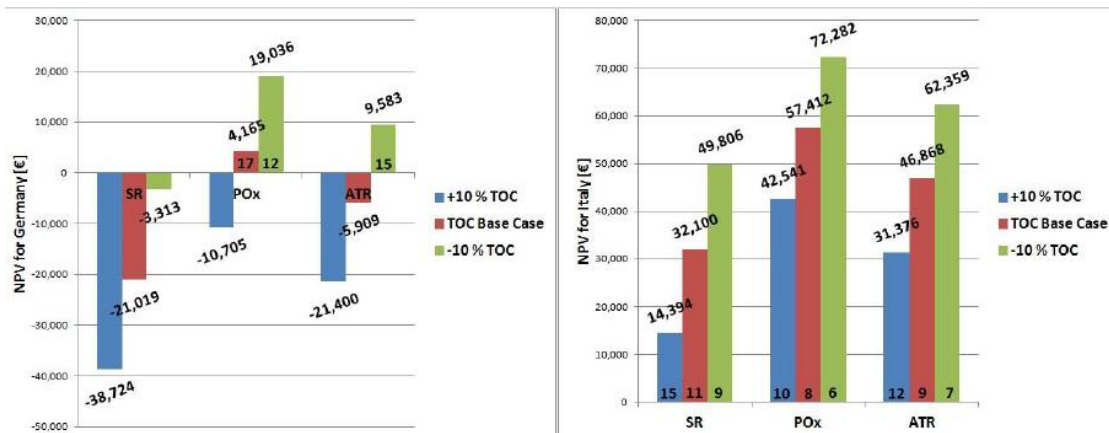
Figure 132. NPV and PBT for varying TOC for Germany and Italy.

As a summary, it can be stated, that POx offers lowest investment costs of approximately 95,000 €, undercutting ATR by around 4,000 € and SR by around 20,000 €. Comparison of German, Italian and Finish biogas subsidy mechanisms clearly show, that all system configurations analyzed in this project generate a positive NPV by applying Italian feed-in tariffs. In Germany, only POx is an economically feasible option at base case conditions. Finish laws do not provide a sufficiently high income for any system layout to break even.

4.4.2 Medium size plants

Partial results on medium size plants have been already published in (Gandiglio et al. 2013), where a detailed plant description and a first system analysis can be found. A 100 kW size plant was analyzed, but the AspenPlus® model and the Excel Economic Calculation File are 100% suitable for scaling-up and thus studies of larger sizes.

While the degradation model was no yet implemented in the small size plant, it is taken into account in the medium size analysis. The same Matlab® methodology develops for the Large size plants has been introduced in the excel file in order to account for the extra spare capacity. The lifetime of the SOFC was not a fixed value but was depending on the chosen degradation rate and the maximum allowable degradation. The resulting lifetime was 5 years, not far from the current industrial values (Table 34).

Figure 133 and Figure 134 show the trend of the installed active area per year (depending on the yearly spare capacity due to degradation and the replacement of the entire initial stack) and the cumulative curve of the same parameter.

Table 34. Degradation model input parameters.

Parameter	Value	Unit
Current density	0.450	A/cm^2
ASR	0.378	Ω cm^2
Area	277661	cm^2
Degradation rate	0.7%	% / 1000h
Maximum acceptable degradation	20%	
Chosen range (yearly hours approximated)	7000	h
Degradation on chosen range	4.9%	
Hours per year	7008	h
Lifetime stack	5	
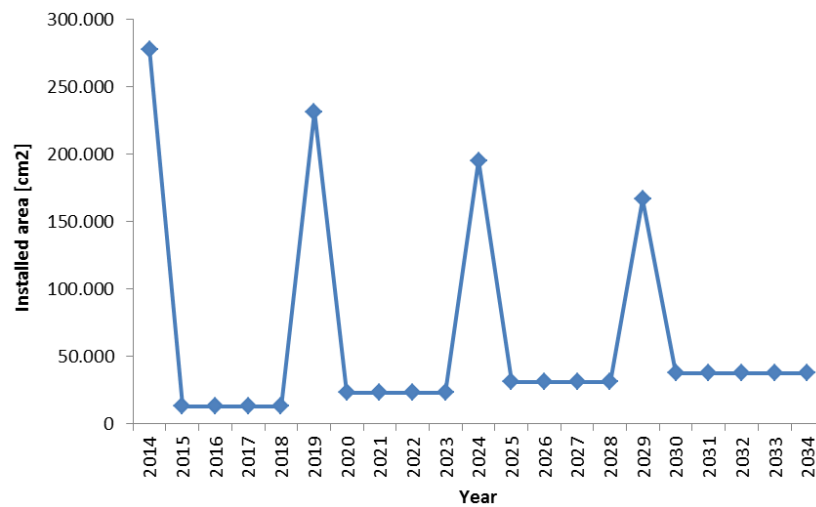
Figure 133. Installed extra active area per year.
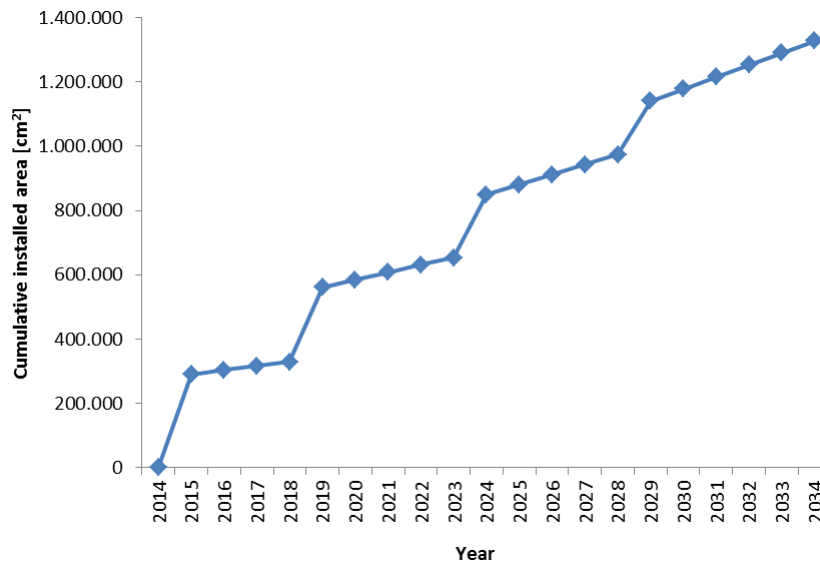
Figure 134. Cumulative installed active area.

Energy analysis

A first analysis has been carried out on the choice of carbon capture with a downstream CCS or CCU.

On Table 35 the results of the implemented electrochemical model developed starting from the one of Van Herle (Van Herle et al. 2003) and further updated, are shown. Values for ASR current density and the total active area can be seen: looking at literature data on ASR the resulting value is in line with target values from the producer. The total required active area, around 26 square meters for 100 kW, is the main input parameter for the SOFC stack cost calculation, as shown in the methodology section.

Table 35. Electrochemical model results.

Electrochemical model		
ASR	0.378	$\Omega \, cm^2$
Current density	0.450	A/cm^2
Total active area	27.76	m^2

Results for the CCS/CCU energy analysis are shown in Table 36. Here the values for efficiencies (electrical and thermal) can be found: the electrical efficiency shows a reduction moving from the non-CCS case to the CCU and finally to the CCS. This is due to the high power consumption of the CO_2 removal stage and the compression stage. Is the carbon separation stage, the oxygen production unit (PSA) and the water/gas pumps and compressors are the reason for the electrical efficiency decrease, and this can be seen both for CCS and CCU.

Table 36. Carbon capture energy results.

Parameter/Case study	NO CCS	CCS	CCU
Electrical Efficiency	57.23%	51.34%	53.54%
Thermal efficiency	26.91%	20.51%	20.51%
Total efficiency	84.14%	71.85%	74.05%
Total auxiliaries power consumption	3.34 kW	12.2 kW	8.4 kW

The compression stage is then the second reason for the efficiency reduction: this influence is obviously higher in the CCS case study where the carbon dioxide needs to be compressed up to 150 bar, while is reduced in the CCU scenario (CO_2 up to 11 bar). Figure 135 shows the share of the auxiliaries power consumption in the NO CCS and CCS case study.
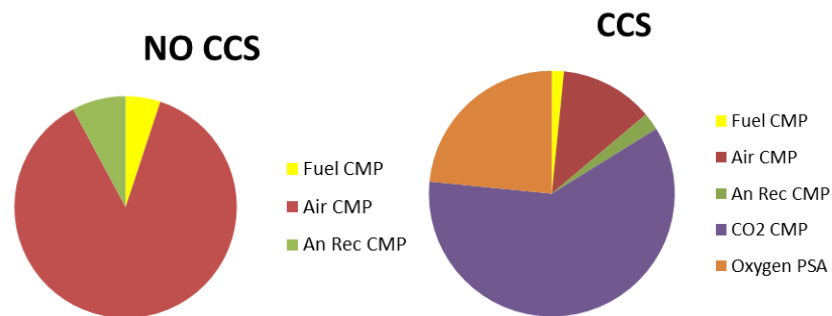
Figure 135. NO CCS and CCS case studies – auxiliaries power consumption.

Economic analysis

From an economic point of view, the energy disadvantage of the carbon capture scenario is confirmed, analyzing a scenario without a CO_2 carbon tax, as currently is.

The higher total system cost (BEC) is due again to the oxygen production unit (PSA), to the condenser and membrane stage and to the compression section.
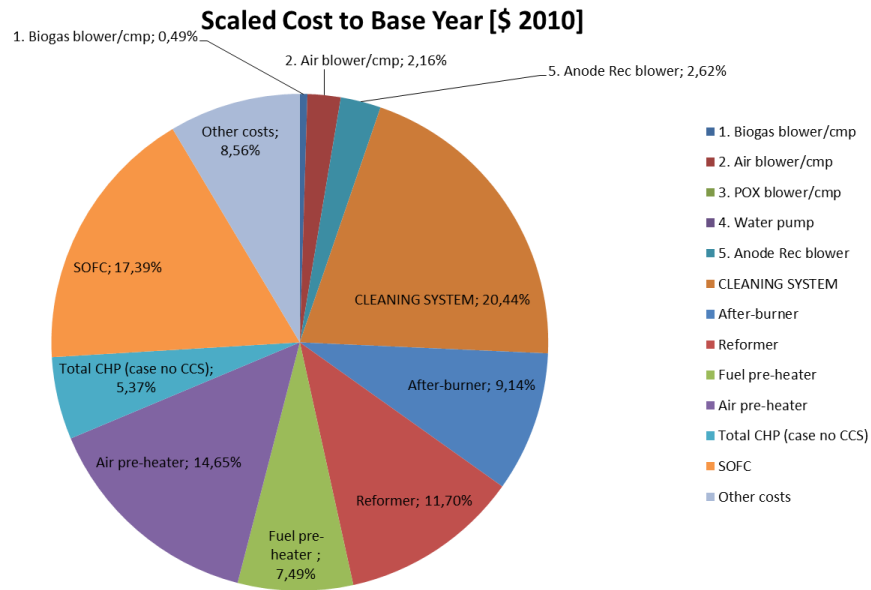
Figure 136. BEC ($243.496) share in the medium size plant - NO CSS scenario.
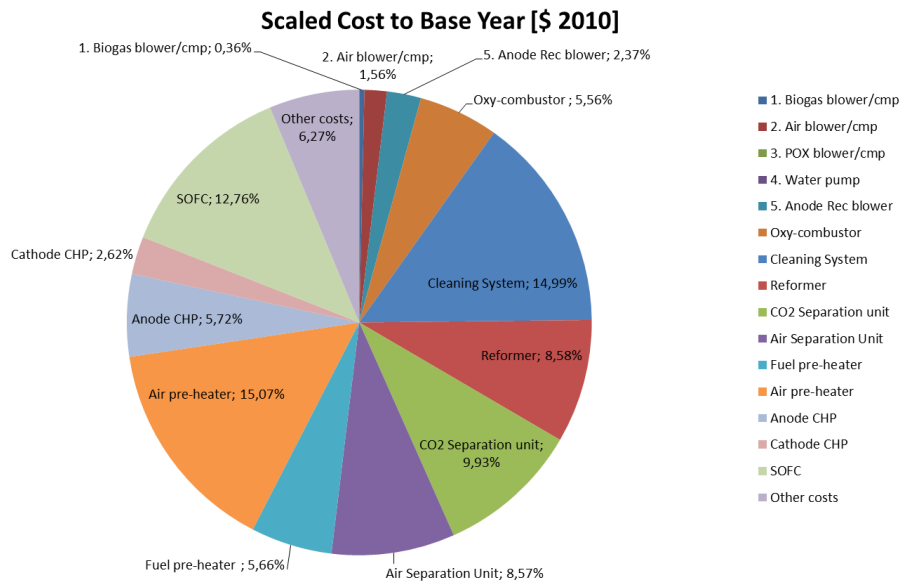
Figure 137. BEC ($331.991) share in the medium size plant - CCU scenario.

Scaled Cost to Base Year [$ 2010]
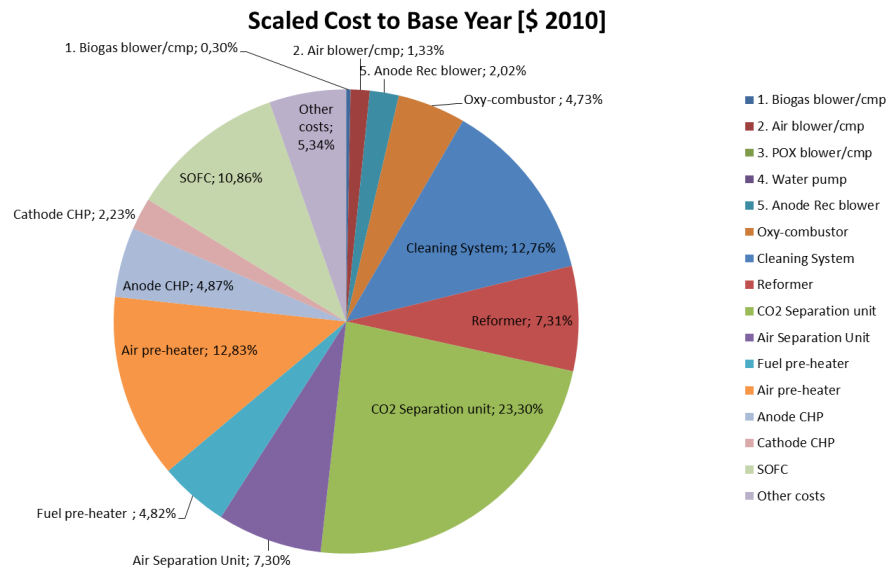
Figure 138. BEC ($389.886) share in the medium size plant - CCS scenario.

Figure 136, Figure 137 and Figure 138 show the BEC cost share between the different system components in the NO CCS, CCU and CCS scenario respectively.

In the first scenario without carbon capture the most important components in the TOC share are the SOFC (which cost is, as explained in the Methodology section, a target future cost quite low compared to current production costs), the cleaning unit (this is mainly depending on biogas type and impurities, a conservative hypothesis has been made), the reactors (reformer and burner) and the air pre-heater (the biggest between all the installed HX). The heat-exchanger network, summing all the heat-exchangers required, accounts for 27%, which is the highest contribution in the plant (see Figure 139). Moving from the first to the second and third scenario, the BEC and the percentages are completely different: the CCU BEC is 36% higher than the NO CCS BEC, and the CCS BEC is again 17% higher than the CCU BEC. Furthermore, looking at the costs share, the higher costs are now related to the CO_2 separation unit and two new costs not very low (5-10%) are now referred to oxy-combustor and PSA.

Plant Cost
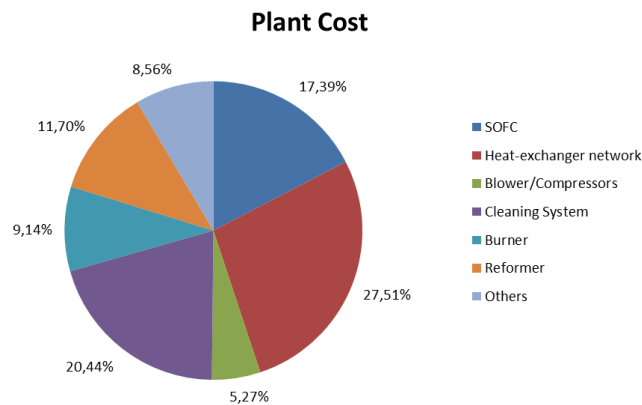
Figure 139. BEC share in NO CCS case.

The BEC cost is then increased with the related percentages about contingencies, engineering and construction costs in order to determine the TOC cost, considered as the real initial investment cost.

Thus, from an investment cost analysis, the carbon capture brings to a high increase of the initial investment which is not repaid with the current operating scenario. The yearly costs and incomes are determined from the operating costs and subsidy revenues + CHP savings (see Figure 140 referred to Italy, WWTP biogas). Yearly, summing the costs and the incomes, the results is thus positive consisting in profit for the plant; the situation is the same both for CCS or not scenarios.
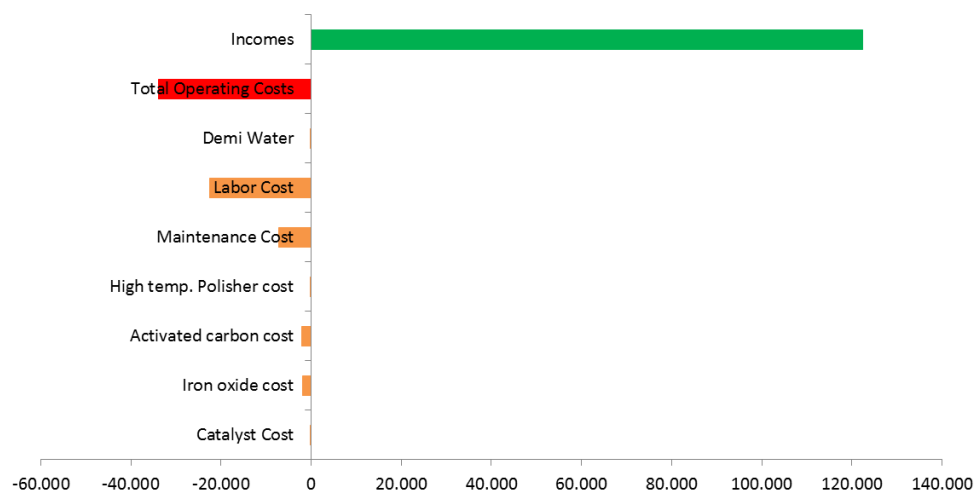
Figure 140. Operating costs.

The good profit achieved is mainly due to the fact that biogas is considered as a free gas in the plant: this hypothesis is always true in the case of biogas from landfills or WWTPs, while can change in case of agricultural plants. If the digester is only fed by waste, the fuel can be considered as free with some electrical/thermal requests for the digestion

process, but if the feeding is a crop, thus the fuel is not free but depends on the crops availability and life.

As will be seen soon in the cash flow, despite the quite good annual incomes, the high initial investment, coupled with a frequent replacement of the SOFC, does not let the cumulative money flow to be repaid very soon.

On Figure 141 a typical cash flow graph is presented. As discussed before, the annual difference between costs and incomes is always positive and can be seen from the blue positive bars, representing the annual profits. These bars are reducing during the years because of the depreciation approach: the WACC chosen value has thus a strong influence on the final results. What is interesting to see from an investor point of view is the cumulative cash flow which points out the PBT and the end of live NPV. The first value is the time in which the initial investment is repaid and here is equal to 8 years, while the second is the amount of money achieved at the end of the plant lifetime, here around 150'000 €.
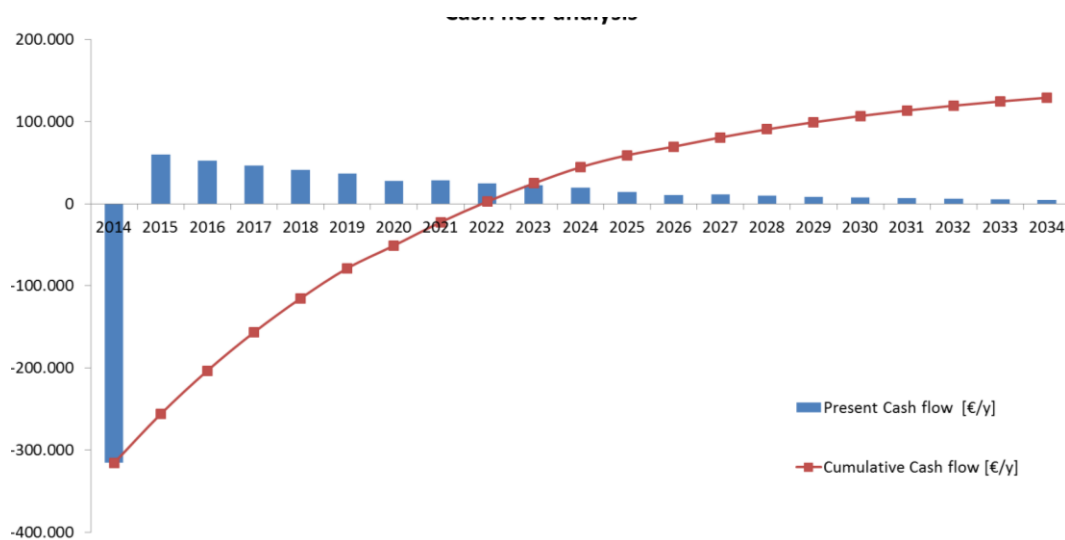
Figure 141.Typical cash flow trend.

Analyzing, for example, the Italian scenario, as can be seen on "Appendix 4 – Economic analysis: functions, cost of biogas and subsidies" (section "A4.3 Subsidy scheme analysis") the subsidies are strongly dependent on the biogas substrate and, for some of them, special bonus for CHP or for nitrogen recovery are issued.

The first analysis is, analyzing only the NO CCS scenario, related to the biogas substrate. As can be seen in Figure 142, the difference between the possible biogas substrates is a very important parameter since it influences the incomes and thus the PBT of the investment. Payback times moves from around 9-10 years in the case of WWTP to

3 years in the case of the biological substrate (agricultural or food industry). In general, biological substrates are mote evaluated than WWTP and landfill biogas. The reason for this is quite unknown and not well justified from the real current scenario: biogas production from landfill and especially from WWTP is an unavoidable process, and fuel is produced by a 100% waste which should be treated anyway. On the other side, agricultural substrates can include food industry waste, animal manure and crops waste which are actually wastes but also energy crops, which use for fuel production brings to the discussion.
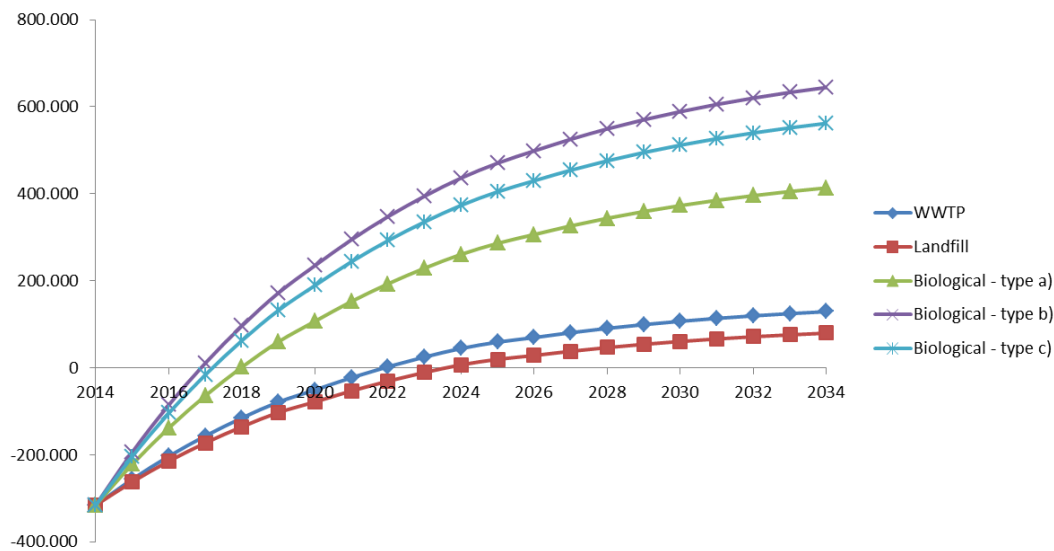
Figure 142. Analysis of different biogas substrates and subsidies – Italy – NO CCS.

Moving from South EU (Italy) to North EU (Finland) it is possible to analyse the Finnish subsidy scheme which is very simple and not depending on the biogas substrate. In Northern countries, the high biomass production is related to wood, and it is usually burned for heat/electricity production. This could be seen as the main reason for such a simple subsidy scheme. Results bring to 13 years PBT, not so desirable from the industrial market (see Figure 143).
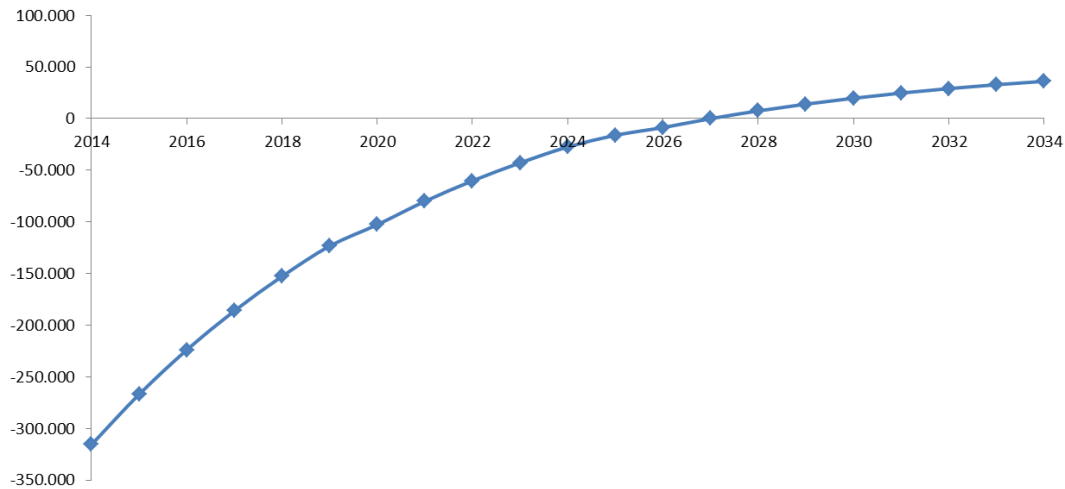
Figure 143. Analysis of biogas subsidy schemes – Finland – NO CCS.
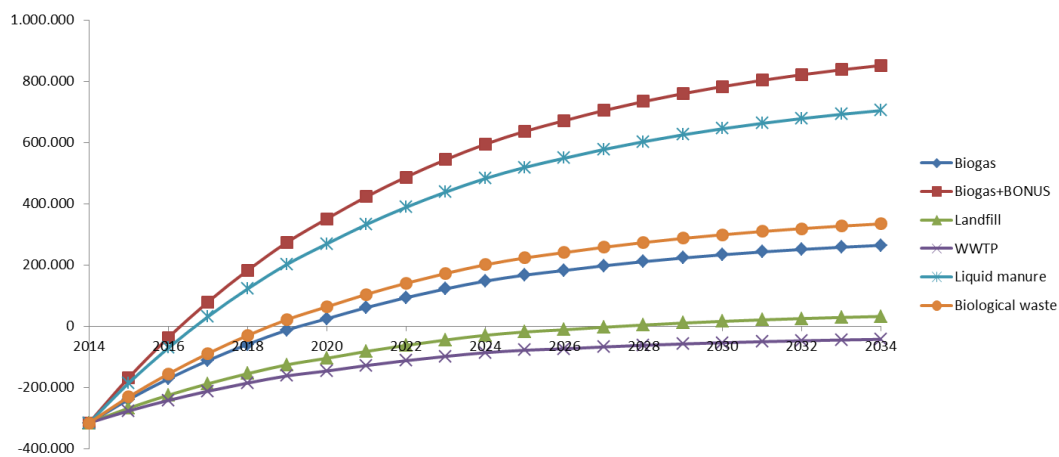
Figure 144. Analysis of biogas subsidy schemes – Germany – NO CCS.

The same analysis on biogas substrates can be done for the Central EU (Germany), and results are shown in Figure 144. On the same line of Italy, also in Germany biological and agricultural substrates are preferable and can access to higher subsidies, while landfill gas and WWTP are still lower than Italian values and PBT results are not acceptable for the industrial market. PBT values move from 2 years for agricultural biogas with a bonus to a too high value (higher than the plant lifetime) for WWTP.

Starting from the subsidy analysis in the different EU countries for the NO CSS scenario, the analysis can be enlarged to the CCU/CCS case study. Figure 145 summarizes the results for Italy analyzing biogas from biological products and WWTP: as can be seen from the graph, WWTP is not any more profitable when carbon capture is performed, while results were still good in the previous NO CCS case.

On the contrary, plants fed with biogas from the biological substrate is still convenient also when carbon capture is performed, because of the very high subsidies given.

Even if results for Finland and Germany are not shown, the behavior will be the same see before with an increase in the initial investment (curves are thus moved down in the graphs): for Finland, the situation was not profitable already with NO CCS, and so it will be worst for carbon capture. For Germany the behavior will be the same as for Italy: acceptable/good PBT for biogas from biological/agricultural substrates and too low PBR for WWTP and landfill gases.
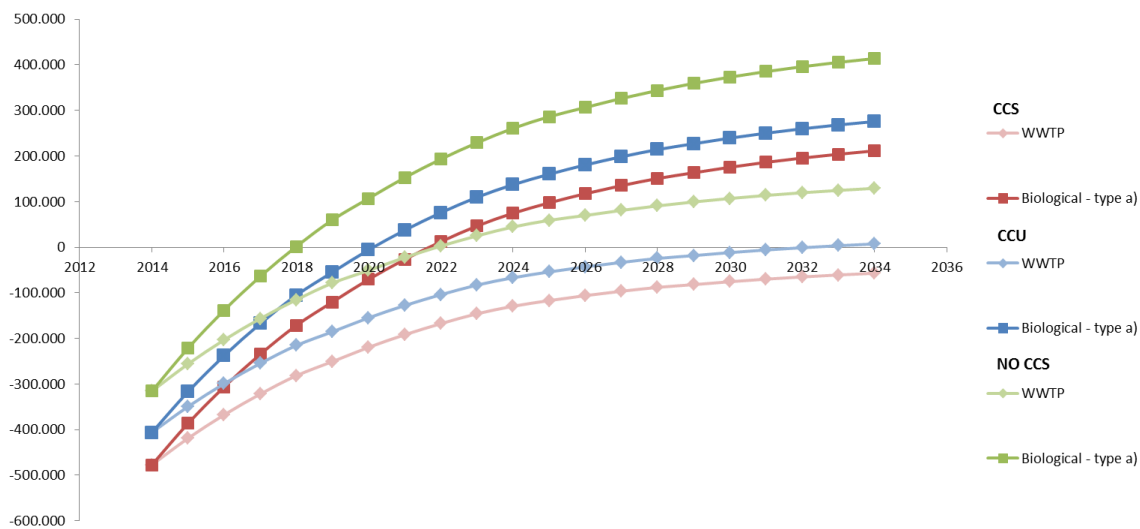
Figure 145. Analysis of carbon capture profitability – Italian Scenario.

Other analysis on Medium Size Plants

Further analyses have been developed on medium size plants, and some of their results will be presented below.

The first analysis was referred to the internal reforming ratio. As can be seen from Figure 146, internal reforming has a positive effect on the electrical and total efficiency: since part of the heat produced in the SOFC is used directly for the reforming reaction, the amount of air is reduced and thus the air compressor power consumption, which is the highest voice in the auxiliaries share (Figure 147). This brings to a positive effect on the electrical, and thus total, efficiency.
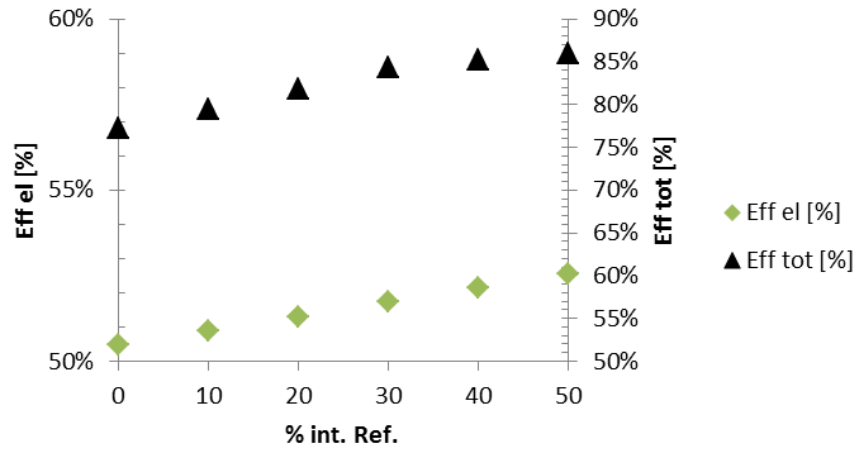
Figure 146. Internal reforming analysis.
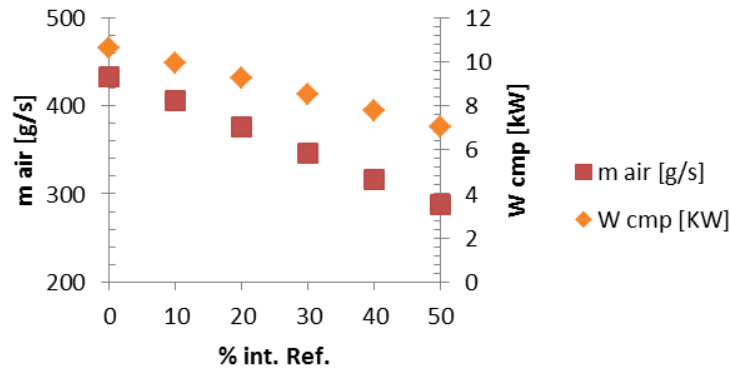
Figure 147. Variation of air flow rate and air compressor consumption with internal reforming ratio.

The maximum limit of 50% of internal reforming was chosen after internal communication with SOFC producers, taking into account that a too high ratio could lead to thermal discontinuity at the SOFC entrance with related electrochemical problems and instabilities.

On Figure 148 a graph on FU analysis can be seen: the reason for this analysis was to show that the electrical efficiency increase with FU tends to be reduced with higher FU, and a horizontal asymptote can be seen. This is the reason why working at high FU up to 85-90% brings to a positive effect on the system, but the choice to develop a too complex system to reach values near 100% is not justified by the energy results. The technical and economic cost for this system development is indeed higher than the earning in terms of efficiency.
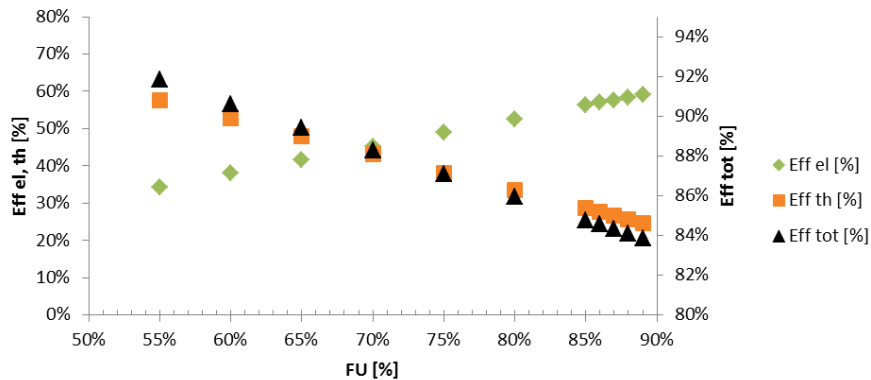
Figure 148. FU analysis.

4.4.3 Large size plants

The works has been published by the author in (Curletti et al. 2015).

Matlab model definition using OSMOSE

All the investigated power plant configurations include a heat exchanger network designed in order to achieve the highest internal energy recovery. The heaters and coolers were not connected in the AspenPlus® model, and the Pinch analysis was developed later in the OSMOSE run to define the composite curves of the plant. The definition of the number of heat exchangers and their physical location in the plant layout requires the implementation of a more sophisticated process that was not performed. Furthermore, sensitivity analysis and MOO could not be made easily with this software.

For these reasons, OSMOSE has been here adopted to provide an interface between Matlab and Aspen Plus®. This tool was then used to implement a method for the construction of a proper heat exchanger network and to perform both sensitivity analysis and MOOs.

The simulations performed are referred to the variation of the following design variables:

- Fuel Utilization Factor (*FU*)
- Operating temperature (T_{SOFC})
- Operating pressure (p_{SOFC})

For the sensitivity and multi-objective optimization (MOO) analysis, an operating range and a reference value for each variable were defined. The feasibility and performance of each configuration are evaluated by the evolution of both technical and economic performance parameters:

- Area Specific Resistance (*ASR*)
- Global Electrical Efficiency (η_{el})
- Net Present Value (*NPV*)

The ASR incorporates the voltage losses due to activation, ohmic and diffusion phenomena. The performance of an integrated SOFC power plant is strongly affected by the conversion efficiency of the stack, and so it is interesting to understand how the variations of the design variables influence the ASR.

Technical performance parameter

The Area Specific Resistance (*ASR*) is the first performance parameter whose behavior is interesting to observe, since, as already seen before, this quantity is related to the degradation effects in the stack over the time and thus it affects the management and replacement of spare capacity.

Figure 149 and Figure 150 show the variations of the *ASR* with respect to the Fuel Utilization, the operating temperature, and the operating pressure.
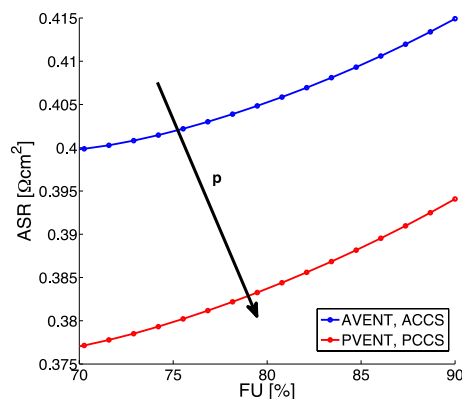
Figure 149. Influence of FU on ASR.

In a fuel cell, when the fuel utilization increases, a higher concentration of H_2 and O_2 is consumed in the cell resulting in more diluted reactants at the electrode. As a consequence, the reversible voltage decreases because of the decreased concentration of the reactants. This also negatively affects the activation kinetics while does not influence sensibly ohmic and diffusion polarizations: the corresponding effect is an increase of the *ASR* and, in Figure 149, this effect is represented.

The operating temperature instead affects the ASR positively because faster electrochemical and reduced resistivity of the ion-conduction electrolyte results in lower stack polarization (as shown in Figure 150).
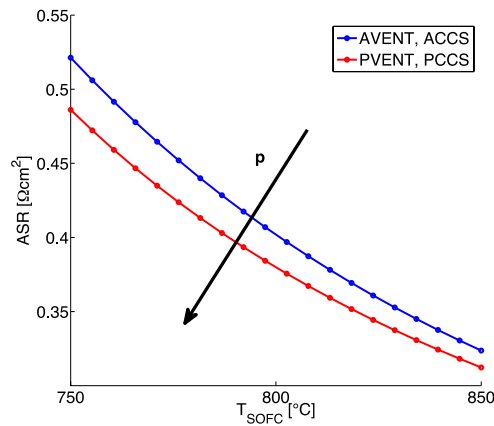
Figure 150. Influence of T_{SOFC} on ASR.

The pressurization of the stack produces an overall increase of the activation kinetics again so that higher operating pressures allow the presence of faster electrochemical reactions: this is the reason why, at the same operating conditions, the *ASR* is lower at pressures higher than the atmospheric one.

This last effect can be observed in both Figure 149 and Figure 150, where the results of the pressurized configurations have trends similar to those atmospheric but are shifted toward lower values.

The global effects of the variation of the three design variables on the technical performance are evaluated through the global electrical efficiency ($\eta_{el,}$).Figure 151, Figure 152 and Figure 153 show the behaviours of $\eta_{el,}$ in respect to *FU*, T_{SOFC} and p_{SOFC}.
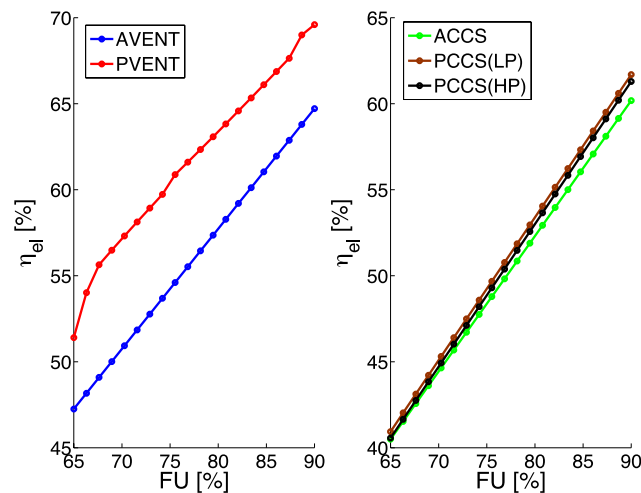
Figure 151. Influence of FU on the plant electrical efficiency η_{el}.
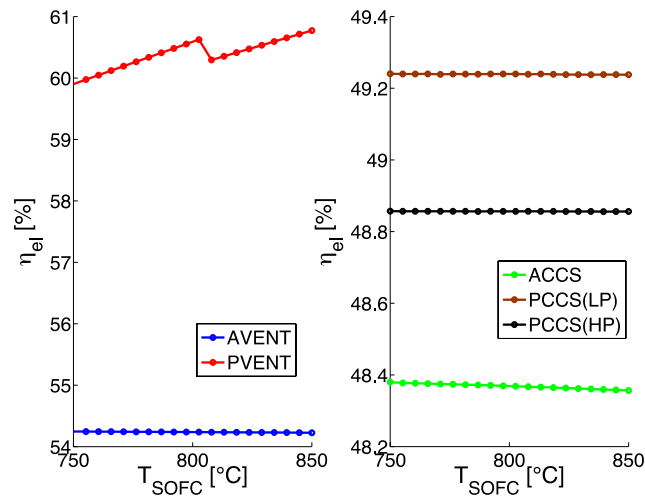
Figure 152. Influence of TSOFC on η_{el}.

The definition of the electrical efficiency shows its dependency essentially on two factors: the net electrical power delivered to the grid and the total fuel consumption. The pressurized configurations are able to achieve higher efficiencies than the atmospheric ones essentially because of the production of additional electrical power in gas turbines or expanders. On the other hand, the extra energy consumption required by the CCS system are so high that the positive effect of the pressurization becomes negligible and then the efficiencies of pressurized plants with CCS are much lower than those atmospheric cases without CO_2 capture. These two aspects are shown in both Figure 151 and Figure 152.

With respect to *FU*, the consumption of fuel decreases very rapidly (see Figure 154) as higher values of *FU* are attained. This behavior influences strongly the evolution of the net electrical efficiency of each plant, which, as a consequence, tends to increase rapidly. As shown in Figure 151, the efficiency varies strongly inside the sensitivity range selected for *FU*: this aspect suggests that this design variable has to be chosen properly during the design of an integrated SOFC power plant.
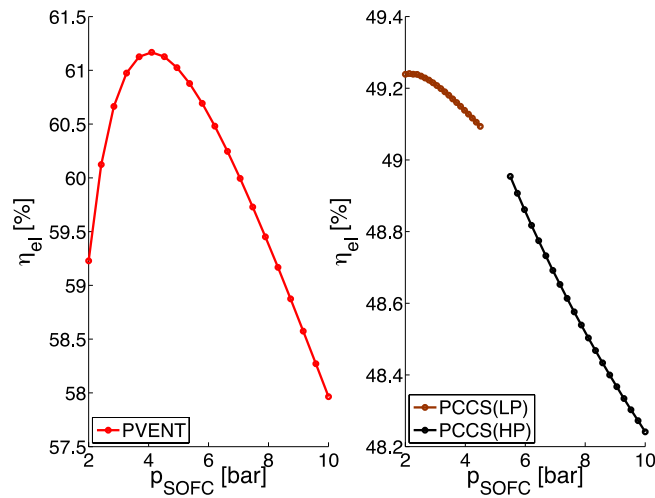
Figure 153. Influence of p$_{SOFC}$ on η$_{el}$.
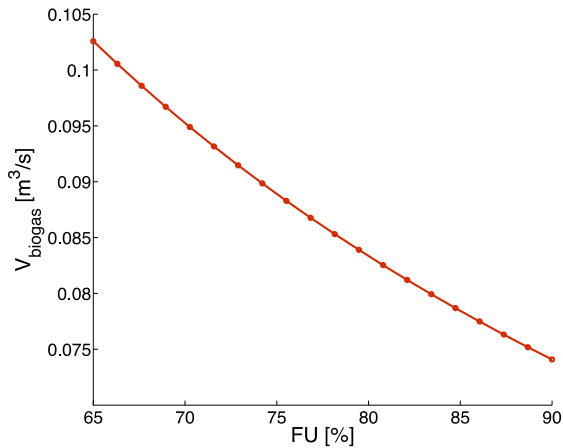
Figure 154. Influence of FU on V$_{biogas}$.

The temperature inside the stack of SOFCs does not affect at all the fuel consumption, and it also has a quite negligible influence on the electrical power required by auxiliary devices. Thus, the global electrical efficiency (Figure 152) is not influenced by this design variable, and inside the sensitivity range, it keeps a nearly constant value. This trend is a direct consequence of the choice made about the imposed constant operation strategy of the SOFC that results in a constant SOFC stack electrical efficiency. The temperature will, on the other hand, influence the economic results (as will be shown in the dedicated paragraph) because the variation of the *ASR* produces a variation of the current density that affects the total active surface required to operate at the constant current imposed.

Figure 155 shows, as example, the evolution of the net electrical power W_{el} sent to the grid with the temperature for the P-VENT configuration: although the variation of power

is not strong, it has the same trend of the efficiency, and this is a consequence of the fact that the consumptions are not influenced by the temperature.
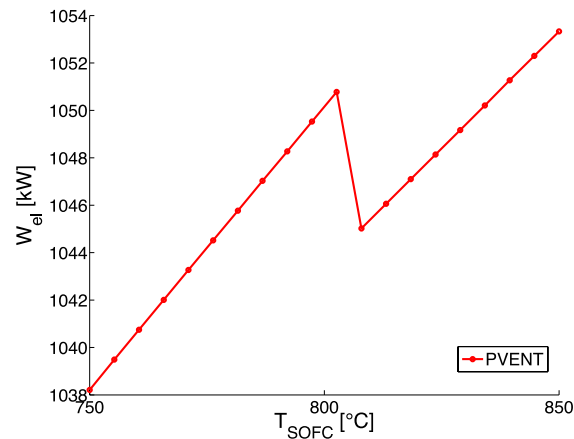
Figure 155. Influence of T_{SOFC} on the net electrical power produced (P-VENT).

The discontinuity point located at 800°C can be explained by the analysis of the electrical power produced by the gas turbine, shown in Figure 156 with the global consumptions of the auxiliary device. This strong variation of power produced is caused by a reduction of the Turbine Inlet Temperature (*TIT*) due to the water injection which occurs inside the after-burner: as already described in the chapter dedicated to the systems layout, the injection of water in the after-burner is required when a temperature higher than 900°C is achieved inside it and, as shown in Figure 157, this condition is reached at SOFC operating temperatures higher than 808°C.
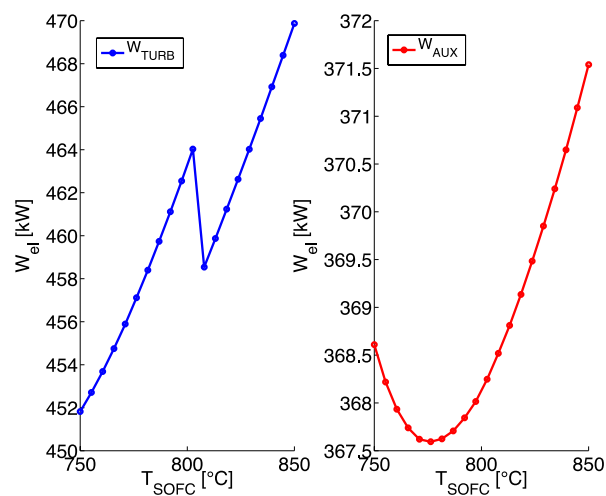
Figure 156. Influence of T_{SOFC} on the electrical power produced by the gas turbine and on the electrical consumption of auxiliaries (P-VENT).
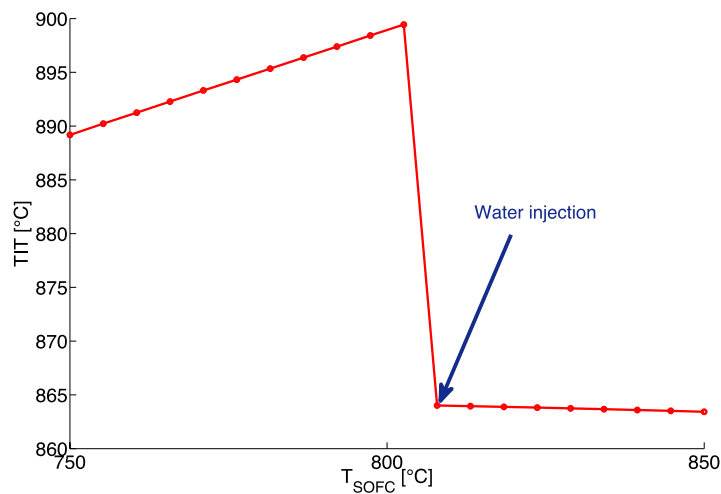
Figure 157. Influence of T_{SOFC} on the Turbine Inlet Temperature (TIT).

The inside pressure of the stack does not influence the fuel consumptions for the same reasons described before and related to the regulation logic adopted, but it has a higher influence on the power consumptions than the one seen for the temperature. Again, the trends of the global electrical efficiency are similar to those of the net electric power sent to the grid (Figure 158), and for both of them, it is possible to identify maximum points located at low-pressure values (e.g. 4.1 bar for P-VENT and 2.4 bar for P-CCS).

As already seen, in the pressurized configurations the production of power occurs in the fuel cells and in the gas turbine, but this last component is used to feed also the auxiliary devices. The maximum point in the efficiency curve corresponds to a situation where the production of the electrical power in the gas turbine does not increase as fast as the electrical consumptions.
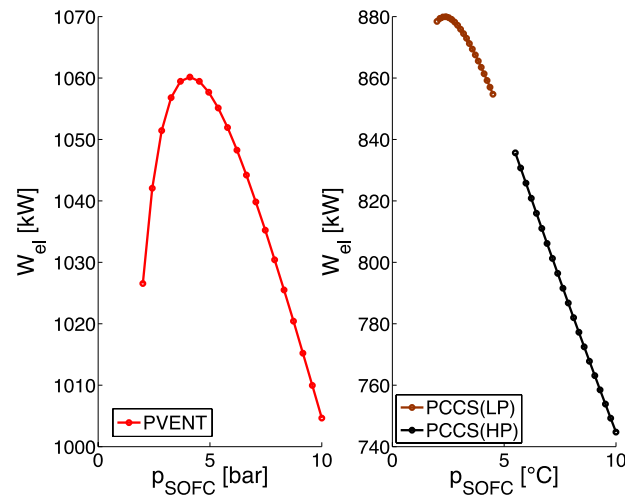
Figure 158. Influence of p_{SOFC} on $W_{el.}$

Figure 159 shows the power production in the gas turbine and the electrical consumptions referred to the P-VENT configuration. It is interesting to note that, from the pressure point where the maximum productivity is achieved (dashed line), the W_{TURB} tends to increase slower than W_{AUX}, while before this point it is faster.

Maximum efficiencies require low operating pressures both for the configuration with and without CCS and, in this second case, the configuration designed for low operating pressures (P-CCSLP) can achieve higher efficiencies than the one designed for high operating pressures (P-CCSHP).

However the variation depending on this design variable is not as strong as the one seen with the *FU*: in fact, in the pressure range simulated, the efficiency can increase not more than 2-3% while with FU slopes of 15-20% were seen.
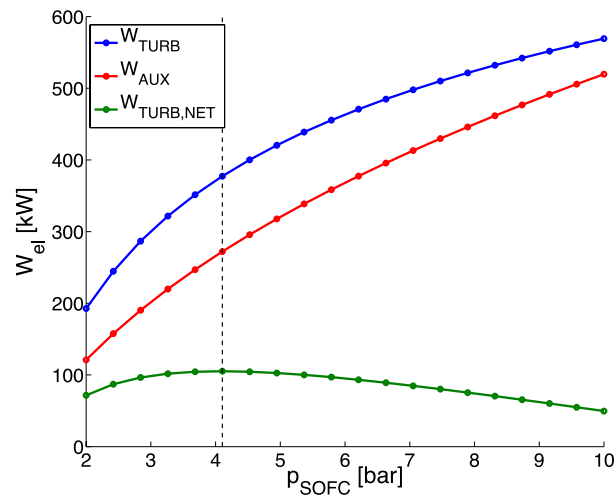
Figure 159. Influence of p_{SOFC} on the electrical power produced by the gas turbine and on the electrical consumptions.

Economic performance parameter

In this section, the main economic results of the investigated plants are shown.

Figure 160, Figure 161 and Figure 162 show the trends of the Net Present Value (NPV) with respect to the three selected design variables while the number of years required to recover the initial capital investment is given in Table 37.

The NPV evaluated at end life depends, as already seen, on many factors correlated to the initial investment and to the annual costs and profits.

During the definition of the economic hypothesis adopted, it was assumed a null cost of the fuel due to the fact that it is produced as waste material (sub-product) in a WTTP. The whole economic analysis has been strongly influenced by this assumption, and its effects are evident especially in the trend of *NPV* with respect to the *FU* (Figure 160). Increasing the *FU*, the system is able to work with a lower consumption of fuel. From a technical point of view, this corresponds to an improvement of the system, however from an economic point of view, there are no real monetary savings. Furthermore, the initial investment has more impact on the final earnings than the annual costs and profits: in fact, although increasing the *FU,* it is possible to decrease the electric consumptions and send more power to the grid, the variations in the initial investment have a bigger impact on the *NPV*.

The effects that can be seen are that the *NPV* has a maximum point at low values of *FU* (around 65-70%) and that the economic convenience decreases with this design variable.

The main Bare Erected Costs (BEC) that affect the initial investment and, consequently, the *NPV* are those of the stack of SOFCs (BEC_{SOFC}) and of the heat exchanger network ($BEC_{Heat\ exchanger\ network}$).
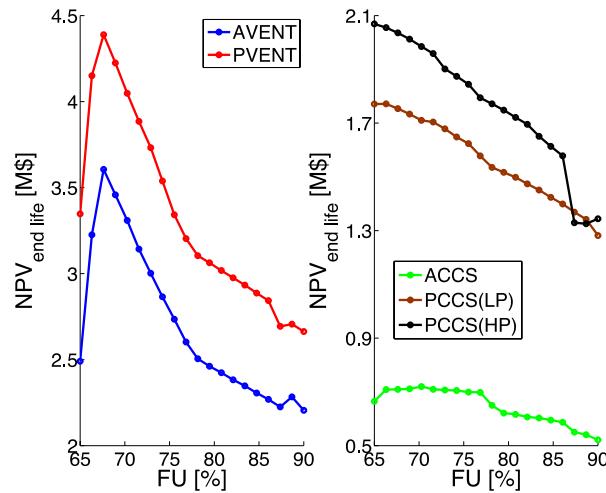
Figure 160. Influence of FU on NPV.
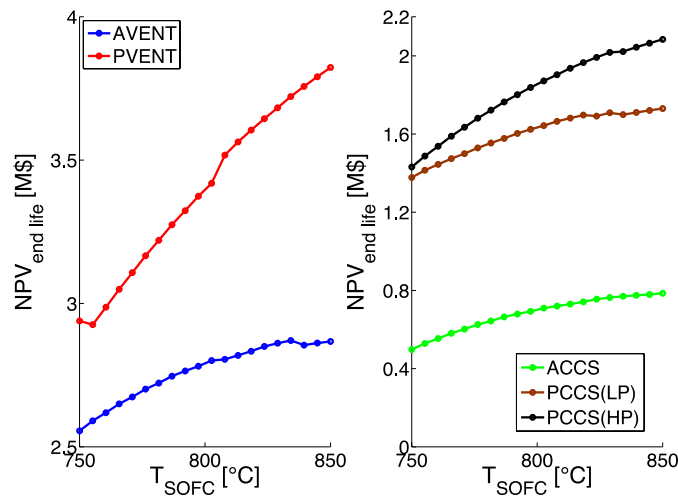
Figure 161. Influence of T_{SOFC} on NPV.

The first cost component influences the trend of NPV strongly*,* and from its analysis, it is possible to understand the reason why the maximum *NPV* is at low values of *FU*. As example, in Figure 163, are shown the results of *BEC$_{SOFC}$* of the A-VENT and P-VENT configurations: around the *FU* where the system is able to gain the highest *NPV* (*FU*=67.6%) it is possible to find a minimum point of the cost of SOFCs and, for higher *Fuel Utilizations*, the *BEC$_{SOFC}$* tends to increase faster producing a respective decrease in the final earnings. This increasing trend of the *BEC$_{SOFC}$* in respect to the *FU* is a

consequence of the increase of the *ASR* and of the losses that occur inside the cells because, in these conditions, the stack will require higher active surfaces to produce the electrical power imposed and then the corresponding investment will be higher too.
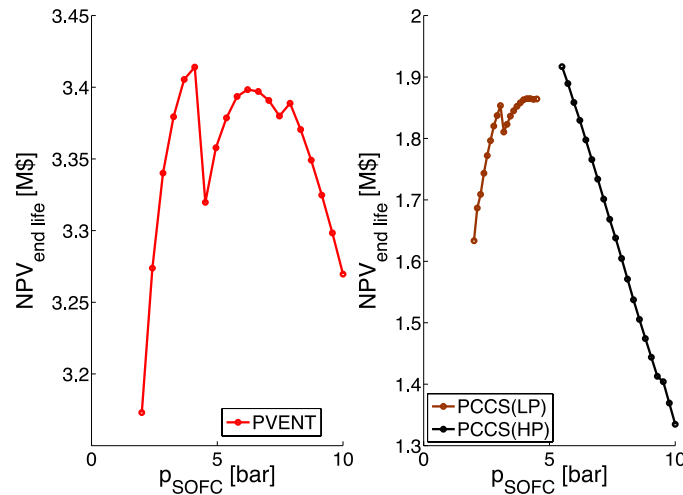
Figure 162. Influence of p$_{SOFC}$ on NPV.

Table 37. Years necessary to recover the initial investment.

Plant Type	Years to recover the initial investment [y]
A-VENT	4-6
P-VENT	3-5
A-CCS	12-14
P-CCS(LP)	8-9
P-CCS(HP)	7-9

The variation in the cost of the heat exchanger network is responsible for the discontinuity points located at high values of *FU*. This aspect is more evident in the P-CCS(HP) configuration and, for this reason, in Figure 164 is shown its *BEC*$_{Heat\ exchanger\ network}$. A discontinuity point can be here found at the same value of *FU* (87.4%), and the strong variation of this cost component is related to the increase in the number of heat exchangers necessary to guarantee a proper heat recovery. For *FU*<87.4% the P-CCS(HP) system is able to work just with 3 heat exchangers but, over that quantity, another one device is needed and must be included in the design that will have a higher investment cost.
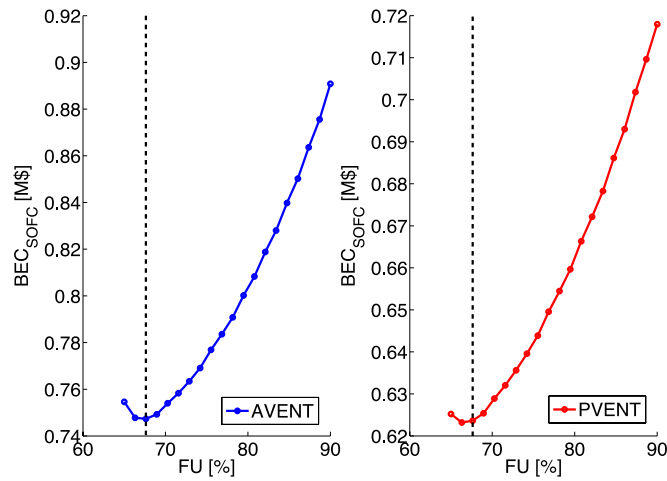
Figure 163. Influence of FU on the BEC of SOFCs (A-VENT and P-VENT).
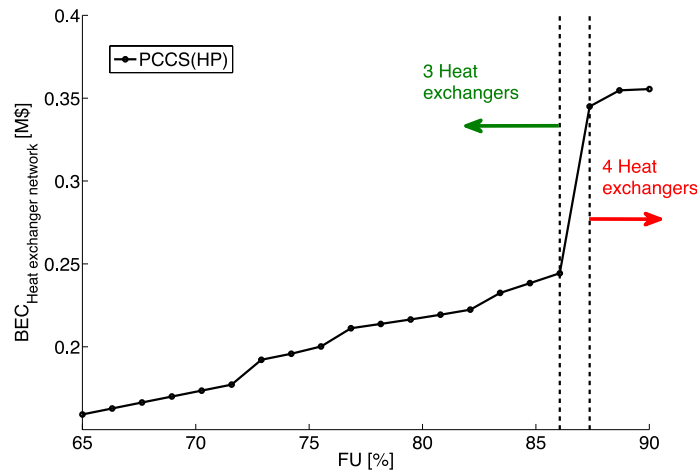
Figure 164. Influence of FU on the BEC of the heat exchanger network (P-CCSHP).

Although the operating temperature does not have a considerable effect on the technical performances, it does have an impact on the economic results (see Figure 161). This trend is a direct consequence of the reduction of the initial investment cost, especially of the component referred to the installation of the stack of SOFCs. In fact, higher operating temperatures support the electrochemical reactions reducing the internal resistance of the cells (*ASR*) and allowing the installation of a smaller active surface in the stack. Also, the spare capacity to be installed over time decreases with the temperature, in fact, it strongly depends on the initial stack.

It is interesting to observe that the pressurized configurations have higher slopes than those atmospheric. This aspect can be explained considering the combined effect of the following two benefits from the pressurization:

- The net electric power sent to the grid is higher thanks to the additional production in the gas turbine
- The reduction of the *ASR* of the cells, due to the increase of the temperature, is more significant when the stack is pressurized. The motivation is due to the fact that the *ASR* tends to decrease with the pressure.
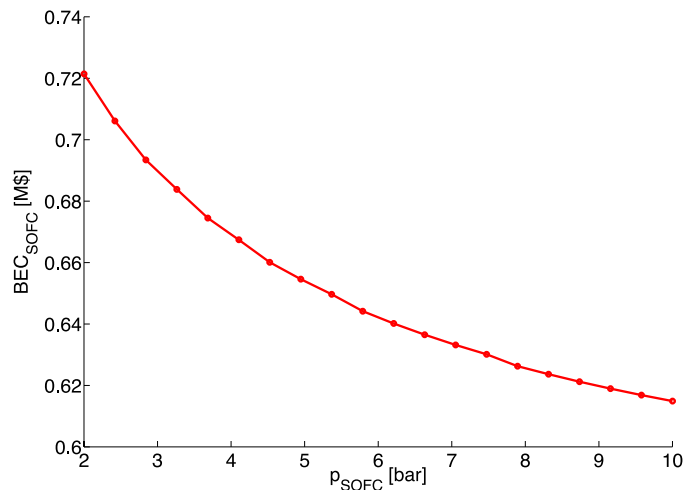
Figure 165. Influence of p_{SOFC} on the BEC of SOFCs.

The evolution of the *NPV* with respect to the last design variable (p_{SOFC}), shown in Figure 162, presents maximum economic revenues at low operating pressures (e.g. 4.1 bar for the P-VENT and for 5.5 bar for the P-CCS). This trend is similar to the one of the global electrical efficiency, and this suggests that the economic results are strongly influenced by the amount of electrical power that the system is able to produce and sell to the grid. Furthermore, it is really interesting that the pressure is the only design variable whose variation produces, more or less, the same positive (and negative) effects on both technical and economic performance parameters.

Again, the investment costs of the stack of SOFCs and of the heat exchanger networks affects the final earnings. In Figure 163 is shown the evolution of BEC_{SOFC} for the P-VENT configuration (which is the same of P-CCS).

This cost decreases with the pressure, and so it influences the NPV positively. Again, the evolution of the BEC_{SOFC} can be understood from the behavior of the *ASR*: the *ASR* and the electrochemical losses inside the cells tend to decrease with the operating pressure and so, increasing this control variable, the total active surface required will decrease, and the investment of the entire stack will be lower too.
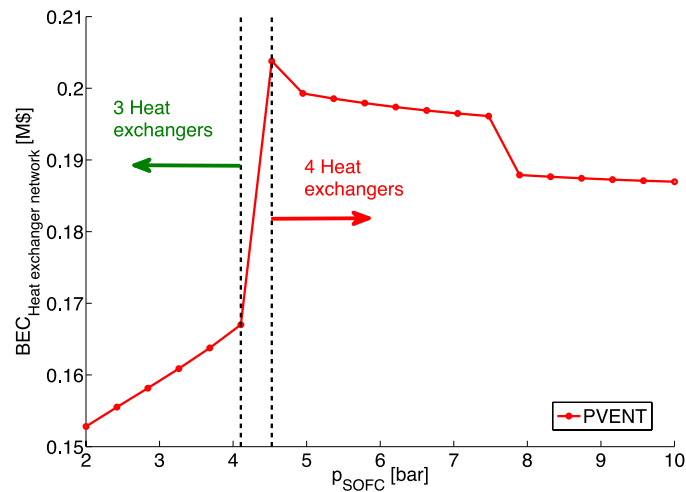
Figure 166. Influence of p$_{SOFC}$ on the BEC of the heat exchanger network (P-CCSHP).

This behavior allows explaining the little differences between the trends of NPV and those of the global electrical efficiency. Especially in the P-CCS configurations, at low pressures, the decrease of the cost of SOFCs is faster than the decrease of the net electrical power sent to the grid, and so the final earnings tend to increase; on the other hand, at high pressures, what occurs is the opposite situation and the *NPV* tends to decrease quickly.

The evolution of the cost of the heat exchanger network (shown in Figure 166 for P-VENT configuration) produces discontinuity points again on the NPV, for the same reasons already explained before.

MOO Optimization Results

The Multi-Objective Optimization (MOO) is useful to identify an operating space of design variables that can deliver the best-operating conditions, highlighting possible trade-off among energy and economic performances.

The MOO analysis first requires the definition of the objective functions to be maximized/minimized. In this study the objectives are:

- maximization of the net electrical efficiency;
- maximization of the net present value at the end of life.

As it was already shown with sensitivity analysis, the two selected functions have conflicting objectives: the optimization procedure has thus to find the set of operating points corresponding to the best compromise solutions (i.e., the so-called Pareto's front (Caramia & Dell'Olmo 2008))

The results of the Multi-Objective Optimization are shown in Figure 167. Each point of the Pareto fronts corresponds to a combination of the chosen design variables that achieves an optimized situation.

The Pareto front is an interesting representation of the results because it does not just show the optimal points but also feasible and not feasible working points in two different regions of the graph, respectively above and below the front of the curve.

Another useful information given by the comparison of different Pareto fronts concerns the choice of the most convenient configuration among those simulated. It is, in fact, possible to identify, for each analyzed system, the highest values of electric efficiency and NPV achievable if the plant is pushed to obtain the best technical or economic benefits.

As expected, the pressurized configuration without the CCS is the best one from both the points of view, followed by the atmospheric configuration without CCS, the pressurized one with CCS and the atmospheric one with CCS. The pressurization of the stack of fuel cells is then always convenient but, also considering the results obtained in the Sensitivity Analysis, too high operating pressures could affect the system performances negatively.
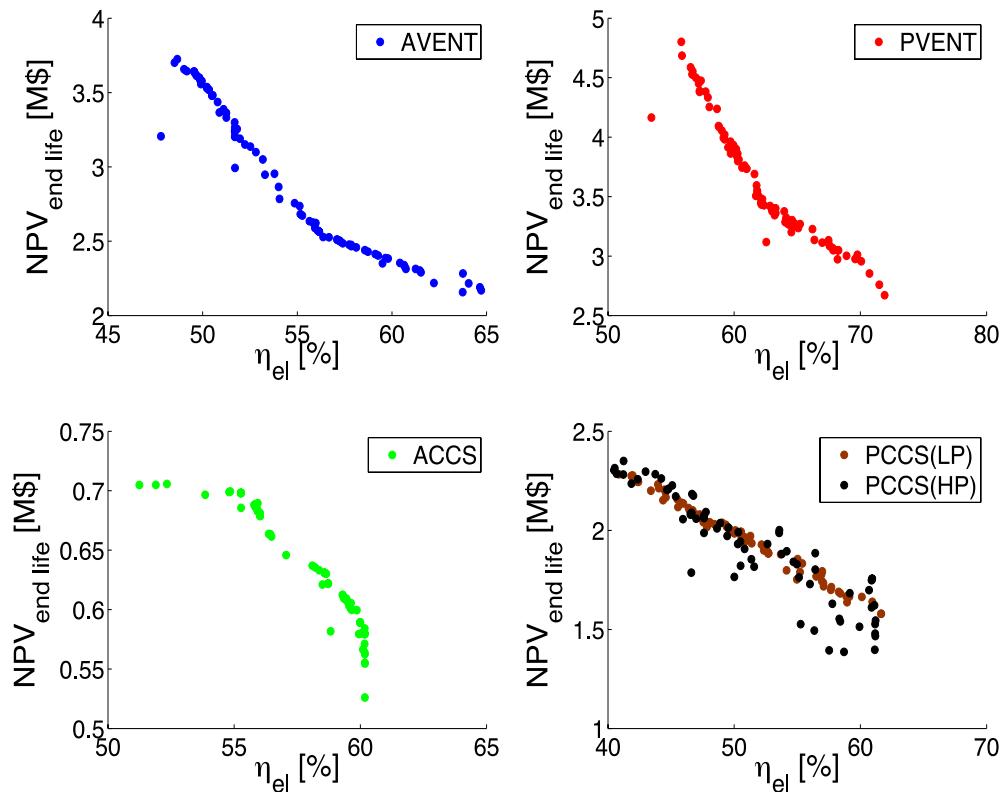
Figure 167. Pareto curves.

At this point, it is appropriate to make some considerations about the trade-offs between technical and economic issues. As the first step, the designer could be more encouraged to follow just the economic optimum (maximizing the *NPV*), because if a system is feasible, there is no reason not to adopt the configuration with the highest possible earnings. However, in a real case study, the efficiency cannot be taken away from the analysis, because it is important to consider that, although the fuel is practically free, it is not guaranteed its unlimited availability. In Table 38 three possible optimized operating points for both the P-VENT and P-CCS plants are given. Two of them correspond to limit situations where the *NPV* and the net efficiency are maximized; the last one is a reasonable energy-economic trade-off chosen by the author as an example.

Table 38. Result of MOO with selected energy-economic trade-off combinations.

Power Plant	Design Variable/Performance Parameter	Scenario		
		Maximization of NPV	*Maximization of η_{el}*	*Energy-economic trade-off*
P-VENT	*FU [%]*	67.12	89.11	76.69
	T_{SOFC} [°C]	850	839.17	847.27
	p_{SOFC} [bar]	7.9844	3.4593	4.4639
	NPV [M$]	4.8021	2.6707	3.4215
	η_{el} [%]	55.81	71.93	62.84
P-CCS	*FU [%]*	65.74	90.00	79.63
	T_{SOFC} [°C]	849.14	832.33	840.64
	p_{SOFC} [bar]	5.7077	3.084	6.2237
	NPV [M$]	2.3501	1.5786	1.9308
	η_{el} [%]	41.24	61.65	52.65

The MOO implemented by OSMOSE also includes graphical representations of the performance parameters expressed respect to each design variable, so that, once the optimal point has been chosen, it is possible to identify its corresponding FU, $T_{SOFC,}$ and p_{SOFC}. In this work are not reported all these results because most of them are just scattered points without any interesting meaning but, in Table 38, are shown those concerning the *FU* (just for the A-VENT configuration) because its trends are the only one worth to be discussed. Results of *FU* produce two continuous curves with predictable trends and not families of scattered points. Especially the curve FU-NPV is really interesting because an evolution

similar to the one of its corresponding Pareto front can be seen. In fact, the x-axis of the Pareto front displaying the net electrical efficiency is linear with *FU*.

This information is useful because it means that the optimized configurations of the power plants are strongly affected by the Fuel Utilization, while the other two design variables are less influential. Already the Sensitivity Analysis suggested that the choice of FU has to be made accurately, but here the MOO has proven, once for all, the importance of an accurate control of this parameter.
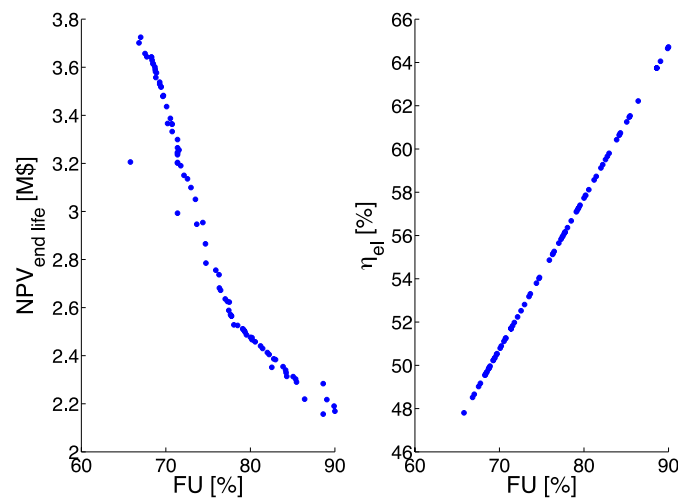
Figure 168. Distribution of the optimized points in respect of the FU and the NPV (A-VENT).

4.4.4 Results discussion

In the present work, different sizes and configurations have been analyzed for the same chosen layout developed in the framework of the SOFCOM project: biogas fed SOFC plants.

The analysis started from small size plants, below 100 kW: this class is mainly related to biogas from agricultural waste/crops, quite small plant to be installed in family farms. For this reason, the simplest configuration was studied: atmospheric SOFC without carbon capture. The analysis was then focused on the different reforming agents and on the choice of the most suitable working parameters; results point out how, for a small size plant, POx is a good choice for the reforming reactor and that biogas compositions variations during the year are not so affecting the performance parameters. The economic analysis confirms the results given by the energy one.

The second analyzed plant type was the medium size one, which size was around "hundreds of kW". As will be discussed better in the exploitation plan document, <u>small and medium size plants are the best field for the growing market of fuel cells</u>: at these low sizes, in fact, ICE are not competitive, very expensive and the investment for installing an ICE or a GT is not profitable anymore. On the other side, as confirmed by this analysis, if SOFC producers will be able to reduce their selling prices, thanks to EU and national subsidies/funding for fuel cells, the high efficiency of SOFCs, not touched by the reduced size, will bring to positive results from both an energy and economic point of view. The electrical production is good and higher than an ICE; the thermal production is still high and enough to cover the plant thermal requirements; the maintenance costs, very reduced respect to traditional systems, are another important positive issue which leads to a positive economic analysis for atmospheric vented plants.

When <u>carbon capture</u> is analyzed, results are worst since the increase of energy consumptions and economic costs for the carbon capture process is not currently re-paid by a real CO_2 market and a real price for this third plant product. During future works, the focus will be given to possible <u>carbon taxes</u> on the emissions at EU/national level and to the deeper analysis of the <u>current CO_2 potential industrial users</u> in order to find investors for this solution.

Finally, <u>large size plants</u> (MW size) have been discussed introducing the <u>pressurized SOFC configuration</u>: this choice has higher performance compared to the high costs, and thus the investment seems to be still convenient. Anyway, it is important to remind that, in the current industrial scenario, atmospheric SOFC are currently available and their manufacturing process is well-known; on the other side, pressurized SOFC are still under test, and they will need some years to become really commercial. Nowadays, the chosen price for this technology is thus a very target future value.

The last part of the analysis was related to the <u>optimization tool</u>, in order to define the best set of working parameters able to maximize efficiency and minimize costs.

Because of the good energy and economic results, and because of the very low emissions of SOFCs, these prime movers seem to be a very attractive alternative to traditional ICE in the biogas field.

Starting from medium and small size plants, where ICE are not currently profitable, a new market could grow and plant roots in order to become a best common practice for biogas plants, not just in terms of environmental and energy benefits, but because it is a good economic opportunity. After this first step, the large size market could be approached to demonstrate to all the industrial sector the advantages of SOFC. All the path should anyway be supported by EU and national regulations and subsidies in order to grow

potential clients confidence in fuel cells and to help manufacturers to reduce their production costs.

Chapter 5

Design and criticalities of industrial SOFC plants

The final part of the presented work has been devoted to the analysis of large size industrial SOFC. The positive experience of the SOFCOM project generated a growing interest, inside SMAT s.p.a., on fuel cells. A new project proposal was presented and won in 2014, related to the installation of the largest industrial size SOFC fed by biogas in Europe. The system will be installed in the SMAT Collegno WWTP, located in the Turin premises (Figure 169).

The project is devoted to the installation of a 174 kWe SOFC system fed by biogas, with thermal recovery from exhaust gases. The activities, in which the thesis has been involved, have been mainly related to the technical design of the system, in cooperation with SMA and Risorse Idriche (an engineering society owned by SMAT), techno-economic evaluation of the plant and communication activities.

The activities are still ongoing, and the first SOFC module will be operated from April 2017. The DEMOSOFC plant (Figure 170) is composed of:

- Biogas processing unit. The unit will include biogas dehumidification, contaminants removal and compression. Biogas from WWTP, even if relatively clean respect to other biofuels, still contains hydrogen sulfide and siloxanes, both harmful for the fuel cell. These contaminants are removed through an adsorption system with activated carbons, in a ultra-safe lead and lag configuration. Before the clean-up system, biogas is cooled and water is removed in a chiller, in order to guarantee the carbon optimal operation

parameters. Later, biogas is compressed up to 4 bar(g) to fed the flow controller placed inside the SOFC unit. A gas analyzer, able to detect both H_2S and siloxanes, is installed to online measure macro-composition and contaminants concentration both at the inlet and outlet of the clean-up system (Anon 2016).

- SOFC modules. The system is composed of 3 modules, able to produce 58 kW AC each. The total amount of installed power is 174 kWe, able to cover around 30% of the plant electrical needs. Thermal recovery from exhaust is used to partially cover the anaerobic digester thermal load, with a percentage depending on the season. SOFC modules are provided by Convion, and technical datasheet guarantee 53% electrical efficiency from compressed biogas to AC power (Anon 2016).

- Heat recovery system. As mentioned, hot exhaust from the SOFC modules heat a water -glycol loop, able to provide partial heating to the sludge entering the digester (50% average yearly coverage). A new heat recovery loop is integrated with an existing one, where heat is provided by a boiler fed by extra biogas or natural gas from the grid (Anon 2016).

Figure 169. SMAT Collegno WWTP.
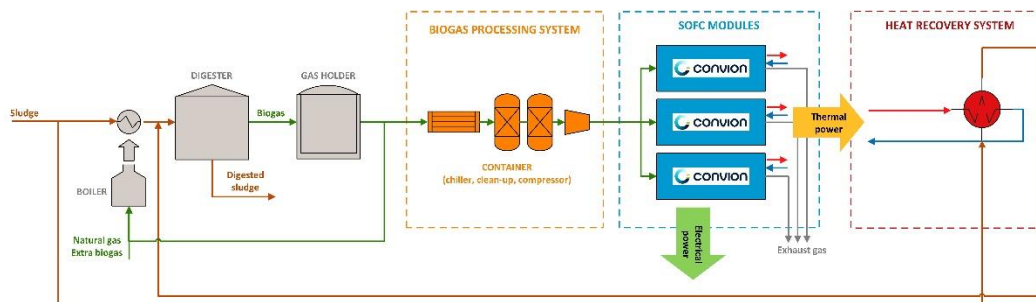
Figure 170. DEMOSOFC plant layout.

The site is currently producing biogas from sludge. Biogas is then exploited in two boiler for thermal production only. Thermal production only devoted to the digester heating. The digester is not directly heated up (as happen in more recent digesters where hot water pipelines are installed in the digester walls) but sludges entering the digester are heated up and mixed with a recirculation loop before entering the digester. The system is thus indirectly heated. The sludge heating line is shown in Figure 171.
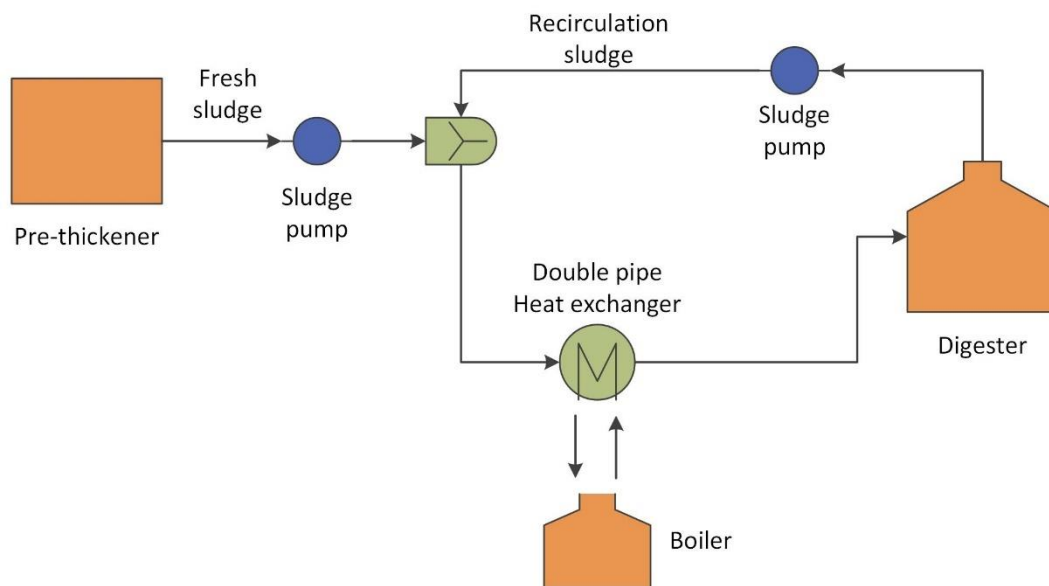
Figure 171. Current digester heating loop in SMAT Collegno.

Hourly biogas production is show in Figure 172 for 2014 and 2015. As can be seen, the average production is between 60 and 70 m^3/h on a yearly basis. The SOFC modules nominal requirement (with a CH$_4$% of around 65%) is 52 m^3/h, lower than the average value produced. The only reduction in the trend can be seen during summer months: this is due to the holiday season, where inhabitants are leaving the city and industries are closed; for this reason the entering waste water to be treated is reduced and consequently the biogas recovered is lower. This will require a modulation of the SOFC modules, as will be discussed later.

The loads of the entire WWTP have also been analysed, in order to understand the current energy consumption within the site. Electrical load (Figure 173) is varying between 600 and 680 on a monthly basis. The SOFC (174 kWe) will be able to supply around 25/30% of the total energy consumption. WWTPs are generally considered energy intensive systems, and a works is under development by the author on this topic, in order to review the analysis of energy consumption in WWTP and analyse possible ways to reach the self-sufficient WWTPs.
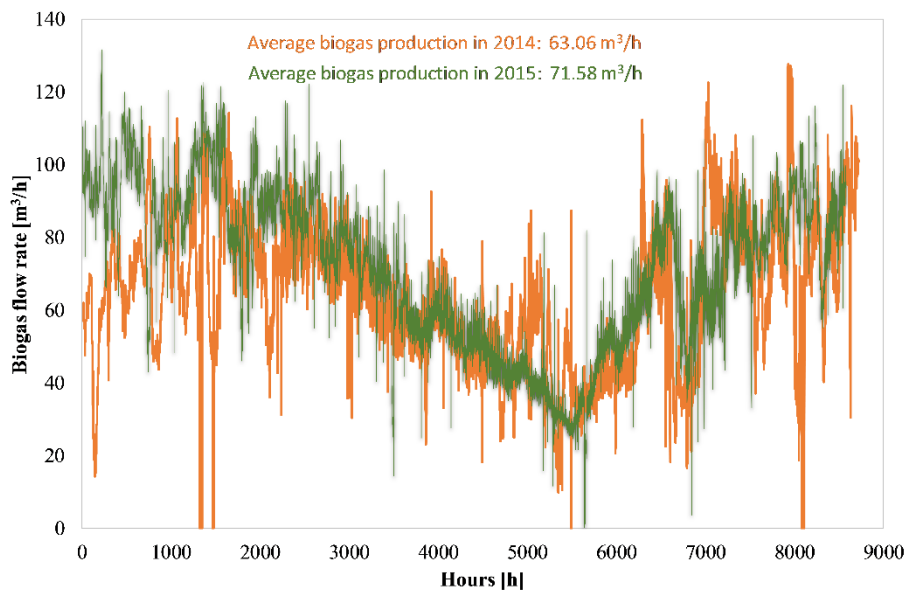
Figure 172. Hourly biogas production in SMAT Collegno.
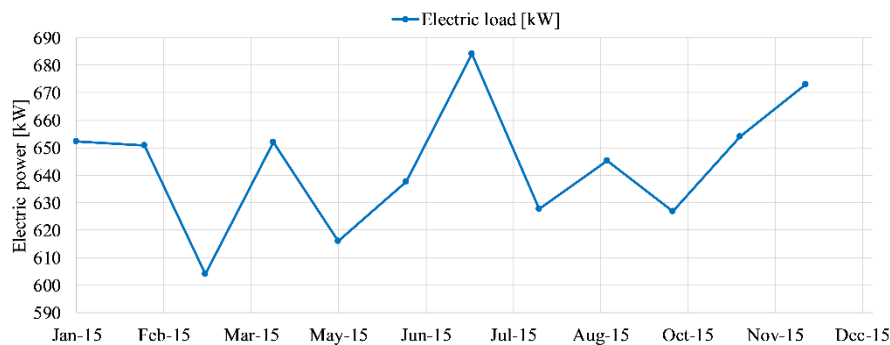
Figure 173. Electrical energy consumption in SMAT Collegno.

In recent years the Electric Power Research Institute (EPRI) declared that roughly 4% of the United States' overall electric consumption was utilized for the treatment and transportation of water and wastewater related processes (altogether accounting for 80% of the nation's overall electric consumption) (R. Goldstein & W. Smith 2002). Furthermore, in 2014 the U.S. Congressional Research Services estimated that between 4-13% of the nation's electricity consumption was related to the water industry. At that time it was stipulated that wastewater treatment processes were the largest consumers of the water related energy capacity (R. Goldstein & W. Smith 2002). In comparison, Europe's wastewater treatment plants (WWTPs) account for more than 1% of the electrical consumption, with a total estimated electricity consumption f 15,021 GWh/year spread among 22.558 plants (Anon n.d.)(Longo et al. 2016).

Different studies have focused on solutions to increase the energy efficiency of WWTPs. The goal of having WWTPs as net energy producers is an ambitious yet feasible

one (Mccarty et al. 2011)(Hao et al. 2015). The self-sufficienty target is deemed an achievable one since wastewater already contains two to four times the amount of energy needed for the wastewater treatment process (WERF (Water Environment Research Foundation) 2016)(Tchobanoglous et al. 2009).

Reducing energy consumption and increasing the efficiency of energy production are both required to have positive energy WWTPs. Measures to reach self-sufficient WWTPs are listed below.

- Process optimization: this approach consists in installing smart meters (Longo et al. 2016) within the plant and developing control systems for the optimal operation of aeration systems and water pumps (aeration is part of the secondary biological treatment, which takes more than 50% of the overall electrical consumption (Environmental Protection Agency (EPA) 2013) (Daw et al. 2012)). EPRI has estimated that, in wastewater facilities, 10-20% energy savings are possible through better process control and optimization (Copeland 2014).
- Enhanced biogas yield: currently, anaerobic digestion (AD) biogas can only provide around 50% of the total energy consumption (Hao et al. 2015). However, sludge pre-treatments (WERF (Water Environment Research Foundation) 2016) can lead to an increase of the biomethane yield.
- Efficient on-site combined power and heat (CHP) generation: the use of fuel cell systems (e.g., SOFC plants) can increase further the on-site electricity generation, which is key to self-sufficiency.
- Co-digestion of sludge with food waste is also an interesting option to increase the overall biogas output.

Self-sufficiency has been already achieved, for example, in the Strass im Zillertal Wastewater Treatment Plant in Austria (WERF (Water Environment Research Foundation) 2010). Here, thanks to sludge pre-thickening systems, improvement of the aeration system, development of an innovative nitrogen removal equipment and increasing the CHP efficiency, energy self-sufficiency has been reached already in 2005 (WERF (Water Environment Research Foundation) 2010) when the onsite production overtook electrical consumption.

Besides electrical consumption, thermal requirement could also be a problem in WWTPs. Thermal load is related to the digester heating and the current scenario is shown in Figure 174. As can be seen, even in the current scenario where biogas is completely burned for thermal production, some extra NG is required to keep the digester at the nominal temperature. This extremely high thermal load is due to two main reasons:

- Low solid content in the inlet sludge. The sludge entering the digester shows a Total Solid (TS) Content lower than 2%: this means that the system is heating

up an entering stream made up more than 90% of water, while the biological part, which is the one where biogas is produced, is only a portion of the 2% (Total Volatile Solids, which are usually around 70% of the Total Suspended Solids). This is the main inefficiency of the sludge line. A pre-thickener, a commercial system devoted to the reduction of the water content, could be installed to avoid this problem. Usually TS are increased up to 5/8% depending on the pre-thickening technology chosen (centrifugal, gravitational, or others). Higher ST are avoided because problems could occur in the pumping system when the sludge density starts increasing. Figure 175 shows the benefits of the use of pre-thickening on the thermal load. A strong reduction could be obtained, and a related better match between a CHP thermal recovery and the load. Coverage around 90% could be reached with a pre-thickening up to 8% TS and the DEMOSOFC concept.

- Mesophilic-thermophilic digester temperature. A second problem could be linked with the high current temperature in the digester. Measurements show values around 40-42 °C. Even if temperature measurements could be difficult in the digester internal environment, because of the acid atmosphere, and thus values found not reliable, the digester seems to work in conditions close to thermophilic digestion. This is enhancing the biogas specific production but also increasing the digester thermal requirement.

The detailed calculation of the digester thermal load can be found in one of the authors publications (Mehr et al. 2017).
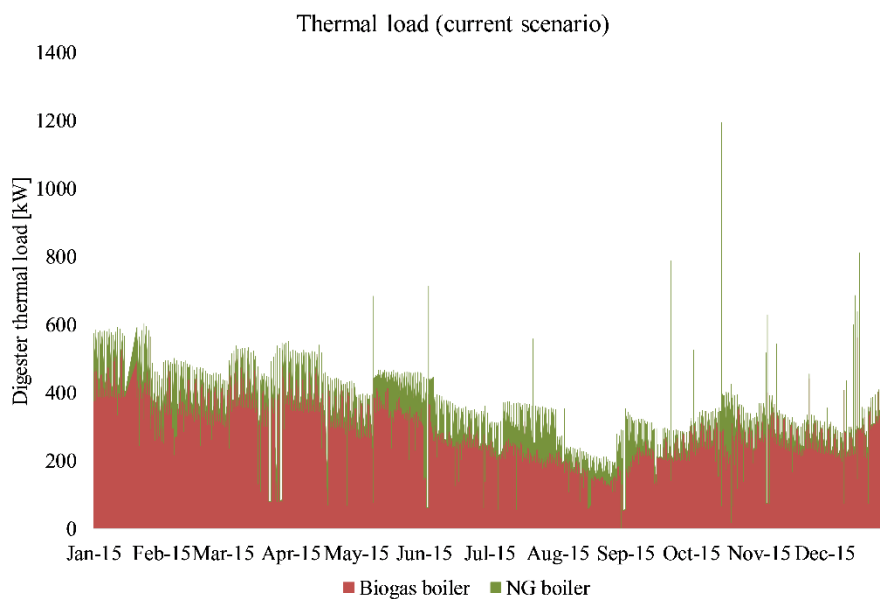
Figure 174. Thermal load (for digester) in SMAT Collegno.
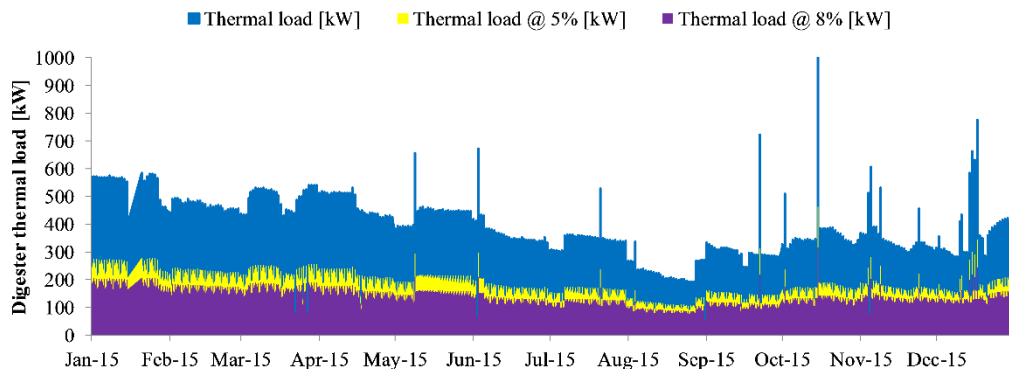
Figure 175. Effect of pre-thickening on the thermal load.

Biogas processing system

The biogas processing system aims to provide to the SOFC unit clean, compressed and de-humidified biogas.

The system is composed of two main sections:

- Biogas collection system, placed closer to the digester, where biogas is de-humidified thanks to a chiller (working with a 8/10 °C dew point) and the sent to a blower. The blower is able to flow biogas until the second section of the biogas processing system.
- Biogas container. This is a unique container where biogas is cleaned from harmful contaminants and compressed up to 4 bar (g). Cleaning is performed via adsorption in activated carbon beds. A detailed description of the carbons type and performance is provided in chapter 5.1.

The system has been designed after a 8 months analysis on the SMAT Collegno biogas, performed by an external lab: results are show in Table 39. As can be seen, most abundant and harmful contaminants found are sulphur, in the form of H_2S, and siloxanes, mainly D4 and D5. This trend confirms the results found in the gas analysis performed during the SOFCOM project in the Castiglione WWTP. WWTP biogas is quite 'clean', with controlled/ reduced amount of sulphur (in the form of H_2S, 20-100 ppm) and some ppm of siloxanes, mainly D4/D5.

From these data, the clean-up system has been designed and is shown in Figure 176.

Table 39. Gas analysis in SMAT Collegno, July 2015 – March 2016.

Compound	Formula		09/07/15	24/04/15	07/08/15	16/09/15	28/09/15	20/10/15	26/01/15	12/02/16	01/03/16
Methane	CH_4	[%]	65.5	64.7	63.4	63.8	63.1	64.4	65.9	61.61	62.78
Carbon dioxide	CO_2	[%]	32.2	30.39	30.15	31.6	33.3	35.1	33.2	37.98	36.14
Oxygen	O_2	[%]	0.33	0.22	0.17	0.11	0.06	0.02	0.02	0.01	0.04
Carbon monoxide	CO	[mg/m^3]	2.7	3.1	2.1	1.8	1.2	0.8	0.5	0.3	0.2
Hydrogen sulfide	H_2S	[mg/m^3]	25.2	27.2	25.9	25.5	22.7	32.9	26.1	22.5	25.8
Sulphur - Mercaptans	-	[mg/m^3]	2.7	2.9	2.4	2.3	2.1	2.6	1.5	1.3	1.4
Ammonia	NH_3	[mg/m^3]	0.132	0.112	0.039	0.091	0.052	0.032	0.03	0.01	0.01
Total siloxanes			0.82	5.67	17.4	43.8	13.4	12.8	4.55	13.81	17.2
(D6) Dodecamethylcyclohexasiloxane	$C_{12}H_{36}O_6Si_6$	[mg/m^3]	0.00	0.17	0.61	1.92	0.95	0.89	0.25	1.26	0.5
(D5) Decamethylcyclopentasiloxane	$C_{10}H_{30}O_5Si_5$	[mg/m^3]	0.75	4.08	13.57	33.15	9.80	9.34	3.47	10.41	14.4
(D4) Octamethylcyclotetrasiloxane	$C_8H_{24}O_4Si_4$	[mg/m^3]	0.07	1.42	2.87	8.10	2.21	2.25	0.75	2.14	2.3
(L3) Octamethyltrisiloxane	$C_8H_{24}O_2Si_3$	[mg/m^3]	0.00	0.00	0.35	0.63	0.44	0.32	0.08	0.00	0.00
Si tot (calculated)	-	[mg/m^3]	0.31	2.14	6.56	16.52	5.05	4.83	1.72	5.21	6.49
Hexane	C_6H_{14}	[mg/m^3]	0.23	0.31	0.29	0.61	0.31	0.36	0.17	0.32	0.26
Heptane	C_7H_{16}	[mg/m^3]	0.2	0.26	0.19	0.58	0.12	0.35	0.2	0.16	0.18
Toluene	C_7H_8	[mg/m^3]	6.12	5.67	9.41	3.21	8.75	8.76	2.63	2.98	1.86
Xylene	C_8H_{10}	[mg/m^3]	0.48	0.77	0.4	0.55	0.17	0.21	0.15	0.14	0.11
Limonene	$C_{10}H_{16}$	[mg/m^3]	5.11	4.08	3.81	7.95	8.15	6.76	14.07	13.72	10.37
Aliphatic Hydrocarbons	-	[mg/m^3]	118.5	114.2	112.7	116	76.7	46.00	48.3	21.4	33.67
Aromatic Hydrocarbons	-	[mg/m^3]	3.22	24.5	6.81	6.57	3.98	1.85	2.94	2.24	5.55
Alicyclic Hydrocarbons	-	[mg/m^3]	21.4	0.5	22.7	16.3	11.7	9.13	3.17	2.03	8.7
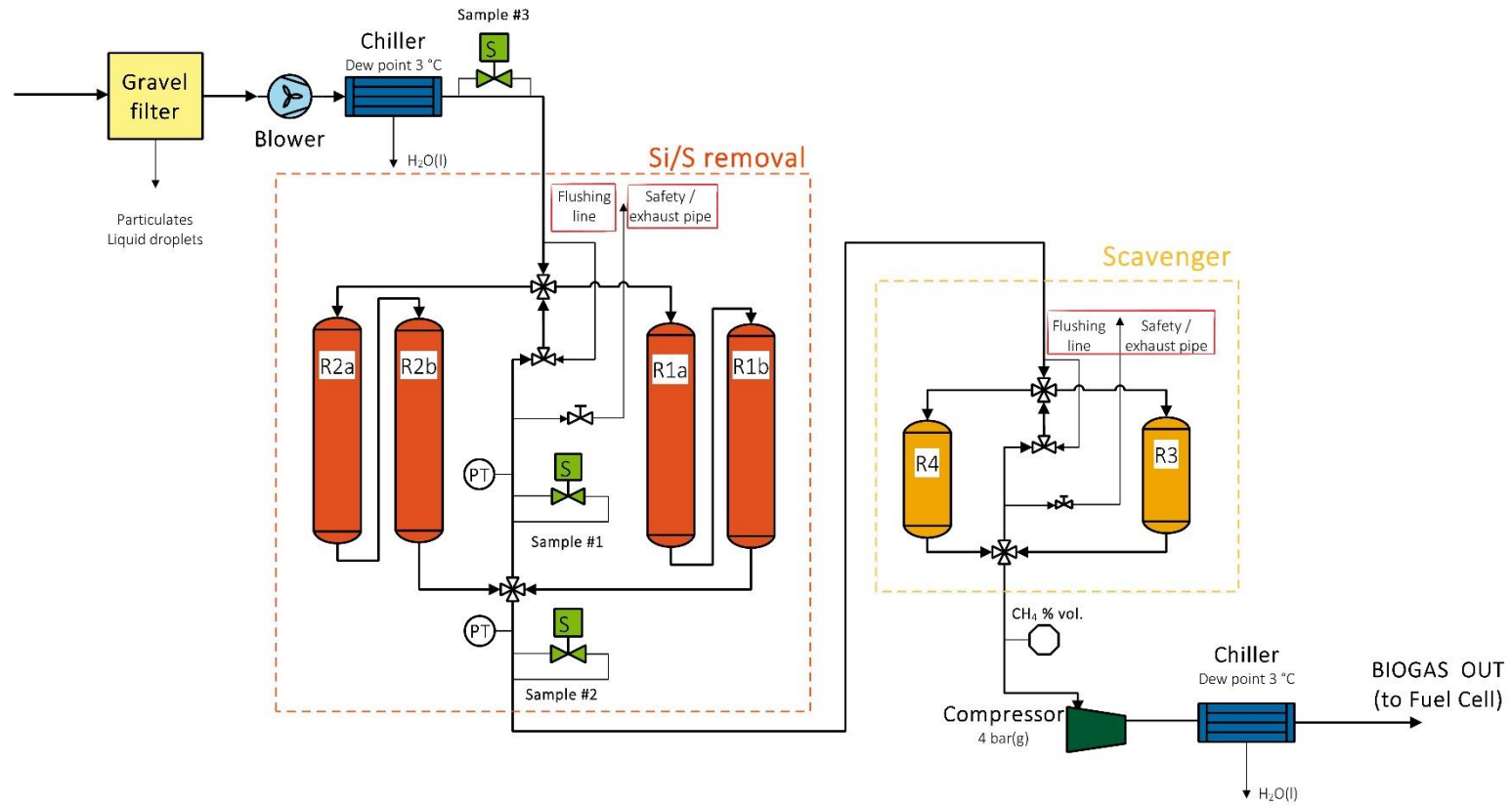
Figure 176. Processing unit layout.

The first section, located outside the container, includes blower and chiller. A gravel filter for condensed water removal is already installed in the SMAT biogas line. All the other components will be placed inside the container.

A high-purity level is required for the fuel gas of a fuel cell generator. The gas purity requirements for the SOFC modules is <30 ppb(v) for total sulfur (corresponding to < 0.045 mg tot. S / Nm^3), and <10 ppb(v) for siloxanes compounds (corresponding to < 0.06 mg tot. Si / Nm^3). The biogas is also required at a pressure of 4 bar(g).

Either reactors R1 ('a' and 'b') or R2 are the lead ones, while the other are the lag reactors. The lead reactors are responsible for removing the most of the contaminants. The lag reactor, instead, act as guard beds in case of temporary high loads of contaminants that reach the clean-up section. Once the breakthrough concentration is measured in Sample Port #1, the current lag reactors become the new lead vessels (the switch is realized by changing the positon of the 4-way valves). The catalyst is then replaced in the original lead reactors in order to restore their full functionality. A flushing line is also included to purge vessels in which the adsorbent catalyst has been replaced. The lead and lag configuration let the user to work with a series configuration during nominal operation, in order to have safety guard beds, and in parallel operation during maintenance, in order to replace the carbons without stopping the entire plant.

Two different adsorbent materials for each leg of the clean-up section are used. One material should be specific for the removal of siloxanes (i.e., the catalyst for reactors R1a and R1b), while the second one should be specific for H_2S removal (reactors R1b and R2b). Scavenger reactor will be filled with siloxanes removal carbon since silica is the most detrimental material for the fuel cell. The chosen carbons for the system are discussed in chapter 5.1.

The precise detection of the breakthrough of H_2S and siloxanes from the clean-up beds should be monitored constantly in order to decide when a change of the adsorbent material is due. For this reason, a continuous gas analyser will be installed, able to detect both sulphur and siloxanes.

SOFC modules

Convion C50 is a modular solid oxide fuel cell power generator with a nominal power output of 58kWe (AC Net). The product can be configured for operating with different fuel gas compositions and has a readiness for exhaust heat recovery. By its modular architecture, multiple C50 units can be installed in parallel to achieve higher power outputs. Nevertheless, each module is a separate generator, able to operate autonomously. C50 is designed to be installed parallel to power grid but is capable of island mode, thus securing

critical power loads within a micro grid. C50 is intended for continuous operation in a base load type generating mode. Table 40 below specifies ambient conditions.

Table 40. Generic operating conditions.

Ambient conditions	
Seismic vibration	IBC 2003: Site class D
Rain	IP54
Temperature [°C]	-20 – +45
Altitude [m]	0 – 1000
Ambient humidity RH, %	0 – 99
Installation	Indoor / Outdoor

A standard C50 fuel cell unit consists of a stack module as well as process, automation and power conversion equipment for facilitating power generation from the unit. At the C50 module interface, pre-cleaned and pressurized fuel and clean, non-condensing pressurized air is required. Process air is taken in by C50 at ambient pressure. Inside of C50 system enclosure there is an interface for a heat recovery. The heat-exchanger will be place inside the unit.
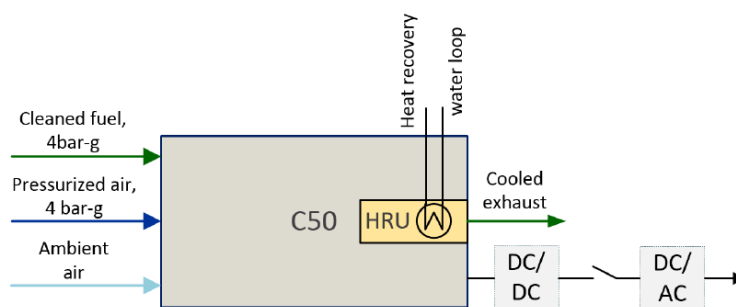
Figure 177. Schematic of C50 interfaces.

Output of a single C50 module is summarized below in Table 41. Total efficiency depends on heat recovery effectiveness and temperature.

Table 41. Summary of typical C50 system output.

Energy output	
Fuel	NG or biogas
Nominal AC power [kWe]	58
Electrical efficiency [%-LHV]	> 53
Exhaust temperature @ rated power, [°C]	222
Exhaust flow rate @ rated power [kg/h]	650
Specific heat capacity of exhaust flow [J/kg, K]	1072
Allowable back pressure [mbar]	25
CHP capability	Optional
Overall efficiency (CHP @ 60 °C), %	> 80
Noise level (dB(A) at 1 m)	< 70
Island mode operation	Optional

Modes of operation

C50 SOFC system has five different operating modes – off mode, heating and loading mode, hot standby mode, cooling mode and failure mode. These modes are described in Figure 178.

When the system operates in a given state, it maintains that state according to internal control constraints and operating set-point. Figure 178 illustrates mode transitions and signals required to trigger mode transients.

Start-up

Start-up is initiated by an operator command to instigate a mode transition from off mode to heating and loading mode. System heat-up is carried out by circulating electrically heated air while heating up the fuel cell stacks and system. At a pre-determined temperature minimum fuel flow needed for maintaining necessary thermal and chemical conditions in the system is initiated. The heating continues until the fuel cell stacks reach approximately 700 °C. Then electrical loading of the stacks is ramped up while increasing fuel feed. Figure 179 illustrates negative efficiency of the system at start-up mode, when electrical heating is used for heating up the system. Heat-up of a cold system to full load takes over 24 hours.

Whenever fuel is supplied to the system the cathode air feed is maintained at a level causing dilution to below LEL at the afterburner and thus, effectively avoiding a possibility of accumulation of explosive gas mixture anywhere in the system.
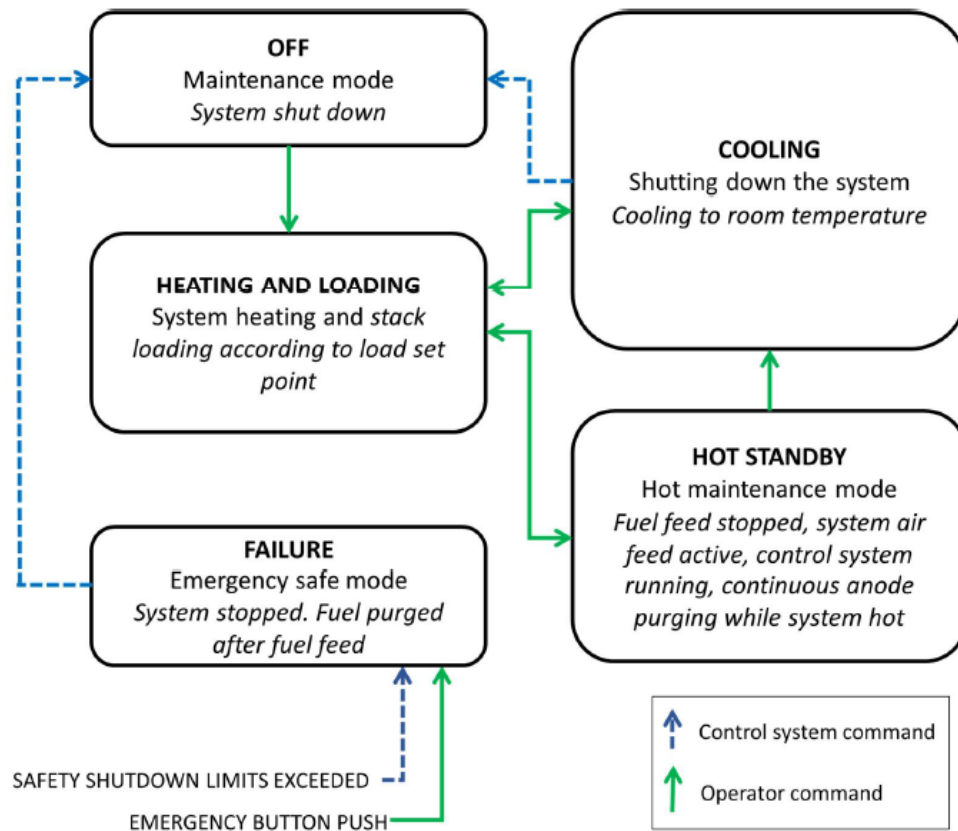
Figure 178. C50 system modes of operation and transitions between modes.

Normal operation

In normal operation the system is kept at as steady conditions as possible, regulating the air feed according to measured stack temperatures. In normal operation, loading of the system is based on operator set point.

By nature, a high temperature fuel cell system is best suited for steady loading and has a limited load following capability due to thermal inertial of the stacks. Maximum stack current ramp up/down rate is 4% of total range per minute. Recommended current modulation range 100%-30% is illustrated in Figure 179.
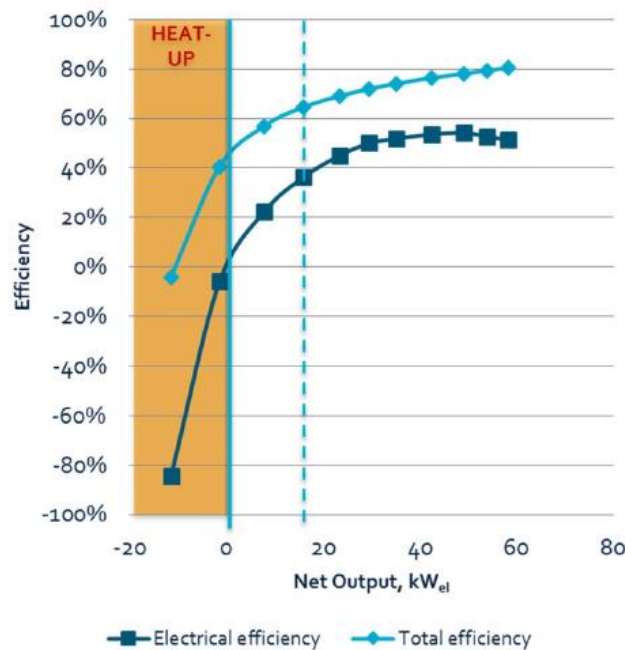
Figure 179. Efficiency of C50 at partial load, including heat-up stage when efficiency is negative due to electrical heating.

Modulated normal operation

By nature, a high temperature fuel cell system is best suited for steady loading

protective atmosphere is maintained in the stacks. During a short term hot-stand by, system cools down passively but does not experience a full thermocycler and can be and has a limited load following capability due to thermal inertial of the stacks. Maximum stack current ramp up/down rate is 4% of total range per minute. Recommended current modulation range 100%-30% is illustrated in Figure 179.

Temporary hot stand-by

Due to long heat-up times and a preference to avoid thermos-cycling of the system, an operator may choose to take the system to a hot stand-by mode for example to facilitate short term maintenance actions that require disconnection of fuel flow. In hot-stand by, system is not actively cooled but instead, only a brought back to full power relatively quickly.

Shut-down

In normal shutdown, the start-up procedure is essentially reversed. This is triggered by an operator command to instigate mode transition from heating and loading mode to cooling mode and eventually a control system command to bring the system to off mode.

In this sequence, stack current is first ramped down to zero. Then fuel supply does not stop when net power generation reaches zero but is needed for maintaining necessary thermal and chemical conditions in the system until system cool down has reached a point when fuel supply can be closed and the fuel system is flushed with air to remove any carbonaceous species that form harmful compounds by chemical reactions. Thereafter cathode air cooling continues until stacks have cooled down to below 100 °C.

Emergency Shutdown

In case of a gas alarm or other failure preventing normal operation or shutdown, the emergency shutdown sequence is triggered. In this case cathode air feed is discontinued, cathode air feed valves closed and the fuel system is flushed for a predefined time with nitrogen. The system then cools down passively without any feed.

In case of a gas alarm all non-ex equipment in the process module is de-energized and the SOFC stacks in the stack module are disconnected from the DC/DC converters. Ventilation of the process module continues approximately 12 hours by means of an explosion safe suction blower with power backup.

Convion C50 is CHP ready, i.e. heat of its hot exhaust flow can be recovered by means of a heat exchanger for a maximum total efficiency. For the most compact arrangement Convion can supply the C50 unit equipped with heat exchanger fitted inside C50 enclosure. Alternatively, heat exchanger may be placed outside of the C50 enclosure. Exhaust gas pipe size at connection points is DN150. Exemplary counter flow arrangement of the heat exchanger is illustrated in Figure 180.

Table 42. SOFC module procedures.

1 module C50				
Procedure - Time	Fuel [kg/h]	Compressed Air [kg/h]	NH-mix (95% N_2, 5% H_2) [kg/h]	Power [kW]
START-UP				
5-8 h	0	≥ 9	0	40 all time
10-16 h	3	≥ 9	0	
SHUT-DOWN				
10-16 h	3	≥ 9	0	5 all time
24 h	0	≥ 9	0	
Emergency SHUT-DOWN				

| Immediately de-powered, ~48h to cool down | 0 | 0 | 3 | 0 |
| HOT STAND-BY | 0 | 0 | 3 | 2 |
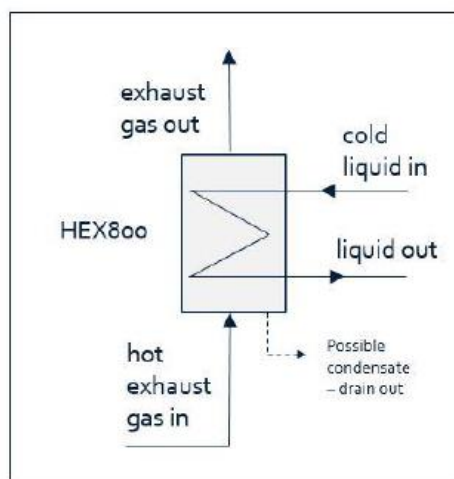
Figure 180. Flow arrangement of a heat recovery heat exchanger.

Maximum allowable pressure drop on the exhaust gas side incurred by exhaust gas flowing through a heat exchanger is 25 mbar. While exhaust gas temperature in all normal full or partial load operating points is below 250°C, an instantaneous peak temperature of 500°C during a rare event of emergency shutdown may be experienced, although duration of peak temperature is short, order of 120s, and during that period exhaust gas flow drops to a low level of about 20kg/h.

Aside of the pressure drop caused by the heat exchanger, operation of heat recovery shall not affect fuel cell system operation in any way. Control and mitigation of possible abnormal operation of the heat recovery system shall be taken care of by an external heat recovery system and its controls. It is not advisable to combine exhaust flows of more than one unit for a common heat recovery instead of using individual heat exchangers. Should an integrator wish to do so please consult Convion during the planning phase.

The technical C50 commercial datasheet is finally shown on Figure 181.

Performance	Targets
Net power output	58kW (3x400-440V AC 50/60Hz)
Energy efficiency (LHV)	
Electrical (net , AC)	> 53 %
Total (exhaust 40°C)	> 80 %
Heat recover	
Exhaust gas flow	650 kg/h
Exhaust gas temperature	222 °C
Emissions	
NOx	< 2 ppm
Particulates(PM10)	< 0.09 mg/kWh
CO_2 (NG, nominal load)	354 kg/MWh
CO_2 (with heat recovery)	234 kg/MWh
Fuels	Natural gas, City gas, Biogas
Dimensions (L x W x H)	
power unit	3,5 x 1,9 x 2,3 m
aux. equipment	2,4 x 0,6 x 2,2 m
Noise level	< 70 dB(A) at 1 m
Installation	Indoor / outdoor
Temperature	-20 – +40°C

Figure 181. Convion SOFC modules datasheet.

Heat recovery system

The thermal recovery loop P&ID is shown on Figure 182.

SOFC modules are represented on the left, fed by biogas (blue line) or auxiliary gas (NH-mix, blue line). Inside the SOFC modules, the first heat-exchanger (gas-liquid) will be placed. Heat released for the hot exhaust gas stream (green line) is transferred to a water+glycol loop (brown lines).

The three water+glycol streams, one per each module, are then connected together and sent to the second heat-exchanger (liquid-liquid), fed on the other side by the incoming sludges to the digester (orange line). The thermal loop is designed to work at constant temperatures and so regulation is available on the flow rates. Concerning the water+glycol loop, regulation is reached through three-way valves installed both on the three single module loops and on the main loop (yellow circles in the figure). The sludge flow, on the other side, is regulated through a variable speed pump (yellow circle) controlled by and inverter.

In order to guarantee a continuous operation of the HRU and avoid the risk of module over-heating, two actions have been implemented:

- All the pumps in the water+glycol loop are doubled and installed in a parallel mode in order to have continuous heat removal also in case of a pump failure.

- The second heat-exchanger is not only connected to the sludge line but also to an industrial water line (light blue line). In case sludges are not available, heat removal is always guaranteed by the possibility to use industrial water in the same heat-exchanger.
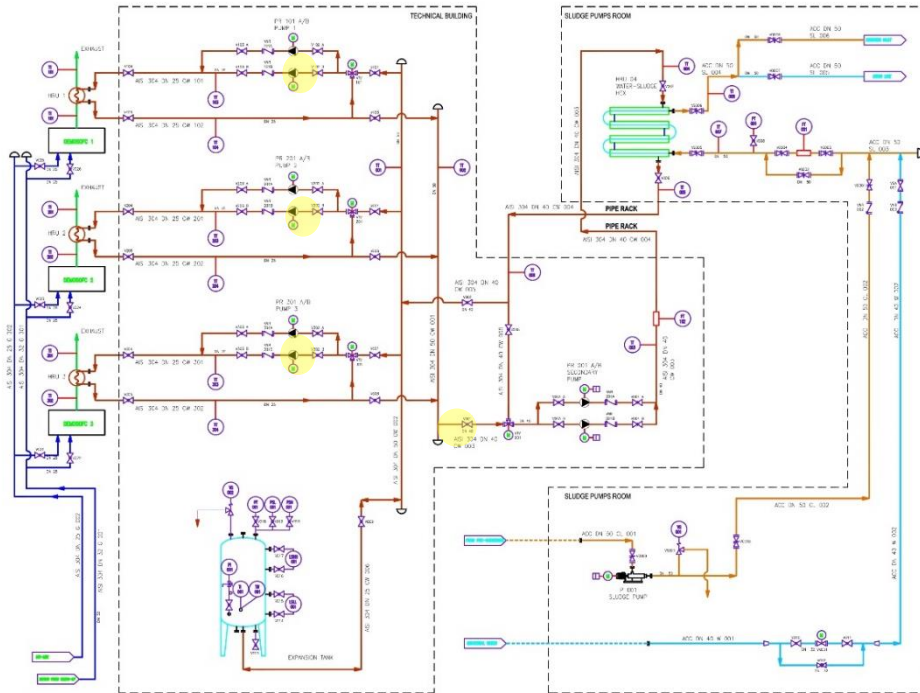
Figure 182. Thermal recovery system.

From an engineering point of view, the existing system will be integrated with the new DEMOSOFC HRU loop. The integration is underlined in the figure below. From the existing sludge line (orange dashed line), a new pipe (orange continuous line) will be detached and connect to the new sludge-water HEX, probably a double pipe heat-exchanger. Part of incoming sludges (flow rate depending on the variable velocity of the feeding pump) are thus sent to the HEX and heated up thanks to the SOFC thermal recovery system (water+glycol loop). The remaining sludge flow is heated in a second, already existing, HEX after being mixed with the recirculation line from the digester. The two flow rates are then mixed again and send to the digester.

The regulation of the heat recovery loop will be guaranteed from the general PLC in order to keep a digester temperature as stable as possible.

On Figure 184 is also shown the total amount of sludge entering the digester. Part of this flow will be, with the DEMOSOFC installation, be sent to the new sludge-water/glycol HEX.
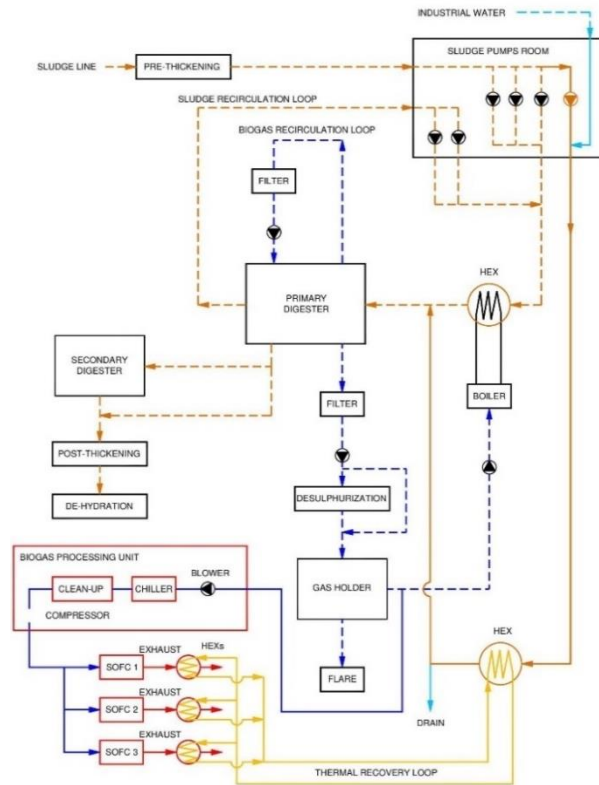
Figure 183. General scheme with focus on the heat integration system.
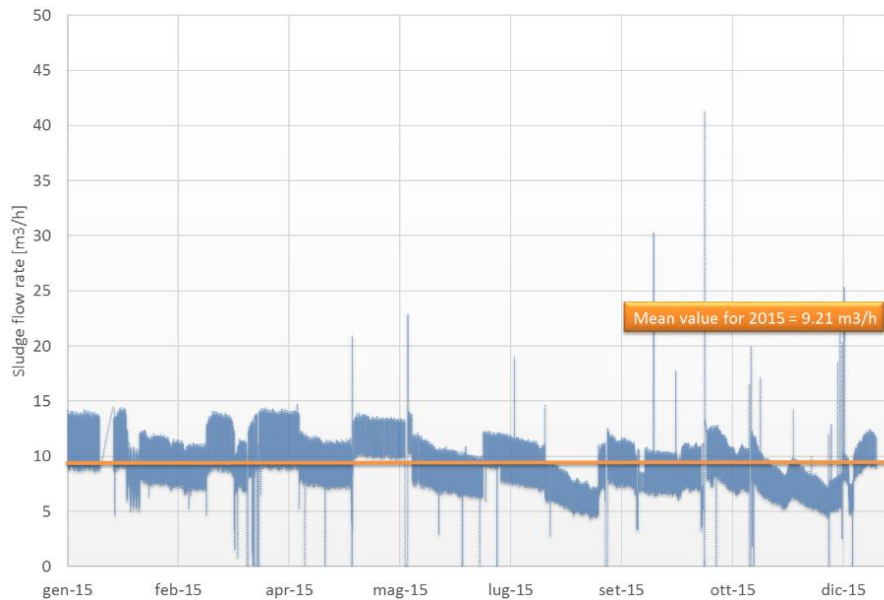
Figure 184. Sludge inlet flow to WWTP.

Activities

In the framework of the PhD, different activities have been developed related to DEMOSOFC project. In particular:

- Analysis of the optimal operation point of view for the fuel cell. A PID controller has been developed to control the SOFC outlet power according to the biogas level in the gas holder (storage between digester and users). During winter and transition seasons, where average biogas production is higher than nominal C50 request, SOFC will be always operated at full load. During summer season, because of the reduced biogas production, the system will be modulated in the available range (30-100%) in order to avoid shut-downs as much as possible.
- Experimental activity on activated carbons, devoted to the selection of material for the DEMOSOFC application. First results are shown in chapter 5.1
- Techno-economic analysis of the DEMOSOFC concept. The analysis has been developed with production of different scenarios. Activities are ongoing together with Imperial College of London and results will be published in the next months. Another techno-economic analysis of the system is provided in two works already published (Marta Gandiglio et al. 2016; Mehr et al. 2017). The analysis has been focused also in other biogas sites like agricultural plants and first results have been published in (M. Gandiglio et al. 2016).
- Engineering design. The main current activity of the author in the project is related to the development, together with SMAT engineers, of the plant design and control system. Concerning the design, a final layout has been proposed while the work is still ongoing for what concerning the PLC logics definition.

Figure 185. DEMOSOFC plant 3D layout.

5.1 Biogas pre-conditioning for SOFC applications

The experimental campaign ongoing in the POLITO laboratories is devoted to the selection of the best activated carbons for the biogas cleaning system designed in the framework of the DEMOSOFC project. The most abundant and harmful contaminants found are H_2S and siloxanes with average values of 20 and 1 ppm (Figure 186).
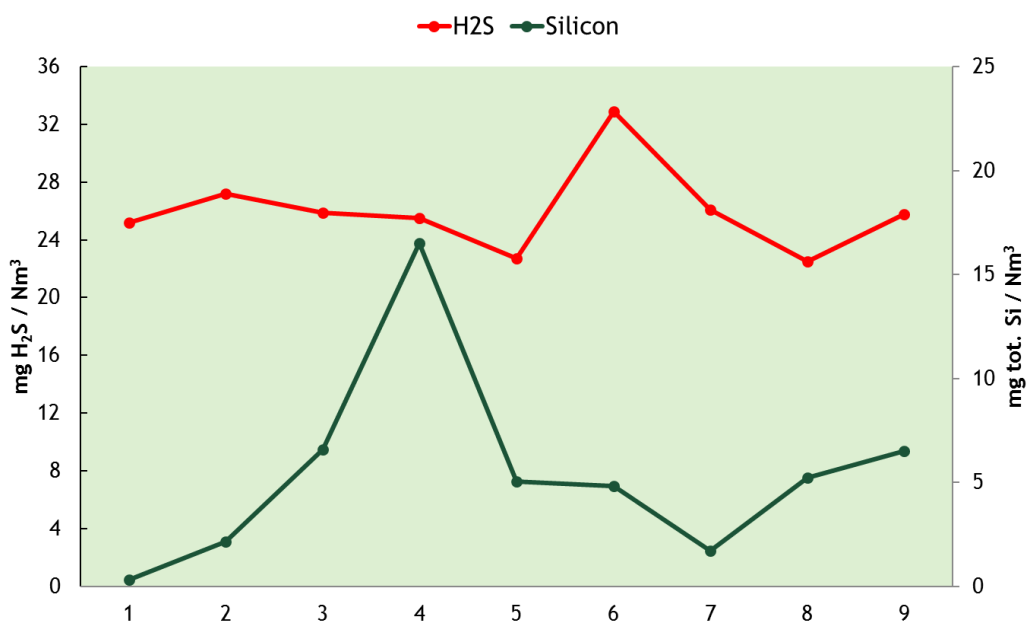
Figure 186. Biogas contaminants concentrations in SMAT Collegno, from July 2015 to March 2016. Data available also in Table 39.

The required purification levels for the SOFC module, given by Convion are:

- H_2S: 30 ppb
- Siloxanes: 10 ppb

The PhD thesis activities have been involved only in tests with sulphur compounds, performed in the laboratories of the Department of Energy of Politecnico di Torino. Tests on siloxanes have been performed by a member of the research group in an external lab located near Trento (IT), because of the specific gas analysers available there.

5.1.1 Materials & Methods

The analysed activated carbons (AC) are listed in Table 43. Two main suppliers have been considered;:

- Sulfatrap: a US company specific in high efficiency activated carbons, which has already developed experimental systems for fuel cell applications, in cooperation with D.O.E. (Alptekin 2014a; Alptekin 2014b; Alptekin et al. 2011; TDA Research Inc 2015)
- Airdep: a IT company, suggested by the cleaning system supplier, which provides commercial activated carbons.

Table 43. Activated carbon included in the lab activities.

Producer & Product	Suggested for:	Datasheet performance	Cost	Unit
SulfaTrap R8G	Siloxanes, large size sulphur compounds and low H_2S levels removal	30-70 mgS/g on biogas @ 2000 ppm(v) H_2S	15.88	€/kg
SulfaTrap R7E	Bulk sulphur removal (high H_2S levels)	180-270 mgS/g on biogas depending on moisture/ oxygen @ 2000 ppm(v) 163 mgS/g on biogas under dry conditions @ 2000 ppm (v)	7.83	€/kg
AirDep CKC	H_2S removal	> 200 mgS/g on air	2.80	€/kg
AirDep CKI	H_2S removal	> 200 mgS/g on air	5.00	€/kg
AirDep C64	Siloxanes removal	600 mgCCl$_4$/g on air	2.20	€/kg

The procedure for the preparation of the micro-reactors is described below.

1) Reduction of the activated carbons (found in the form shown in Figure 187) in powder. The reduction is performed manually by means of a mortar.
2) The powder is then sieved to guarantee a certain particles range. The range, usually between 53 and 75 μm, is defined in order to keep constant the ratio $d_{particle/pellet}$ on $d_{reactor}$.

Figure 187. Activated carbons: from left to right hand: Airdep ACs, Sulfatrap R7E, Sulfatrap R8G.

Figure 188. Micro-reactors for AC testing.

3) The sieved powder is then filled into the micro-reactors. Internal diameter is 4 mm, external diameter 6 mm (Figure 188). The micro-reactors is weighted before and after filling the carbons and micro-reactors are filled with almost the same quantity of material for having a better test comparison. Different quantities have been used only to investigate the influence of the GHSV.

4) The micro-reactor was then inserted in the simple experimental setup developed for these specific tests and shown in Figure 189. A by-pass line was available to purge and clean the lines and the analyser without damaging the sample.
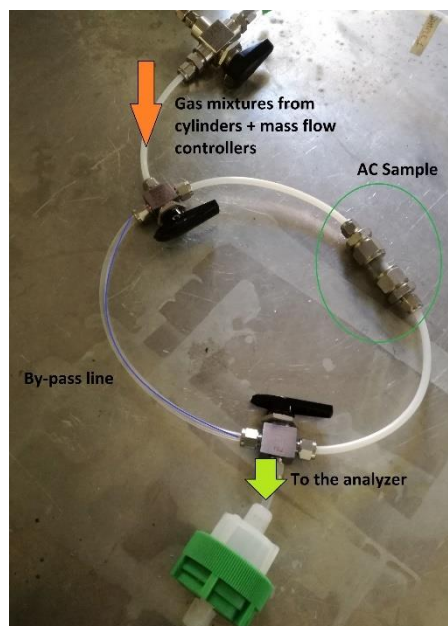
Figure 189. Experimental setup for activated carbons testing.

5) After having completed passage 1 to 4, the test can start. The gas was flown through the sample and then reached the analyser. A filter was inserted to avoid solid particles to reach the gas analyser. Two gas detectors were used in the presented tests:
   - Hiden mass spectrometer. This instrument was used for the first months of experimental activities, mainly for the screening of the different carbons and the analysis on AirDep CKC at different concentrations. The instrument was able to detect all chosen compounds, at macro and micro-level. The MasSoft software was available to follow the instrument and log data. Tests were then stopped because of instabilities problems due to malfunctioning of the vacuum pumps. Because of these problems, the instrument has been sent back to the producer for maintenance.
   - Siegrist H_2S electrochemical analyser. This instrument is a dedicated analyser for hydrogen sulphide only. Different sensors could be placed inside with different detection ranges: the one installed is a 0-200 ppm sensor. The main advantages compared to the mass spectrometer is the easiness of the instrument, less sensible to environmental factors and internal components, because of the simple layout and design. An in-house developed Simulink software is used to follow the tests and log the data.
6) After having launched the test, the typical detected curve was the one shown in Figure 190. The outlet H_2S was first zero, because the carbon was fully

adsorbing the contaminants. From the breakthrough time on, the carbon start releasing some sulphur and the concentration increases up to the stable level called saturation time: in this condition the carbon is not adsorbing anymore and the inlet sulphur concentration is equal to the outlet one. Because of the low concentration admitted at the fuel cell inlet, the carbons will be replaced as soon as the breakthrough time will be detected, in order to avoid to send contaminants to the SOFC modules. For this reason the tests were mainly devoted to the detection of the breakthrough time and many curves were stopped after this moment without reaching the saturation point.
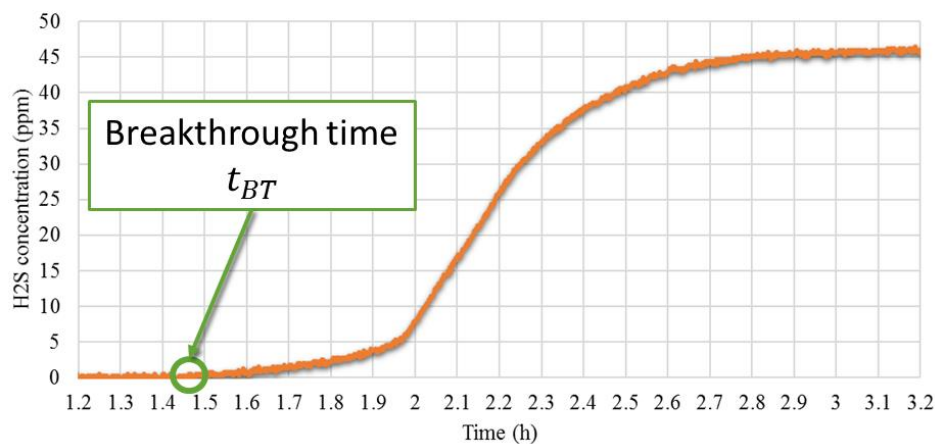
Figure 190. Adsorption curve for a single test with a micro reactor.

7) The adsorption capacity of the material in terms of sulphur (Ads_S, in mg of sulphur per g of AC) can be finally determined as:

$$Ads_S = \frac{\dot{m}_{biogas} \cdot c_S \cdot t_{BT}}{m_{AC}}$$

Eq. 32

Where $\dot{m}_{biogas}$ is the biogas flow rate (m3/s), c_S the sulphur concentration in biogas (mg/m3), t_{BT} the breakthrough time (s) and m_{AC} the mass of AC in the micro reactor (g).

The tests, which will be presented in this thesis, are related to:

- Screening of different commercial activated carbons
- Analysis of the Langmuir isotherm for a specific carbon
- Influence of oxygen on the adsorption capacity
- Influence of GHSV on the adsorption capacity
- Siloxanes preliminary results

The final configuration for the DEMOSOFC system is then proposed and evaluated in terms of investment cost, replacement time and replacement costs.

More details and recent tests will be available in the PhD thesis of Davide Drago (Drago 2017), devoted specifically to this topic. Furthermore, a publication from the author and the research group involved is under development.

5.1.2 Results

The first two sections of the results are related to the analysis of the AC performance in terms of sulphur and siloxanes adsorption with a fixed contaminant inlet concentration. Test on sulphur were first conducted at 95 ppm and then repeated at 50 ppm, to better simulate the real SMAT biogas. Test on siloxanes were done at 20 ppm D4, a concentration higher than the average one in SMAT (~ 1 ppm), because of limitations in the feeding system.

Adsorption capacity on H_2S

The first experimental campaign was related to a screening of the different available activated carbons for sulphur removal. Results are presented for three selected carbons: Airdep CKC and CKI and Sulfatrap R8G, since they were pointed out from producers as the best choice for hydrogen sulphide removal. Activities are still ongoing in order to test also Airdep C64 and Sulfatrap R7E, even if their performance are expected to be lower in terms of sulphur adsorption.

The common parameters for the three tests are:

- H_2S inlet concentration: 50 ppm
- Total flow rate: 750 ml/min
- Composition CH_4/CO_2: 62.5/37.5 %
- Sample diameter: 4 mm (internal)
- Spatial velocity: 0.995 m/s

Results are shown in Figure 191 and Table 44. From the analysis of the curves, R8G is pointed out as the best choices in terms of adsorption capacities. In fact, from a qualitative point of view only, similar reactors (filled with similar quantities of AC) show strong differences in terms of breakthrough time: Airdep ACs, both CKC and CKI, reach breakthrough more than four hours before Sulfatrap R8G. this is confirmed by the low adsorption capacities, both at breakthrough and saturation time (Table 44).
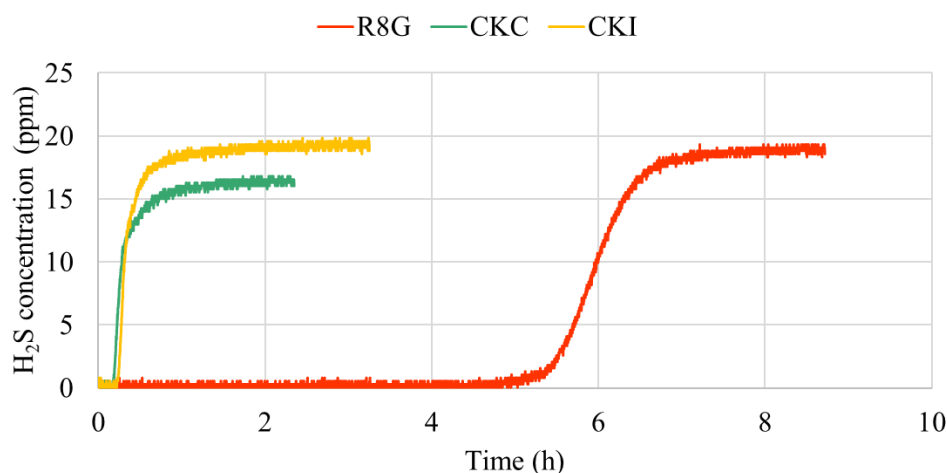
Figure 191. Results on the adsorption capacity evaluation in terms of H_2S with a fixed 50 ppm concentration.

Table 44. Adsorption capacities for the selected activated carbons.

	Adsorption capacity (mg/g)	
	@ Breakthrough	@ Saturation
R8G	40.17	61.13
CKC	1.16	13.75
CKI	1.51	14.35

Sulfatrap R8G can provide adsorption capacities at breakthrough forty times higher than Airdep AC. The low performance of the Airdep carbons, as will be discussed later, are mainly due to the 'extreme' testing conditions in terms of simulated biogas. Standard biogas from anaerobic digestion usually shows humidity and a small quantity of oxygen. These two factors have been partially analysed in the presented experimental campaign (effect of oxygen) and their positive effect is also confirmed by literature works (Huang et al. 2006; Sitthikhankaew et al. 2014). In particular, the work from Sitthikhankaew et al. (Sitthikhankaew et al. 2014) provides an interesting experimental work on the effect humidity, oxygen and carbon monoxide on impregnated activated carbons.

Adsorption capacity on Siloxanes (D4)

From the external experimental work performed mainly by Davide Papurello, data on adsorption performance for siloxanes are presented. Test have been performed in the following setup conditions:

- D4 concentration: 20 ppm (in H_2)
- Total flow rate: 200 ml/min

- Spatial velocity: 0.27 m/s
- Sample diameter: 4 mm (internal)

Results are shown in Figure 192 with data on adsorption capacities at breakthrough time. Looking at the overall range of values, it is clear that siloxanes removal is 'easier' than sulphur removal, since adsorption capacities are higher and almost all the carbons are able to partially remove D4 with acceptable performance. The best performance is related to Airdep C64, specifically devoted to siloxanes removal.
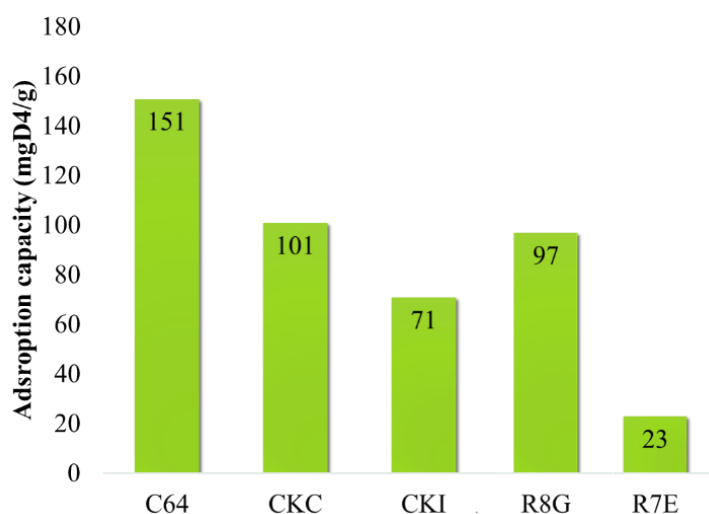
Figure 192. Results on the adsorption capacity evaluation in terms of D4 with a fixed 20 ppm concentration

Even if further analysis have been performed, to better understand the phenomena from a scientific point of view, from this first screening, R8G and C64 have been pointed out as the better carbons for sulphur and siloxanes removal respectively. As will be discussed later, these are the chosen materials for the DEMOSOFC installation.

The second section of the results is related to the analysis of some specific factors which are influencing the adsorption capacity detected in the first tests. There are indeed fluid-dynamic and chemical factors which can increase or reduce the nominal performance measured in the standard conditions.

Effect of O$_2$

Sitthikhankaew et al. (Sitthikhankaew et al. 2014) already analysed the positive effect of oxygen on impregnated activate carbons, especially the ones impregnated with iodine and potassium, like the Airdep ACs. Experimental test conditions for the tests are:

- H$_2$S concentration: 95 ppm
- Total flow rate: 200 ml/min

- Composition CH_4/CO_2: 62.5/37.5 %
- Sample diameter: 4 mm (int.)

Results are shown in Figure 193. As anticipated, the presence of oxygen, evne in low quantities (0.1%) strongly enhance the performance of the AirDep CKC impregnated carbon. Adsorption capacity at breakthrough increases from around 1 to more than 80 mg/g.
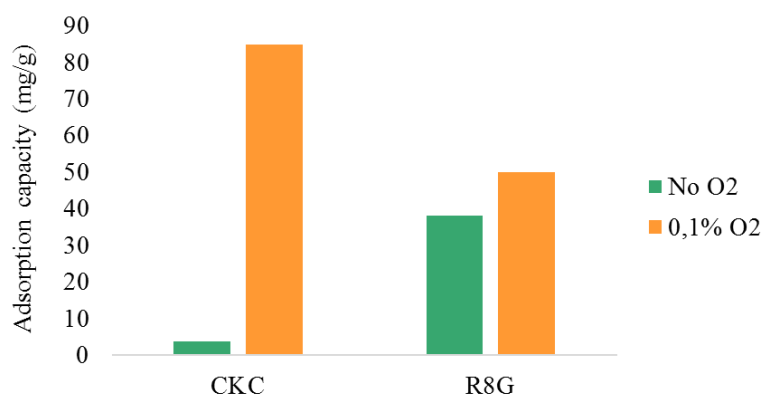
Figure 193. Effect of oxygen on CKC and R8G carbons.

Sulfatrap R8G also shows a 30% increase compared to the standard test conditions. In some traditional anaerobic digester plants, oxygen can be found in the inlet biogas, usually because of air leakages into the digester. The analysis on oxygen was also performed in the SMAT biogas during the eight months gas analysis shown before. As can be seen on Figure 194, the oxygen content changes rapidly during the months, from more than 0.3 to less than 0.05.

Oxygen, as pointed out by (Sitthikhankaew et al. 2014), strongly enhance the performance of impregnated activated carbons because chemically reacts with hydrogen sulphide and generate elemental sulphur. A second mechanism, besides pure adsorption, is thus generated by the presented of O_2.

Because of this instability in the measurement, Airdep AC were not considered for the first reactor filling at the DEMOSOFC site. The continuous gas analyser which will be installed in the clean-up container will give information on the real oxygen amount during system operation. In case a constant minimum oxygen amount will be detected, when the first carbon fill will be replaced, another type could be chosen and inserted in the system.
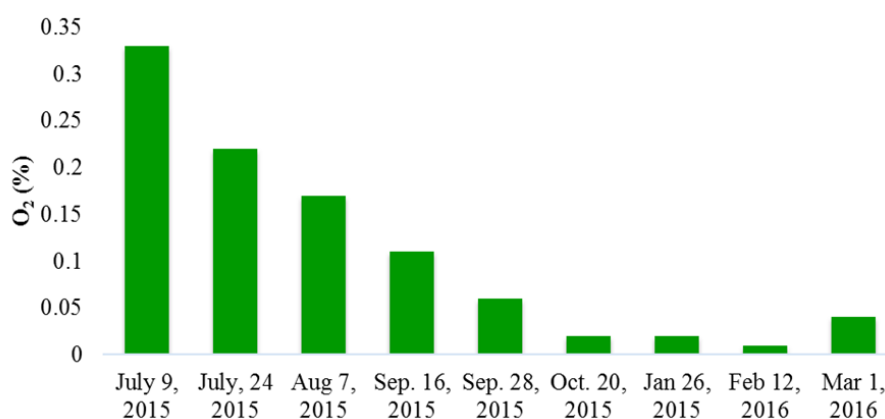
Figure 194. Oxygen concentration in the SMAT biogas. Measurements from the analysis shown in Table 39.

Effect of the Spatial Velocity

The second analysed parameter is the gas spatial velocity. Laboratory experiments are usually performed using micro-reactors, in order to reduce the total experiment time. In the presented experiments, by using a 4 mm sample, the spatial velocity of the gas was 0.995 m/s. On the other side, the spatial velocity on the real DEMOSOFC site will be 0.04 m/s. For this reason, it is interesting to know the effect of this parameter in order to understand the relationship between the performance measured in the laboratory and the real performance expected on the plant site. A lower spatial velocity was reached by using a large sample, 10 mm internal. Test duration also increases since the L/D ratio was kept constant.

Expected results were better performance at lower spatial velocity. A similar analysis has been proposed by Sisani et al. (Sisani et al. 2014) where the influence of the Gas Hourly Space Velocity (GHSV) was analysed . GHSV is directly linked with the spatial velocity, and is directly proportional in case the reactor length is kept constant. This specific test has been performed for R8G carbon only. The reduced velocity tested is 0.159 m/s, still four times higher than the real one. The reason is linked with the duration of tests when the velocity is decreased at values lower than 0.1 m/s: increasing the sample diameter, but trying to keep a constant L/D ratio, generates long duration tests, with breakthrough times in the order of weeks.

The test conditions for the analysis on GHSW are the following:

- H_2S concentration: 50 ppm
- Total flow rate: 750 ml/min
- Composition CH_4/CO_2: 62.5/37.5 %

Results are shown in Figure 195 and . As can be seen, the adsorption capacity increases of 97% when the velocity is decreased from 0.995 to 0.159 m/s. The increase is due to the increase in the contact time between the gas stream and the activated carbons surface: the adsorption performance are consequently improved.
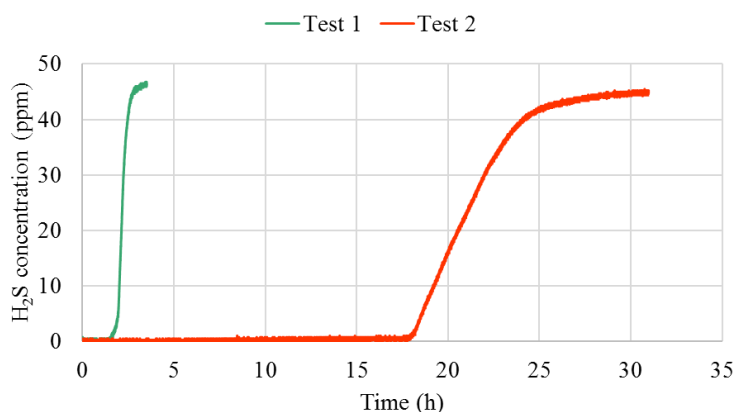
Figure 195. Effect of GHSV on the performance of R8G.

Table 45. Effect of GHSV on the performance of R8G.

	Sample Φ_{int} (mm)	GHSV (h-1)	Velocity (m/s)	Adsorption capacity at breakthrough (mg/g)
Test 1	4.00	155,695	0.995	31.38
Test 2	10.00	25,000	0.159	61.82

The last section of the results chapter is devoted to a general view on the other ongoing tests, fundamental for the deep understanding of the adsorption phenomena involved in the real plant, but still under development. A more detailed description of these tests with updated results will be included in the PhD thesis of Davide Drago (Drago 2017).

Other results

An interesting results, obtained in the external tests with siloxanes, is related to the decrease of the adsorption capacity when the carbon is fed with a mixture of different compounds. This has been investigated for R8G, fed by a mixture of D4 and various sulphur-based contaminants, by analysing the adsorption capacity in terms of siloxanes.
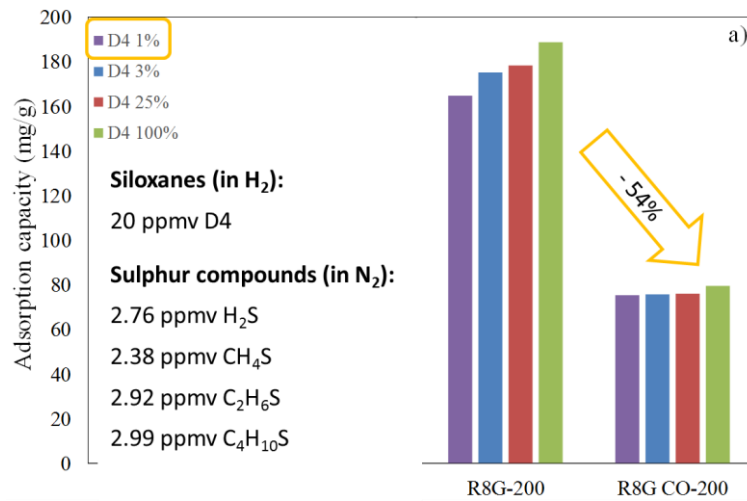
Figure 196. Multiple compounds effect on D4 adsorption capacity.

Results are shown in Figure 196. A reduction of more than 50% is detected when various sulphur species are contained in the biogas flow. This effect needs to be analysed more in detail since, as shown in Table 39, the analysis of SMAT biogas reveals that H_2S and D_4 are the most significant compounds in terms of SOFC degradation but other compounds non detrimental for the fuel cell, such as organic compounds, could be influencing the performance of the activated carbon.

The second results shown (Figure 197) is related to variation of performance of a single carbon (CKC in this case) when the inlet H_2S concentration is varying. this curve is currently under development also for the chosen R8G carbon. By knowing this trend, it is possible to estimate the performance, and consequently the lifetime, of the selected carbon when the inlet sulphur concentration is varying.
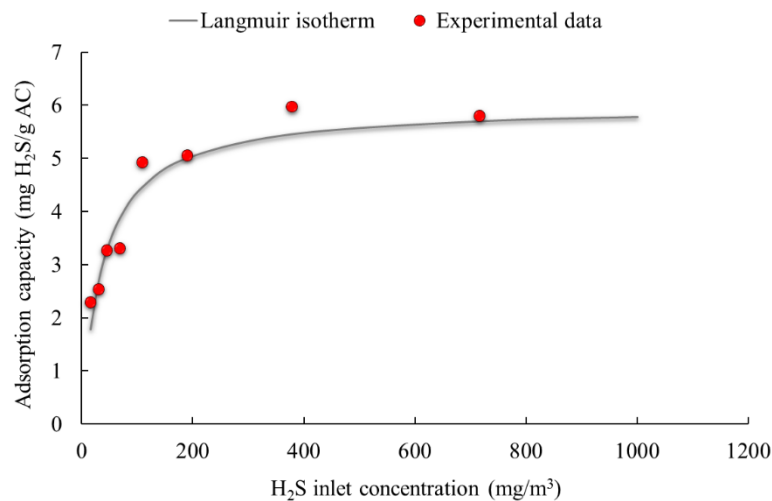
Figure 197. Concentration curve for CKC.

5.1.3 DEMOSOFC cleaning system layout

From the results of the first experimental test campaign in the POLITO laboratories, the selection of the first vessel filling was done (Figure 198). The first and second lead and lag sections will be filled with the same sequence: first C64 for siloxane removal and then R8G for sulphur removal. This choice was due to the analysis on multiple compounds performed also in terms of H2S. R8G adsorption capacity in terms of sulphur was in fact decreasing more, in presence of multiple compounds, than C64 adsorption capacity in terms if siloxanes. C64 performance were halved but the absolute value was anyway higher than 60 mg/g at breakthrough, which corresponds to a high replacement time (more than 12 months). On the contrary sulphur capacity, already lower in terms of mg/g, was reduced to a non-acceptable value.

The last two reactors, placed as ultrafiltration and safety beds, will be filled by C64 only, for two reasons: first, siloxanes are more detrimental than sulphur for the fuel cell; second, based on previous knowledge of the Airdep carbons, C64 should be able to partially remove sulphur (test on C64 fed by H2S will be performed).
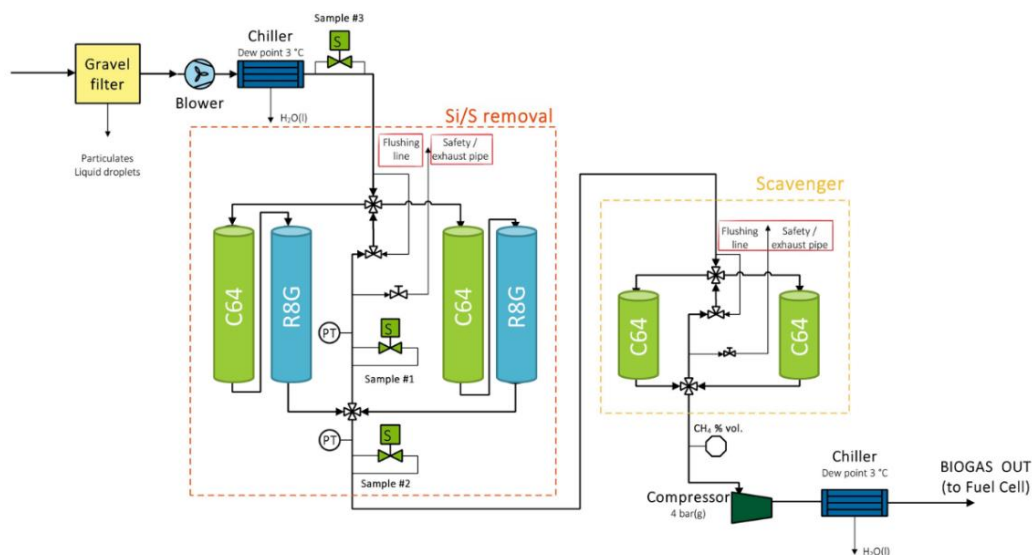
Figure 198. DEMOSOFC cleaning system final layout.

Some final economic considerations are presented in order to show the investment cost for the chosen solution and the replacement times and costs.

Costs presented here will be referred to the activated carbons only. Investment costs and maintenance for the overall clean-up unit have been analysed in one of the author

publication were the entire system is analysed from an economic point of view (Mehr et al. 2017).

The cost for the initial fill of the six reactors is equal to 10,138 € (Table 46), and more than 78% is due to the two reactors filled with R8G.

The replacement time for one reactor, with the current performance from the experimental campaign, is more than 16 months for R8G (sulphur removal) and 49 months for C64 (siloxanes removal). This corresponds on a yearly average cost (calculated on a 10 years lifetime) of 3,340 €, which is acceptable for the plant owner and is considerably lower than literature data (Argonne National Lab reports values around 0.1 c$/kWh that, for a 174 kWe is around 15,000 $). Even if labour cost and disposal should be included besides the value of material only, the final cost should be acceptable. Disposal cost, in particular, is hard to be known and could strongly influence the final cost of activated carbon since they are classified as 'special waste'.

Table 46. Investment cost for the first vessels filling with the selected ACs.

Reactor	AC	Costs (€/reactor)
Lead reactor 1	C64	€ 550
Lag reactor 1	R8G	€ 3'969
Lead reactor 2	C64	€ 550
Lag reactor 2	R8G	€ 3'969
Scavenger reactor A	C64	€ 550
Scavenger reactor B	C64	€ 550
Total AC Cost		**€ 10,138**

Table 47. Replacement time and cost for one reactor of R8g and one of C64.

Parameter	Value	Unit
1 Reactor of R8G		
Adsorption capacity H_2S @ 20 ppm	61.82	mg/g
Entering H_2S value	20	ppm
Duration	16.12	months
Number of substitutions per lifetime (10 y)	7.55 (8)	
Yearly cost	3'175	€/y
1 Reactor of C64		

Adsorption capacity D4 @ 20 ppm	97.00	mg/g
Entering D4 value	1	ppm
Duration	48.85	months
Number of substitutions per lifetime (10 y)	2.49 (3)	
Cost	165	€/y

5.2 Challenges for biogas-fed industrial SOFC systems

The activities already performed and ongoing in the framework of the DEMOSOFC project have pointed out technical and economic challenges and benefits for biogas-fed industrial size SOFC systems. Specific topics are listed below.

- **Biogas cleaning system**. As described in the previous chapter, biogas cleaning system is a challenging technical issue from both technical and economic aspects. From the technical point of view, scientific knowledge on adsorption phenomena and contaminants removal technique is available, but a complete cleaning system able to reach the requested purification limit for fuel cells is not yet commercially available. Cleaning unit designed for specific installations are available, but a complete on-field experience on these systems is missing. The DEMOSOFC proposed layout is probably over-sized and with a very high safety design coefficient, being the first for this kind of applications. Future similar system should be optimized in terms of total number of reactors in order to also reduce the total area required for biogas processing. Furthermore, a flexible cleaning system able to remove contaminants in more than one biogas site is fundamental to commercialize SOFC in the biogas sector. Depending on the level of contaminants, some low-medium-high ranges should be defined and for each of them, a standard solution should be available. Replacement costs are not impacting too much on the total system cost, but more information are required on the carbon disposal or, eventually, regeneration.

- **Thermal integration**. WWTPs usually show higher thermal loads for digester heating compared to other biogas sites. This is, as discussed before, due to the low solid content in the entering biomass. This could be a problem when a high electrical efficiency CHP system is installed, such an SOFC. To better match the thermal production and the thermal requirement, some improvement in the anaerobic digestion are fundamental, such as sludge pre-thickening to reduce the liquid content and consequently the thermal load of the digester.

- **SOFC module**. The SOFC modules available in the market are already quite close to an early commercial product, since they are able to provide directly AC power from inlet biogas. Main criticalities for the diffusion of the SOFC technology are related to the system costs and lifetime. Demonstration projects, like DEMOSOFC, are fundamental to gain on-field experience, to test the system in real operating conditions and get results on the real system lifetime and degradation rate. Furthermore, dedicated policies are required for the commercialization of these systems. Biogas is an interesting application market since subsidies for electricity production from biogas are already available in many EU countries, thus creating benefits in the system economic performance.

Chapter 6

Conclusions

The presented work has been focused on the analysis of biogas-fed SOFC systems, with the 'option' of carbon capture. The analysis has been divided into different section: first a general introduction and motivation of the work, followed by the analysis of potential biogas market in EU (*Chapter 2 - Potential for SOFC in biogas applications*).

Biogas is proposed as a first promising market for SOFCs. The reasons for biogas can be found in the low average size of the sites, which better fits fuel cells than traditional internal combustion engines since SOFCs can guarantee a high electrical efficiency despite the size. Furthermore, policies and subsidy schemes are already available for electricity production from biogas, thus providing a positive effect on the economics of the installation. The calculation of the size of the biogas market in EU is thus a key indicator of the potential impact of fuel cell installations in this specific field.

A biogas potential of around 32 Mtoe/yr has been found, confirmed by Aebiom report for biogas potential (Aebiom 2009), which stated a potential of 40 Mtoe in 2020 as compared to a production of 5,9 Mtoe in 2007. According to the 40 Mtoe proposed, in 2020 biogas could deliver more than a third of Europe's natural gas production or around 10% of the European consumption (433,7 Mtoe in 2007).

After having analyzed the area of the analysis (biogas) and its size (potential market), the work focuses on the SOFCOM specific case study (*Chapter 3 - The SOFCOM proof-of-concept: Experimental activities*): the first demonstration, at proof-of-concept level, of a tetra-generation system able to produce electricity, heat, algae and clean water is presented. The chapter is related to a real experimental activity on an SOFC based system

with carbon capture and re-use. The system has been in operation for more than six months in the Turin premises (IT) and single components tests have been performed before running the whole plant. Results show good performance regarding electricity production from SOFC and carbon capture. CO_2 could be easily separated from the anode exhaust, and a pipeline-quality CO_2 stream was obtained, with a water content around 100 ppm. On the contrary, the performance of the photobioreactor for algae production were lower than target values from literature and the management of the system was hard and unstable, because of fluctuating parameters such as weather conditions, algae growing rates, and quality of the inlet wastewater (in terms of nutrients and impurities). The SOFCOM project and thesis objective was the demonstration of the feasibility of carbon capture from SOFC at a proof-of-concept level, in an non-laboratory environment: the goal was reached and carbon dioxide was not only separated but also re-used to fix available carbon in form of microalgae.

The same concept of carbon capture from SOFC systems has been then analyzed, from a techno-economic point of view, in *Chapter 4 - The SOFCOM proof-of-concept: Modeling of biogas-fed SOFC systems*. The modeling activity has examined different biogas sites according to inlet biomass and plant size, and for each of the size ranges, specific bottom processes and sensitivity analyses have been proposed. An initial roadmap shows the map of the activities performed. Results pointed out the advantages of fuel cells, for what concerning electrica production and overall system efficiency. On the contrary, the economic analysis shows a still hard market entry for fuel cells, due to low production volumes and related hard costs. Use of target costs (defined by the SOFC manufacturers) leads to better economic profiles, especially when biogas subsidies are considered. Subsidy schemes have been analyzed for four different countries and results compared. Germany and Italy seem to be the most interesting markets for what concerning SOFC applications in biogas sites.

Finally, *Chapter 5 - Design and criticalities of industrial SOFC plants* is devoted to the analysis of a real industrial size biogas-fed SOFC system. The plant is under construction in the framework of an EU project, DEMOSOFC, in the Turin premises. The plant will include three SOFC modules able to produce 58 kWe each, for a total installed power of 174 kWe. The work is devoted to the description of the system layout, which is different from a traditional ICEs plant especially because of the biogas cleaning unit, strongly impacting the whole plant design. Experimental activities on contaminants adsorption by activated carbons are also presented as a key activity for the definition of the biogas cleaning unit design. Main criticalities encountered during the system design and analysis are also listed and discussed.

The work proposed in this PhD thesis will be continued in the next months in the framework of the DEMOSOFC project. Activities related to installation, start-up, and

operation of the plant will be fundamental to face and understand real problems when SOFC systems move from laboratories to a real industrial environment. Economic analysis will also be performed to include all actual costs for site preparation and installation found during this real experimental activity. The DEMOSOFC project will give an extraordinary opportunity of understanding the SOFC performance and criticalities in a real industrial environment. Literature data have provided us with many data on SOFC performance and lifetime, but only a real industrial installation can confirm these predictions. Furthermore, the understanding of the possibility of market entry of this promising technology should be analyzed, and dedicated policies should be proposed to reach a number of installations able to reduce the costs and make SOFCs finally competitive.

Appendix

Appendix 1 – Biogas potential calculation method

A1.1 Biogas substrates

This section is related to the analysis of the possible biogas substrates and the general AD plant layout. The work is developed to analyze biogas production from a high number of available substrates (Figure 23).

<u>Energy crops</u>

Despite being a controversial biomass, crops are one of the highest possible sources for biomass, since they present one of the highest methane conversion yields. Because of the '100%' organic content, not exploited in crops, the biogas conversion rate is high compared to 'wastes': here, the organic content has been already partially exploited in the digestion process inside the human/ animal being, and thus the biogas yield is reduced.

Different literature works have been analyzed to find a mean value for the crops yield. First of all, every single crop (maize, wheat, triticale) has a proper biogas yield, expressed in Nm^3 biogas per tons of inlet biomass. Since the values, as will be shown later, are similar, a mean value as been used thus avoiding to define the quantity of every single crop.

As can be seen from the table above, values for the most common crops used for biogas (corn, maize, triticale, sorghum) are similar. For this reason, the author chose a mean value equal to 150 Nm^3 biogas/tons of crops. This value, if converted with a general Total Solid (ST) of 27.5 % and Solid Volatile ratio (SV/ST) of 90% (both values confirmed as mean values by (Kothari et al. 2014), (Grignani et al. 2006)), is equal to a yield of 650 Nm^3/t SV.

It is fundamental to underline that the values above refer to cereal silage: this means that all the vegetable is harvested and fed to the digesters. On the other side, in the case of food production, the cereal is collected in a way to keep separated the grain and the waste part (straw). The agricultural wastes section will analyze these residual substrates.

The methodology shown below will include the calculation of the chosen % of arable land for biogas and the cereals production per hectare. This value is strongly depending on the growing method followed by the plant operator, the geographical location, and the soil type. If the crop is fertilized and irrigate, the production yield could be the double of non-treated crops. Furthermore, weather conditions could influence the yearly cost of treatments. Since we analyze different cereals, a brief discussion on their production cycle should be defined:

1 Maize, rice, and sorghum are "summer" cereals: being cold-intolerant, they must be planted in the spring and usually harvested in September.

2   Wheat, Triticale, and Barley are "autumn-winter" cereals and are thus planted in autumn and harvested in the late spring.

As can be seen from the list above, the two bowls of cereal groups refer to two different seasons of the year. This means that a field could be used for the production, in the same year, of a cereal of group #1 during spring and summer, and a cereal of group #2 during autumn and winter. The two growing phases are not 100% separated, and thus this could be done for energy purposes since the plants do not require the total maturity of the kernel. On the other side, this technique could be difficult. Even if some plants perform this procedure, we have performed the calculation with a unique cereal production per year, to have a conservative energy potential from crops.

Table 48. Analysis of yield values available on the literature for different crops.

Substrate	Reference	Biogas yield [Nm³/t SV]	Biogas yield [Nm³/t fresh]
Crops (general)	(Reale et al. 2009)	550 – 750	
	(Kothari et al. 2014)	650	
	(Biocombustibili n.d.)	550 – 560	
Maize silage	(Reale et al. 2009)	600 – 680	190 – 210
	(Aebiom 2009)		200 – 220
	(Adani 2008)	647 – 689	
	(Grignani et al. 2006)	660 – 770	
	(Appels et al. 2011)	480 – 600	
Sorghum silage	(Reale et al. 2009)	500 – 560	140 – 160
	(Aebiom 2009)		100 – 130
	(Adani 2008)	557 – 631	
	(Grignani et al. 2006)	660 – 670	
	(Appels et al. 2011)	485 – 535	
Triticale silage	(Reale et al. 2009)	550 – 650	170 – 200
	(Appels et al. 2011)	535 – 565	
Grass silage	(Reale et al. 2009)	500 – 550	130 – 140
	(Aebiom 2009)		160 – 170
	(Appels et al. 2011)	485 – 535	

	(Biocombustibili n.d.)	400-520	
Rye silage	(Aebiom 2009)		170 – 180
Wheat	(Appels et al. 2011)	585 – 635	

Sewage Sludge

Sewage sludge is the sludge produced by the wastewater treatment. Wastewater is collected from domestic and industrial sites and is treated in a wastewater treatment plant (WWTP); sedimentation and chemical processes clean the entering water and produce sludges as a by-product. Due to their high biological concentration, sludges cannot be discharged as they are and the anaerobic digestion is the common way to cut down their bacterial load. The yield of WWTP biogas is taken from real plants in the Turin premises. SMAT (Anon n.d.), which is the municipality which supplies clean water and collects and discharge wastewater, has been a partner of Politecnico di Torino in different projects. The biogas yield available from their plants (in particular Castiglione and Collegno plants, which are presented in Chapter 3 and 5) is 390 Nm^3 of biogas per ton of SV. The SV/ST ratio is usually 70%.

The methodology section will explain the calculation of the production of waste water and thus biogas per capita per day.

Municipal Solid Waste – OFMSW and LBG

Biogas can be derived from different part of what is normally called "MSW". From the literature, it is known that the domestic wastes are normally recycled or landfilled. The recycled quota is then divided into paper, plastic, metals, and an organic fraction. Biogas can be generated or in a landfill, thanks to the aerobic digestion of the organic parts contained in the mixed wastes, or in a dedicated anaerobic digestion plant for OFMSW.
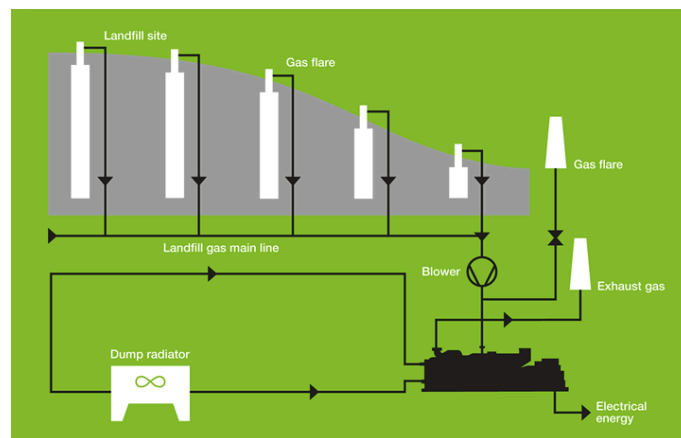
Figure 199. Layout of a landfill.

From (Themelis & Ulloa 2007), some data are available on the MSW composition in the US. From the data (Figure 200), it seems that around 30% of the MSW is recycled, 13% sent to energy purposes and 55% landfilled. The situation is slightly different in EU. Denmark and Germany (Kjaer 2013) (Fischer 2013) have more than 50% recycling (value imposed by EU for 2020), Austria is near 60% (Herczeg 2013). In Italy, the value was 34.9 % in 2012, with peaks of 79.5% in Pordenone and minimum of 3% in Siracusa[1]. The mean value for EU is around 36%[2][3], which is also the value used for the calculations.

	14th SOG survey [3,4]		USEPA 2001 survey [5]	
	Million tonnes/yr	(%)	Million tonnes/yr	(%)
Amount generated	336	100	211	100
Amount recycled and composted	90	26.7	65	30.8
Amount to waste-to-energy	26	7.7	27	12.8
Amount landfilled	220	65.6	119	56.4

Figure 200. Generation and fate of MSW in the USA. (Themelis & Ulloa 2007)
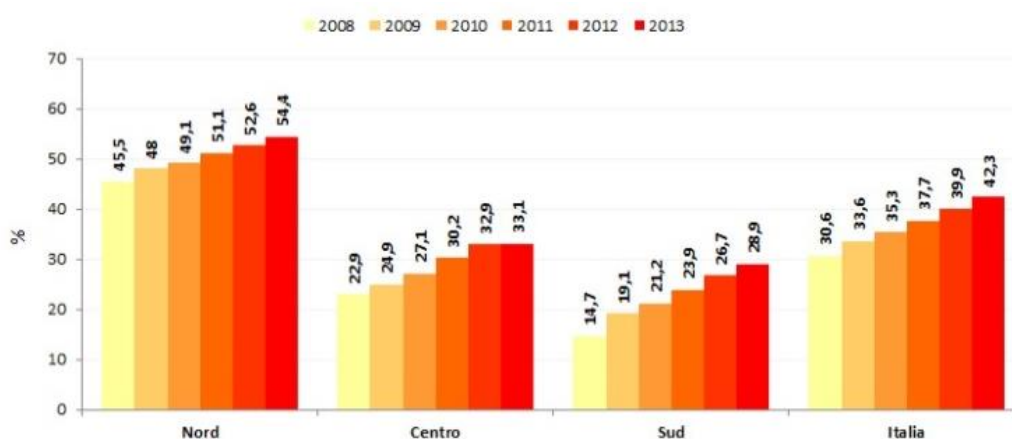
Figure 201. Italian recycled rate in North, Centre, and South, from 2008 to 2013.[4]

---

[1] http://dati.istat.it/Index.aspx?DataSetCode=DCCV_INDRACDIFF
[2] http://www.eea.europa.eu/media/newsreleases/highest-recycling-rates-in-austria
[3] http://ec.europa.eu/eurostat/statistics-explained/index.php/Waste_statistics
[4] Rapporto ISPRA 2014
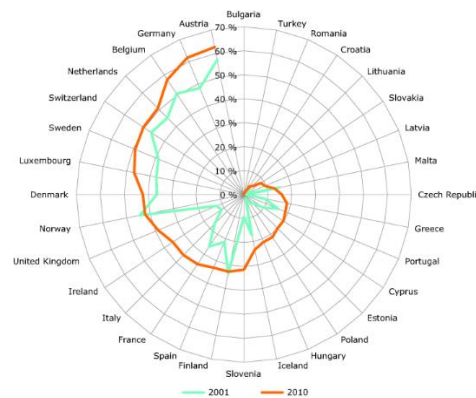
Figure 202. Percentage of recycling in different EU countries (European Environmental Agency (EEA) 2013).

Among the recycled wastes, we also need to determine the OFMSW percentage. This value is thus a sub-percentage of the recycled quota. From different sources (Erler n.d.) (Kjaer 2013) (Novamont S.p.a. n.d.) (Themelis & Ulloa 2007) and[5], the % of OFMSW over total waste has been found, and a mean value, with a lower than 5% error, of 15% has been chosen. Only some country like Austria (Herczeg 2013), in which recycling is at high percentages, can reach up to 30% OFMSW.
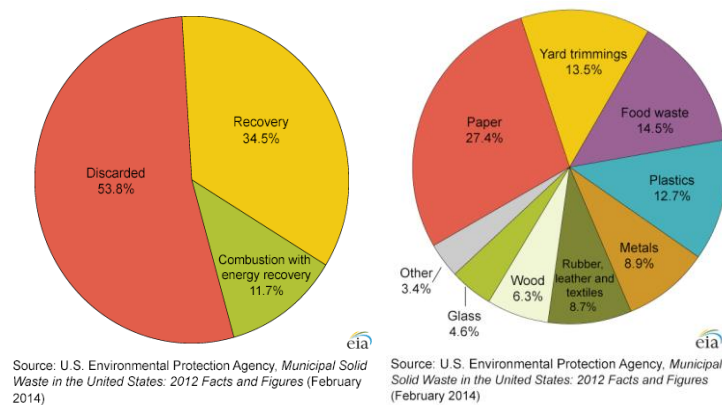
Figure 203. Management of MSW in the USA in 2012 (left) and Total MSW generation by material in 2012 (right).

Due to the probable impossibility of collecting 100% MSW (because of rural areas with diffused low productions where probably the transport cost would be higher than the profit), the 15% value has been chosen for the analysis.

The biogas yield from LBG and OFMSW has also been determined. For what concerning LBG, as discussed in the previous paragraphs, the gas production is not constant during the landfill site lifetime (Figure 204), but is rapidly increasing from zero to a

---

[5] http://www.epa.gov/wastes/nonhax/municipal

maximum value in the first years and then slowly decreasing in the remaining years until landfill shut-down.

Furthermore, often the gas production is measured but not directly linked to the amount of MSW introduced since this happens in a batch mode. Values of methane production as a function of the inlet MSW are available from:

- (Anon n.d.) 30 m^3 biogas/t MSW, calculated using a methane percentage of 50%
- (Surroop & Romeela 2011) 59.9 m^3 biogas/t MSW, calculated with the same CH_4 %
- (Lohila et al. 2007) 39.4 m3 biogas/t MSW

A mean value of 43.1 m^3 biogas/t MSW has been determined and used for the calculations. The three reference data are close to the same value, and thus the error will be acceptable compared to the results data precision.

For the OFMSW the data was easier to be found and more in line between various literature sources. The chosen reference value, 123 m^3 of biogas for tons OFMSW (Cvetković et al. 2014), has been confirmed by different literature sources. (Biocombustibili n.d.) shows 100-120 m^3 of biogas per ton of biomass and the Turin integrated waste treatment plant "Acea Pinerolese" reports a value of 134 m^3 of biogas per ton OFMSW (Organica & Territoriale n.d.).
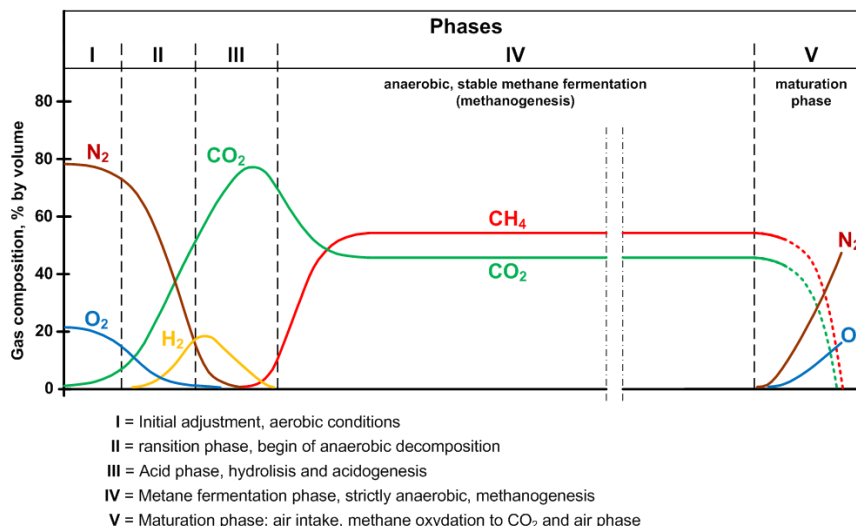
Figure 204. Landfill life cycle related to CH4/CO2 production. (Green Energy 2014)

Livestock effluents

Many AD plants have been installed during last years fed by a mix of energy crops and livestock effluents. Livestock effluents potential is usually low if biomass pre-treatments

are avoided and has a quite high thermal request because of its low density. This reduced biogas yield is the reason why usually is mixed with crops, to enhance the anaerobic digestion productivity. Nevertheless, in last years, plants fed by 100% livestock effluents can be found in the EU area. This is due to the reduction in incentives for energy crops but especially to the expensive and environmentally challenging disposal of effluents. Problems are in fact related both to the application of the EU directive 91/676/CEE on nitrates (Directive 1991) and on the odor control. The directive sets a maximum of kg N per hectare depending on the area and, as known, effluents are rich in N and P. Furthermore, the odor could be a problem in touristic areas or fields close to residential districts. Anaerobic digestion could be an answer to these problems since the ammonia compounds, responsible for the odor, are here removed, and the digested biomass is still available for fertilization.

The potential from livestock effluents has not been determined using an average value for all animals types but taking into account the single animal numbers per country and the related biogas yield. For each animal species, the effluents production per day regarding kg SV per day has been determined from (Biocombustibili n.d.) where data were available on the effluents medium production (kg/day) and mean SV and ST percentages. From the same reference, we also estimate the biogas yield.

Table 49. Effluents generation per day per animal and SV content.

Pig		
Pig medium weight	180	kg
Pig medium effluents	10.35	kg/day
Pig medium organic effluents	0.714	kgSV/day
Cattle		
Cattle medium weight	600	kg
Cattle medium effluents	42.6	kg/day
Cattle medium organic effluents	4.463	kgSV/day
Buffalo		
Buffalo medium weight	600	kg
Buffalo medium effluents	54.8	kg/day
Buffalo medium organic effluents	5.400	kgSV/day
Chicken + Poultry + Turkey		
Chicken + Poultry medium weight	5	kg
Chicken + Poultry medium organic effluents	0.0015	kgSV/day

Rabbit		
Rabbit medium weight	7.3	kg
Rabbit medium effluents	0.118	m³/day
Rabbit medium organic effluents	0.033	kgSV/day
Horse		
Horse medium weight	450.0	kg
Horse medium effluents	40	kg/day
Horse medium organic effluents	2.700	kgSV/day
Sheep		
Sheep medium weight	57.5	kg
Sheep medium effluents	3.675	kg/day
Sheep medium organic effluents	0.303	kgSV/day

The main hypothesis is the percentage of livestock which can be exploited for energy purposes since a part is commonly used as fertilizers. Even if, using the manure for biogas production, generate a secondary stream of digested biomass which is used as fertilizer, usually not 100% of the manure fed to the anaerobic digestion. In our calculation, a value of 50% of livestock for energy production has been chosen: even if in some reports values around 30% can be found (Aebiom 2009), the choice is due to the digested biomass production from anaerobic digestion. Existing plants are in fact able to fertilize their fields only with digested biomass from anaerobic digestion, thus avoiding direct use of effluents on the field. Currently, the main substrates for biogas production are cattle liquid and solid manure, pigs liquid manure (pigs only produce liquid manure) and chicken manure.

Table 50. Biogas yields for livestock effluents.

Animals	**Reference**	**Biogas yield [Nm³/tSV]**
Cattle		295
	(Reale et al. 2009)	215 – 230
	(Grignani et al. 2006)	200 – 292
	(Biocombustibili n.d.)	350
Buffaloes		295
Sheep + Goats	(Reale et al. 2009)	370
Pigs		396
	(Reale et al. 2009)	355 – 400
	(Adani 2008)	387
	(Grignani et al. 2006)	340 – 400

Horses	(Reale et al. 2009)	300
Chickens + Turkeys + Poultry		383
	(Reale et al. 2009)	300 – 400
	(Adani 2008)	416
Rabbits	(Adani 2008)	351

Agricultural wastes

Agricultural wastes include all the wastes and residues derived from the cropping of the cereals for food production.
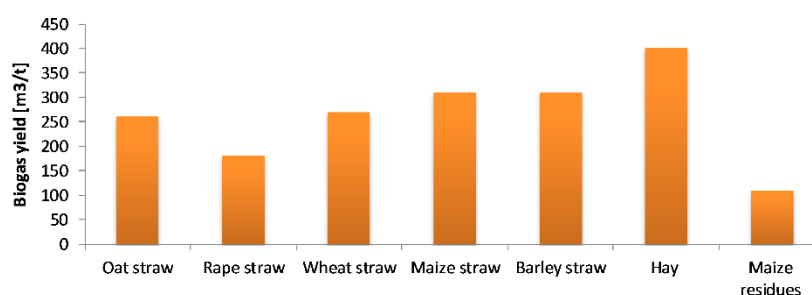
Figure 205. Biogas potential from different agricultural wastes.

This group includes straw, stalks, and cobs. These materials, despite of a low specific weight and a limited biogas yield, are a free substrate for biogas production. For collecting these residues, plant owner should equip harvesting and threshing machines with an optional part able to collect such residues and not letting them on the field. As for the energy crops, this substrate can be stored during winter and used through all the year.

Table 51. Biogas yields for different biogas residues. (TPEnergy n.d.)

Substrate	Biogas yield [m^3/t]
Oat straw	260
Rape straw	180
Wheat straw	270
Maize straw	310
Barley straw	310
Hay	400
Maize residues (stalks, cobs)	110
Mean value	263

Industrial wastes/residuals

The analysis of the agro-industrial wastes for biogas production has been conducted, starting from the work of (Biocombustibili n.d.), according to different sectors:

- Milk industry
- Fruit and vegetable industry
- Wine industry
- Beer industry
- Distillation industry for alcoholic beverages
- Slaughterhouse industry
- Beer industry
- Cereal industry

Dairy industry

The dairy industry is usually related to the processing of fresh milk for the production and supply of long-life milk, cheese, yogurt, and butter. From cheese production, a residual product called serum is generated, with a high organic load, and it is usually sent to WWTPs. Because of the high organic content, plant owners need to treat the serum before sending it to the wastewater treatment plant, according to D. Lgs 22/1997. Serum could thus be an optimal substrate for biogas production as mentioned in the Directive CE 1774/2002, after pasteurization at 70 °C. From yogurt and butter production, furthermore, other residuals are generated which are usually sent to WWTP or used for animal feed production or composting.

All these residual are classified as "sub-products coming from an animal source", and are thus usually granted with high incentives in case of biogas production. The production rate is variable during the year according to the seasonal market request: an anaerobic digestion plant located on the site should thus be able to store the residuals or to have other feeding streams to guarantee a continuous operation of the system. The table below shows the residuals production and biogas yields for the milk industry.

Table 52. Serum biogas yield. (Biocombustibili n.d.)

Sub-product	Production [kg/ton milk]	Biogas [m^3/t]
Serum	500	25
Other residual	5,4	500

Fruit and vegetable industry

The fruit and vegetables processing industry also generate many residuals. Excluding the case of processing for fresh products market, which generates almost no residuals, when fruits and vegetables are treated to obtain juices, pulps, and soups, the process creates many sub-products like peels, kernels and filtration residuals. These residual are used for animal feed, composting, boilers or AD. It is important to remind that the quantity of residual is highly changing depending on the fruit/vegetable type. For example, red fruits have almost zero residuals.

In this analysis, we have analyzed the fruits and vegetables shown in Table 53, since these are the ones that are mainly produced in EU and processed for juices, soups and transformed food. Among the total values of production in each EU country, the quota related to the fresh market (no processing) should be defined. Furthermore, we considered that not all the residuals are exploited for energy. For this reason, only 40% of each product is producing residuals in the analysis. The 40% is not a literature number since no data is available at a national/ European level on this value. Furthermore, the chosen vegetables and fruits certainly do not cover to EU production. The table below shows the residual percentages over the initial product quantity.

In Europe, many countries as Spain, Portugal, Italy, Poland, and Germany are the worldwide leader in specific vegetables/fruits products, and thus a high interest in residual treatment for energy purposed can be found. Grapes have not been included in this calculation since the wine industry section includes them (we only made the hypothesis that most of the grape production goes into wine process).

The biogas yields for different residuals have been taken from a work of Regione Lombardia on the biogas production from wastes (Regione Lombardia 2013).

Table 53. Residual quota for different fruits and vegetables. (Rossi & Piccinini 2009)

Fruits / Vegetables	% Residue
Potatoes	22.5%
Tomatoes	3.1%
Olives	45.0%
Onions	28.1%
Citrus	37.5%
Apples + pears	4.3%
Peaches	4.3%
Plums	4.3%
Watermelon + melon	4.3%

Table 54. Biogas yields from fruits and vegetables. (Regione Lombardia 2013)

Sub-product	Biogas [m³/t]
Potatoes pulp	75
Marc without stalk	90
Olives virgin residues	95
Apples residues	105
Tomatoes peels	105
Fruits residues	205
Bread residues	585
Oil residues	675
Onion peels	269
Mixed food wastes	120

Wine industry

The wine industry is generating different residuals from the fermentation of the grapes into wine. These residual include peels and branches of the grape itself. Currently, they are sent to distillation industry (according to CE 479/2008 and CE 555/2008 it is mandatory to send a part of the grape branches to the distillation industry) or used for agronomic purposes. Since the highest production (18 kg/hl wine over 2.5 and 4) is related to the peels, they are considered as the only substrate available for AD.

Table 55. Grapes residual biogas yield. (Biocombustibili n.d.)

Sub-product	Production [kg/hl wine]	Biogas [m³/t]
Peels	18	62
Branches	4	n.a.
Seeds	2,5	n.a.

Slaughterhouse industry

The slaughterhouse industry potential is related to the residual from the animal processing. Main residuals are:

- Rumen contents
- Blood
- Stomach

Table 56. Slaughterhouse residues biogas yield. (Biocombustibili n.d.)

	CATTLE	SHEEP+GOAT	PIG	Biogas yield [m³/t]
Medium weight – kg per cap	100	24.5	160	
Rumen contents - % of weight	1.6%	0.0%	0.0%	188.5
Blood - % of weight	2.4%	5.5%	2.9%	70
Stomach - % of weight	0.0%	7.8%	7.0%	43.5
TOT - % of weight	4.00%	13.30%	9.81%	

Other residuals are produced from the processing, but their use is not allowed for energy scope, according to Directive CE 1774/2002 and CE 1069/2009 (according to this directive, only type II and III animal sub-products can be used for AD). Furthermore, and this is one of the main obstacles to their use for energy, is the requirement of a pasteurization at 70 °C for 60 minutes before the AD plant. While this request was not a challenging problem in the milk industry, where pasteurization is a standard part of the milk treatment process, the request in this scenario is economically and energetically expensive.

Furthermore, these residuals usually already have their processing for animal feed, fertilizers or chemical industry.

Beer industry

The EU beer industry is concentrated in specific EU countries like Belgium, Czech Republic, and Germany. From the beer production process two main residuals are available:

- Malt residuals (spent grain) coming from the malt decantation procedure, mainly made by the grain peel.
- Yeast, used for the beer fermentation.

Both of these residuals are currently widely used in the animal feed industry or for chemical processes (extraction of vitamin B12 from yeast). Nevertheless, the beer process requires energy regarding electricity and heat thus making interesting the analysis of the alternative scenario with AD.

Yields value for the two residuals is shown in the table below.

Table 57. Beer residues biogas yield. (Biocombustibili n.d.)

Sub-product	Production [kg/hl beer]	Biogas [m³/t]
Spent grain	18	131

Yeast	3	66

Cereals industry

The cereal industry is related to the processing of raw cereals to obtain flours for human food, animals feed and processed cereals. The cereals processing, especially during the grinding, which produces the bran, generates many residues. Typically the bran is used for animal feed production; nevertheless, especially due to the high transportation cost respect to the bran final price, this process is not always convenient. Data for the waste quota from cereals industry were available from the literature[6]. Thus, from the table below, only the biogas yield has been used. Because of the traditional use of brain for animal feed, only the 50% of the available wastes has been considered to be user for AD.

Table 58. Cereal residues biogas yield. (Biocombustibili n.d.)

Sub-product	Production [kg/t final product]	Biogas [m^3/t]
Bran	60-70	478
Production residual	20	400
Washing and other residuals	5-10	400

Confectionery industry

The production of confectionery, bread, and sweets is producing a relatively high number of residues: old bread, residues from manufacturing (flour, dough), frying oil. Expect the oil, these products usually have a good nutritional content and are thus requested by the animal feed industry. The competition with biogas could thus not be attractive in general.

Due to the difficulties in finding data on this production, and on the current, reliable exploitation of these residues, this substrate has not been considered.

Table 59. Confectionery industry residues biogas yield. (Biocombustibili n.d.)

Sub-product	Production [kg/ton flour]	Biogas [m^3/t]
Old bread	50	500
Residuals from production	50	675
Flour	50	612

---

[6] FAOstat database

Other industrial wastes

The following section is related to other possible substrates for biogas production from an industrial process which has not been considered in the study since too many data were missing.

Sugar can be produced alternatively from sugar beets or sugar canes. Sugar beets are usually exploited also for bio-oil production. Furthermore, from the sugar production, some residues are produced, and the molasses is the most important for weight and nutritional value. The molasses from sugar cane is usually exploited in industrial rum production and sometimes for the vodka production. The one from sugar beets is lees precious and is used for brewer's yeast production or feeds.

Aspects	Vinasse	Filter cake	Bagasse	Straw
Reactor type	Biomass immobilization system (e.g., UASB)	CSTR or combination with biomass immobilization system	CSTR with high HRT (>35 days)	CSTR with high HRT (>40 days)
Pre-treatment	Not necessary	Recommended	Highly recommended	Highly recommended
Macronutrients	Phosphorous addition to balance C:P ratio at autonomous plant	Sulfur addition to balance C:S ratio	Nitrogen, sulfur and phosphorus addition to balance C:N:P:S ratio	Nitrogen, sulfur and phosphorus addition to balance C:N:P:S ratio
Trace elements	Lack of Fe, Ni, Co, Mo, W, Mn, Cu, Se, and Zn	Lack of Mo, W, and Se	Lack of Fe, Ni, Co, Mo, W, Mn, Cu, Se, and Zn	Lack of Fe, Ni, Co, Mo, W, Mn, Cu, Se, and Zn
Major challenge	High sulfur content, especially at annexed plants	Storage in case of use during sugarcane offseason	Low biomass availability; High lignin content;	Substrate logistic; High lignin content

Figure 206. (Janke, Leite, Nikolausz, Schmidt, et al. 2015)

Other sugar industry residues have also been evaluated from different literature works. (Janke, Leite, Nikolausz, Schmidt, et al. 2015) and (De Souza et al. 2011), analyzed the biogas production for sugar cane wastes, and considered different residues: vinasse, filter cake, bagasse, and straw.

As shown in Figure 206, the highest potential in methane is the one related to the bagasse. The bagasse digestion is also discussed in (Janke, Leite, Nikolausz & Stinner 2015), where the utilization of filter cake as a single substrate for biogas production and the combination with bagasse in a co-digestion system was studied.
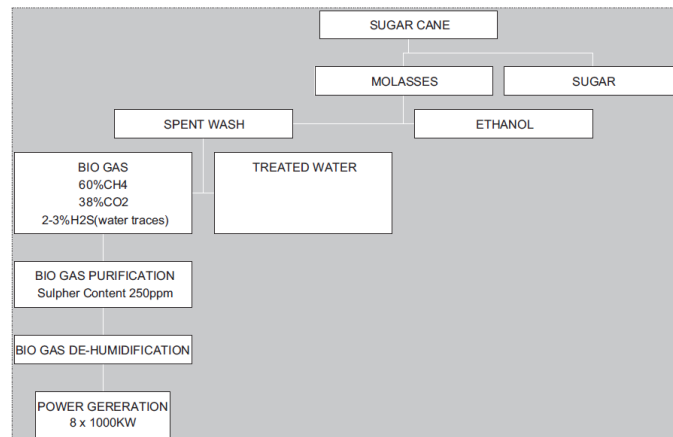
Figure 207. Sugar cane residuals. (Yasar et al. 2015)

Other studies are related to the recovery of the waste water from sugar industry (Hossain & Das 2010) (Yasar et al. 2015) because of its high chemical oxygen demand. As can be seen from the figure above, the wastewater treatment generates wastes and biogas, in a way similar to standard WWTPs. The worldwide sugar production has also been analyzed, and Europe is a relatively small producer (around 10-15% of world sugar production), only from sugar beet, as shown in the figures below.

Despite the good potential in biogas from sugar residues, few data are available on the ratio between the waste water generated and the sugar production. Concerning the molasses, the production is known but is not considered in the study since many exploitation pathways are already available for this sub-product.

Figure 208. Sugar production map.

World Centrifugal Sugar

1,000 Metric Tons, Raw Value

	2010/11	2011/12	2012/13	2013/14	2014/15	May 2015/16
Production						
Brazil	38,350	36,150	38,600	37,800	35,850	36,000
India	26,574	28,620	27,337	26,605	29,483	29,050
European Union	15,939	18,320	16,655	16,020	16,750	15,500
Thailand	9,663	10,235	10,024	11,333	10,970	11,400
China	11,199	12,341	14,001	14,263	11,000	10,820
United States	7,104	7,700	8,148	7,676	7,735	7,665
Mexico	5,495	5,351	7,393	6,382	6,360	6,360
Pakistan	3,920	4,520	5,000	5,630	5,230	5,430
Australia	3,700	3,683	4,250	4,380	4,700	4,800
Russia	2,996	5,545	5,000	4,400	4,350	4,500
Guatemala	2,048	2,499	2,778	2,862	2,900	2,965
Philippines	2,520	2,400	2,400	2,500	2,500	2,500
Turkey	2,274	2,262	2,130	2,300	2,055	2,300
Argentina	2,030	2,150	2,300	1,780	2,150	2,250
Colombia	2,280	2,270	1,950	2,300	2,350	2,250
Indonesia	1,770	1,830	2,300	2,300	2,100	2,250
Egypt	1,830	1,980	2,000	2,013	2,067	2,125
South Africa	1,985	1,897	2,020	2,435	2,116	2,050
Vietnam	1,240	1,400	1,650	1,700	1,650	1,700
Cuba	1,150	1,400	1,525	1,600	1,650	1,665
Ukraine	1,540	2,300	2,400	1,196	2,135	1,445
Iran	1,380	1,370	1,300	1,350	1,370	1,370
Peru	1,069	1,072	1,080	1,150	1,220	1,240
Sudan	750	750	760	700	780	780
Nicaragua	506	615	712	745	728	770
Other	12,907	13,699	13,837	14,143	14,109	14,220
Total	162,219	172,359	177,550	175,563	174,308	173,405

Figure 209. World sugar production. (USDA 2015)

The distillation industry is the processing of fruits or wine residuals (grape branches) for the production of alcoholic products, called distilled beverages. This process generates different residuals types depending on the primary input: if grape branches are used, the residual is solid, and with a fair calorific value (use for burners and thermal energy production, or for animal feed), if fruits is chosen, the residual is liquid and is usually sent to a WWTP.

This sector is presented since could be an interesting application of AD plants, but is not inserted in the calculations since too many data are missing: it is unknown the quota of distilled liquors among all alcoholic beverages, it is unknown the quota of distilled liquors from grapes among all the distilled liquors. Furthermore, (Biocombustibili n.d.) reports that grape branches residuals are generally burned in a traditional boiler to provide the required thermal energy for the distillation process. In this case, there would be no need and no economic advantage in having biogas production.

Table 60. Distillation residual biogas yields. (Biocombustibili n.d.)

Sub-product	Production [kg/l product]	Biogas [m^3/t]
Branches	20	122,5
Other residuals	20	30

Pulp and paper production requires high amounts of water for:

- suspension as well as for transport of fibers and fillers;
- as solvent for chemical additives;
- as a medium to build hydrogen bridge bonds between the fibers, what creates the stability of the paper.
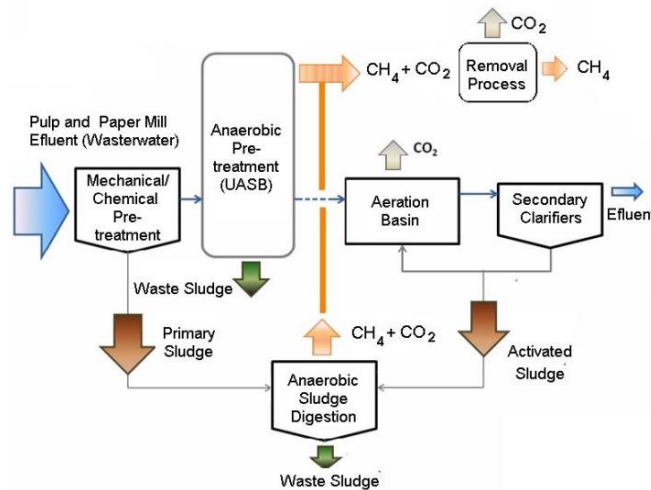
Figure 210. Wastewater from the paper industry and anaerobic digestion plant. (Pontual et al. 2015)

At conditioning and formation fiber fleece 250 and 1000 L/kg of water of the product are required, depending on the type of product. A mean value of 500 liters of water per kg of paper has been chosen.

Substrate	Temp. °C	VS %WW	TS %WW	Methane potential dm³ kgVS$_{added}$$^{-1}$	Reference
Primary sludge					
TMP	37	1.4–2.8	2.3–6.2	45	Jokela *et al.* (1997)
Kraft	35	2.9	3.4	210	This study
	55			230	
Secondary sludge					
Mechanical	37	-	1.3	138	Karlsson *et al.* (2011)
	37	-	1.3	197	Karlsson *et al.* (2011)
Sulphite	37	-	0.9	159	Karlsson *et al.* (2011)
	35	-	1.1	320[a]	Wood *et al.* (2009)
CTMP/kraft	37	-	1.1	97	Karlsson *et al.* (2011)
Kraft/CTMP	37	-	0.7	167	Karlsson *et al.* (2011)
TMP	37	0.8–0.9	1.2–1.3	85	Jokela *et al.* (1997)
Kraft	37	-	0.6	145	Karlsson *et al.* (2011)
	35	-	2.4	90[a]	Wood *et al.* (2009)
	35	3.3	4.0	50	This study
	55			100	
	55	3.9	4.7	108	

[a]biogas dm³ kgVSS^{-1}
TMP = thermo-mechanical pulp

Figure 211. Methane potential from paper and pulp industry from the different reference source. (Bayr 2014)

The biogas production from wastewater from paper and pulp industry has been discussed in many literatures works, mainly related to the area of the world in which paper is produced (Central Asia, South America, and North Europe). (Ericsson et al. 2011) (Hagelqvist 2013) (Priadi et al. 2014) (Cvetković et al. 2014). For this analysis, mean values for the ST content and the methane yield have been chosen and are summarized in the table below. The calculation has been performed only for Sweden and Finland since are the only two country, among the analyzed ones, contained in the biggest ten worldwide paper and pulp producers, as shown below.

The hypothesis has also been confirmed by results which show that, also for the two biggest EU paper producers, the quantity of biogas potential is reduced, thus meaning that the potential for the other EU countries can be neglected.

Table 61. Chosen yields for biogas from paper and pulp industry.

Data	Value	Unit
Sludge yield	500	l sludge /kg paper
SV Percentage	2.29	%
CH$_4$ yield	143	dm^3/ kg SV
%CH$_4$	60%	
Biogas yield	5.45	m^3/ton

Rank 2011	Country	Production in 2011 (1,000 ton)	Share 2011	Rank 2010	Production in 2010 (1,000 ton)
1	China	99,300	24.9%	1	92,599
2	United States	75,083	18.8%	2	75,849
3	Japan	26,627	6.7%	3	27,288
4	Germany	22,698	5.7%	4	23,122
5	Canada	12,112	3.0%	5	12,787
6	South Korea	11,492	2.9%	8	11,120
7	Finland	11,329	2.8%	6	11,789
8	Sweden	11,298	2.8%	7	11,410
9	Brazil	10,159	2.5%	10	9,796
10	Indonesia	10,035	2.5%	9	9,951
	World Total	398,975	100.0%		394,244

Figure 212. Paper and Pulp production, ten biggest worldwide producers.[7]

Biogas production plant layout

---

[7] http://www.jpa.gr.jp/en/

A general layout of an anaerobic digestion plant is shown in Figure 213. The layout is valid for all the chosen substrates expect the landfill gas, which extracting procedure was shown in the related figure in the previous section.

Figure 213. General layout of an anaerobic digestion plant.

1   The substrate is collected and sent to the anaerobic digestion plant. The plant can be located on-site (distributed generation) or can be in a centralized plant. Depending on the site, transport costs could be influencing or not the economic feasibility of the plant.

2   The substrate is usually stocked in a specific area of the plant. Not all substrates can be stocked.

3   Some substrates require pre-treatments before the anaerobic digestion. Pre-treatments could be chemical (chemical reaction involved), thermal (heat requirement) or mechanical (electricity requirement). Generally pre-treatments are included by law (for example in case of milk serum or slaughterhouse residue, a thermal treatment is mandatory) or in order to increase the substrate biogas yield (sewage sludge could have a pre-thickening system to reduce the digester thermal need, straw or other agricultural products could have a mechanical treatment to break the ligneous-cellulosic bonds and increase the biogas yield).

4   A feeding system is then required to feed the substrate into the digester. This system is depending on the substrate density. If it is liquid, a normal pump could be installed. Otherwise, a cochlea is required. Electricity is thus required to move the feeding system.

5   The substrate is then fed to the digester. As well-known in literature, anaerobic digestion can be performed by:
    - Psychrophilic bacteria (20 °C)
    - Mesophilic bacteria (35-37 °C)
    - Thermophilic bacteria (>55 °C)

6   The digestion can be wet/humid (TSS[8] 5-8%), semi-dry (TSS 8-20%), dry (TSS < 20%). The biological process can be performed in one single reactor or in two reactors. Anaerobic digestion thus requires heat, depending on the working conditions, and electricity. The second is needed to have a continuous mixing effect of the substrate and the gas which is produced: this is usually performed via mechanical mixers or using gas injection from the top to the bottom of the digester. Residence time can vary between 15 and more than 40 days, and the digestion can be continuous or in batch.

7   From the anaerobic digestion two products are generated: biogas (CH_4 40-70%, CO_2 30-60%), which is usually stored in a gas holder, and digested biomass.

8   The digested substrate can be used as it is from the digestion (for examples in the case of agricultural residue) or can need post-treatments before being sold or disposed of (for example in the case of sewage sludge, OFMSW, industrial wastes).

9   Biogas can be exploited in different pathways. The most common are:

    • Cogeneration systems: usually Internal Combustion Engines (ICE), rarely micro-Gas Turbines (mGT) or Fuel Cells (FC). In this case, biogas needs pre-treatments which are depending on the cogeneration technology but are always related to contaminants removal. Most dangerous biogas contaminants are sulfur and siloxanes.

    • Boilers: this simpler choice is made to produce heat only.

    • Biogas upgrading: biogas can also be upgraded to biomethane by removing CO_2 and other components. Biomethane can be used on site for vehicles fueling or injected to the grid.

    A comparison between the different biogas exploitation path has been presented in the author's work (M. Gandiglio et al. 2016).

A1.2 Methodology for biogas potential evaluation

The following section shows the methodology and the hypothesis for the potential calculation related to the different substrates. The analysis has been performed by always using, when available, data from the FAOstat and World Bank Database in order to have a common reference database for all the substrates analyzed. The analysis has been applied to selected specific EU countries: Finland, Sweden, and Norway (North EU), France, Germany and Italy (Central EU) , Spain (South EU), Poland (East EU) and the overall European Union.

---

[8] TSS = total suspended solid

Energy crops

The arable land area has been taken from the FAOstat database (FAOstat n.d.). As can be seen from Figure 214, the arable land area is reduced in North Europe, due to the high forest area, while peaks are referred to France, Germany, Spain and Poland. Currently, around 50% of the arable land area is used for cereal production (FAOstat n.d.).

Figure 214.Arable land and land currently under cereal production in the EU region.

In different reference source, the percentage of land area which could be used for energy crops, without influencing the food production, is discussed. The food request is assumed to be decreasing in next decades since the developing countries should increase their internal production and reduce import from Europe. The chosen percentage in this work is 5%, as also mentioned in (Aebiom 2009). As was also discussed in the substrates description section, a safety hypothesis has also been included: each hectare of land has been assumed to be planted which one type of crop/cereal per year, even if often two cultivations per year are admissible.

The cereal yield per hectare has been assumed equal to 500 q/ha[9], which is a precautionary value assuming to have a quite high number of hectares without irrigation (with irrigation this number can also reach 700-800 q/ha).

The biogas yield, as discussed before, has been assumed equal to 170 Nm^3 biogas per tons of crop, as a mean value from different literature sources. The resulting TOE per year is shown in Figure 215. Peaks are related to Germany, France, Spain, and Poland.

$$Pot_{crops}\left[m^3/y\right] = AL[ha] \cdot \%En \cdot CY\left[t/(ha \cdot y)\right] \cdot BY\left[m^3/t\right] \qquad \text{Eq. 33}$$

---

[9] http://www.terraevita.it/trinciato-di-mais-allarme-rese/
http://www.terraevita.it/trinciato-di-mais-annata-doro/
http://www.yara.it/nutrizione-delle-colture/colture/mais/resa/incremento-della-resa-del-mais-da-trinciato/

Where:

- $Pot_{crops}\left[m^3/y\right]$ is the resulting potential biogas production
- $AL[ha]$ is the arable land
- $\%En$ is the chosen percentage of arable land which is exploited for biogas production
- $CY\left[t/ha \cdot y\right]$ is the cereal yield, cereal production per hectare
- $BY\left[m^3/t\right]$ is the biogas yield, biogas production per ton of substrate (cereal)

Figure 215. Biogas production from energy crops in the EU region.

Sewage Sludge

The biogas from waste water potential has been determined from the population value. This data is taken from the World Bank Database (World Bank Data n.d.) for the year 2013 (Figure 216). The EU countries with the highest population are France and Germany.

Figure 216. Population in 2013 for the EU region.

From the Turin WWTP owner and operator, SMAT s.p.a., the value of waste water volume per capita, sludge production and related biogas production, has been determined. Results are shown in Table 62. The biogas potential in TOE per year has thus been calculated (Figure 217).

$$Pot_{WWTP}\left[m^3/y\right] = Pop[capita] \cdot WW\left[l/_{capita \cdot day}\right] \cdot 365\left[day/_y\right] \cdot SY\left[m^3/_l\right]$$
$$\cdot BY\left[m^3/_{m^3}\right] \qquad \text{Eq. 34}$$

Where:

- $Pot_{WWTP}\left[m^3/y\right]$ is the resulting potential biogas production
- $Pop[capita]$ is the population value per country
- $WW\left[l/_{capita \cdot day}\right]$ is the daily waste water production per capita
- $SY\left[m^3/_l\right]$ is the sludge yield, sludge production per litre of waste water
- $BY\left[m^3/_{m^3}\right]$ is the biogas yield, biogas production per m³ of substrate (sludge)

Table 62. Wastewater, sludge and biogas production from WWTP per capita.

Production	Value	Unit
Waste water	220	l/day/capita
Sludge feed	0.50	m³/year/capita
Biogas	2.62	Nm³/year/capita

Figure 217. Biogas potential from sewage sludges.

OFMSW

For the OFMSW, the percentage calculation and the biogas yields have been discussed before and are shown in Table 72.

Table 63. Parameters used for the OFMSW percentage calculation and biogas yield.

Parameter	Value
Percentage of waste used for biogas production - OFMSW	15%
Dry Matter(DM) content	40%
Biogas yield [m³/t DM]	308
Biogas yield [m³/t]	123

From the MSW total production, which will be discussed in next section, the quota referred to OFMSW (15%) has been determined and thus the potential in case of biogas production. All the production could be exploited for energy purposes since the substrate is a 100% waste.

$$Pot_{OFMSW}\left[m^3/y\right] = Pop[capita] \cdot WP\left[t/_{capita \cdot y}\right] \cdot \%OFMSW \cdot BY\left[m^3/_t\right] \qquad \text{Eq. 35}$$

Where:

- $Pot_{OFMSW}\left[m^3/y\right]$ is the resulting potential biogas production
- $Pop[capita]$ is the population value per country
- $WP\left[t/_{capita \cdot y}\right]$ is the yearly waste production per capita
- $\%OFMSW$ is the quota of OFMSW among all waste production
- $BY\left[m^3/_t\right]$ is the biogas yield, biogas production per ton of substrate (OFMSW)

Figure 218. Biogas potential from OFMSW.

LBG

The landfill gas is a gas extracted from landfill sites. In order to calculate the potential from LBG, the total municipal solid waste generation (MSW) was determined. Figure 219 shows the MSW generation in the analyzed EU countries between 2000 and 2009. The

production is almost stable for EU, with a first decrease and then a low increase between 2007 and 2008 (European Environmental Agency (EEA) 2007) , (European Environmental Agency (EEA) 2013). The chosen data, referred to 2009, are shown in Table 64. Furthermore, in Figure 220, the MSW per area of the world is shown: For developing countries, this value is reduced respect to EU mean value, while is higher for USA, Canada, and Australia. The quota of MSW which is landfilled should be determined to calculate the LBG potential. The chosen value is 40%. This number is a mean value for the entire EU: in fact, for Italy, this value was 42% in 2012 (Ciafani et al. 2013), while lower values are referred to northern countries (Kjaer 2013) (Fischer 2013).

Figure 219. MSW generation calculated from European Environmental Agency EEA with data on Municipal waste generated (Eurostat), and Average population (Eurostat). (Eea 2001) and (European Environmental Agency (EEA) 2013)

A general composition of MSW is shown in Figure 221. As can be seen, MSW to landfill is composed of materials which promote the aerobic/anaerobic digestion (around 70%) and by other which are not biomass (30%).

Table 64. Waste generation per capita

Country	Waste generation rate [kg/capita/year] - 2009
Finland	480
France	535
Germany	587
Italy	540
Norway	473
Spain	547
Sweden	482
Poland	316
European Union	512

Figure 220. MSW generation in different world area (Bingemer & Crutzen 1987)

Figure 221. MSW composition. (Themelis & Ulloa 2007)

From a mean composition knowledge, the biogas yield can be determined and the value assumed was discussed in the substrate description section. The biogas potential can finally be determined from the knowledge of the MSW landfilled and the biogas yield.

$$Pot_{LBG} \left[{m^3}/{y} \right] = Pop[capita] \cdot WP \left[{t}/{capita \cdot y} \right] \cdot \%LBG \cdot BY \left[{m^3}/{t} \right] \qquad \text{Eq. 36}$$

Where

- $Pot_{OFMSW} \left[{m^3}/{y} \right]$ is the resulting potential biogas production
- $Pop[capita]$ is the population value per country
- $WP \left[{t}/{capita \cdot y} \right]$ is the yearly waste production per capita
- $\%LBG$ is the quota of landfilled wastes among all wastes production
- $BY \left[{m^3}/{t} \right]$ is the biogas yield, biogas production per ton of substrate (landfilled wastes)

Figure 222. Biogas potential from LBG.

Livestock effluents

Livestock effluents are another important substrate for the biogas production. Even if they were usually exploited as fertilizers, in the last years many plants started to use effluents for biogas production. This is due to the tight regulations on the effluents use for field fertilizing, which is limited in terms of quantity and season due to nitrogen content and odor control. Because of this directive, many farms started to have unexploited effluents which were turned into biogas substrates.

Biogas is generally produced from pig, cattle and poultry caps. Figure 223 show the animal caps per country in 2012. As can be seen from the graph, high concentrations are related to pig, cattle and sheep and goats in central and southern UE countries.

Figure 223. Animal caps per country. (FAOstat n.d.)

In order to evaluate the potential from livestock effluents, the daily production per caps is required, together with the biogas yield. On the table below these values are shown per each animal group. The analysis is done for the total effluents production even if some animals like cattle produce both liquid and solid manure which are collected separately. Others produce only liquid manure (like pigs) or only solid manure (like poultry). The production and the humidity content is also strongly dependent on the method was chosen for the collection: in case water is used, the biogas yields per unit of weight will be reduced.

As discussed above, the chosen percentage of effluents for energy production has been fixed to 50%. With this data it is possible to evaluate the biogas potential from livestock effluents.

$$Pot_{LE}\left[m^3/y\right] = \%En \cdot \sum_i Animals_i[cap] \cdot EP_i\left[t/_{cap \cdot day}\right] \cdot 365\left[day/_y\right] \cdot BY_i\left[m^3/_t\right] \qquad \text{Eq. 37}$$

Where:

- $Pot_{LE}\left[m^3/y\right]$ is the resulting potential biogas production
- $\%En$ is the percentage of livestock effluents considered to be exploited for biogas and energy production
- $Animals_i[cap]$ is the number of caps per each animal category per country
- $EP_i\left[t/_{cap \cdot day}\right]$ is the daily effluents production per cap per each animal category
- $BY\left[m^3/_t\right]$ is the biogas yield, biogas production per ton of substrate (livestock effluents) for each animal category

Table 65. Effluents production per caps per day. (Colonna et al. 2009)

Animals	Effluents production [kgSV/day]	Biogas yields [Nm³/t SV]
Cattle	4.463	295
Buffaloes	5.400	295
Sheep + Goats	0.303	370
Pigs	0.714	396
Horses	2.700	300
Chickens + Turkeys + Poultry	0.001	383
Rabbits	0.033	351

Figure 224. Biogas potential from livestock effluents.

Agricultural waste

Agricultural residue potential has been determined from the waste production from different cereals families in different countries. Data are available from (FAOstat n.d.) and are summarized in Figure 225. The main cereals, and thus wastes, producers are France, Germany, and Poland.

From the knowledge of the yearly residue production (determined to account only one production per year, which is a conservative hypothesis) and the mean biogas yield discussed before (263 Nm^3/t), the biogas potential can thus be determined.

$$Pot_{AGR-W}\left[{m^3}/{y}\right] = AW\left[{t}/{y}\right] \cdot \overline{BY}\left[{m^3}/{t}\right] \qquad \text{Eq. 38}$$

Where:

- $Pot_{AGR-W}\left[{m^3}/{y}\right]$ is the resulting potential biogas production
- $AW\left[{t}/{y}\right]$ is the total yearly waste production from various cereals
- $\overline{BY}\left[{m^3}/{t}\right]$ is mean the biogas yield, biogas production per ton of substrate (agricultural wastes)

Figure 225. Agricultural waste from cereals in different EU countries. (FAOstat n.d.)
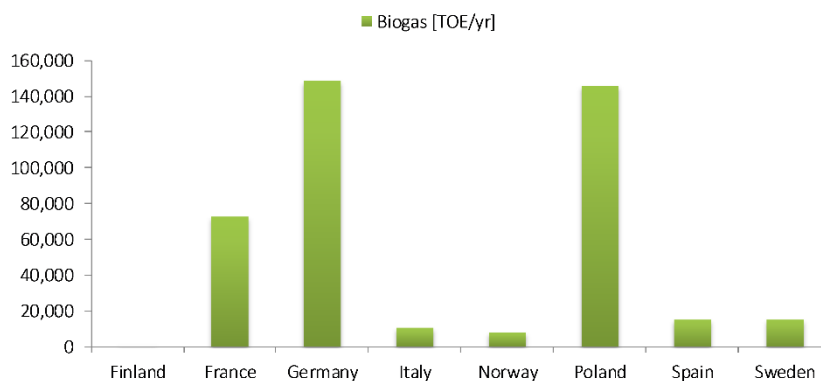
Figure 226. Biogas potential from livestock effluents.

Industrial wastes/residuals

The industrial residuals and wastes have been analyzed for each chosen area with related biogas yields. Calculations are discussed below. Equations are not included anymore since the method used is always the same: from the production quantities, available from the database, literature data are used to determine the waste generation and biogas yield to calculate the potential biogas production.

<u>Milk industry</u>

The serum is the residue from the milk production which could be exploited for biogas production. As discussed before, per each ton of milk are produced:

- 500 kg of serum with a biogas yield of 25 m^3/t
- 5.4 kg of other residuals with a biogas yield of 500 m^3/t

From the FAO database, it is possible to extract the production quantity for different processed materials. Results for milk are shown in Figure 227. Unfortunately, the data for EU was not available in this case. Once the milk production, expressed in tons per year, is known, the residuals quantity can be determined and finally the biogas potential from milk.
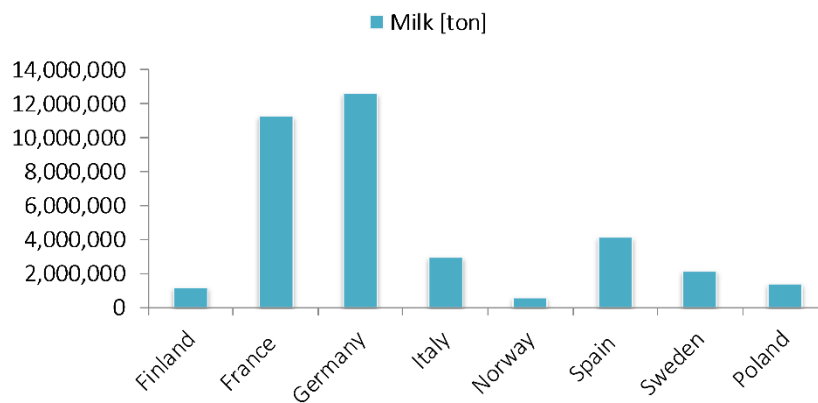
Figure 227. Milk production in different EU countries. (FAOstat n.d.)

Fruit and vegetable industry

Fruits and vegetables production has been determined from the FAO data on crops production per country. As can be seen in Figure 228, the highest production is related to potatoes in France, Germany, and Poland. Italy and Spain show a large variety of products while Northern Country have near zero production mainly because of the severe weather.
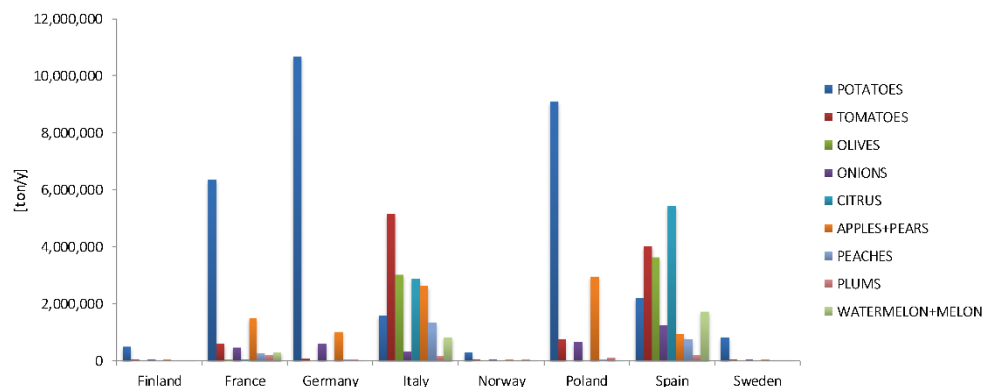
Figure 228. Fruits and vegetable production in the EU area. (FAOstat n.d.)

As discussed in the previous section, biogas could be probably made by other fruits and vegetable residuals, for example from leguminous vegetables; in this study, the choice has been made according to a wide literature research trying to analyze the substrate which is already under use in some plants. The biogas potential from these substrates could thus be higher depending on the development of this industry sector in the future.

The quota of products which is transformed, and thus not sold as fresh on the market, has been assumed 60% as previously discussed. Then, according to the residual percentages, the quantity of available substrate has been determined and the biogas potential calculated.

Wine industry

The wine industry biogas potential is related to the wine production per country. As for the other substrates, on FAO database, the wine production can be found (Figure 229). From one hl of wine, 18 kg of peels and branches are produced, as shown before, with a biogas yield of 62 m^3/t. The biogas potential can thus be determined.

Beer industry

The beer production per country is shown in Figure 229, compared to the one of wine. For each hl of beer are produced:

- 18 kg of spent grains of malt with a relatively high biogas yield (131 m^3/t)
- 3 kg of spent yeast with a lower biogas yield (66 m^3/t)

Breweries have also been indicated by the Roland Berger report (Roland Berger Strategy Consultants 2015) as a potential and interesting market for biogas and fuel cells. Their analysis was based on biogas production not only from spent grains but also from waste water on breweries (excluding all the micro-breweries).
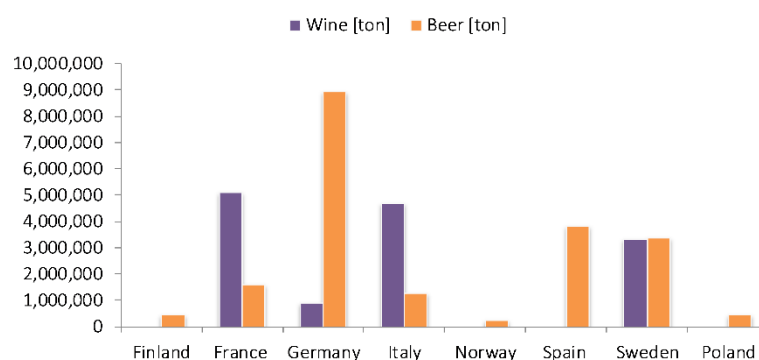
Figure 229. Beer VS Wine production per country (FAOstat n.d.)

Slaughterhouse industry

From each transformed animal cap, different quantity of slaughterhouse residual is available (rumen content, stomach, and blood mainly). Data were available for pigs, sheep and cattle caps. The data of the animal number per country is thus required and was found in FAO database. It has been assumed that almost every year new animals are similar to dead animals.

From this evaluation, and taking into account the biogas yields discussed before, the biogas potential has thus been determined.
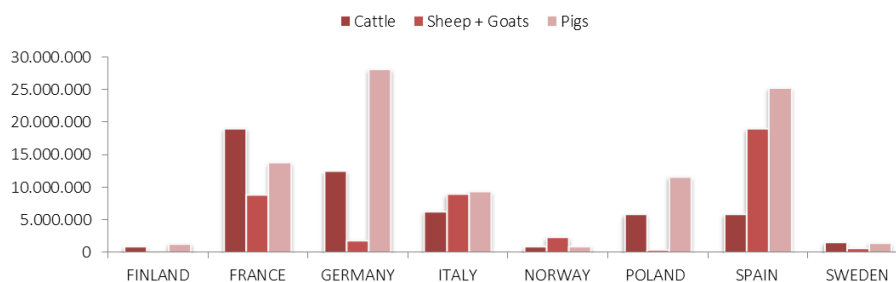
Figure 230. Animals per country (FAOstat n.d.)

Cereal industry

From the FAO database, waste quantities from different cereals production are also available. Data are shown in the table below.
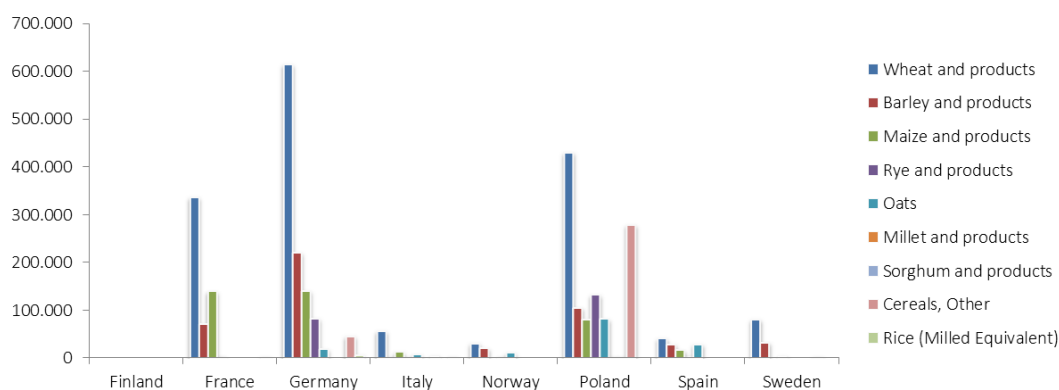
Figure 231. Cereal wastes (FAOstat n.d.)

The calculation of the biogas potential has been done on the total waste quantity since the literature data available were referred to the bran for a general cereal processing.

Industrial wastes

The overall biogas potential from industrial wastes can thus be determined as the sum of the above-mentioned substrates potential. Results are shown in Figure 232. In countries where arable land is found, the climate is Mediterranean, and fruits and vegetables are produced, this is the largest share in biogas potential from food industry waste. In the same geographical areas, cereals processing industry and milk industry are also quite large contributions. Lowest values are indeed related to Northern EU countries. Beer potential is relevant only in Germany, where the largest breweries and beer production are located. Industrial wastes related to wine, slaughterhouse. and paper is indeed the lowest potential contributions.
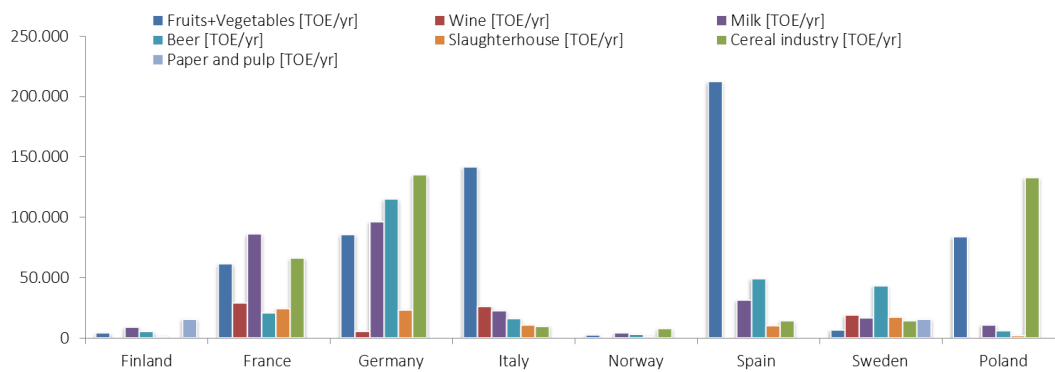
Figure 232. Total biogas potential from industrial wastes.

Appendix 2– SOFCOM units testing

A2.1 Clean-up unit test

The biogas macro-composition was checked on almost a daily basis during the plant operation. A portable gas analyzer (see Figure 233) was used for the analysis, able to measure CH_4, CO_2, O_2 vol. % and H_2, CO, H_2S at the ppm(v) level. N_2 was calculated as the balance of the previous components. SMAT also provides the raw biogas composition measurements from the digesters, which are made with the same instrument as above.

Figure 234 shows the trends for the biogas composition during January and February 2015 for selected sampling points after SMAT digesters. As it can be seen, methane content was almost constant and always higher than 60% vol. in monitored period. The same values, between 60 and 63%, were measured at the demo plant inlet. For what concerns H_2S, values are higher at the digester outlet than at the demo plant. From the figure, the mean value is around 110 ppm(v) with peaks around at 180 ppm(v). At the biogas plant inlet, H_2S concentration has always been between 2 and 30 ppm(v). This can be due to the long pipe connecting the biogas feeding from chillers and the demonstration plant.

Figure 233. Geotech gas analyzer.

From the external laboratory analysis, other compounds were monitored during the plant operation:

- Siloxanes
- Total sulfur compounds
- Hydrogen sulphide
- Methane
- Oxygen
- Carbon dioxide

The standard followed for the analysis are:

- Hydrogen sulfide: UNICHIM 634 method;
- Siloxanes: EPA TO-15 1999 (sampling with vacuum bottle);
- Total sulfur compounds (post-combustion): sampling with an activated carbon phial according to NIOSH 6013, determination according to EPA 9056A 2007 with Mahler bomb;
- Methane, Oxygen and Carbon Dioxide: portable analyzer with electrochemical cells.

The sampling points analyzed are (see Figure 235):

- S1: biogas inlet to the demo plant, coming from SMAT chillers.
- S2: biogas after the first cleaning vessel (ZnO).
- S3: biogas after the second cleaning vessel (AC) before the reformer inlet.
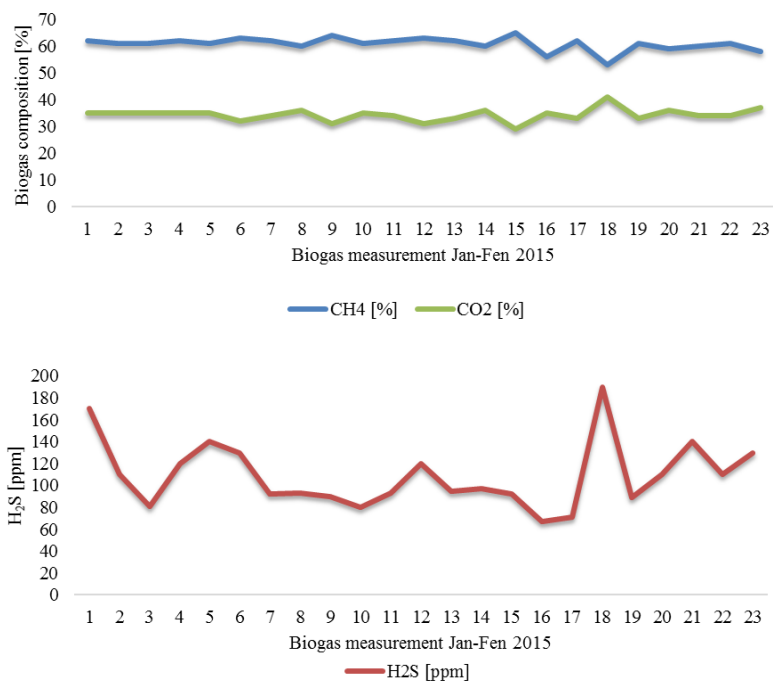
Figure 234. CH_4/CO_2 and H2S content at the digester outlet – SMAT data.

Figure 235. Sampling points.

In Table 66 the trace compounds concentrations measured in the three different sampling points S1, S2 and S3 are given.

Table 66. Gas composition for sampling points.

Component	S1	S2	S3	Unit
Hexamethyldisiloxane(HMDSO)	< 4.47	< 4.47	< 4.47	ppb V
1.1.3.3.5.5-hexamethyltrisiloxane	< 2.02	< 2.02	< 2.02	ppb V
Decamethylcyclopentasiloxane (D5)	10.5	46.5	6.32	ppb V
Decamethyltetrasiloxane (L4)	< 2.37	< 2.37	< 2.37	ppb V
Dodecamethylpentasiloxane (L5)	< 24	< 24	< 24	ppb V
Hexamethylcyclotrisiloxane (D3)	9.59	6.97	< 5.36	ppb V
Octamethylcyclotetrasiloxane (D4)	57.1	128	43.4	ppb V
Octamethyltrisiloxane (L3)	< 6.36	< 6.36	< 6.36	ppb V
Pentamethyldisiloxane (PMDSO)	< 4.29	< 4.29	< 4.29	ppb V
Tetramethylsilane (TMS)	< 6.37	< 6.37	< 6.37	ppb V
Trimethylsilanol	26.8	< 13.9	< 13.9	ppb V
CO_2	36.6	36.3	36.1	% V
O_2	< 0.1	< 0.1	< 0.1	% V
CH_4	63.3	63.6	63.8	% V
H_2S	15.7	7.84	6.96	mg/m3
Stot	32.9	28.1	39.8	mg/m3

The first cleaning bed, filled with ZnO, removes mainly H_2S, from 50 to 70% up to achieve the total removal in the second bed. The ZnO bed also removes some siloxanes: the D3 concentration (Hexamethylcyclotrisiloxane) shows a reduction of 27%. The second bed, filled with activated carbons, is able to remove mainly siloxanes and H_2S down to ppbv units: D5 (Decamethylcyclopentasiloxane) shows a reduction of 87%, D4 (Octamethylcyclotetrasiloxane) a reduction of 70.
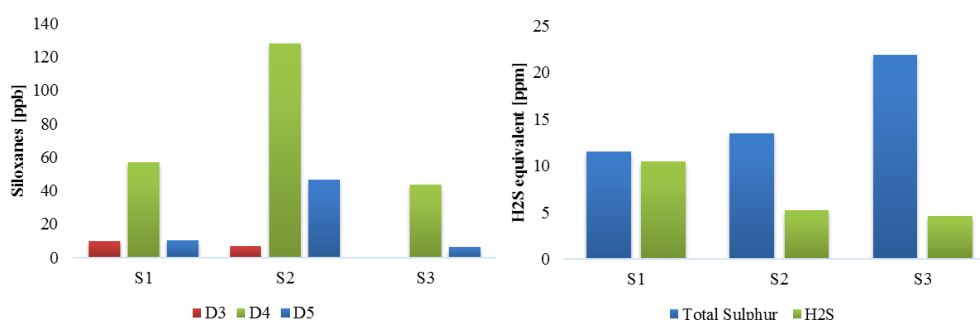
Figure 236. Siloxanes and sulfur compounds trend in the cleaning system.

As can be seen from Figure 236 siloxanes are removed, as expected, in the AC bed. Despite this, siloxanes trend in the first bed (ZnO) shows an increasing concentration concerning D4 and D5. This behavior is due to the competitive adsorption of siloxanes and other volatile trace compounds contained in the biogas mixture. As also reported from Wood et al. (Wood 2002), the competitive adsorption of more than one elements shows the "roll-up" phenomenon. When there is co-presence of two compounds in the clean-up bed, compared to the case with only a single, breakthrough times are decreased since each vapor wavefront moves through the bed faster as the other vapor is taking up some adsorption volume. Also, the more weakly and previously adsorbed vapor will be partially displaced by the other one, thus resulting in a higher maximum concentration of the former compared to its inlet concentration; this is the so-called 'rollup' or 'overshoot' phenomenon. Figure 237 better explains the phenomena described above.
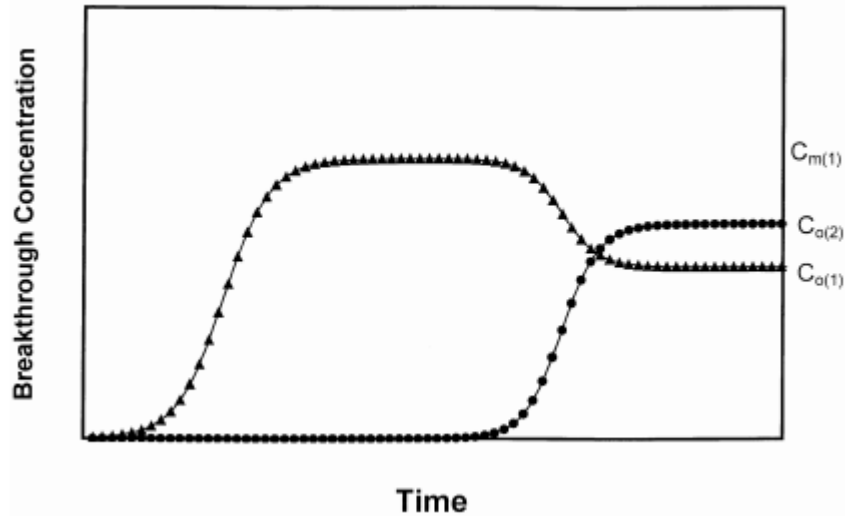
Figure 237. Hydrogen measurement. Multiple vapors breakthrough curve characteristics. Circles represent the vapor (2) which has the higher adsorption capacity at its inlet vapor concentration Co (2). Triangles represent the first-eluting vapor (1), whose maximum rollup concentration Cm(1) exceeds its entering vapor concentration Co(1) due to displacement by vapor 2 (Wood 2002).

H_2S is also removed in ZnO as designed, but not completely. Furthermore, a high concentration of non-sulphur compounds has been detected. The same phenomena described for silicon compounds, 'rollup,' can also be considered for sulfur compounds. It follows that much more attention should be taken for the trace compounds monitoring and then foresee a sorbent material changing.

The biogas cleaning process is discussed in detail in chapter 5.1.

A2.2 Reformer test session #1

After some days of a start-up in NH-mix (usually defined as 95% N_2, 5% H_2) where the processing unit (evaporator + reformer) was just working as a heater, the first outdoor test with biogas was performed, analyzing the working points shown in Table 67. The starting mixture fed to the system was 60% N_2 / 40% H_2, as required in the SOFC start-up procedure.

Table 67. Reformer test points.

Test	Biogas % respect to nominal	Biogas flow [NLPM]	S/C	H$_2$O [g/h]	O/C	O$_2$ [ml/min]
1	20%	1.67	2.5	132	0	0
2	40%	3.35	2.5	250	0	0
3	40%	3.35	2.5	250	0.05	100
4	40%	3.35	2.5	250	0.10	200
5	40%	3.35	2.5	250	0.15	300

As can be seen from the table, the biogas reforming has been tested up to 40% since the reformer temperature profile was quite low compared to nominal data, even by adding oxygen to the reaction. The presented results are referred to the temperature profile within the evaporator, and the reformer during the tests 1-5 and the influence of oxygen is also analyzed.

From tests 1 to 5, while increasing biogas, hydrogen and nitrogen were reduced accordingly keeping the rate 60/40 % N$_2$/H$_2$ at the SOFC inlet constant.

Tests results are shown in Figure 238 and Figure 239 for the evaporator and the reformer respectively. As can be seen, reforming has been tested at 20% and 40% of reforming and, in the 40% test condition, water was increased up to the content related to 60%, to test the evaporator performance.

The evaporator performance has been in accordance with the specifications during these first tests with a quite constant temperature profile both inside the reactor and on the electrical resistance. The evaporator internal temperature was always kept constant not depending on the increasing water flow rate. Furthermore, the electric heater was using a low amount of the available power (around 15% of the total installed power, 4 kW).

At the end of the test, water flow for the 60% reforming point has also been tested in order to see the temperature profile and results were still good: stable temperature without high power requirement (resistance temperature always below 600 °C).

Concerning the reformer test results, initial conditions were stable and close to nominal values with a mean reformer temperature around 800 °C and not overheating on the electrical heaters (resistance @ 850 °C).
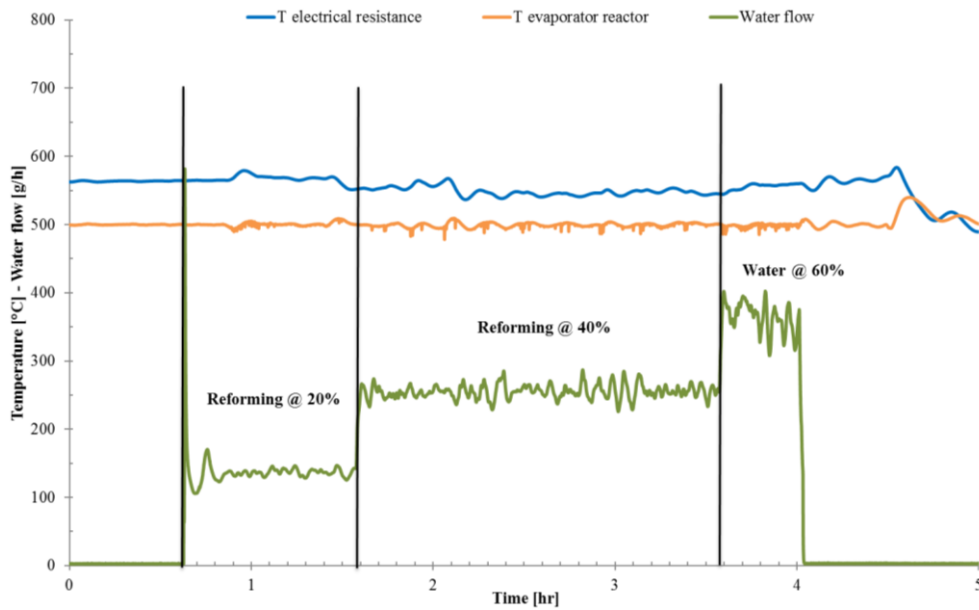
Figure 238. Evaporator test results
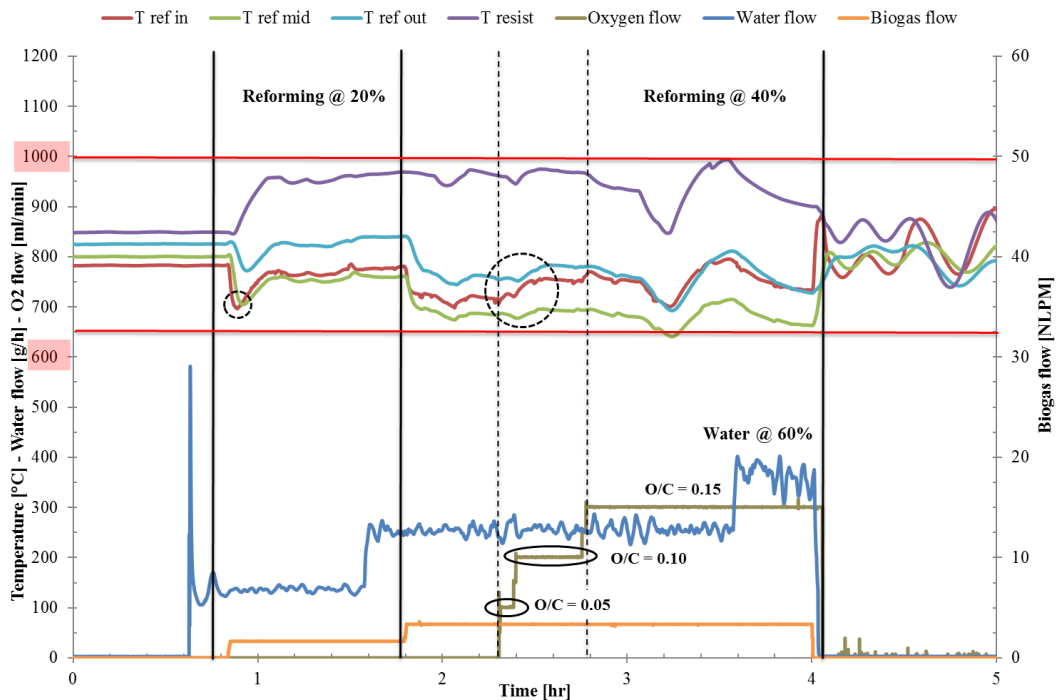
Figure 239. Evaporator test results.

When 20% biogas has been sent to the system, a decrease up to 700 °C can be seen in the profile temperature, especially for the inlet and mean thermocouples. As is also known from the CFD modeling (Pret et al. 2015), the reaction takes place in the very first section of the reactor, generating a high heat requirement and a related temperature decrease. The reformed gas is then heated up again in the final reactor section, and thus the outlet

temperature is high and quite stable during all tests. Admissible minimum and maximum temperature for the reformer reactor, required in order to avoid carbon deposition (minimum 600 °C) and electrical resistance overheating (maximum, 1000 °C) are also shown in the figure.

At the minimum temperature value in the 20% test, an inversion in the temperature profile can also be seen (first dashed round): from this moment the colder thermocouples are not the inlet one but the mean one, probably because here is the section in which the reaction takes place. Thanks to a high increase in the resistance temperature (up to 960 °C), the system was able to get back to good temperature values, between 750 and 800 °C.

In this stable conditions, the water and then the biogas flow rates were increased up to 40% reforming. The temperature decrease which can be seen in the thermocouples is similar to the previous one but, despite the further increased power of the resistance, the system was not able to reach a temperature above 700 °C in all its sections. In particular, the colder mean temperature was stable at around 680 °C.

Since the lower limit for avoiding carbon deposition was set to 600/650 °C, before moving to the 60% working point, the influence of oxygen has been analyzed in order to see the related temperature increase. As suggested by reformer models, in this first test the O/C ratio has been varied in the low range between 0.05 and 0.15. In the O/C = 0.05 test, since the oxygen injection is done at the top of the reactor, its influence is visible on the inlet thermocouple (temperature increase) and not in the mean one. Increasing the O/C ratio up to 0.15 (third oxygen level) the influence was higher on the inlet thermocouple were a 50 °C temperature increase can be seen. On the other side, the cold thermocouple 'T ref mean' was still below 700 °C. This target value was reached once, but the resistance temperature was close to 1000 °C. Thus this condition should be avoided for a longer period.

Because of the low reformer inlet temperate this first reforming test was stopped here. The system was working properly, but further considerations on the real low-temperature limit to avoid carbon deposition should be done: in order to reach 60, 80 and 100% biogas rate, the risk of achieving 600 °C inside the reformer cannot be avoided. Final results on the overall system will show the performance of the unit at full load.

A2.3 Reformer test session #2

A series of preliminary tests with simulated biogas mixture (CH_4= 60%, CO_2 = 40%) were performed in order to confirm the functional capability of the complete reforming unit before to carry out the test with the real biogas. At the same time, the suitability of the

catalyst selected by precedent micro-scale tests and the possibility to use the Steam Reforming (SR) or the Oxy steam Reforming (OSR) process has been verified.

The operating conditions of the preliminary tests were selected to fit the acceptance tests with the real biogas mixture, considering, therefore, also the nominal working condition (biogas = 10.45 Nl/min, H_2O = 480-725 g/h with H_2O/CH_4= 2-3 under SR and O_2= 250 -1240 Nl/min with O_2/CH_4= 0.05-0.25 under OSR).

The reformer acceptance test and the procedure (1-4) for the nominal working condition reported in Table 68.

Several kinds of tests were performed following the operating condition and the procedure reported in the user manual and in the acceptance test. A safety strategy has been used about the heaters utilization:

Vaporizer/mixer:

    a) 90% if $T_{evap} < 650$ °C
    b) 50% if $T_{evap} > 650$ °C
    c) 0% if $T_{evap} > 700$ °C

Reforming reactor:

    a) 90% if $T_{ref} < 900$ °C
    b) 50% if $T_{ref} > 900$ °C
    c) 0% if $T_{ref} > 950$ °C

In addition to this safety hierarchy, the PIDs system was active to activate/deactivate the heaters based on the set point.

The operating conditions are reported in detail in Table 69

.

Table 68. Acceptance test with operating condition and procedure steps (1-4).

Gas from feeding system	Biogas from cylinders					
Procedure	H_2 [Nl/min]	N_2 [Nl/min]	CH_4 [Nl/min]	CO_2 [Nl/min]	H_2O [g/h]	O_2 [Nl/min]
Mixture identifier						

1	N$_2$-H$_2$ mix Heat up (RT --> 800 °C)	3.00	57.00	0.00	0.00	0	0
2	N$_2$-H$_2$ mix (800 °C) Catalyst reduction	20.10	30.10	0.00	0.00	0	0
3	Simulated Biogas (600-700 °C) SR	0.00	0.00	6.27	4.18	725	0
4	Simulated Biogas (600-700 °C) OSR	0.00	0.00	6.27	4.18	725	500

Table 69. Preliminary tests operative conditions.

Test	H$_2$O/CH$_4$	H$_2$O(g/h)	O$_2$/CH$_4$	O$_2$ (ml/min)
0	2	484	0	0
1	2	484	0,05	250
2	2	484	0,1	500
3	3	725	0,1	500
4	3	725	0,15	750
5	3	725	0,2	1000
6	2	484	0,25	1240
7	2	484	0	0

Figure 240 shows the behavior of the temperatures for the vaporizer/mixer during the tests (0-7), the analysis evidences that despite the variations in the different working points (see the flow rate of H$_2$O and O$_2$), the evaporator is always maintained at temperature between 400 and 700 ° C maximum (on the resistance). This temperature values are optimal to ensure a complete vaporization of the steam.
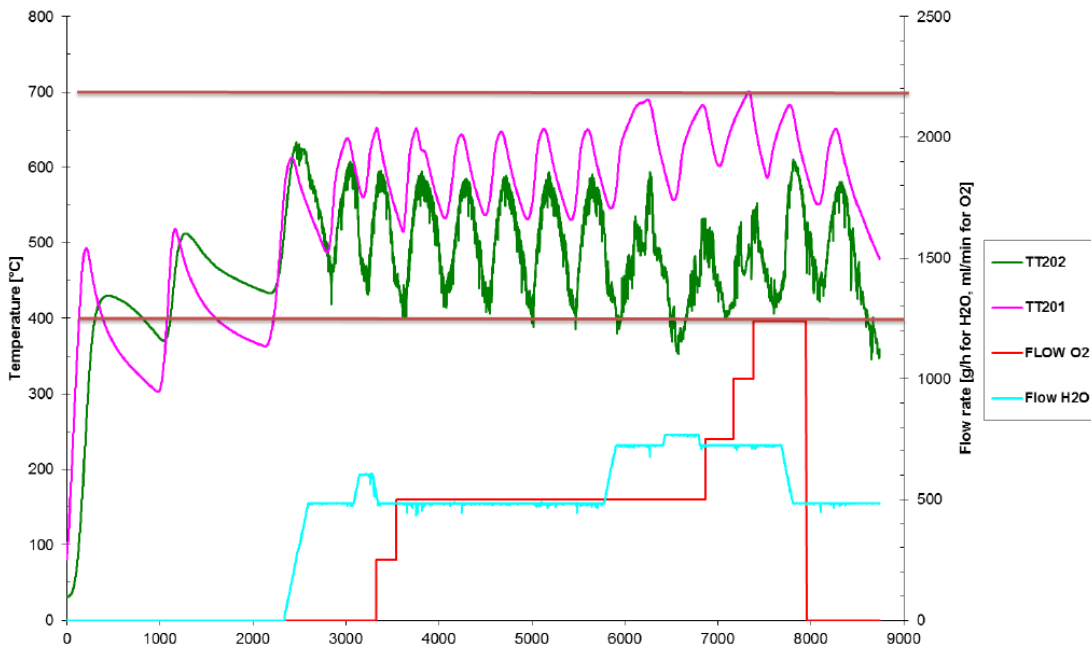
Figure 240. Temperature profile of the vaporizer/mixer.
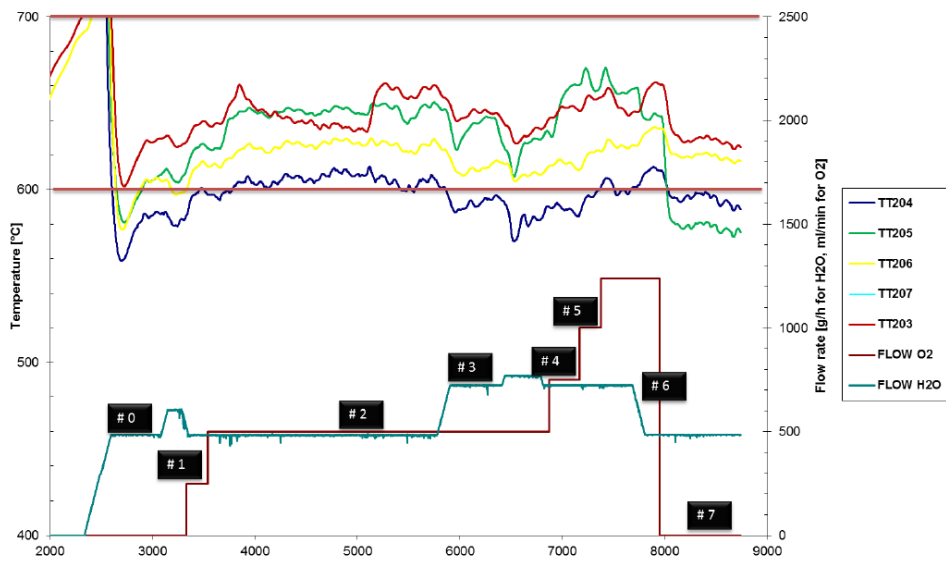
Figure 241. Temperature profile trough the reforming reactor.

Figure 241 shows the axial temperature profile through the reforming reactor; the diagram also shows the different operating conditions (table 10, 0–7) of the tests performed. The results evidence that adding water and/or its increase causes a decrease in reactor temperature.

The oxygen effect results in an increase of the catalytic bed temperature. In the conditions 2 and 3, the temperatures are above 600 ° C with an O_2/CH_4 ratio equal to 0.10;

these conditions appear adequate for the reformer operation as confirmed by the analysis of the composition of the syngas mixture at the outlet of the reformer reported in Table 70.

Table 70. Syngas composition

Test	H_2O/CH_4	O_2/CH_4	% CO	% CO_2	% H_2	% CH_4	H_2/CO
0	2	0.00	17.59	18.03	56.30	7.16	3.20
1	2	0.05	19.13	17.11	56.70	5.64	2.96
2	2	0.10	20.07	16.82	56.65	4.95	2.82
3	3	0.10	16.23	19.36	60.35	3.29	3.72
4	3	0.15	15.85	20.05	60.55	2.85	3.82
5	3	0.20	15.93	20.45	60.53	2.39	3.80
6	2	0.25	19.64	18.47	57.25	3.61	2.91
7	2	0.00	18.54	17.19	56.00	7.33	3.02

Moreover, the introduction of the O_2 in the reaction mixture has a beneficial effect not only on the endothermic nature of the process but also on the syngas composition, in fact, the CH_4 concentration decreases in the outlet products increasing the O_2/CH_4 molar ratio. The low CH_4 concentration and the correspondent H_2/CO molar ratio (2.8-3.72) are appropriate for the SOFC downstream process.

Summarizing, the preliminary test with the simulated biogas mixture has demonstrated that the reforming unit and the related peripheral components, which are necessary for the operation of the system (e.g. pump, mass flow, valves, measurement and safety devices, etc..) operated as desired. Moreover, the tests in OSR condition have evidenced that the oxygen utilization is useful for the efficiency of the process and the final performances of the reformer.

Influence of oxygen feeding to reformer reactor

The specific test on the reformer reactor has been performed in order to analyze the effect of oxygen feed to the reactor.

During first acceptance test for the reformer, low temperatures have been detected inside the reactor's catalytic bed, thus resulting in a high risk of carbon deposition. During a stop of the system, solid carbon powder was detected in the outlet pipe of the reformer.

The problem was not related to the electric ovens: the power available from the heaters was indeed double compared to the theoretical one needed for the reactions.

In order to assist the reforming reaction and increase its temperature, an oxygen pipe was added to the reformer inlet, controlled by an MFC, as shown in the figure below.
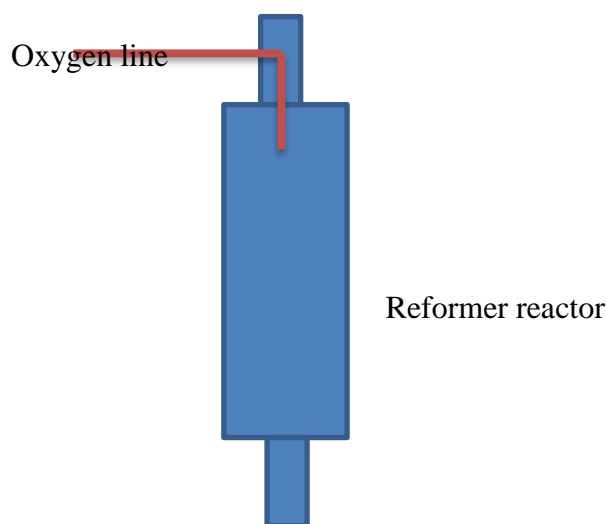
Figure 242. Simple layout of the oxygen added line to the reformer.

The oxygen was fed directly into the reformer reactor in order to avoid high temperatures in the evaporator (since AISI 316L, evaporator material, was not suitable for high temperatures). The oxygen flow rate was defined from a chosen O/C ratio. Test results are presented below.

Before oxygen injection, at time 18-19, and without biogas feed, the reformer temperature was acceptable for what concerning T1 and T2 (> 700 °C), and near the minimum level for T3 (~ 650 °C). From partner specifications and reformer user manual, the reactor temperature should always be higher than 650-700 °C to avoid carbon deposition.

The biogas flow rate was increased from 0 NLPM to 8.36 NLPM (see the purple line in Figure 243).

Figure 243 and Figure 244 show the trend of the reforming temperatures with biogas increase and oxygen effect. The three steps for the biogas increase up to 100% have been:

- 1/3 of the biogas nominal flow rate
- 2/3 of the biogas nominal flow rate
- 3/3 = 100% working point

When a certain O2 flow was added to the system, biogas flow was increased in order to have a constant FU in the SOFC: since part of the methane reacts with oxygen in the reactor, the hydrogen equivalent content to the fuel cell is reduced. An extra-biogas and water flows were thus calculated and summed (Table 71).

Table 71. Calculation of the extra-biogas and water content for 3 O/C conditions.

Biogas-Nl/min	H_2O g/h	O_2 ml/min	O/C	Extra biogas-Nl/min	Biogas new-Nl/min	Steam new-g/h
8.36	604.45	501.60	0.10	0.42	8.78	634.67
8.36	604.45	752.40	0.15	0.63	8.99	649.78
8.36	604.45	852.72	0.17	0.71	9.07	655.82

As can be seen in the figures below the main problem of the oxygen feeding is related to the local effect that has been noticed on the reactor. When oxygen is fed, even in lower concentrations, the temperature close to the O_2 pipe (T1) shows a strong and high increase in temperature, while the effect on others thermocouples is very limited. The O/C ratio has not been increased too much since the limit on the maximum temperature of the Ni-base catalyst were also required, and thus an internal temperature higher than 900 °C was not recommended.

Therefore, a constant and low O/C was chosen and used to run the reformer in nominal conditions, even if its effect was mainly related to the feeding point.
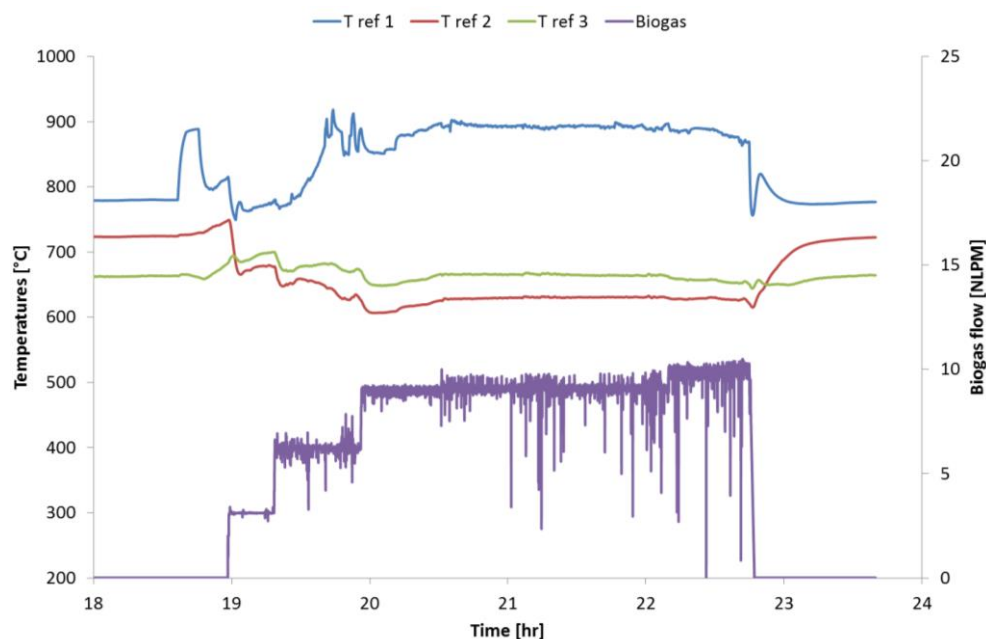
Figure 243. Biogas flow rate and temperatures trend
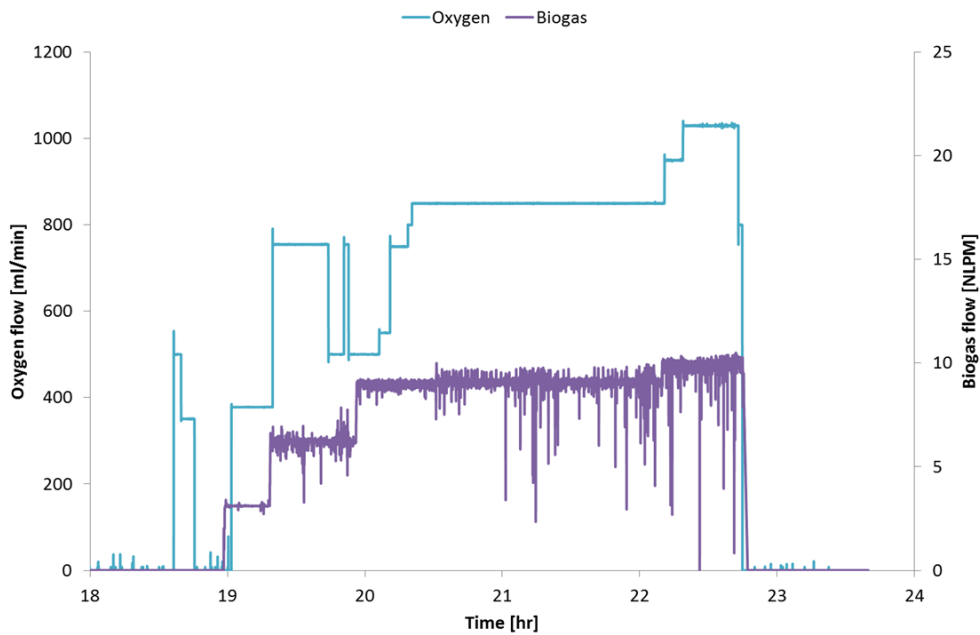
Figure 244. Oxygen increase.

A2.4 SOFC unit test results

Below are shown the polarization and power curves obtained during the test.
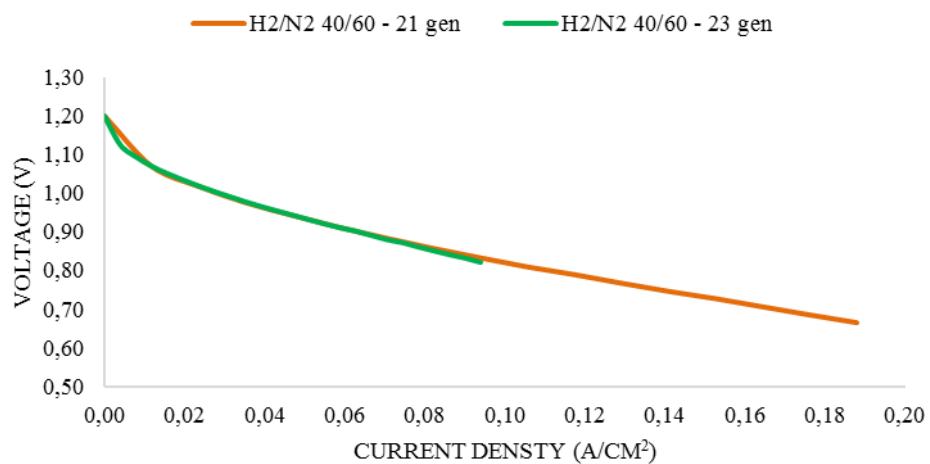
Figure 245. Polarization curve.
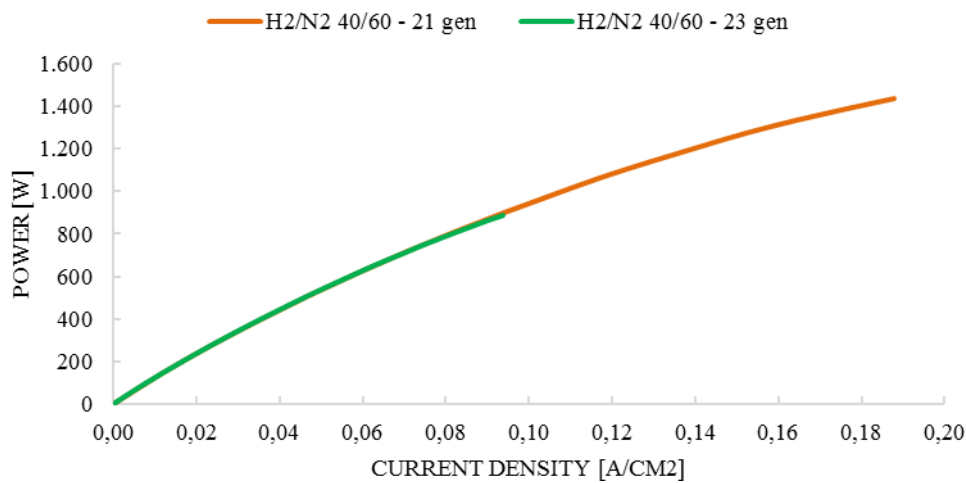
Figure 246 Power curve.

Both tests were done on 21 and 23 January 2015 are a reporter in this work, in order to make a benchmark between the data obtained.

The curves have been obtained by gradually increasing the current load, with steps of 0.5 A for a time, from OCV condition to the target chosen value (usually 24 A).

As can be seen from the graph, the second test was conducted up to 12 An instead of 24 An in order to achieve the optimum conditions for testing the oxy-combustor unit. Thus, keeping constant the inlet fuel flow, a mixture richer in hydrogen in order to facilitate the ignition of the anode exhausted was then obtained.

The steps followed for the implementation of the test are summarized below (see Figure 247 as reference).

(6) <u>Heat-up</u>. The test starts with a fuel composition of H_2/N_2 5/95%, as reported on the test procedures documentation, in order to complete the heat-up phase of the ISM. The chosen flow rates were 20 NLPM N_2 and 1 NLPM H_2. For the heat-up phase, anode inlet temperature was set to 750 °C and cathode inlet temperature to 820 °C with a high air flow (250 NLPM) in order to have a high heat carrier for the stack heating.

(7) <u>Gas composition variation</u>. When a stack temperature close to 800°C is reached, the composition of the inlet fuel was changed from 5/95 % to 40/60%, sending 30 NLPM of nitrogen and 20 NLPM of hydrogen; Notice that the heat-up phase was carried out under OCV conditions.

(8) <u>Current load increase</u>. After gas composition change, when temperatures were in steady state conditions, the electrical load was applied, imposing a step current of 0.5 A. (see point An on Figure 247). By imposing the load, as expected, it has been noted the drop in cell voltage due to the internal irreversibilities, from around 113 V (in OCV condition) to 57-58 V at 24 A.

The temperature of the cells, on the other side, tends to increase due to the heat delivered by the hydrogen's oxidation reaction and the internal resistance of the electrolyte. Therefore, it was necessary to reduce the temperature of the air input as is shown in the circle box (B) and (C) in .

(9) While decreasing the cathode inlet temperature from 820 to 650 °C, in order not to cool down too much the stack, the air flow rate was reduced and regulated in order to maintain a stable temperature inside the stack between 820 and 840 °C.

(10)   SOFC under full current load. Completed the test, reaching the goal of 24 A, the stand-by procedure has been applied again in order to perform the gradual reduction of the load and bring the stack under OCV condition (E). During this step, the air flow has been reported to its initial value (250 NLPM) and also increasing the intake temperature.

In fact, it is noted that due to the removal of the load, the internal temperature of the cell tends to decrease rapidly. This is mainly due to two causes:

- Eliminating the load, lacking both the heat input of the oxidation reaction of hydrogen and the heat generated by the internal irreversibility of the electrolyte;
- The air flow and temperature, previously reduced to avoid overheating, need to be restored to the initial condition to prevent the cooling of stack;

The test is expiring bringing back the flow of fuel in the initial conditions.

The switch from N/H mixture to biogas, from producer specification, should always be performed under load, after the current increase. For this reason, the polarization curve has been obtained for the N-H mix gas composition and then the stream was switched to biogas. Under biogas conditions, the voltage had a decrease from 75.6 to 61.9 V going to 40% biogas reforming (see Figure 248).

Further tests will be analyzed more deeply the SOFC stack performance under different load conditions and biogas rates.
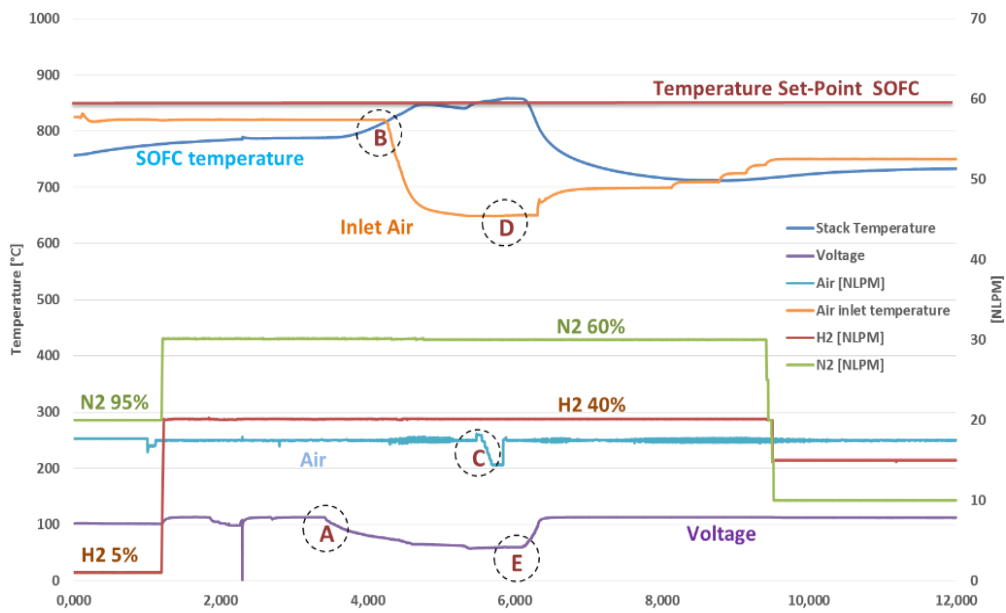
Figure 247 SOFC test. Horizontal axis is showing time.
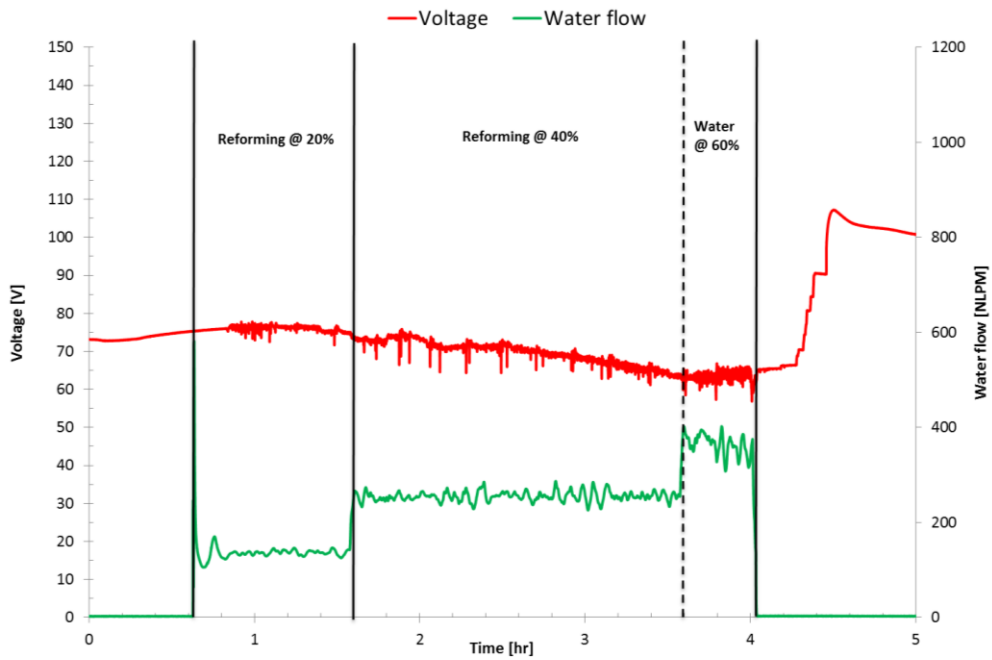
Figure 248 SOFC test with biogas.

A2.5 Oxy-combustor test results

The oxy-combustor was designed with two inlet pipes for oxygen (Figure 249). This choice was because the geometry of the reactor should be able to spread the combustion across the entire length.
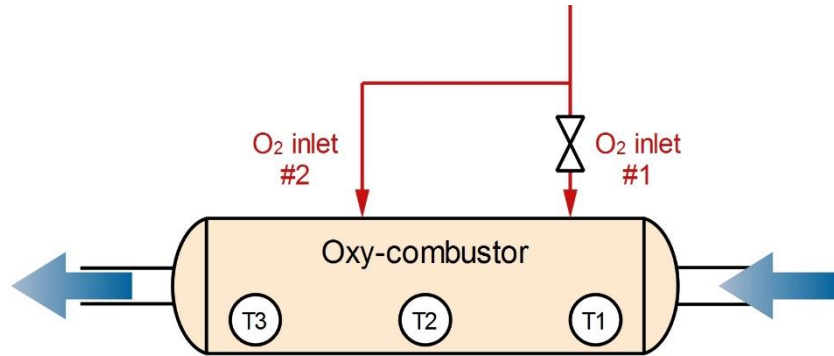
Figure 249. Oxy-combustor oxygen inlets layout.

Results from the first test with oxygen sent only to inlet #1 (nominal system configuration) are shown in the figure below (Figure 250). The maximum temperature achievable in the reactor should be 1200°C to avoid problems for materials. With this configuration, anyway, in a standard nominal condition, temperature T1 was higher than the maximum allowable value. Furthermore, the temperature change across the reactor was high: from T1 @ 1300°C to T3 @ 700°C: the combustion reaction was thus taking place only in the first combustor section.
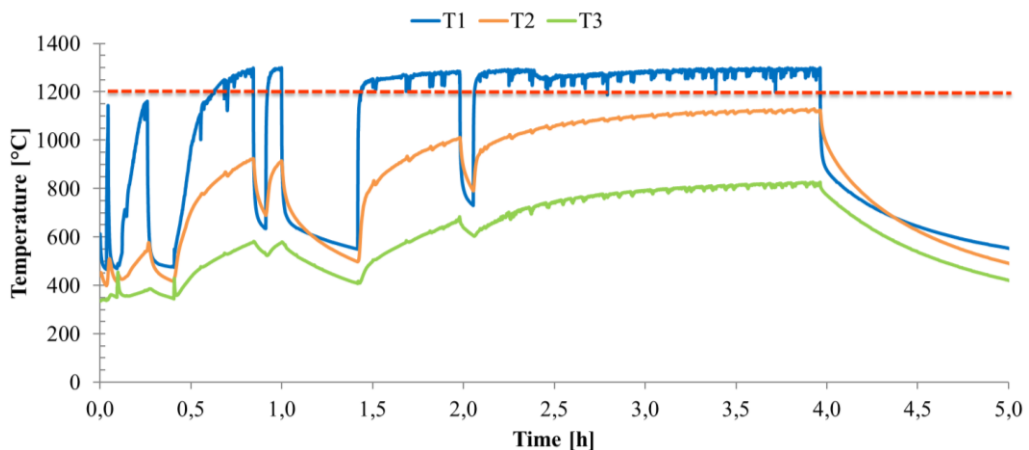
Figure 250. Oxygen feed #1. Vertical axis: temperature in °C. Horizontal axis: time in hours.

The final layout chosen for the tests was to use both inlet #1 and #2 since the reactor design seemed not able to spread the combustion across the overall length. The inlets were

already placed and connected in the system, so the flow would not be split in equal part since the inlet #2 pipe was longer and thus with higher pressure drops. For this reason, a manual needle valve was inserted before inlet #1, to create the same pressure drop as for inlet #2 and have a similar flow rate going into the two pipes.

Results for this final layout are shown in Figure 251. All the temperature are lower than the acceptable max. value (1200°C) and the temperature difference across the combustor was reduced from 500 to less than 300°C. A staged combustion seems to be achieved with this new layout, with a diffusion of the flame along all the combustion chamber.
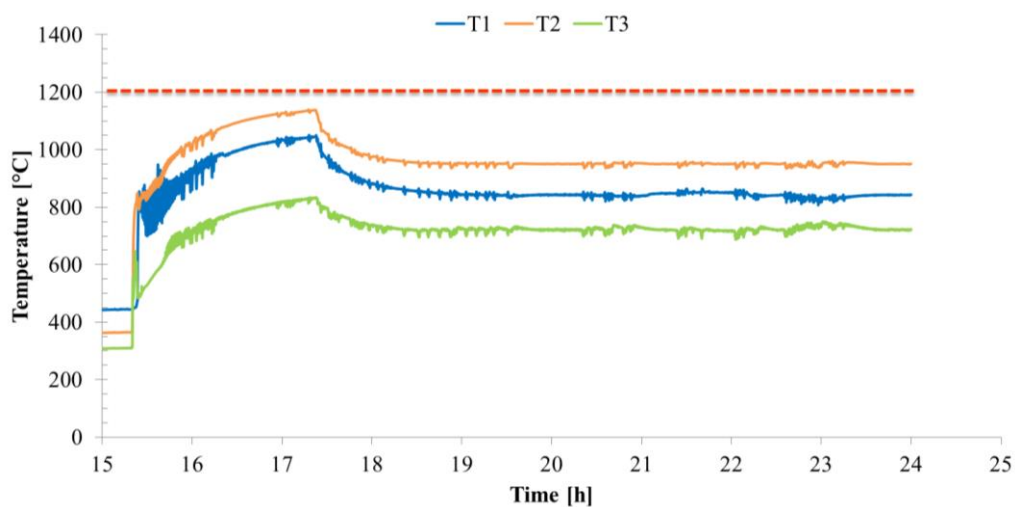
Figure 251. Oxygen feed #1 + #2. Vertical axis: temperature in °C. Horizontal axis: time in hours.

A2.6 Condenser unit test results

The condenser system has been tested for several times during the demo working period. No specific test has been performed in this unit since its working mode was suitable for the system and no change was needed. The only modification, respect to the nominal working conditions set in its user manual, is related to the compressor outlet pressure.

The flow rate reaching the condenser was lower than the one for which the system was designed since the major part of the water was already condensed in the anode CHP cooler. Furthermore, a long run @ 50% of nominal power has been performed. In these low-flow conditions, the compressor showed some difficulties in reaching a stable operation since a too low rotation speed was required and the system was going in continuous on/off operation. One of the solutions adopted for reducing this problem was to increase the compressor outlet pressure from 5 to 7 barg.
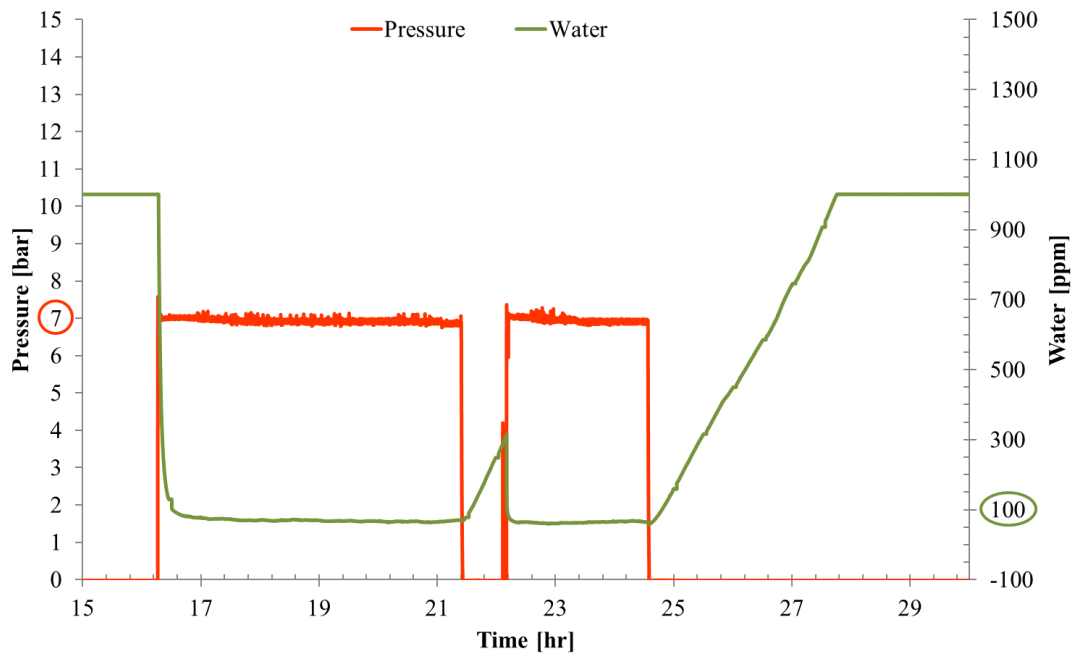
Figure 252. Condenser test results.

The global CCS institute stated that existing long-distance US CO_2 pipelines typically operate with a maximum specified water content around 25–30 lb/MMscf (which corresponds to approximately 200-245 ppm w/w) (International Energy Agency-Greenhouse Gas R&D Programme (IEAGHG) 2010) Buit el al. (Buit et al. 2011) have also analyzed different references for the limiting water concentrations in CO2 pipelines, which ranges from 40 to over 500 ppm (Thomas & Benson 2005; Det Norske Veritas 2010). As a conclusion, the authors confirm that under normal operating conditions, dense phase CO_2 can be transported when containing 500 ppm water without any risk of free water formation, because the water solubility is at least 1,500 ppm under these circumstances (International Energy Agency- Greenhouse Gas R&D Programme (IEAGHG) 2010). For this reason, the lower extremes of 40 and 50 ppm are probably rather conservative values.

The water content inside the outlet CO_2 stream was extremely low in the proposed SOFCOM system: the water content in the outlet stream reaches a value around and lower than 100 ppm (v) (Figure 252). Hence, the water content that was achieved is safe in term of water condensation and related corrosion issues.

A2.7 Photobioreactor test

The operating results are obtained after two weeks of test, where the system setup was developed and first problems solved especially linked to the electro-vales. Table 72 shows the desired values settled into the system.

Table 72. Low and full-scale values with desired values for sensor transmitter and scaling of the analog signal.

Measure/Display	Lower Value	Value desired	Upper Value
LIT 430	0 cm	50 cm	100 cm
TI 428	>0 °C	20-30 °C	140 °C
FI 208	0 l/h	200 l/h	1500 l/h
L 326	0 kLux	60-100 kLux	270 kLux
PI 436	0 bar	0.1-1.5 bar	10 bar
PI 412	0 bar	0.1-1.5 bar	10 bar
PI 128	0 bar	3 bar	10 bar

Stable performance are achieved during the first days of operation.
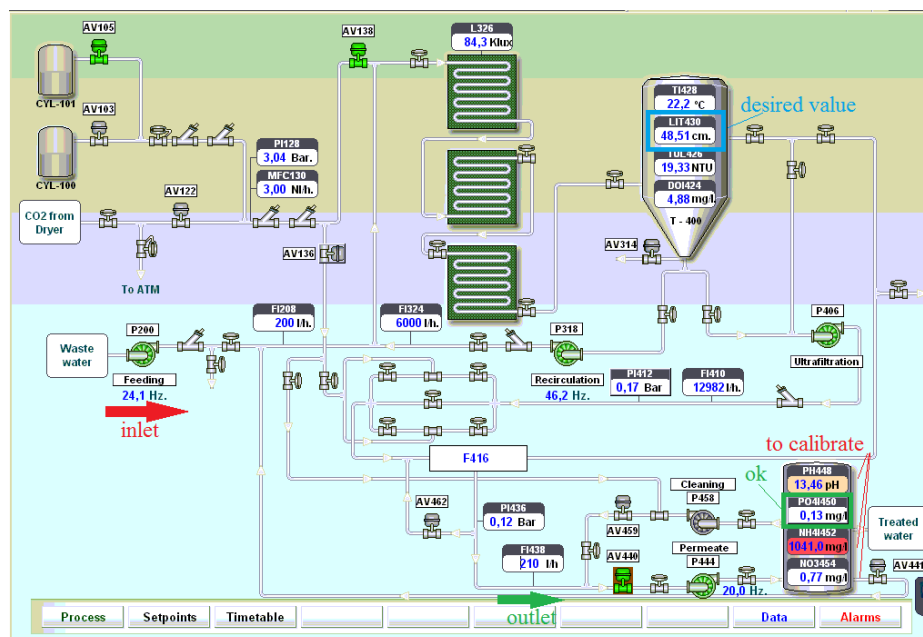
Figure 253. Process screen which allows the direct supervision of the photobioreactor – stable performance achieved.

First results obtained after two weeks of operation are reported below. The sun irradiation is reported in Figure 254 and correlated to the temperature increasing inside tubes exposed to the sun.
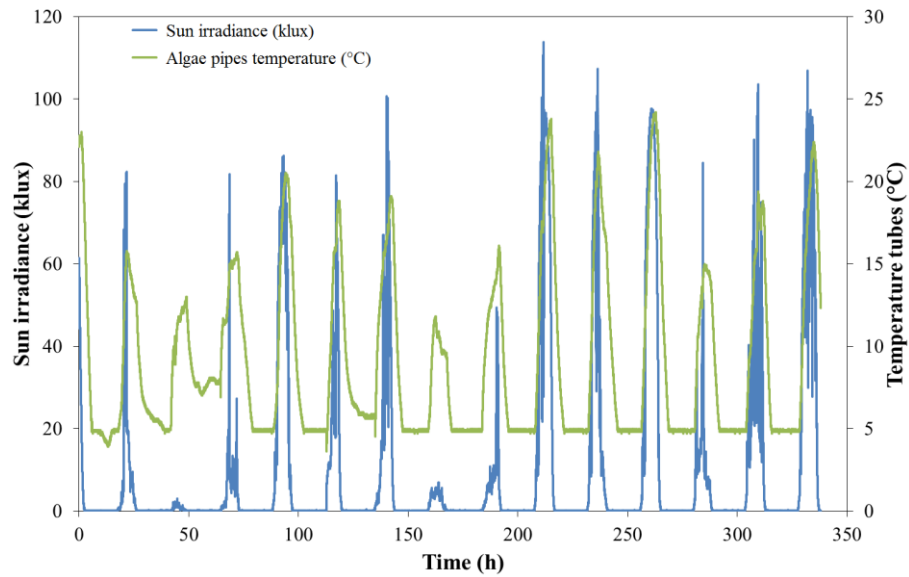
Figure 254. Sun irradiance variation correlated to the algae temperature.

There is a correlation between the sun irradiance and temperature. The sun irradiance changes from to 50-60 klux to 110 klux while the temperature changes between 5 to 25 °C.

Figure 255 shows results of PO4 removal, detected from the clean tank, during the test with sun irradiance and the CO_2 injection, 3 Nl/h. Preliminary results are in agreement with results obtained in the laboratory. The figure shows how increasing the sun irradiance increase the phosphate removal from 90% to 94%.
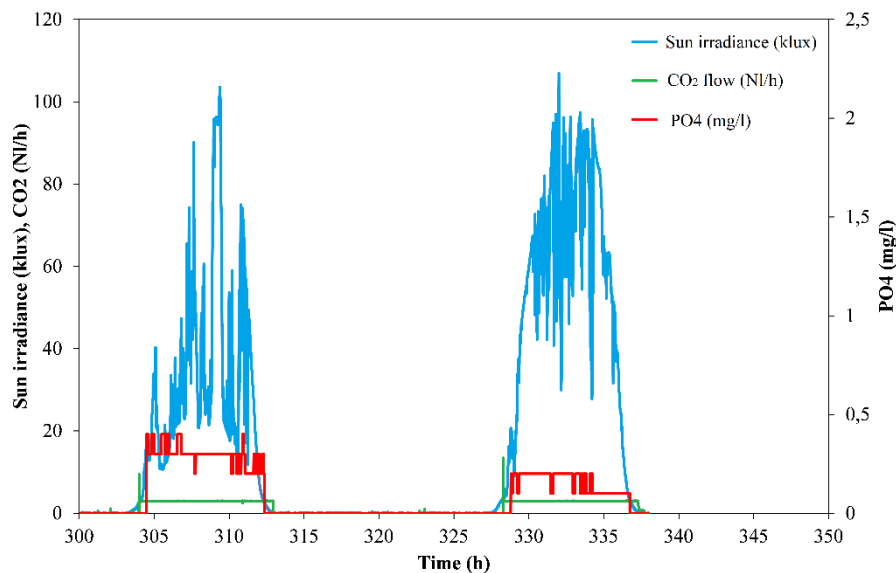
Figure 255. Sun irradiance variation correlated to the CO_2 injection and PO4 removal.

Preliminary results of the algae growth are reported in Figure 256 where CO_2 bubbles are showed with the first algae sedimentation on the tube.
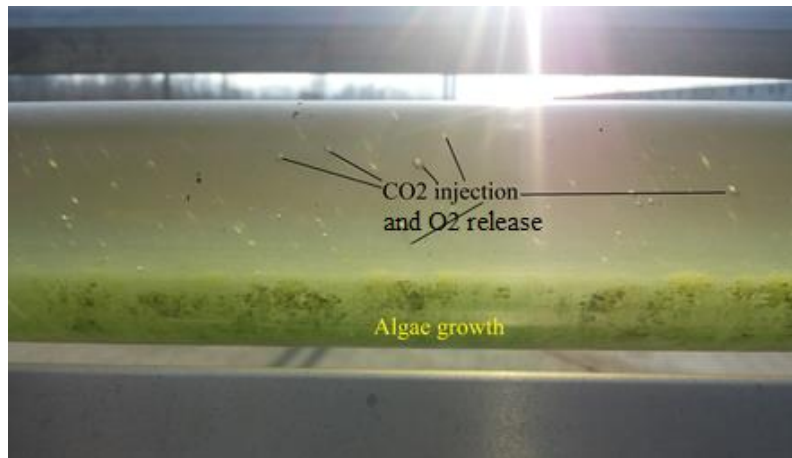
Figure 256. Preliminary results of the CO_2 injection and algae growth.

The following figure shows the oxygen dissolved into the degasification tank; these preliminary results show the oxygen production during the day related to the algae photosynthesis process also related to the sun irradiance. The oxygen dissolved peak seems to be related to the sun irradiance peak while the temperature is still high due to the thermal inertia of the system.
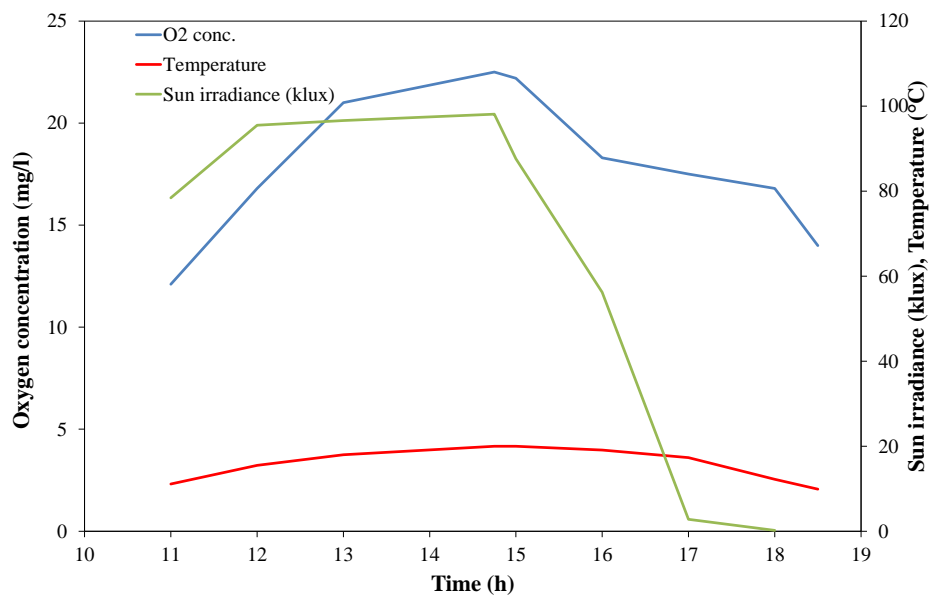
Figure 257. Oxygen dissolved into the degasification tank produced from algae.

Appendix 3 – Plant modeling

A3.1 Clean-up system

The cleaning unit has been sized and defined mainly according to the work of the US Argonne Laboratory. A detailed work on the biogas impurities has been developed in the framework of the small size plant analysis, and a journal paper has been published on it (Papadias et al. 2012).

Depending on the substrate used for biogas production, the type and amount of contained impurities vary largely. This is illustrated by Table 73 and Table 74, which list detailed biogas compositions produced from different substrates including wastewater treatment plants. Concentrations of CH_4 and CO_2 vary, even though the same classification of the substrate is used. This is also valid for other biogas constituents such as sulfur and halogen compounds.

Table 73. Biogas Composition for Different Biogas Plant Types (Fuel Cell Energy 2012) (Trendewicz & Braun 2013).

Composition	Natural gas	Biogas			
		Wastewater	Food waste	Animal waste	Landfill
Methane [% vol.]	80 – 100	50 – 60	50 – 70	45 – 60	40 – 55
Carbon dioxide [% vol.]	< 3	30 – 40	25 – 45	35 – 50	35 – 50
Nitrogen [% vol.]	< 3	< 4	< 4	< 4	< 20
Oxygen [% vol.]	< 0.2	< 1	< 1	< 1	< 2
H_2S [ppm]	< 0.1	< 400	< 10'000	< 300	< 200
Non H_2S sulfur [ppm]	< 10	< 1	< 1'000	< 30	< 30
Halogens [ppm]	< 0.1	< 0.2	< 0.2	< 0.2	< 100
Moisture [%]	< 0.02	~ 3	~ 3	~ 3	~ 3

Table 73 also shows that type and amount of impurities within biogas depends on the originating substrate. Combining data presented in the table with the biogas substrate considered in this project, the following conclusions can be drawn:

(1) The main contaminants in biogas produced from agricultural wastes and biological substrates are **sulfur compounds**, among which hydrogen sulfide (H_2S) is the most dominant one; this conclusion is also validated in other references (Arnold 2009; Van Herle et al. 2004; Papadias et al. 2012).

(2) In biogas stemming from food and animal waste as well as wastewater (Table 73), **halogenated compounds** are present in very small trace amounts.

(3) **Organic silicon compounds** are only detected in landfill gas and gas from WWTPs (Pfeifer et al. 2013; Arnold 2009).

Table 74. Average and Maximum Values of the Main Contaminants in Biogas from WWTP (Du & Parker 2011).

	Contaminants	Average value [ppm]	Maximum value [ppm]
Sulfur compounds	H2S	400	2897
Siloxanes	D4	0.825	20'144
	D5	1.689	18'129
Halogens	Dichloromethane	0.052	0.052
	Chlorobenzene	0.255	0.693
	Dichlorobenzene	0.254	0.61

Therefore, the following paragraphs describe the origin, concentration levels, and possible impact of sulfur and halogen compounds on biogas-fueled SOFC plants, in which the focus lies on anode side contamination. Sulfur is present in nearly all biological compounds as part of amino acids such as methionine and cysteine (Du & Parker 2011). In addition, biomass itself is made up by <2% (on a weight basis of dry and ash-free biomass) of sulfur taken up through the soil and air (Vassilev et al. 2010). During digestion, sulfur is converted into gaseous compounds including H_2S, carbonyl sulfide (COS), mercaptans, and disulfides, among which H_2S is the most common one (Arnold 2009). Concentration levels of H_2S in biogas along with the overall chemical build-up of biogas vary significantly depending not only on the substrate but also on operating conditions. Sklorz et al. observed the following three correlations of H_2S concentration fluctuations in a 45 kWel biogas plant using a gas engine for power generation (Bayerisches Institut für Angewandte 2003):

- As soon as the integrated gas engine stops running, H_2S concentration in biogas decreases; this is explained by microorganisms or chemical reactions of H_2S with galvanized steel tubing, which reduce more H_2S in coordination with a slower gas flow and longer residence time of the gas inside the digester system.
- Due to mechanical stirring starting every 4 h for 20 min, fresh biogas with a higher loading of H_2S is released from the digested biomass; the time for

desulfurization reactions to take place is not sufficient to absorb the increasing H_2S concentration effectively.

- When a new batch of the substrate is added to the digester, a continuous increase in H_2S concentration is observed due to the injection of fresh, sulfur-containing matter.

However, not only H_2S is present within biogas but also several other sulfur compounds (Papurello et al. 2012): in this project, kitchen waste is digested in a pilot-scale anaerobic digester while gas quality is monitored over a period of 30 days. Besides H_2S, other sulfur compounds such as methanethiol (CH_3SH), propanethiol (C_3H_7SH), butanethiol (C_4H_9SH), and dimethylsulfide (DMS) are detected, with levels that at times even surpass concentration levels of H_2S. As a consequence, at least two gas cleaning steps are needed for effective biogas cleaning: one step to remove bulk H_2S concentration and the second step to remove remaining sulfur compounds from the biogas, because H_2S removal systems do not necessarily remove other sulfur compounds (Arnold 2009). Halogens are contained within waste in the form of kitchen salts and polymers (polytetrafluoroethylene: PTFE; polyvinyl chloride: PVC). As such, these compounds are mostly found in biogas stemming from landfills (Arnold 2009; Pfeifer et al. 2013). In ref (Papadias et al. 2012), halogenated compounds measured in landfill gas and biogas produced from anaerobic digestion of sewage sludge are compared with each other. It is shown that average concentrations in landfill gas are higher than maximum values detected in gas stemming from sewage sludge (compare Table 74). Table 73 also indicates that halogen content in biogas from WWTUs lies in the same range as biogas produced on farms.

An explanation for halogen content in biological substances is that small quantities of chlorine are taken up by plants through salts which are washed out of soils. On average, chlorine build-up in plants amounts to <1%wtdb (Vassilev et al. 2010). As a result, trace amounts of halogens can be detected in biogas produced from the substrate considered in this paper. The quantities of halogens reported in the literature are below 1 ppm_{mol}, as shown in Table 73.

It is now clear that integration of biogas fuel with solid oxide fuel cell systems can only be realized via an effective gas-cleaning system. Consequently, several cleaning steps are necessary to ensure risk-free operation.

The following list gives a basic summary of gas-cleaning stages applied in the system analysis:

(1) **In situ H_2S precipitation** by injecting 2 mol % to 6 mol % of air directly into the digester; this way, bacteria oxidize H_2S into elemental sulfur, which is enriched in

the digested biomass lowering hydrogen sulphide concentrations in the gas stream to <100 ppm$_{mol}$ (Ryckebosch et al. 2011; Krich et al. 2005);

(2) Saturated biogas leaving the digester is dried by **condensation** using cold water to avoid corrosion in power plant parts and then reheated again with incoming biogas; calculations show that a relative humidity of approximately 60% is achieved;

(3) The remaining content of H$_2$S, which is not removed by bacterial activity, is cleaned by **adsorption on ZnO**, ideally reaching concentrations levels of <1 ppm$_{mol}$ (Anttila et al. 2013);

(4) Trace impurities such as other sulfur and halogen compounds are removed in a final polishing step by an **adsorption bed of activated carbon (AC)**, aiming for concentrations levels of <1 ppm$_{mol}$ (Papurello et al. 2014).
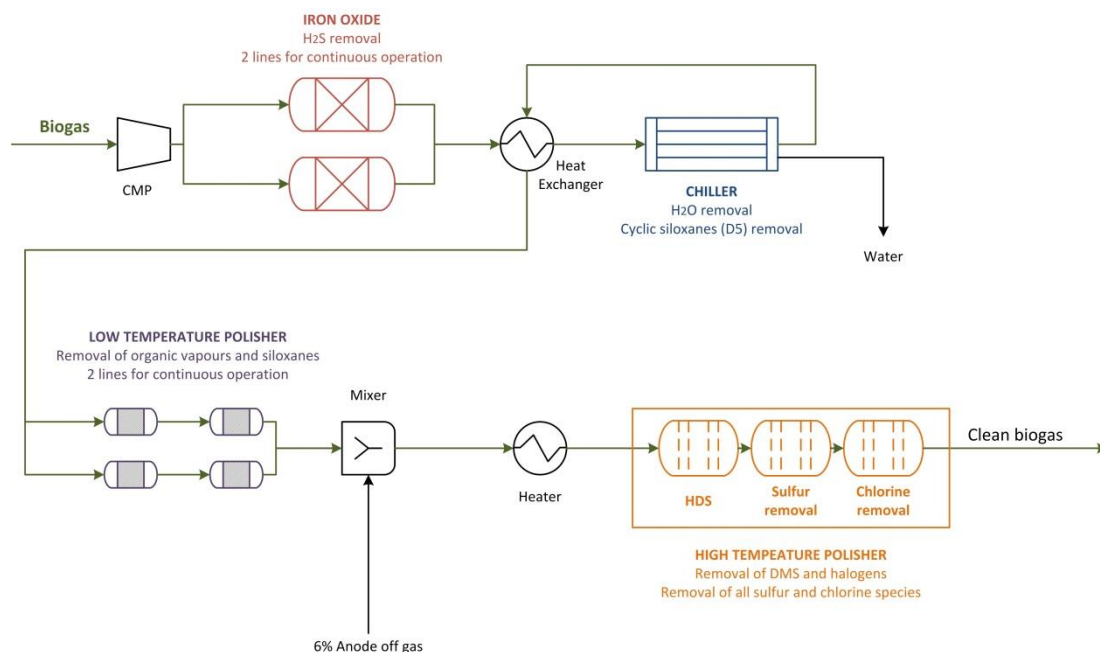
Figure 258. General cleaning system layout.

It is suggested that the cleaning system comprises two parallel adsorption vessels for each filter to ensure continuous operation during bed material change or breakdown. After gas cleaning, contamination levels of biogas impurities are considered to be below 1 ppm$_{mol}$ and thus do not pose any threat to power plant components during system operation.

The biogas cleaning system is not included in the Aspen Plus® model because it does not give any sensitive contribution related to the thermodynamic of the system: there are no changes in macro-components composition, temperature, pressure, and flow rate. The inlet biogas to the model is supposed to be already clean. Yet, the gas-cleaning system is included in the form of pressure drops along the cleaning columns.

Since larger size plants should also be considered, coming from different substrates and containing different contaminants, a more detailed cleaning system compared to the base one has been chosen for the medium and large size plants. It is taken from the work of Argonne Laboratory (Papadias et al. 2012) and it is able to remove all the impurities contained in the biogas completely. The biogas used in the SOFCOM demonstration, for example, after a 6 months analysis was found to be quite clean compared to the literature values presented above and thus the complete cleaning system can be considered a conservative. Figure 258 shows the general layout of the analyzed cleaning system.

The system from (Papadias et al. 2012) is composed of:

Iron oxide: iron oxide media (SulfaTreatHP®)for the hydrogen sulfide removal. Desulfurization is achieved by reaction with mixed-metal oxides forming a stable metal sulfide. Even if other media are available for this purpose, SulfaTreat® was chosen because many information can be found on it in case studies and literature, which are helpful for developing a model for design purposes and qualitatively assess the adsorption capacity. The maximum adsorption capacity was estimated as 12 wt% (g-S/g-adsorbent). The temperature was also found to be very important for the adsorption capacity value. See Table 75 for design details.

Gas drying: the gas need to be dried before entering the next polisher. Moisture, especially at a relative humidity (RH) exceeding 40% can significantly reduce the capacity of adsorbents like activated carbon. Other adsorbents, such as silica gel or zeolites, are even more sensitive to RH. The gas is thus passed through a chiller/condenser that cools it down to a dew point of 4°C; after, the gas is reheated at 25 °C (RH = 25%) in a heat exchanger, by using the warm biogas coming from the hydrogen sulfide removal bed. The only species that were predicted to condensate out by cooling are cyclic siloxanes, especially D5. Table 76 shows design parameter for the chiller/condenser.

Low-temperature polisher: activated carbon (AC) is frequently used for the removal of organic vapors, and it has also been demonstrated to be efficient in removing siloxanes. Design parameters can be found in Table 77. The lead and lag configuration was chosen again.

High temperature polisher: in this system, all the sulfur and chlorinated species not captured by the carbon bed are removed by the high temperature polisher. Organic sulfur and chloride are first reacted with hydrogen over a hydrogen processing catalyst (HDS) and converted to H_2S and HCl respectively. These species are then removed by using sulfur and chlorine adsorbents (ZnO and Al_2O_3). Design parameters can be found in Table 78.

Table 75. Iron oxide bed design parameters (Papadias et al. 2012).

Parameter	Value	Unit
Contact time	60 - 120	Sec
Vessels design	2 vessel design (lead and lag)	-
Lead vessel breakthrough H$_2$S concentration	15	ppm
Temperature	38	°C
Removal	All H$_2$S and mercaptans	

Table 76. Design parameters for chiller/condenser (Papadias et al. 2012).

Parameter	Value	Unit
Dew point	4	°C
Rh at 25 °C	25	%
COP for refrigeration cycle	3.4	-
Removal	Water and cyclic siloxanes	

Table 77. Design parameters for low temperature polisher (Papadias et al. 2012).

Parameter	Value	Unit
Pressure	1.1	atm
Temperature	25	°C
Moisture at RH 25%	Not affecting adsorption capacity	-
Carbon media	Calgon BPL (700 kg/bed, 2 bed in series)	-
Limiting species	Siloxane D4	-
Bed replacement	164	-

Table 78. Design parameters for high temperature polisher (Papadias et al. 2012).

Parameter	Value	Unit
Temperature	330	°C
H$_2$ partial pressure for HDS	5	kPa

Sulfur removal media	G-72E (5 wt% capacity before breakthrough)	-
Chlorine removal media	G-92C (5 wt% capacity before breakthrough)	-
Vessel design	2 beds for continuous adsorption	-

A3.2 Processing unit

The processing unit has been deeply analyzed in the framework of the presented analysis. Special attention has been devoted to the different reforming agents and to the different reforming heat integration within the plant.

Concerning the **reforming agents**, three main case studies have been analyzed (Tjaden et al. 2014):

- Steam reforming (SR).
    - External demi water.
    - Anode exhaust recirculation.
- Partial Oxidation (POx) with external air.
- Auto-thermal reforming using anode recirculation and external air (ATR).

All the analyzed reforming types will be mixed with a portion of dry reforming, having carbon dioxide contained in the biogas.

In relation to the possible **heat integration of the reformer** within the stack, three main configurations have been discussed:

- External reformer (heat supplied by exhaust).
- Indirect internal reformer (heat supplied by the stack, without having internal reforming).
- Direct internal reformer (heat supplied by the stack through internal reforming) .

This first analysis was performed mainly related to the small size plants in order to find an optimal solution to be applied for medium and large plants. The second one can be easily performed on each plant modeled, but results will be presented mainly related to medium size scale. Furthermore, some technical analyses with a related literature research on patents and commercial products have been carried out on small size plants for:

- Reformer technical design for small size plants (1 – 100 kWe)
- Anode recirculation devices
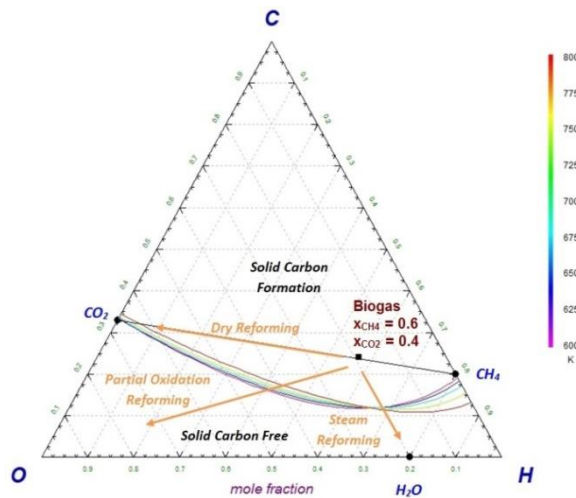
Figure 259. Ternary C−H−O diagram for biogas reforming options (equilibrium calculations for 600 to 800 °C) (Tjaden et al. 2014).

In the first analysis, as mentioned above, three reforming options are considered: steam reforming (SR) with simultaneous dry reforming (DR), partial oxidation reforming (POx), and auto-thermal reforming (ATR), where steam and dry reforming run in parallel as well. The amount of either reforming agents, which is needed to avoid carbon deposition on the anode, can be estimated by equilibrium calculations, as shown in Figure 259. The three options are briefly outlined below.

Steam Reforming

Under steam reforming, H_2O is used as a reforming agent to convert CH_4 into an H_2- and CO-rich synthesis gas. For a small-scale system, no external supply of any kind of reforming agent is implemented. Consequently, steam is provided to the reformer by anode exhaust gas recirculation from anode exhaust stream back into the reformer. Aside from H_2O, CO_2 is present in the recirculated gas as well as in the biogas itself.

As deployed catalysts favor steam as well as dry reforming, both reforming options are considered to run in parallel under SR. The mass flow of steam is adjusted in such a way, that steam to carbon ratio (S/C) of two is reached in the reformer. S/C ratio is calculated using the following equation:

$$S/C = \frac{\dot{n}_{H2O}}{\dot{n}_{CH4}}$$

Eq. 39

In which can be defined:

- S/C   steam to carbon ratio [-]
- $\dot{n}_{H2O}$ molar flow rate of steam [mol/s]

- $\dot{n}_{CH4}$ molar flow rate of methane [mol/s]

Despite the carbon dioxide contained in the biogas, the S/C ratio is defined in its general equation as the ratio between the methane and the water. Figure 260 shows a ternary diagram of the inlet composition as a function of S/C ratio. It is visible that at temperatures above 675 °C, no carbon deposition is caused even at low S/C ratios of one. Thus, the nominal chosen value of two leaned on parameters used in the literature (such as in refs (Galvagno et al. 2013; Chiodo et al. 2012)) is safe when the reformer temperature lies higher than 700 °C, which is always guaranteed in this analysed plant. Steam is injected into the reformer by recirculating anode off-gas back into the reformer to meet the S/R ratio.
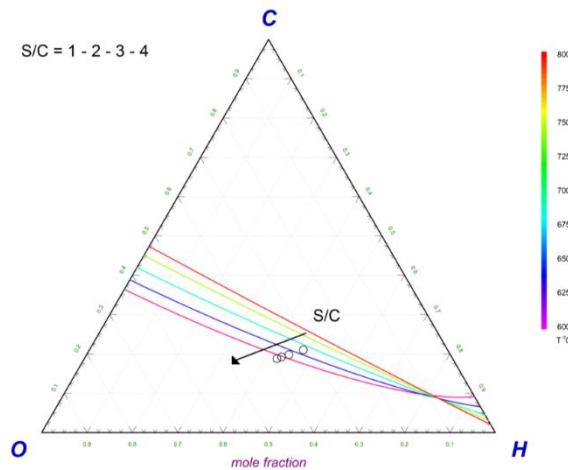
Figure 260. Ternary C−H−O diagram for the steam reformer inlet composition varying the S/C ratio (Tjaden et al. 2014).

Partial oxidation

Partial oxidation reforming combusts a part of the fuel by adding air as the reforming agent. Due to partial combustion and dilution with N_2 contained in air, system efficiency is expected to be lower compared to steam reforming. Yet, POx offers lower system complexity and thus economic advantages. The lambda air ratio in the reformer λ_{POx} is assumed to be a constant value amounting to 0.25.

$$\lambda_{POx} = \frac{\dot{n}_{Air}}{\dot{n}_{Air,st}}$$ Eq. 40

In which can be defined:

- λPOx   lambda air ratio [-]
- $\dot{n}_{Air}$ actual air flow rate [mol/s]

- $\dot{n}_{Air,st}$ stoichiometric air flow rate for complete combustion [mol/s]

In order to avoid the carbon formation risk when POx is performed, the inlet gas composition is modified by varying the lambda air ratio (as shown in the ternary diagram of Figure 261). With a reduced air flow rate (low oxygen-to-carbon ratio in the reformer), the risk of solid carbon formation can be reached at a temperature lower than 800 °C. On the other hand, the analysis shows that with the chosen nominal conditions of 0.25, the risk is reduced and the safety area is guaranteed at the chosen reformer nominal temperature (Galvagno et al. 2013; Chiodo et al. 2012).
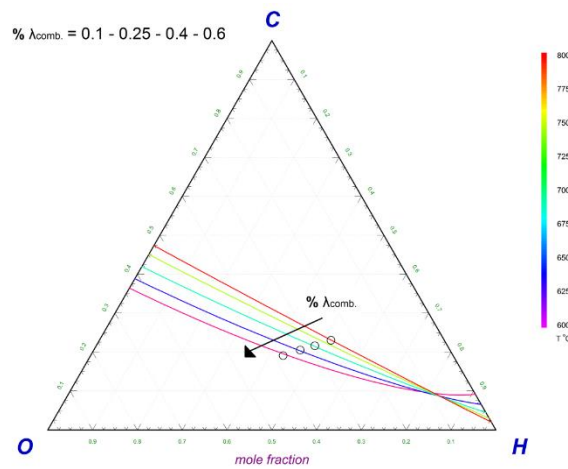
Figure 261. Ternary C−H−O diagram for the POx reformer inlet composition varying the λPOx (Tjaden et al. 2014).

Auto-thermal reforming

Auto-thermal reforming is a combination of all aforementioned reforming options, which means that exothermic partial oxidation reforming drives endothermic steam and dry reforming reactions. In the end, reforming agents are combined in such a way that overall enthalpy of reaction amounts to zero. Reforming reactions and corresponding enthalpies of reactions at standard conditions are shown in the following equations:

$$CH_4 + CO_2 \rightarrow 2CO + 2H_2 \quad \Delta^r h^o = 247 \; kJ/mol \qquad \text{Eq. 41}$$

$$CH_4 + H_2O \rightarrow CO + 3H_2 \quad \Delta^r h^0 = 206 \; kJ/mol \qquad \text{Eq. 42}$$

$$CH_4 + \frac{1}{2}O_2 \rightarrow CO + 2H_2 \quad \Delta^r h^0 = -36 \; kJ/mol \qquad \text{Eq. 43}$$
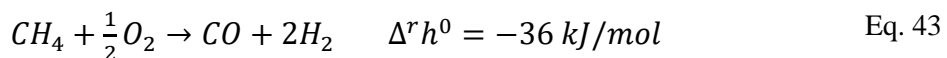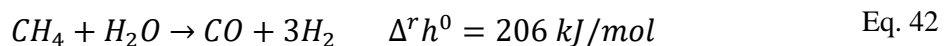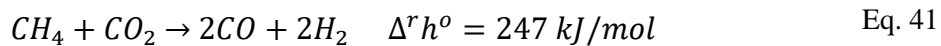
In which can be defined:

- $\Delta^r h^0$ specific reaction enthalpy at standard conditions [kJ/mol]

The system analysis compares SR, POx, and ATR in which the amount of internal reforming for SR is varied. DR is considered to take place in parallel to SR and ATR due to elevated CO_2 content present in the biogas stream as well as in recirculated anode exhaust gas stream and because of applied catalysts.

Once the biogas flow rate is determined (DR fixed), infinite possible combinations of S/C and Lambda could be determined in order to have a zero heat duty of the reformer: for this reason in the model, the S/R ratio has been fixed to its nominal value.

Small size plant reformer design

Depending on the reforming agent, a different reactor design is needed. A detailed literature analysis on the reformer layout for small size systems (0 – 100 kWe) has also been performed in the framework of the analysis (Tjaden et al. 2014). Due to the small system scale analyzed in this project, only a few manufacturers offer adequate solutions. Nevertheless, the following paragraphs summarize solutions on applicable reformer options:

- *Steam reforming* is feasible in the 450−900 °C range, but the best results are achieved between 550 and 800 °C. Because of the endothermic nature of the process, an external heat source is always required when performing SR. On the other hand, this process leads to the highest electrical efficiency of the three solutions. A commercial small size steam reformer for fuel cell applications is presented on the Web site of the manufacturer (see ref (Anon n.d.)). In order to provide the required amount of thermal power, two possible technical solutions are available: combustion heated reformer and indirect internal reformer. In combustion heated reformer, the reformer chamber is set inside a combustion chamber in which exhaust gases (together with NG if needed) are burned with spent air in order to provide the heat required. In ref (Antonini et al. 2012), the following layout can be found: a first combustion chamber made of a metal material for the first combustion stage is connected to a second combustion chamber defining a second combustion stage. The reaction unit also comprises one or more reaction elements housed partly inside the combustion chambers so that the heat generated inside them is transferred by thermal heat conduction to these elements (Antonini et al. 2012). The chosen catalyst is nickel-based, which is the most common catalyst suitable for these applications. The chosen system size lies below the one proposed in the work so that an SR could be considered a viable solution for the analyzed plant. From other patents, a similar layout with packages of tubes is also found (Mizuno & Hatada 2008; Sammes 2002). In indirect internal reformer, the reformer is located on the premises of the SOFC in a position where it is able to receive heat radiation from the SOFC. This combination is able to compensate for the

endothermic heat requirement of the reforming with the surplus of heat generated in the SOFC, yielding a reduction in the cathode air flow and blower consumption.

- *Partial oxidation reformer*: POx is an exothermic reaction, and thus no heating requirement is needed. Despite this first advantage, the reaction consumes a part of the fuel and thus leads to a reduced electrical efficiency. Some commercial products can be found in the fuel cell market using catalytic POx (Anon n.d.; Anon n.d.).

- *Auto-thermal reformer*: When a low S/C ratio and a low temperature are coupled together, as seen before in the ternary diagram, the risk of coke formation cannot be avoided. This problem can be overcome by adding air or oxygen to the hydrocarbon/steam fuel mixture. An auto-thermal reforming catalyst is a catalyst which promotes a steam reforming as well as partial oxidation reforming. In general, high-activity nickel reforming catalysts containing 15−25 wt% nickel on a α-alumina or magnesia-doped alumina are used, but higher efficiency products with rhodium on an impregnated alumina support are also be found in practice (Herbert J. Setzer et al. 1984). Catalyst materials are different for each reforming solution because a material able to activate the chosen reforming agent is needed. Higher efficiency catalysts can be rhodium- or platinum-based ones, even if this will lead to a high-cost increase (Mizuno & Hatada 2008). Catalysts are usually filled in the reformer in pellet or honeycomb form.

For start-up purposes, for the high-efficiency SR, an external hydrogen cylinder is necessary to start the endothermic reforming reactions and subsequently start up the SOFC. In recent studies in the field of SOFC start-up, more complex but more flexible system layouts were introduced such as in ref (Yukihiro Sugiura 2013). Here, the system is composed of a first steam reformer heated by the SOFC itself which works under nominal operating conditions and a second reformer heated by an NG combustor for the start-up procedure. Another option for system start-up is presented in ref (IWao Anzai 2014), where a first thermally auto-sustained POx phase is followed by an SR for nominal operation. The two stages can be operated as one single reformer with an auto-thermal catalyst or as two separate reformers. This way the system can be initiated in a short time without losing the advantages of SR. In this work, the reforming reactor is modeled using a Gibbs equilibrium reactor. This choice is justified by literature findings which validated reforming models by comparing calculated equilibrium gas compositions with experimental findings (Marsano et al. 2004; Hakala 2012). For this reason, the choice of an equilibrium reactor, as done in the presented work, is a good approximation of the real reforming behavior despite the technical and sometimes even complex flow and thermal design arrangements proposed by the manufacturers of fuel-processing units for SOFC systems.

Anode Off-Gas Recirculation: technical analysis

For anode recirculation purposes under steam reforming, two possible pathways can be considered:

- **Hot recirculation blower**: This was historically the preferred solution for molten carbonate fuel cells due to its simple working principle and the availability of materials which can withstand temperatures of up to 700 °C (Anon n.d.; Grillo et al. 2003). For SOFC systems, the temperatures could be higher (up to 900 °C), and thus, new expensive and innovative materials are required. Commercial solutions can be found on the market which focuses on applications in the automotive sector (Massardo & Bosio 2001; Chick et al. 2013).
- **The ejector (Venturi device):** Ejectors are a promising solution for the future of fuel cell plants. They operate without moving parts, which results in considerably lower stress. As a result, conventional materials can be applied for which no lubrication is needed, which might pose a risk of anode poisoning (Marsano et al. 2004). In the ejector, a primary fluid at high pressure expands in a nozzle and enters a duct at high velocity, where it mixes with another gas coming from a second line. The ejector aims at to maintaining required pressure in the fuel cell while enough exhaust gas is recirculated to obtain the desired S/ C ratio. The main disadvantage of the presented solution is related to the poor availability of commercial high temperature solution and the difficulty of responding to load variations in the fuel cell (Hakala 2013; Hakala 2012).

Reformer heat integration

As mentioned in the introduction section, different heat integrations are possible when analyzing the reforming process.

Steam reforming reactions, being endothermic, require some heat provided by external and this lead to different possible configurations. On the contrary, POx reforming involves exothermic reactions, and thus some heat is generated and has to be removed in order to control the vessel temperature. From the heat integration point of view, the best solution is thus related to the ATR reforming, where the exothermic and endothermic reactions are balanced.

Looking at the SR reforming, which will be outlined as the best solution looking at energy and economic aspects, three different possible integrations can be performed:

- **External reforming** (Figure 262)**:** in this configuration, the reformer is a separated vessel set outside the stack hot box. This is the most common solution in case of POx and ATR since the heat generated in the first can be easily removed while the second has a zero heat output/input. On the contrary, when analyzing SR, the endothermic reaction need a certain amount of heat to take place keeping the

temperature constant (in order to avoid coke deposition). The heat required can be provided in two ways depending on the system layout and size:

- o **Heat from an auxiliary device:** usually an NG fed burner, place in contact with the reformer, which is able to provide the required heat. This is the less convenient solution since NG is required and it is adopted just for small size plants, especially micro-CHP. Electrical heater is used just for laboratory purposes.
- o **Heat from exhaust:** the fuel cell exhausts, after they burn with air/oxygen in a combustor, has to pre-heat the fresh inlet streams (biogas and air). Usually, the high temperature of the exhaust and the high potential which they can contain, make possible also the coverage of the reformer heat duty. In this case it is thus possible to heat the reformer at 700/800 °C and then pre-heat the inlet streams, always using the exhaust from the cells. As will be presented in next chapters, this solution is possible when a vented plant without CCS is analyzed while becomes more difficult in the case of carbon capture.
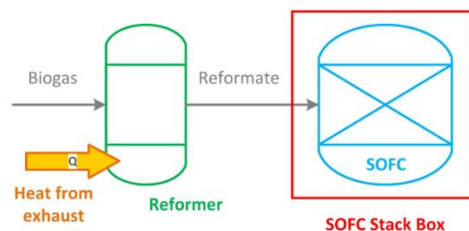
Figure 262. External reformer layout.

- **Internal reforming:** this configuration simply means that the reforming process takes place inside the stack box. Depending on the configuration, two possible solutions are available:
  - o **Indirect internal reforming** (Figure 263) **:** in this case, the reformer is set inside the stack box, but the two processes are still performed inside different vessels. The heat required for the SR can be thus supplied by the stack itself being closely placed. This is one of the best achievable solutions since it not only solves the problem of the reformer heat but also reduces the net heat generated within the stack. This amount of net reaction heat has to be removed by the cathode air flow: performing indirect internal reforming, it is thus possible to reduce the air flow rate and consequently the auxiliary consumptions, mainly related to the air blower. Furthermore, the indirect reforming is able to avoid lots of the thermal issues related to the direct one.
  - o **Direct Internal Reforming** (Figure 264)**:** direct internal reforming is the direct conversion of methane into hydrogen inside the stack. From the heat integration point of view, the configuration is optimal since in the same

vessel both the reforming and SOFC reactions occur and the heat is directly transferred from one to the other. From the literature, it is also well known about the problem with thermal gradients inside the stack when performing it. Because of the exothermic SR reaction, when methane is fed to the stack, a strong decrease in temperature can be seen nearby the entrance, with a risk of sealing break and thus stack damage. In order to guarantee a good thermal balance, it is important to send to the stack a portion of hydrogen already converted so that the two reactions are balanced: the limit from producers is usually imposed a maximum 50% of internal reforming. The only possible configuration is thus a mix between the direct internal reforming and an external or indirect internal reformer which can convert part of the inlet methane.
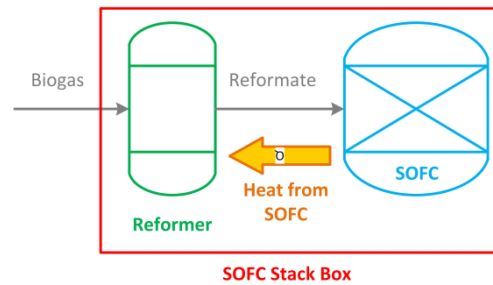
Figure 263. Indirect internal reformer layout.
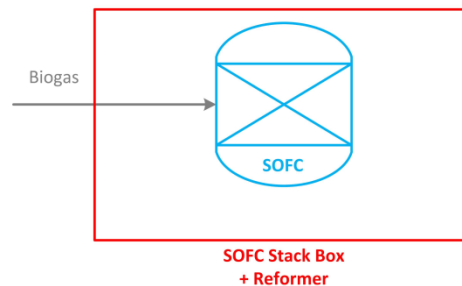
Figure 264. Direct internal reformer layout.

When performing SR, the steam to carbon ratio between CH_4 in biogas and external demineralized water has been set to 2 in order to avoid carbon deposition (Novosel et al. 2012; Yu et al. 2012). The nominal composition of the reformate is thus: >50% H_2, 10% CO_2, 19% H_2O, 19% CO, and <0.3% CH_4. For POx the lambda value is 0.25. sensitivity analysis on this parameters has been performed for small and medium size plants.

Inside AspenPlus® the reformer has been modeled as a Gibbs equilibrium reaction, since, as mentioned before, the hypothesis of a final composition close to the equilibrium

one, is an acceptable hypothesis confirmed by experimental results (Galvagno et al. 2013; Chiodo et al. 2012).

On Table 79 the nominal values of the processing unit input parameters have been summarized.

Table 79. Main design parameter for the processing unit.

Parameter	Value	Unit
Reformer temperature	750	°C
S/C ratio for steam reforming	2	-
λ_{POx} ratio for partial oxidation	0.25	-

A3.3 SOFC stack

In this section, a detailed description of the SOFC modeling is reported. The work starts with the electrochemical model definition, the choice of the operating strategy with a final part on the AspenPlus® modeling.

Electrochemical model

Comparing the fuel cell to an electrical circuit, where current flows through different voltage values three equivalent resistances (R_{act}, R_{ohm}, and R_{diff}) associated with each loss term can be defined:

1) **Activation losses** connected to overcoming energy barriers of involved reactions;
2) **Ohmic losses** caused by resistance of migrating electrons and ions in cell material;
3) **Diffusion losses** arising due to mass transport limitations of reactants.

Figure 265 shows a graphical explanation of the equivalent electrical circuit.

$$ASR = R_{act} + R_{ohm} + R_{dif}$$

$$\Delta V_{loss} = ASR \cdot j$$
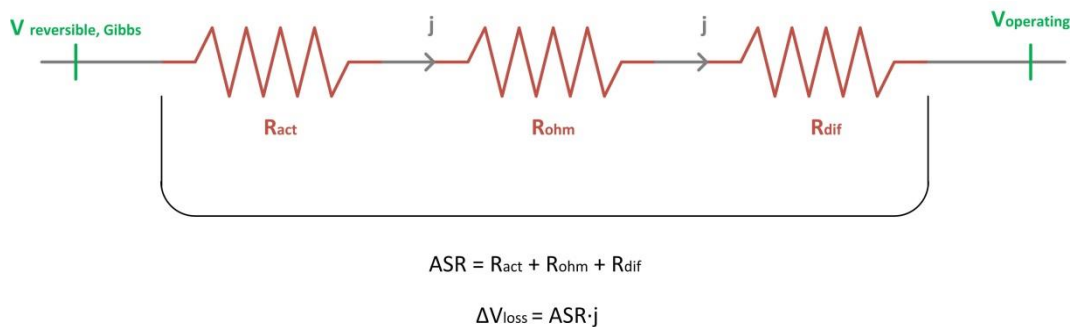
Figure 265. Fuel Cell equivalent electrical circuit.

Once these equivalent resistances are defined, the determination of the Area Specific Resistance (ASR) can be made with the following relation:

$$ASR = R_{act} + R_{diff} + R_{ohm}$$

The electrochemical model definition can also be found in two publication by POLITO (Tjaden et al. 2014) (Gandiglio et al. 2013).

Activation losses

The activation overvoltage is associated with the energy required to overcome the energy barriers in the two interfaces between each electrode and the electrolyte. The version of the Butler- Volmer equation implemented by J. Van Herle (Van Herle et al. 2003) has been used:

$$j = j_{0,an} \left[e^{\frac{2F}{RT}\eta_{act,an}} - e^{-\frac{F}{RT}\eta_{act,an}} \right]$$

$$j = j_{0,cat} \left[e^{\frac{F}{2RT}\eta_{act,cat}} - e^{-\frac{F}{2RT}\eta_{act,cat}} \right]$$

The exchange current densities are defined as:

$$j_{0,an} = \frac{RT\sigma_{an}}{3F}$$

$$j_{0,cat} = \frac{2RT\sigma_{cat}}{F}$$

Where:

$$\sigma_{an} = \sigma_{0,an} \cdot e^{\left(-\frac{E_{a,an}}{RT} \right)}$$

$$\sigma_{cat} = \sigma_{0,cat} \cdot e^{\left(-\frac{E_{a,cat}}{RT} \right)}$$

The pre-exponential factors σ_0 and the activation energies E_a are constant parameters that, again, depend on the kind of fuel cell and on its properties. On Table 80 input values for the model are reported (some of them are from the report form J. Van Herle (Van Herle et al. 2003), some in (Gandiglio et al. 2013) others derive from internal communications with EPFL, partner of the SOFCOM project (Anon 2014)).

Table 80. Activation losses parameters.

Parameter	Value	Unit	Reference
$\sigma_{0,an}$	433'033	S/cm	(Van Herle et al. 2003)
$\sigma_{0,cat}$	61'527'821	S/cm	(Van Herle et al. 2003)
$E_{a,an}$	106'000	J/mol	(Anon 2014)
$E_{a,cat}$	101'205	J/mol	(Anon 2014)

The main problem with the Butler-Volmer equations is that they are in an implicit form and so they should be converted in explicit respect to the activation overvoltage. The equation referred to the cathode can be solved easily using the hyperbolic sinus:

$$\eta_{act,cat} = \frac{2RT}{F}\,\text{asinh}\left(\frac{j}{2j_{0,cat}}\right)$$

Eq. 51

On the other hand, the one referred to the anode is more complicated to solve, because the different values of the coefficients in the exponentials do not allow the use of the hyperbolic sine. A simplified form of its solution is given by this equation 15 and demonstrated on the ref. (Lisbona et al. 2007):

$$\eta_{act,an} = \frac{RT}{2F}\,\text{asinh}\left(\frac{j}{2j_{0,an}}\right)$$

Eq. 52

Figure 266 shows a comparison in order to validate the approximated equation from literature: the red line is the approximated form of the sin hyperbolic while the blue line is the implicit form of the Butler-Volmer equation. Results confirm the validity of the chosen equation.
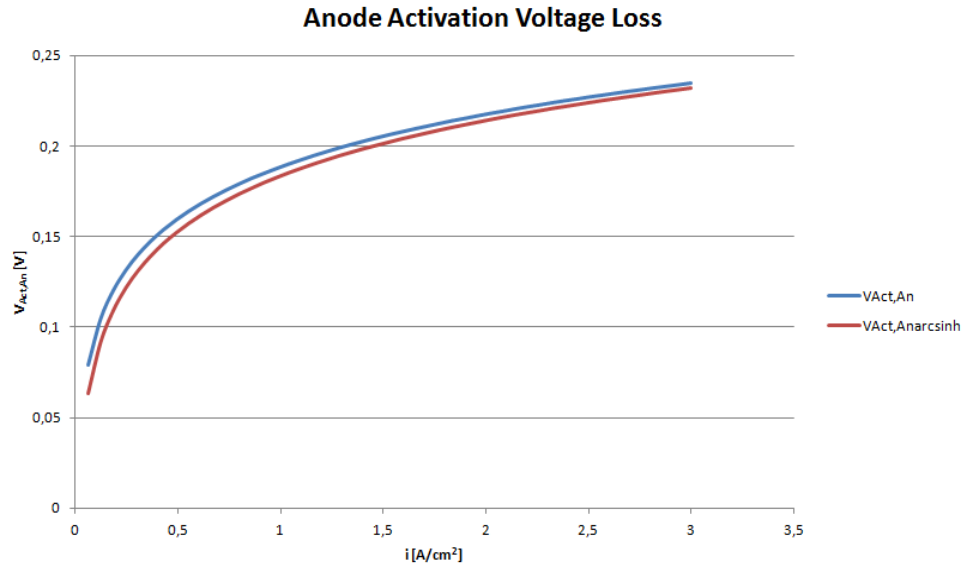
Figure 266. Equation 15 validation.

Once we have defined the anode and cathode voltage drops related to the activation phenomena, the related equivalent resistance of the fuel cell referred is given by the following relationship:

$$R_{act} = \frac{\eta_{act,an} + \eta_{act,cat}}{j}$$

Eq. 53

Ohmic losses

Although the electrodes and the external circuit are made of materials with high electronic conductivities and the electrolyte with a high ionic one, it is not possible to avoid the presence of a voltage loss due to the natural resistance of each component to the movement of the electrons and of ions.

Using again the correlations implemented in the analysis made by J. Van Herle (Van Herle et al. 2003), the equivalent resistance of the fuel cell due to the ohmic losses can be defined:

$$R_{ohm} = R_{an} + R_{cat} + f_{cc} \cdot R_e$$

Eq. 54

where:

- R_{ohm} $[\Omega cm^2]$ is the total resistance due to ohmic losses
- R_{an} $[\Omega cm^2]$ is the equivalent resistance due to ohmic losses in the anode

- R_{cat} $[\Omega cm^2]$ is the equivalent resistance due to ohmic losses in the cathode
- R_e $[\Omega cm^2]$ is the equivalent resistance due to ohmic losses in the electrolyte
- f_{cc} is the current correction factor

The ohmic resistance referred to the electrolyte can be calculated by its resistivity σ_e, defined by J. Van Herle (Van Herle et al. 2003) with the Arrhenius relationship for the 8YSZ (Yttria – Stabilized – Zirconia) and its thickness *Lel*:

$$R_e = \frac{L_e}{\sigma_e}$$

Eq. 55

$$\sigma_e = \sigma_{0,e} \cdot e^{\left(-\frac{E_{a,e}}{RT}\right)}$$

Eq. 56

From the total ohmic resistance, the voltage drop due to this phenomenon can be determined, using the total current density of the fuel cell.

$$\eta_{ohm} = j \cdot R_{ohm}$$

Eq. 57

On Table 81 the reference values used for the definition of the total ohmic resistance are reported.

Table 81. Ohmic losses parameters.

Parameter	Value	Unit	Reference
R_{an}	0.02	Ωcm^2	(Anon 2014)
R_{cat}	0.03	Ωcm^2	(Anon 2014)
f_{cc}	4	-	(Van Herle et al. 2003)
L_e	10	μm	Assumption
$\sigma_{0,e}$	372.2	S/cm	(Van Herle et al. 2003)
$E_{a,e}$	79'535	J/mol	(Van Herle et al. 2003)

Diffusion losses

The diffusion losses are due to the higher concentrations of reactants around the catalysts, which bring to pressure differences between the chemical species in the electrodes and so to a voltage drop. This phenomenon can be observed especially at high operating currents, while it can be avoided at low values. In our analysis, we will not consider the diffusion losses at the cathode (Singhal & Dokiya 2003), because, typically, in an SOFC they are so low in respect to those at the anode that can be neglected.

Again, the definition of the diffusion overvoltage is made used the method implemented by J. Van Herle. These equations derive from a discretization of the multicomponent Fickian model that is a simplification of a complete diffusion models (such as the dusty – gas model or the mean – transport pore model).

First of all, we need to define which chemical species should be considered in the definition of the diffusion losses. The analysis of this phenomenon could be really difficult if we don't use some other simplifications. For this reason, in the anode will be considered a mixture composed just of two chemical species, the equivalent hydrogen (reagent) and the equivalent water (product).

Considering that the fuel sent to the anode is a mixture especially made of hydrogen, carbon monoxide and methane, the concentration of the equivalent hydrogen in the anodic mixture can be evaluated in this way:

$$x_{H2,eq} = x_{H2} + x_{CO} + 4 \cdot x_{CH4}$$ Eq. 58

where the x_i is the concentration of the gaseous species *i-th* in the anodic mixture.

On the other hand, considering that the main products achievable during the oxidation reactions are water and carbon dioxide, we can find easily the concentration of the equivalent water using this relationship:

$$x_{H2O,eq} = x_{H2O} + x_{CO2}$$ Eq. 59

Then, for each species it's necessary to define its diffusion coefficient with the Bosanquet formula:

$$D_{eff,i} = \frac{\varepsilon}{\tau} \cdot \frac{D_{Kn,i} D_{i,m}}{D_{i,m} + D_{Kn,i}}$$ Eq. 60

Where ε is the porosity of the anode, τ the tortuosity, $D_{Kn,i}$ is the Knudsen diffusion term of the gaseous species *i-th* and $D_{i,m}$ is the mixture diffusion coefficient of the gaseous species *i-th* evaluated by the Wilke equation.

The Knudsen diffusion term for each gaseous species can be expressed as:

$$D_{Kn,i} = \frac{\overline{d_p}}{3} \cdot \sqrt{\frac{8RT}{\pi M_i}}$$ Eq. 61

Where $\overline{d_p}$ is the mean pore diameter and M_i the molecular weight of the gaseous species *i-th*. The mixture diffusion coefficients are evaluated by the Wilke equation, using the mole fraction of gases in the boundary layer:

$$D_{i,m} = \frac{1 - x_i}{\sum_{\substack{j=1 \\ j \neq i}}^{n} \frac{x_i}{D_{i-j}}} \qquad \text{Eq. 62}$$

Where x_i are the mole fraction in the boundary layer of the gaseous species *i-th* and D_{i-j} are the binary diffusion coefficients which are computed with Fuller equation.

The general form the Fuller equation is:

$$D_{i-j} = \frac{1.43 \cdot 10^{-7} T^{1.75}}{p \sqrt{\frac{2}{M_i^{-1} + M_j^{-1}} \left(V_{d,i}^{1/3} + V_{d,j}^{1/3}\right)^2}} \qquad \text{Eq. 63}$$

where:

- $V_{d,i}$ and $V_{d,j}$ are the diffusion volumes for the chemical species *i-th* and *j-th*
- p is the partial pressure of the considered species at the electrolyte layer

The effective diffusion coefficient is then applied to determine the partial pressure of considered species at the electrolyte layer which finally results in the voltage drop due to diffusion polarization on the anode side as shown in the following equations:

$$p_{H2,Ely} = x_{H2eq} * p_{An} - \frac{R * T_{An} * j * \delta_{An}}{2 * F * D_{eff,H2}} \qquad \text{Eq. 64}$$

$$p_{H2O,Ely} = x_{H2Oeq} * p_{An} + \frac{R * T_{An} * j * \delta_{An}}{2 * F * D_{eff,H2O}} \qquad \text{Eq. 65}$$

$$\eta_{diff,An} = \frac{R * T}{2 * F} * \ln \left(\frac{x_{H2eq} * p_{An} * p_{H2O,Ely}}{p_{H2,Ely} * x_{H2Oeq} * p_{An}}\right) \qquad \text{Eq. 66}$$

Where p_{An} is the pressure at the anode side, T_{An} is the anode temperature and δ_{An} is the anode thickness. The total voltage drop due to polarization losses in the fuel cell is $V_{Diff,An}$.

The input parameters for the diffusion model are shown in Table 82.

Polarization and power density curves as a function of current density under steam reforming are shown in Figure 267. Furthermore, Figure 268 shows a general distribution of the three losses within the polarization curve.

Table 82. Input parameters for the diffusion model.

Parameter	Value	Unit	Reference
ε	0.5	-	(Anon 2014)
τ	5	-	(Anon 2014)
d_p	1µm	µm	(Anon 2014)
δ_{An}	200 µm	µm	(Anon 2014)
M_{H2}	2.016	g/mol	-
M_{H2O}	18.015	g/mol	-
$V_{D,H2}$	7.07	-	(Fogler & Gurmen n.d.)
$V_{D,H2O}$	12.7	-	(Fogler & Gurmen n.d.)

The equivalent electric resistance can be determined as:

$$R_{diff} = \frac{\eta_{diff}}{j} = \frac{\eta_{diff,An}}{j} \qquad \text{Eq. 67}$$
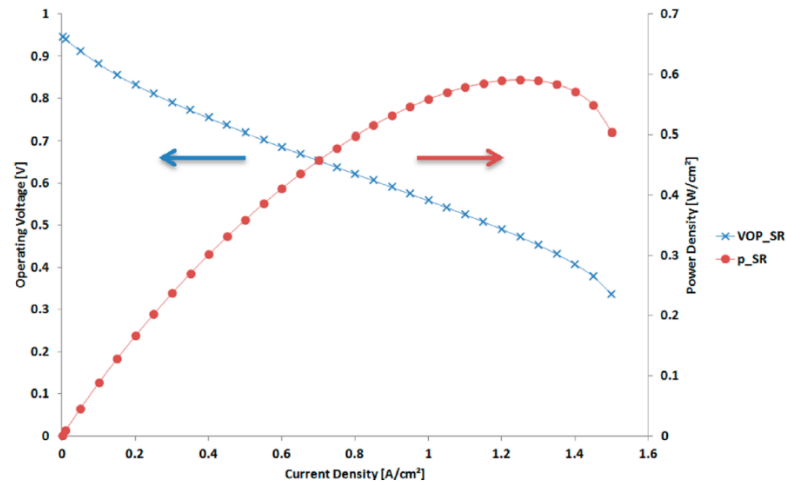
Figure 267. Polarization (×) and power density (●) curve for steam reforming in anode-supported cell operating at 800 °C.
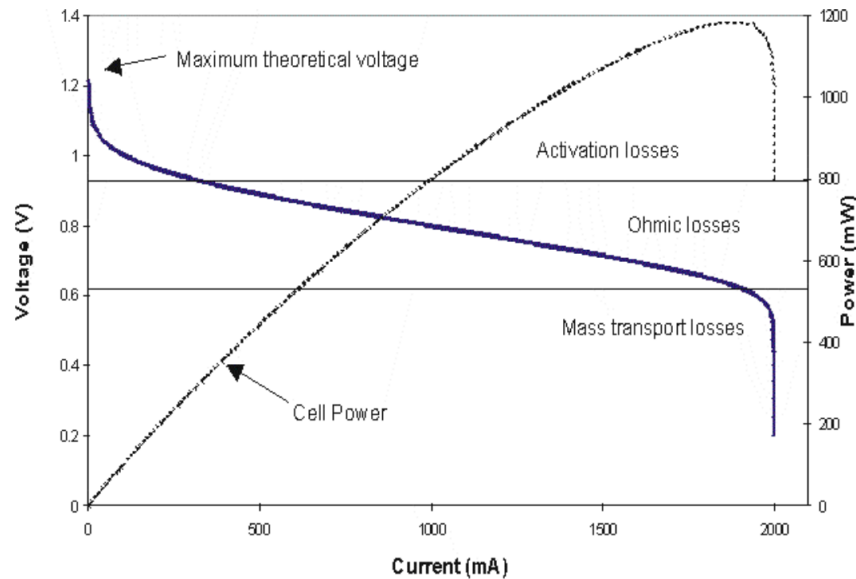
Figure 268. Typical polarization curve of a fuel cell.

Operating strategy

The control strategy for the operation of an SOFC integrated into a power plant strictly affects the evolution of the degradation rate and, consequently, the stack lifetime. Two main regulations can be adopted:

- Constant current operation
- Constant voltage operation

For the analyzed models, constant voltage operating strategy has been chosen, because it maintains high plant efficiency even during cell degradation; in previous work by Thjssen (DOE NETL & Thjissen 2007), a comparison between constant voltage and constant current strategies is presented. It is made clear that a constant voltage operating strategy reduces stresses to the stack caused by degradation due to the decreasing current in order to ensure the chosen operating voltage. As operating current is decreased during cell degradation, efficiency is kept constant. In order to provide constant power output while the cell current decreases, the installation of an excess spare capacity is required. Nevertheless, this results in up to 5 times longer operating lifetime of the stack when a constant voltage is carried out in the system compared to constant current operating strategy. An example will be presented to discuss more in detail the control strategy choice.

Let's suppose that an SOFC produces, in four years, electrical power and that, in this period, the ASR increases. Imposing an Open Circuit Voltage equal to 0,997 V (a typical value for SOFC at 800 °C (Chiodelli & Malavasi 2013)), it is possible to define the

polarization curves associated with different values of ASR. On Figure 269 these trends are shown for four increasing values of ASR. If in the period considered, the ASR changes from ASR1 to ASR4, the working point will translate vertically if the control is made to maintain a constant current density or horizontally to maintain a constant voltage.

In a first moment, the regulation that guarantees a constant voltage could appear as the worst one, because it is characterized by the highest deviation from the original working condition. However, it was observed, during experimental tests (DOE NETL & Thjissen 2007), that, under constant current mode, the net power produced and the system performance degrade very rapidly. Moreover, the only strategy which can be adopted to keep the same productivity is the overdesign of the BoP so that it can accommodate increased airflow.
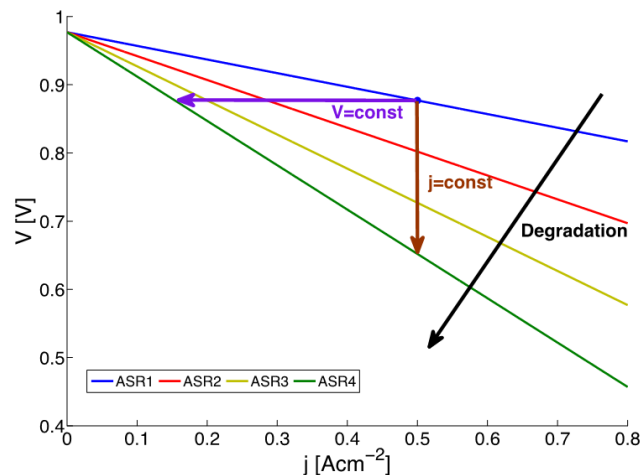
Figure 269. Evolution of the operating point for the different regulation strategies.

The stack replacement can be done just when the system output is lower than an imposed threshold, about 90% of the initial capacity, while the installation of an excess of stack capacity is not included because has no benefit. On the other hand, if the operation is at a constant voltage, the productivity and the performances can be not affected during the degradation if the system is designed with spare stack capacity that increases, periodically, the total active surface. The initial stack is then overdesigned but, this configuration allows to use each cell till the 30 – 50 % of the initial capacity. At a degradation rate of 1%, in a constant current mode, the lifetime of the stack is lower than 4000 hours, while in a constant voltage one it is higher than 20'000 hours (DOE NETL & Thjissen 2007).

The sizing of the fuel cell stack and the active area requirement calculation are thus presented under a constant operating voltage working conditions.

Correlation between operating voltage V_{op}, area-specific resistance ASR, and current density j is presented in the following equation:

$$V_{op} = V_r - ASR \cdot j$$

<div align="right">Eq. 68</div>

In which can be defined:

- V_{op} is the stack operating voltage [V]
- V_r is the ideal Gibbs reversible voltage of cell [V]
- ASR is the area-specific resistance of the cell [Ωcm^2]
- j is the current density in the cell [A/cm^2].

For calculating ASR and j, Gibbs (thermodynamic) voltage rather than Nernst voltage is used as reversible voltage V_r. The reason for this is that Nernst voltage is dependent on the molar fractions of educts and products in the fluid streams entering and exiting the cell. Consequently, Nernst voltage is highest when there is no electrochemical reaction occurring in the cell. However, this only takes place when no current is drawn from the cell and thus when no load is connected to it (Van Herle et al. 2003). From a power plant operation point of view, such a scenario is of limited practical use. Gibbs voltage on the other hand provides the maximum (reversible) work that can be extracted from a control volume after a certain amount of fuel and oxidant stream have reacted and eventually mixed.

Gibbs reversible voltage can be expressed as:

$$V_r = -\frac{\Delta G_{stack}/N_{cells}}{n \cdot F \cdot \dot{n}_{fuel}/N_{cells}} = \frac{\Delta G_{stack}}{n \cdot F \cdot \dot{n}_{fuel}}$$

<div align="right">Eq. 69</div>

Aside from operating voltage, the installed power capacity of the fuel cell is fixed. As a result, the current density is varying according to operating conditions and applied reforming option.

The main problem related to the constant voltage operation is that on Eq. 68 ASR in function of j. For this reason, the definition of the current density cannot be performed in a direct way, but an iterative procedure is required. The easiest way to implement this calculation is with the following procedure:

$$find\ j\ \in [j_{min}\ ;\ j_{max}]\ so\ that\ \Delta_{ASR} < toll$$

<div align="right">Eq. 70</div>

$$\Delta_{ASR} = |ASR_1 - ASR_2|$$

$$ASR_1 = \frac{V_r - V_{op}}{j}$$

$$ASR_2 = \sum R_{losses}(j)$$

where *toll* is an absolute tolerance that has to be chosen properly. With this iterative procedure, it is finally possible to estimate the correct j.

Once the current density and the ASR have been determined via the electrochemical correlations introduced above, the active area of the stack can be calculated from the knowledge of the total faradic current.

$$A_{act} = \frac{I_{Farad,tot}}{j} = \frac{W_{DC}/V_{op}}{j} \qquad\qquad \text{Eq. 71}$$

Where:

- A_{act} is the total active area of stack [cm^2]
- $I_{Farad,tot}$ is the total faradic current of stack [A]
- W_{DC} is the SOFC DC power output [W]

Equation 33 indicates that another fixed parameter in this SOFC model is the power output W_{DC} generated by the stack. Together with a fixed operating voltage, W_{DC} is the main input parameter to solve the electrochemical model of the SOFC and calculate ASR and j.

Degradation phenomena

Any kind of fuel cell suffers from degradation phenomena which usually bring to an increasing ASR and thus a reducing power output of the cell. In order to understand the phenomena and to identify the main phenomena responsible for the degradation of the SOFC, we need to focus our attention on each part of a cell (WUILLEMIN 2009).

In the **anode**, the main deterioration mechanisms that can be identified are:

- Coarsening: the microstructure of the anode evolves with time due to the operation at high temperatures, and the Nickel particles are subject to coarsening phenomena. This results in a loss of percolation and in a decrease in the conductivity of the electrons, and so the active sites available for the electrochemical reactions are lower.

- Pollutants: anode materials are sensitive to pollutants species, especially those containing sulfur. The poisoning effect of the H_2S is one of the worst because, being adsorbed by the Nickel particles, it affects the electrochemical reactions strongly and alters the kinetics of steam reforming reactions. Other pollutants that can be sent with the fuel are chlorine, siloxanes, and boron (this last one seems to promote particle coarsening). Other pollutants can also be generated inside the fuel cells or can be even released by sealing materials.

- Redox – cycling: this is the most damaging situation that can occur in the anode and corresponds to the partial or complete oxidation of the Nickel used as a catalyst. In fact, when these reactions occur, the Nickel increases its density strongly and, in the layer, grow the mechanical stresses. Repeated redox cycles can happen especially in anode – supported cells and it's needed just the failure of a single cell to have the failure of the complete stack.

In the **cathode**, the main degradation mechanisms are:

- Chemical reactions: not all the cathode materials are intrinsically stable, but some of them tend to react with other materials spontaneously. During these reactions, can occur changes of phases that worsen the electrochemical properties, such as the ionic and electronic conductivities. Besides the interactions between the materials, the cathode can experience morphological changes due to the sintering of its materials, which is related to a degradation of performances. This kind of degradation could be easily limited with an appropriate choice of the materials of the cathode.

- Current – induced activation and degradation: the passage of currents affects the performance of the cathode materials strongly. Although this mechanism is not, nowadays, completely clarified, it was observed that, in the first period of polarization, is generated a current, induced by the activation phenomena, that influences the degradation of the layer. This kind of degradation produces an alteration of the interface between the particles of LSM and YSZ, reducing the contact area between the electrode and the electrolyte. It was reported that this effect is more pronounced at lower temperatures (<750°C) and that tends to be limited increasing the partial pressure of the oxygen or its purity. In order to limit this problem, it is necessary to choose appropriate operating conditions.

- Pollutants: as was observed in the anode, this problem is related to the purity level of the inlet flow (in this case the air) and to the pollutants contained in the materials of the stack. The pollutants that affect this electrode's performances are the chromium – containing volatile species such as CrO_3 (abundant in dry air) and $CrO_2(OH)_2$ (predominant even at low levels of humidity). Due to the fact that the metallic interconnects have been considered as the principal sources of chromium, were developed and applied protective layers to avoid its evaporation from them.

Other pollutants were identified, such as magnesium (segregated in zirconia), silica, alkaline species and sulfur. However, at this moment, the main identified sources of pollutants that can significantly affect the performances of the cathode are the metallic parts and the sealing materials.

The **seal materials** produce degradation too and the main mechanisms identified are the following:

- Chemical interactions: seal materials are known to react with the metallic interconnect they are in contact with. The reactions that occur could cause an anomalous oxidation of the alloy that is accompanied by a release of volatile chromium – containing species, which, as we have already seen, produce an intense poisoning effect at the cathode. These components containing chromium are the more dangerous but there are many other volatile species that can be released from the materials of seals, and that can cause degradation.
- Loss of gas tightness: the loss of gas tightness with the time is an important issue for seal materials, and it strongly depends on the raw material and on its form. Different geometries and different materials can be used to reduce this negative effect, for example, silver rings are considered a good choice of sealing materials.
- Insulating properties: seals have to be electrically insulated in order to avoid losses of power to the outside. Unfortunately, it was reported that the insulating properties of glass – ceramic seals tend to degrade during the cell's life, due to the migration of conducting species in the material. In addition, if glass – ceramic sealants are supposed to provide mechanical support, local overheating over the glass transition can lead to catastrophic loss of support and short – circuiting.

Finally, the last components where degradation phenomena can occur are the **metallic interconnectors**, and the main mechanisms are:

- Oxidation: on the interconnector can occur oxidation reactions that increase the ohmic resistance and release pollutant species.
- Creep: at high temperatures or at high temperature gradients, the thermal stresses at the interconnectors tend to increase with the time, due to the creep phenomenon. The resulting deformation affects the diffusion of gases inside the cells, and so it influences the electrochemical reactions negatively and reduces the total active area. Although the knowledge of all these mechanisms are useful to understand not only for which reasons the degradation can occur but also how could we intervene to reduce, during the sizing, this problem, we are more interested in identifying of a reference parameter that can be used to implement the negative effects on the electrochemical model.

From a *thermodynamic point of view*, the degradation can be seen as a reduction of the efficiency of the SOFC and so, consequently, of the global efficiency of the entire power plant. A reduction of the performances corresponds to a higher consumption of fuel, for the production of the same amount of power, so this is the main negative effect that can be observed in a deteriorated stack.

From an *electrochemical point of view*, the worst utilization of the fuel corresponds to an increase of the internal resistance of the cells, which, as already seen during the description of the electrochemical model, is defined by the Area Specific Resistance (ASR). For this reason, in our analysis, the effects of the degradation will be associated with the variation, during the lifetime of the plant, of the ASR.

In order to maintain a constant electrical power production during lifetime, which is one of the main objectives of a power generation plant, it is necessary to overdesign the stack of fuel cells, so that the negative effects on the performances due to the degradation are compensated by the utilization of new active surface.

This excess of area represents the <u>spare capacity</u> and can be integrated into the stack or when the plant is made, or periodically during substitutions. From an economical point of view, it is better to depreciate the investment as much as possible, so the situation where extra spare capacity is installed each year has been chosen.

This technique does not eliminate the possibility to use the original stack for the entire lifetime. In fact, with respect to the degradation rate and to the maximum degradation allowed, during the years one or more stacks of fuel cells can be replaced.

First of all, we need to define a relationship that expresses the increase, during the time, of the ASR:

$$ASR(t) = ASR_0 \cdot \left(1 + \frac{d_{ASR}}{100} \cdot t \right) \qquad\qquad \text{Eq. 72}$$

where:

- $ASR(t)$ is the Area Specific Resistance at the time *t*
- ASR_0 is the initial Area Specific Resistance (*t*=0)
- *t* is the time
- d_{ASR} [%] is the percentage of degradation of the ASR expressed per unit of time

The degradation is usually referred to a temporal time such as 100 or 1000 hours, so that means that each 100, 1000 hours the ASR increases of a certain percentage. In this

relationship, it is important to take care of *t* because it is the time expressed in the same reference unit of the d_{ASR}.

Due to the fact that the control mode imposed is at a constant voltage, from the evolution of the ASR, it is possible to define that one of the current density:

$$j(t) = \frac{V_r - V_{op}}{ASR(t)} = \frac{V_r - V_{op}}{ASR_0 \cdot \left(1 + \frac{d_{ASR}}{100} \cdot t\right)} \qquad \text{Eq. 73}$$

The ASR evolution is a linear expression, while the one of *j* is a hyperbolic one.

In Figure 270, it is shown an example of the evolutions of ASR and *j* referred to the atmospheric power plant, working in the following design and operating conditions:

- FU = 0.75
- T$_{SOFC}$ = 800°C
- d_{ASR} = 0.2 % (every 1000 h)
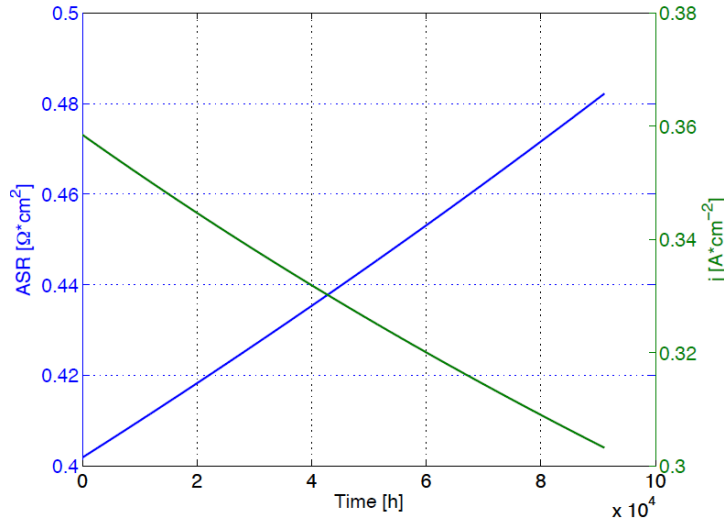
Figure 270. Evolution of the ASR and of j with time, due to degradation of the cell.

The value chosen of the degradation percentage respects the target value for the SOFC technology that has been imposed on the new plants under construction (future scenario) (Anon 2014). For this reason, we will adopt this reference in all the simulations.

The spare capacity that has to be integrated each year can be calculated considering the excess of active area needed to cover the current losses. Obviously, the electrochemical properties of the new cells are in a non-degraded condition, so for the current density and the ASR are used the initial values (j_0 and *ASR$_0$*).

To calculate the surface needed each year $A_{add}(t)$, it is sufficient to define the current drops to be covered $\Delta I_{op}(t)$:

$$\Delta I_{op}(t) = I_{op} - \overrightarrow{J(t)} \cdot \overrightarrow{A_{tot}(t)} \qquad \text{Eq. 74}$$

$$A_{add}(t) = \frac{\Delta I_{op}(t)}{j_0} \qquad \text{Eq. 75}$$

On Eq. 74 vectors for current densities and of total surfaces are used because in the definition of the current drop we need to consider the evolutions of each active surface installed from the moment of its installation. For example, if the lifetime is 20 years and the strategy was chosen requires to install capacity once a year, when the plant is dismissed the stack has inside itself 20 different groups of cells, each one with different surfaces and different values of operating current densities (the lowest j are referred to the oldest cells).

Although this assessment enables the use, as much as possible, of cells in non-optimal conditions, it is necessary to impose a limit degradation under that the stack has to be replaced.

The reason why this operation cannot be avoided is that, at a certain point, the cell is so degraded that the utilization could bring at its break. Each year is defined the relative difference, from the original state, of the ASR of every cell:

$$\overrightarrow{\Delta_{ASR}(t)} = \left| \frac{\overrightarrow{ASR(t)} - ASR_0}{ASR_0} \right| \qquad \text{Eq. 76}$$

If one or more differences are lower than a limit value, then the new spare capacity has to be defined in order to include the replacement of those cells unusable.

$$\overrightarrow{\Delta_{ASR}(t)} < \Delta_{ASR\,max} \qquad \text{Eq. 77}$$

In the simulations, the limit chosen is 20% (Anon 2014), because, although in a constant voltage regulation mode each cell could work until 30-50% of its initial capacity, a conservative choice has been preferred.

In Figure 271, it is represented the evolution of the active area that has to be installed each year and of the total surface installed in the entire stack of fuel cells. The simulation was made using the same operating conditions defined before to implement the variation of the j and ASR.
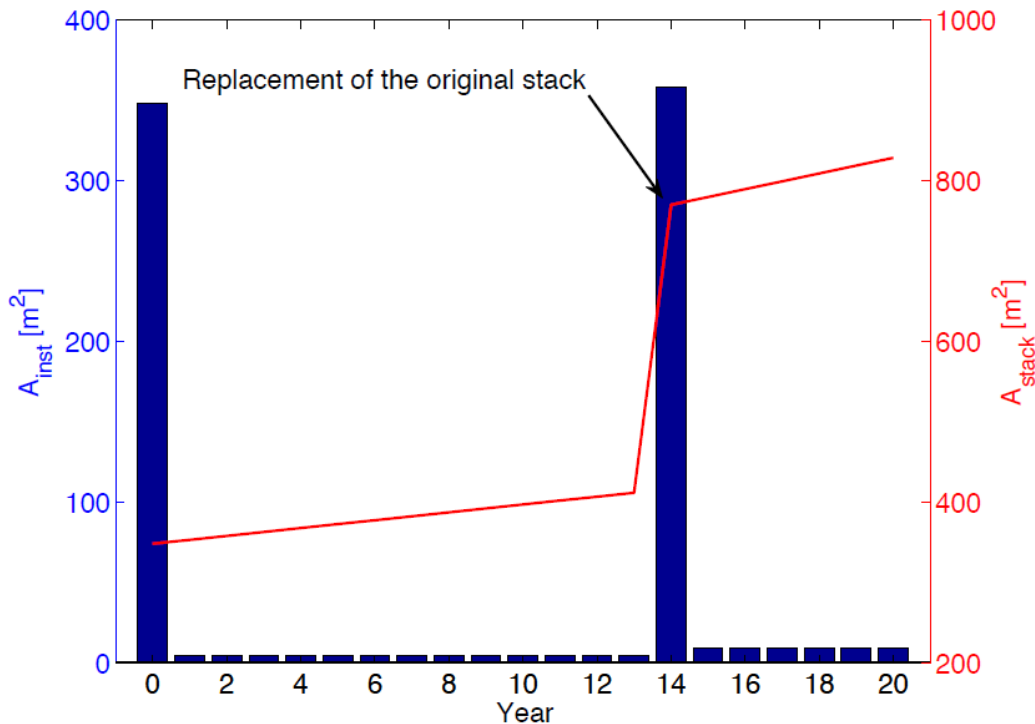
Figure 271. Evolution of the spare capacity with time.

The year 0 corresponds to the time when the power plant starts to produce, and its active surface is the one sized during the initial design.

In the first year of productivity, the degradation decreases the performances of the fuel cells, then, to compensate this negative effect, additional capacity is installed.

From the second year on, also the new active areas degrade, and so the new spare capacity required will have to take care of what happen both in the original stack and in the new cells. However, the negative effects of degradation are more intense where larger surfaces are involved, so, for this reason, it seems that each year is installed the same spare capacity (although from one to another a little increase occurs).

At the fourteenth year, the active surface required is much higher than those of the previous years, in fact, this time corresponds to the moment when the degradation of the original stack is so high that a replacement is required. This particular trend shows us the lifetime of the SOFC involved, and we can say that 14 years is a reasonable value, not far from the future scenario for SOFC.

The cumulative function (red line on Figure 271) was added to give an idea of the total space required in twenty years of operation. Although the spare capacities are integrated every year, during the initial design phase, it is necessary to understand how much space will be occupied, so that the external coating can be properly designed. For this purpose,

an engineer could choose to reuse the space dedicated to the initial group of cells that has to be replaced: this choice could reduce a lot the volume required but technically it is preferred to provide new spaces, since in this way the design is less complicated.

The degradation phenomenon obviously affects the convenience of an integrated SOFC power plant strongly. Especially, the variations of the degradation rate influence the economic analysis results. Although we have not already defined the economic analysis method that will be implemented in this work, we anticipate that the decisional parameter that will be used to evaluate the economic feasibility of the plant is the Net Present Value (NPV) at the end of life: the highest this value is, the more convenient the plant is. In Figure 272 it is shown the variation of the NPV with respect to the degradation rate of the ASR.

The trend presents two discontinuity points where the NPV strongly decreases: in these conditions the degradation is so high that it is necessary to perform a replacement in respect of what is required in the previous state. This is interesting because, if we are, for example, in the case d_{ASR}=0.2 %, a deviation around this value does not change heavily the NPV but, if we have d_{ASR}=0.25%, a deviation could force the engineer to make two replacement instead of one during lifetime, and so the NPV would decrease a lot.

Thus, if the operating point is near to a discontinuity, the effects of a small variation can be really sensitive from the economic point of view.
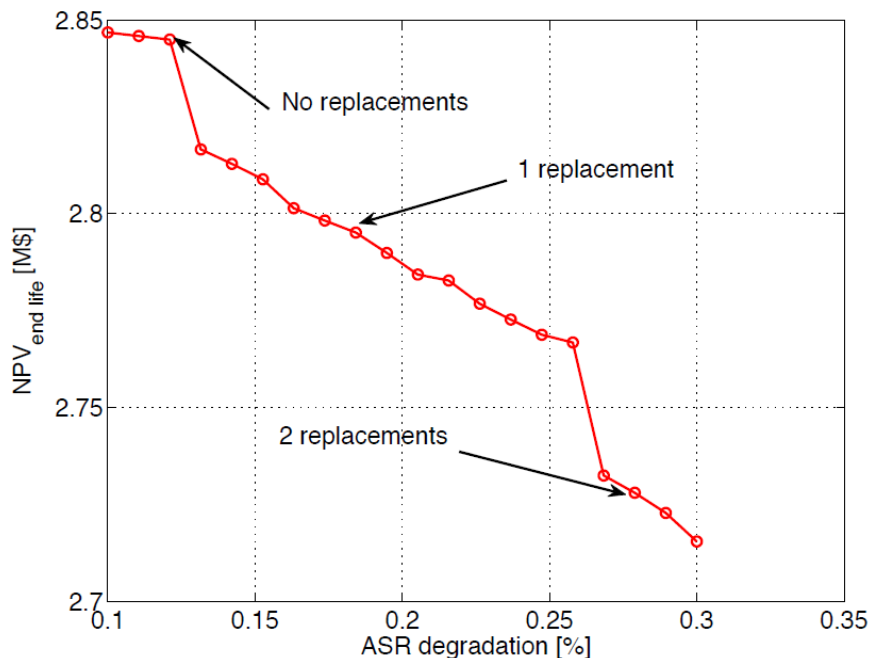
Figure 272. Variation of the NPV with the degradation rate.

SOFC modelling

The SOFC have also been modelled with the Aspen Plus software. As can be seen from Figure 273, the software does no present e specific component representing the fuel cell. Since oxygen ions are moving from cathode to anode, the cells have been modeled using two separated blocks:

- a separator for the cathode which exports from the inlet air the stoichiometric oxygen for the electrochemical reaction
- a Gibbs reactor for the anode in which the oxygen and the hydrogen-rich reformate stream are sent: here the electrochemical reaction takes place, and chemical and physical equilibrium are reached. The Gibbs reactor heat duty will be the *ΔH* of the electrochemical reaction.

Furthermore, since the fuel is entering the stack at 750 °C and the air at 650 °C, while the SOFC is working at 800 °C, the sensible heat related to the temperature increase of the two streams is simulated using two dummy heaters.
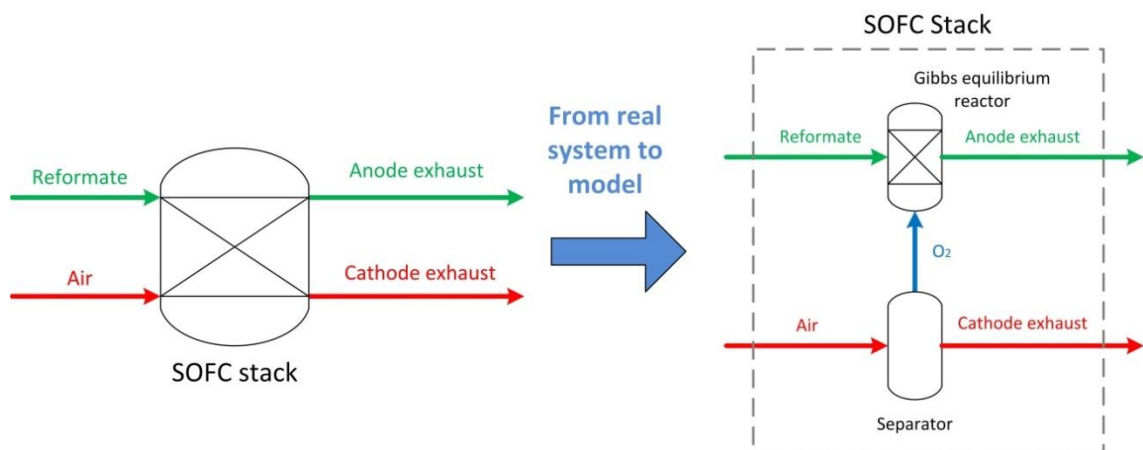
Figure 273. SOFC stack model in Aspen Plus®.

Fuel Utilization Factor

In a generic fuel cell, the production of power involves just a fraction of the inlet fuel that depends on many operating factors. Imposing a constant fuel mass flow, with the variation of other design conditions (such as the power produced) we could verify that the quantity of fuel is reacting and that one which goes out from the stack with the flue gases are not constant.

The parameter that expresses the fraction of fuel converted in the Redox reactions is the Fuel Utilization Factor (FU) (Nehrir & Wang 2009). With pure hydrogen is used as fuel, the FU is defined as:

$$FU = \frac{\dot{n}_{H2,consumed}}{\dot{n}_{H2,inlet}}$$
<div align="right">Eq. 78</div>

where the ratio is expressed in terms of molar flows.

Considering that, for the Faraday law, there is a relationship between the hydrogen molar flow consumed and the total current generated in the cell, we can express the fuel utilization in this form:

$$FU = \frac{I}{2 \cdot F \cdot \dot{n}_{H2,inlet}}$$
<div align="right">Eq. 79</div>

From Eq. 79 it is possible to calculate the molar flow required to obtain a certain value of current. If the inlet flow is a mixture where the hydrogen is bonded in hydrocarbons, the flows of these species can be easily found using the corresponding charge number. For the methane this is the correct relationship:

$$\dot{n}_{CH4,inlet} = \frac{I}{8 \cdot F \cdot FU}$$
<div align="right">Eq. 80</div>

Typically, a fuel cell is designed to operate at a constant fuel utilization and so it is important to define its influences on the plant performances.

The Nernst equation, expressed in the form where are explicited the concentrations of the species involved in the Redox reactions (see (Tjaden et al. 2014)), gives us some information about the behavior of a cell in respect of the variation of the FU.

In fact, the term that corresponds to the voltage drop depends strictly on the reactants involved. If we increase the fuel utilization factor, the anodic mixture will have a higher concentration of products than one of reactants. This behavior corresponds to a growing trend of the ASR in respect to the FU.

If the ASR increases, in order to maintain a constant value of voltage it is necessary to decrease the operating current density. On the other hand, if we want an operation where the current density has to be fixed at a constant value, the corresponding effect is a decrease in the operating voltage.

The implications of choice between the regulation logics based on the maintaining of a constant voltage and of a constant current have been already discussed before. Although the negative behavior of the ASR in respect to the increasing of the FU, the global electrical efficiency tends to increase too because a higher value of fuel utilization corresponds to a better use of the internal chemical energy of the fuel. So its trend will be growing.

Excess of air at the cathode

The definition of the inlet air at the cathode has to consider, simultaneously, two different requirements for the correct operation of the SOFC.

First of all, the air flux has to contain a minimum amount of oxygen, so that a sufficient number of O_2 ions, required for the oxidation of the hydrogen, is released during the reduction reactions. This stoichiometric flow can be easily calculated with the Faraday law modified considering that, in the external air, the oxygen volume concentration is 21%.

$$\dot{n}_{air,st} = \frac{I}{4 \cdot F} \cdot \left(\frac{1}{0.21}\right)$$

Eq. 81

This value has to be considered as a lower limit, but a cell requires a quantity of air much higher than this one.

In fact, the second condition to take care of is the requirement of a continuous cooling of the cell, in order to take out the heat generated during the exothermic Redox reactions and guarantee a constant stack temperature. Without a cooling air flux, the temperature inside the cell would increase at very high values and bring to the break of the stack.

For the definition of the real airflow, it is necessary to understand the dynamic of the heat generation inside the cell (Gandiglio et al. 2013). In an SOFC, during the electrochemical reaction, the production of electrical and thermal power is due to an enthalpy variation of the stack:

$$\Delta H_{stack} = W_{el} + \dot{Q}_w + \dot{Q}_{loss}$$

Eq. 82

The total thermal power produced ($\dot{Q}_w + \dot{Q}_{loss}$) considers the heat generated in the two electrodes for the Redox reactions and to that absorbed in the reforming processes:

$$\dot{Q}_w + \dot{Q}_{loss} = \dot{Q}_{an} + \dot{Q}_{cat} + \dot{Q}_{ref}$$

Eq. 83

$\dot{Q}_{loss}$ is the thermal power that the fuel cell exchanges with the environment for the transmission of the heat through the stack. Due to the fact that we want to recover as much heat as possible, this quantity is considered as a losses. On the other hand, $\dot{Q}_w$ represents the heat recovered that increase the temperature of the cooling air.

Usually, the losses are expressed as a ratio of the power of the fuel:

$$\dot{Q}_{loss} = \frac{r_{loss}}{100} \cdot \dot{Q}_{fuel,in} = \frac{r_{loss}}{100} \cdot LHV_{fuel} \cdot \dot{V}_{fuel,in}$$

Eq. 84

In this work, the ratio used is 1% because it represents a target value (Anon 2014). The real air flux can be determined, from this last thermal power, with the imposition of its thermodynamic state (temperature) outside the cathode:

$$\dot{n}_{air} = \frac{\dot{Q}_w}{\dot{c}_{p,air} \cdot \Delta T_{air,cat}} = \frac{\dot{Q}_w}{\Delta H_{air,cat}}$$

Eq. 85

where $\dot{c}_{p,air}$ and $\Delta H_{air,cat}$ are the heat capacity and the enthalpy variation of the air, both of them expressed per unit of mole.

Once the real air flow and the stoichiometric one have been defined, the cathode air excess can be found:

$$\lambda_{air} = \frac{\dot{n}_{air}}{\dot{n}_{air,st}} > 1$$

Eq. 86

The air excess is not a decisional variable, such as the fuel utilization, because its value is imposed by the design of the SOFC stack, but can be considered as a performance parameter.

Recirculation of the exhausts

Some SOFC can be designed to allow the partial recirculation of the flue gases produced in the anode and in the cathode. This operation has the effect of dilute the reactants sent to the two electrodes. From an electrochemical point of view, the dilution always brings to a decrease of the Nernst voltage so a configuration of this kind could be considered not convenient in respect to the traditional one. However, there are different reasons to include, in some SOFC stacks, the exhaust recirculation.

The anode recirculation can be made to supply the quantity of steam required for the reforming processes, both internal and external, as explained before, thus avoiding the use of external water and demineralized; furthermore, both anode and cathode recirculation help in preheating the inlet streams.

With the definition of the Steam to Carbon ratio (see Reformer description), it is possible to define the molar flow of the water to send and, accordingly, the fraction *y* of anodic exhausts to be re-circulated (see Figure 274):

$$\dot{n}_{H_2O} = SC \cdot \dot{n}_{CH_4}$$

Eq. 87

$$\dot{n}_{an,recirc} = \frac{\dot{n}_{H_2O}}{x_{H_2O}}$$

Eq. 88

$$y = \frac{\dot{n}_{an,recirc}}{\dot{n}_{an,out}}$$

Eq. 89

where x_{H_2O} is the concentration of water in the anodic exhausts.
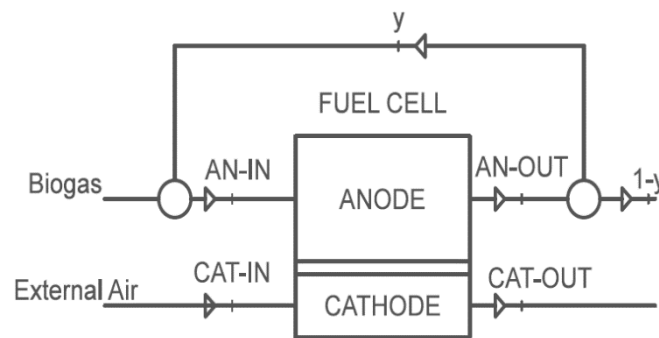
Figure 274. Anode recirculation.

The anodic re-circulation dilutes the inlet biogas so that the molar flow of hydrogen which enters in the anode changes. For this reason, we can define a global Fuel Utilization factor that considers the new molar flows involved:

$$FU_{glob} = \frac{FU \cdot (1 - y)}{1 - y \cdot FU}$$

Eq. 90

A3.4 Case NO CCS: afterburner and heat recovery

In case no carbon capture is performed within the system, the anode and cathode exhaust are simply burned together in an after-burner .The combustor has been simply modeled as an adiabatic Gibbs equilibrium reactor where the generated energy is all transferred to the outlet stream as thermal energy.

Depending on the analyzed operating conditions the air flow from the cathode can be lower or higher than the stoichiometric value required for the complete combustion of the anode exhaust, which depends on the chosen FU.

In order to solve this problem an extra air flow rate has been inserted to feed the after-burner (solution already adopted in other systems (Papadias et al. 2012)). This flow is varied by a specific function of AspenPlus® in order to have complete combustion and thus is higher than zero only in off-design conditions.

Furthermore, in the after-burner the chemical energy still contained in the anode exhaust is converted into thermal energy, thus producing a temperature increase in the outlet stream. Depending on the chosen operating condition the temperature inside the combustor and at its outlet can reach values too high for commercial alloys (temperature around 1500 °C).

This second problem can be practically solved in two ways:

- Using ceramic pipes and heat exchanges: this solution has not been adopted since it would require the adoption of non-commercial and very expensive materials.
- Including a water quenching inside the burner in order to control the outlet temperature. A demineralized water flow rate has thus been inserted to feed the burner, and its flow rate is controlled in order to keep the temperature inside the combustor at a certain fixed value, usually 900 °C (maximum allowable temperature for Ni alloy). With this option, the negative effect is that, by reducing the temperature increase, the recovered heat duty is also reduced.

The hot stream from the after-burner is then sent to inlet streams pre-heating and then to the cogeneration heat exchangers. Figure 275 shows a general scheme of this downstream section of the plant. The first stream to be heated up is the fresh biogas, which should enter the reformer at 750 °C but, since also anode recirculation is performed, the outlet temperature from the gas-gas heat exchangers will be lower (600 - 700 °C). Then the exhaust streams go to pre-heat the fresh air up to 650 °C since no cathode recirculation in considered in this analysis. This is the highest thermal contribution because of the high air mass flow. Finally, the remaining heat duty is transferred to a water stream for cogeneration purposes: water is usually heated from 70 to 90 °C. The exhaust gases are cooled down until 110 °C and then sent to the chimney; the temperature has been set in order to avoid condensation.
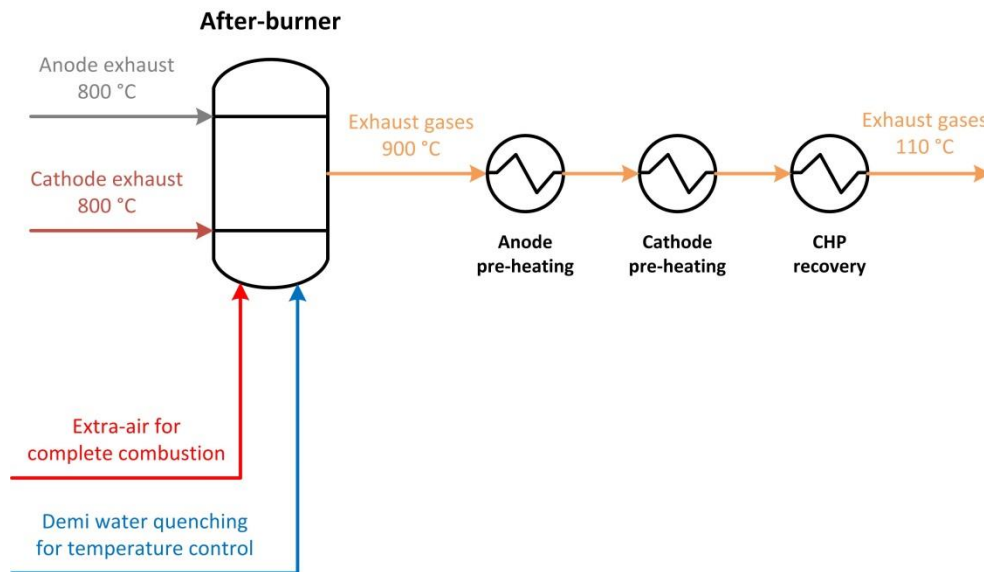
Figure 275. Afterburner and heat recovery layout.

Generally, in a waste water treatment plant, a high thermal power is required to pre-heat the sludges going to the anaerobic digester, since mesophilic process at around 30-40 °C is the best choice between low temperatures (and efficiency) and too high temperatures. If no heat is required by the digester because of the summer season or because the system is not installed in a WWTP, the heat generated can be used for heating the offices and the workshops, for the domestic how water and finally used to run adsorption chillers. This contribution will be fundamental for the determination of the thermal efficiency of the plant.

On Table 83 the main design parameters for this section of the plant are summarized.

Table 83. Afterburner and heat recovery design parameters.

Parameter	Value	Unit
After-burner temperature	900	°C
Exhaust to chimney temperature	110	°C
Water for CHP temperatures	65/75	°C

A3.5 Case CCS: oxy-combustor and CO_2 separation

If the carbon dioxide needs to be extracted, anode and cathode shall be treated separately.

Since nitrogen should be avoided, cathode exhaust is simply used for pre-heating the fresh air inlet and then for cogeneration in a water-gas heat-exchanger until 110 °C before being sent to the chimney.

The anode exhaust in, on the other hand, are burnt with pure oxygen (always for avoiding nitrogen) in order to yield a pure H_2O-CO_2 mixture. Complete combustion is always guaranteed since oxygen flow is modified in order to reach this objective. Oxygen is produced locally, in this work a Pressure Swing Adsorption (PSA) has been considered since it can be considered a commercial solution for producing medium quality oxygen (Kuramochi et al. 2011). Purity reached with PSA is around 95% O_2 since the process is not able to remove the Argon from the air (Anon n.d.; Goldstein et al. 2003). Another option for oxygen production is the Cryogenic Separation which can reach purities up to 99% (Smith & Klosek 2001) but, because of its complexity and high cost, it is usually adopted only in the in the chemical industry, where oxygen with very high level of purity is required. The energy cost of the oxygen production has been taken from (Wilkinson et al. 2003; Smith & Klosek 2001) and values are shown in Table 84.
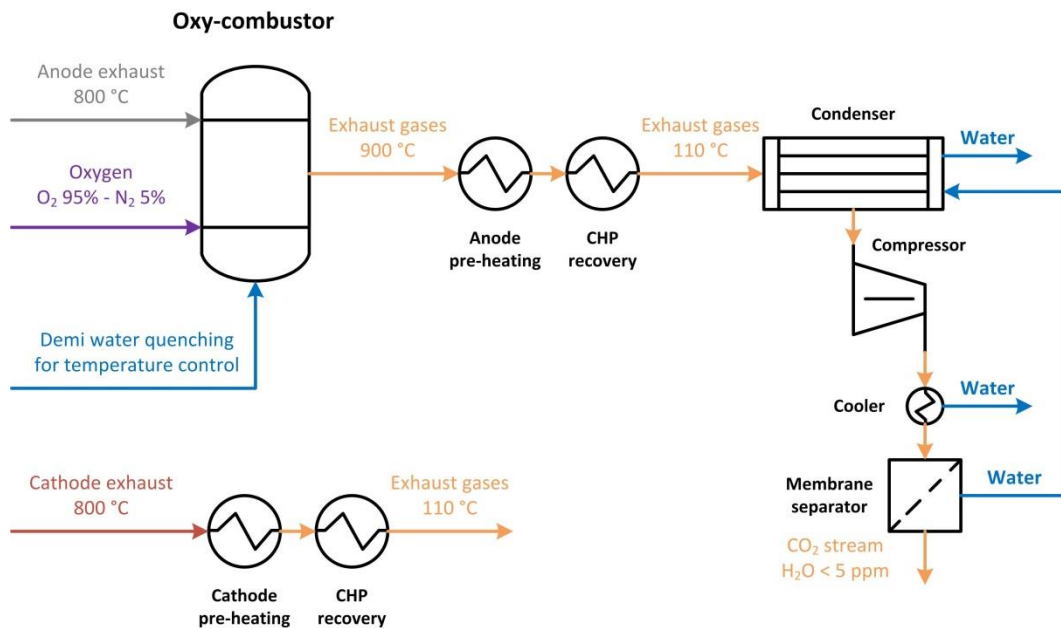
Figure 276. Oxy-combustor and heat recovery layout.

The molar flow of the oxygen required can be simply calculated considering that, in the oxy-combustor, the inlet exhaust are made, especially of water, carbon monoxide, carbon dioxide, hydrogen and methane and that occur mainly these combustion reactions:

$$CH_4 + 2O_2 \rightarrow CO_2 + 2H_2O$$

Eq. 91

$$H_2 + \frac{1}{2} O_2 \rightarrow H_2 O \qquad \text{Eq. 92}$$

$$CO + \frac{1}{2} O_2 \rightarrow CO_2 \qquad \text{Eq. 93}$$
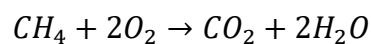
So, the molar flow of oxygen required, in stoichiometric conditions, for the complete combustion is given by:

$$\dot{n}_{O_2}^{st} = 2\dot{n}_{CH_4} + \frac{1}{2} \dot{n}_{H_2} + \frac{1}{2} \dot{n}_{CO} \qquad \text{Eq. 94}$$

It is not suggested to supply just the stoichiometric flow because it could be not sufficient to ensure the full oxidation of the entire fuel (Kuramochi et al. 2011). Then, a certain oxygen excess e_{O_2} has to be defined (typically $1 - 3$ %) and the real molar flow is given by:

$$\dot{n}_{O_2} = \dot{n}_{O_2}^{st} \cdot \left(1 + \frac{e_{O_2}}{100} \right) \qquad \text{Eq. 95}$$

The higher concentration of CO_2 and H_2O allows a simpler capture of CO_2, but the combustion made with pure oxygen presents two additional problems to take care of. The first one is related to the oxygen production, already discussed above.

The second one is related to the combustion itself: a complete combustion of the flue gases generates high temperatures (up to 1000-1200 °C) that could be not tolerated by the materials. From a thermodynamic point of view, we would be very interested in them because the heat recoveries and the production of hot water should improve. On the other hand, the only way to make work the system at these temperatures is the adoption of ceramic materials that are too much expensive and should be avoided.

A very good Ni alloy could be made to work properly up to 2000 °F (1093 °C) (Anon n.d.), but we have imposed a limit temperature of 900 °C so that it was considered the use of a material of medium-high quality and not of the best one achievable.

The best way to control the combustion temperature is to pump in the oxy-combustor fresh demineralized water taken from the environment (quenching process, as for the afterburner).

After the combustion, the stream is sent to a water gas heat exchanger to recover the available heat for cogeneration (digester heating in WWTP). Since water temperatures are around 60/80 °C and are preferred to avoid condensation in the heat exchanger, below 100

°C the gas is directly sent to a condenser to remove the major part of the water contained in it.

Since a pipeline quality CO_2 is the objective of the CCS, condensation is not sufficient for the water removal, and a pressurized membrane is used. The stream is thus compressed at around 8 bars and then cooled down by an air fan since membrane cannot stand temperatures higher than 60/65 °C.

Before entering the membrane, liquid water, if present, is removed by a fog condenser since it is not suitable for the membrane long term operation.

These membranes (Dortmundt & Doshi 1999) are not porous like other separation devices, such as the filters, because they allow a selective diffusion of just some chemical components that have a tendency to dissolve and to diffuse, through the membrane, higher than that one of others. The driving force of this separation is the pressure of the mixture fed, which cannot be the atmospheric one. This aspect can be seen directly from the Fick's law:

$$J = \frac{k \cdot D \cdot \Delta p}{l}$$ Eq. 96

where:

- J is the molar flow of the component that passes through the membrane
- k is the solubility of the component in the membrane
- D is the diffusion coefficient of the component through the membrane
- Δp is the difference between the partial pressure of the component and that at the permeate side of the membrane
- l is the membrane thickness

Table 84. Oxy-combustor and heat recovery design parameters.

Parameter	Value	Unit
Oxy-combustor temperature	900	°C
Oxygen purity	95%	O2
	5%	N2
Oxygen energy production cost with PSA	300	kWh/ton
Condenser temperature	15/200	°C
Compressor outlet pressure	5	bar

Membrane outlet water	< 5	ppm
Exhaust to chimney temperature	110	°C
Water for CHP temperatures	65/75	°C

So the molar flow separated is proportional to the inlet pressure of the flue gas.

In the analyzed membrane the water is the component passing through the membrane and going back to the condenser inlet, while the pure CO_2 stream is exiting the membrane.

At this point we have obtained a stream of almost pure carbon dioxide with a very high level of purity and, depending on what is the CO_2 pathway, different downstream configurations can be designed. If the stream is locally required, for different uses which will be analyzed in next chapters, then nothing else is required. Sometimes a blower can just be required if the membrane pressure is not sufficient to win the pressure drops on the line.

The second possible solution for the CO_2 is the geological sequestration or carriage to another site: in both cases, carbon dioxide needs to be liquefied. The liquefaction of the CO_2 at the ambient temperature requires its compression up to, at least, 110 bars. A single compressor is never used because it is too expensive from an energetic point of view, while a Multi-Stage Compressor (MSC) where the flow is compressed and cooled in a certain number of stages is more appropriate for this application.

The system has been modeled in AspenPlus® using double stream heat-exchangers, a flash separator for the condenser in order to divide the liquid fraction from the vapor one and a separator for the membrane to achieve the desired carbon dioxide purity in the outlet stream. the multi-stage compression has been modeled using five compression stages (Figure 277).
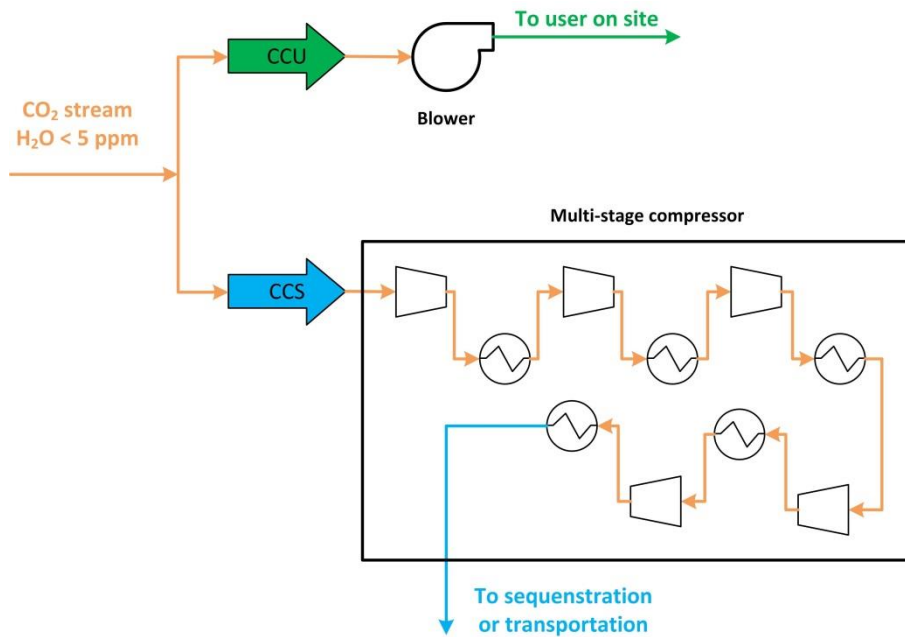
Figure 277. CO_2 compression processes.

A3.6 Atmospheric and pressurized plants

In this section, the main technical differences between atmospheric and pressurized plants will be discussed.

As suggested by its name, in the <u>atmospheric plant</u> the fuel cells are supplied with biogas and external air at near ambient pressures. The blowers for inlet biogas and air are just included to win the pressure drops of the components. In fact, if the streams have, in any point of the plant, the pressure under the atmospheric one, the circulation stops, and there is no production of power. For this reason, the two lines (anode and cathode) need the presence of pressure control systems, so that each drop is coped with an adequate pressurization given by the blowers.

Furthermore, the two electrodes of the cell should be maintained, as much as possible, at equal pressures because large differences between them may influence the electrochemical activity or even lead to the destruction of electrolyte and of the whole cell. For a correct and an appropriate operation, when running atmospheric cells, it is necessary to have inside the cell a pressure drop lower than 500 mbar (Willich et al. n.d.). In the atmospheric plant the blowers are sized with respect to this limits:

$$p_{an,in} = p_{cat,in}$$ Eq. 97

$$\Delta p_{biogas,blw} = \Delta p_{clean-up} + \Delta p_{HXan} + \Delta p_{reformer} + \Delta p_{SOFC,an} \\ + \Delta p_{burner/combustor} + \Delta p_{CHP}$$

Eq. 98

$$\Delta p_{air,blw} = \Delta p_{HXcat} + \Delta p_{SOFC,cat} + \Delta p_{burner} + \Delta p_{CHP}$$

Eq. 99

where each Δp represents the pressure drop of the corresponding device.

In the case of a non-CCS plant, the pressure balance is easier since the two inlet streams are burned together in the after-burner, and their pressures are thus leveled inside the burner itself.

In the case of CCS plants, on the other hand, the two exhaust streams are kept separated during the downstream process. On the anode exhaust side, the blower has just to cover the pressure drops until the CHP heat-exchanger since, from the condenser on, the membrane compressor I able to guarantee the flow. On the cathode side, no burner is included: consequently pressure drops are lower. The important limit set by the first equation has always to be respected.

In the case of <u>pressurized plants</u> blowers are replaced with compressors in order to pressurize the entire system.

Concerning the plant without CCS, the most important variation in the design concerns the presence of a Micro Gas Turbine (MGT) that expands the flue gases leaving the after-burner and recovers mechanical energy that can be reused within the plant. The connections involving this device has to be defined in the most appropriate way since the feasibility, and the performances of the whole plant could be affected.

In a plant, where there are both turbines and compressors, it is unusual that these devices are not connected between them in pairs (turbo-compressor system). For this reason, in our design, the turbine is directly connected to a compressor.

First of all, it was necessary to identify the compressor that requires the larger amount of energy: in a first approximation, this device is the one where is treated a larger volume flow. As was described before, in order to supply both the stoichiometric oxygen for the Redox reaction and the cooling flow at the SOFC, a large amount of air is required, and its volume flow is much higher than that of biogas. Considering this, the air compressor is assumed to be the one with the highest consumptions. This hypothesis is totally confirmed by the simulations performed.

The second point was to understand if it is more convenient that the gas turbine produces electrical or mechanical power. This could be understood easily considering the energy conversions involved.

When analyzing the pressurized plant with CCS, two possible situations can occur:

1. $p_{SOFC} < p_{membrane}$
2. $p_{SOFC} > p_{membrane}$

Where p_{SOFC} is the pressure of the system defined by the SOFC and $p_{membrane}$ the pressure of the membrane, usually around 5 bars.

In the situation where the pressure of the flue gases is under the value required to the membrane, this plant has the same features already seen for the pressurized one without CCS since:

- On the cathode side, exhaust gases are expanded with a turbo-compressor group.
- On the anode side, no turbine is inserted, and the membrane compressor is required to guarantee the correct working of the separator.

On the other side, if pressurization is so intense that the pressure of the flue gases overcomes the value required to the separator, on the anode side the compressor can be avoided, but the pressure has to be decreased to the one of the membranes, so the gas needs to be expanded.

The expansion of the hot flue gases can be done using an expander or another gas turbine. The adoption of a gas turbine allows to recover other mechanical energy that can be reused to feed the biogas compressor but, on the other hand, it requires a connection between them and so a higher complexity of the system. The choice between the two devices was made trying to verify if the energy recoveries are, or are not, worth the more complexity.

Considering that the membrane works at pressures around 5 bar, that an SOFC will not be pressurized more than 10 bars (to avoid excessive mechanical stresses) and that the mass flow expanded is much lower than the one sent to the other gas turbine on cathode side, the energy that can be recovered during the expansion is very low and there is not a valid motivation to adopt a more complex system. For this reason, an expander is adopted and, during the simulations, was verified that the mechanical power produced by the expansion is ten times lower than the one produced by the gas turbine, so it is recovery is not worth.

Possible uses of CO_2

Nowadays, the use of CO_2 is limited to small markets and applications, most of which are still at the level of scientific research. Analyzing, through a detailed literature research from MATGAS, a Spanish company and a SOFCOM partner who is working on this topic (Vega n.d.; Vega n.d.; Torres & Vega 2011; Torres 2013), a lot of possible uses in different areas of the industrial words have been pointed out. Even if currently it is difficult to talk about a CO_2 market, and thus a CO_2 price, in the next decades it could become an interesting investment for the industries. Below, some possible uses of carbon dioxide are summarized, divided by industrial area. Some of them, like the food industry, are currently an industrial user of CO_2 while others, like the supercritical one, are still on the scientific research stage (summary on Figure 278).

Direct use in the food industry

- Gas beverages
- Food preservation (modified atmosphere)
- Freezing with cryogenic CO_2
- Acidification of milk and dairy products
- Control of parasites

Use in processes

- Synthesis/extrusion of polymers
- Carbonation process of industrial waste

CO_2 supercritical

- Substitution of organic solvents
- Extraction of caffeine from tea/coffee and hops, and of pesticides from cereals
- Beverages de-alcoholization
- Degreasing (cocoa, skin)
- Dry-cleaning (clothes, electronics)
- Removal of TCA from cork
- Crystallization/micronization
- Co-precipitation/encapsulation
- Sterilization/pasteurization
- Synthesis of new materials (Aerogels)

Biological use

- Enrichment of the environmental CO_2 in greenhouses
- Carbon fertirrigation
- Microalgae growth (bio-fuels, cosmetic industry)

- Waste water treatment with microalgae

Chemical use

- Acetylsalicylic acid
- Production of powdered carbonates (filler for paper, plastics, and paintings)
- Methanol production
- Polymers production
- Artificial photosynthesis (new photo-catalytic materials)

Figure 278. CO_2 possible uses summary.

Appendix 4 – Economic analysis: functions, cost of biogas and subsidies

A4.1 Cost functions definition

Fans and compressors

The estimation of the capital cost for fans and compressors is made using a unique cost function, implemented by professor R. Turton (Turton et al. 2012). From the data that he collected during the period from May to September 2001, a general expression of the investment cost, which can be applied to different devices just changing a series of constants, was obtained:

$$\text{BEC} = C_p^0 \cdot F_m \cdot F_P \qquad \text{Eq. 100}$$

where:

- C_p^0 [$] is the purchased cost of equipment referred to base conditions
- F_m is the material factor
- F_P is the pressure factor

The base conditions of the purchased cost are referred to a device working at ambient temperature and pressure and using, as material, carbon steel. The expression that was used to fit the economic data is the following:

$$\log_{10} C_p^0 = K_1 + K_2 \log_{10} A + K_3 (\log_{10} A)^2 \qquad \text{Eq. 101}$$

where:

- *A* is the operating condition chose as reference for the device considered
- *K₁, K₂,* and *K₃* are three constants that R. Turton defined, for some devices, to fit the expression to the real costs of the devices sold

For fans and compressors, the independent variable adopted is the inlet volumetric flow:

$$A = \dot{V}_{inlet} \left[\frac{m^3}{s} \right] \qquad \text{Eq. 102}$$

The purchased cost expression, as already told, is valid just inside a range of the independent variable. In operating conditions outside the limit imposed it is necessary to

use the scaling factor (that, for some devices, is again evaluated by R. Turton (Turton et al. 2012)).

The material factor takes care of the real material that should be used to allow the appropriate thermal resistance of the device.

In this work has been assumed that a device can be made of one of the three materials, shown in and that the choice of which one should be adopted depends just on the highest temperature reached inside the component.

Table 85. Materials and thermal limits.

Material	Max. temperature
Carbon Steel – CS	350 °C
Stainless Steel – SS	600 °C
Ni Alloy – Ni	900 °C

R. Turton (Turton et al. 2012) has defined some reference values of the material factors in respect of the component and of the material.

The pressure factors consider the mechanical resistance that must have the material so that the device can stand the mechanical stresses caused by the pressures drops. Another logarithmic formula was implemented to estimate this last coefficient:

$$\log_{10} F_P = C_1 + C_2 \log_{10} P + C_3 (\log_{10} P)^2 \qquad \text{Eq. 103}$$

where:

- P is the independent variable that expresses the pressure field, but its definition is not unique and depends on the component considered
- C_1, C_2, and C_3 are three constants defined to fit the expression to the real data

For the fans and the compressors, the pressure factor depends on the pressure difference, in bar, between the outlet and inlet fluids:

$$P = \Delta p[bar] = p_{out}[bar] - p_{in}[bar] \qquad \text{Eq. 104}$$

On Table 86 all the data required for the adoption of this cost function are reported.

Table 86. Constants for the fans and compressors cost function.

Parameter	Symbol	Value	
Purchased cost at base conditions	K_1	3.5391	
	K_2	-0.3533	
	K_3	0.4477	
	$\dot{V}_{inlet,min}$	$1\ m^3/s$	
	$\dot{V}_{inlet,max}$	$100\ m^3/s$	
	Scaling factor	0.6	
Material factor	$F_m - CS$	2.75	
	$F_m - SS$	5.8	
	$F_m - Ni$	11.7	
Pressure factor		$\Delta p < 0.01$	$\Delta p \geq 0.01$
	C_1	0	0
	C_2	0	0.20889
	C_3	0	-0.0328
BEC Actualization	Year	2001	
	$CEPCI_{2001}$	394	
	$CEPCI_{2010}$	551	

Cleaning system

The calculation of the capital cost for the cleaning system was made using the scaling method, starting from some reference data referred to the purification of biogas produced in an anaerobic digester (Papadias et al. 2012).

The total investment cost can be divided into four components, each of one referred to a step of the treatment device:

- C_{IO}: cost of the Iron Oxide system for the H_2S capture.
- C_{MR}: cost of the Moisture Removal system.
- C_{LTP}: cost of the Low Temperature Polisher based on Active Carbon that removes the organic sulphur, siloxanes and, halogens.

- C_{HTP}: cost of the high temperature polisher for the residuals removal, especially sulphur and chlorine compounds are transformed into H$_2$S and HCl and the removed.

The independent variables adopted for the scaling are:

- C_{H2S} $[ppm]$: concentration, in the biogas, of the hydrogen sulphide to scale the C_{MR}
- $\dot{V}_{biogas}$ $\left[Nm^3/day\right]$: daily volume flow of the biogas to scale all the other cost components

In Table 87 are reported all the quantities required for the calculation.

Table 87. Constants for the cleaning system cost function.

Parameter	Symbol	Value
Reference Condition	C_{IO}	27'500 $
	C_{MR}	36'600 $
	C_{LTP}	48'800 $
	C_{HTP}	12'800 $
	H$_2$S concentration	400 ppm
	Daily volume flow	2570 $\left[Nm^3/day\right]$
	Scaling factor	0.7
BEC Actualization	Year	2012
	$CEPCI_{2012}$	551
	$CEPCI_{2010}$	551

External reformer

The external reformer is a simple vessel sized with a volume that considers both the inlet flow to reformate and the presence of the catalyst, which activate the reactions. Considering this, the cost function chosen to estimate its capital cost derives again from the methodology implemented by R. Turton for horizontal vessels (Turton et al. 2012).

The purchase cost, at base conditions, is defined in respect of the total volume of the reformer:

$$A = V_{reformer}[m^3]$$

<div align="right">Eq. 105</div>

The definition of the volume of the vessel requires a scaling method starting from available results referred to real operating reformers. In the following table all the required data found in the literature (DOE NETL et al. 2011), referred to an experimental reformer are reported.

Table 88. Properties of the experimental reformer.

Parameter	Value
CH$_4$ inlet molar fraction (C_{in})	93.10 %
Inlet flow ($\dot{V}_{in}$)	1556 kmol/h
CH$_4$ outlet molar fraction (C_{out})	1.32 %
Outlet flow ($\dot{V}_{out}$)	6167 kmol/h
Initial fill ($V_{fill,r}$)	1341 m^3

With initial fill, the volume of the reformer occupied by the inlet biogas during the whole reforming reaction was considered. The reformer has in fact been considered as fully filled by the catalyst.

The variable chosen for the scaling is the flow of methane converted in the reformer, which can be, for the reference conditions, found as:

$$\dot{V}_{conv,r} = \dot{V}_{in} \cdot C_{in} - \dot{V}_{out} \cdot C_{out}$$

<div align="right">Eq. 106</div>

A scaling factor equal to 1 has been chosen since volume is supposed to be proportional to the quantity of reformate.

$$V_{fill,op} = V_{fill,r} \cdot \left(\frac{\dot{V}_{conv,op}}{\dot{V}_{conv,r}}\right)$$

<div align="right">Eq. 107</div>

where $\dot{V}_{conv,op}$ is the molar flow of methane reformed in operating conditions.

It has been assumed that there is a ratio 1:2 between the initial fill and the volume occupied by the catalyst, so the total volume of the reformer can be estimated in the following way:

$$V_{ref} = V_{fill,op} \cdot 1.5$$

<div align="right">Eq. 108</div>

Due to the high temperatures involved in the reforming reactions, the only material that can be used is the Ni alloy, so the material factor will be referred to a horizontal vessel made of Ni.

The logarithmic law that allows the calculation of the pressure factor cannot be used for vessels. However, another empiric relationship is available:

$$F_p = \frac{\dfrac{\left((p+1) \cdot D\right)}{2 \cdot \left(850 - 0.6 \cdot (p+1)\right)} + 0.00315}{0.0063}$$

Eq. 109

Where:

- p [barg] is the operating relative pressure
- D [m] is the diameter of the vessel

Table 89. External reformer cost function input data.

Parameter	Symbol	Value
Purchased cost at base conditions	K_1	3.5565
	K_2	0.3776
	K_3	0.0905
	$V_{vess,min}$	0.1 m^3
	$V_{vess,max}$	628 m^3
	Scaling factor	0.7
Material factor	$F_m - Ni$	7.05
BEC Actualization	Year	2001
	$CEPCI_{2001}$	394
	$CEPCI_{2010}$	551

If the pressure factor found is lower than 1, it is replaced with 1. The diameter of the vessel can be evaluated from the volume just if the height (H) is hypothesized. A value of H = 1 m has been assumed, and thus the diameter can be calculated:

$$V_{ref} = \pi \cdot \frac{D^2}{4} \cdot H$$

Eq. 110

$$D = \sqrt{\frac{4 \cdot V_{ref}}{\pi \cdot H}} \qquad \text{Eq. 111}$$

In T the constants used for the application of the Turton cost function to the external reformer are reported.

SOFC Stack

The cost function used to estimate the capital cost of the entire SOFC module is a function of the total area occupied by the cells and of the insulation volume needed to limit the thermal losses:

$$BEC = c_{mod} + c_{ins} \qquad \text{Eq. 112}$$

where:

- c_{mod} is the capital cost referred to the installation of the module of the fuel cells
- c_{ins} is the capital cost referred to the integration of the insulating (Alumina) required

On Table 90 the reference costs of an SOFC stack expressed per unit of active surface and electrical power produced are reported (DOE NETL 2011a).

In order to have all the cost components expressed per unit of active surface, it is necessary to convert those referred to the unit of power using the power density of the stack:

$$W_{dens} \left[\frac{kW}{m^2}\right] = \frac{W_{DC}}{A_{tot}} \qquad \text{Eq. 113}$$

$$c_i \left[\frac{\$}{m^2}\right] = c_i \left[\frac{\$}{kW}\right] \cdot W_{dens} \qquad \text{Eq. 114}$$

The total area of the stack does not correspond exactly to the active surface because it depends on the disposition chosen of the cells. For this reason, it is necessary to implement, during the economic analysis, a function that defines the geometry of the entire SOFC stack.

The planar configuration has been chosen for the stack, so a parallelepiped can be shaped. The single cell has a a square and thickness t; thus the module is made of a number of stacks that contain a constant number of cells, $n_{cells,mod}$. For square base SOFC module

of 1-2 MW, for example, it is recommended to have both more or less 80 cells 33, value used as a reference in the large scale analysis.

From the total active surfaces and the geometric properties of the cells and of the modules, it is possible to estimate the number of modules necessary:

$$A_{cell} = a \cdot a$$
<div align="right">Eq. 115</div>

$$n_{cells} = round\left(\frac{A_{tot}}{A_{cell}}\right)$$
<div align="right">Eq. 116</div>

$$n_{mod} = round\left(\frac{n_{cells}}{n_{cells,mod}}\right)$$
<div align="right">Eq. 117</div>

Table 90. SOFC stack cost component.

Cost component	Value
Integrated block	540 $/m^2
Enclosure (vessel only)	100 $/m^2
Transport and placement	60 $/m^2
Foundation at the site	185 $/m^2
Improvement to site	255 $/m^2
Building and structures	235 $/m^2
Piping	68 $/m^2
Power conditioning (inverter)	82 $/kW
Electrical accessories	79.75 $/kW
Instrumentation and controls	50 $/kW

Obviously the ratios must be rounded up to define the number of cells and modules: for this reason, the module will be a little oversized. The stacks can be disposed of in the module in different ways, adopting an interspace *i* between each two.

To simplify the design has been assumed that there are relationships between the dispositions towards the three Cartesian directions: defining with *H, L* and *W* the numbers of cells respectively towards *x,y* and *z*, a constant value of *W* (it can be 1,2 or 3) and the ratio between *L* and *H* (usually 2) have been imposed.

With these assumptions, the number of modules *H*, *L,* and *W* are:

$$
\left[
\begin{array}{l}
n_{mod} = round\left(\dfrac{n_{cells}}{n_{cells,mod}}\right) \\[3ex]
H = round\left(\sqrt{\dfrac{n_{mod}}{W \cdot \left(\frac{L}{H}\right)}}\right) \\[4ex]
L = H \cdot \left(\dfrac{L}{H}\right)
\end{array}
\right.
\qquad\text{Eq. 118}
$$

$$W, \left(\frac{L}{H}\right) \; inpu\; data$$

The value of *H* must be again rounded up, so this causes another oversizing.

In the following figure is represented a summary of the geometrical properties of modules and cells.
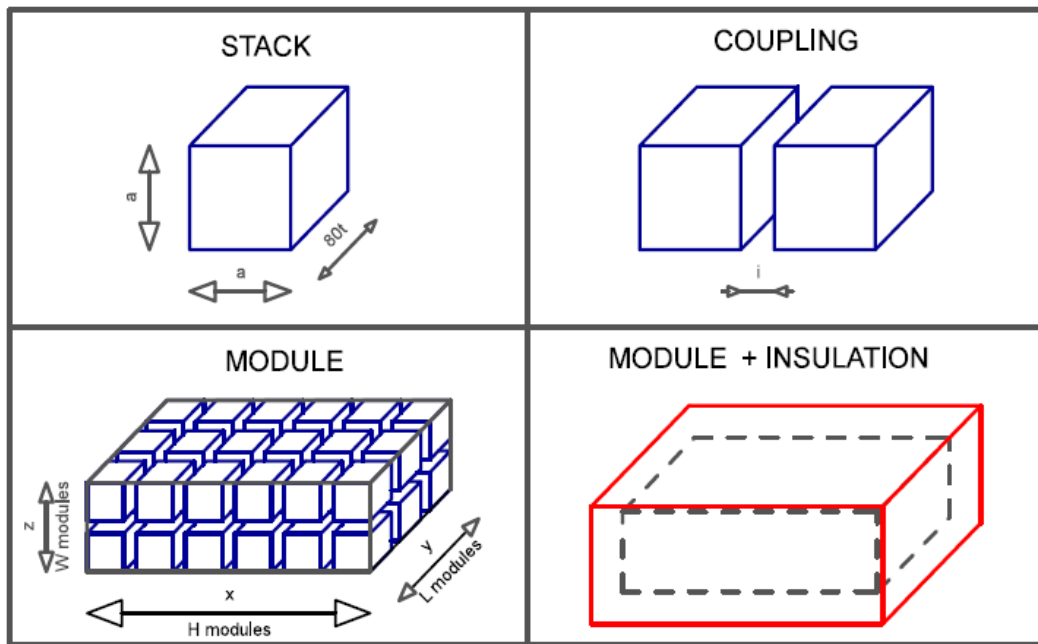
Figure 279. Geometrical properties of modules and of the stack.

Defining with *x,y,* and *z* the three edges towards the three directions, the total area of the module can be found in the following way:

$$A_{mod} = 2 \cdot x \cdot y + 2 \cdot x \cdot z + 2 \cdot y \cdot z \qquad\text{Eq. 119}$$

$$x = H \cdot a + (H - 1) \cdot i \qquad \text{Eq. 120}$$

$$y = L \cdot a + (L - 1) \cdot i \qquad \text{Eq. 121}$$

$$z = W \cdot t + (W - 1) \cdot i \qquad \text{Eq. 122}$$

Then, the total area has to be multiplied to each cost component, expressed per unit of surface, so that the total cost for the installation of the module can be estimated:

$$c_{mod} = \left(\sum c_i \right) \cdot A_{mod} \qquad \text{Eq. 123}$$

In Table 91 all the geometrical assumptions required for the surfaces calculation are reported.

Table 91. Reference geometrical values of the cells, modules, and stack.

Geometrical property	Value	Unit
a	10	cm
t	0.1	cm
$n_{cells,mod}$	80	-
i	3.33	cm
L/H	2	-
W	1	-

The capital cost also depends on a second variable, the volume of the insulating (alumina) required.

First of all, it is necessary to identify the thickness of the insulation material to limit the thermal losses at a certain value.

During the definition of the electrochemical model it was shown a way to correlate the thermal losses with the potential power of the inlet fuel:

$$\dot{Q}_{loss} = \frac{r_{loss}}{100} \cdot \dot{Q}_{fuel,in} \qquad \text{Eq. 124}$$

The heat is transferred to the environment by the conduction through the alumina. This material has a conductivity very low so that the losses are controlled, and its thickness

required depends strongly on the quantity of power that we accept to lose. The thickness can be easily found from the conduction equation:

$$\dot{Q}_{loss} = \frac{\lambda_{al}}{s_{al}} \cdot A_{mod} \cdot (T_{SOFC} - T_a) \qquad \text{Eq. 125}$$

$$s_{al} = \frac{\lambda_{al} \cdot A_{mod} \cdot (T_{SOFC} - T_a)}{\dot{Q}_{loss}} \qquad \text{Eq. 126}$$

Where:

- $\lambda_{al} \left[\frac{W}{mK}\right]$ is the alumina thermal conductivity
- $T_{SOFC}[°C]$ is the SOFC operating temperature
- $T_a[°C]$ is the environment temperature
- $s_{al}[m]$ is the required thickness

The losses cannot be completely avoided; a certain fraction occurs ever. The quantity of material bought depends on the losses accepted, in fact, as can be seen from the last relationship, lower values of Q_{loss} correspond to higher thicknesses.

In order to simplify the calculation of the alumina volume, required for the cost function, a subdivision of the total insulation volume in three portions has been performed, as can be seen on Figure 280.
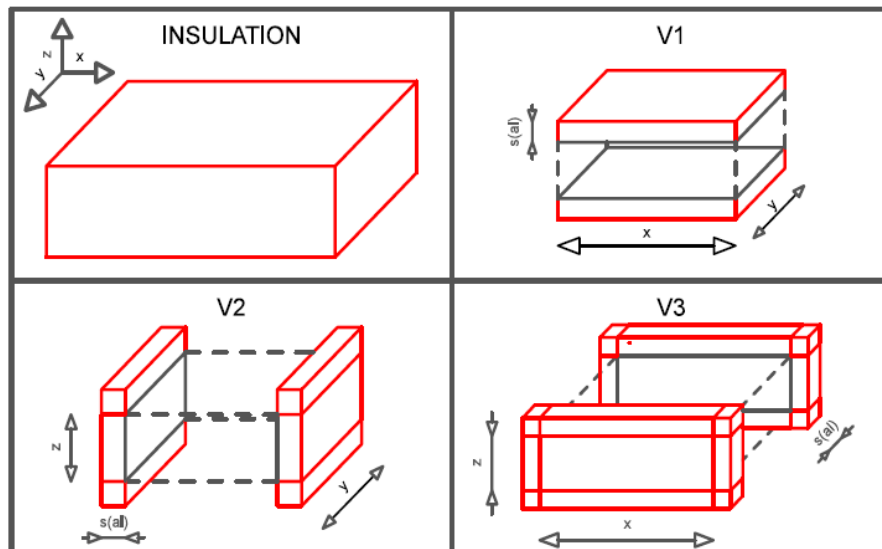
Figure 280. Alumina volume layout.

The total insulation volume can be thus determined as the sum of *V1, V2,* and *V3*.

$$V_{al} = V_1 + V_2 + V_3 \qquad \text{Eq. 127}$$

$$V_1 = 2 \cdot x \cdot y \cdot s_{al} \qquad \text{Eq. 128}$$

$$V_2 = 2 \cdot y \cdot (z + 2 \cdot s_{al}) \qquad \text{Eq. 129}$$

$$V_3 = 2 \cdot (x + 2 \cdot s_{al}) \cdot (z + 2 \cdot s_{al}) \qquad \text{Eq. 130}$$

From the total alumina volume the specific cost of the material, the second cost component for the SOFC module is given by:

$$c_{al} = c_{al,sp} \cdot V_{al} \qquad \text{Eq. 131}$$

In Table 92 all the reference values required to complete the calculation of the second capital cost are reported.

Table 92. Constants for the alumina cost calculation.

Geometrical property	Value	Unit
$c_{al,sp}$	5	c\$/m^3
λ_{al}	0.036	W/(mK)
T_a	25	°C

Each cost component implemented is referred to the year 2007, then for the actualization of the BEC, it is necessary to use the corresponding value of CEPCI, equal to 525.

Afterburner and oxy-combustor

The after-burner and the oxy-combustor are combustion chambers that do not present so many technological complexities and can thus be studied as simple horizontal vessels. The cost function that allows estimating their capital costs is then the one developed by R. Turton and already explained in the paragraph dedicated to the external reformer.

The main problem is the definition of the maximum volume of the chamber since this value is the independent variable that influences the capital cost.

A simple method of estimation of this volume involves the knowledge of the average reaction time. This quantity is defined as the time necessary for the reactants to react

between them and produce the final products. These combustion reactions are really fast and, in literature, are available many reference values related to different operating conditions. However a reaction of this kind tends to be fully completed between 0 and 1 s, so, considering this range, an average reaction time of 0.5 s was assumed.

The only parameter needed at this point, for the definition of the maximum volume, is the total volume flow that enters in the vessel. For the after-burner it will be given by the flue gases from the anode, from the cathode and the cooling water for the quenching; on the other hand, for the oxy-combustor, instead of the flue gases from the cathode, will be used the oxygen flow produced in the PSA unit.

The total volume is then:

$$V_{vessel}[m^3] = t_{react}[s] \cdot \dot{V}_{in}\left[m^3/s\right]$$

Eq. 132

From now on, the procedure is the same one applied in the external reformer.

Micro gas turbine

The costs of the gas turbines installed in the pressurized plants cannot be estimated with the cost functions implemented by R. Turton, because these relationships are more appropriate for devices of medium – large size, while, in our case, the production of power from the expansion of exhausts is low. The use of these functions could oversize too much the total investment cost and cause mistakes that influence the whole work.

These components are not standard gas turbines but are micro-turbines, and so it was necessary to use a more specific cost function.

In general, the capital cost of a micro-turbine depends on three main factors:

- Inlet mass flow
- TIT (Turbine Inlet Temperature)
- Pressure ratio

From available economic data, it has been possible to define a relationship with a fitting operation between the three values. In this analysis, the equation defined by L. Galanti and A. Massardo was chosen (Galanti & Massardo 2011):

$$BEC = \frac{t_1 \cdot \dot{m}_g \cdot \sqrt{\dfrac{R_g}{R_{ref}}} \cdot \ln \beta}{t_2 - \eta_{pol,turb}}$$

Eq. 133

where:

- t_1 and t_2 are reference coefficients
- $\dot{m}_g \left[\frac{kg}{s}\right]$ is the inlet mass flow
- $R_g \left[\frac{J}{kg\ K}\right]$ is the real gas constant
- $R_{ref} \left[\frac{J}{kg\ K}\right]$ is the reference gas constant for air
- β is the pressure ratio
- $\eta_{pol,turb}$ is the polytrophic efficiency of the turbine

Although the TIT is not included in the relationship, this equation is valid just for operating temperatures not higher than 900 °C. Around this value, the material used requires a high thermal resistance, and so it will be more expensive. The operating temperatures of the turbines are around 800 °C; then this expression can be used because we have already overcome the possibility of adopting cheaper materials.

In Table 93 the constants required for the application of this cost function are reported.

Table 93. Constants for the cost function of micro-gas turbines.

Parameter	Value	
t_1	376.1 $	
t_2	0.903	
BEC Actualization	Year	2003
	$CEPCI_{2001}$	402
	$CEPCI_{2010}$	551

PSA unit and MSC

The cost functions of the Pressure Swing Adsorption (PSA) unit and of the Multi-Stage Compressor are both developed with the scaling method, using as initial data the values found in the same reference (Novosel et al. 2012). The independent variable of the PSA is the daily productivity of the oxygen. This parameter can be found from the inlet oxygen flow in the oxy-combustor:

$$Q_{PSA} = P_{O_2} \left[\frac{ton}{d}\right] = \dot{m}_{O_2} \left[\frac{g}{s}\right] \cdot 3600 \left[\frac{s}{h}\right] \cdot 24 \left[\frac{h}{d}\right] \cdot 10^{-6} \left[\frac{ton}{g}\right] \qquad \text{Eq. 134}$$

On the other hand, the independent variable for the MSC is the net electrical work required for the whole compression:

$$Q_{SMC} = W_{el,net} [MW]$$
<div align="right">Eq. 135</div>

In Table 94 the constants required for the use of the scaling method are reported.

Table 94. Constants for the cost function of the PSA unit and of the MSC.

Parameter	Symbol	PSA	MSC
Reference values	C_r	9.15 x 10⁴ $	1.56 x 10⁶ $
	Q_r	1 ton/d	0.7 MW
	Scaling factor	0.83	0.67
BEC Actualization	Year	2011	2011
	$CEPCI_{2011}$	551	551
	$CEPCI_{2010}$	551	551

Depending on the different studied scenarios, the heat exchanger network can be defined in the design procedure or determined automatically through the minimization of the external heat requirement. The second methodology has been implemented in the OSMOSE function (large size plants), while the first one is used for small and medium size plants. Once defined the HX network, anyway, the methodology chosen for the cost evaluation has always been maintained during the analyses.

Below the more complex methodology with the HX network definition is explained: for small and medium size plants, the cost function was simply implemented without the first design process.

The total investment cost depends on the configuration of the network adopted. Unfortunately, when the HX network is not known a priori, this dependence is not simple to implement in a code because the whole function changes with the design itself. For this reason, it was then necessary to adopt a simplified approach based on the discretization of the cumulative curves.

First of all, let's define the cost function of a simple heat exchanger. Again, we adopt the methodology developed by R. Turton, where the BEC depends on the purchase cost at base conditions, the pressure factor and the material factor.

The independent variable that defines the purchase cost is the heat exchange surface:

$$A = A_{HX}[m^2]$$

Eq. 136

This value can be determined from the knowledge of the net thermal power exchanged between the hot and cold flows and their inlet/outlet temperatures:

$$\dot{Q}_{net} = U \cdot A_{HX} \cdot LMTD$$

Eq. 137

$$A_{HX} = \frac{\dot{Q}_{net}}{U \cdot LMTD}$$

Eq. 138

$$LMTD = \frac{\left(\left(T_{h,in} - T_{c,out}\right) - \left(T_{h,out} - T_{c,in}\right)\right)}{\ln\frac{\left(T_{h,in} - T_{c,out}\right)}{\left(T_{h,out} - T_{c,in}\right)}}$$

Eq. 139

where:

- $\dot{Q}_{net}[kW]$ is the net thermal power exchanged
- $U\left[\frac{kW}{m^2 K}\right]$ is the global heat transfer coefficient
- $LMTD$ is the logarithmic mean temperature difference
- $T_{h,in}, T_{c,out}, T_{h,out}, T_{c,in}$ [°C] are the inlet and outlet temperatures of the hot and cold flows

In the analyzed plants, the heat exchangers are fed by gas or water and the global heat transfer coefficients used depends on which of them flows (Bonacina et al. 1989):

- Water – Gas HX, U_{wg}=0.130 $\frac{kW}{m^2 K}$
- Gas – Gas HX, U_{gg}=0.025 $\frac{kW}{m^2 K}$

In the pressure factor, the *P* value assumes the meaning of the highest relative pressure of the operative fuels.

The material factor can depend on the temperatures of both the fuels. In fact, the heat exchanger can be made of different materials in the hot and cold side if the temperatures of the respective flows allow it. The definition of the material factor is, in this cost function, made with the following relationship:

$$F_m = B_1 + B_2 \cdot F'_m \cdot F_p$$

<div align="right">Eq. 140</div>

where B_1 and B_2 are constants defined for the heat exchanger device and F'_m depends on the materials used in the two sides.

The heat exchanger chosen is the double pipe one, which was the most suitable solution analyzing the limits of the HXs cost functions. In Table 95 the constants required for the use of this cost function are reported.

At this point, the methodology would be finished in case of small and medium size plants. For large size plants, let's define the discretization approach adopted for the calculation of the investment cost of the total network.

The pinch analysis is the first step for the design of a heat exchanger's network. This procedure estimates the maximum thermal recoveries achievable in a system, minimizing the consumptions of energy provided by external sources. This method is based on the construction of two cumulative curves; one referred to the internal hot sources and the other one for those cold. From the comparison of the two curves and from the imposition of a minimum temperature difference from the flows, it's then possible to evaluate the necessary external heat (both cold and hot) corresponding to the highest thermal recovery achievable.

Although the design of the network could be done starting from the results obtained in the pinch analysis, from an economical point of view, it could be less convenient to adopt just this approach. The reason why it's not sufficient is due to the fact that a network well designed, from the point of view of thermal recoveries, could require the adoption of many heat exchangers: in general, if it's necessary to exchange a certain quantity of thermal power, a larger heat exchanger is much cheaper than many smaller devices.

Table 95. Constants for the cost function of the heat exchangers.

Parameter	Symbol	Value
Purchased cost at base conditions	K_1	3.3444
	K_2	0.2745
	K_3	- 0.0472
	$A_{HX,min}$	1 m^2
	$A_{HX,max}$	10 m^2
	Scaling factor	0.59
Material factor	B_1	1.74
	B_2	1.55

	$F'_m - CS - CS$	1
	$F'_m - CS - SS$	1.8
	$F'_m - CS - Ni$	2.65
	$F'_m - SS - Ni$	2.75
	$F'_m - Ni - Ni$	3.75
Pressure factor	C_1	0.6072
	C_2	- 0.912
	C_3	0.3327
BEC Actualization	Year	2001
	$CEPCI_{2001}$	394
	$CEPCI_{2010}$	551

A most appropriate design requires another information, the minimum number of heat exchanger that can be installed. A simple relationship relates this number with the process streams involved in the heat recovery (N_s), the number of utility streams used to close the energy balance of the system ($N_{s,u}$) and the number of streams that cross the pinch point (N_p) (Gassner 2010):

$$N_{HX,min} = \left(N_s + N_{s,u} - 1 \right) + \left(N_p - 1 \right)$$

Eq. 141

Unfortunately, although the number of devices can be easily obtained, the configuration of the network requires a further step that is too complicated to implement in a program. Usually, the definition of the network is made by hand, trying the different connections until the best one is achieved. However, in this work, it's required to analyses the behavior of a model at different operating conditions, so it's unthinkable to perform a correct design of the network for each case (especially during the Multi-Objective Optimization this should be really absurd). The discretization approach consists on the subdivision of the cumulative curves (resulting in the pinch analysis) in a number of subintervals equal to to the minimum number of connections found.

The discretization walk can be calculated from the number of connections and from the highest value of power in the cumulative:

$$\Delta \Phi = \frac{\Phi_{cumul,max}}{n_{conn}}$$

Eq. 142

Each subinterval will be considered as a heat exchanger where $\Delta \Phi$ is the net power exchanged and the limit temperatures are the inlet and outlet temperatures of the hot and

cold flows. To help the understanding of this method, in Figure B3 an example of discretization applied for a network involving 3 cold flows and a hot one and defined by a minimum number of connections is equal to 3 is given.

Although this procedure is clearly a simplification, its use does not cause sensible mistakes, on the contrary the investment cost applied on this network will be ever oversized but never underestimated: in fact this discretization generates a good network ever, because it's based on the minimum number of devices, but surely it's not the best one achievable with the appropriate procedure made by hand.

The only problem with the application of the heat exchanger's cost function on this network is that it's not possible a priori to define the global heat transfer coefficient of each heat exchanger, in fact, we cannot recognize at every subinterval the state of the flows involved. To solve this problem, it was necessary another simplification, based on the determination of the fraction f_{wg} of the power fluxes exchanged by gaseous flows (in our case the exhausts) respect to the total:

$$f_{wg} = \frac{\sum \Phi_{gas}}{\Phi_{tot}}$$

Eq. 143

This fraction corresponds, more or less, to the ratio of heat exchanged between gas and water, and then it is possible to estimate a constant value of the global heat transfer coefficient in this way:

$$U = f_{wg} \cdot U_{wg} + \left(1 - f_{wg}\right) \cdot U_{gg}$$

Eq. 144

A4.2 Estimation of the cost of biogas

The biogas that feeds the designed power plants is produced locally in treatment and purification units. The definition of its cost is not simple and, from literature, this aspect was not fully investigated for the reasons already given before. Due to the fact that it seems interesting to show the influence in the economic results of a biogas cost, a simplified procedure to estimate a reasonable value will be implemented in this appendix.

The procedure is based on the determination of a sale price of biogas so that the investment required for the construction of an anaerobic digester is recovered in 10 years.

First of all, it was necessary to find an appropriate reference for the assumption of a Total Plant Cost of the digester (Buratti et al. n.d.):

Table 96. Reference value for the calculation of the biogas cost.

Parameter	Value
TPC_r	1 M€
Daily biogas production	1640 m^3/d
annual operating hours	8000 h/y

With the daily production and the annual operating hours, it is possible to define the annual production (simply multiplying them). This parameter is used in a scaling method to define the TPC referred to an anaerobic digester that can produce, annually, the real biogas flow necessary to the large size plants:

$$TPC = TPC_r \cdot \left(\frac{V_{bio,y}}{V_{bio,y,r}}\right)^{sf}$$

Eq. 145

Where:

- $V_{bio,y}$ and $V_{bio,y,r}$ are the annual consumptions/productions of biogas in current and reference conditions
- sf is the scaling factor (here assumed equal to 0.7)

The construction of the cash flow is made in the same way that was defined for power plants, assuming annual costs for the maintenance equal to 2% of the TPC and an interest rate of 3%. If in 10 years, the sum of each annual cost (actualized) is equal to $C_{a,tot}$ and the annual production of biogas is $V_{bio,y}$, then the price cost, that has to be imposed to have the return of the investment, is:

$$c_{bio}\left[\frac{c€}{Nm^3}\right] = \frac{C_{a,tot}[€]}{V_{bio,y}[Nm^3]} \cdot 100$$

Eq. 146

Usually, the cost is expressed per unit of inlet energy, then, using the Lower Heating Value of biogas:

$$c_{bio}\left[\frac{c€}{kWh}\right] = \frac{C_{bio}\left[\frac{c€}{Nm^3}\right]}{LHV\left[\frac{kWh}{Nm^3}\right]}$$

Eq. 147

The cost obtained using the consumptions of the analyzed large size plant is:

$$c_{bio} = 14 \frac{c€}{Nm^3} = 2.63 \frac{c€}{kWh} = 3.62 \frac{c\$}{kWh}$$
<div align="right">Eq. 148</div>

A4.3 Subsidy scheme analysis

As the subsidy systems for the analyzed countries are differing substantially from each other, a brief outline for each is summarized in the following paragraphs. Countries considered in the analysis are Germany, Italy, and Finland.

Germany

In order to encourage the deployment of renewable energy sources in Germany, the German Renewable Energy Act was revised in 2012 and provides an elaborate subsidy system for electricity generated using biogas. The amount of subsidy which is paid in the form of a feed-in tariff depends on the substrate used for biogas production, the installed electric power capacity as well as the full load hours of the plant. However, the granted subsidy is guaranteed to be paid for the duration of 20 years and does not vary during the overall payment period (Anon n.d.). Table 97 lists the different levels of feed-in tariffs for the different capacity and substrate classes.

As mentioned above, the amount of subsidy granted is depending on the used substrate which is why the German Renewable Energy Act stipulates a set of substrate classifications. Although this list is extensive, the following classification gives a condensed summary of substrate classes considered in the law:

a) Substrate Class 0: receives only basic compensation; agricultural products for human consumption;
b) Substrate Class I:receiving basic compensation plus bonus according to Class I; wheat, Grasses;
c) Substrate Class II: receiving basic compensation plus bonus according to Class II; solid manure;
d) Landfill Gas;
e) Sewage Sludge Gas;
f) Liquid manure of small plants;
g) Biological waste: garden and park waste, household waste, biological waste of markets; only receives the specified subsidy;

Table 97. German biogas subsidy system

Renewable Energy	Type	Rated Power [kW$_{el}$]	Base Incentive [ct/kWh$_{el}$]
Biogas	Basic Subsidy	1-150	14.01
		150-500	12.05
		500-5,000	10.75
		5,000-20,000	5.88
	Subsidy Bonus Substrate Class I	1-500	6.00
		500-5,000	2.50
	Subsidy Bonus Substrate Class II	1-500	8.00
		500-5,000	6.00
Landfill Gas		1-500	8.47
		500-5,000	5.80
Sewage Sludge Gas		1-500	6.69
		500-5,000	5.80
Biogas from Liquid Manure		1-75	24.50
Biogas from Biological Waste		1-500	15.68
		500-20,000	13.72

In addition to the substrate classifications above, the plant power output is used to determine the accurate amount of subsidy received. Hereby, not the installed capacity is used, but rather a rated plant power which is calculated via the following equation:

$$P_{rated} = \frac{P_{installed} * \tau_{FLH}}{8760} \qquad \text{Eq. 149}$$

In which can be defined:

- P_{rated}: rated power plant capacity used for subsidy calculation [kWel]
- $P_{installed}$: installed power plant capacity [kWel]
- τ_{FLH}: full load hours of plant [hrs/y]

The amount of subsidy is then determined using the rated power output of the plant and the type of substrate used. Hereby it has to be pointed out, that an additional bonus can be obtained by upgrading the biogas to grid quality and injecting it into the natural gas

network. Moreover, the amount of subsidy received for each kWh$_{el}$ supplied to the grid increases, if the plant is certified as a combined heat and power plant (Anon n.d.)

Italy

The Italian subsidy law exhibits certain similarities compared to the German law: the subsidy in the form of a feed-in tariff for electricity generated using biogas is paid for the duration 20 years. Also, to determine the amount of subsidy, the installed plant electric power output and substrate are deciding parameters. Below is a summarized list of substrate classification applied by the Italian subsidy law (Ministero dello Sviluppo Economico 2012):

a) Biological products: agricultural products for human consumption such as wheat, corn, barley, oat, vegetables and fruit products as well as grasses;
b) Sub-products of biological origin including:
   - *Sub-products of animal origin*: manure (liquid and solid), meat and bone meal, carcasses, blood and all animal sub-products, food industry waste, sea animals sub-products;
   - *Sub-products from agriculture, breeding, and green area management*: manure, straw, hay, waste from forestry, trees and prunings, residuals from fields;
   - *Sub-products from food and agro-food industry*: sub-products of vegetable, fruit, cereal, bread, beer, coffee, oil and algae processing;
   - *Sub-products from industry*: sub-products from wood industry for furniture production;
c) Waste with a certain biodegradable fraction: urban waste from waste collection, special waste from mechanical waste treatment and separation, secondary solid fuel from urban waste, sanitary and veterinary waste, old tires;
d) None collected waste which is different of type c) and organic fraction of municipal waste;
e) Landfill Gas;
f) Sewage Sludge Gas;

Depending on biomass substrate listed above, the subsidies shown in Table 98 can be claimed accordingly. Hereby, it has to be pointed out, that the amount of subsidy is determined by the following correlation:

- Feed-in tariff for plants with a capacity < 1 MW$_{el}$, is calculated using the following equation:

$$T_{Subsidy} = T_{Basic} + T_{Bonus}$$

Eq. 150

- Feed-in tariff for plants with a capacity > 1 MW$_{el}$, is calculated using the following equation:

$$T_{Subsidy} = T_{Basic} + T_{Bonus} - T_{Grid} \qquad \text{Eq. 151}$$

In which can be defined

- T$_{subsidy}$ total amount of subsidy received [€/MWhel]
- T$_{basic}$ basic subsidy for respective substrate [€/MWhel]
- T$_{bonus}$ bonus on top of T$_{Basic}$ for CHP plants [€/MWhth]
- T$_{grid}$ grid electricity price [€/MWh$_{el}$]

In comparison to the German subsidy system, the Italian one holds certain specificities. The process of requesting a subsidy for a biogas plant on the plant size:

- Plants with an installed capacity < 100 kW$_{el}$ the plant owner can directly apply for admission to the feed-in tariff;
- Plants of the capacity between 100 kW$_{el}$ and 5 MW$_{el}$ have to inscribe in a special register with limited available installation capacity;
- Plants with a capacity of > 5 MW$_{el}$ public "auction" of available subsidies;

These application processes are connected to a maximum limit of available plant installations. This means that as soon as the amount of installed biogas plant capacities reaches the limit, no further subsidy is granted for any additional plant. In addition to the bonus for heat generation, a further bonus is granted for N$_2$ recovered from the digested biomass for fertilizer production.

Table 98. Italian biogas subsidy system.

Renewable Energy	Type	Power [kW$_{el}$]	Base Incentive [€/MWh$_{el}$]	High-Efficiency CHP [€/MWh$_{th}$]
Biogas	Biological products type a)	1-300	180	40
		300-600	160	40
		600-1'000	140	40
		1'000-5'000	104	40
		> 5'000	91	40
	Biological subproducts and waste of	1-300	236	10
		300-600	206	10
		600-1'000	178	10

	type b) and d)	1'000-5'000	125	10
		> 5'000	101	10
	MSW c)	1-600	216	10
		600-1'000	216	10
		1'000-5'000	109	10
		> 5'000	85	10
Landfill Gas		1 -1'000	99	-
		1'000-5'000	94	-
		> 5'000	90	-
Sewage Sludge Gas		1-1'000	111	-
		1'000-5'000	88	-
		> 5'000	85	-

Finland

Compared to the subsidy schemes in Germany and Italy the Finish system is formulated in a more compact way. A biogas plant operator can decide to either receive a fixed feed-in tariff or a subsidy on plant investment costs. Plants with a rated power output of > 100 kVA are eligible for a fixed price of electricity amounting to 83.50 €/MWh$_{el}$. The subsidy will cover the difference between the actual grid electricity price and the guaranteed price. In addition to this, 50 €/MWh$_{th}$ for heat generation are granted. In this case, total plant efficiency has to be > 50 % for plants with a power output of < 1 MW$_{el}$ and > 75 % for plants with an electric capacity > 1 MW$_{el}$, respectively. The feed-in tariff is granted for a maximum period of 12 years as long as the total installed power of biogas plants does not exceed 19 MVA (Anon n.d.). If a biogas plant is not applicable for the feed-in tariff, an application for a subsidy on investment costs of the plant which amounts to a maximum of 40 % can be requested (Anon n.d.). The actual amount of investment cost subsidy depends on the applied technologies and the local authorities. Table 99 summarizes the Finish biogas subsidy system.

Table 99. Finish biogas subsidy system.

Feed-In Tariff				
Plant Capacity	Subsidy Duration	Amount	CHP Bonus	
100 kVA	up to 12 years	83.50 €/MWh$_{el}$	50 €/MWh$_{th}$	
			< 1 MW$_{el}$	>1 MW$_{el}$

			$\eta_{tot} > 50\ \%$	$\eta_{tot} > 75\ \%$
Investment Costs Subsidy				
Maximum of 30 % - 40 % of Investment Costs				
Typical Values 15 % – 20 % of Investment Costs				

Appendix 5 - OSMOSE optimization tool

As will be discussed in the methodology chapter, one of the main tool used in this work is OSMOSE (Palazzi et al. 2010), a Matlab-based package developed by EPFL (Anon n.d.) that allows to create an interface between Matlab itself and a process modelling software (e.g., Aspen Plus® or Vali®). In this work, OSMOSE is employed to perform thermal integration of hot/cold streams via pinch analysis methodology, sensitivity analysis, and MOO optimizations. The effectiveness of this tool has been proved in other scientific reports where complex energy systems were studied and optimized. For example, the software (Morandin et al. 2011) has been used to optimize the design conditions of a sugarcane process integrated to a CHP system fuelled by bagasse (main by-product from juice extraction) or, in (Palazzi et al. 2007), it allowed the optimization of different SOFC systems from a thermo-economic point of view.

Each plant configuration has been modeled with Aspen Plus®. Its library does not include fuel cells. For this reason, it was necessary to integrate the electrochemical model of the SOFCs: the relationships used were those implemented by Van Herle et al. for an SOFC co-generator fuelled by biogas (Van Herle et al. 2003). This electrochemical model has been validated in its original form: only, some material parameters have been updated with current values that are referred to the actual state-of-art of SOFCs technology and materials.

All the investigated power plant configurations include a heat exchanger network (HEN) designed in order to achieve the highest internal energy recovery. The definition of the number of heat exchangers and their physical location in the plant layout requires the implementation of a more sophisticated process that was not performed.

Furthermore, sensitivity analysis and MOO could not be made easily with this software. For these reasons, OSMOSE has been here adapted to provide an interface between Matlab and Aspen Plus®. This tool was then used to implement a method for the construction of a proper heat exchanger network and to perform both sensitivity analysis and MOOs. In Figure 281 is represented, in a flow chart, the approach based on the interface between Aspen Plus® and OSMOSE that is adopted to study the different SOFC power plants designed in this work. From the chart can be recognized:

- A first phase dedicated to the modelling of each system and to the definition of the main design variables and performance parameter to be controlled: the models have to be defined in Aspen Plus® with Fortran code, because this is the only programming language which allows creating an interface between Aspen Plus® and OSMOSE.

-   Once the systems have been designed and the proper interface has been implemented, sensitivity and MOO analysis can be performed in Matlab.
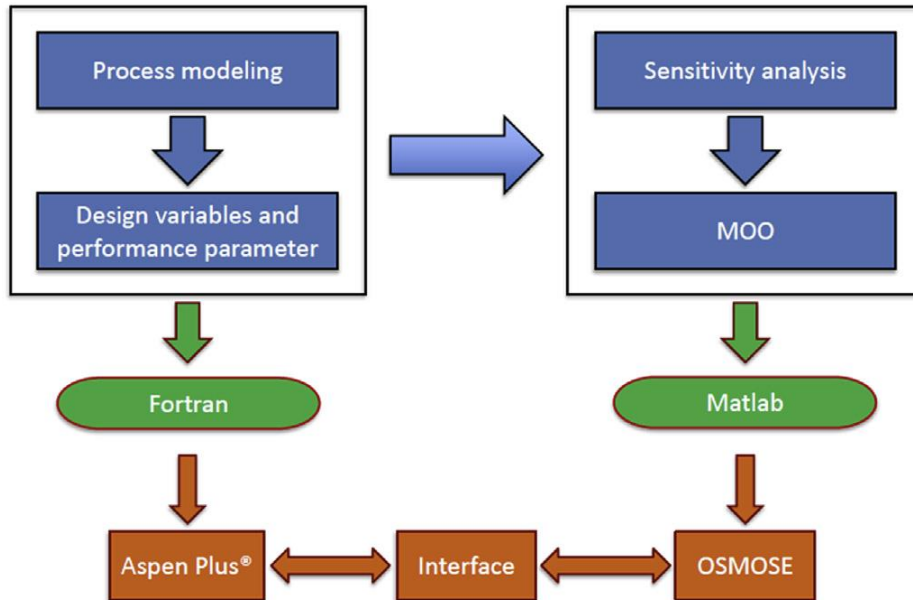
Figure 281. Interface between Aspen Plus® and OSMOSE.

In this work, five different plant configurations were studied for the large size plants and, for each one of them, the plant layout has been defined. During each plant simulation at a given operating point, heat and cold streams are identified. Subsequently, the HEN design is established based on a discretization of the resulting composite curve (with hot and cold streams) that allows determining the overall heat exchange area required and the number of heat exchangers necessary to minimize the external energy requirement. A proper HEN design can be implemented based on one of the following criteria (Linnhoff & Hindmarsh 1983):

-   Minimum (external) utility usage
-   Minimum overall surface area requirement
-   Minimum number of units (heat exchangers)
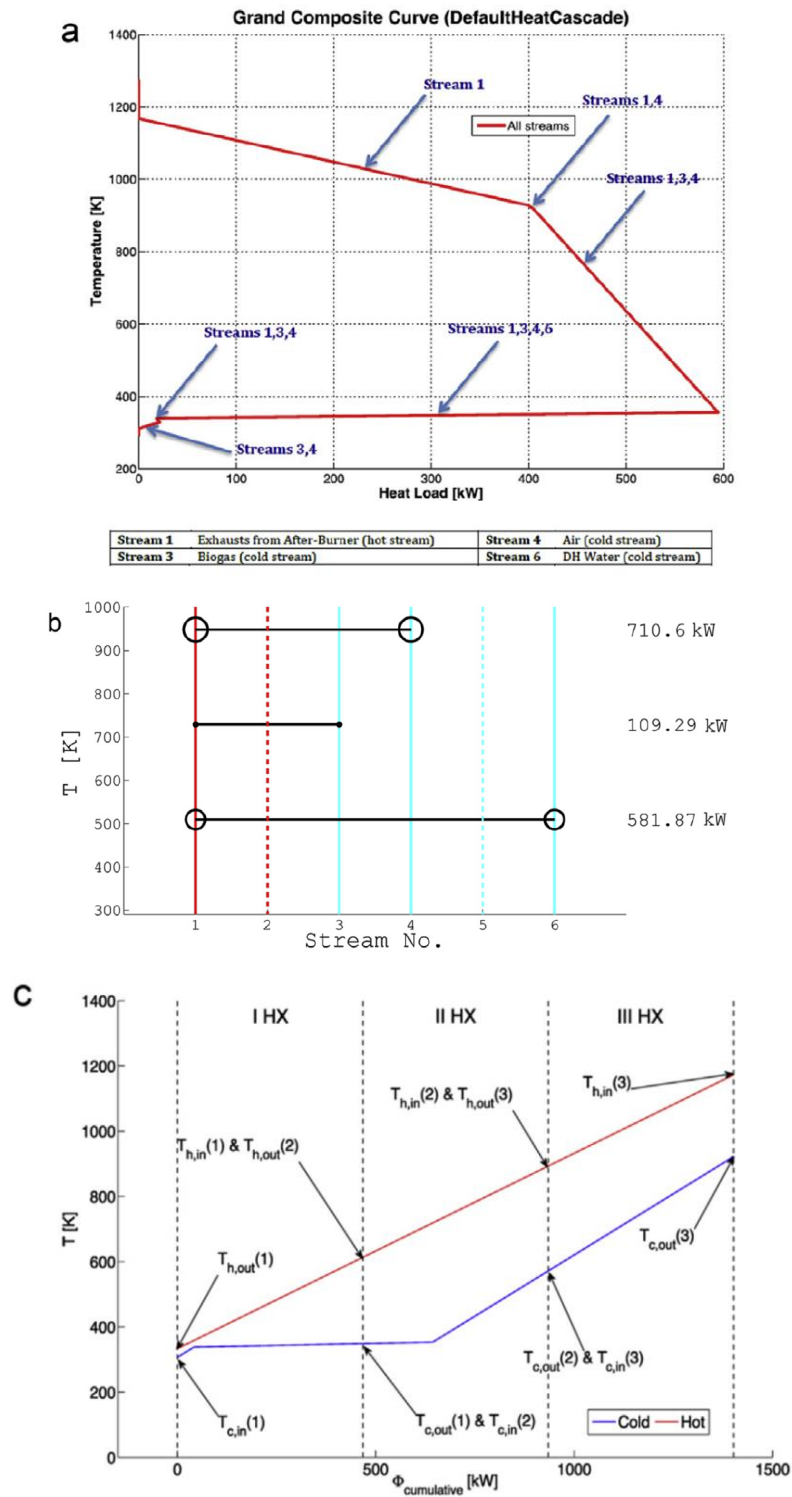
Figure 282. a: Grand Composite Curve (A-VENT). b: Graphical representation of the Heat Exchanger Network (A-VENT). c: Discretized cumulative curve (A-VENT).

Here the design is based on the minimization of the number of heat exchangers.

The configuration of an efficient HEN does not depend just on the number heat streams exchanged, but it is also related to the design of the whole plant and to its specifications. For this reason, it was necessary to adopt a different approach, based on the discretization of the cumulative curves obtained from the pinch analysis.

OSMOSE allows activating an EI (Energy Integration) mode which performs a pinch analysis and gives the results needed to build the composite curves. In Figure 282-a an example of the Grand Composite curve achieved by the implementation of the EI function is shown. This example was extrapolated from one of the simulations performed for the A-VENT configuration. OSMOSE also produces a graphical representation of the matching between hot and cold streams. In Figure 282-b an example is shown that refers to the same simulation of Figure 282-a. Utility and process streams involved are the listed below:

- Stream 1 is the exhaust gas from the afterburner that requires cooling
- Stream 2 is the utility stream for hot water (not needed here)
- Streams 3 and 4 are biogas and cathode air, respectively, that required pre-heating
- Stream 5 is the utility stream of cold water (not needed here)
- Stream 6 is the water district heating

The EI, as shown in Figure 282-b, is able to provide a representation of the matching between hot and cold streams. However, this procedure requires a high computational cost when applied for each simulation run, and it does not provide the heat exchangers properties necessary for the definition of the HEN. This is another reason why the approach based on the discretization of the cumulative curves was chosen instead. First of all, the composite curves have been built from the results of the EI just to perform the pinch analysis. The minimum number of the heat exchanger was then defined according to Eq. 152 (Gassner 2010):

$$N_{HE,min} = (N_S + N_{S,u} - 1) - (N_P - 1) \qquad \text{Eq. 152}$$

where:

- $N_{HE,min}$ is the minimum number of heat exchangers
- N_S is the number of process streams involved in the heat recovery network
- $N_{S,u}$ is the number of utility streams involved to close the energy balance of the system
- N_P is the number of streams crossing the pinch point

The composite curves are then discretized in a number of subintervals, equal to $N_{HE,min}$, that is used to estimate the properties of the heat exchangers defined for the best network achievable. This approach is conservative because the real network achievable from the minimization of the number of heat exchangers is more efficient than this one approximated. In Figure 282-c an example of how the composite curves are discretized in subintervals, each one corresponding to a heat exchanger, is shown. This example has been extrapolated from the same simulation performed for the A-VENT configuration, with the results shown in Figure 282-a and b. The red and blue curves correspond respectively to the hot and cold stream curves while the boundaries of each subinterval give the inlet and outlet temperatures.

From the resulting properties, it is possible to size the heat exchangers using the following equations.

$$LMTD = \frac{\left(\left(T_{h,i} - T_{c,o}\right) - \left(T_{h,o} - T_{c,i}\right)\right)}{\ln\left(\dfrac{T_{h,i} - T_{c,o}}{T_{h,o} - T_{c,i}}\right)} \qquad \text{Eq. 153}$$

$$A_{HX} = \frac{\dot{Q}_{net}}{U \cdot LMTD} \qquad \text{Eq. 154}$$

where:

- *LMTD* is the logarithmic mean temperature difference
- $T_{h,i}, T_{h,o}, T_{c,i}, T_{c,o}$ T [°C] are the inlet and outlet temperatures of the hot and cold flows
- A_{HX} [m^2] is the heat exchanger surface
- $\dot{Q}_{net}$ [kW] is the net thermal power exchanged
- *U* [W/m^{2}K] is the global heat transfer coefficient

The methodology, used for the costing of the heat exchanger network and the sizing of each device, includes correction factors (>1) to account for the materials required (Ni alloy, CS, SS,) to build the HX depending on its operating temperature (that depends on the inlet and outlet temperatures of hot and cold streams). Combinations of different materials are also possible.

Acknowledgments

E come accade con ogni percorso che volge verso il termine, è giusto fermarsi a ringraziare chi ne ha preso parte e chi lo ha reso tale.

Grazie innanzitutto ai miei relatori. Grazie al professor Santarelli, che ama le montagne come me e che mi ha insegnato a mettere la passione nel proprio lavoro e a puntare sempre un po' più in alto, che ha sempre creduto in me dandomi opportunità e responsabilità. Grazie ad Andrea, che mi ha seguita giorno per giorno in tutti i miei anni al Poli, a partire dalla tesi, che mi ha insegnato gran parte di quel che oggi posso dire di sapere: grazie per l'esempio e per i momenti condivisi. Grazie a tutto il gruppo STEPS e agli amici del Poli, chi è solo passato di qua e chi c'è sempre stato e ci sarà anche dopo, grazie per i tre anni in compagnia. Grazie allo zio palestrato dei Bauducchi, all'egregio Domenico e al buon Papu, grazie ad Arpilio Mascarpone, a Raffy e Laura, al buon Giglio, a Marco, a Matteo, Luiggggi e Annalisa e a tutti quelli che ho dimenticato. Grazie a chi ha passato qui solo un periodo ma sufficiente a donarmi qualcosa e a farmi conoscere nuovi mondi senza dover viaggiare: grazie a Paruyr, a Yongchun, a Mahrokh e ad Ali. E grazie a tutti i tesisti che hanno lavorato con me: a Bernhard, a Rosamaria, a Marco e a Giuseppe.

Grazie poi a tutte le persone con cui ho avuto la possibilità di collaborare in questi tre anni: grazie a Claudia che mi ha sempre supportata e ha riso con me durante i viaggi, grazie a tutte le persone incontrate in SMAT, grazie a tutti le persone incontrate nell'ambito dei progetti regionali ed europei, con cui ho avuto modo di condividere esperienze scientifiche e divertenti momenti insieme: da ognuno di loro ho certamente imparato qualcosa.

"*Ogni persona che incontri è migliore di te in qualcosa; in quella cosa impara.*"

E poi grazie a tutti quelli che al Poli forse non sono mai venuti, ma che hanno reso meno pesanti le ore di lavoro con la loro presenza nella mia vita, quella vera. Grazie alla mia famiglia, che mi ha sempre appoggiata nel fare questo lavoro che forse non ha ancora capito bene cosa sia, che mi ha donato quest'anima agricola che mi porto dietro ogni giorno e di cui vado fiera, grazie a tutti: ai miei genitori, ai nonni, agli zii e cugini, grazie a Cami e grazie ad Albi, che è molto più di un fratello. Grazie a Fra, che ha condiviso questo percorso con me dall'inizio dalla fine, supportandomi e sopportandomi, grazie perché mi ha insegnato che la vita vera non è davanti al computer né in ufficio, e dev'essere al primo posto, sempre. Grazie perché c'è sempre stato e so che ci sarà.

Grazie agli amici di sempre, quelli che si sono già beccati tre ringraziamenti in dieci anni e non ne potranno più, ma che so apprezzeranno come sempre: grazie alle amiche di sempre, Giulia Alessia Ilaria e Ilaria, che stanno arrivando ai trenta insieme a me, fianco a fianco. Grazie ai Cisti, alla sexyssima Agne, a Noem e Fede #sposi, a Zampetta, alla lady Giulz, a Zupy, a Bea, ad Eri&Je, a Tabby e Cioccio&Momo, grazie perché so che comunque vada la vita potrò sempre trovare qualcuno di voi che si trovi alle 9.30 ai Cisti per una birra e due chiacchiere. Grazie infine a tutti quelli di cui non scrivo il nome ma che mi hanno regalato un sorriso!

Grazie a chiunque ha reso più sereni e allegri questi tre anni, o anche solo un'ora. Grazie perché il dottorato è stata un'esperienza importante, dove ho imparare qualcosa da ogni persona incontrare nel percorso, e sommando ogni contributo alla fine ho imparato molto, ma soprattutto ho imparato che fare quel che ci piace è l'unico modo per 'fare bene', 'fare del bene', e farlo col sorriso.

"*Un pianeta migliore è un sogno che inizia a realizzarsi quando ognuno di noi decide di migliorare se stesso*"

Reference

2G, Combined Heat & Power Generation. Available at: http://www.2-g.com/en/.

4th Energy Wave, 2016. *The Fuel Cell and Hydrogen Annual Review, 2016*, Available at: http://www.4thenergywave.com/#!blank-1/c1p8.

Adani, F., 2008. I fattori che rendono ottimale la razione per il digestore. *L'informatore Agrario*.

Advanced Power and Energy Program, 2012. TRI-GENERATION FROM BIOGAS. *Advanced Power and Energy Program.* Available at: http://www.apep.uci.edu/3/research/partnership_TRI-GEN.aspx [Accessed January 5, 2017].

Aebiom, 2009. A Biogas Road Map for Europe. , p.22.

Alptekin, D.G.O., 2014a. Novel sorbent to clean biogas for fuel cell combind heat&power systems. In *US DOE Advanced Manufacturing Office Peer Review Meeting*.

Alptekin, D.G.O., 2014b. Sulfatrap Sorbents for Effective Sulfur Removal for Fuel Cells: Dimethyl Sulfide, Mercaptan and COS Adsorption. In *AIChE 2014 Annual Meeting*.

Alptekin, G. et al., 2011. Sulfur Removal Sorbents for Fuel Cell Applications. In *North American Catalysis Society*.

Anon, Aerodyne Alloys - Nickel Alloy properties - Products section. Available at: http://www.aerodynealloys.com/.

Anon, AVL Electrification Solutions website. Available at: https://www.avl.com/home.

Anon, Bloomenergy official website.

Anon, Bundestag der Bundserepublik Deutschland (2002), Gesetz für die Erhaltung, die

Modernisierung und den Ausbau der Kraft-Wärme-Kopplung: KWKG 2002, BGBl. I S. 1092.

Anon, Bundestag der Bundserepublik Deutschland (2008), Gesetz für den Vorrang Erneuerbarer Energien: EEG, BGBl. I S. 2074.

Anon, Canta Forda Computer Laboratory. Available at: http://www.cfcl.com/.

Anon, 2006. Decreto Legislativo 3 aprile 2006, n. 152 - Norme in materia ambientale. Available at: http://www.camera.it/parlam/leggi/deleghe/06152dl.htm.

Anon, 2016. DEMOSOFC project official website. Available at: www.demosofc.eu [Accessed December 20, 2015].

Anon, Ecole Polytechnique Federale de Lausanne (EPFL). Available at: www.epfl.ch.

Anon, Enerwater EU project official website. Available at: http://www.enerwater.eu.

Anon, *EUROSTAT Energy price statistics*, Available at: http://ec.europa.eu/eurostat/statistics-explained/index.php/Energy_price_statistics.

Anon, Hexis official website. Available at: http://www.hexis.com/en/hexis-ag.

Anon, 2014. Internal communication with EPFL on updated data from lab test.

Anon, Landfill biogas.

Anon, Plant Cost Index - Chemical Engineering. Available at: http://www.chemengonline.com/pci-home.

Anon, SMAT, Società Metropolitana Acque Torino S.p.A., Turin, IT. Available at: http://www.smatorino.it/.

Anon, 2012. *SOFCOM Project: Analysis of the Operation of the SMAT (Torino) Sewage Plant and Record of Historical Data. Deliverable 4.1*,

Anon, SOLIDpower official webiste. Available at: http://www.solidpower.com/en/home/.

Anon, Suomen Eduskunta (2010), Laki uusiutuvilla energialähteillä tuotetun sähkön tuotantotuesta, 1396/2010.

Anon, Suomen Eduskunta (2012), Valtioneuvoston asetus energiatuen myöntämisen yleisistä ehdoista, 1063/2012.

Anon, Universal Industrial Gases Inc. - Industrial Gases Production, Supply Systems and Services. Available at: http://www.uigi.com/.

Antonini, M. et al., 2012. Endothermic reaction unit and steam reforming device

comprising   this   reaction   unit.   Available   at:
https://www.google.com/patents/EP2519342A1?cl=en.

Anttila, P. et al., 2013. *SOFCOM Project No. 278798 - Deliverable: Fuel Cleaning Guidelines for Implementation of Proofs-of-Concepts, SOFC CCHP with Poly-Fuel: Operation and Maintenance*,

Appels, L. et al., 2011. Anaerobic digestion in global bio-energy production: Potential and research challenges. *Renewable and Sustainable Energy Reviews*, 15(9), pp.4295–4301. Available at: http://dx.doi.org/10.1016/j.rser.2011.07.121.

De Arespacochaga, N., Valderrama, C., Peregrina, C., Mesa, C., et al., 2015. Evaluation of a pilot-scale sewage biogas powered 2 . 8 kW e Solid Oxide Fuel Cell : Assessment of heat-to-power ratio and in fl uence of oxygen content. *Journal of Power Sources*, 300, pp.325–335. Available at: http://dx.doi.org/10.1016/j.jpowsour.2015.09.086 [Accessed January 10, 2017].

De Arespacochaga, N., Valderrama, C., Peregrina, C., Hornero, A., et al., 2015. On-site cogeneration with sewage biogas via high-temperature fuel cells : Benchmarking against other options based on industrial-scale data. *Fuel Processing Technology*, 138, pp.654–662. Available at: http://dx.doi.org/10.1016/j.fuproc.2015.07.006 [Accessed January 10, 2017].

Aresta, M., Dibenedetto, A. & Angelini, A., 2013. The changing paradigm in CO2 utilization. *Journal of CO2 Utilization*, 3–4, pp.65–73. Available at: http://dx.doi.org/10.1016/j.jcou.2013.08.001.

Arnold, M., 2009. *Reduction and monitoring of biogas trace compounds*,

Bayerisches Institut für Angewandte, 2003. *Untersuchungen zum Einsatz von Oxidationskatalysatoren an landwirtschaft- lichen Biogas-Verbrennungsmotoren*,

Bayr, S., 2014. *Biogas Production from Meat and Pulp and Paper Industry Suvi Bayr Biogas Production from Meat and Pulp and Paper Industry By-Products*,

Bazmi, A.A. & Zahedi, G., 2011. Sustainable energy systems: Role of optimization modeling techniques in power generation and supply—A review. *Renewable and Sustainable Energy Reviews*, 15(8), pp.3480–3500.

Becker, W.L., Braun, R.J. & Melaina, M.W., 2011. Design and technoeconomic performance analysis of a 1 MW solid oxide fuel cell polygeneration system for combined production of heat , hydrogen , and power. , (March 2016).

Benito, M. et al., 2007. Development of biogas reforming Ni-La-Al catalysts for fuel cells. *Journal   of   Power   Sources*,   169(1),   pp.177–183.   Available   at: http://linkinghub.elsevier.com/retrieve/pii/S0378775307002042   [Accessed November 18, 2016].

Berhad, D., 2009. Annual Report | 2009. , pp.1–136.

Bilek, A., 2011. The German Biogas Experience : Opportunities and Key Experiences for Future US Deployment.

Bingemer, H.G. & Crutzen, P.J., 1987. The production of methane from solid wastes. *Journal of Geophysical Research*, 92(1), p.2181.

Biocombustibili, P.N., Mappatura delle biomasse anaerobica in Alto Adige avviabili a digestione - Relazione conclusiva - Partner Ministero delle Politiche Agricole , Agrarie e Forestali. , pp.1–113.

Bloomenergy, Energy Server 5 Technical Datasheet. , pp.5–6.

Bonacina, A., Cavallini, A. & Mattarolo, L., 1989. *Trasmissione del calore* CLEUP Editore, ed.,

Brouwer, J., Bekemohammadi, R. & Margalef, P., 2012. Tri-Generation of Hydrogen, Heat and Power From a High Temperature Fuel Cell. In *2012 AIChE Annual Meeting*. Available at: https://www3.aiche.org/Proceedings/Abstract.aspx?PaperID=261312 [Accessed January 5, 2017].

Buit, L. et al., 2011. CO2 EuroPipe study of the occurrence of free water in dense phase CO2 transport. *Energy Procedia*, 4, pp.3056–3062. Available at: www.elsevier.com/locate/procedia [Accessed December 29, 2016].

Buratti, C., Barbanera, M. & Fantozzi, F., Studio di fattibilità di un impianto di digestione anaerobica nel comune di castiglione del lago.

California Stationary Fuel Cell Collaborative (CaSFCC), 2016. Stationary Fuel Cell Installations in California. Available at: http://casfcc.org/STATIONARY_FC_MAP/ [Accessed January 10, 2017].

Caramia, M. & Dell'Olmo, P., 2008. *Multi-objective Management in Freight Logistic. Chapter 2: Multi-objective Optimization* Springer, ed.,

Chen, C.-Y. et al., 2011. Cultivation, photobioreactor design and harvesting of microalgae for biodiesel production: A critical review. *Bioresource Technology*, 102, pp.71–81.

Chen, Y., Adams II, T.A. & Arton, P.I., 2011. Optimal design and operation of static energy polygeneration systems. *Industrial & Engineering Chemistry Research*, 50(5099–5113), p.319. Available at: http://dspace.mit.edu/handle/1721.1/79192.

Chen, Y., Adams II, T.A. & Barton, P.I., 2011. Optimal design and operation of flexible energy polygeneration systems. *Industrial & Engineering Chemistry Research*, 50, pp.4553–4566. Available at: http://dspace.mit.edu/handle/1721.1/79192.

Chicco, G. & Mancarella, P., 2008. A unified model for energy and environmental

performance assessment of natural gas-fueled poly-generation systems.

Chicco, G. & Mancarella, P., 2009. Distributed multi-generation: A comprehensive view. *Renewable and Sustainable Energy Reviews*, 13(3), pp.535–551.

Chicco, G. & Mancarella, P., 2007. Trigeneration primary energy saving evaluation for energy planning and policy development. *Energy Policy*, 35, pp.6132–6144.

Chick, L.A. et al., 2013. SOLID OXIDE FUEL CELL STEAM REFORMING POWER SYSTEM.

Chiodelli, G. & Malavasi, L., 2013. Electrochemical open circuit voltage (OCV) characterization of SOFC materials. *Ionics*, 19, pp.1135–1144.

Chiodo, V. et al., 2012. Analysis of biogas reforming process for molten carbonate fuel cells. *Journal of Power Sources*, 206, pp.215–221. Available at: http://dx.doi.org/10.1016/j.jpowsour.2012.01.114.

Chiu, S.-Y. et al., 2008. Reduction of CO2 by a high-density culture of Chlorella sp. in a semicontinuous photobioreactor. *Bioresource Technology*, 99, pp.3389–3396.

Ciafani, S., Zampetti, G. & Mancini, M., 2013. Ridurre e riciclare prima di tutto.

Colonna, N. et al., 2009. La stima del potenziale di biogas da biomasse di scarto del settore zootecnico in Italia.

Convion Fuel Cell Systems, 2016. Convion product focus. Available at: http://convion.fi/.

Copeland, C., 2014. *Energy-Water Nexus: The Water Sector's Energy Use*,

Cuéllar-Franca, R.M. & Azapagic, A., 2015. Carbon capture, storage and utilisation technologies: A critical analysis and comparison of their life cycle environmental impacts. *Journal of CO2 Utilization*, 9, pp.82–102.

Curletti, F. et al., 2015. Large size biogas-fed Solid Oxide Fuel Cell power plants with carbon dioxide management : Technical and economic optimization. *Journal of Power Sources*, 294, pp.669–690.

Cvetković, S. et al., 2014. Potentials and status of biogas as energy source in the Republic of Serbia. *Renewable and Sustainable Energy Reviews*, 31, pp.407–416.

Daw, J. et al., 2012. *Energy Efficiency Strategies for Municipal Wastewater Treatment Facilities*,

Day, D., 2014. A demonstration project at Orange County Sanitation District tests the viability of using a fuel cell to generate electricity, hydrogen fuel and heat. *TPO - Treatment Plant Operator Magazine*. Available at: http://www.tpomag.com/editorial/2014/07/sustainable_operations_three_for_one

[Accessed January 5, 2017].

Det Norske Veritas, 2010. *RECOMMENDED PRACTICE DNV-RP-J202: DESIGN AND OPERATION OF CO2 PIPELINES*,

Directive, C.C., 1991. Directive 91/676/CEE concerning the protection of waters against pollution caused by nitrates from agricultural sources. *Official Journal of the European Communities*, pp.1–8.

DOE NETL, 2011a. Analysis of Integrated Gasification Fuel Cell Plant Configurations.

DOE NETL et al., 2011. *Analysis of Natur al Gas Fuel Cell Plant Configurations*,

DOE NETL, 2011b. *Cost Estimation Methodology for NETL Assessments of Power Plant Performance*,

DOE NETL & Thjissen, J., 2007. The Impact of Scale-Up and Production Volume on SOFC Manufacturing Cost.

Dong, L., Liu, H. & Riffat, S., 2009. Development of small-scale and micro-scale biomass-fuelled CHP systems – A literature review. *Applied Thermal Engineering*, 29(11), pp.2119–2126.

Dortmundt, D. & Doshi, K., 1999. *Recent Developments in CO2 Removal Membrane Technology*,

Drago, D., 2017. *The sulfur issue in fuel cell based cogenerative systems*. Politecnico di Torino.

Du, W. & Parker, W., 2011. Modeling volatile organic sulfur compounds in mesophilic and thermophilic anaerobic digestion of methionine. *Water Research*, 46(2), pp.539–546. Available at: http://dx.doi.org/10.1016/j.watres.2011.11.043.

E4Tech, 2015. *The Fuel Cell Industry Review*,

Eea, 2001. Biodegradable waste in landfills. , pp.1–4.

Environmental Protection Agency (EPA), 2013. *Energy Efficiency in Water and Wastewater facilities - A guide for developing and implementing greenhouse gas reduction programs*,

Ericsson, K., Nilsson, L.J. & Nilsson, M., 2011. New energy strategies in the Swedish pulp and paper industry-The role of national and EU climate and energy policies. *Energy Policy*, 39(3), pp.1439–1449.

Erler, R., Sustainable Biogas Potentials in Germany.

Eta Florence & Environment Park, National Report on current status of biogas production

– Italy.

European Commission, 2016. *Implementing the Paris Agreement: Progress of the EU towards the at least -40% target*,

European Environment Agency, 2015. Urban Waste Water Treatment maps. Available at: http://www.eea.europa.eu/data-and-maps/uwwtd/interactive-maps/urban-waste-water-treatment-maps-1 [Accessed January 12, 2017].

European Environmental Agency (EEA), 2007. *Estimating the environmentally compatible bioenergy potential from agriculture*, Available at: http://www.eea.europa.eu/publications/technical_report_2007_12.

European Environmental Agency (EEA), 2013. *Managing municipal solid waste*,

European Technology Platform for Zero Emission Fossil Fuel Power Plants, 2012. *Biomass with CO2 Capture and Storage (Bio-CCS)*,

FAOstat, FOOD AND AGRICULTURE ORGANIZATION OF THE UNITED NATIONS. Available at: http://faostat.fao.org/.

FCCC United Nations, 2015. *Adoption of the Paris Agreement under the United Nations Framework Convention on Climate Change, FCCC/CP/2015/L.9/Rev.1*,

Fischer, C., 2013. Municipal waste management in Germany. , (February).

Fisher, B.S., N. Nakicenovic, K. Alfsen, J. Corfee Morlot, F. de la Chesnaye, J.-Ch. Hourcade, K. Jiang, M. Kainuma, E.L.R. & A. Matysek, A. Rana, K. Riahi, R. Richels, S. Rose, D. van Vuuren, R.W., 2007. Issues related to mitigation in the long term context. In C. Cambridge University Press, ed. *Climate Change 2007: Mitigation. Contribution of Working Group III to the Fourth Assessment Report of the Inter-governmental Panel on Climate Change*. Cambridge University Press.

Fogler, H.S. & Gurmen, M.N., Chapter 11: External Diffusion Effects on Heteregeneous Reactions. In *4th Edition Elements of chemical reaction engineer*. Available at: http://umich.edu/~elements/index.htm.

Foreest, F. Van, 2012. *Perspectives for biogas in Europe*, Available at: http://www.oxfordenergy.org/wpcms/wp-content/uploads/2012/12/NG-70.pdf.

Fuel Cell Energy, 2012. *Fuel Cell Power Plants: Biofuel Case Study – Tulare, CA (DOE-NREL Workshop)*,

FuelCellEnergy, 2017. U.S. Deployment Programs - Fuel Cell Energy. Available at: http://www.fuelcellenergy.com/applications/financial-incentives/u-s-incentives/ [Accessed January 11, 2017].

Galanti, L. & Massardo, A.F., 2011. Micro gas turbine thermodynamic and economic

analysis up to 500 kWe size. *Applied Energy*, 88(12), pp.4795–4802. Available at: http://dx.doi.org/10.1016/j.apenergy.2011.06.022.

Galvagno, A. et al., 2013. Biogas as hydrogen source for fuel cell applications. *International Journal of Hydrogen Energy*, 38(10), pp.3913–3920. Available at: http://dx.doi.org/10.1016/j.ijhydene.2013.01.083.

Gandiglio, M. et al., 2016. DESIGN, ENERGY MODELING AND PERFORMANCE OF AN INTEGRATED INDUSTRIAL SIZE BIOGAS SOFC SYSTEM IN A WASTEWATER TREATMENT PLANT. *Proceedings of the ASME 2016 14th International Conference on Fuel Cell Science, Engineering and Technology FUELCELL2016 June 26-30, 2016, Charlotte, North Carolina*.

Gandiglio, M. et al., 2013. Design and balance of plant of a demonstration plant with a Solid Oxide Fuel Cell fed by biogas from Waste-water and exhaust carbon recycling for algae growth. *Journal of Fuel Cell Science and Technology*, 11(June), p.14. Available   at: http://proceedings.asmedigitalcollection.asme.org/data/Journals/JFCSAU/27238/1_1 .pdf%5Cnhttp://fuelcellscience.asmedigitalcollection.asme.org/pdfaccess.ashx?Reso urceID=4508201&PDFSource=13.

Gandiglio, M., Drago, D. & Santarelli, M., 2016. Techno-economic Analysis of a Solid Oxide Fuel Cell Installation in a Biogas Plant Fed by Agricultural Residues and Comparison with Alternative Biogas Exploitation Paths. *Energy Procedia*, 101(September),   pp.1002–1009.   Available   at: http://linkinghub.elsevier.com/retrieve/pii/S1876610216313364.

Gassner, M., 2010. *Process Design Methodology for Thermochemical Production of Fuels from Biomass . Application to the Production of Synthetic Natural Gas from Lignocellulosic Resources*. ÉCOLE POLYTECHNIQUE FÉDÉRALE DE LAUSANNE.   Available   at: https://infoscience.epfl.ch/record/147963/files/EPFL_TH4693.pdf   [Accessed December 28, 2016].

General Electric, Reciprocating Engines. Available at: http://www.2-g.com/de/biogas-module/.

Goldstein, L. et al., 2003. *Gas-Fired Distributed Energy Resource Technology Characterizations*,

Green Energy, 2014. Landfill gas to energy.

Grignani, C. et al., 2006. Produzione di energia e uso agronomico di biomasse agroalimentari e reflui zootecnici. , pp.46–49.

Grillo, O., Magistri, L. & Massardo, A.F., 2003. Hybrid systems for distributed power generation based on pressurisation and heat recovering of an existing 100 kW molten

carbonate fuel cell. *Journal of Power Sources*, 115, pp.252–267.

Hagelqvist, A., 2013. *Sludge from pulp and paper mills for biogas production treatment and sludge management Sludge from pulp and paper mills for biogas production Strategies to improve energy performance in wastewater*,

Hakala, T., 2012. Method and arrangement for controlling anode recirculation. Available at: https://google.com/patents/EP2494641A1?cl=ko.

Hakala, T., 2013. Method and arrangement for controlling anode recirculation for fuel cells using a steam jet ejector. Available at: https://www.google.com/patents/US8580443.

Hamelinck, C.N. et al., 2004. Production of FT transportation fuels from biomass; technical options, process analysis and optimisation, and development potential. *Energy*, 29(11), pp.1743–1771.

Hao, X., Liu, R. & Huang, X., 2015. Evaluation of the potential for operating carbon neutral WWTPs in China. *Water Research*, 87, pp.424–431. Available at: http://dx.doi.org/10.1016/j.watres.2015.05.050 [Accessed November 22, 2016].

Hauptmeier, K., Penkuhn, M. & Tsatsaronis, G., 2016. Economic assessment of a solid oxide fuel cell system for biogas utilization in sewage plants. *Energy*, 117, pp.361–368.

Herbert J. Setzer, E. et al., 1984. AUTOTHERMAL REFORMING CATALYST AND PROCESS.

Herczeg, M., 2013. Municipal waste management in Austria. , (February).

Van Herle, J. et al., 2003. Energy balance model of a SOFC cogenerator operated with biogas. , 118, pp.375–383.

Van Herle, J. et al., 2004. Process flow model of solid oxide fuel cell system supplied with sewage biogas. , 131, pp.127–141.

Hill, R. et al., 2015. Application of molten carbonate fuel cell for CO2 capture in thermal in situ oil sands facilities. *International Journal of Greenhouse Gas Control*, 41, pp.276–284.

Hossain, S.M. & Das, M., 2010. Anaerobic biogas generation from sugar industry wastewaters in three-phase fluidized-bed bioreactor. *Canadian Journal of Chemical Engineering*, 88(6), pp.1085–1090.

Http://www.sofcom.eu., SOFCOM Project, SOFC CCHP with Poly-fuel Operation and Maintenance.

Huang, C.C., Chen, C.H. & Chu, S.M., 2006. Effect of moisture on H2S adsorption by copper impregnated activated carbon. *Journal of Hazardous Materials*, 136(3),

pp.866–873.

International Energy Agency, 2011. *Combining Bioenergy with CCS: Reporting and Accounting for Negative Emissions under UNFCCC and the Kyoto Protocol*,

International Energy Agency- Greenhouse Gas R&D Programme (IEAGHG), 2010. *Corrosion and materials selection in CCS systems*,

International Energy Agency (IEA), 2011. *Co-Generation and Renewables: Solutions for a low-carbon energy future*,

International Energy Agency (IEA), 2016. *Energy, Climate Change and Environment: 2016 Insights*,

IWao Anzai, Y., 2014. METHOD FOR STARTING-UP SOLID OXIDE FUEL CELL SYSTEM.

Janke, L., Leite, A., Nikolausz, M. & Stinner, W., 2015. Biogas production from sugarcane filter cake : Start-up strategies , co-digestion with bagasse and plant design.

Janke, L., Leite, A., Nikolausz, M., Schmidt, T., et al., 2015. Biogas Production from Sugarcane Waste : Assessment on Kinetic Challenges for Process Designing. , pp.20685–20703.

Jasmin Kemper, 2016. Biomass with carbon capture and storage (BECCS or Bio-CCS). In *CCS Leaders Forum, 10-12 February 2016*.

Jradi, M. & Riffat, S., 2014. Tri-generation systems: Energy policies, prime movers, cooling technologies, configurations and operation strategies. *Renewable and Sustainable Energy Reviews*, 32, pp.396–415.

Jungbluth, T. and De Baey-Ernsten, H., 2012. Online European Feedstock Atlas basis version.   Available   at: http://daten.ktbl.de/euagrobiogasbasis/substratemischung.do?selectedKateg=Energy +crops&selectedAction=kategGruppe.

Khoiyangbam, R.S. et al., 2004. Methane emission from fixed dome biogas plants in hilly and plain regions of northern India. , 95, pp.35–39.

Kjaer, B., 2013. Municipal waste management in Denmark. , (February).

Kothari, R. et al., 2014. Different aspects of dry anaerobic digestion for bio-energy: An overview. *Renewable and Sustainable Energy Reviews*, 39, pp.174–195. Available at: http://linkinghub.elsevier.com/retrieve/pii/S1364032114004638 [Accessed January 12, 2015].

Krich, K. et al., 2005. *Biomethane from Dairy Waste A Sourcebook for the Production and Use of Renewable Natural Gas in California*,

Kupecki, J. et al., 2016. Experimental and numerical analysis of a serial connection of two SOFC stacks in a micro-CHP system fed by biogas. *International Journal of Hydrogen Energy*.

Kuramochi, T., Turkenburg, W. & Faaij, A., 2011. Competitiveness of CO2 capture from an industrial solid oxide fuel cell combined heat and power system in the early stage of market introduction. *Fuel*, 90(3), pp.958–973. Available at: http://linkinghub.elsevier.com/retrieve/pii/S0016236110005685 [Accessed January 12, 2015].

Lackey, J., Champagne, P. & Peppley, B., 2016. Use of wastewater treatment plant biogas for the operation of Solid Oxide Fuel Cells (SOFCs). *Journal of Environmental Management*, pp.1–7. Available at: http://linkinghub.elsevier.com/retrieve/pii/S0301479716306557 [Accessed January 10, 2017].

Lackner, K.S., 2003. A Guide to CO2 Sequestration. *Science*, 300(5626).

Leung, D.Y.C., Caramanna, G. & Maroto-Valer, M.M., 2014. An overview of current status of carbon dioxide capture and storage technologies. *Renewable and Sustainable Energy Reviews*, 39, pp.426–443. Available at: http://creativecommons.org/licenses/by/3.0/ [Accessed January 5, 2017].

Linnhoff, B. & Hindmarsh, E., 1983. The pinch design method for heat exchanger networks. *Chemical Engineering Science*, 38(5), pp.745–763.

Lisbona, P. et al., 2007. Analysis of a solid oxide fuel cell system for combined heat and power applications under non-nominal conditions. *Electrochimica Acta 53*, 53, pp.1920–1930.

Liu, P., Gerogiorgis, D.I. & Pistikopoulos, E.N., 2007. Modeling and optimization of polygeneration energy systems. *Catalysis Today*, 127(1), pp.347–359.

Liu, P., Pistikopoulos, E.N. & Li, Z., 2009. A mixed-integer optimization approach for polygeneration energy systems design. *Computers and Chemical Engineering*, 33, pp.759–768.

Liu, P., Pistikopoulos, E.N. & Li, Z., 2010a. A multi-objective optimization approach to polygeneration energy systems design. *AIChE Journal*, 56(5), pp.1218–1234. Available at: http://doi.wiley.com/10.1002/aic.12058 [Accessed January 3, 2017].

Liu, P., Pistikopoulos, E.N. & Li, Z., 2010b. Decomposition Based Stochastic Programming Approach for Polygeneration Energy Systems Design under Uncertainty. *Industrial & Engineering Chemistry Research*, 49(7), pp.3295–3305. Available at: http://pubs.acs.org/doi/abs/10.1021/ie901490g [Accessed January 3, 2017].

Lohila, A. et al., 2007. Micrometeorological measurements of methane and carbon dioxide

fluxes at a municipal landfill. *Environmental science & technology*, 41(8), pp.2717–2722.

Longo, S. et al., 2016. Monitoring and diagnosis of energy consumption in wastewater treatment plants. A state of the art and proposals for improvement. *Applied Energy*, 179(October), pp.1251–1268.

De Lorenzo, G. et al., 2016. Thermoelectric characterization of an intermediate temperature solid oxide fuel cell system directly fed by dry biogas. *Energy Conversion and Management*, 127, pp.90–102.

MacKay, D.J., 2009. *Sustainable Energy - without the hot air (Version 3.5.2. November 3)*,

Malpei, F., 2016. Digestione anaerobica fanghi : benchmark e modalità di ottimizzazione. In *OTTIMIZZAZIONE DELLA DIGESTIONE ANAEROBICA - ComoNext, 28 ottobre 2016*.

Mantripragada, H.C. & Rubina, E.S., 2009. CO2 reduction potential of coal-to-liquids (CTL) plants. *Energy Procedia*, 1(1), pp.4331–4338.

Margalef, P. et al., 2011a. Conceptual design and configuration performance analyses of polygenerating high temperature fuel cells. *International Journal of Hydrogen Energy*, 36(16), pp.10044–10056.

Margalef, P. et al., 2011b. Efficiency of poly-generating high temperature fuel cells. *Journal of Power Sources*, 196(4), pp.2055–2060.

Marsano, F., Magistri, L. & Massardo, A.F., 2004. Ejector performance influence on a solid oxide fuel cell anodic recirculation system. *Journal of Power Sources*, 129, pp.216–228.

Massardo, A.F. & Bosio, B., 2001. Assessment of Molten Carbonate Fuel Cell Models and Integration With Gas and Steam Cycles. *J. Eng. Gas Turbines Power*, 124(1), pp.103–109.

Mccarty, P.L., Bae, J. & Kim, J., 2011. Domestic Wastewater Treatment as a Net Energy Producer - Can This be Achieved? *Environ. Sci. Technol*, 45, pp.7100–7106.

Meerman, J.C., Faaij, A.P.C. & Turkenburg, W.C., 2009. Flexible integrated gasification co-generation facilities A technical and energy analysis. *Energy Procedia*, 1(1), pp.4241–4248.

Mehr, A.S. et al., 2017. Solar-assisted integrated biogas solid oxide fuel cell (SOFC) installation in wastewater treatment plant: energy and economic analysis. *Accepted for publication on Applied Energy*, 191, pp.620–638.

Ministero dello Sviluppo Economico, 2016. DECRETO 23 giugno 2016 - Incentivazione dell'energia elettrica prodotta da fonti rin- novabili diverse dal fotovoltaico.

GAZZETTA UFFICIALE DELLA REPUBBLICA ITALIANA, pp.1–26.

Ministero dello Sviluppo Economico, 2012. *Decreto 6 luglio 2012 - Attuazione dell'art. 24 del decreto legislativo 3 marzo 2011, n. 28, recante incentivazione della produzione di energia elettrica da impianti a fonti rinnovabili diversi dai fotovoltaici,*

Mizuno, Y. & Hatada, S., 2008. Solid oxide fuel cell and reformer. Available at: http://google.com/patents/EP2009726A1?cl=und.

Morandin, M. et al., 2011. Synthesis and parameter optimization of a combined sugar and ethanol production process integrated with a CHP system. *Energy*, 36(6), pp.3675–3690.

Murphy, J.D. & McKeogh, E., 2004. Technical, economic and environmental analysis of energy production from municipal solid waste. *Renewable Energy*, 29, pp.1043–1057.

Nehrir, M.H. & Wang, C., 2009. *Modeling and Control of Fuel Cells: Distributed Generation Applications* Wiley, ed., Available at: http://eu.wiley.com/WileyCDA/WileyTitle/productCd-0470233281.html.

Norsker, N.-H. et al., 2012. On Energy Balance and Production Costs in Tubular and Flat Panel Photobioreactors. *SCHWERPUNKT*, 1.

Novamont S.p.a., RIFIUTI ORGANICI I sistemi e i contenitori.

Novosel, B., Marinšek, M. & Maček, J., 2012. Deactivation of Ni-YSZ Material in Dry Methane and Oxidation of Various Forms of Deposited Carbon. *J. Fuel Cell Sci. Technol*, 9(6)(6), p.61003. Available at: http://fuelcellscience.asmedigitalcollection.asme.org/article.aspx?doi=10.1115/1.4007272 [Accessed November 18, 2016].

NREL, 2013. Biogas Potential in the United States. , pp.1–4.

Organica, D.F. & Territoriale, I.L.C., Il polo ecologico acea: un esempio all'avanguardia nel trattamento della frazione organica. , pp.1–3.

Palazzi, F. et al., 2007. A methodology for thermo-economic modeling and optimization of solid oxide fuel cell systems. *Applied Thermal Engineering*, 27(16), pp.2703–2712.

Palazzi, F. et al., 2010. *OSMOSE user manual,*

Papadias, D.D., Ahmed, S. & Kumar, R., 2012. Fuel quality issues with biogas energy - An economic analysis for a stationary fuel cell system. *Energy*, 44(1), pp.257–277. Available at: http://dx.doi.org/10.1016/j.energy.2012.06.031.

Papurello, D. et al., 2014. Influence of co-vapors on biogas filtration for fuel cells monitored with PTR-MS (Proton Transfer Reaction-Mass Spectrometry). *Fuel Processing Technology*, 118, pp.133–140. Available at:

http://dx.doi.org/10.1016/j.fuproc.2013.08.011.

Papurello, D. et al., 2012. Monitoring of volatile compound emissions during dry anaerobic digestion of the Organic Fraction of Municipal Solid Waste by Proton Transfer Reaction Time-of-Flight Mass Spectrometry. *Bioresource Technology*, 126, pp.254–265. Available at: http://dx.doi.org/10.1016/j.biortech.2012.09.033.

Pfeifer, T. et al., 2013. System design and process layout for a SOFC micro-CHP unit with reduced operating temperatures. *International Journal of Hydrogen Energy*, 38(1), pp.431–439. Available at: http://dx.doi.org/10.1016/j.ijhydene.2012.09.118.

Piccinini, S., 2010. State of the art of biogas in Italy. , pp.1–8.

Pino, L. et al., 2014. Hydrogen from biogas: Catalytic tri-reforming process with Ni/LaCeO mixed oxides. *Applied Catalysis B: Environmental*, 148–149, pp.91–105. Available at: http://linkinghub.elsevier.com/retrieve/pii/S0926337313006681 [Accessed November 18, 2016].

Pino, L. et al., 2011. Hydrogen production by methane tri-reforming process over Ni–ceria catalysts: Effect of La-doping. *Applied Catalysis B: Environmental*, 104(1–2), pp.64–73. Available at: http://linkinghub.elsevier.com/retrieve/pii/S092633731100097X [Accessed November 18, 2016].

Pontual, L., Mainier, F.B. & Lima, G.B.A., 2015. The Biogas Potential of Pulp and Paper Mill Wastewater : An Essay. , 5(3), pp.53–57.

Pöschl, M., Ward, S. & Owende, P., 2010. Evaluation of energy efficiency of various biogas production and utilization pathways. *Applied Energy*, 87, pp.3305–3321.

Pret, M.G. et al., 2015. Thermal design , modeling and validation of a steam-reforming reactor for fuel cell applications. *Chemical Engineering Research and Design*, 104, pp.503–512. Available at: http://dx.doi.org/10.1016/j.cherd.2015.09.016.

Priadi, C. et al., 2014. Biogas Production in the Anaerobic Digestion of Paper Sludge. *Procedia - Social and Behavioral Sciences*, 9(Icbee 2013), pp.65–69. Available at: http://dx.doi.org/10.1016/j.apcbee.2014.01.012.

R. Goldstein & W. Smith, 2002. *Water & Sustainability (Volume 4): U.S. Electricity Consumption for Water Supply & Treatment -The Next Half Century*,

Raj, N.T., Iniyan, S. & Goic, R., 2011. A review of renewable energy based cogeneration technologies. *Renewable and Sustainable Energy Reviews*, 15(8), pp.3640–3648.

Rasi, S., Läntelä, J. & Rintala, J., 2011. Trace compounds affecting biogas energy utilisation – A review. *Energy Conversion and Management*, 52(12), pp.3369–3375. Available at: http://dx.doi.org/10.1016/j.enconman.2011.07.005.

Reale, F. et al., 2009. Analisi e stima quantitativa della potenzialità di produzione

energetica da biomassa digeribile a livello regionale . Studio e sviluppo di un modello per unità energetiche Parte 1 - Metodologia. , p.129.

Rechberger, P. & Lötjönen, T., 2009. Introduction. *Energy from field energy crops – a handbook for energy producers*, pp.6–12.

Regione Lombardia, 2013. La Digestione Anaerobica Di Rifiuti E Biomasse : Rassegna Delle Potenzialità Specifiche Di Produzione.

Rhodes, J.S. & Keith, D.W., 2008. Biomass with capture: negative emissions within social and environmental constraints: an editorial comment. *Climatic Change*, 87, pp.321–328.

Roland Berger Strategy Consultants, 2015. *Advancing Europe's energy systems: Stationary fuel cells in distributed generation. A study for the Fuel Cells and Hydrogen Joint Undertakinng*,

Rong, A. & Lahdelma, R., 2007. Efficient algorithms for combined heat and power production planning under the deregulated electricity market. *European Journal of Operational Research*, 176(2), pp.1219–1245.

Rong, A. & Lahdelma, R., 2016. Role of polygeneration in sustainable energy system development challenges and opportunities from optimization viewpoints. *Renewable and Sustainable Energy Reviews*, 53, pp.363–372. Available at: http://dx.doi.org/10.1016/j.rser.2015.08.060.

Rossi, L. & Piccinini, S., 2009. Caratteristiche di sottoprodotti e scarti dell'industria agro-alimentare avviabili a recupero di energia e/o materia.

Rubin, E. et al., 2013. *Toward a Common Method of Cost Estimation for CO2 Capture and Storage at Fossil Fuel Power Plants*, Available at: http://cdn.globalccsinstitute.com/sites/default/files/publications/85761/toward-common-method-cost-estimation-ccs-fossil-fuel-power-plants-white-paper.pdf.

Ryckebosch, E., Drouillon, M. & Vervaeren, H., 2011. Techniques for transformation of biogas to biomethane. *Biomass and Bioenergy*, 35(May 2011), pp.1633–1645.

Sammes, N.M., 2002. Integrated solid oxide fuel cell and reformer. Available at: https://www.google.com/patents/US6492050.

Santarelli, M. et al., 2017. Carbon recovery and re-utilization (CRR) from the exhaust of a solid oxide fuel cell (SOFC): analysis through a proof-of-concept. *Accepted for publication on Journal of CO2 utilization*, 18, pp.206–221.

Santarelli, M., Lanzini, A. & Gandiglio, M., 2014. *Technical report on the potential impact of biogas exploitation with the SOFC technology in waste-water treatment plants - Deliverable 4.5 of SOFCOM Project n° 278798 "SOFC CHP WITH POLY-FUEL: OPERATION AND MAINTENANCE,"*

Seadi, T. Al et al., 2008. *Biogas handbook*,

SEVA Energy AG, Heat&Power systems catalogue. Available at: http://www.simonsgreenenergy.com.au/pdf/SEVA Brochure.pdf.

Sevigné Itoiz, E. et al., 2012. Energy balance and environmental impact analysis of marine microalgal biomass production for biodiesel generation in a photobioreactor pilot plant. *Biomass and Bioenergy*, 39, pp.324–335. Available at: www.sciencedirect.com [Accessed December 29, 2016].

Shiratori, Y. & Sakamoto, M., 2016. Performance improvement of direct internal reforming solid oxide fuel cell fuelled by H2S-contaminated biogas with paper-structured catalyst technology. *Journal of Power Sources*, 332, pp.170–179.

Sigot, L. et al., 2016. Comparing the performance of a 13X zeolite and an impregnated activated carbon for H2S removal from biogas to fuel an SOFC: Influence of water. *International Journal of Hydrogen Energy*, 41(41), pp.18533–18541.

Singh, R.N. & Sharma, S., 2012. Development of suitable photobioreactor for algae production – A review. , 16(4), pp.2347–2353.

Singhal, S.C. & Dokiya, M., 2003. *Solid Oxide Fuel Cells VIII: (SOFC VIII) : Proceedings of the International Symposium, Volume 8* T. E. Society, ed.,

Singhal, S.C. & Kendall, K., 2003. *High-temperature solid oxide fuel cells : fundamentals, design, and applicatons*, Elsevier Advanced Technology.

Sisani, E. et al., 2014. Adsorptive removal of H2S in biogas conditions for high temperature fuel cell systems. *International Journal of Hydrogen Energy*, 39(36), pp.21753–21766.

Sitthikhankaew, R. et al., 2014. Effects of humidity, O2, and CO2 on H2S adsorption onto upgraded and KOH impregnated activated carbons. *Fuel Processing Technology*, 124.

Slade, R. & Bauen, A., 2013. Micro-algae cultivation for biofuels : Cost , energy balance , environmental impacts and future prospects. *Biomass and Bioenergy*, 53(0), pp.29–38. Available at: http://dx.doi.org/10.1016/j.biombioe.2012.12.019 [Accessed December 29, 2016].

Smith, A.R. & Klosek, J., 2001. A review of air separation technologies and their integration with energy conversion processes. *Fuel Processing Technology*, 70, pp.115–134.

Song, C. & Pan, W., 2004. Tri-reforming of methane: a novel concept for catalytic production of industrially useful synthesis gas with desired H2/CO ratios. *Catalysis Today*, 98(4), pp.463–484. Available at: http://linkinghub.elsevier.com/retrieve/pii/S0920586104005644 [Accessed November 18, 2016].

De Souza, S.N.M., Santos, R.F. & Fracaro, G.P.M., 2011. Potential for the Production of Biogas in Alcohol and Sugar Cane Plants for Use in Urban Buses in the Brazil. *Production*, pp.418–424. Available at: http://www.ep.liu.se/ecp_article/index.en.aspx?issue=57;vol=1;article=56.

Styring, P. et al., 2011. Carbon Capture and Utilisation in the green economy. *Centre for Low Carbon Futures*, p.60.

Surroop, D. & Romeela, M., 2011. Power Generation From Landfill Gas. *2nd International Conference on Environmental Engineering and Applications*, 17(November 1997), pp.238–241. Available at: http://www.ipcbee.com/vol17/45-L30010.pdf.

Tchobanoglous, G., Leverenz, H. & Gikas, P., 2009. IMPACTS OF NEW CONCEPTS AND TECHNOLOGY ON THE ENERGY SUSTAINABILITY OF WASTEWATER MANAGEMENT. In *Climate Change, Sustainable Development, and Renewable Energy Sources*.

TDA Research Inc, 2015. *Novel Sorbent to Clean Up Biogas for CHPs*,

The Royal Society, 2009. Geoengineering the climate: science, governance and uncertainty.

Themelis, N.J. & Ulloa, P. a., 2007. Methane generation in landfills. *Renewable Energy*, 32, pp.1243–1257.

Thomas, D.C. & Benson, S., 2005. *Carbon dioxide capture for storage in deep geologic formations: results from the CO_2 capture project*, Elsevier.

Tjaden, B. et al., 2014. Small-scale biogas-SOFC plant: Technical analysis and assessment of different fuel reforming options. *Energy and Fuels*, 28(6), pp.4216–4232.

Torres, J., 2013. *Utilización de CO2*,

Torres, J. & Vega, L., 2011. *Documento elaborado por MATGAS para la Plataforma Española del CO2 - USOS INDUSTRIALES DEL CO2*,

TPEnergy, DATI MEDI DI PRODUZIONE BIOGAS - ENERGIA ELETTRICA / TERMICA. , pp.1–2.

Tredici, M.R. et al., 2015. Energy balance of algal biomass production in a 1-ha Green Wall Panel plant: How to produce algal biomass in a closed reactor achieving a high Net Energy Ratio. *Applied Energy*, 154, pp.1103–1111.

Trendewicz, A.A. & Braun, R.J., 2013. Techno-economic analysis of solid oxide fuel cell-based combined heat and power systems for biogas utilization at wastewater treatment facilities. *Journal of Power Sources*, 233, pp.380–393. Available at: http://dx.doi.org/10.1016/j.jpowsour.2013.01.017.

Turton, R. et al., 2012. *Analysis, Synthesis and Design of Chemical Processes (4th Edition)*,

USDA, U. states D. of A., 2015. Sugar: World Markets and Trade. Available at: https://public.govdelivery.com/accounts/USDAFAS/subscriber/new.

Vassilev, S. V et al., 2010. An overview of the chemical composition of biomass. *Fuel*, 89(5), pp.913–933. Available at: http://dx.doi.org/10.1016/j.fuel.2009.10.022.

Vega, L.F., *La utilización del CO2 en el contexto industrial y energético actual*,

Vega, L.F., *Proyectos estratégicos en usos industriales sostenibles del CO2 en España: visión industrial*,

Vita, A. et al., 2014. Biogas as renewable raw material for syngas production by tri-reforming process over NiCeO2 catalysts: Optimal operative condition and effect of nickel content. *Fuel Processing Technology*, 127, pp.47–58. Available at: http://linkinghub.elsevier.com/retrieve/pii/S0378382014002513 [Accessed November 18, 2016].

Wang, X. et al., 2008. Predicting the Performance of System for the Co-production of Fischer-Tropsch Synthetic Liquid and Power from Coal. *Journal of Engineering for Gas Turbines and Power*, 130(1), p.11401. Available at: http://gasturbinespower.asmedigitalcollection.asme.org/article.aspx?articleid=14256 56 [Accessed January 3, 2017].

WERF (Water Environment Research Foundation), 2010. *Sustainable Treatment: Best Practices from the Strass im Zillertal Wastewater Treatment Plant*,

WERF (Water Environment Research Foundation), 2016. *WERF Energy Factsheet*,

Wilkinson, M.B. et al., 2003. Oxyfuel Conversion of Heaters and Boilers for CO 2 Capture. In *Second National Conference on Carbon Sequestration, May 5th – 8th 2003, Washington, DC*. pp. 1–13.

Willich, C. et al., Pressurized Solid Oxide Fuel Cells: Operational Behavior.

Witzke, H.P., Zintl, a. & Tonini, a., 2009. *The Common Agricultural Policy SIMulation (CAPSIM) Model: Dairy Reform and Western Balkan Countries Accession Scenarios*, Available at: ftp://139.191.159.34/users/publications/public/EURdoc/EURdoc/JRC50411.pdf.

Wood, G.O., 2002. A review of the effects of covapors on adsorption rate coefficients of organic vapors adsorbed onto activated carbon from flowing gases. *Carbon*, 40(5), pp.685–694.

World Bank Data, data.worldbank.org. Available at: http://data.worldbank.org/italian.

Wu, B. et al., 2016. Energetic-environmental-economic assessment of the biogas system

with three utilization pathways : Combined heat and power , biomethane and fuel cell. *Bioresource Technology*, 214, pp.722–728. Available at: http://dx.doi.org/10.1016/j.biotech.2016.05.026 [Accessed January 10, 2017].

WUILLEMIN, Z., 2009. *Experimental and Modeling Investigations on Local Performance and Local Degradation in Solid Oxide Fuel Cells*. ÉCOLE POLYTECHNIQUE FÉDÉRALE DE LAUSANNE.

Yasar, A. et al., 2015. Waste to energy analysis of shakarganj sugar mills; biogas production from the spent wash for electricity generation. *Renewable and Sustainable Energy Reviews*, 43, pp.126–132. Available at: http://linkinghub.elsevier.com/retrieve/pii/S1364032114009691.

Yu, J., Wang, Y. & Weng, S., 2012. Numerical Analysis of the Possibility of Carbon Formation in Planar SOFC Fueled With Syngas. *J. Fuel Cell Sci. Technol*, 9(2)(2), p.21011. Available at: http://fuelcellscience.asmedigitalcollection.asme.org/article.aspx?articleid=1472393 [Accessed November 18, 2016].

Yukihiro Sugiura, K., 2013. INDIRECT INTERNAL REFORMING SOLID OXIDE FUEL CELL SYSTEM.